

**NIST Technical Note 1952**

**LTE Impacts on GPS  
Final Report**

William F. Young  
Ari Feldman, Sheryl Genco, Aziz Kord, Daniel G. Kuester,  
John Ladbury, Duncan A. McGillivray, Audrey K. Puls, Andre Rosete,  
Adam Wunderlich, and Wen-Bin Yang

This publication is available free of charge from:  
<https://doi.org/10.6028/NIST.TN.1952>

**NIST Technical Note 1952**

# **LTE Impacts on GPS**

## **Final Report**

William F. Young  
Ari Feldman, Sheryl Genco, Aziz Kord, Daniel G. Kuester,  
John Ladbury, Duncan A. McGillivray, Audrey K. Puls, Andre Rosete,  
Adam Wunderlich, and Wen-Bin Yang  
*Communications Technology Laboratory*

This publication is available free of charge from:  
<https://doi.org/10.6028/NIST.TN.1952>

February 2017



National Institute of Standards and Technology  
*Kent Rochford, Acting NIST Director and Under Secretary of Commerce for Standards and Technology*

Certain commercial entities, equipment, or materials may be identified in this document in order to describe an experimental procedure or concept adequately. Such identification is not intended to imply recommendation or endorsement by the National Institute of Standards and Technology, nor is it intended to imply that the entities, materials, or equipment are necessarily the best available for the purpose.

**National Institute of Standards and Technology Technical Note 1952**  
**Natl. Inst. Stand. Technol. Tech. Note 1952, 425 pages (February 2017)**  
**CODEN: NTNOEF**

**This publication is available free of charge from:**  
**<https://doi.org/10.6028/NIST.TN.1952>**

NASCTN Report 1

NIST Technical Note 1952

# LTE Impacts on GPS

## Final Test Report

William F. Young, Ari Feldman, Sheryl Genco, Aziz Kord, Daniel G. Kuester,  
John Ladbury, Duncan A. McGillivray, Audrey K. Puls, Andre Rosete,  
Adam Wunderlich, and Wen-Bin Yang

February 15, 2017



# NASCTN

National Advanced Spectrum and  
Communications Test Network

## National Advanced Spectrum and Communications Test Network (NASCTN)

The mission of the National Advanced Spectrum and Communications Test Network (NASCTN) is to provide, through its members, robust test processes and validated measurement data necessary to develop, evaluate and deploy spectrum sharing technologies that can increase access to the spectrum by both federal agencies and non-federal spectrum users.

The U.S. Department of Commerce's National Institute of Standards and Technology (NIST) and National Telecommunications and Information Administration (NTIA) established the Center for Advanced Communications (CAC) in Boulder, Colorado, to address, among other challenges, the increasing need for spectrum sharing testing and evaluation capabilities to meet national needs. As part of CAC's mission to provide a single focal point for engaging both industry and other government agencies on advanced communication technologies, including testing, validation, and conformity assessment, NASCTN was formed under the umbrella of the CAC. NIST hosts the NASCTN capability at the Department of Commerce Boulder Laboratories in Boulder, Colorado. NASCTN is a membership organization under a charter agreement. Members

- Make available, in accordance with their organization's rules policies and regulations, engineering capabilities and test facilities, with typical consideration for cost.
- Coordinate their efforts to identify, develop and test spectrum sharing ideas, concepts and technology to support the goal of advancing more efficient and effective spectrum sharing.
- Make available information related to spectrum sharing, considering requirements for the protection of intellectual property, national security, and other organizational controls, and, to the maximum extent possible, allow the publication of NASCTN test results.
- Ensure all spectrum sharing efforts are identified to other interested members.

Current charter members are:

- National Telecommunications and Information Administration (NTIA)
- National Institute of Standards and Technology (NIST)
- Department of Defense Chief Information Officer (DoD CIO)

# LTE Impacts on GPS

## FINAL TEST REPORT

**Dr. Sheryl Genco**  
Project Manager

*NASCTN/Test Coordination Office  
Communications Technology Lab  
NIST*

**Dr. William F. Young**  
Testmaster

*Shared Spectrum Metrology Group  
RF Technology Division  
Communications Technology Lab  
NIST*

**Dr. Ari Feldman**

*High-Speed Measurements Group  
RF Technology Division  
Communications Technology Lab  
NIST*

**Aziz Kord**

*Shared Spectrum Metrology Group  
RF Technology Division  
Communications Technology Lab  
NIST*

**Dr. Daniel G. Kuester**

*Shared Spectrum Metrology Group  
RF Technology Division  
Communications Technology Lab  
NIST*

**John Ladbury**

*RF Fields Group  
RF Technology Division  
Communications Technology Lab  
NIST*

**Dr. Duncan A. McGillivray**

*Shared Spectrum Metrology Group  
RF Technology Division  
Communications Technology Lab  
NIST*

**Audrey K. Puls (Assoc.)**

*Shared Spectrum Metrology Group  
RF Technology Division  
Communications Technology Lab  
NIST*

**Andre Rosete (Assoc.)**

*Shared Spectrum Metrology Group  
RF Technology Division  
Communications Technology Lab  
NIST*

**Dr. Adam Wunderlich**

*NASCTN/Test Coordination Office  
Communications Technology Lab  
NIST*

**Dr. Wen-Bin Yang**

*Wireless Networks Division  
Communications Technology Lab  
NIST*

February 15, 2017



**NASCTN**

National Advanced Spectrum  
and Communications Test Network



## Acknowledgments

The development and execution of this test methodology and data parsing and analysis required input from multiple types of expertise. Integrating and leveraging a wide range of technical skills was critical to the overall success of the project. Team members, while responsible for specific areas in their domain of expertise, were called upon to contribute to other technical and programmatic areas as needed to ensure the overall project success.

Within the technical team, Dr. Daniel G. Kuester led the RF testbed design, including the automation and calibration processes; Dr. Adam Wunderlich headed up the data analysis, investigation into measurand behaviors, and presentation of collected data; Dr. Duncan A. McGillivray led the integration of devices under test (DUTs), optimization of the test operations for efficiency, and establishment of the GPS test conditions with Carlos Ruiz of the Electronic Proving Grounds at Fort Huachuca<sup>1</sup>; John Ladbury led the RF uncertainty analysis and supported calibration of the RF signaling chain; and Dr. Ari Feldman led the database construction, and supported data parsing and automated data acquisitions from DUTs. Other key members of the technical team include Aziz Kord, who focused on extracting data from DUTs; Andre Rosete, who supported the parsing of data and DUT-to-testbed interfacing; and Audrey K. Puls, who supported the calibration of the testbed and organization of the testing process. Dr. Wen-Bin Yang performed simulation analysis on  $C/N_0$  algorithm behavior and Frank Sanders of ITS<sup>2</sup> provided technical feedback during the test method development.

Success of a project of this complexity requires strong technical management. Dr. Sheryl Genco coordinated this elaborate effort, resolved scheduling challenges, and enabled productive exchanges with all the stakeholders, including manufacturers, the sponsor, and government agencies; Dr. Mike Janezic led critical outreach efforts with both NASCTN members and external stakeholder agencies; and Eric Fisher of the Electronic Proving Grounds made available GPS technical material and personnel support necessary to complete the testing.

Finally, the technical team thanks NIST management, Dr. Kent Rochford, Associate Director for Laboratory Programs; Dereck Orr, Acting Communication Technical Laboratory Director, Dr. Michael Kelley, RF Technology Division Chief; and Dr. Stefania Romisch, Group Leader of the Atomic Standards Group, for their support, which made the project success possible.

---

<sup>1</sup>The Electronic Proving Ground is the US Army's organization for testing command, communications, control, computer, and intelligence systems and equipment including testing of global positioning system (GPS) receivers.

<sup>2</sup>The Institute for Telecommunications Sciences (ITS), located in Boulder, Colorado, is the research and engineering arm of the National Telecommunications and Information Administration (NTIA).



## Executive Summary

**Project Submittal** In April of 2016, Ligado Networks submitted a project proposal to the National Advanced Spectrum and Communications Test Network (NASCTN) [1]. The request was for NASCTN to (1) develop a test method to investigate the impact of adjacent-band long-term evolution (LTE) signals on global positioning system (GPS) devices that operate in the L1 frequency band, and (2) perform radiated measurements on a representative set of GPS devices to validate the test method.

**Test Plan Development** After screening the proposal and initiating this project, NASCTN convened a panel of technical experts to develop a test plan with these following objectives:

- develop a test plan that is transparent, reproducible, and well-calibrated,
- develop sound, statistically-valid data retrieval and processing techniques,
- provide a clear path from measurement setup, to data collection, to processed results, and
- provide data to inform discussions between different interested parties on proper measurement requirements.

The test method was designed to make reproducible measurements under clearly-defined test conditions in order to isolate impacts of radiated LTE signals on GPS receivers, and to allow others to make comparable measurements if desired. To accomplish this, the approach aimed to measure the response of selected GPS devices given well-controlled GPS and LTE power levels under fixed, stable thermal noise conditions, while limiting the number of other extraneous variables. This report describes key test setup and process details so that a reasonably knowledgeable technical team can expect their execution of the same tests on the same devices to yield measurand responses within the calculated uncertainty bounds.

In May of 2016, the NASCTN team completed the draft test plan and distributed it to a cross-section of GPS manufacturers, federal agencies, and spectrum regulators to obtain technical feedback on the proposed method. Over a two-month period, NASCTN received 159 comments from 10 different organizations, including spectrum regulators, federal agencies, GPS manufacturers and members of the general public. The NASCTN test team reviewed the comments and developed a revised test plan in July of 2016 that addressed the technical issues raised in the comments. The draft test plan, the revised test plan, and the adjudicated comments from the review process are all publicly available on the NASCTN website.

**Key Aspects of the Test Method** In this test method, a well-characterized, simulated satellite constellation was presented to each GPS receiver. The GPS receiver was then also exposed to

a stepped range of LTE power levels in three proposed frequency bands adjacent to GPS L1. Measurand data, as reported by the GPS receiver, were collected at a baseline condition (i.e., no LTE adjacent-band activity) and for each LTE power level in the covered LTE power range. The time spent collecting data at the baseline condition and at each LTE power level was generally of sufficient length for the GPS receiver measurand outputs to reach steady state. Collected raw measurand data were formatted for additional analysis and presentation. The next several paragraphs highlight key aspects of the test method and data analysis that are discussed in detail within the body of the report.

In order to support a broad understanding of GPS receiver performance, the test plan focused on a variety of measurands, including carrier-to-noise-density ratio ( $C/N_0$ ), 3D position error (3DPE), timing error, number of satellites in view, time to first fix (TTFF), and time to first reacquisition (TTFR). The tests assessed each of these measurands across a large range of adjacent-band LTE power levels.

As discussed in Section 2.1, the NASCTN test plan considered four classes of GPS receivers – general location and navigation (GLN), high-performance positioning (HPP), real-time kinematic (RTK), and GPS-disciplined oscillator (GPSDO). Each class is differentiated by a general set of GPS features that is geared towards some common type of end-user application. The set of devices in each class was selected for 1) the ability to output an adequately broad variety of GPS and device state data, 2) recommendations from the test plan review process, and 3) device representation in prior test campaigns.

To help ensure that any interference during testing was attributable to LTE and not other sources of electromagnetic interference (EMI), each device under test (DUT) was tested individually within a shielded chamber.

The LTE communication waveforms emulated in these tests required some assumptions about basic signal parameters. The LTE network deployment under study was intended to be generic and architecture agnostic; this informed test conditions for parameters like power level, resource block usage, and data transfer rate. As was typical in previous testing, the LTE downlink signal was assigned a 10 MHz frequency-division duplex (FDD) LTE channel with fully-allocated resource blocks, making the 10 MHz band allocation fully occupied. The uplink bands were allocated 10 MHz of LTE, with resource block loading of 70%. This represented a realistic degree of heavy uplink data throughput from user equipment.

The test focused on collecting measurement data from a stationary GPS device exposed to a simulated moving constellation of GPS satellites. There were two test case scenarios, which were differentiated by the extent of satellite exposure at the DUT:

- Nominal GPS exposure: Each DUT was exposed to target levels of -128.5 dBm EIIP (defined in Section A.1) from each satellite. Each DUT reported baseline  $C/N_0$  values ranging between 40 dB-Hz and 50 dB-Hz when no LTE activity was present.

- Limited GPS exposure: This exposure condition was included in order to stress the DUT. The implementation reduced the number of satellites below nominal, and reduced the GPS signal strength of remaining satellites to various levels, as far as 15 dB below nominal exposure. Both the nominal and limited satellite conditions are described in more detail in Section 2.2.

Key features of the test method include:

- use of composite LTE waveforms that include both in-band activity and proposed out-of-band emission (OOBE) masks (Subsection 2.3.2 and Section 3.1),
- thorough calibration and characterization of the radio frequency (RF) transmission system (Section 3.5 and Section 3.6),
- reset and initialization of DUTs to a known state prior to each test condition (Subsubsection 2.1.3.1),
- LTE exposure times of stepped power levels that are generally sufficient to achieve a steady-state operating condition in the DUT (Subsection 4.3.1 and Section 5.4),
- TTFF and TTFR response of DUTs based on 100 repeated trials (Subsection 2.4.2, Subsection 4.3.2, and Subsection 4.3.2),
- simultaneous activity on the proposed LTE uplink and LTE downlink bands (Subsection 2.4.1), and
- time stability of pulse-per-second output from each DUT relative to a cesium atomic clock (Subsection 3.1.4, Subsubsection 4.3.1.3, and Subsection 5.5.3).

These features enabled a wide variety of response data for each DUT that was supported by extensive testbed characterization data.

**Measurement Campaign** Using the revised test plan, NASCTN coordinated and performed the radiated measurements associated with this project at two facilities – a semi-anechoic chamber at National Technical Systems (NTS) in Longmont, CO and at a fully-anechoic chamber at the NIST Broadband Interoperability Testbed (NBIT) facility in Boulder, CO. NASCTN relied on technical staff from NIST and the U.S. Army’s Electronic Proving Grounds to perform and validate the measurements and collect the data. The team was multi-disciplinary, including experts in GPS devices and simulation, radiated radio-frequency measurements, timing measurements, microwave metrology, statistical analysis, and data processing.

Automation was vital to achieving repeatability by enforcing consistency of test conditions and synchronous data acquisition. Initial set-up was carried out during the month of July, and testing was executed nearly continuously from August through the end of October. The total testbed operation time for the results presented in this report was 1,476 hours. These data represent 968 LTE exposure tests at discrete power levels (including nominal and limited GPS satellite condition), 891 TTFR tests, 5,155 TTFF tests, and 83 timing receiver tests. Over the three months of the measurement campaign, 38,222 data capture files (including testbed state and DUT reporting) were acquired, from which 19,220 parsed data files were generated. Subsequent data processing yielded a set of 3,859 anonymized data files (780 MB) that is available along with this report.

**Measurement Results** The measurement data collected for this project are summarized in a series of plots provided in Chapter 6. The plots include:

- LTE power level sweeps for general location and navigation (GLN) and high-performance positioning (HPP) including real-time kinematic (RTK) devices:
  - scatter plots versus LTE power for 3DPE,  $C/N_0$ , and the number of satellites in view
  - plots of 95% confidence regions for the median versus LTE power for 3DPE and  $C/N_0$
- LTE power level sweeps for GPSDO devices:
  - time-series plots of warmed-up time interval counter (TIC) output
  - plots of Allan time Deviation (TDEV) for the warmed-up TIC data
  - time-series plots of the number of satellites in view
  - $C/N_0$  scatterplots and 95% confidence regions for median versus LTE power
- TTFF and TTFR tests
  - scatter plots of TTFF or TTFR versus LTE power
  - plots of empirical cumulative distribution functions (CDFs) for TTFF and TTFR at each tested power level.

The uncertainties in the data values, described in Section 5.4, depended on DUT factors (internal processing algorithms, output data rate, output data resolution, hardware capabilities), as well as test factors such as measurement duration (hence, number of data samples). Post-processing and statistical analysis techniques took these aspects into account and provided uncertainty estimates for the DUT data outputs. These estimates included detailed uncertainty analyses of the strength of GPS and LTE exposure at the plane of the DUT.

NASCTN provided briefings to federal agencies in order to summarize the test method and preliminary measurement data: one on September 27, 2016, and another on November 15, 2016.

**Comparisons with Previous Measurements** Comparison among results of different test campaigns (including this study and [2–5]) requires an understanding of any differences in test conditions, devices, and parameters. Specific examples include GPS and LTE signal parameters, power levels, and test environments. Understanding these factors is crucial to drawing conclusions based on the aggregate of these heterogeneous test results. These types of analyses are beyond the scope of this project, but may be undertaken by other interested parties such as the GPS and cellular communications industry, government agencies, or spectrum regulators.

# Contents

Acknowledgments . . . . .	v
Executive Summary . . . . .	vii
List of Acronyms . . . . .	xx
List of Figures . . . . .	xxxvi
List of Tables . . . . .	xxxix
<b>1 Introduction</b>	<b>1</b>
1.1 Objective . . . . .	1
1.2 Scope . . . . .	2
1.3 Anonymization of Data . . . . .	4
1.4 Background . . . . .	4
1.5 Stakeholder Outreach . . . . .	5
1.6 Overview . . . . .	6
<b>2 Test Parameters</b>	<b>9</b>
2.1 GPS Receivers . . . . .	9
2.1.1 Test Population . . . . .	9
2.1.1.1 General Location and Navigation (GLN) . . . . .	9
2.1.1.2 High-Precision Positioning (HPP) . . . . .	12
2.1.1.3 Real-Time Kinematic (RTK) . . . . .	12
2.1.1.4 GPS-Disciplined Oscillators (GPSDO) . . . . .	12
2.1.1.5 External Antennas . . . . .	14
2.1.2 Measurands . . . . .	14
2.1.2.1 Focus and Scope . . . . .	14
2.1.2.2 Statistical Analysis and Reporting . . . . .	15
2.1.3 Test Capabilities . . . . .	15
2.1.3.1 Support for Warm and Cold Start . . . . .	15
2.1.3.2 Data Formats . . . . .	16
2.1.4 Incident Power at the Receiver . . . . .	16
2.2 GPS Constellation Characteristics . . . . .	18
2.2.1 Base Signal Parameters . . . . .	19
2.2.2 LTE Power Level Sweep Test Scenarios . . . . .	20
2.2.2.1 Nominal (GLN, HPP, RTK) . . . . .	20
2.2.2.2 Limited (GLN, HPP, RTK) . . . . .	20
2.2.2.3 Timing (GPSDO) . . . . .	22
2.2.3 TTFF and TTFR Test Scenarios . . . . .	22

2.2.3.1	TTFB . . . . .	22
2.2.3.2	TTFR . . . . .	23
2.2.4	Augmentation Signals . . . . .	23
2.2.4.1	WAAS . . . . .	23
2.2.4.2	GPS L2 . . . . .	23
2.2.4.3	Other GNSS Systems . . . . .	23
2.2.5	Track Modifications for Daily Constellation Reuse . . . . .	24
2.3	Long Term Evolution (LTE) Signal Characteristics . . . . .	24
2.3.1	LTE Bands Under Consideration . . . . .	24
2.3.2	Radiated Emissions Mask . . . . .	25
2.3.3	LTE Baseband Signal Characteristics . . . . .	25
2.4	Test Sweeps of GPS Receiver Response . . . . .	28
2.4.1	LTE Power Level Sweeps . . . . .	28
2.4.1.1	Positioning Classes (GLN, HPP, and RTK) . . . . .	28
2.4.1.2	Timing Classes (GPSDO) . . . . .	29
2.4.2	Time to First Fix (TTFF) and Time to First Reacquisition (TTFR) Swept with LTE Power . . . . .	30
2.4.2.1	GLN, HPP, and RTK . . . . .	30
2.5	Test Campaign Execution and Scope . . . . .	32
2.5.1	Phase 1: LTE Power Level Sweeps for Nominal GPS Power Exposure . . . . .	32
2.5.2	Phase 2: TTFF and TTFR Tests . . . . .	33
2.5.3	Phase 3: LTE Power Level Sweeps for Limited GPS Power Exposure . . . . .	33
<b>3</b>	<b>GPS and LTE Transmission System</b> . . . . .	<b>35</b>
3.1	System Overview . . . . .	35
3.1.1	GLN/Base Test Configuration . . . . .	35
3.1.2	HPP Test Configuration . . . . .	36
3.1.3	RTK Test Configuration . . . . .	37
3.1.4	GPSDO Test Configuration . . . . .	37
3.1.5	Top-Level Manifest of Equipment . . . . .	39
3.2	Radiated Test Setup . . . . .	42
3.2.1	Test Chambers . . . . .	42
3.2.2	Chamber Layout . . . . .	43
3.2.3	Single-Antenna Transmission . . . . .	43
3.2.3.1	LTE Polarization Correction . . . . .	45
3.2.3.2	Signal Coupling Considerations . . . . .	45
3.3	Measurement Transmitter Design . . . . .	45
3.3.1	Level, Combine, and Monitor Network . . . . .	45
3.3.2	Design Priorities . . . . .	46
3.3.3	Coupled GPS “Tap” Output . . . . .	46
3.3.4	Manifest of Instrumentation and Test Parts . . . . .	46
3.4	Waveform Synthesis . . . . .	49

3.4.1	LTE OOB DL . . . . .	49
3.4.2	LTE OOB UL . . . . .	49
3.5	Calibration and Leveling . . . . .	50
3.5.1	Conducted GPS . . . . .	50
3.5.2	Conducted LTE . . . . .	50
3.5.3	Radiated Losses . . . . .	51
3.5.4	Radiated GPS . . . . .	52
3.5.5	Power Level Uncertainty . . . . .	52
3.6	Transmitter Performance Characterization and Validation . . . . .	52
3.6.1	LTE Modulation Fidelity . . . . .	53
3.6.2	Dynamic Range . . . . .	53
3.6.2.1	Maximum Output Power . . . . .	53
3.6.2.2	Output Noise Floor . . . . .	54
3.6.2.3	Conducted and Radiated Levels . . . . .	55
3.6.2.4	Noise Output Mitigation . . . . .	55
3.6.3	Signal Path Isolation . . . . .	56
3.6.4	LTE Filtering and Spectral Regrowth . . . . .	58
3.6.4.1	Review of Spectral Regrowth . . . . .	58
3.6.4.2	Out-of-Band Outputs of the LTE IB DL Signal Path . . . . .	58
3.6.4.3	Out-of-Band Outputs of the LTE IB UL Signal Path . . . . .	59
3.6.4.4	Intermodulation Between LTE Signal Paths . . . . .	59
3.7	Summary . . . . .	61
<b>4</b>	<b>GPS Receiver Test Processes</b>	<b>63</b>
4.1	Automation . . . . .	63
4.1.1	Backend . . . . .	64
4.1.2	Frontend . . . . .	67
4.1.3	Extension and Customization . . . . .	68
4.2	DUT Placement, Orientation and System Level Checks . . . . .	71
4.2.1	General Location and Navigation Units (GLN) . . . . .	71
4.2.1.1	Fixturing . . . . .	71
4.2.1.2	System Level Checks . . . . .	71
4.2.2	High Precision Positioning and Real Time Kinematic Units (HPP & RTK) . . . . .	71
4.2.2.1	Fixturing . . . . .	71
4.2.2.2	System Level Checks . . . . .	72
4.2.3	GPS Disciplined Oscillator Units (GPSDO) . . . . .	72
4.2.3.1	Fixturing . . . . .	72
4.2.3.2	System Level Checks . . . . .	72
4.3	Test Procedure . . . . .	72
4.3.1	Power Level Sweeps . . . . .	72
4.3.1.1	General Location and Navigation (GLN) . . . . .	73

4.3.1.2	High Precision Positioning and Real Time Kinematic Units (HPP & RTK) . . . . .	76
4.3.1.3	GPS Disciplined Oscillator Units (GPSDO) . . . . .	80
4.3.2	TTFR Sweeps . . . . .	82
4.3.3	TTFF Sweeps . . . . .	82
4.4	Data Acquisition . . . . .	85
4.4.1	General Location and Navigation (GLN) . . . . .	85
4.4.2	High Precision Positioning and Real Time Kinematic Units (HPP & RTK) . . . . .	87
4.4.3	GPS Disciplined Oscillator Units (GPSDO) . . . . .	87
<b>5</b>	<b>Data Processing and Analysis Methods</b>	<b>93</b>
5.1	Data Parsing . . . . .	93
5.1.1	NMEA . . . . .	96
5.1.1.1	NMEA Preprocessor . . . . .	96
5.1.1.2	NMEA to Output CSV Conversion . . . . .	98
5.1.2	BINEX . . . . .	99
5.1.3	GPSDO Formats . . . . .	99
5.1.4	TTFF and TTFR . . . . .	99
5.1.5	Time Interval Data and Cesium Clock Log File . . . . .	100
5.2	Database Creation . . . . .	100
5.3	Data Wrangling . . . . .	103
5.3.1	Aggregation, Sorting, and Cleaning . . . . .	103
5.3.2	Position Error Calculation . . . . .	104
5.4	Statistical Analysis Methods . . . . .	104
5.4.1	LTE Power Sweep Tests . . . . .	104
5.4.1.1	Warm-up Time Estimation . . . . .	105
5.4.1.2	Steady-state Median Estimation . . . . .	105
5.4.2	TTFF and TTFR Tests . . . . .	107
5.4.3	Timing Tests . . . . .	107
5.5	Data Visualization . . . . .	107
5.5.1	LTE Power Sweep Tests . . . . .	107
5.5.2	TTFF and TTFR Tests . . . . .	113
5.5.3	Timing Tests . . . . .	113
5.6	Data Files Accompanying This Report . . . . .	118
<b>6</b>	<b>Test Results</b>	<b>119</b>
6.1	Summary . . . . .	119
6.2	Frequency Response of DUT Antennas . . . . .	120
6.3	LTE Power Level Sweeps for Nominal GPS Power Exposure . . . . .	124
6.3.1	GLN Exposure to LTE DL . . . . .	125
6.3.2	GLN Exposure to LTE UL1 . . . . .	130
6.3.3	GLN Exposure to LTE UL2 . . . . .	135

6.3.4	GLN Exposure to LTE Combination DL + UL1 . . . . .	140
6.3.5	HPP Exposure to LTE DL . . . . .	145
6.3.6	HPP Exposure to LTE UL1 . . . . .	150
6.3.7	HPP Exposure to LTE UL2 . . . . .	155
6.3.8	HPP Exposure to Combination LTE DL + UL1 . . . . .	160
6.3.9	HPP Exposure to Combination LTE DL + UL1 (DUT 7 repeat for validation)	165
6.3.10	RTK Exposure to LTE DL . . . . .	170
6.3.11	RTK Exposure to LTE UL1 . . . . .	175
6.3.12	RTK Exposure to LTE UL2 . . . . .	180
6.3.13	RTK Exposure to LTE Combination DL + UL1 . . . . .	185
6.3.14	GPSDO Exposure to LTE DL . . . . .	191
6.3.15	GPSDO Exposure to LTE UL1 . . . . .	198
6.3.16	GPSDO Exposure to LTE UL2 . . . . .	205
6.3.17	GPSDO Exposure to LTE Combo . . . . .	212
6.4	<b>TTFF and TTFR Tests . . . . .</b>	<b>219</b>
6.4.1	GLN Exposure to LTE DL . . . . .	221
6.4.2	GLN Exposure to LTE UL1 . . . . .	223
6.4.3	HPP Exposure to LTE DL . . . . .	225
6.4.4	HPP Exposure to LTE UL1 . . . . .	227
6.4.5	RTK Exposure to LTE DL . . . . .	229
6.4.6	RTK Exposure to LTE UL1 . . . . .	231
6.5	<b>LTE Power Level Sweeps for Limited GPS Power Exposure . . . . .</b>	<b>233</b>
6.5.1	GLN DL . . . . .	234
6.5.2	GLN UL1 . . . . .	239
6.5.3	HPP DL . . . . .	244
6.5.4	HPP UL1 . . . . .	249
6.5.5	RTK DL . . . . .	254
6.5.6	RTK UL1 . . . . .	259
<b>7</b>	<b>Conclusions . . . . .</b>	<b>265</b>
7.1	Future Considerations . . . . .	266
<b>A</b>	<b>Radiated Signal Levels: Test and Application to Practical Scenarios . . . . .</b>	<b>267</b>
A.1	Definition of Power Incident Upon DUTs . . . . .	267
A.2	Single-Antenna Test Technique for Controlling Signal-to-Interference Ratio . . . . .	268
<b>B</b>	<b>Variability due to Choice <math>C/N_0</math> Estimator: A simulation study . . . . .</b>	<b>271</b>
B.1	Introduction . . . . .	271
B.2	Methods . . . . .	271
B.3	Results . . . . .	274
B.4	Summary . . . . .	275

<b>C</b>	<b>Testbed Configuration and Calibration</b>	<b>277</b>
C.1	Test Instrument Configuration . . . . .	277
C.1.1	GPS Simulation . . . . .	277
C.1.1.1	Almanac Modification . . . . .	277
C.1.2	LTE IB DL Signal Generator . . . . .	278
C.1.3	LTE IB UL Signal Generator . . . . .	279
C.1.4	LTE OOB DL Signal Generator . . . . .	280
C.1.5	LTE OOB UL Signal Generator . . . . .	280
C.1.6	Spectrum Analyzer . . . . .	280
C.2	Procedures . . . . .	281
C.2.1	Amplifier Signal Level Limits . . . . .	281
C.2.1.1	LTE IB DL . . . . .	281
C.2.1.2	LTE IB UL . . . . .	282
C.2.1.3	LTE OOB UL . . . . .	282
C.2.2	Conducted Testbed Output Levels . . . . .	283
C.2.2.1	GPS . . . . .	284
C.2.2.2	Spectrum Analyzer . . . . .	285
C.2.3	Relative OOBE Levels . . . . .	285
C.2.3.1	LTE OOB DL . . . . .	285
C.2.3.2	LTE OOB UL . . . . .	286
C.2.4	Radiated Levels . . . . .	287
C.2.4.1	Radiated correction to the plane of the DUT . . . . .	287
C.2.4.2	Nominal GPS output level . . . . .	288
C.3	Calibration Records . . . . .	288
C.4	Power Level Uncertainty Estimation . . . . .	291
C.4.1	Antenna Gain . . . . .	291
C.4.2	Spectrum Analyzer Power Measurement Uncertainty Components . . . . .	293
C.4.3	Power Level Time Stability Uncertainty Components . . . . .	294
C.4.4	Coupled Output Power Calibration Uncertainty Components . . . . .	295
C.4.5	Antenna Gain Uncertainty Components . . . . .	295
C.4.6	Programmable Attenuators . . . . .	296
C.4.7	Uncertainty Budgets . . . . .	296
<b>D</b>	<b>Validation of Conducted Transmitter Performance</b>	<b>307</b>
D.1	Validation Test Uncertainties . . . . .	307
D.2	Isolation Between Signal Paths . . . . .	307
D.2.1	Overview . . . . .	307
D.2.2	Measurements at Each Test Point . . . . .	309
D.3	Signal Fidelity of LTE Output Modulation . . . . .	321
D.3.1	In-Band Downlink . . . . .	321
D.3.2	In-Band Uplink . . . . .	323
D.4	Conducted Testbed Noise Floor Output . . . . .	325

D.5	Tests for Testbed Intermodulation . . . . .	331
D.5.1	Two-Tone Excitation . . . . .	331
D.5.1.1	DL+UL1 . . . . .	332
D.5.1.2	DL . . . . .	332
D.5.1.3	UL1 . . . . .	332
D.5.2	LTE Excitation . . . . .	336
D.5.2.1	DL . . . . .	336
D.5.2.2	UL . . . . .	337
D.6	Components . . . . .	340
D.6.1	Testbed Filters . . . . .	340
<b>E</b>	<b>Validation of Radiated Chamber Performance</b>	<b>343</b>
E.1	Chamber Performance . . . . .	343
E.2	Chamber Environmental Stability . . . . .	346
E.3	DUT Test Locations . . . . .	347
<b>F</b>	<b>Supplemental Test Results: Development Board Devices (DEV)</b>	<b>349</b>
F.1	Development Board Setup . . . . .	349
F.2	LTE Power Level Sweeps (Nominal GPS Scenario) . . . . .	352
F.2.1	DEV Exposure to LTE DL . . . . .	353
F.2.2	DEV Exposure to LTE UL1 . . . . .	356
F.2.3	DEV Exposure to LTE UL2 . . . . .	359
F.2.4	DEV Exposure to Combination LTE DL + UL1 . . . . .	362
F.2.5	DEV Exposure to LTE DL . . . . .	366
F.2.6	DEV Exposure to LTE DL . . . . .	367
F.2.7	DEV Exposure to LTE DL . . . . .	368
F.2.8	DEV Exposure to LTE UL1 . . . . .	369
F.2.9	DEV Exposure to LTE UL1 . . . . .	370
F.2.10	DEV Exposure to LTE UL1 . . . . .	371
F.3	TTFF and TTFR (Nominal GPS Scenario) . . . . .	372
F.3.1	DEV Exposure to LTE DL . . . . .	373
F.3.2	DEV Exposure to LTE UL1 . . . . .	374
F.4	LTE Power Level Sweeps (Limited GPS Scenario) . . . . .	375
F.4.1	DEV Exposure to LTE DL . . . . .	376
F.4.2	DEV Exposure to LTE UL1 . . . . .	379
	<b>References</b>	<b>383</b>



## Acronyms

<b>3DPE</b>	3D position error	<b>EMI</b>	electromagnetic interference
<b>3GPP</b>	3rd-generation partnership project	<b>EVM</b>	error vector magnitude
<b>API</b>	application programming interface	<b>FCC</b>	Federal Communications Commission
<b>ASCII</b>	American standard code for information interchange	<b>FDD</b>	frequency-division duplex
<b>AWG</b>	arbitrary waveform generation	<b>FFT</b>	fast Fourier transform
<b>AWGN</b>	additive white Gaussian noise	<b>GLONASS</b>	global navigation satellite system
<b>BINEX</b>	binary exchange	<b>GLN</b>	general location and navigation
<b>BPSK</b>	binary phase-shift keying	<b>GNSS</b>	global navigation satellite system
<b>BW</b>	bandwidth	<b>GPS</b>	global positioning system
<b>C/A</b>	coarse/acquisition	<b>GPSDO</b>	GPS-disciplined oscillator
$C/I_0$	carrier-to-interference-density ratio	<b>HDOP</b>	horizontal dilution of precision
$C/N_0$	carrier-to-noise-density ratio	<b>HPP</b>	high-performance positioning
<b>CDF</b>	cumulative distribution function	<b>IB</b>	in-band
<b>CRADA</b>	cooperative research and development agreement	<b>IF</b>	intermediate frequency
<b>Cs</b>	cesium	<b>IMD</b>	intermodulation distortion
<b>CSV</b>	comma-separated values	<b>IMD3</b>	third-order intermodulation distortion
<b>CW</b>	continuous-wave	<b>ITS</b>	Institute for Telecommunications Sciences
<b>DC</b>	direct current	<b>I/O</b>	input/output
<b>DEV</b>	development board	<b>IP</b>	internet protocol
<b>DGPS</b>	differential global positioning system	<b>IQ</b>	in-phase and quadrature
<b>DL</b>	downlink band	<b>KPI</b>	key performance indicator
<b>DLL</b>	dynamic link library	<b>LHCP</b>	left-hand circularly-polarized
<b>DOP</b>	dilution of precision	<b>LO</b>	local oscillator
<b>DOT</b>	U.S. Department of Transportation	<b>LOS</b>	line-of-sight
<b>DUT</b>	device under test	<b>LP</b>	linearly-polarized
<b>ECEF</b>	earth-centered earth-fixed	<b>LTE</b>	long-term evolution
<b>EIIP</b>	effective isotropic incident power	<b>MM</b>	moments method
<b>EIRP</b>	effective isotropic radiated power	<b>MSER-5</b>	marginal standard error rule-5
<b>EMC</b>	electromagnetic compatibility	<b>NASCTN</b>	National Advanced Spectrum and Communications Test Network

<b>NBIT</b>	NIST Broadband Interoperability Testbed	<b>RHCP</b>	right-hand circularly-polarized
<b>NIST</b>	National Institute of Standards and Technology	<b>RMS</b>	root mean square
<b>NLOS</b>	non-line-of-sight	<b>RNSS</b>	radio navigation satellite services
<b>NMEA</b>	National Marine Electronics Association	<b>RSCN</b>	real signal-complex noise
<b>NPEF</b>	National Space-Based Positioning, Navigation, and Timing Systems Engineering Forum	<b>SIR</b>	signal-to-interference ratio
<b>NTIA</b>	National Telecommunications and Information Administration	<b>SNR</b>	signal-to-noise ratio
<b>NTS</b>	National Technical Systems	<b>SNV</b>	signal-to-noise variance
<b>NWPR</b>	narrowband-wideband power ratio	<b>SQL</b>	structured query language
<b>OOB</b>	out-of-band	<b>TCP</b>	transmission control protocol
<b>OOBE</b>	out-of-band emission	<b>TDEV</b>	Allan time deviation
<b>PAR</b>	peak-to-average ratio	<b>TDOP</b>	time dilution of precision
<b>PC</b>	personal computer	<b>TOW</b>	time of week
<b>PDOP</b>	position (3D) dilution of precision	<b>TIC</b>	time interval counter
<b>PIM</b>	passive intermodulation	<b>TL1</b>	transaction language 1
<b>PN9</b>	9-bit pseudo-random noise	<b>TTFB</b>	time to first fix
<b>PPS</b>	pulse-per-second	<b>TTFR</b>	time to first reacquisition
<b>PRN</b>	pseudo-random noise	<b>TWG</b>	technical working group
<b>PSD</b>	power spectral density	<b>UE</b>	user equipment
<b>RF</b>	radio frequency	<b>UI</b>	software user interface
<b>QPSK</b>	quadrature phase-shift keying	<b>UL</b>	uplink bands
<b>RB</b>	resource block	<b>UL1</b>	uplink band 1 (low)
<b>RTK</b>	real-time kinematic	<b>UL2</b>	uplink band 2 (high)
<b>RINEX</b>	receiver independent exchange	<b>USB</b>	universal serial bus
		<b>UTC</b>	coordinated universal time
		<b>VNA</b>	vector network analyzer
		<b>VRB</b>	virtual resource block
		<b>WAAS</b>	wide-area augmentation system
		<b>WGS84</b>	World Geodetic System 1984

## List of Figures

1.1	Spectrum allocations showing radio navigation satellite services (RNSS), which includes the GPS L1 band, and the various adjacent bands proposed for LTE use. . . . .	2
2.1	Friis equation relationship between effective isotropic incident power (EIIP) (power at the plane of DUT) and the free-space distance from LTE operating at maximum emissions levels (Figure 2.4). The displayed downlink band (DL) (blue) and uplink bands (UL) (green) spans represent the output capability of the testbed (Table 3.6). . . . .	18
2.2	Satellite Constellations Nominal & Limited . . . . .	21
2.2a	Nominal scenario . . . . .	21
2.2b	Limited exposure scenario . . . . .	21
2.2c	GPSDO scenario . . . . .	21
2.3	Satellite Constellations TTFF & TTFR . . . . .	22
2.3a	Time to first fix scenario . . . . .	22
2.3b	Time to first reacquisition scenario . . . . .	22
2.4	Emissions masks under study in this test report, reflecting proposals to the Federal Communications Commission (FCC) [11] for (a) LTE downlink and (b) LTE uplink bands. . . . .	27
2.5	LTE Power Level sweep profile . . . . .	28
2.6	GPSDO:LTE Power Level sweep profile . . . . .	29
2.7	TTFF and TTFR sweep profile . . . . .	31
2.7a	Time to first fix sweep profile for HPP and RTK units. . . . .	31
2.7b	Time to first reacquisition sweep profile for GLN units. . . . .	31
3.1	Measurement system configuration for testing a GLN device (and base configuration for testing all other device classes). The “level, combine, monitor” block is expanded in Figure 3.9. . . . .	36
3.2	Measurement system configuration for testing a HPP (high precision positioning) device. The “level, combine, monitor” block is expanded in Figure 3.9. . . . .	37
3.3	Measurement system configuration for testing an RTK device. The “level, combine, monitor” block is expanded in Figure 3.9. . . . .	38
3.4	Measurement system configuration for testing GPSDO devices. The “level, combine, monitor” block is expanded in Figure 3.9. . . . .	39
3.5	Photographs of rackmounted instrumentation and test circuits. . . . .	42
3.5a	Longmont, CO test site . . . . .	42
3.5b	Boulder, CO test site . . . . .	42
3.6	Test chambers used in radiated testing for this report. . . . .	43
3.6a	Semi-anechoic chamber at the National Technical Systems (NTS) test facility in Longmont, CO. . . . .	43
3.6b	Anechoic chamber at the NIST Broadband Interoperability Testbed (NBIT) facility at National Institute of Standards and Technology (NIST) in Boulder, CO. . . . .	43
3.7	Side view of chamber layout in the NTS and NBIT facilities. The reference position of the transmit antenna corresponds with that of its gain calibration; exact positioning of the DUT varied slightly between units, but we estimate the indicated box bounds a center point with edges $\pm 0.08$ m. . . . .	44

3.8	Use of the single-antenna test configuration (a) reduces the number of orientation variables in the test configuration applied to the DUT compared to the two-antenna setup (b) used in previous tests such as [2–4]. . . . .	45
3.9	The level, combine, and monitor network amplifies and combines GPS and LTE signals, and monitors leveling across all GPS and LTE bands. It is common to all test configurations in this report. . . . .	47
3.9a	Block diagram schematic . . . . .	47
3.9b	Implemented combine circuits at the output of leveling and amplification stages (off-frame). . . . .	47
3.10	Custom arbitrary waveform generation (AWG) waveform designed to emulate LTE out-of-band (OOB) DL signals by shaping circular additive white Gaussian noise (AWGN) in the frequency domain. . . . .	49
3.11	Custom AWG waveform designed to emulate LTE OOB UL signals by shaping circular AWGN in the frequency domain. . . . .	50
3.12	Intermodulation products of simple two-tone input signals illustrated (a) in general, (b) at the band edges of LTE in-band (IB) DL, and (c) at each of LTE IB DL and uplink band 1 (low) (UL1). . . . .	58
3.13	High dynamic range measurements of LTE IB DL and LTE DL OOB conducted output signals performed with the downlink test diplexer. Output power spectral density (PSD) standard uncertainty varies with relative level: $\pm 0.5$ dB at 0 dB relative level, and $\pm 3.1$ dB below -70 dB relative level. . . . .	59
3.14	Measurements of LTE IB UL1 and LTE UL OOB conducted output spectra. Output PSD standard uncertainty varies with relative level: $\pm 0.5$ dB at 0 dB relative level, and $\pm 3.1$ dB at -70 dB relative level. . . . .	60
3.15	Measurements of LTE IB uplink band 2 (high) (UL2) and LTE UL OOB conducted output spectra. In-band measurements were generated from UL1 data. Output PSD standard uncertainty varies with relative level: $\pm 0.5$ dB at 0 dB relative level, and $\pm 3.1$ dB at -70 dB relative level. . . . .	60
4.1	Data connections with the personal computer (PC) that executes test automation. . . . .	64
4.2	Class relationships that define the structure of DUT implementation in test automation software. . . . .	65
4.3	Class relationships that define the structure of instrumentation implementation in test automation software. . . . .	66
4.4	Class relationships that define the structure of software user interface (UI) implementation in test automation software. . . . .	67
4.5	Frontend user interface for monitor and control of instruments and DUTs. . . . .	68
4.6	Frontend user interface for customizing, selecting, and starting automated measurements. . . . .	70
4.7	Test Procedure Flowchart: GLN . . . . .	75
4.8	Test Procedure Flowchart: HPP & RTK . . . . .	79
4.9	Test Procedure Flowchart: GPSDO . . . . .	81
4.10	Test Procedure Flowchart: TTFR . . . . .	83
4.11	Test Procedure Flowchart: TTFF . . . . .	84
4.12	Data Stream: GLN . . . . .	88
4.13	Data Stream: RTK . . . . .	88
4.14	1 sec. capture of the Arbiter 1088B ASCII data stream. . . . .	89
4.15	1 sec. capture of the MicroSemi SyncServer S650 American standard code for information interchange (ASCII) data stream. . . . .	89

4.16	1 sec. capture of the MicroSemi TimeSource 3050 ASCII data stream. . . . .	90
4.17	ASCII state file of the timing reference cesium clock. . . . .	90
4.18	1 sec. capture of receiver independent exchange (RINEX) v2.11 converted from binary exchange (BINEX), acquired during standalone mode with L1 frequency only. . . . .	90
4.19	1 sec. capture of RINEX v2.11 converted from BINEX, acquired during RTK mode with L1 and L2 frequencies. . . . .	91
5.1	Flowchart for raw data parsing. . . . .	94
5.2	Relational Database Layout . . . . .	102
5.3	Warm-up Time Examples . . . . .	106
5.4	Example Position Error Plots . . . . .	109
5.5	Example $C/N_0$ Plots - Nominal Condition . . . . .	110
5.6	Example $C/N_0$ Plots - Limited Condition . . . . .	111
5.7	Example Plot for the Number of Satellites in View . . . . .	112
5.8	Example plots for TTFF and TTFR tests. . . . .	114
5.9	Example plot of warmed-up TIC output for a timing test. . . . .	115
5.10	Example plots of Allan time deviation (TDEV) for a timing test. . . . .	116
5.11	Example plot of Number of Satellites in View for a timing test. . . . .	117
6.1	DUT antenna response . . . . .	121
6.2	DUT antenna response . . . . .	122
6.3	DUT antenna response . . . . .	123
6.4	Scatterplots of reported $C/N_0$ from GLN receivers, swept with LTE power level. The GPS scenario is nominal, and the type of incident LTE is DL. . . . .	125
6.5	Estimated 95% confidence regions of the median of reported $C/N_0$ from GLN receivers, swept with LTE power level. The GPS scenario is nominal, and the type of incident LTE is DL. . . . .	126
6.6	Scatterplots of error in reported 3-D position compared to simulator truth from GLN receivers, swept with LTE power level. The GPS scenario is nominal, and the type of incident LTE is DL. . . . .	127
6.7	Estimated 95% confidence regions of the median error in reported 3-D position from GLN receivers, swept with LTE power level. The GPS scenario is nominal, and the type of incident LTE is DL. . . . .	128
6.8	Scatterplots of the number of satellites in view from GLN receivers, swept with LTE power level. The GPS scenario is nominal, and the type of incident LTE is DL. . . . .	129
6.9	Scatterplots of reported $C/N_0$ from GLN receivers, swept with LTE power level. The GPS scenario is nominal, and the type of incident LTE is UL1. . . . .	130
6.10	Estimated 95% confidence regions of the median of reported $C/N_0$ from GLN receivers, swept with LTE power level. The GPS scenario is nominal, and the type of incident LTE is UL1. . . . .	131
6.11	Scatterplots of error in reported 3-D position compared to simulator truth from GLN receivers, swept with LTE power level. The GPS scenario is nominal, and the type of incident LTE is UL1. . . . .	132
6.12	Estimated 95% confidence regions of the median error in reported 3-D position from GLN receivers, swept with LTE power level. The GPS scenario is nominal, and the type of incident LTE is UL1. . . . .	133
6.13	Scatterplots of the number of satellites in view from GLN receivers, swept with LTE power level. The GPS scenario is nominal, and the type of incident LTE is UL1. . . . .	134

6.14	Scatterplots of reported $C/N_0$ from GLN receivers, swept with LTE power level. The GPS scenario is nominal, and the type of incident LTE is UL2. . . . .	135
6.15	Estimated 95% confidence regions of the median of reported $C/N_0$ from GLN receivers, swept with LTE power level. The GPS scenario is nominal, and the type of incident LTE is UL2. . . . .	136
6.16	Scatterplots of error in reported 3-D position compared to simulator truth from GLN receivers, swept with LTE power level. The GPS scenario is nominal, and the type of incident LTE is UL2. . . . .	137
6.17	Estimated 95% confidence regions of the median error in reported 3-D position from GLN receivers, swept with LTE power level. The GPS scenario is nominal, and the type of incident LTE is UL2. . . . .	138
6.18	Scatterplots of the number of satellites in view from GLN receivers, swept with LTE power level. The GPS scenario is nominal, and the type of incident LTE is UL2. . . . .	139
6.19	Scatterplots of reported $C/N_0$ from GLN receivers, swept with LTE power level. The GPS scenario is nominal, and the type of incident LTE is Combination DL + UL1. The UL level was swept, and the DL level was fixed at -50 dBm EIIP unless otherwise annotated. The horizontal axis reports the linear sum of DL and UL power. . . . .	140
6.20	Estimated 95% confidence regions of the median of reported $C/N_0$ from GLN receivers, swept with LTE power level. The GPS scenario is nominal, and the type of incident LTE is Combination DL + UL1. The UL level was swept, and the DL level was fixed at -50 dBm EIIP unless otherwise annotated. The horizontal axis reports the linear sum of DL and UL power. . . . .	141
6.21	Scatterplots of error in reported 3-D position compared to simulator truth from GLN receivers, swept with LTE power level. The GPS scenario is nominal, and the type of incident LTE is Combination DL + UL1. The UL level was swept, and the DL level was fixed at -50 dBm EIIP unless otherwise annotated. The horizontal axis reports the linear sum of DL and UL power. . . . .	142
6.22	Estimated 95% confidence regions of the median error in reported 3-D position from GLN receivers, swept with LTE power level. The GPS scenario is nominal, and the type of incident LTE is Combination DL + UL1. The UL level was swept, and the DL level was fixed at -50 dBm EIIP unless otherwise annotated. The horizontal axis reports the linear sum of DL and UL power. . . . .	143
6.23	Scatterplots of the number of satellites in view from GLN receivers, swept with LTE power level. The GPS scenario is nominal, and the type of incident LTE is Combination DL + UL1. The UL level was swept, and the DL level was fixed at -50 dBm EIIP unless otherwise annotated. The horizontal axis reports the linear sum of DL and UL power. . . . .	144
6.24	Scatterplots of reported $C/N_0$ from HPP receivers, swept with LTE power level. The GPS scenario is nominal, and the type of incident LTE is DL. . . . .	145
6.25	Estimated 95% confidence regions of the median of reported $C/N_0$ from HPP receivers, swept with LTE power level. The GPS scenario is nominal, and the type of incident LTE is DL. . . . .	146
6.26	Scatterplots of error in reported 3-D position compared to simulator truth from HPP receivers, swept with LTE power level. The GPS scenario is nominal, and the type of incident LTE is DL. . . . .	147
6.27	Estimated 95% confidence regions of the median error in reported 3-D position from HPP receivers, swept with LTE power level. The GPS scenario is nominal, and the type of incident LTE is DL. . . . .	148

6.28	Scatterplots of the number of satellites in view from HPP receivers, swept with LTE power level. The GPS scenario is nominal, and the type of incident LTE is DL. . . . .	149
6.29	Scatterplots of reported $C/N_0$ from HPP receivers, swept with LTE power level. The GPS scenario is nominal, and the type of incident LTE is UL1. . . . .	150
6.30	Estimated 95% confidence regions of the median of reported $C/N_0$ from HPP receivers, swept with LTE power level. The GPS scenario is nominal, and the type of incident LTE is UL1. . . . .	151
6.31	Scatterplots of error in reported 3-D position compared to simulator truth from HPP receivers, swept with LTE power level. The GPS scenario is nominal, and the type of incident LTE is UL1. . . . .	152
6.32	Estimated 95% confidence regions of the median error in reported 3-D position from HPP receivers, swept with LTE power level. The GPS scenario is nominal, and the type of incident LTE is UL1. . . . .	153
6.33	Scatterplots of the number of satellites in view from HPP receivers, swept with LTE power level. The GPS scenario is nominal, and the type of incident LTE is UL1. . . . .	154
6.34	Scatterplots of reported $C/N_0$ from HPP receivers, swept with LTE power level. The GPS scenario is nominal, and the type of incident LTE is UL2. . . . .	155
6.35	Estimated 95% confidence regions of the median of reported $C/N_0$ from HPP receivers, swept with LTE power level. The GPS scenario is nominal, and the type of incident LTE is UL2. . . . .	156
6.36	Scatterplots of error in reported 3-D position compared to simulator truth from HPP receivers, swept with LTE power level. The GPS scenario is nominal, and the type of incident LTE is UL2. . . . .	157
6.37	Estimated 95% confidence regions of the median error in reported 3-D position from HPP receivers, swept with LTE power level. The GPS scenario is nominal, and the type of incident LTE is UL2. . . . .	158
6.38	Scatterplots of the number of satellites in view from HPP receivers, swept with LTE power level. The GPS scenario is nominal, and the type of incident LTE is UL2. . . . .	159
6.39	Scatterplots of reported $C/N_0$ from HPP receivers, swept with LTE power level. The GPS scenario is nominal, and the type of incident LTE is DL + UL1. The UL level was swept, and the DL level was fixed at -50 dBm EIIP unless otherwise annotated. The horizontal axis reports the linear sum of DL and UL power. . . . .	160
6.40	Estimated 95% confidence regions of the median of reported $C/N_0$ from HPP receivers, swept with LTE power level. The GPS scenario is nominal, and the type of incident LTE is DL + UL1. The UL level was swept, and the DL level was fixed at -50 dBm EIIP unless otherwise annotated. The horizontal axis reports the linear sum of DL and UL power. . . . .	161
6.41	Scatterplots of error in reported 3-D position compared to simulator truth from HPP receivers, swept with LTE power level. The GPS scenario is nominal, and the type of incident LTE is DL + UL1. The UL level was swept, and the DL level was fixed at -50 dBm EIIP unless otherwise annotated. The horizontal axis reports the linear sum of DL and UL power. . . . .	162
6.42	Estimated 95% confidence regions of the median error in reported 3-D position from HPP receivers, swept with LTE power level. The GPS scenario is nominal, and the type of incident LTE is DL + UL1. The UL level was swept, and the DL level was fixed at -50 dBm EIIP unless otherwise annotated. The horizontal axis reports the linear sum of DL and UL power. . . . .	163

6.43	Scatterplots of the number of satellites in view from HPP receivers, swept with LTE power level. The GPS scenario is nominal, and the type of incident LTE is DL + UL1. The UL level was swept, and the DL level was fixed at -50 dBm EIIP unless otherwise annotated. The horizontal axis reports the linear sum of DL and UL power. . . . .	164
6.44	$C/N_0$ response from DUT 7 (HPP), swept with LTE power, for the combination DL + UL1 LTE scenario. Top row are the scatterplots and the bottom row is that of the estimated 95% confidence regions of the median. Left column: Downlink LTE signal, middle column: Uplink 1, right column: Combination DL + UL1. The UL level was swept, and the DL level was fixed at -50 dBm EIIP unless otherwise annotated. The horizontal axis reports the linear sum of DL and UL power. . . . .	165
6.45	Repeat test of $C/N_0$ from DUT 7 (HPP), swept with LTE power, for the combination DL + UL1 LTE scenario. The repeat was after several days and tests of other DUTs. The trend of the $C/N_0$ response of the repeated measurement (right column) follows the initial (left column) measurement closely. The UL level was swept, and the DL level was fixed at -50 dBm EIIP unless otherwise annotated. The horizontal axis reports the linear sum of DL and UL power. . . . .	166
6.46	Error in reported 3-D position from DUT 7 (HPP), swept with LTE power, for the combination DL + UL1 LTE scenario. Top row are the scatterplots and the bottom row is that of the estimated 95% confidence regions of the median error in reported 3-D position. Left column: Downlink LTE signal, middle column: Uplink 1, right column: Combination DL + UL1. The UL level was swept, and the DL level was fixed at -50 dBm EIIP unless otherwise annotated. The horizontal axis reports the linear sum of DL and UL power. . . .	167
6.47	Repeat test of error in reported 3-D position from DUT 7 (HPP), swept with LTE power, for the combination DL + UL1 LTE scenario. The repeat was after several days and tests of other DUTs. The trend of the repeated measurement result (right column) follows the initial (left column) measurement closely. The UL level was swept, and the DL level was fixed at -50 dBm EIIP unless otherwise annotated. The horizontal axis reports the linear sum of DL and UL power. . . . .	168
6.48	Repeat test the number of satellites in view to from DUT 7 (HPP), swept with LTE power, for the combination DL + UL1 LTE scenario. The repeat was after several days and tests of other DUTs. The trend of the repeated measurement result (right column) follows the initial (left column) measurement closely. The UL level was swept, and the DL level was fixed at -50 dBm EIIP unless otherwise annotated. The horizontal axis reports the linear sum of DL and UL power. . . . .	169
6.49	Scatterplots of reported $C/N_0$ from RTK receivers, swept with LTE power level. The GPS scenario is nominal, and the type of incident LTE is DL. . . . .	170
6.50	Estimated 95% confidence regions of the median of reported $C/N_0$ from RTK receivers, swept with LTE power level. The GPS scenario is nominal, and the type of incident LTE is DL. . . . .	171
6.51	Scatterplots of error in reported 3-D position compared to simulator truth from RTK receivers, swept with LTE power level. The GPS scenario is nominal, and the type of incident LTE is DL. . . . .	172
6.52	Estimated 95% confidence regions of the median error in reported 3-D position from RTK receivers, swept with LTE power level. The GPS scenario is nominal, and the type of incident LTE is DL. . . . .	173
6.53	Scatterplots of the number of satellites in view from RTK receivers, swept with LTE power level. The GPS scenario is nominal, and the type of incident LTE is DL. . . . .	174

6.54	Scatterplots of reported $C/N_0$ from RTK receivers, swept with LTE power level. The GPS scenario is nominal, and the type of incident LTE is UL1. . . . .	175
6.55	Estimated 95% confidence regions of the median of reported $C/N_0$ from RTK receivers, swept with LTE power level. The GPS scenario is nominal, and the type of incident LTE is UL1. . . . .	176
6.56	Scatterplots of error in reported 3-D position compared to simulator truth from RTK receivers, swept with LTE power level. The GPS scenario is nominal, and the type of incident LTE is UL1. . . . .	177
6.57	Estimated 95% confidence regions of the median error in reported 3-D position from RTK receivers, swept with LTE power level. The GPS scenario is nominal, and the type of incident LTE is UL1. . . . .	178
6.58	Scatterplots of the number of satellites in view from RTK receivers, swept with LTE power level. The GPS scenario is nominal, and the type of incident LTE is UL1. . . . .	179
6.59	Scatterplots of reported $C/N_0$ from RTK receivers, swept with LTE power level. The GPS scenario is nominal, and the type of incident LTE is UL2. . . . .	180
6.60	Estimated 95% confidence regions of the median of reported $C/N_0$ from RTK receivers, swept with LTE power level. The GPS scenario is nominal, and the type of incident LTE is UL2. . . . .	181
6.61	Scatterplots of error in reported 3-D position compared to simulator truth from RTK receivers, swept with LTE power level. The GPS scenario is nominal, and the type of incident LTE is UL2. . . . .	182
6.62	Estimated 95% confidence regions of the median error in reported 3-D position from RTK receivers, swept with LTE power level. The GPS scenario is nominal, and the type of incident LTE is UL2. . . . .	183
6.63	Scatterplots of the number of satellites in view from RTK receivers, swept with LTE power level. The GPS scenario is nominal, and the type of incident LTE is UL2. . . . .	184
6.64	Scatterplots of reported $C/N_0$ from RTK receivers, swept with LTE power level. The GPS scenario is nominal, and the type of incident LTE is Combination DL + UL1. The UL level was swept, and the DL level was fixed at -50 dBm EIIP unless otherwise annotated. The horizontal axis reports the linear sum of DL and UL power. . . . .	185
6.65	Estimated 95% confidence regions of the median of reported $C/N_0$ from RTK receivers, swept with LTE power level. The GPS scenario is nominal, and the type of incident LTE is Combination DL + UL1. The UL level was swept, and the DL level was fixed at -50 dBm EIIP unless otherwise annotated. The horizontal axis reports the linear sum of DL and UL power. . . . .	186
6.66	Scatterplots of error in reported 3-D position compared to simulator truth from RTK receivers, swept with LTE power level. The GPS scenario is nominal, and the type of incident LTE is Combination DL + UL1. The UL level was swept, and the DL level was fixed at -50 dBm EIIP unless otherwise annotated. The horizontal axis reports the linear sum of DL and UL power. . . . .	187
6.67	Estimated 95% confidence regions of the median error in reported 3-D position from RTK receivers, swept with LTE power level. The GPS scenario is nominal, and the type of incident LTE is Combination DL + UL1. The UL level was swept, and the DL level was fixed at -50 dBm EIIP unless otherwise annotated. The horizontal axis reports the linear sum of DL and UL power. . . . .	188

6.68	Scatterplots of the number of satellites in view from RTK receivers, swept with LTE power level. The GPS scenario is nominal, and the type of incident LTE is Combination DL + UL1. The UL level was swept, and the DL level was fixed at -50 dBm EIIP unless otherwise annotated. The horizontal axis reports the linear sum of DL and UL power. . . . .	189
6.69	Plots of stability of 1 PPS output of a GPSDO receiver measured against that of the GPS simulator from GPSDO receivers, swept with LTE power level. The GPS scenario is timing, and the type of incident LTE is DL. . . . .	191
6.70	Allan time deviation plots from GPSDO receivers, swept with LTE power level. The GPS scenario is timing, and the type of incident LTE is DL. . . . .	192
6.71	Zoom of Allan time deviation for DUT 13. Shaded regions indicate pointwise 95% confidence bands. Each curve corresponds to a tested LTE power level. The GPS scenario is timing, and the type of incident LTE is DL. . . . .	193
6.72	Zoom of Allan time deviation for DUT 14. Shaded regions indicate pointwise 95% confidence bands. Each curve corresponds to a tested LTE power level. The GPS scenario is timing, and the type of incident LTE is DL. . . . .	194
6.73	Zoom of Allan time deviation for DUT 15. Shaded regions indicate pointwise 95% confidence bands. Each curve corresponds to a tested LTE power level. The GPS scenario is timing, and the type of incident LTE is DL. . . . .	195
6.74	$C/N_0$ scatter plots and median, with estimated 95% confidence region of the median from GPSDO receivers, swept with LTE power level. The GPS scenario is timing, and the type of incident LTE is DL. . . . .	196
6.75	Number of satellites in view from GPSDO receivers, swept with LTE power level. The GPS scenario is timing, and the type of incident LTE is DL. . . . .	197
6.76	Plots of stability of 1 PPS output of a GPSDO receiver measured against that of the GPS simulator from GPSDO receivers, swept with LTE power level. The GPS scenario is timing, and the type of incident LTE is UL1. . . . .	198
6.77	Allan time deviation plots from GPSDO receivers, swept with LTE power level. The GPS scenario is timing, and the type of incident LTE is UL1. . . . .	199
6.78	Zoom of Allan time deviation for DUT 13. Shaded regions indicate pointwise 95% confidence bands. Each curve corresponds to a tested LTE power level. The GPS scenario is timing, and the type of incident LTE is UL1. . . . .	200
6.79	Zoom of Allan time deviation for DUT 14. Shaded regions indicate pointwise 95% confidence bands. Each curve corresponds to a tested LTE power level. The GPS scenario is timing, and the type of incident LTE is UL1. . . . .	201
6.80	Zoom of Allan time deviation for DUT 15. Shaded regions indicate pointwise 95% confidence bands. Each curve corresponds to a tested LTE power level. The GPS scenario is timing, and the type of incident LTE is UL1. . . . .	202
6.81	$C/N_0$ scatter plots and median, with estimated 95% confidence region of the median from GPSDO receivers, swept with LTE power level. The GPS scenario is timing, and the type of incident LTE is UL1. . . . .	203
6.82	Number of satellites in view from GPSDO receivers, swept with LTE power level. The GPS scenario is timing, and the type of incident LTE is UL1. . . . .	204
6.83	Plots of stability of 1 PPS output of a GPSDO receiver measured against that of the GPS simulator from GPSDO receivers, swept with LTE power level. The GPS scenario is timing, and the type of incident LTE is UL2. . . . .	205
6.84	Allan time deviation plots from GPSDO receivers, swept with LTE power level. The GPS scenario is timing, and the type of incident LTE is UL2. . . . .	206

6.85	Zoom of Allan time deviation for DUT 13. Shaded regions indicate pointwise 95% confidence bands. Each curve corresponds to a tested LTE power level. The GPS scenario is timing, and the type of incident LTE is UL2. . . . .	207
6.86	Zoom of Allan time deviation for DUT 14. Shaded regions indicate pointwise 95% confidence bands. Each curve corresponds to a tested LTE power level. The GPS scenario is timing, and the type of incident LTE is UL2. . . . .	208
6.87	Zoom of Allan time deviation for DUT 15. Shaded regions indicate pointwise 95% confidence bands. Each curve corresponds to a tested LTE power level. The GPS scenario is timing, and the type of incident LTE is UL2. . . . .	209
6.88	$C/N_0$ scatter plots and median, with estimated 95% confidence region of the median from GPSDO receivers, swept with LTE power level. The GPS scenario is timing, and the type of incident LTE is UL2. . . . .	210
6.89	Number of satellites in view from GPSDO receivers, swept with LTE power level. The GPS scenario is timing, and the type of incident LTE is UL2. . . . .	211
6.90	Plots of stability of 1 PPS output of a GPSDO receiver measured against that of the GPS simulator from GPSDO receivers, swept with LTE power level. The GPS scenario is timing, and the type of incident LTE is DL + UL1. The UL level was swept, and the DL level was fixed at -50 dBm EIIP unless otherwise annotated. The colorbar reports the linear sum of DL and UL power. . . . .	212
6.91	Allan time deviation plots from GPSDO receivers, swept with LTE power level. The GPS scenario is timing, and the type of incident LTE is DL + UL1. The UL level was swept, and the DL level was fixed at -50 dBm EIIP unless otherwise annotated. The colorbar reports the linear sum of DL and UL power. . . . .	213
6.92	Zoom of Allan time deviation for DUT 13. Shaded regions indicate pointwise 95% confidence bands. Each curve corresponds to a tested LTE power level. The GPS scenario is timing, and the type of incident LTE is DL + UL1. The UL level was swept, and the DL level was fixed at -50 dBm EIIP unless otherwise annotated. The colorbar reports the linear sum of DL and UL power. . . . .	214
6.93	Zoom of Allan time deviation for DUT 14. Shaded regions indicate pointwise 95% confidence bands. Each curve corresponds to a tested LTE power level. The GPS scenario is timing, and the type of incident LTE is DL + UL1. The UL level was swept, and the DL level was fixed at -50 dBm EIIP unless otherwise annotated. The colorbar reports the linear sum of DL and UL power. . . . .	215
6.94	Zoom of Allan time deviation for DUT 15. Shaded regions indicate pointwise 95% confidence bands. Each curve corresponds to a tested LTE power level. The GPS scenario is timing, and the type of incident LTE is DL + UL1. The UL level was swept, and the DL level was fixed at -50 dBm EIIP unless otherwise annotated. The colorbar reports the linear sum of DL and UL power. . . . .	216
6.95	$C/N_0$ scatter plots and median, with estimated 95% confidence region of the median from GPSDO receivers, swept with LTE power level. The GPS scenario is timing, and the type of incident LTE is DL + UL1. The UL level was swept, and the DL level was fixed at -50 dBm EIIP unless otherwise annotated. The horizontal axis reports the linear sum of DL and UL power. . . . .	217
6.96	Number of satellites in view from GPSDO receivers, swept with LTE power level. The GPS scenario is timing, and the type of incident LTE is DL + UL1. The UL level was swept, and the DL level was fixed at -50 dBm EIIP unless otherwise annotated. The colorbar reports the linear sum of DL and UL power. . . . .	218

6.97	CDF plots of TTFR from lock acquisition reported by GLN receivers at different LTE power levels. The GPS scenario is TTFR, and the type of incident LTE is DL. . . . .	221
6.98	Scatterplots of TTFR from lock acquisition reported by GLN receivers at different LTE power levels. The GPS scenario is TTFR, and the type of incident LTE is DL. . . . .	222
6.99	CDF plots of TTFR from lock acquisition reported by GLN receivers at different LTE power levels. The GPS scenario is TTFR, and the type of incident LTE is UL1. . . . .	223
6.100	Scatterplots of TTFR from lock acquisition reported by GLN receivers at different LTE power levels. The GPS scenario is TTFR, and the type of incident LTE is UL1. . . . .	224
6.101	CDF plots of TTFF from lock acquisition reported by HPP receivers at different LTE power levels. The GPS scenario is TTFF, and the type of incident LTE is DL. . . . .	225
6.102	Scatterplots of TTFF from lock acquisition reported by HPP receivers at different LTE power levels. The GPS scenario is TTFF, and the type of incident LTE is DL. . . . .	226
6.103	CDF plots of TTFF from lock acquisition reported by HPP receivers at different LTE power levels. The GPS scenario is TTFF, and the type of incident LTE is UL1. . . . .	227
6.104	Scatterplots of TTFF from lock acquisition reported by HPP receivers at different LTE power levels. The GPS scenario is TTFF, and the type of incident LTE is UL1. . . . .	228
6.105	CDF plots of TTFF from lock acquisition reported by RTK receivers at different LTE power levels. The GPS scenario is TTFF, and the type of incident LTE is DL. . . . .	229
6.106	Scatterplots of TTFF from lock acquisition reported by RTK receivers at different LTE power levels. The GPS scenario is TTFF, and the type of incident LTE is DL. . . . .	230
6.107	CDF plots of TTFF from lock acquisition reported by RTK receivers at different LTE power levels. The GPS scenario is TTFF, and the type of incident LTE is UL1. . . . .	231
6.108	Scatterplots of TTFF from lock acquisition reported by RTK receivers at different LTE power levels. The GPS scenario is TTFF, and the type of incident LTE is UL1. . . . .	232
6.109	Scatterplots of reported $C/N_0$ from GLN receivers, swept with LTE power level. The GPS scenario is limited, and the type of incident LTE is DL. . . . .	234
6.110	Estimated 95% confidence regions of the median of reported $C/N_0$ from GLN receivers, swept with LTE power level. The GPS scenario is limited, and the type of incident LTE is DL. . . . .	235
6.111	Scatterplots of error in reported 3-D position compared to simulator truth from GLN receivers, swept with LTE power level. The GPS scenario is limited, and the type of incident LTE is DL. . . . .	236
6.112	Estimated 95% confidence regions of the median error in reported 3-D position from GLN receivers, swept with LTE power level. The GPS scenario is limited, and the type of incident LTE is DL. . . . .	237
6.113	Scatterplots of the number of satellites in view from GLN receivers, swept with LTE power level. The GPS scenario is limited, and the type of incident LTE is DL. . . . .	238
6.114	Scatterplots of reported $C/N_0$ from GLN receivers, swept with LTE power level. The GPS scenario is limited, and the type of incident LTE is UL1. . . . .	239
6.115	Estimated 95% confidence regions of the median of reported $C/N_0$ from GLN receivers, swept with LTE power level. The GPS scenario is limited, and the type of incident LTE is UL1. . . . .	240
6.116	Scatterplots of error in reported 3-D position compared to simulator truth from GLN receivers, swept with LTE power level. The GPS scenario is limited, and the type of incident LTE is UL1. . . . .	241
6.117	Estimated 95% confidence regions of the median error in reported 3-D position from GLN receivers, swept with LTE power level. The GPS scenario is limited, and the type of incident LTE is UL1. . . . .	242

6.118	Scatterplots of the number of satellites in view from GLN receivers, swept with LTE power level. The GPS scenario is limited, and the type of incident LTE is UL1. . . . .	243
6.119	Scatterplots of reported $C/N_0$ from HPP receivers, swept with LTE power level. The GPS scenario is limited, and the type of incident LTE is DL. . . . .	244
6.120	Estimated 95% confidence regions of the median of reported $C/N_0$ from HPP receivers, swept with LTE power level. The GPS scenario is limited, and the type of incident LTE is DL.	245
6.121	Scatterplots of error in reported 3-D position compared to simulator truth from HPP receivers, swept with LTE power level. The GPS scenario is limited, and the type of incident LTE is DL. . . . .	246
6.122	Estimated 95% confidence regions of the median error in reported 3-D position from HPP receivers, swept with LTE power level. The GPS scenario is limited, and the type of incident LTE is DL. . . . .	247
6.123	Scatterplots of the number of satellites in view from HPP receivers, swept with LTE power level. The GPS scenario is limited, and the type of incident LTE is DL. . . . .	248
6.124	Scatterplots of reported $C/N_0$ from HPP receivers, swept with LTE power level. The GPS scenario is limited, and the type of incident LTE is UL1. . . . .	249
6.125	Estimated 95% confidence regions of the median of reported $C/N_0$ from HPP receivers, swept with LTE power level. The GPS scenario is limited, and the type of incident LTE is UL1. . . . .	250
6.126	Scatterplots of error in reported 3-D position compared to simulator truth from HPP receivers, swept with LTE power level. The GPS scenario is limited, and the type of incident LTE is UL1. . . . .	251
6.127	Estimated 95% confidence regions of the median error in reported 3-D position from HPP receivers, swept with LTE power level. The GPS scenario is limited, and the type of incident LTE is UL1. . . . .	252
6.128	Scatterplots of the number of satellites in view from HPP receivers, swept with LTE power level. The GPS scenario is limited, and the type of incident LTE is UL1. . . . .	253
6.129	Scatterplots of reported $C/N_0$ from RTK receivers, swept with LTE power level. The GPS scenario is limited, and the type of incident LTE is DL. . . . .	254
6.130	Estimated 95% confidence regions of the median of reported $C/N_0$ from RTK receivers, swept with LTE power level. The GPS scenario is limited, and the type of incident LTE is DL.	255
6.131	Scatterplots of error in reported 3-D position compared to simulator truth from RTK receivers, swept with LTE power level. The GPS scenario is limited, and the type of incident LTE is DL. . . . .	256
6.132	Estimated 95% confidence regions of the median error in reported 3-D position from RTK receivers, swept with LTE power level. The GPS scenario is limited, and the type of incident LTE is DL. . . . .	257
6.133	Scatterplots of the number of satellites in view from RTK receivers, swept with LTE power level. The GPS scenario is limited, and the type of incident LTE is DL. . . . .	258
6.134	Scatterplots of reported $C/N_0$ from RTK receivers, swept with LTE power level. The GPS scenario is limited, and the type of incident LTE is UL1. . . . .	259
6.135	Estimated 95% confidence regions of the median of reported $C/N_0$ from RTK receivers, swept with LTE power level. The GPS scenario is limited, and the type of incident LTE is UL1. . . . .	260
6.136	Scatterplots of error in reported 3-D position compared to simulator truth from RTK receivers, swept with LTE power level. The GPS scenario is limited, and the type of incident LTE is UL1. . . . .	261

6.137	Estimated 95% confidence regions of the median error in reported 3-D position from RTK receivers, swept with LTE power level. The GPS scenario is limited, and the type of incident LTE is UL1. . . . .	262
6.138	Scatterplots of the number of satellites in view from RTK receivers, swept with LTE power level. The GPS scenario is limited, and the type of incident LTE is UL1. . . . .	263
B.1	Histograms of $C/N_0$ estimates with an AWGN GPS channel. Top: true $C/N_0 = 20$ dB-Hz, Bottom: true $C/N_0 = 40$ dB-Hz. The LTE power at the plane of DUT is -20 dBm (Left) and -40 dBm (Right). The vertical dashed line indicates the true $C/N_0$ value. . . . .	274
B.2	Histograms of $C/N_0$ estimates with a Rician GPS channel. Top: true $C/N_0 = 20$ dB-Hz, Bottom: true $C/N_0 = 40$ dB-Hz. The LTE power at the plane of DUT is -20 dBm (Left) and -40 dBm (Right). The vertical dashed line indicates the true $C/N_0$ value. . . . .	275
C.1	General User Interface of the GPS Simulator. The Setup shows the configuration for “Day 1” of the nominal GPS scenario. . . . .	277
C.2	Antenna gain checks performed by the two-antenna method to 1) compare measured gain values with those reported by the manufacturer, and 2) estimate uncertainty introduced by assuming a constant gain over frequency. . . . .	293
C.3	Output power relative to the average final power. Typical drift in the output of the high-power amplifier after the output is enabled and an LTE downlink signal applied. Results show that the worst drift occurs when the amplifier is set to maximum output power, but is still significant even if the LTE signal is 100 dB below maximum. . . . .	294
C.4	Testbed programmable attenuator validation measurements, 1540 MHz (near LTE DL). . . . .	297
C.5	Testbed programmable attenuator validation measurements, 1580 MHz (near GPS L1 band center). . . . .	298
C.6	Testbed programmable attenuator validation measurements, 1640 MHz (near LTE UL1 and LTE UL2). . . . .	299
D.1	Test points probed in tests of isolation between signal paths. . . . .	308
D.2	GPS isolation tests: Test circuit for comparing reverse coupled power against forward power	310
D.2a	Reverse coupled power . . . . .	310
D.2b	Forward power . . . . .	310
D.3	GPS isolation tests: Comparison of reverse and forward power spectra . . . . .	311
D.3a	Reverse coupled power at GPS amplifier output, with all LTE signals at maximum . . . . .	311
D.3b	Forward power at GPS amplifier output . . . . .	311
D.4	LTE IB UL1 and UL2 isolation tests: Test circuit for comparing reverse coupled power against forward power. Switching between tests of bands UL1 and UL2 is achieved by substituting the indicated cavity filter block. . . . .	312
D.4a	Reverse coupled power . . . . .	312
D.4b	Forward power . . . . .	312
D.5	LTE IB UL1 isolation tests: Comparison of forward and reverse power spectra . . . . .	313
D.5a	Reverse coupled power at LTE IB UL amplifier output; all other LTE signals at maximum . . . . .	313
D.5b	Forward power at LTE IB UL amplifier output . . . . .	313
D.6	LTE IB UL2 isolation tests: Comparison of forward and reverse power spectra . . . . .	314
D.6a	Reverse coupled power at LTE IB UL amplifier output, all other LTE signals at maximum . . . . .	314
D.6b	Forward power at LTE IB UL amplifier output . . . . .	314
D.7	LTE IB DL isolation tests: Test circuit for comparing reverse coupled power against forward power . . . . .	315

D.7a	Reverse coupled power . . . . .	315
D.7b	Forward power . . . . .	315
D.8	LTE IB DL isolation tests: Comparison of forward and reverse power spectra . . . . .	316
D.8a	Reverse coupled power at LTE IB DL amplifier output, all other LTE signals at maximum . . . . .	316
D.8b	Forward power at LTE IB DL amplifier output . . . . .	316
D.9	LTE OOB DL isolation tests: Test circuit for comparing reverse coupled power against forward power . . . . .	317
D.9a	Reverse coupled power . . . . .	317
D.9b	Forward power . . . . .	317
D.10	LTE OOB DL isolation tests: Comparison of forward and reverse power spectra . . . . .	318
D.10a	Reverse coupled power at LTE OOB DL signal generator output, all other LTE signals at maximum . . . . .	318
D.10b	Forward power at LTE OOB DL signal generator output . . . . .	318
D.11	LTE OOB UL isolation tests: Test circuit for comparing reverse coupled power against forward power . . . . .	319
D.11a	Reverse coupled power . . . . .	319
D.11b	Forward power . . . . .	319
D.12	LTE OOB UL isolation tests: Comparison of forward and reverse power spectra. Note that “reverse power” scale in (a) is 70 dB weaker than that of the forward power (b). . . . .	320
D.12a	Reverse coupled power at LTE OOB UL amplifier output, all other LTE signals at maximum . . . . .	320
D.12b	Forward power at LTE OOB UL amplifier output . . . . .	320
D.13	Spectrum analyzer capture of LTE Evaluation Suite. DL signal drive level 20 dB below maximum, low-distortion amplifier response. . . . .	321
D.14	Spectrum analyzer capture of LTE Evaluation Suite. DL signal drive level at maximum, distorted amplifier response. . . . .	322
D.15	Spectrum analyzer capture of LTE Evaluation Suite. DL signal drive level 50 dB below maximum, dominated by amplifier noise. . . . .	323
D.16	Spectrum analyzer capture of LTE Evaluation Suite. UL signal drive level 10 dB below maximum, low-distortion amplifier response. . . . .	324
D.17	Spectrum analyzer capture of LTE Evaluation Suite. UL signal drive level at maximum, distorted amplifier response. . . . .	324
D.18	Spectrum analyzer capture of LTE Evaluation Suite. UL signal drive level 60 dB below maximum, dominated by amplifier noise. . . . .	325
D.19	Test setups for testbed noise floor . . . . .	326
D.20	Noise floor of the spectrum analyzer used to measure noise floor . . . . .	326
D.21	Spectrum analyzer capture of GPS noise floor test (amplifier on, signal off, attenuator at nominal operating level). Output signals and amplifiers in other paths were disabled. . . . .	328
D.22	Testbed LTE DL output noise floors. All outputs of non-indicated paths are disabled. . . . .	329
D.22a	LTE IB DL (amplifier on at maximum gain; signal off) . . . . .	329
D.22b	LTE OOB DL (signal on, level corresponds to maximum DL output of testbed) . . . . .	329
D.23	Testbed LTE UL output noise floors. All outputs of non-indicated paths are disabled. This was the strongest output noise floor measured, and motivated the use of the medium power amplifier for low power levels. The LTE OOB DL output spectrum shown is shown for comparison. . . . .	330
D.23a	LTE IB UL (amplifier on; signal off) . . . . .	330

D.23b	LTE OOB UL (amplifier on, signal off)	330
D.24	Two-tone intermodulation test setup.	331
D.25	Wideband tests of two-tone intermodulation for input tones at the DL band center (1536 MHz) and UL1 band center (1632.5 MHz).	333
D.25a	No output filtering; display DL level 41.9 dBm, display UL1 power 34.8 dBm	333
D.25b	Notch filters remove input tones; third-order intermodulation distortion (IMD3) products at -138 dBc (lower) and -136 dBc (upper)	333
D.26	Two-tone intermodulation distortion (IMD) tests of LTE IB DL output. Output is at maximum testbed power split between 1531 MHz $\pm$ 5 MHz.	334
D.26a	Unfiltered: input tone levels 40.5 dBm	334
D.26b	Filtered: IMD levels -109.7 dBc $\pm$ 1.5 dB at 1646 MHz, -129.9 dBc $\pm$ 1.5 dB at 1656 MHz, and -152.8 dBc $\pm$ 1.5 dB at 1666 MHz.	334
D.27	Two-tone intermodulation tests of the LTE IB UL1. The testbed output tones split maximum testbed output power between 1627.5 MHz and 1634.5 MHz. 7 MHz bandwidth corresponds with 70% resource block loading across the proposed 10 MHz channel.	335
D.27a	Unfiltered: input tone levels 20.4 dBm	335
D.27b	Filtered: IMD levels -43 dBc $\pm$ 1.5 dB at 1620.5 MHz, -75 dBc $\pm$ 1.5 dB at 1613.5 MHz, and -101 dBc $\pm$ 1.5 dB at 1606.5 MHz.	335
D.28	Two-tone intermodulation tests of the LTE IB DL output. Output tones are at maximum testbed power, split between 1526 MHz and 1536 MHz.	336
D.28a	Setup to measure testbed LTE IB DL output inside of the intended band	336
D.28b	Setup to measure testbed LTE IB DL output outside of the intended band	336
D.29	Transmission and matching characteristics of the low-passive intermodulation (PIM) diplexer used for high-dynamic range tests of LTE DL outputs	338
D.29a	Transmission	338
D.29b	Matching	338
D.30	Spectrum analyzer captures of spectra detected from the two diplexer tests of LTE IB DL performed according to Figure D.28.	339
D.30a	Measurements of testbed LTE IB DL output inside of the intended band	339
D.30b	Measurements of testbed LTE IB DL output outside of the intended band	339
D.31	Measurements of testbed LTE IB DL performed by diplexer output spectra (Figure D.30) with network analyzer data of (Figure D.29). Levels are normalized to average in-band PSD.	340
D.32	Full 2-port S-parameter measurements of LTE IB DL bandpass cavity filter.	341
D.33	Full 2-port S-parameter measurements of LTE IB UL1 bandpass cavity filter.	341
D.34	Full 2-port S-parameter measurements of LTE IB UL2 bandpass cavity filter.	342
E.1	Test method for wideband multipath check in the anechoic chamber.	344
E.2	Multipath response (both H-Pol and V-Pol) in the NTS chamber.	345
E.3	Multipath response (both H-Pol and V-Pol) in the NIST NBIT chamber.	345
E.4	Temperature fluctuations during the test campaign at the NTS and NBIT facilities.	346
E.5	Humidity variability during the test campaign at the NTS and NBIT facilities.	347
F.1	Data Stream: DEV	349
F.2	DUT antenna response	351
F.3	Scatterplots of reported $C/N_0$ , and estimated 95% confidence regions of the median of reported $C/N_0$ from DEV receivers, swept with LTE power level. The GPS scenario is nominal, and the type of incident LTE is DL.	353

F.4	Scatterplots of error in reported 3-D position compared to simulator truth, and estimated 95% confidence regions of the median error in reported 3-D position from DEV receivers, swept with LTE power level. The GPS scenario is nominal, and the type of incident LTE is DL. . . . .	354
F.5	Scatterplots of the number of satellites in view from DEV receivers, swept with LTE power level. The GPS scenario is nominal, and the type of incident LTE is DL. . . . .	355
F.6	Scatterplots of reported $C/N_0$ , and estimated 95% confidence regions of the median of reported $C/N_0$ from DEV receivers, swept with LTE power level. The GPS scenario is nominal, and the type of incident LTE is UL1. . . . .	356
F.7	Scatterplots of error in reported 3-D position compared to simulator truth, and estimated 95% confidence regions of the median error in reported 3-D position from DEV receivers, swept with LTE power level. The GPS scenario is nominal, and the type of incident LTE is UL1. . . . .	357
F.8	Scatterplots of the number of satellites in view from DEV receivers, swept with LTE power level. The GPS scenario is nominal, and the type of incident LTE is UL1. . . . .	358
F.9	Scatterplots of reported $C/N_0$ , and estimated 95% confidence regions of the median of reported $C/N_0$ from DEV receivers, swept with LTE power level. The GPS scenario is nominal, and the type of incident LTE is UL2. . . . .	359
F.10	Scatterplots of error in reported 3-D position compared to simulator truth, and estimated 95% confidence regions of the median error in reported 3-D position from DEV receivers, swept with LTE power level. The GPS scenario is nominal, and the type of incident LTE is UL2. . . . .	360
F.11	Scatterplots of the number of satellites in view from DEV receivers, swept with LTE power level. The GPS scenario is nominal, and the type of incident LTE is UL2. . . . .	361
F.12	Scatterplots of reported $C/N_0$ , and estimated 95% confidence regions of the median of reported $C/N_0$ from DEV receivers, swept with LTE power level. The GPS scenario is nominal, and the type of incident LTE is DL + UL1. The UL level was swept, and the DL level was fixed at -50 dBm EIIP unless otherwise annotated. The horizontal axis reports the linear sum of DL and UL power. . . . .	362
F.13	Scatterplots of error in reported 3-D position compared to simulator truth, and estimated 95% confidence regions of the median error in reported 3-D position from DEV receivers, swept with LTE power level. The GPS scenario is nominal, and the type of incident LTE is DL + UL1. The UL level was swept, and the DL level was fixed at -50 dBm EIIP unless otherwise annotated. The horizontal axis reports the linear sum of DL and UL power. . . . .	363
F.14	Scatterplots of the number of satellites in view from DEV receivers, swept with LTE power level. The GPS scenario is nominal, and the type of incident LTE is DL + UL1. The UL level was swept, and the DL level was fixed at -50 dBm EIIP unless otherwise annotated. The horizontal axis reports the linear sum of DL and UL power. . . . .	364
F.15	$C/N_0$ scatter plots and median, estimated 95% confidence region of the median, and number of satellites in view from DEV receivers, swept with LTE power level. The GPS scenario is timing, and the type of incident LTE is DL. . . . .	366
F.16	Plots of stability of GPSDO receiver 1 PPS output measured against the GPS simulator, and Allan time deviation plots from DEV receivers, swept with LTE power level. The GPS scenario is timing, and the type of incident LTE is DL. . . . .	367
F.17	Zoom of Allan time deviation for DUT 18. Shaded regions indicate pointwise 95% confidence bands. Each curve corresponds to a tested LTE power level. The GPS scenario is timing, and the type of incident LTE is DL. . . . .	368

F.18	<i>C/N<sub>0</sub></i> scatter plots and median, estimated 95% confidence region of the median, and number of satellites in view from DEV receivers, swept with LTE power level. The GPS scenario is timing, and the type of incident LTE is UL1. . . . .	369
F.19	Plots of stability of GPSDO receiver 1 PPS output measured against the GPS simulator, and Allan time deviation plots from DEV receivers, swept with LTE power level. The GPS scenario is timing, and the type of incident LTE is UL1. . . . .	370
F.20	Zoom of Allan time deviation for DUT 18. Shaded regions indicate pointwise 95% confidence bands. Each curve corresponds to a tested LTE power level. The GPS scenario is timing, and the type of incident LTE is UL1. . . . .	371
F.21	TTFF CDF plots and TTFF scatterplots of TTFF from lock acquisition reported by DEV receivers at different LTE power levels. The GPS scenario is TTFF, and the type of incident LTE is DL. . . . .	373
F.22	TTFF CDF plots and TTFF scatterplots of TTFF from lock acquisition reported by DEV receivers at different LTE power levels. The GPS scenario is TTFF, and the type of incident LTE is UL1. . . . .	374
F.23	Scatterplots of reported <i>C/N<sub>0</sub></i> , and estimated 95% confidence regions of the median of reported <i>C/N<sub>0</sub></i> from DEV receivers, swept with LTE power level. The GPS scenario is limited, and the type of incident LTE is DL. . . . .	376
F.24	Scatterplots of error in reported 3-D position compared to simulator truth, and estimated 95% confidence regions of the median error in reported 3-D position from DEV receivers, swept with LTE power level. The GPS scenario is limited, and the type of incident LTE is DL. . . . .	377
F.25	Scatterplots of the number of satellites in view from DEV receivers, swept with LTE power level. The GPS scenario is limited, and the type of incident LTE is DL. . . . .	378
F.26	Scatterplots of reported <i>C/N<sub>0</sub></i> , and estimated 95% confidence regions of the median of reported <i>C/N<sub>0</sub></i> from DEV receivers, swept with LTE power level. The GPS scenario is limited, and the type of incident LTE is UL1. . . . .	379
F.27	Scatterplots of error in reported 3-D position compared to simulator truth, and estimated 95% confidence regions of the median error in reported 3-D position from DEV receivers, swept with LTE power level. The GPS scenario is limited, and the type of incident LTE is UL1. . . . .	380
F.28	Scatterplots of the number of satellites in view from DEV receivers, swept with LTE power level. The GPS scenario is limited, and the type of incident LTE is UL1. . . . .	381

## List of Tables

2.1	List of General Navigation and Location Devices . . . . .	10
2.2	List of High Precision Positioning (Including Real Time Kinematic) Devices . . . . .	11
2.3	List of GPS Disciplined Oscillator Devices . . . . .	13
2.4	List of Antennas Used for Testing . . . . .	13
2.5	List of Data Reported for Each DUT When Available . . . . .	14
2.6	List of Measurands that are the Focus of Additional Statistical Analysis and of Particular Interest to the Stakeholder Community . . . . .	15
2.7	List of LTE Bands Under Study . . . . .	25
2.8	Phase 1 Tests by DUT: LTE Power Sweeps with Nominal GPS Satellite Exposure . . . . .	32
2.9	Phase 2 Tests by DUT: TTFF or TTFR Tests . . . . .	33
2.10	Phase 3 Tests by DUT: LTE Power Sweeps with Limited GPS Satellite Exposure . . . . .	34
3.1	Top-Level Equipment Manifest . . . . .	40
3.1	Top-Level Equipment Manifest . . . . .	41
3.2	Measurement Transmitter Components . . . . .	48
3.3	List of Calibrations Performed to Establish Conducted Signal Levels . . . . .	51
3.4	Correction from Conducted Power Output by the Testbed to Power at the Plane of the DUT (EIIP). Values Use The Measured Separation Distance 3.32 m. . . . .	51
3.5	Summary of LTE output error vector magnitude (EVM) . . . . .	53
3.6	Output Power Capability of the Testbed at the Conducted Output and at the Plane of the DUT (EIIP). The Quoted Uncertainties Correspond to the 97.5% Confidence Interval. . . . .	54
3.7	Summary of Noise Impacts on an Idealized Reference DUT at 3.32 m Test Distance . . . . .	55
3.8	Isolation: Forward Power Available From a Coupling Source Relative to Reverse Coupled Power Absorbed in a Victim Test Point . . . . .	57
3.9	Coupled power ratio: Coupled Power Relative to Intended Forward Power at the Victim Test Point . . . . .	57
4.1	HPP & RTK Configuration Command Structures Configuration Commands for HPP and RTK DUTs . . . . .	76
4.1	HPP & RTK Configuration Command Structures Configuration Commands for HPP and RTK DUTs . . . . .	77
4.1	HPP & RTK Configuration Command Structures Configuration Commands for HPP and RTK DUTs . . . . .	78
4.2	GPSDO Configuration Command Structures . . . . .	80
4.3	NMEA Strings Collected for the Various DUTs . . . . .	86
4.4	Non-NMEA Data Formats Collected for the Various DUTs . . . . .	87
5.1	Data Parsing Capability by Message in Supported Formats. Not All Supported Messages in Each Format are Output by Every DUT. . . . .	95
5.2	Fix Flag Indicators, Leap Second Accounting, and Source of the Timestamp for Each DUT. . . . .	97
5.3	List of Parsed NMEA Sentences. . . . .	98

5.4	Measurands (Subject to Availability) Provided in Data Files. . . . .	118
6.1	LTE Powers by DUT for the Timing Test. The Uncertainty Corresponds to the 95% Confidence Interval. . . . .	190
6.2	LTE Power by DUT for the Time-to-First Fix Test. The Uncertainty Corresponds to the 95% Confidence Interval. . . . .	220
B.1	Parameters used for Eq. (B.5). . . . .	273
C.1	Testbed LTE IB DL Signal Generator Configuration . . . . .	279
C.2	Testbed LTE IB UL Signal Generator Configuration . . . . .	279
C.3	Testbed LTE OOB DL Signal Generator Configuration . . . . .	280
C.4	Testbed LTE OOB UL Signal Generator Configuration . . . . .	280
C.5	Testbed Spectrum Analyzer Configuration . . . . .	281
C.6	Conducted Level Calibration Procedure: Limit LTE IB DL Maximum Output Levels . . . . .	282
C.7	Conducted Level Calibration Procedure: Limit LTE IB UL Maximum Input Level . . . . .	283
C.8	Conducted Level Calibration Procedure: Limit LTE OOB UL Maximum Input Level . . . . .	283
C.9	Conducted Level Calibration Procedure: GPS Output Power . . . . .	284
C.10	Conducted Level Calibration Procedure: Spectrum Analyzer . . . . .	285
C.11	Conducted Level Calibration Procedure: LTE OOB DL Relative to LTE IB DL . . . . .	286
C.12	Conducted Level Calibration Procedure: LTE OOB UL Relative to LTE IB UL . . . . .	287
C.13	Corrections from Conducted Power to Radiated EIIP at the Plane of the DUT . . . . .	288
C.14	Conducted Level Calibration Procedure: LTE OOB UL Relative to LTE IB UL . . . . .	288
C.15	Power Level Calibration Data Taken During the Course of the Test Campaign. <u>Underline</u> Indicates Reuse of Previous Calibration Runs, and <b>Bold</b> Values are Measurement Results. . . . .	290
C.16	Serial Number of the Programmable Attenuator Used in Each Signal Path . . . . .	300
C.17	Uncertainty Budget of the High Power LTE IB DL EIIP. . . . .	301
C.18	Uncertainty Budget of the Low Power LTE IB DL EIIP. . . . .	302
C.19	Uncertainty Budget of the LTE IB UL EIIP. . . . .	303
C.20	Uncertainty Budget of the LTE OOB UL EIIP. . . . .	304
C.21	Uncertainty Budget of the GPS EIIP. . . . .	305
D.1	Reverse Power Across Signal Paths . . . . .	308
D.2	Forward Power at each Signal Test Point . . . . .	309
D.3	Offset Corrections from Signal PSD to Total Signal Power . . . . .	309
D.4	Summary of Output Noise Floor Test Results by Signal Path . . . . .	327
D.5	Summary of Two-Tone IMD3 Test Tone Inputs and Output Products . . . . .	331
E.1	DUT Test Locations ▲ Denotes NTS Longmont and ▼ Denotes NBIT Boulder. . . . .	347
E.1	DUT Test Locations ▲ Denotes NTS Longmont and ▼ Denotes NBIT Boulder. . . . .	348
F.1	DEV Test Matrix. The DEV DUTs were Evaluated for the Following GPS and LTE Signal Combinations. . . . .	350
F.2	Development Board Interfacing, Initialization Commands and National Marine Electronics Association (NMEA) Strings Collected. <i>Italicized NMEA strings</i> are Used for Data Analysis	350
F.3	Dev: Time to First Fix Parsing . . . . .	350
F.4	LTE Powers by DUT for the Timing Test. The Uncertainty Corresponds to the 97.5% Confidence Interval. . . . .	365

F.5 LTE Power by DUT for the Time-to-First-Fix Test. The Uncertainty Corresponds to the 97.55% Confidence Interval. . . . . 372



# 1 Introduction

## 1.1 Objective

The objective of this project was to establish a test method to investigate the impact of adjacent-band long-term evolution (LTE) transmissions on global positioning system (GPS) L1 receivers in tracking and reacquisition modes. We present here the resulting test method and data, which could be used to:

1. establish the integrity of this and other test methods and ensure the quality of the collected data, including detailed uncertainty analysis of both the test conditions and the device under test (DUT) response,
2. enable a connection to previous testing efforts focused on adjacent band activity impacts on GPS device performance, and/or
3. support additional, in-depth testing by other interested parties on measurand behavior as reported by the DUTs.

The methods, testing, results, and analyses neither assumed nor identified pass/fail thresholds. Instead, several GPS receiver outputs were recorded and analyzed over a range of adjacent-band LTE power levels. Results are plotted in this report and an anonymized set of test data is available along with it.

This document encompasses key test setup and process details so that a reasonably knowledgeable technical team should expect their execution of the same tests on the same devices to yield measurand responses within the calculated uncertainty bounds. The details on the data processing, uncertainty analysis, and data plot generation are included to aid the readers' understanding of the plots in this report as well as support the portability of the data analysis techniques to other similar data sets.

The underlying goal was rigorous testing of each DUT configured for typical use. The statistical analyses are focused on outputs of individual DUTs, not the population as a whole. The resulting details and descriptions are meant to facilitate similarly rigorous testing of additional units. Testing a broad subset of GPS devices helped to establish the applicability of our test method beyond our test population, and demonstrated a variety of key response characteristics.

Comments received during the review of the test plan noted that there are tens of millions of GPS devices in circulation. The distribution and quantity of units, models, or manufacturers necessary to achieve a DUT population that is "representative" of this complete market has not been established. The relationship between the comprehensive market and our test population (or that of previous tests) is therefore not clear. However, GPS receivers representing both narrow and broadband response were included in the test population and reported data.

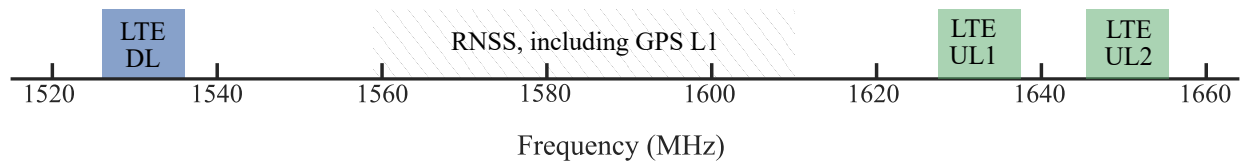


Figure 1.1: Spectrum allocations showing RNSS, which includes the GPS L1 band, and the various adjacent bands proposed for LTE use.

## 1.2 Scope

The purpose of this measurement project was to develop a rigorous (repeatable, calibrated, and well-documented) test method and collect data to analyze impacts of proposed adjacent-band LTE signals on GPS devices using the L1 band. The test method aims to be independent of LTE network architecture and expandable to a variety of GPS device types and use cases. Our execution of the detailed test method focused on L1 GPS scenarios, proposed adjacent band LTE activity, and a set of twenty different GPS-device configurations. Testing was carried out in both an anechoic and semi-anechoic chambers, with well-characterized, radiated, simulated GPS L1 signals, and simultaneously radiated, emulated LTE signals. The GPS receiver was exposed to a stepped range of adjacent-band LTE power levels.

The spectrum allocations in question are illustrated by Figure 1.1. The GPS L1 signal occupied  $1575.42 \text{ MHz} \pm 12 \text{ MHz}$  in the 1559 MHz – 1610 MHz RNSS band allocated by the Federal Communications Commission (FCC). The simulated GPS constellation corresponds with a stationary GPS receiver, and provides two exposure level scenarios, “nominal” and “limited.” Test time limitations did not allow for more dynamic DUT-in-motion simulation scenarios. However, in future investigations the methodology is adaptable to other definitions of GPS use cases.

Adjacent-band LTE activity was represented through emulated, modulating LTE waveforms occupying proposed downlink (1526 MHz – 1536 MHz, “DL”) and uplink (1627.5 MHz – 1637.5 MHz “UL1” and 1646.5 MHz – 1656.5 MHz “UL2”) bands. The fully-utilized downlink activity occupied 10 MHz bandwidth with fully-allocated resource blocks. The uplink LTE modulation was created by emulating a 10 MHz band at approximately 70% resource-block allocation, concentrated in the lower 7 MHz nearest to the GPS L1 signal.

We investigated four types of LTE waveforms. In order of test priority, they were 1) DL, 2) UL1, 3) UL2, and 4) simultaneous DL and UL1. The downlink band (DL) band transmits the most power and is closest to 1575.42 MHz, and therefore received the most attention in previous tests. Emissions from uplink band 1 (low) (UL1) may also be of concern, however, because the proposed waveform contains less stringent out-of-band emission (OOBE) emissions masks. Moreover, in a typical use case, an LTE user equipment (UE) may be much closer to a victim receiver than a cellular base station. We added tests of simultaneous activity in DL and UL1 to imitate more realistic emissions that might be seen in a deployment, and capture any impacts receiver linearity or digital filter performance. In sweeps involving this combination signal, DL power was held at a

constant reduced level, and only UL1 was stepped across power levels, because maximum power level is not expected in both bands at the same time.

Tests were meant to emulate attenuation over distance, so sweeps of LTE power levels are sweeps of both in-band levels and their corresponding OOB. The *relative* levels of the OOB masks is therefore held constant.

Test conditions such as LTE exposure dwell times, number of repetitions and test iterations were chosen to acquire a statistically rich measurand data set and support rigorous analysis of device response. A key aspect in testing was the quality and availability of measurands such as carrier-to-noise-density ratio ( $C/N_0$ ), position, pseudorange, carrier phase, and loss-of-lock (reported by the GPS receiver) or pulse-per-second time output relative to the simulator (reported by a time interval counter instrument). Each of these data was collected at both 1) a baseline condition without LTE adjacent band activity and 2) each LTE power level in the covered LTE power range.

The results were based on sweeps of LTE power levels defined as equivalent output of an isotropic antenna at the plane of the DUT antenna. These levels, together with antenna performance specifications, and assumptions about ambient RF noise, device orientation, separation distances, and radio frequency (RF) propagation, can be used to estimate the GPS device response to LTE transmission power levels in deployment scenarios.

The categories of GPS receiver DUTs encompassed general location and navigation (GLN), high-performance positioning (HPP) including real-time kinematic (RTK), and GPS-disciplined oscillator (GPSDO). For some devices that supported multiple, detachable antenna options, compatible antennas of different designs were tested. In the test setup, systems with embedded antennas were oriented, to the extent practical, to provide consistent test conditions. Calibrated, three-dimensional antenna radiation patterns, including cross-polarization characteristics, for the DUTs were not typically known or available.

Devices specific to aviation, space-based, cellular, or military applications were outside of the scope. The test procedure may require modification to include those additional categories of devices (base station connectivity for cellular devices or test capabilities to meet certified aviation requirements). However, as pointed out in the outreach process during the test plan development, previous testing [2, 3] suggested that the basic GPS receiver RF architecture is the distinguishing feature, e.g., a narrowband versus wideband receiver, in determining susceptibility to LTE activity outside of the GPS band.

Three key test considerations influenced the data that could be collected from the DUTs. This limited the data produced in this report and affected the reported uncertainty estimates. First, some DUTs did not provide a mode of operation that allowed collection of all the desired measurands. Secondly, some DUTs did not provide an appropriate interface for automated testing. Lastly, DUTs generally do not collect measurand data in a metrology-grade manner — for example, many devices only reported  $C/N_0$  values rounded (or truncated) to the nearest 1 dB. These factors were mitigated

in the test setup and execution to the extent that was practical.

### 1.3 Anonymization of Data

The DUT and antenna product identifiers are anonymized in the data presentation. This allows the reader to make informed decisions on DUT performance independent of manufacturer knowledge. Although the GPS receiver products are listed in the report, product names will not be reported in conjunction with the data. Moreover, the intent of this report is to focus on the effects of LTE signals on GPS based receivers as classified by device functional capability of devices instead of by manufacturer. Therefore, devices are simply given an identification number as well as an antenna identification letter. For example, DUT 12 was tested with both antenna C and antenna D.

### 1.4 Background

The National Advanced Spectrum and Communications Test Network (NASCTN) was established to support four key functions [1]:

- facilitate and coordinate spectrum sharing and engineering capabilities,
- create a trusted capability for evaluating spectrum-sharing technologies,
- perform outreach activities to identify spectrum-related testing and modeling needs, and
- protect proprietary, classified and sensitive information while facilitating maximum dissemination.

In support of these functions, this National Advanced Spectrum and Communications Test Network (NASCTN) effort has focused on potential impacts of proposed LTE activities adjacent to GPS L1 receivers in tracking and reacquisition modes. The resulting test methods and data are intended to provide sound and transparent technical information that can support the technical dialogue between affected parties. In January of 2011, the FCC granted a conditional waiver for the operation of a terrestrial communications network in a frequency band adjacent to that used by the GPS. This waiver required the users of the spectrum to prove that their transmissions would not interfere with existing GPS receivers. The resulting four-month (March to June, 2011) measurement effort brought together experts from the fields of communications, GPS, and electromagnetic compatibility (EMC), referred to as a GPS technical working group (TWG). The TWG formed sub-teams to evaluate different types of GPS receivers (e.g., aviation, cellular, general location and navigation, precision timing, etc.) for possible interference effects [2].

In addition, testing was performed by the National Space-Based Positioning, Navigation, and Timing Systems Engineering Forum (NPEF) in October 2011 to January 2012 [3]. Moreover, in 2015 Roberson and Associates [4] performed testing focused on the potential impacts of adjacent band LTE activity on GPS receivers, and in 2016 the U.S. Department of Transportation (DOT) Volpe Center performed testing on adjacent band compatibility to the GPS band [5]. These efforts, including their test plans, paved the way for future efforts to assess potential interference between transmitters and GPS receivers.

Even after the testing above, consensus on the definition of interference to a GPS receiver has yet to be achieved. Stakeholders in the GPS industry proposed interference should be defined as a 1 dB decrease in  $C/N_0$  as reported by the receiver. This implies a slight redefinition of  $C/N_0$  as the ratio of the carrier power to spectral density of noise *plus interference*, and that the ratio of interference density to noise density is -6 dB.

The potential user of the spectrum adjacent to the GPS bands has proposed an interference definition based on the end-user experience. The measurands under test in this case could include degradation in accuracy of the device-reported position, accuracy of timing output, or number of satellites in view. Beyond the lack of consensus on a quantitative definition of interference, many GPS receivers do not readily output or fully define parameters such as pseudorange error or  $C/N_0$ . In these cases, users and license holders who wish to assess potential adjacent-band interference impacts require assistance and cooperation from GPS manufacturers. This situation, when it arises, presents an obstacle to third-party interference testing that may limit users' ability to check for a 1 dB decrease in  $C/N_0$ .

## 1.5 Stakeholder Outreach

Testing of adjacent-band activity involves multiple systems by its very nature, and stakeholders often view testing from different perspectives and data needs. The test method that NASCTN has developed and executed here is to inform stakeholders such as the spectrum regulators, the GPS community, and proposers of nearby LTE activity. The draft test plan was distributed to stakeholders and posted on the NASCTN website. Additionally, federal stakeholders were briefed in June of 2016. Comments were received and adjudicated. Over a two-month period, NASCTN received 159 comments from spectrum regulators, Federal agencies, GPS manufacturers and members of the general public. The adjudication was posted on the NASCTN website. As a result of the comments, the test plan was revised and posted on the NASCTN website in July of 2016. Changes included but were not limited to the addition of GPSDO timing receiver and real time kinematic (RTK) tests and development of the limited satellite condition.

As part of the test development, the test team met with GPS manufacturers to discuss aspects of the test such as simulated satellite conditions, RTK configurations, and GPSDO setup. In addition, manufacturers participated in the development of DUT automated control and data acquisition during the test campaign. To assist with long-lead-time procurements and maintain the project schedule, manufacturers provided additional devices and licenses for testing under equipment loan agreements. These devices are all commercially available units. When necessary, non-disclosure agreements were signed to secure access to software application programming interface (API) and documentation resources.

The final test setup reflects incorporation of comments from a wide range of stakeholders during the test plan development and review process. The US Army's Electronic Proving Ground, an experienced GPS test facility, met with the test team prior to the release of the draft test plan

and became a participant of this NASCTN test team. In addition, other individuals in the GPS community provided historical context and their perspectives on GPS testing via teleconferences.

Due to the interest in the findings, NASCTN provided two pre-briefings of the data collected during the test, one on September 27th and one on November 15th, 2016. These pre-briefings were restricted to federal employees due to the rules under which the project was operating. NASCTN set the boundaries for these pre-briefings in accordance with its technical review process and the rules defined in the cooperative research and development agreement (CRADA):

- Prior to the release of data or reports, the NASCTN process for the release of technical reports requires a technical review by NIST and ITS. The pre-briefings were conducted in the midst of the test campaign and prior to the reviews. Therefore, no data was distributed electronically or in hard copy, and those in attendance were bound by confidentiality agreements.
- The timing of a data or report release on completion of the NASCTN review process was defined in the CRADA.

## 1.6 Overview

Twenty different GPS-device configurations were tested, comprised of devices classified as GLN, HPP, RTK, or GPSDO timing. Each class is differentiated by a general set of GPS features that is advertised to some common type of end-user application<sup>1</sup>. The receiver test population and antenna population are outlined in Table 2.1, Table 2.2, and Table 2.3 (pages 10 – 13). Testing was executed in three phases, the corresponding test matrices are presented in Table 2.8, Table 2.9, Table 2.10 (pages 32 – 32):

- Phase 1 – Stepped power level sweeps: Nominal satellite constellation, testing of DL, UL1, UL2, and DL + UL1 LTE waveforms
- Phase 2 – TTFF and TTFR tests: Nominal satellite constellation, testing of DL, and UL1 LTE waveforms
- Phase 3 – Stepped power level sweeps: Limited satellite constellation, testing of DL, and UL1 LTE waveforms

Supplemental tests were also performed on development board (DEV) devices (see Table F.1 for a test matrix of supplemental tests and Table F.2 for a device list).

This main structure of the report is as follows:

- statement of parameters of the test campaign (Chapter 2 starting on page 9),
- test hardware design, control, calibration, and validation (Chapter 3 starting on page 35),
- the automation and testing process (Chapter 4 starting on page 63),
- data processing and analysis methods (Chapter 5 starting on page 93), and

---

<sup>1</sup>Some documents refer to real-time kinematic (RTK) units as a subcategory or specialization of high-performance positioning (HPP).

- plotted results of the collected data (Chapter 6 starting on page 119).

The appendices provide additional calculations, calibration data, and supporting analysis:

- the physical definition of DUT exposure conditions (Appendix A starting on page 267)
- a simulation investigation on the behavior of  $C/N_0$  estimators impacted by LTE waveforms (Appendix B starting on page 271),
- detailed transmitter calibration procedures and data (Appendix C starting on page 277),
- detailed procedures and results for conducted transmitter performance (Appendix D starting on page 307),
- detailed procedures and results for conducted transmitter performance (Appendix E starting on page 343),
- supplemental results obtained by testing GPS DEV (Appendix F starting on page 349).



## 2 Test Parameters

This chapter summarizes the devices under test (DUTs), the characteristics of the simulated global positioning system (GPS) constellation, the strength and structure of GPS and long-term evolution (LTE) signals, and the tests performed on each DUT.

### 2.1 GPS Receivers

#### 2.1.1 Test Population

We organized the DUTs into four device classes: general location and navigation (GLN), high-performance positioning (HPP), real-time kinematic (RTK), and GPS-disciplined oscillator (GPSDO). Each class was defined according to application criteria like tightly specified positioning accuracy, or support for external active antennas, differential position solutions, or time synchronization outputs.

The set of devices in each class was selected for the ability to output an adequately broad variety of GPS and device state data, as well as test plan feedback and device representation in prior test campaigns.

Devices were purchased new-in-box, shipped directly to a National Advanced Spectrum and Communications Test Network (NASCTN) test facility. The receiver units were configured according to their most common deployment, with the addition of any necessary software licenses to allow for automating data collection.

##### 2.1.1.1 General Location and Navigation (GLN)

General location and navigation devices are the most common type in use by the general public. The selected set of devices was based on hand-held receivers that consumers typically encounter as hiking GPS units. The list encompassed legacy products as well as current market offerings. Where applicable, the units were specified to include necessary cables or personal computer (PC) interface solutions for streaming data sold together as part of a kit. Moreover, the devices used external power supplies to allow for long test periods without the need for battery changes. Our GLN device population is found in Table 2.1.

Table 2.1: List of General Navigation and Location Devices

<b>Unit<sup>1</sup></b>	<b>Model ID</b>	<b>Antenna</b>	<b>Mode</b>	<b>Interface</b>	<b>Data</b>	<b>Cold-Start</b>	<b>Relevant KPI(s)</b>
Garmin eTrex H	s/n: 190-00818-10 Rev A f/w: 3.40	Integrated	N/A	Serial	NMEA	No	Time, position, $C/N_0$ , # sats in view
Garmin eTrex 30x	s/n: 3907308647 f/w: 2.30	Integrated	N/A	USB mass storage	GPX	No	Time, position
Garmin GPSMAP 78	s/n: 3916298284 f/w: 6.40	Integrated	N/A	Serial	NMEA	No	Time, position, $C/N_0$ , # sats in view
Garmin Montana 650t	s/n: 3873599505 f/w: 5.30	Integrated	N/A	Marine Mount to Serial	NMEA	No	Time, position, $C/N_0$ , # sats in view
Garmin Montana 680t	s/n: 3913704347 f/w: 2.20	Integrated	N/A	Marine Mount to Serial	NMEA	No	Time, position, $C/N_0$ , # sats in view
Garmin Montana 680t	s/n: 3923469238 f/w: 2.54	Integrated	N/A	Marine Mount to Serial	NMEA	No	Time, position, $C/N_0$ , # sats in view

<sup>1</sup>Certain commercial equipment, instruments, or materials are identified in this report in order to specify the experimental procedure adequately. Such identification is not intended to imply recommendation or endorsement by NIST nor is it intended to imply that the materials or equipment identified are necessarily the best available for the purpose.

Table 2.2: List of High Precision Positioning (Including Real Time Kinematic) Devices

Unit <sup>1</sup>	Model ID	Antenna	Mode	Interface	Data	Cold-Start	Relevant KPI(s)
Leica GR50	s/n: 1870346 f/w: 4.00.335	External	Standalone	Ethernet	NMEA	Yes	Time, position, $C/N_0$ , # sats in view, fix type
Novatel FlexPak 628	s/n: NKC13100010 f/w: OEM060700RN0000 h/w: 2.01	External	Standalone, RTK (base)	Serial	NMEA	Yes	Time, position, $C/N_0$ , # sats in view, fix type, pseudorange, carrierphase
Novatel FlexPak 628	s/n: NKC14160016 f/w: OEM060700RN0000 h/w: 2.01	External	RTK (rover)	Serial	NMEA	Yes	Time, position, $C/N_0$ , # sats in view, fix type, pseudorange, carrierphase
Novatel ProPak 6	s/n: NMCP16240010E f/w: OMP060601RN0000 h/w: 1.07	External	Standalone	Serial	NMEA	Yes	Time, position, $C/N_0$ , # sats in view, fix type, pseudorange, carrierphase
Trimble NetR9	s/n: 5616R50136 f/w: 5.03 h/w: 3.2	External	Standalone, RTK (base)	Ethernet	NMEA, BINEX	Yes	Time, position, $C/N_0$ , # sats in view, fix type, pseudorange, carrierphase
Trimble R9S	s/n: 5616R03026 f/w: 5.14 h/w: 3.2	External	RTK (rover)	Ethernet	NMEA, BINEX	Yes	Time, position, $C/N_0$ , # sats in view, fix type, pseudorange, carrierphase

<sup>1</sup>Certain commercial equipment, instruments, or materials are identified in this report in order to specify the experimental procedure adequately. Such identification is not intended to imply recommendation or endorsement by NIST nor is it intended to imply that the materials or equipment identified are necessarily the best available for the purpose.

### 2.1.1.2 High-Precision Positioning (HPP)

Often referred to as GPS reference receivers, high precision positioning devices are commonly used in surveying, geodetic, and scientific applications. The test devices were purchased as a commercially available kit. These kits were representative of the most commonly specified end user configurations and included antenna, cabling, as well as software licenses to allow for programmatic interfacing with the DUT. The HPP device population is found in Table 2.2.

### 2.1.1.3 Real-Time Kinematic (RTK)

We treated RTK devices as a subset of HPP devices with additional features. The RTK devices make use of a fixed receiver (base) and a roaming receiver (rover)<sup>1</sup>. The base and rover communicate so as to improve positioning calculations.

The RTK subsystems (base and rover) communicated with each other by either RS-232 serial or TCP/IP over ethernet.

The RTK kits were provided for testing by their manufacturers; the units were tested as standalone HPP devices and in the RTK mode. The RTK mode test population is in Table 2.2.

### 2.1.1.4 GPS-Disciplined Oscillators (GPSDO)

High precision timing receivers are commonly used in network architectures for time syncing. The timing receivers were configured as kits which included cabling, external antennas, and DUT setups that were representative of most common use cases. The specification exception however was in the timing crystal. The GPSDOs were configured with their fastest responding/shortest long term stability crystal oscillators so as to facilitate reasonable measurement times. Precision timing devices were configured in steering mode, where their time estimate is directly related to GPS timing information at a known fixed position. In addition to the receiver key performance indicators (KPIs), the GPSDOs were also evaluated for their pulse per second output. The GPSDO population is given in Table 2.3.

---

<sup>1</sup>In this test, only the rover will be exposed to LTE signals.

Table 2.3: List of GPS Disciplined Oscillator Devices

Unit <sup>1</sup>	Model ID	Antenna	Mode	PC Interface	Data	Cold-Start	Relevant KPI(s)
Arbiter 1088B	s/n: A1222 f/w: Nov 30 2015	External	Steering	Serial	NMEA, ASCII	No	Time, position, # sats in view, 1 PPS
MicroSemi SyncServer S650	s/n: SCA162600014 f/w: 1.1.5	External	Steering	Serial	ASCII	Yes	Time, position, $C/N_0$ , # sats in view, fix type, 1 PPS
MicroSemi TimeSource 3050	s/n: SCA15410000C f/w: 1.0.7 f/w: DEV:34	External	Steering	Serial	ASCII	Yes	Time, position, $C/N_0$ , # sats in view, fix type, 1 PPS

<sup>1</sup>Certain commercial equipment, instruments, or materials are identified in this report in order to specify the experimental procedure adequately. Such identification is not intended to imply recommendation or endorsement by NIST nor is it intended to imply that the materials or equipment identified are necessarily the best available for the purpose.

Table 2.4: List of Antennas Used for Testing

Manufacturer <sup>1</sup>	Model	Part Number
Arbiter	GPS Active Timing	AS0087800
Javad	GrAnt-G3T	01-570200-01
Leica	AR20	794207
Microsemi	Kit Antenna	32-3372-14-01
Microsemi	Kit GNSS DTI Roof Top Antenna	090-72510-71 Rev C
Novatel	GPS-702-GGL	01017939
Novatel	GPS-704-WB	01019436
Trimble	Zephyr Geodetic Antenna Model 2	57971-00
Trimble	Zephyr Geodetic Antenna Model 2	77971-00

<sup>1</sup>Certain commercial equipment, instruments, or materials are identified in this report in order to specify the experimental procedure adequately. Such identification is not intended to imply recommendation or endorsement by NIST nor is it intended to imply that the materials or equipment identified are necessarily the best available for the purpose.

Table 2.5: List of Data Reported for Each DUT When Available

Data Source	Recorded Parameters
DUT only	UTC date/time, latitude, longitude, height, 3D position, fix indicator, $C/N_0$ , pseudorange, carrier phase, TTFF, TTFR
DUT referenced to GPS simulator “truth”	3D position error, pseudo-range error
DUT referenced to GPS simulator “truth” and external instruments	1 PPS output error

### 2.1.1.5 External Antennas

Where applicable, external antennas were selected as part of a kit in conjunction with the DUT. Some DUTs were tested with two antenna solutions. A comprehensive list of GPS antennas is given in Table 2.4.

### 2.1.2 Measurands

The key focus of this study was the response of DUT output “measurands” (defined for example in [6]) at different levels of LTE signal. In our context, measurands were data that are

1. observable to users (or third-party testers) from digital outputs of the DUT,
2. made available from the GPS simulator as the reference “truth,” and/or
3. measurable at electrical outputs of the DUT.

We collected a combination of these types of measurands. In some cases, collaboration with vendor technical support was required to extract device data. Previous efforts focused heavily, if not exclusively, on carrier-to-noise-density ratio ( $C/N_0$ ) as the key performance measurand.

#### 2.1.2.1 Focus and Scope

Table 2.5 lists the data that were the focus of this study, along with the sources of these data. When available, DUT configuration options were set to enable the output of these measurands. No special effort was made to collect or analyze measurands that are not in Table 2.5 (though they were collected and recorded if part of the output stream).

Many types of collected data originated entirely from the DUT’s data streams. We augmented the DUT measurands with data from the GPS simulator and the time interval counter (TIC). The use

Table 2.6: List of Measurands that are the Focus of Additional Statistical Analysis and of Particular Interest to the Stakeholder Community

Central Location Type	Measurand
Median	Receiver-reported $C/N_0$
Median	3-D position error
Stability	1 PPS output
—	Observed number of satellites
—	Time to first fix
—	Time to first reacquisition

of the GPS simulator provided insights into the GPS constellation and “true” DUT position against which to compare DUT output data. Information about the time synchronization signal stability was enabled by TIC measurements, which compared the output of the DUT against the Cesium timebase input to the GPS simulator.

During tests, raw data were collected and recorded, then timestamped according to the most recently available coordinated universal time (UTC) date and time reported by the DUT. For consistency, among different kinds of DUTs and instruments, some values were translated to a common system of units, such as converting values to floating point number representation, or converting position coordinates. No other changes were made to the actual data values produced by the DUT.

### 2.1.2.2 Statistical Analysis and Reporting

The measurands listed in Table 2.6 were the subject of additional statistical study. We chose this subset of data for added focus based on stakeholder feedback received during outreach.

The resulting uncertainty statement added another layer of insight for stakeholders: 1) limits on the strength of the results imposed by test method and DUT variability, and 2) the repeatability that can be reasonably expected during future implementations of our test method. The statistical techniques used to estimate the reported measurement value and uncertainty are discussed in Chapter 5. Uncertainties in LTE power are expressed with 97.5% confidence intervals, unless otherwise noted.

The results are presented graphically in Chapter 6.

### 2.1.3 Test Capabilities

#### 2.1.3.1 Support for Warm and Cold Start

At the beginning of a data acquisition sequence the DUTs were initialized to remove device memory. Devices with cold-start command capability were initialized from test automation scripts to ensure

that the device calculated its initial conditions without relying on prior data. Cold starts typically deleted ephemeris and almanac data, forcing the device to recalculate its position from freshly acquired almanac and ephemeris information. We chose this procedure with the intention to force the device to initialize without hysteresis or bias from previous test conditions.

The automated testbed could not automatically perform a cold-start for GLN DUTs. We ran these through an alternate initialization procedure. Prior to a test sweep, GLN DUTs were manually reset through menu driven functionality and manual power cycling. In the case where manual intervention was impractical, such as time to first reacquisition tests, a “warm-start” procedure was implemented with a specialized “warm-start” GPS simulator scenario that introduced a change of the “true” position to the DUT. The support for automated cold-start in the test population is listed in Table 2.1-Table 2.3.

### 2.1.3.2 Data Formats

The collected data formats were determined by the DUT. The most common were the standardized National Marine Electronics Association (NMEA) stream in American standard code for information interchange (ASCII) format. We collected as many types of NMEA sentences as possible, but GPGGA sentences, containing fix information, and GPGSV sentences, containing detailed satellite information, were the highest priority. Together, these sentences gave UTC time, position, satellite specific  $C/N_0$ , number of satellites in view, and fix type (Standalone, differential global positioning system (DGPS), or RTK).

Some DUTs also supported binary exchange (BINEX) data, which provided lower-level satellite information such as high precision  $C/N_0$ , pseudorange, and carrier phase. When available, these low-level data were also collected within manufacturer-specific NMEA sentences.

The GPSDO devices output other types of ASCII-formatted data via TL1, or another manufacturer-dependent tabular representation. Raw data provided in these formats included only the most basic of information, time, position, number of satellites in view, and in some cases satellite specific  $C/N_0$  and fix type.

### 2.1.4 Incident Power at the Receiver

The subject of this report is the impact of radiated LTE signals upon GPS device KPIs. This means we need to consider the impacts of these emissions at the position of the DUT, not the radiator. This test condition needs to be defined clearly for each GPS or LTE signal.

The incident field strength test condition at the DUT is defined and reported in this study as “power at the plane of the DUT,”<sup>2</sup> or abbreviated effective isotropic incident power (EIIP).

---

<sup>2</sup>For the purposes of this test DUT is defined as the whole system, where the “plane of the DUT” is defined as the plane of the RF-front end.

The EIIP parameter is already in use by other test reports and cellular industry standards for characterizing GPS power levels [2, 4, 7] and for wireless communications including LTE [4, 8, 9]. Sometimes, it has been referred to simply as “power.” Our use of “EIIP at the plane of the DUT” is to create a distinction compared to any actual power quantity that could be measurable in the DUT.

The EIIP is the incident power that would be received by an idealized (non-physical) reference receiver system with the following properties:

- its antenna is lossless with isotropic gain,
- its antenna is co-polarized with respect to a reference polarization (we define right-hand circularly-polarized (RHCP) for GPS signals and linearly-polarized (LP) for LTE signals),
- its antenna is loaded by a receiver that has a conjugate (reflectionless) impedance match,
- its receiver adds no noise (i.e., has a noise figure equal to 0 dB), and
- its receiver reports calibrated root mean square (RMS) power across the signal bandwidth that is traceable to power standards.

Substituting this reference ideal in place of an actual DUT is the reference condition for EIIP. Similarly, the spectral density reported by this receiver could be interpreted as “power spectral density (PSD) at the plane of the DUT,” or EIIP PSD.

A more mathematical discussion of EIIP is in Section A.1. The details include the relationship between total incident field strength and the transmit effective isotropic radiated power (EIRP) by means of the Friis transmission equation [10].

Some previous efforts give results in terms of the equivalent separation distance between a DUT and a LTE transmitter radiating at the LTE DL or UL emissions mask maximum limits. Equation A.3 gives a means to map the power at the plane of a DUT to the equivalent separation distance at maximum LTE power in free space. This mapping is plotted in Figure 2.1. The curves are valid for free space propagation as long as antenna geometries allow reasonable far field assumptions.

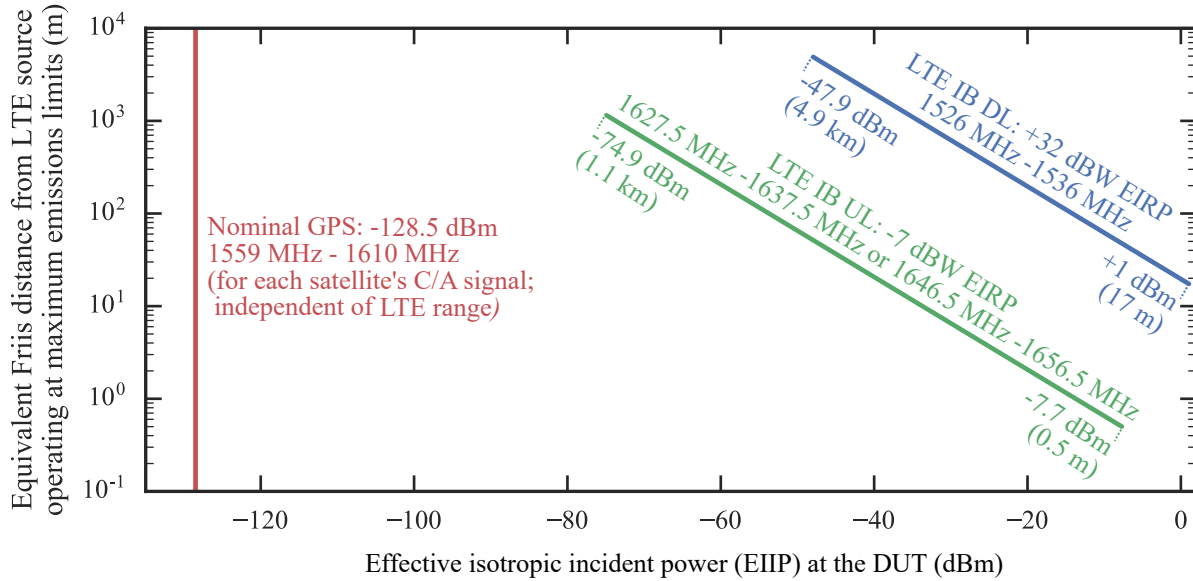


Figure 2.1: Friis equation relationship between EIIP (power at the plane of DUT) and the free-space distance from LTE operating at maximum emissions levels (Figure 2.4). The displayed DL (blue) and UL (green) spans represent the output capability of the testbed (Table 3.6).

## 2.2 GPS Constellation Characteristics

In evaluating the effects of LTE on GPS receivers most tests have three options: 1) utilize continuous live-sky, 2) make use of a pre-recorded live-sky, or 3) simulate the GPS environment. There are advantages with each method but they can mostly be categorized into faithfulness to a real-world scenario, repeatability, or complete control over the GPS signals and constellation.

The first solution of using live-sky directly, would use a stationary environment without the ability to control GPS constellation repeatability, environmental factors (ionospheric, tropospheric), and spurious external noise sources. However, this method would channel augmentation signals such as WAAS or other manufacturer specific protocols into the test environment.

The second solution pertains to playback of pre-recorded live-sky data. These recordings may be taken under kinematic conditions such as a recording carried out by a survey vehicle driving on a predefined path. These collected GPS conditions present inherent challenges in repeatability measurements and statistical analysis of measurands. In particular the “true” position for 3-D position error calculations will be very difficult to discern in a kinematic environment.

Furthermore, the pre-recorded track would need to be completed numerous times in order to get a statistically meaningful distribution of baseline behavior of the DUT. This means that the test time needs to be long enough for the track to be run through numerous times (e.g., the survey vehicle would complete several laps of the same test loop) or that the DUT needs to be re-initialized at the beginning of every playback (e.g., DUT initialization begins at the start of the playback and the

sequence is iteratively repeated).

Both pre-recorded GPS emulations or live-sky signals also present inherent challenges to the evaluation of DUT performance based on  $C/N_0$  estimation. Live-sky data contain stratified GPS-signal strengths on a per satellite basis. From an end user perspective this means that the DUT reports  $C/N_0$  levels that depend on the satellite position in the sky. Consequently, evaluations of receiver performance based on  $C/N_0$  alone are troublesome, as natural shifts in a satellite constellation such as a transition over the horizon can affect mean  $C/N_0$  calculations.

While it is possible to account for the effects of these transitions (GPS satellite tracks are very well defined) it is impractical to continuously adjust baseline receiver performance in the presence of stratified  $C/N_0$  data.

Therefore, it is most practical to control as many GPS-conditions as possible. We made use of a GPS simulator which gave us greater control over the GPS environment. In general we utilized:

- a stationary position,
  - alleviated long test time requirements over kinematic tests
  - simplified predicting satellite transitions over the horizon during data analysis
- identical GPS power level across all satellites (nominal case),
  - simplified statistical analysis of  $C/N_0$  data
  - included Wide area augmentation system
- control over environmental effects, such as
  - tropospheric
  - ionospheric
  - clean, non-multipath environment
- and minimization of the number of satellite transitions over the horizon.

### 2.2.1 Base Signal Parameters

GPS signals were simulated with a dedicated global navigation satellite system (GNSS) simulator. The scenario configurations accommodated various test conditions as outlined in the following sections. However, all the power level sweep tests had the following attributes:

- The GPS L1 (center frequency of 1575.42 MHz) is the only GNSS signal under investigation.
- Signal codes: L1 C/A, L1C pilot, Pseudo Y, and M-code.
- Stationary location: N 31° 35.893636', W 110° 16.670841', height 1352.30 m. The location corresponds to a surveyed marker location at US Army Fort Huachuca's Electronic Proving

Grounds.

- Two wide-area augmentation system (WAAS) augmentation signals (pseudo-random noise (PRN) 135, PRN 138).
- A satellite elevation mask of  $5^\circ$  above the horizon.
- Tropospheric and ionospheric propagation effects.
- Initial constellation and geometry of July 4, 2016 at UTC time 01:35:18. Normally there is a slight variation in satellite constellation due to diurnal cycles. This variation was accounted for by modifying simulated almanac data. This allowed for identical constellations at 24 hour intervals.

## 2.2.2 LTE Power Level Sweep Test Scenarios

Test scenarios made use of either the nominal, limited, or timing GPS scenarios.

### 2.2.2.1 Nominal (GLN, HPP, RTK)

The nominal scenario for positioning receivers simulated the actual GPS satellite constellation of July 4th, 2016.

Two WAAS satellites were included in the simulation. There were 11 satellites transmitting L1; each provided coarse/acquisition (C/A) codes specified with a target level of -128.5 dBm EIIP at the plane of the DUT antenna (calibrated according to Subsection 3.5.4). During test implementation the exposure level and corresponding uncertainty was found to be  $-128.5 \text{ dBm} \pm 2.7 \text{ dB}$  EIIP at the plane of the DUT antenna. A polar plot of the satellite tracks for the Nominal condition are shown in Figure 2.2a.

The scenario ran from 01:35:18 UTC until 02:10:18 UTC. Some key properties of the constellation over this chosen timespan included:

1. Satellite movement without transitions over the horizon for 35 minutes
2. Low dilution of precision (DOP) (a key indicator of constellation quality)

The nominal test condition was designed to test DUT response to LTE without the influence of satellite transitions, poor constellation geometry, or sparsely populated GPS-receiver channels.

### 2.2.2.2 Limited (GLN, HPP, RTK)

The “limited” scenario for positioning receivers was an adjustment to the “normal” nominal scenario constellation and has reduced power and fewer satellites. This exposure stressed the ability of GPS receivers to acquire lock through reduced  $C/N_0$  levels. The adjusted constellation was limited to eight L1 C/A and two WAAS signals. The satellite exposure levels at the DUT were

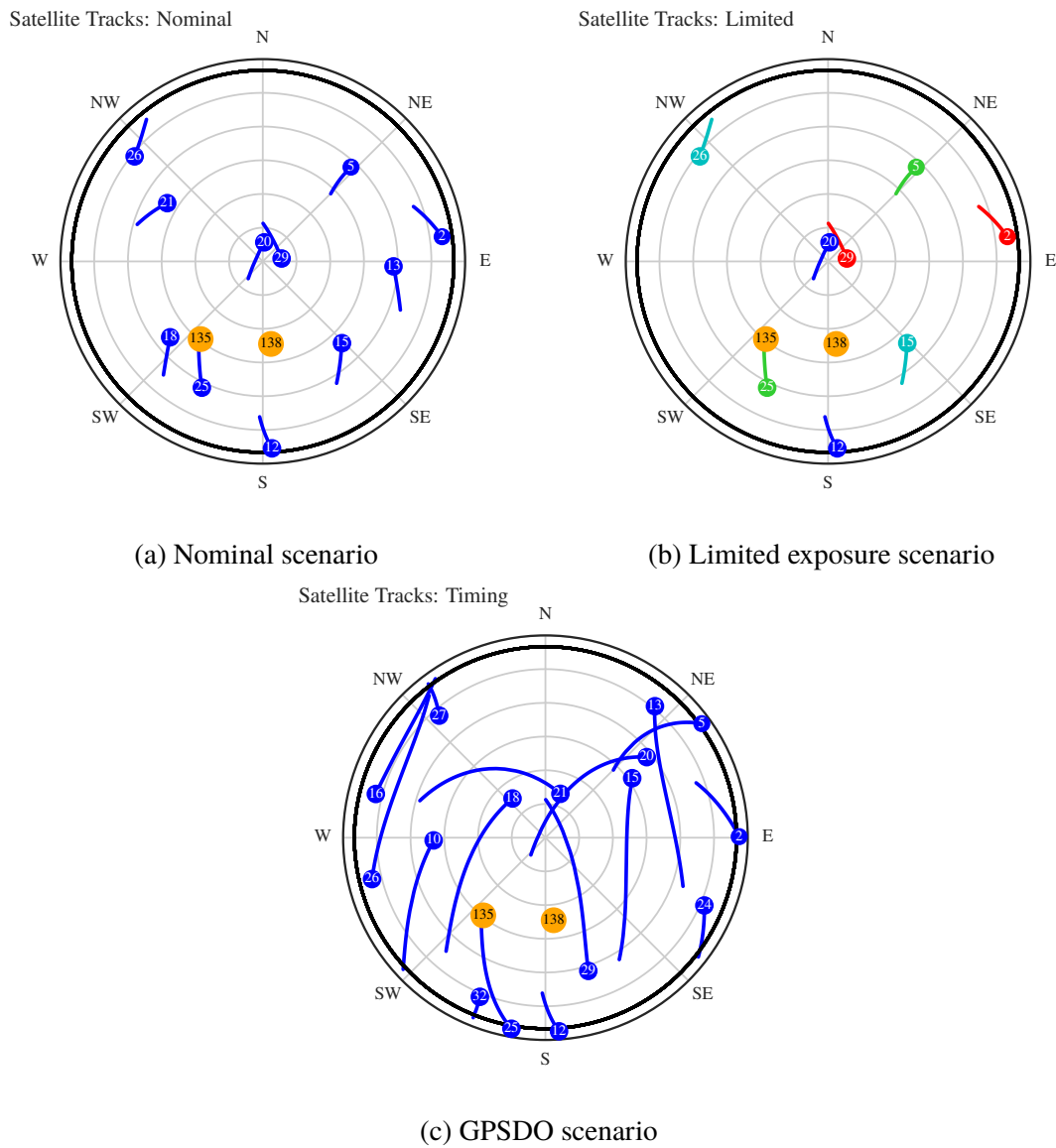


Figure 2.2: Simulated satellite tracks for nominal and limited exposure constellations and timing tests. The satellite PRN marker denotes the final position of the satellite along its track. Marker and track colors correspond to GPS power level at the plane of the DUT, with the exception of ●, which denotes a WAAS satellite. The circumferential black line shows the 5° elevation mask angle of the simulation.

- -128.5 dBm ± 2.7 dB, ● -133.5 dBm ± 2.7 dB,
- -138.5 dBm ± 2.7 dB, and ● -143.5 dBm ± 2.7 dB.

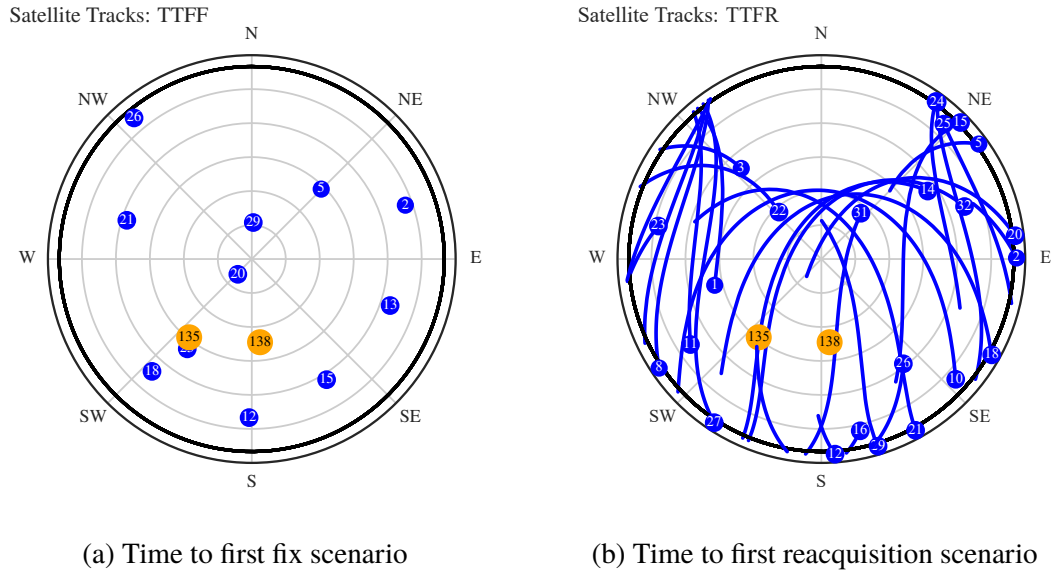


Figure 2.3: Simulated satellite tracks for TTFF and TTFR constellations. The satellite power levels were nominal at  $-128.5 \text{ dBm} \pm 2.7 \text{ dB EIIP}$ . The satellite PRN marker denotes the final position of the satellite along its track. The TTFF tracks were very short, a period of 2 min for HPP DUTs and 3 min for RTK DUTs. The TTFR tests required a long test period of 8 hrs, therefore satellite transitions over the horizon occur.

distributed across four target values — a pair of satellites at each of  $-128.5 \text{ dBm}$ ,  $-133.5 \text{ dBm}$ ,  $-138.5 \text{ dBm}$ , and  $-143.5 \text{ dBm EIIP}$  at the DUT (in test implementation, satellite exposure values were  $-128.5 \text{ dBm} \pm 2.7 \text{ dB}$ ,  $-133.5 \text{ dBm} \pm 2.7 \text{ dB}$ ,  $-138.5 \text{ dBm} \pm 2.7 \text{ dB}$ , and  $-143.5 \text{ dBm} \pm 2.7 \text{ dB EIIP}$  at the DUT). The satellite tracks for the limited scenario are shown in Figure 2.2b.

### 2.2.2.3 Timing (GPSDO)

The timing test scenario for GPSDO devices ran for 150 minutes, which included satellite transitions over the horizon. The satellite tracks for the timing test are shown in Figure 2.2c.

## 2.2.3 TTFF and TTFR Test Scenarios

### 2.2.3.1 TTFF

The TTFF tests made use of the constellation from the nominal scenario. The test time for individual fix acquisition is shortened (2 to 5 mins). Figure 2.3a shows the satellite constellation tracks across this time span, which are so short that the satellites appear stationary.

### 2.2.3.2 TTFR

The TTFR scenario introduced a “warm start” state in the DUT. The scenario emulated idealized signals experienced by a DUT that enters a tunnel, where it lost signal, then exits the tunnel after traveling 1595 m in 3 min.

The scenario was composed of many repeated toggles between two stationary DUT locations:

1. Tunnel entrance: N 31° 35.3333775', W 110° 17.0257599', height 1372.00 m.
2. Tunnel exit: N 31° 35.8077487', W 110° 17.0257599', height 1356.45 m.

These correspond to surveyed ground marker locations at the U.S. Army Fort Huachuca Electronic Proving Grounds.

In each iteration of the tunnel test, the DUT was first exposed to location 1) for 2 minutes. The GPS satellite power transmission is disabled for 3 minutes while the DUT was “in the tunnel.” Finally, the DUT was exposed to the second position for 2 minutes followed by an additional 3 minutes without satellite coverage and position change to the initial location.

The full scenario includes 50 iterations, or 100 total opportunities for acquisition by the DUT, lasting approximately 8 hours total. This extended run time required satellite transitions over the horizon as in Figure 2.3b.

## 2.2.4 Augmentation Signals

### 2.2.4.1 WAAS

Two geostationary WAAS sources were included in the simulation. The first WAAS satellite had PRN 135 at 133° W longitude, and EIIP at the DUT equal to  $-128.8 \text{ dBm} \pm 2.7 \text{ dB}$ . The second satellite W2 with PRN 138 at 107° 18' W longitude was configured to a power level setting that produces DUT EIIP exposure of  $-128.9 \text{ dBm} \pm 2.7 \text{ dB}$ .

### 2.2.4.2 GPS L2

One DUT required L2 signals to report RTK solutions. Simulated L2 Pseudo-Y and M-noise codes were transmitted at -6 dB with respect to L1 signals, when testing this DUT. Therefore, nominal L2 signals were at  $-134.5 \text{ dBm} \pm 2.7 \text{ dB}$  EIIP at the plane of the DUT, limited L2 signals were  $-134.5 \text{ dBm} \pm 2.7 \text{ dB}$ ,  $-139.5 \text{ dBm} \pm 2.7 \text{ dB}$ ,  $-144.5 \text{ dBm} \pm 2.7 \text{ dB}$ , and  $-149.5 \text{ dBm} \pm 2.7 \text{ dB}$ .

### 2.2.4.3 Other GNSS Systems

No other GNSS augmentation signals were simulated in these tests. Signals that were not simulated or transmitted included GPS L5-band, Galileo, BeiDou, and global navigation satellite system

(GLONASS).

## 2.2.5 Track Modifications for Daily Constellation Reuse

Initially there was a concern that subjecting a DUT to unrepeatable satellite constellations during testing may have an affect on DUT baseline performance. Moreover, simply repeating the same constellation during testing could confuse DUTs as the devices may not be able to handle backward discontinuities in time. Modifications to the simulated almanac alleviated GPS satellite track concerns.

As the LTE power levels were incremented, the GPS-simulator time was advanced by 24 hrs. A modified almanac was used to obtain identical satellite constellations between the 24 hour intervals. This allowed for additional repeatability in the measurement. Furthermore, this modification ensured that DUTs were exposed to identical GPS condition without having backward discontinuities in time.

In order to keep the same geometry in the constellation, all scenarios must have the same static position and the same dynamic profile. Additionally, the almanac files were modified by recalculating the “Right Ascension at Week” and adjusting “Time of Applicability” to the initial scenario time. The updated almanac files were loaded into the GPS simulator.

## 2.3 Long Term Evolution (LTE) Signal Characteristics

### 2.3.1 LTE Bands Under Consideration

The LTE waveforms emulated for signaling in these tests were generic because the authors of this test plan do not know details of the proposed LTE deployment architecture.

Emulated LTE waveforms and power levels were chosen to mirror those in a few key scenarios relevant to the topic under study:

1. LTE downlink (base station transmission) only, radiated toward a GPS L1 receiver,
2. LTE uplink (user equipment (UE) transmission) only, radiated in close physical proximity to a GPS L1 receiver, and
3. dual LTE uplink and LTE downlink activity, 1 and 2, (above) superimposed.

The LTE uplink and downlink frequency bands were each 10 MHz allocations as specified in Table 2.7. Another LTE downlink band (1670 MHz — 1680 MHz) proposed in Federal Communications Commission (FCC) filings was not tested in this work because a cavity filter was not currently available with this passband.

Table 2.7: List of LTE Bands Under Study

Description	Test Abbreviation	LTE Band (MHz)
LTE Downlink	DL	1526.0 - 1536.0
LTE Uplink 1	UL1	1627.5 - 1637.5
LTE Uplink 2	UL2	1646.5 - 1656.5

### 2.3.2 Radiated Emissions Mask

Radiated waveforms in this study were designed to match the emissions masks proposed in [11]. The masks specified EIRP PSD limitations for LTE user equipment (UE) devices and base stations. They were illustrated by Figure 2.4 in relation to the GPS L1 and LTE operating bands under consideration.

The radiated signals were intended to match the emissions masks that could be received by a DUT. These waveforms matched Figure 2.4, where both the in-band (IB) and corresponding out-of-band (OOB) power levels were scaled up or down by the same propagation loss. During testing, this meant adjustments to LTE IB DL or LTE IB UL power required the same adjustment to LTE OOB DL and LTE OOB UL levels. In other words, the relative emissions levels for OOB signals shown on the right axis are forced to apply at any IB power level.

### 2.3.3 LTE Baseband Signal Characteristics

This test campaign made a departure from previous work by use of LTE modulated signaling instead of band-limited Gaussian noise. The resulting device responses should therefore be more representative of a realistic deployment scenario.

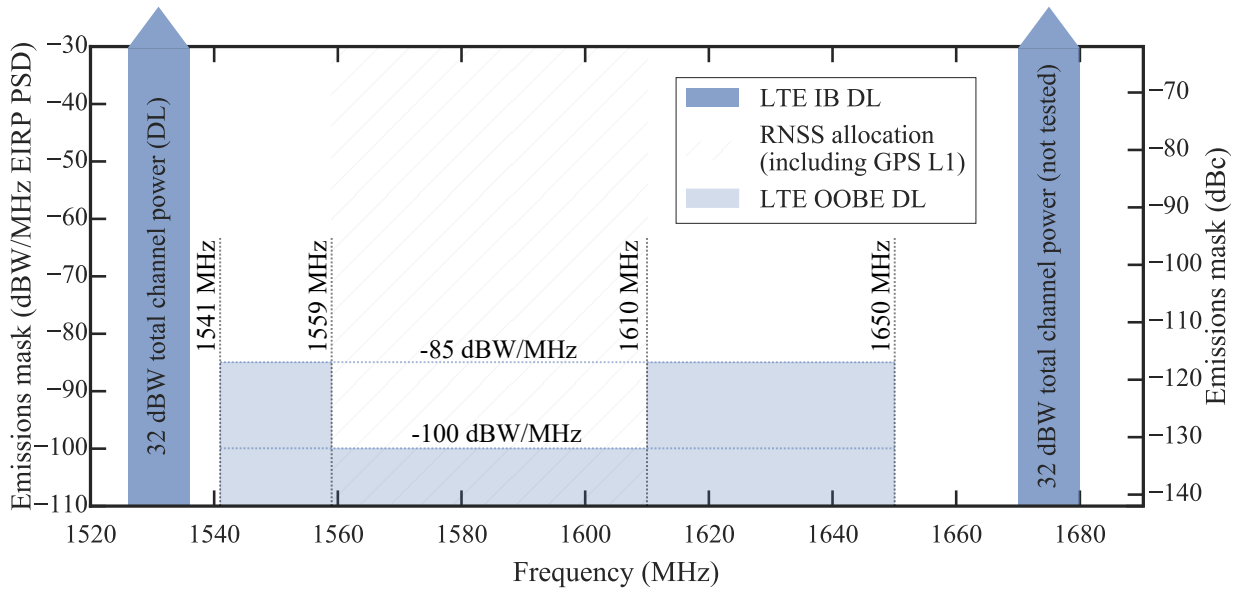
The proposed LTE deployment is frequency-division duplex (FDD), because the uplink and downlink bands are in separate frequency allocations.

The parameter space of LTE configuration settings is very large; at the same time, the shortest test of a single DUT in this report (LTE power level sweeps) takes more than 30 minutes. Together, these facts made expansive testing across many LTE configurations impractical — the ability to sweep across LTE power levels was a higher priority. We therefore chose configuration parameters to represent two “generic” FDD LTE configurations:

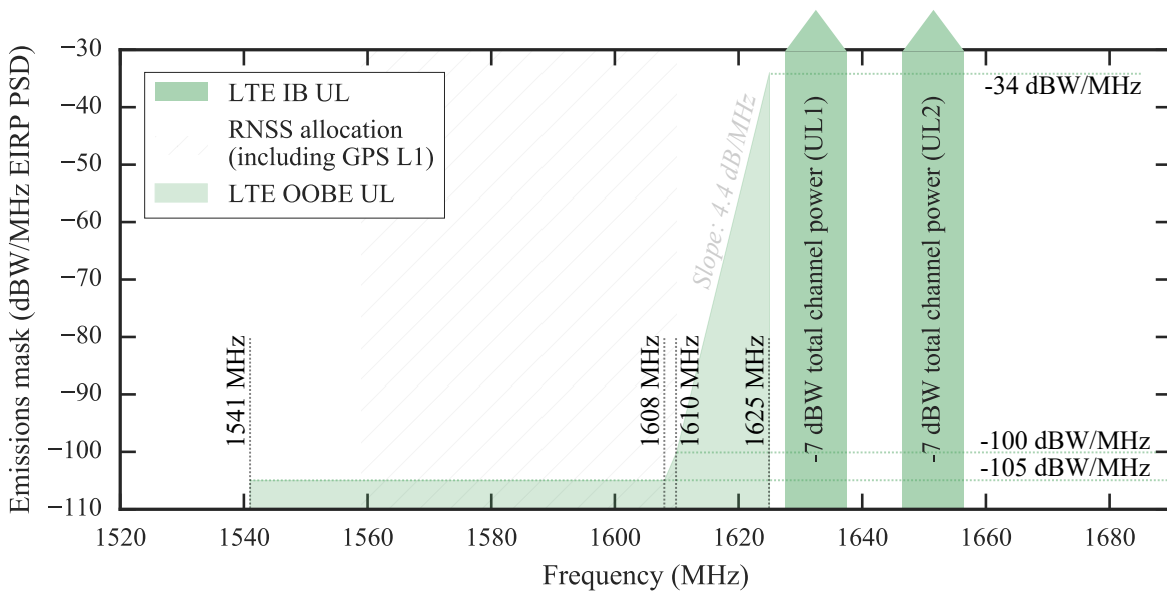
- one signal parameter configuration for LTE IB DL FDD, to be tested at various power levels, detailed in Appendix C.1.2, and
- one signal parameter configuration for LTE IB UL FDD, to be tested at various power levels and at both uplink band 1 (low) (UL1) and uplink band 2 (high) (UL2) bands, detailed in Appendix C.1.3.

We selected a vector signal generator to produce communication signals corresponding to eNodeB

downlink and UE uplink traffic. The instrument upconverts LTE baseband signaling to radio frequency (RF) at configurable frequencies; this was crucial because actual LTE networking hardware that can operate at these frequencies was not available. The output includes LTE protocol layers to sufficient depth that we could customize the data transmitted over the channel, which we set to a high entropy PN9 bit stream. The instrument also enabled automation with our test software.



(a)



(b)

Figure 2.4: Emissions masks under study in this test report, reflecting proposals to the FCC [11] for (a) LTE downlink and (b) LTE uplink bands.

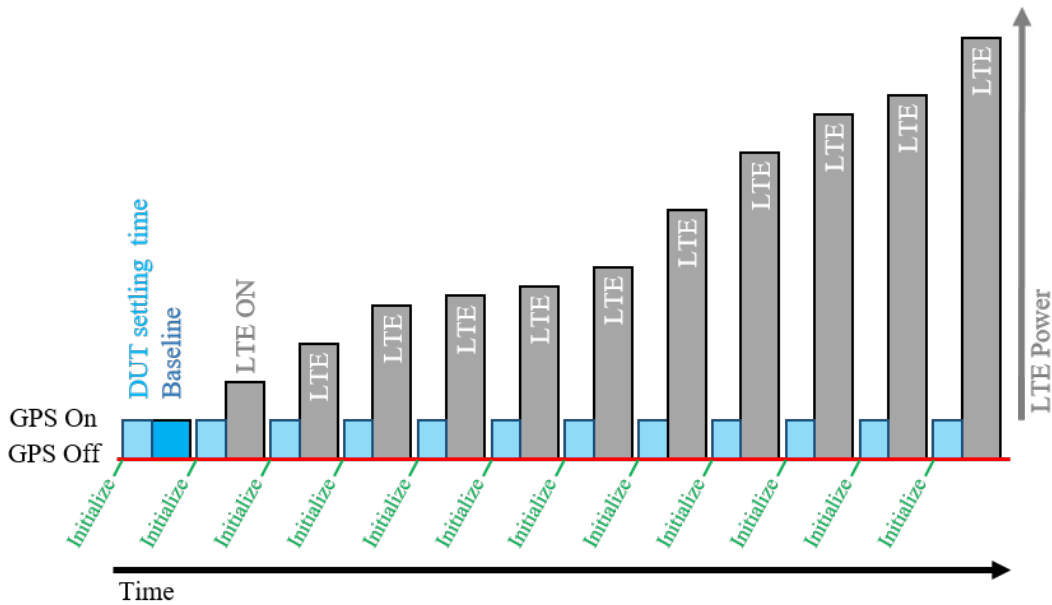


Figure 2.5: Diagram of the LTE power level sweep procedure for GLN, HPP, and RTK DUTs. Power level sweeps were initialized with a cold-start if available. The DUT was then exposed to 15 mins of GPS only and subsequently to 20 minutes of GPS and LTE. Power level sweep parameters were designed to invoke major DUT responses.

## 2.4 Test Sweeps of GPS Receiver Response

Signal sweep profiles were developed to encompass LTE power level sweeps, TTFF, TTFR, as well as GPSDO specific tests.

### 2.4.1 LTE Power Level Sweeps

#### 2.4.1.1 Positioning Classes (GLN, HPP, and RTK)

Power Level sweeps as shown in Figure 2.5 were initialized with a cold-start (if available) at the start of each power level step. DUTs without remote cold-start initialization capability (GLN) were reset and power cycled prior to the baseline test (at the very beginning of a power level sweep) and did not receive a reinitialization at subsequent power levels. At each power level, the DUT was first exposed to 15 min GPS-only signal (No-LTE). This gave the DUTs sufficient time to download ephemeris and almanac data. After the 15 min soak time, LTE was turned on for 20 min. For the purposes of analyzing DUT response, only the 20 min duration with LTE was used for statistical consideration. Test time amounted to 37 mins per power level per LTE waveform sweep.

The testbed was capable of providing LTE power throughout the range outlined in Figure 2.1. The actual range tested varied on a DUT basis, and primarily depended on preliminary observations on DUT response. The LTE power levels were chosen to outline a progression in DUT response to the

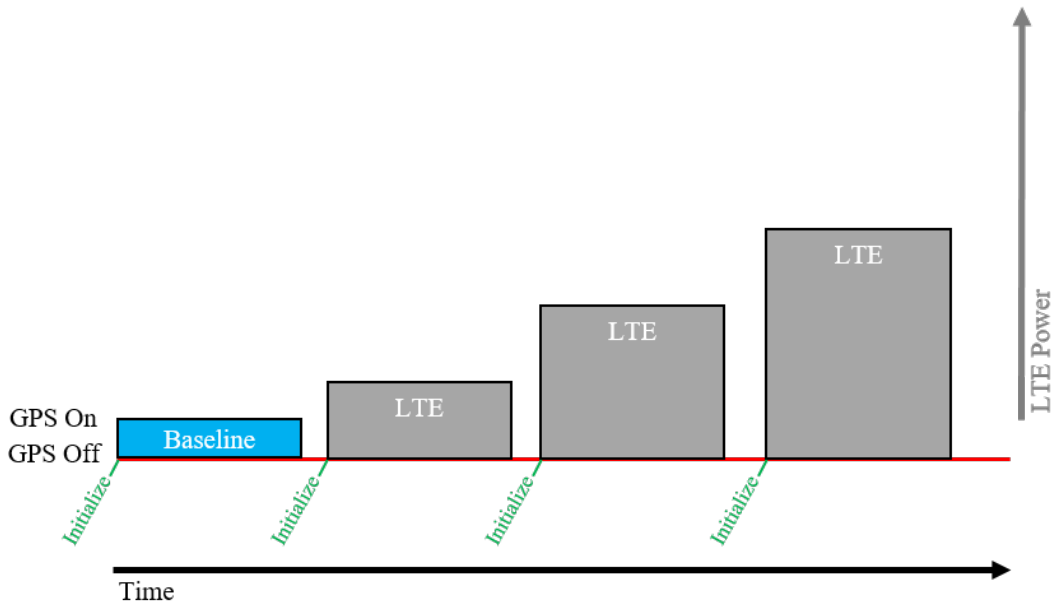


Figure 2.6: Diagram of the LTE Power Level sweep procedure for GPSDO DUTs. LTE level sweeps were initialized with a cold-start or power cycle procedure. The DUT was then exposed to 150 mins of GPS and LTE. Power level sweep parameters were designed to observe major DUT responses.

LTE signal.

DL, UL1, and UL2 were tested through a range of power levels. The combination signal of DL + UL1 were tested by holding the DL power fixed at a targeted -50 dBm EIIP, and varying the UL1 EIIP through a range. Devices that were not able to perform during combination tests with a fixed target DL power level of -50 dBm EIIP were subsequently tested with a fixed target DL power level at -65 dBm EIIP while varying UL1 EIIP.

The LTE power level sweep procedure applied to the nominal and limited satellite constellations.

#### 2.4.1.2 Timing Classes (GPSDO)

Unlike the LTE power sweep testing for positioning devices, GPSDO devices were not exposed to a preconditioning phase and had to achieve timing solutions post initialization in the presence of a LTE signal (see Figure 2.6). GPSDO data were collected for 150 mins to observe timing crystal responses in 1 pulse-per-second output measurand. GPSDO receiver measurands were observed for a long time period in order to isolate responses due to LTE from the long-term stability of internal crystals.

The power-levels were chosen in a fashion to show a representative set of DUT responses to LTE power.

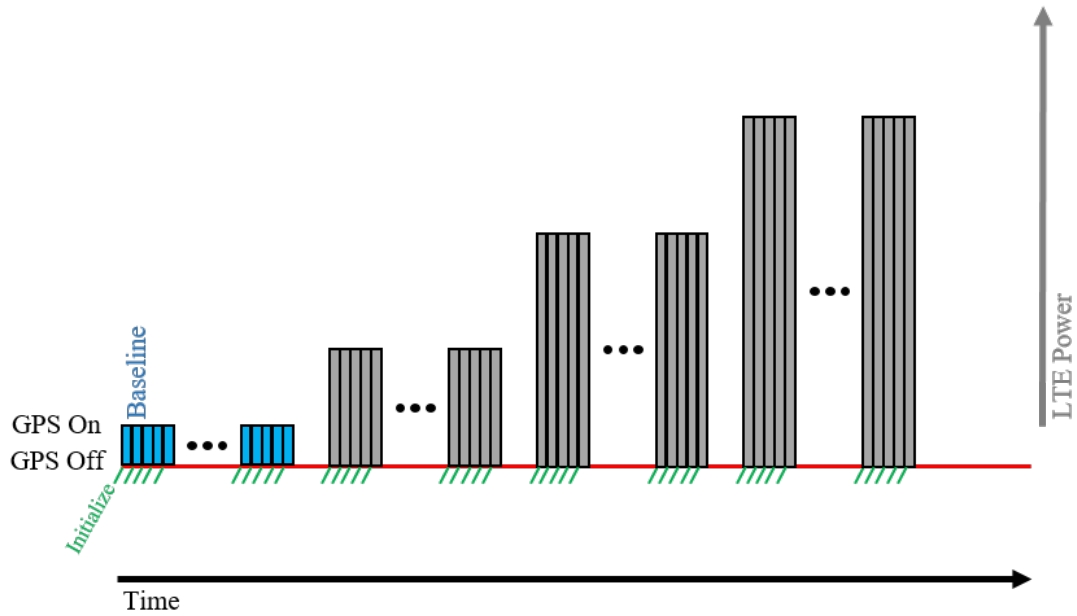
## **2.4.2 Time to First Fix (TTFF) and Time to First Reacquisition (TTFR) Swept with LTE Power**

### **2.4.2.1 GLN, HPP, and RTK**

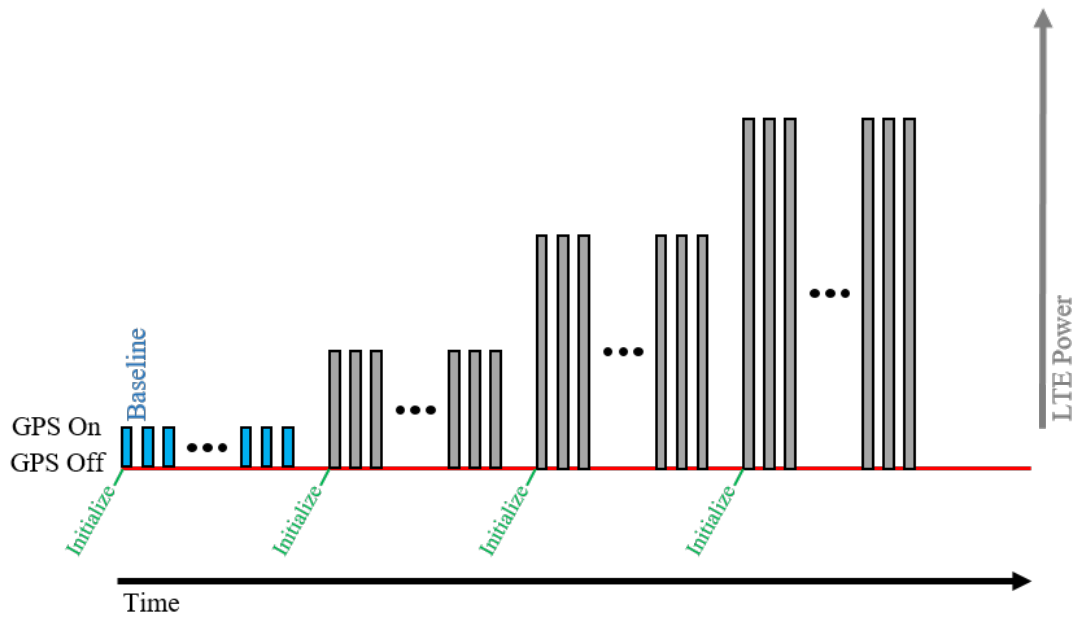
Power sweep profiles for TTFF and TTFR are shown in Figure 2.7. For repeatability, a high degree of automation was necessary to achieve these tests. TTFF tests for HPP and RTK units were initialized with a cold-start and data were acquired for 2 mins for HPP units and 5 mins for RTK units. RTK units typically required a longer and more complex cold-start procedure, therefore data were acquired for 5 mins. For each LTE waveform, the test time amounted to 5 hrs per power level for HPP units, and 10 hrs per power level for RTK units.

The GLN units did not allow for programmatic initialization, therefore a TTFR test procedure was devised, as discussed in Section 2.2. TTFR test time amounted to 8 hrs per power level per LTE waveform.

The DUTs response to LTE power level sweeps informed on the LTE power levels chosen for the TTFF and TTFR tests.



(a) Time to first fix sweep profile for HPP and RTK units.



(b) Time to first reacquisition sweep profile for GLN units.

Figure 2.7: Diagram of the TTFF (top) and TTFR (bottom) sweep procedures. Each LTE power level consisted of 100 cycles. LTE power levels were selected after analyzing the DUT's LTE power sweep response.

Table 2.8: Phase 1 Tests by DUT: LTE Power Sweeps with Nominal GPS Satellite Exposure

Device	Type	GPS Scenario	Test Sweep	LTE Waveform			
				DL	UL 1	UL 2	DL + UL 1
DUT 1	GLN	Nominal	LTE power	✓	✓	✓	✓
DUT 2	GLN	Nominal	LTE power	✓	✓	✓	✓
DUT 3	GLN	Nominal	LTE power	✓	✓	✓	✓
DUT 4	GLN	Nominal	LTE power	✓	✓	—	—
DUT 5 <sup>†</sup>	GLN	Nominal	LTE power	✓	✓	—	—
DUT 6 <sup>‡</sup>	GLN	—	—	—	—	—	—
DUT 7	HPP	Nominal	LTE power	✓	✓	✓	✓
DUT 8	HPP	Nominal	LTE power	✓	✓	✓	✓
DUT 9, Ant C	HPP	Nominal	LTE power	✓	✓	✓	✓
DUT 9, Ant D	HPP	Nominal	LTE power	✓	✓	✓	✓
DUT 10	HPP	Nominal	LTE power	✓	✓	✓	✓
DUT 11, Ant A	RTK	Nominal	LTE power	✓	✓	✓	✓
DUT 11, Ant B	RTK	Nominal	LTE power	✓	✓	✓	✓
DUT 12, Ant C	RTK	Nominal w/ L2	LTE sweep	✓	✓	✓	✓
DUT 12, Ant D	RTK	Nominal w/ L2	LTE sweep	✓	✓	✓	✓
DUT 13	GPSDO	Timing	LTE power	✓	✓	✓	✓
DUT 14	GPSDO	Timing	LTE power	✓	✓	✓	✓
DUT 15	GPSDO	Timing	LTE power	✓	✓	✓	✓

<sup>†</sup> DUT 5 did not provide sufficient measurands to present a complete dataset for the purpose of this study .

<sup>‡</sup> DUT 6 data reporting did not include sufficient number of key measurands of interest to this study, and its control capability presented challenges for third-party testbed automation.

## 2.5 Test Campaign Execution and Scope

Some DUT receivers were tested with multiple antennas and/or in both standalone and RTK modes. Each mode accounted for a separate DUT entry. For example a HPP receiver with RTK capability was tested once as a standalone unit and then again as an RTK unit. Test deliverables were acquired in three phases. Phase 1 focused on LTE power level sweeps under a nominal satellite constellation profile. Phase 2 performed TTFB and TTFR tests with nominal satellite constellations. Phase 3 evaluated the DUT’s susceptibility to LTE power in a limited satellite scenario.

### 2.5.1 Phase 1: LTE Power Level Sweeps for Nominal GPS Power Exposure

Phase 1 data encompass a power level sweep for a nominal satellite exposure in the presence of either DL, UL1, UL2, or combination DL and UL1. Some data resulted from testing done at National Technical Systems in Longmont, CO, and the remainder are from testing performed at NIST Broadband Interoperability Testbed (NBIT) facility in Boulder, CO.

Table 2.9: Phase 2 Tests by DUT: TTFF or TTFR Tests

Device	Type	GPS Scenario	Test Sweep	LTE Waveform			
				DL	UL 1	UL 2	DL + UL 1
DUT 1	GLN	TTFR	TTFR	✓	✓	—	—
DUT 2	GLN	TTFR	TTFR	✓	✓	—	—
DUT 3	GLN	TTFR	TTFR	✓	✓	—	—
DUT 4*	GLN	—	—	—	—	—	—
DUT 5	GLN	—	—	—	—	—	—
DUT 6	GLN	—	—	—	—	—	—
DUT 7	HPP	TTFF	TTFF	✓	✓	—	—
DUT 8	HPP	TTFF	TTFF	✓	✓	—	—
DUT 9, Ant C	HPP	TTFF	TTFF	✓	✓	—	—
DUT 9, Ant D	HPP	TTFF	TTFF	✓	✓	—	—
DUT 10	HPP	TTFF	TTFF	✓	✓	—	—
DUT 11, Ant A	RTK	TTFF	TTFF	✓	✓	—	—
DUT 11, Ant B	RTK	TTFF	TTFF	✓	✓	—	—
DUT 12, Ant C	RTK	TTFF w/ L2	TTFF	✓	✓	—	—
DUT 12, Ant D	RTK	TTFF w/ L2	TTFF	✓	✓	—	—
DUT 13	GPSDO	—	—	—	—	—	—
DUT 14	GPSDO	—	—	—	—	—	—
DUT 15	GPSDO	—	—	—	—	—	—

\* DUT 4 was not sufficiently stable to accommodate test times greater than 3 hrs.

### 2.5.2 Phase 2: TTFF and TTFR Tests

Phase 2 included the TTFR for GLN DUTs and TTFF for HPP and RTK DUTs in the presence of either DL or UL1 in the presence of a nominal GPS constellation. All data from Phase 2 were done at National Institute of Standards and Technology (NIST) NBIT facility in Boulder, CO.

### 2.5.3 Phase 3: LTE Power Level Sweeps for Limited GPS Power Exposure

Phase 3 tests gave the DUT response to reduced  $C/N_0$  conditions by means of the limited satellite constellation in the presence of either DL or UL1. All data from Phase 3 were performed at the NIST NBIT facility in Boulder, CO.

Table 2.10: Phase 3 Tests by DUT: LTE Power Sweeps with Limited GPS Satellite Exposure

Device	Type	GPS Scenario	Test Sweep	LTE Waveform			
				DL	UL 1	UL 2	DL + UL 1
DUT 1	GLN	Limited	LTE power	☑	☑	—	—
DUT 2	GLN	Limited	LTE power	☑	☑	—	—
DUT 3	GLN	Limited	LTE power	☑	☑	—	—
DUT 4	GLN	—	—	—	—	—	—
DUT 5	GLN	—	—	—	—	—	—
DUT 6	GLN	—	—	—	—	—	—
DUT 7	HPP	Limited	LTE power	☑	☑	—	—
DUT 8	HPP	Limited	LTE power	☑	☑	—	—
DUT 9, Ant C	HPP	Limited	LTE power	☑	☑	—	—
DUT 9, Ant D	HPP	Limited	LTE power	☑	☑	—	—
DUT 10	HPP	Limited	LTE power	☑	☑	—	—
DUT 11, Ant A	RTK	Limited	LTE power	☑	☑	—	—
DUT 11, Ant B	RTK	Limited	LTE power	☑	☑	—	—
DUT 12, Ant C	RTK	Limited w/ L2	LTE power	☑	☑	—	—
DUT 12, Ant D	RTK	Limited w/ L2	LTE power	☑	☑	—	—
DUT 13	GPSDO	—	—	—	—	—	—
DUT 14	GPSDO	—	—	—	—	—	—
DUT 15	GPSDO	—	—	—	—	—	—

## 3 GPS and LTE Transmission System

The transmission system was designed to excite a receiver device under test (DUT) with calibrated and computer-controlled levels of emulated global positioning system (GPS) and synthesized long-term evolution (LTE) signals. There were four types of LTE signals, each generated by a separate signaling path before combining: synthesized in-band (IB) downlink band (DL) and IB uplink bands (UL), and Gaussian noise with spectral shaping to represent out-of-band (OOB) DL and OOB UL.

Conducted signals were filtered and combined into a single conducted output, then fed into a single right-hand circularly-polarized (RHCP) transmit antenna. The test environment was a (semi-) anechoic chamber in order to approximate empty space with ambient background noise equivalent to thermal noise at room temperature.

### 3.1 System Overview

One conducted test topology was the basis for each class of DUTs: general location and navigation (GLN), high-performance positioning (HPP), real-time kinematic (RTK), and GPS-disciplined oscillator (GPSDO). This section provides an overview of the system architecture and its application to each class of tested GPS receiver.

#### 3.1.1 GLN/Base Test Configuration

The GLN class of devices tested operated with antennas that were integrated inside the device shell. These devices supported digital communication over a link to the testbed control personal computer (PC). No optional external antennas were connected to the DUT. These characteristics made GLN the simplest test configuration, and the basis from which other device class tests were derived.

The measurement system configured for GLN devices is illustrated in Figure 3.1. Each of these high-level blocks are discussed in later sections of this chapter. Signal leveling, combining, and monitoring, which is identical for each class of DUT, is detailed in Section 3.3. The GPS simulator excites a GPS constellation as defined in Section 2.2.

Four separate signal generators generated calibrated LTE IB DL, LTE OOB DL, LTE IB UL, and LTE OOB UL (as defined in Section 2.3).

The test chamber is discussed in Section 3.2. All functional blocks were controlled by the test

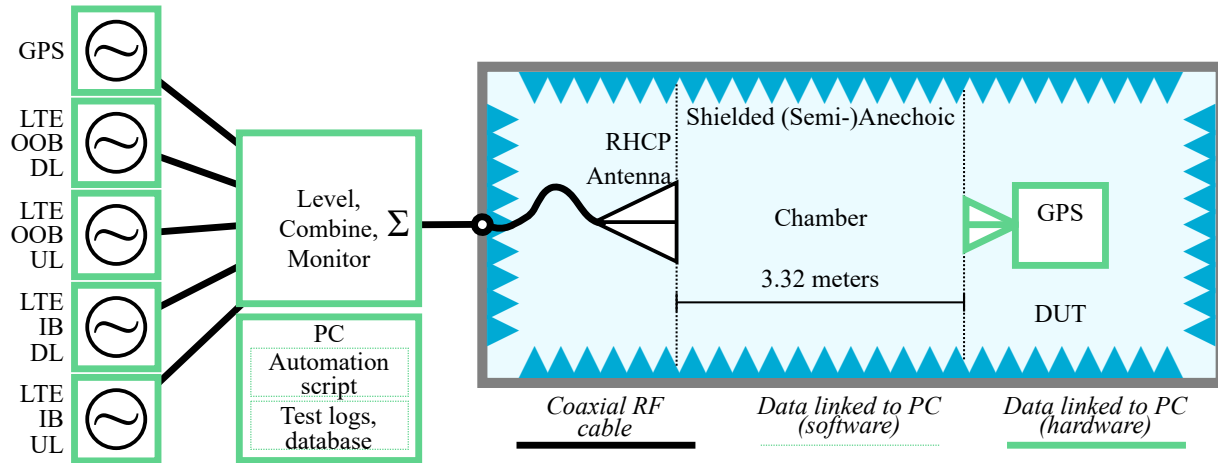


Figure 3.1: Measurement system configuration for testing a GLN device (and base configuration for testing all other device classes). The “level, combine, monitor” block is expanded in Figure 3.9.

automation scripts discussed in Section 4.1.

Unlike tests for other device classes, data link cables and connectors passed under the (shielded) floor of the test chamber, then ran vertically from the floor through test mast inside the chamber to the DUT. This mast was not shielded. Any radio frequency (RF) self-interference components radiated by these data links became part of the RF noise input to the DUT; this type of effect would also be experienced by any user who is streaming data. We did not perform any additional tests to determine the extent of these impacts.

We did not perform tests that include multiple DUTs in the chamber, because:

1. the intended test condition does not incorporate any potential interference from other DUTs,
2. identification and mitigation of interference caused by unintended radiation by GPS receivers would add to test time and (and present risks if suitable mitigation techniques could not be identified),
3. each additional DUT adds additional reflections in the chamber which may alter the test conditions applied to each DUT, and
4. uniform field excitation upon multiple DUTs suitable for sweeping the same power levels across many devices was determined to be impractical.

These problems could make an interesting subject of future study.

### 3.1.2 HPP Test Configuration

The HPP measurement system topology (Figure 3.2) was an adaptation of the GLN configuration. The HPP DUTs used external antennas that connect to the receiver box with a  $50\ \Omega$  coaxial cable.

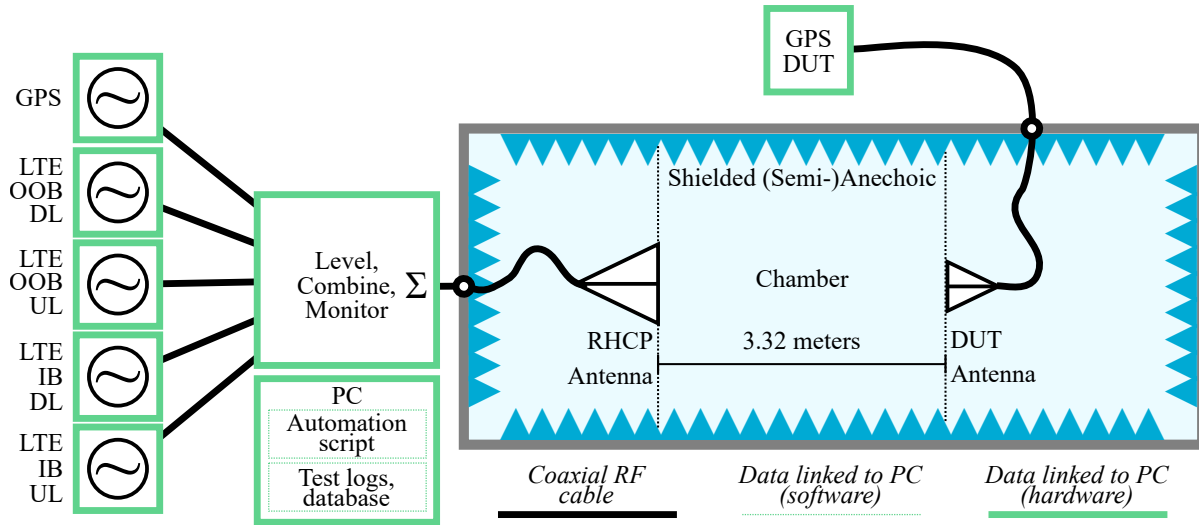


Figure 3.2: Measurement system configuration for testing a HPP (high precision positioning) device. The “level, combine, monitor” block is expanded in Figure 3.9.

We took advantage of the cable to place the receiver unit outside the test chamber, mitigating electromagnetic interference (EMI). All HPP tests in this report used this coaxial cable, specified in the top-level equipment manifest, Table 3.1.5.

### 3.1.3 RTK Test Configuration

The RTK device class test configuration is illustrated in Figure 3.3. Each of these DUTs is a system of two receivers: a base and a rover. The rover was exposed to the combination of GPS and LTE, while the base unit was connected only to GPS.

The base unit connection to GPS passed through 1) a directional coupler, redirecting a small portion of the GPS simulator output, then 2) a variable attenuator. The resulting GPS level at the base approximated that of the rover (when LTE is disabled).

The rover receiver operated outside the chamber (like the HPP devices). Both rover and base were connected by similar cables (the coaxial cable from the testbed GPS tap to base had  $3.33 \text{ dB} \pm 0.10 \text{ dB}$  loss at 1575.42 MHz).

The rover connected to the base unit via a data link cable according to DUT manufacturer operating instructions. This data link provided rover positioning and telemetry data to the base as necessary to compute the RTK position solution.

### 3.1.4 GPSDO Test Configuration

The notable feature of GPSDO receiver tests is the output of timing synchronization signals. Those tested in this report were all configured to accomplish this through 1 pulse-per-second (PPS)

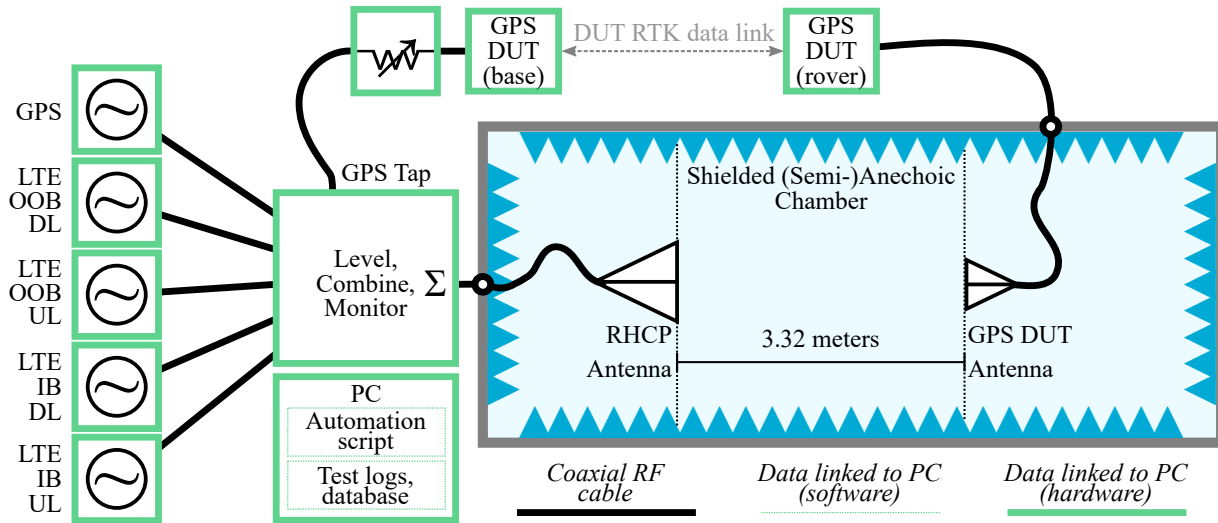


Figure 3.3: Measurement system configuration for testing an RTK device. The “level, combine, monitor” block is expanded in Figure 3.9.

outputs. The key performance characteristic that could impact users of these receivers is 1 PPS output relative to an 1 PPS that of coordinated universal time (UTC) as forwarded through GPS time.

The time reference in these laboratory-based tests was a cesium (Cs) clock taking the place of UTC for the GPS simulator. The most relevant and measurable choice of “correct” reference time for DUT timing accuracy assessment was therefore the 1 PPS signal generated by the Cs clock. The test configuration (Figure 3.4) included a time interval counter (TIC) to compare the DUT 1 PPS output against the 1 PPS output of the Cs clock.

The output of the TIC was the difference between the “correct” reference 1 PPS and GPSDO 1 PPS. We took this difference as the timing error. The timing error includes some fixed delays (propagation, electronics, processing inside the DUT, etc.). The mean value of these delays encapsulates a fixed timing offset delay, which includes the time output stability of the TIC, UTC output by the GPS simulator, Cs clock drift, DUT clock drift, and any LTE signal impacts on the DUT. The manufacturers of these DUTs specified the timing performance in terms of a time output stability which was on the order of tens of nanoseconds.

The time difference was recorded by the testbed PC in addition to any data reported directly by the DUT. The TIC was a calibrated measurement instrument; therefore, unlike the other self-reported data recorded from DUTs in these tests, standard uncertainty estimation practices can be applied to these test results. The single-shot time resolution on standard 1 PPS signals with the TIC model specified in Table 3.1.5 was 100 ps.

As for HPP and RTK testing, the GPSDO receiver DUTs were located outside the chamber and connected to the antenna in the chamber via (shielded) coaxial cables. The 1 PPS coaxial connections

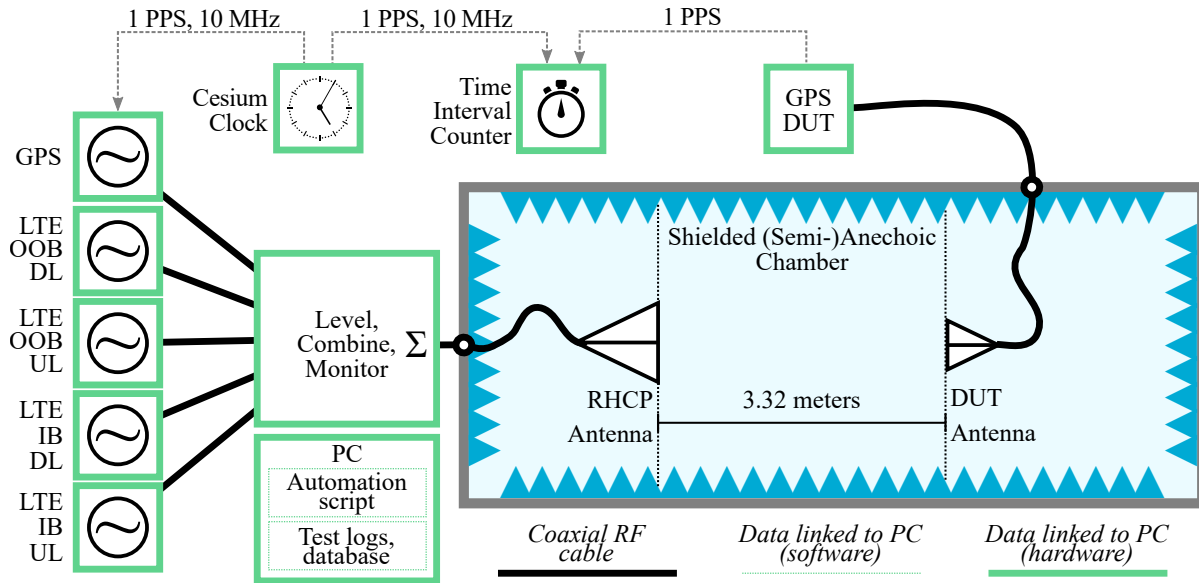


Figure 3.4: Measurement system configuration for testing GPSDO devices. The “level, combine, monitor” block is expanded in Figure 3.9.

between the DUT, the GPS simulator, the Cs clock, and the TIC and approximately length-matched (within centimeters) in order to minimize relative delays between 1 PPS signals.

The RF connection between the GPSDO DUT and its antenna was a coaxial cable with characteristic impedance and length matched to those provided by the manufacturer. Two of the tested devices used a long GPSDO test cable which is specified in Table 3.1.5. The third receiver and antenna were designed for 75  $\Omega$  Type-F connectors, so we used the manufacturer-supplied coaxial cable with Type F connectors.

### 3.1.5 Top-Level Manifest of Equipment

The list of equipment that implemented the top-level architecture blocks of this section is in Table 3.1.5. The list also includes other equipment for the calibration and validation processes in report appendices.

Table 3.1: Top-Level Equipment Manifest

Block	Description	Product <sup>1</sup>	Specification Notes
GPS	 GPS Emulator	Spirent GSS8000	× 1 L1, L2, WAAS
LTE IB DL	 Signal Generator	Rohde Schwarz SMW200A + SMW-K55	× 1 LTE FDD
LTE IB UL	 Signal Generator	Rohde Schwarz SMW200A + SMW-K55	× 1 LTE FDD
LTE OOB DL	 Signal Generator	Rohde Schwarz SMBV100A	× 1 Baseband AWG
LTE OOB UL	 Signal Generator	Rohde Schwarz SMBV100A	× 1 Baseband AWG
	 Level, Combine, and Monitor Network	Custom	× 1 Discussion in Section 3.3
	 Antenna	ETS-Lindgren 3102L	× 2 RHCP Log-Spiral
	 Programmable attenuator	Mini-Circuits RCDAT-6000-110	× 5 110 dB max in 0.25 dB steps
	 Network analyzer	Keysight N5222A + N4433A	× 1 Electronic calibration
	 Time Interval Counter	Keysight 53220A	× 1 Resolution < 500 ps
	 Spectrum Analyzer	Rhode Schwartz FSW26	× 1 LTE Analysis capability
	 Cesium Clock	Hewlett Packard HP5071A	× 1 10 MHz and 1 PPS outputs
	Temperature Logger	Pyle Digital PTHDL170	× 1
	 LTE IB DL Diplexer	K&L WSD-00661-2	× 1 Bandpass and bandstop outputs; -153 dBc PIM at 40 W input
	 Notch 1 Filter	K&L 3TNF-1000/2000-N/N	× 1 Variable, 1000-2000 MHz

Table 3.1: Top-Level Equipment Manifest

Block	Description	Product <sup>1</sup>	Specification Notes
	 Notch 2 Filter	Fairview Microwave SBRF-1000-2000-01-N	× 1 Variable, 1000-2000 MHz
	 Low-PIM Attenuator	Microlab FZ-A10	× 1 -153 dBc PIM at 40 W 110 W max
Coaxial Cable	DUT Antenna→Receiver	<i>HPP and RTK Devices</i> 50 Ω TNC to TNC	Loss 3.12 dB ±0.1 dB, 1575.42 MHz
		<i>GPSDO Devices:</i> 50 Ω TNC to TNC	Loss 5.27 dB ±0.1 dB, 1575.42 MHz
LTE UL OOB 	Amplifier	Mini-Circuits ZHL-4W-422+	× 1 4 W peak out

<sup>1</sup>Certain commercial equipment, instruments, or materials are identified in this report in order to specify the experimental procedures adequately. Such identification is not intended to imply recommendation or endorsement by National Institute of Standards and Technology (NIST) nor is it intended to imply that the materials or equipment identified are necessarily the best available for the purpose.



(a) Longmont, CO test site



(b) Boulder, CO test site

Figure 3.5: Photographs of rackmounted instrumentation and test circuits.

The testbed instrumentation is pictured in each facility in Figure 3.5. The level, equalize, and combine circuit is shown in the lower right, in both cases. The GPS simulator is off frame (behind the testbed shown) in Figure 3.5(a).

## 3.2 Radiated Test Setup

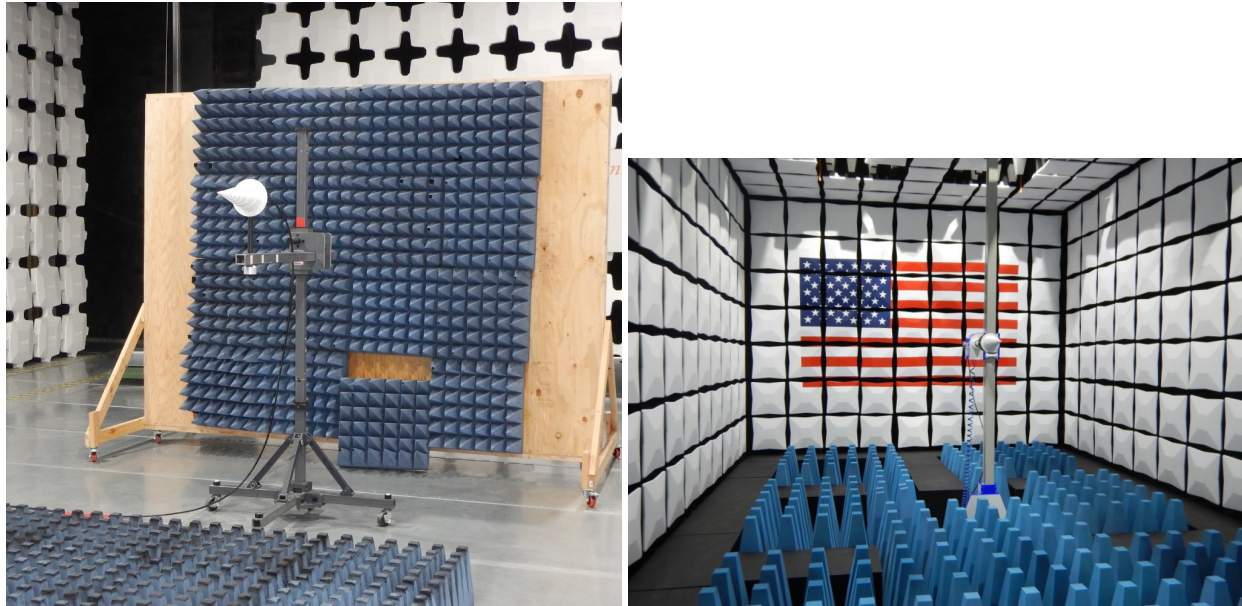
The shielded RF anechoic and semi-anechoic test chambers provided important base capabilities to the testbed:

1. propagation between the transmit antenna and the DUT approximates that of free space,
2. shielding the test from outside noise and interference, and
3. approximating a noise environment defined as thermal noise at room temperature.

### 3.2.1 Test Chambers

Testing was performed at two test facilities. The first test site was a semi-anechoic test chamber in Longmont, CO, operated by NTS. The second was a fully-anechoic chamber at NIST's NBIT facility in Boulder, CO. Both chambers were shielded. Radiated tests are pictured for each of these facilities in Figure 3.6.

The semi-anechoic test environment had less wall absorber coverage compared to the fully-anechoic chamber.



(a) Semi-anechoic chamber at the NTS test facility in Longmont, CO.

(b) Anechoic chamber at the NBIT facility at NIST in Boulder, CO.

Figure 3.6: Test chambers used in radiated testing for this report.

### 3.2.2 Chamber Layout

A side view of the test layout in each chamber is illustrated by Figure 3.7. The nominal intended separation distance at the beginning of the test campaign was approximately 3 m. The separation distance between the DUT and the transmit antenna was  $3.32 \text{ m} \pm 0.08 \text{ m}$ . The discrepancy in the center position was caused by 1) the wide range of DUT mounting adapters required to support the variety of DUT packages, and 2) the location of the amplitude center of the transmit antenna was not known exactly. The  $\pm 0.08 \text{ m}$  uncertainty increased the uncertainty in the effective isotropic incident power (EIIP) at the DUT.

The location and orientation of the cables, transmit antenna, and DUT were the same in both the semi-anechoic and fully-anechoic test facilities (to within the uncertainties given by Subsection 3.5.5). Particular emphasis was placed on maintaining the same separation distance between the testbed transmit antenna and the DUT.

In both test environments, cables ran underneath shielded hatches in the chamber floor to avoid disturbing the test area. We checked the radiated noise characteristics of the electronics in the test area with a spectrum analyzer, but no detectable EMI was detected above 800 MHz.

### 3.2.3 Single-Antenna Transmission

The tests in this report excite GPS and LTE at the DUT by means of a single transmit antenna. It received as its input the conducted sum of both LTE and GPS. The LTE and GPS signals were

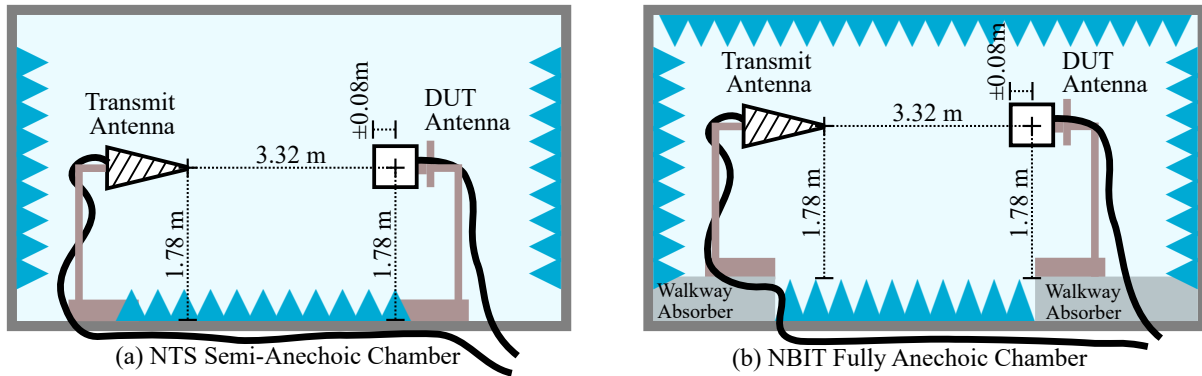


Figure 3.7: Side view of chamber layout in the NTS and NBIT facilities. The reference position of the transmit antenna corresponds with that of its gain calibration; exact positioning of the DUT varied slightly between units, but we estimate the indicated box bounds a center point with edges  $\pm 0.08$  m.

input to the antenna from the conducted level, combine, and monitor network (Section 3.3).

Previous test efforts [2–4] transmitted separately from two antennas, one for GPS, and the other for LTE. Some motivations for this type of setup could include:

1. selection of antennas that corresponds to deployment-like polarizations of RHCP radiated GPS and linear polarized LTE signals,
2. isolation between transmitting antennas may be improved compared to a single antenna with circuit-combined GPS and LTE waveforms.

A key disadvantage of this approach would be caused by the geometric arrangement of GPS and LTE antennas, which has led to incident radiation from different angles, as in Figure 3.8. Moreover, as most DUT antenna patterns are not well reported, a blind test would result in a large uncertainty in the reported signal-to-interference ratio introduced to the DUT receiver. Proper testing would require extensive investigation on DUT antenna patterns which would prove to be impractical for most test campaigns.

Use of a single transmit antenna rather than two ensured precise control over the relative levels of GPS and LTE conducted into the DUT electronics. This advantage led to several practical benefits:

- the test geometry enforces the same definition orientation upon both GPS and LTE (Figure 3.8), simplifying interpretation and application of the test results;
- a relatively compact test zone became suitable for testing without concerns over trade-offs between LTE-to-GPS isolation vs. similar illumination angles from both LTE and GPS;
- antenna characterization was only necessary for one antenna; and
- the relative strength of GPS and LTE (in other words, the signal-to-interference ratio) con-

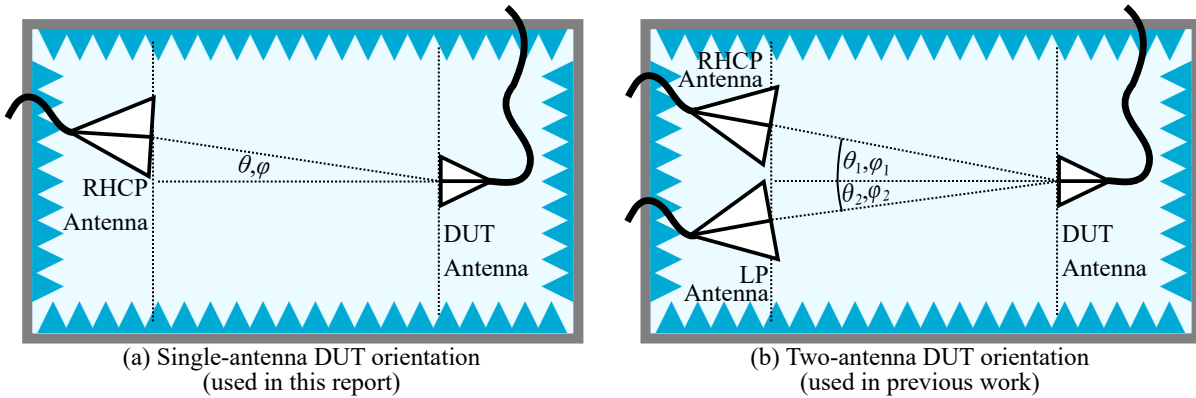


Figure 3.8: Use of the single-antenna test configuration (a) reduces the number of orientation variables in the test configuration applied to the DUT compared to the two-antenna setup (b) used in previous tests such as [2–4].

ducted into the DUT receiver was determined by the transmission system, not the DUT antenna.

A more detailed discussion of the reduction in the number of test variables is provided in Section A.2.

### 3.2.3.1 LTE Polarization Correction

Test methods and results involving LTE interference power were still defined in terms of incident *linear* polarization for this study. Conversion from the RHCP measurement to the equivalent linearly-polarized LTE response was achieved by adding 3 dB. Test results reported in this study were therefore referenced to linear polarization, making the LTE power levels at the plane of the DUT comparable to those of other test efforts.

### 3.2.3.2 Signal Coupling Considerations

Concerns about isolation between the GPS and high-power LTE IB paths were received in feedback from stakeholders. The isolation was addressed through testbed design and validation testing in Subsection 3.6.3 and Section D.2. No isolation problems between these paths were expected based on the design, nor were any discovered after extensive testing.

## 3.3 Measurement Transmitter Design

### 3.3.1 Level, Combine, and Monitor Network

The “level, combine and monitor” block of Section 3.1 took one GPS input (from the GPS simulator) and four LTE signal inputs (from the LTE signal generators). This test network, detailed by Figure 3.9, performed the following functions:

1. amplifies the input signals,
2. enables level control by PC-controlled attenuators for each signal input,
3. combines the amplified and leveled input signals,
4. monitors and measures testbed output signals via coupled output to spectrum analyzer, and
5. provides GPS “tap” output for RTK base units.

The power levels specified in Chapter 2 drove the need for these capabilities.

### **3.3.2 Design Priorities**

The following design priorities were adopted in order to achieve these goals:

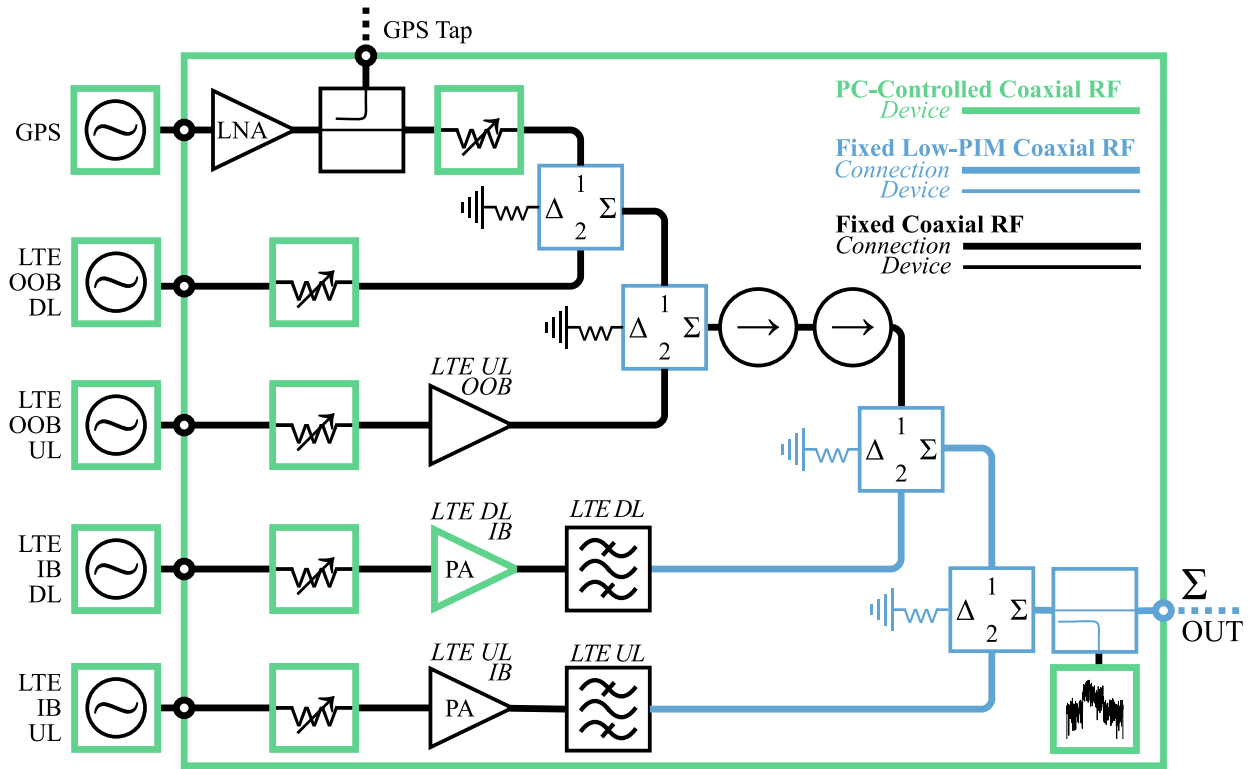
1. operating within safe power handling limits of available parts,
2. isolating amplifiers and signal generators from signals that originate in other signal chains,
3. minimizing passive intermodulation (PIM) along signal paths that carry high-power LTE, and
4. maximizing test system power output.

### **3.3.3 Coupled GPS “Tap” Output**

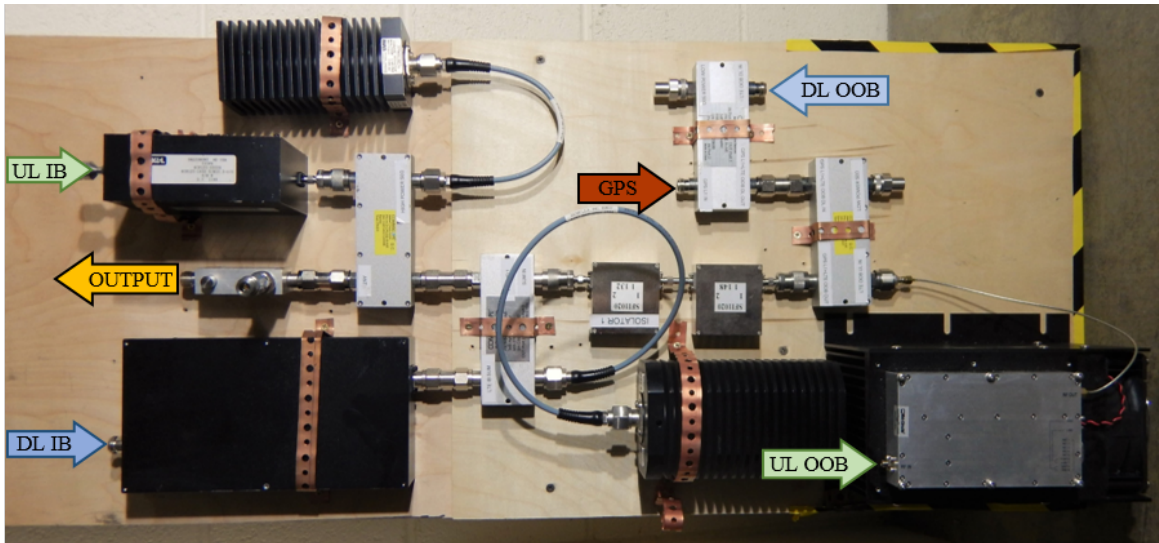
The GPS tap output was connected only in the RTK testbed configuration. The GPS tap coupler remained in the test setup during tests of other device classes; the coupled GPS output was simply terminated with a matched 100 dB attenuator. This convenience avoids additional calibration effort when reconfiguring the measurement system between DUT classes. The termination is omitted from non-RTK configuration schematics for clarity.

### **3.3.4 Manifest of Instrumentation and Test Parts**

Table 3.2 lists the principal functional components needed for the measurement transmitter. Many incidental small and non-electrical parts like mounting hardware, adapters, power supplies and data cables are not included.



(a) Block diagram schematic



(b) Implemented combine circuits at the output of leveling and amplification stages (off-frame).

Figure 3.9: The level, combine, and monitor network amplifies and combines GPS and LTE signals, and monitors leveling across all GPS and LTE bands. It is common to all test configurations in this report.

Table 3.2: Measurement Transmitter Components

Block	Description	Product <sup>1</sup>	Specification Notes
LTE UL IB 	Amplifier	Varian TWTA VZL6941K1	× 1 20 W peak out
LTE DL 	Amplifier	<i>High Power Setup:</i> EMPOWER 2170-00	× 1 1000 W peak out
		<i>Medium Power Setup:</i> Mini-Circuits ZHL-4W-422+	× 1 4 W peak out
LTE UL OOB 	Amplifier	Mini-Circuits ZHL-4W-422+	× 1 4 W peak out
	 Programmable Attenuator	Mini-Circuits RCDAT-6000-110	× 5 110 dB max in 0.25 dB steps
	 Hybrid Coupler	CommScope H-3-CPUSE-N-Ai6	× 4 Max 200 W average power -160 dBc PIM at 40 W
	 Isolator	Fairview SFI1020	× 2 Isolation > 19 dB
LTE DL 	Bandpass Cavity Filter	RF Morecomm RMC1531B10M01	× 1 1526 - 1536 MHz
LTE UL 	Bandpass Cavity Filter	<i>UL1 Setup:</i> K&L 4CP120-1632.7/E10.3	× 1 1627.7 - 1637.7 MHz
		<i>UL2 setup:</i> K&L 4CP120-1651.7/E10.3	× 1 1646.7 - 1656.7 MHz
	 Directional Coupler	E-Meca LP715-30-1.650W	× 2 Coupling 30 dB PIM -155 dBc at 40 W in
	 Calibrated Power Sensor	Keysight	× 1 Specified sensitivity -70 dBm

<sup>1</sup>Certain commercial equipment, instruments, or materials are identified in this report in order to specify the experimental procedures adequately. Such identification is not intended to imply recommendation or endorsement by NIST nor is it intended to imply that the materials or equipment identified are necessarily the best available for the purpose.

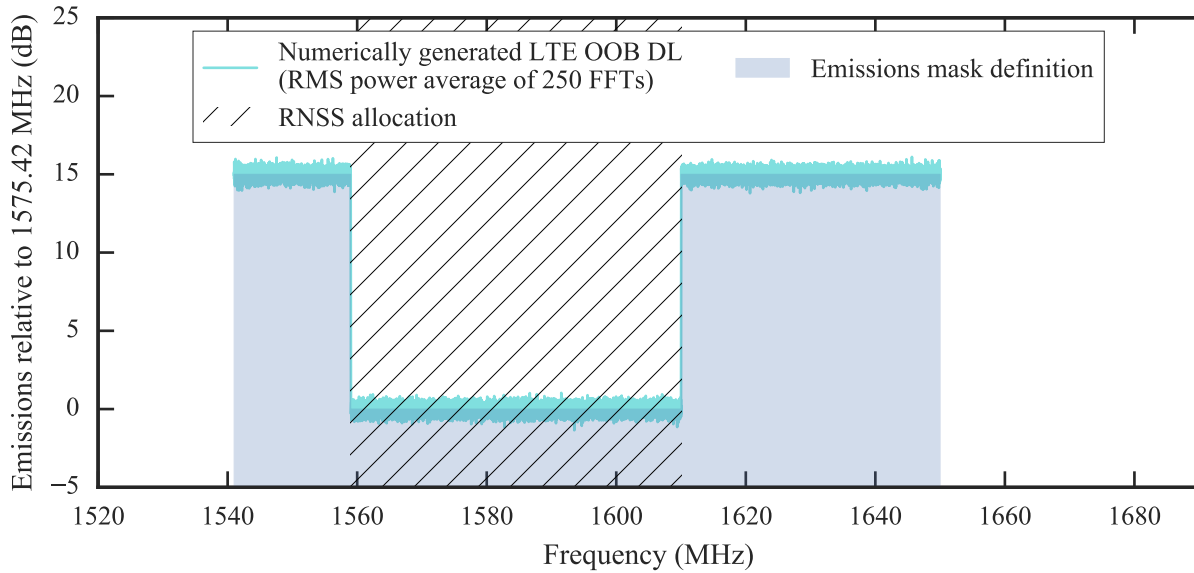


Figure 3.10: Custom AWG waveform designed to emulate LTE OOB DL signals by shaping circular AWGN in the frequency domain.

### 3.4 Waveform Synthesis

#### 3.4.1 LTE OOB DL

Figure 3.10 shows the LTE OOB DL noise power spectral density of the LTE IB DL signal AWG file generated to match that of Figure 2.4. The signal generation procedure began with 100 ms of complex-valued circular AWGN. Its spectral contour was achieved by scaling the waveform in the frequency domain by fast Fourier transform (FFT). The script exported the resulting waveform into a file composed of 16-bit binary in-phase and quadrature (IQ) values uploaded to the signal generator over USB.

#### 3.4.2 LTE OOB UL

The synthesis procedure for the LTE OOB UL waveform was very similar to the procedure outlined for the LTE OOB DL waveform. The power spectral density (PSD) shown in Figure 3.11 followed the emissions mask in Figure 2.4. The resulting spectrum is shown in Figure 3.11.

The LTE OOB UL waveform required substantial dynamic range: the PSD of the peak near 1625 MHz is defined 70 dB above the PSD component inside the radio navigation satellite services (RNSS) band. This presented a challenge for the signal generator, which produced a continuous-wave (CW) peak near -40 dBc at the center (LO) frequency (an undesired DC offset in the baseband signal). To mitigate this problem, the baseband signal was offset to 1620 MHz, where the direct current (DC) offset tone was negligible in comparison to the peak PSD.

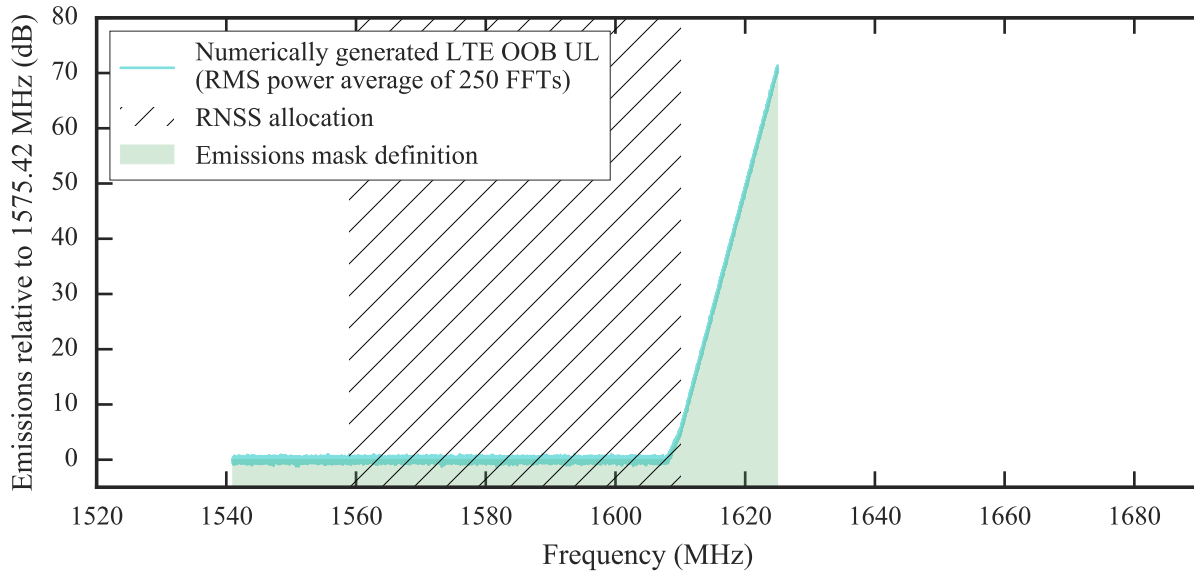


Figure 3.11: Custom AWG waveform designed to emulate LTE OOB UL signals by shaping circular AWGN in the frequency domain.

### 3.5 Calibration and Leveling

The test team developed a nine-step calibration plan. The methods involved are listed in Table 3.3. Detailed procedures and calibration data are in Appendix C.

#### 3.5.1 Conducted GPS

Automated control over the GPS signal levels from the PC was less flexible. Therefore, the GPS signal level was calibrated by determining a calibrated nominal attenuation value of the GPS attenuator. The procedure for determining this value was outlined in the next section, because achieving calibrated levels at the DUT requires calibrated radiation losses.

The levels were calibrated to a power standard traceable to a national metrology institute by means of a power sensor at the conducted output of the testbed. Measurement of GPS power output with the GPS attenuator set to 0 dB (minimum attenuation/maximum transmission) were then taken as the reference output level.

#### 3.5.2 Conducted LTE

The LTE calibrations were implemented on the instruments by saving the instrument state to a file containing the calibrated output power level. Safe amplifier signal level limits were limited further by adding fixed attenuators to the signal generator outputs, preventing damage to amplifiers even at the maximum signal generator output level.

Table 3.3: List of Calibrations Performed to Establish Conducted Signal Levels

Step	Calibration Type	Signal	Appendix
1	Amplifier signal level limit	LTE IB DL	C.2.1.1
2	Amplifier signal level limit	LTE IB UL	C.2.1.2
3	Amplifier signal level limit	LTE OOB UL	C.2.1.3
4	Conducted testbed output level	GPS	C.2.2.1
5	Conducted testbed output level	LTE IB DL, LTE IB UL, and LTE OOB UL	C.2.2.2
6	Relative OOBE level	LTE OOB DL	C.2.3.1
7	Relative OOBE level	LTE OOB UL	C.2.3.2
8	Radiated correction to the plane of the DUT	LTE OOB UL	C.2.4.1
9	Nominal GPS output level	LTE OOB DL	C.2.4.2

Table 3.4: Correction from Conducted Power Output by the Testbed to Power at the Plane of the DUT (EIIP). Values Use The Measured Separation Distance 3.32 m.

Signal	Reference Polarization	Correction from Conducted Power to “Plane of DUT”
GPS	RHCP	-43.2 dB
LTE DL	LP	-39.9 dB
LTE uplink band 1 (low) (UL1)	LP	-40.5 dB
LTE uplink band 2 (high) (UL2)	LP	-40.6 dB

The total power of each of the LTE outputs (except the weak LTE OOB DL) was measured during tests with the “band power” feature of the calibrated spectrum analyzer. The lower and upper frequency bounds of each band were set to match Figure 2.4. The spectrum analyzer levels were calibrated against a power sensor at the testbed output, excited with a 1575.42 MHz CW tone.

The calibration of each out-of-band emission (OOBE) path sets its level to produce the correct *relative* emissions mask relative to the corresponding IB path. During normal test operation, the attenuation level settings for IB and OOB attenuators should then be kept equal to each other in order to maintain the relative levels in Figure 2.4 (for example: LTE IB DL attenuation = LTE OOB DL attenuation). The calibration data in Subsection C.4.6 shows the deviation from ideal for each variable attenuator swept with attenuation setting.

### 3.5.3 Radiated Losses

Table 3.4 lists the correction factors used to convert conducted testbed output to EIIP. The computation of these correction factors is detailed in Subsubsection C.2.4.1. The EIIP of each LTE signal was computed at the plane of the DUT by adding the conducted power output of the testbed to the correction listed in the table.

### 3.5.4 Radiated GPS

The nominal (calibrated) GPS attenuation level was calculated from 1) the calibrated reference GPS output power, 2) the correction to GPS EIIP in Table 3.4, and 3) the desired  $-128.5 \text{ dBm} \pm 2.4 \text{ dB}$  EIIP at the plane DUT. The detailed calibration process is in Subsubsection C.2.4.2.

### 3.5.5 Power Level Uncertainty

The key parameters output by the measurement system were the power levels of the GPS and LTE signals to which the DUTs were exposed. However, the power levels themselves have little value without an accompanying statement regarding the uncertainties associated with those levels. As stated in the NIST Guidelines for Evaluating and Expressing the Uncertainty of NIST Measurement Results [6],

“Results of measurements and conclusions derived from them constitute much of the technical information produced by NIST. It is generally agreed that the usefulness of measurement results, and thus much of the information that we provide as an institution, is to a large extent determined by the quality of the statements of uncertainty that accompany them. For example, only if quantitative and thoroughly documented statements of uncertainty accompany the results of NIST calibrations can the users of our calibration services establish their level of traceability to the U.S. standards of measurement maintained at NIST.”

Stated results indicate our best estimate of the parameter of interest (referred to as a “measurand”). The uncertainties are given as a “standard uncertainty” that can be interpreted as a standard deviation (assuming a normal distribution) about the estimate. Our estimates of uncertainty about the given power levels, as well as the uncertainties about the measurements used to determine power levels and uncertainties, are given in Appendix C.

All power-level uncertainties presented in this report are associated with the exposure system. The DUTs also added associated uncertainties relating to the reception of those power levels (e.g., gain of the DUT antenna, amplification, filtering, loss and mismatch in connecting cables, sensitivity and noise floor of the receiver circuitry, post processing). Analysis of these sources of uncertainty is important, but beyond the scope of this report, since they require additional knowledge of the construction and use of proprietary systems. We instead treated the GPS receiver systems (antenna, cables, and receiver) as a single unit, rather than one member of the entire population of every receiver model.

## 3.6 Transmitter Performance Characterization and Validation

Feedback about the test plan received from stakeholders included concerns about intermodulation distortion (IMD) and PIM. This section outlines our study of the performance of the testbed in

Table 3.5: Summary of LTE output EVM

Signal	Power relative to max.	EVM
LTE DL	-50 dB	26.3%
	-20 dB	1.7%
	0 dB	1.6%
LTE UL	-60 dB	10.9%
	-10 dB	0.8%
	0 dB	6.2%

these areas, as well as LTE modulation fidelity and output noise. The detailed test methods and results are in Appendix D.

### 3.6.1 LTE Modulation Fidelity

There is no established link between the quality of an LTE signal and the potential for coexistence with GPS, but to emulate a realistic LTE deployment, the NASCTN team made efforts to establish signals low enough to operate a cellular network. We also added cavity filters at the outputs of the amplifiers to mitigate potential out-of-band distortion components that might be caused by compression or intermodulation.

The error vector magnitude (EVM) values indicated by the signal analyzer for LTE IB DL and LTE IB UL modulation fidelity are listed in Table 3.5. The EVM is lowest in a range between output compression (at higher power levels) and the noise floor (at lower power levels).

### 3.6.2 Dynamic Range

The maximum output power level that the testbed supported for each signal is listed in Table 3.6. We fixed each OOB emissions mask output level according to the relative mask of Figure 2.4 (right vertical axis). Therefore, for any DL or UL pair, upper- or lower-bounds from either an IB or an OOB component needed to be studied as potential constraints for the usable range of testbed output power levels. The following discussions address various physical sources of these bounds, validation tests that were run, and overall impacts on transmission dynamic range.

#### 3.6.2.1 Maximum Output Power

The maximum output power level of each signal path is limited by:

- the minimum attenuation setting of the in-path variable attenuator,
- the linearity performance of its amplifier near saturation,
- the minimum acceptable output signal fidelity, characterized (for example) as EVM, and

Table 3.6: Output Power Capability of the Testbed at the Conducted Output and at the Plane of the DUT (EIP). The Quoted Uncertainties Correspond to the 97.5% Confidence Interval.

	Max Output (dBm)		
	Conducted	EIP	Constraint
<b>GPS</b>	-47.9 ±1.1 dB	-91.7 ±2.7 dB	Attenuator
<b>LTE IB DL<sup>1</sup></b>	+42.3 ±1.8 dB	+1.9 ±2.7 dB	Coupler
<b>LTE IB DL<sup>2</sup></b>	+10.1 ±1.1 dB	-30.1 ±2.4 dB	Amp. input level
<b>LTE IB UL</b>	+34.2 ±1.1 dB	-6.8 ±2.2 dB	Amplifier

	Min Output (dBm)		
	Conducted	EIP	Constraint
<b>GPS</b>	-157.9 ±1.1 dB	-201.7 ±2.4 dB	Attenuator
<b>LTE IB DL<sup>1</sup></b>	-7.6 ±1.8 dB	-48 ±2.7 dB	Amplifier
<b>LTE IB DL<sup>2</sup></b>	-37 ±1.1 dB	-78 ±2.4 dB	Amplifier
<b>LTE IB UL</b>	-34 ±1.1 dB	-75 ±2.2 dB	Amplifier

<sup>1</sup>Configuration with high power amplifier

<sup>2</sup>Configuration with medium power amplifier

- the power handling capability of downstream components.

The most limiting of these factors is listed as the constraint for each signal path.

### 3.6.2.2 Output Noise Floor

The minimum output power of a testbed signal was determined in general by a combination of

- the noise output of the signal path amplifier, and
- the maximum attenuation (minimum transmission) setting of the variable attenuator.

The signal levels of several paths were controlled by variable attenuators that are upstream of amplifiers. This topology helped to prevent attenuator damage and mitigated signal linearity problems at compression levels. Noise output by these paths was therefore determined by the gain and noise figure of the amplifier (and losses from the amplifier output to the testbed output) and could not be controlled by the attenuator. At very high attenuation settings, the output of these paths was dominated by amplifier output noise.

This type of noise output risks corrupting the emulated output spectral masks. Each path was therefore checked for output noise above the intended mask level. We approached the problem by spectrum measurements to quantify path noise, translated the conducted measurements to radiated levels in order to estimate impacts on idealized DUTs, and checked DUT carrier-to-noise-density ratio ( $C/N_0$ ) response during pre-test checks.

Table 3.7: Summary of Noise Impacts on an Idealized Reference DUT at 3.32 m Test Distance

	Test Band Center MHz	Noise at Idealized DUT		
		Reference Noise Floor <sup>1</sup> dBW/MHz	Noise Density EIRP PSD <sup>2</sup> dBW/MHz	Reference Noise Floor Degradation <sup>1,2</sup> dB
GPS	1575.42	-144	max. -171.5	max. 0.01
LTE IB DL <sup>3</sup>	1531	-144	-93.3	50.7
LTE IB UL1	1632.5	-144	-120.3	23.8
LTE IB UL2	1651.5	-144	-120.3	23.7
LTE OOB DL	1575.42	-144	max. -171.5	max. 0.01
LTE OOB UL	1575.42	-144	-164.0	0.04

<sup>1</sup>Reference antenna noise temperature 298 K with noiseless reference receiver

<sup>2</sup>Noise PSD received by an unfiltered matched isotropic reference antenna

<sup>3</sup>Using the high-power LTE IB DL amplifier.

### 3.6.2.3 Conducted and Radiated Levels

Tests for the conducted noise output of the testbed are detailed in Section D.4. We conclude that the most powerful sources of output noise were the LTE IB DL and LTE IB UL power amplifiers.

In order to estimate the degree of impact these levels might have on a DUT, we needed to consider the noise at the plane of the DUT itself. Because the noise inside the receiver was not directly known (reported  $C/N_0$  was not a calibrated physical quantity in this test process, nor in previous tests for interactions between LTE and GPS), we began by translating the conducted levels to the plane of the DUT according to Subsection C.2.4. The response of an idealized reference DUT to this level of radiated noise is listed in Table 3.7.

The impact of radiated noise was only an estimate, intended to gauge risks of DUT response to the transmitted noise levels. The noise floor degradation estimate on the far right column applies to a hypothetical DUT with no OOB filtering, an isotropic antenna response, and an ideal receiver that adds no noise.

The noise floor degradation of an actual DUT could be estimated relative to the hypothetical values above by accounting for realistic antenna gain (and pattern), higher noise figure (perhaps near 2 dB instead of 0 dB), and realistic OOB filter rejection.

### 3.6.2.4 Noise Output Mitigation

The reference noise floor degradation checks showed that some mitigation was necessary to ensure LTE IB signaling noise was acceptable for test purposes.

1. The high-power LTE IB DL amplifier was disabled during UL signal tests, removing all detectable noise. The testbed automation software included amplifier enable/disable control to support this.
2. Test team members checked  $C/N_0$  reported by DUTs with amplifiers on and off (and LTE input attenuators set to minimum transmission) as a pretest check. The DUT was required to indicate no detectable change in the noise floor within the reporting resolution of National Marine Electronics Association (NMEA) output strings.
3. If a DUT failed the LTE IB DL noise check (previous item), a medium power amplifier was substituted for the high-power amplifier (the same model as the LTE OOB UL path, producing negligible noise impact even for the idealized high-sensitivity receiver in Table 3.7). An appropriate alternative LTE OOB DL calibration was applied according to procedures in Subsection C.2.3.

### 3.6.3 Signal Path Isolation

The testbed was designed to isolate high power LTE IB DL or LTE IB UL signals from lower-power LTE OOB or GPS paths. The design included aggressive use of isolators, high-isolation hybrid couplers, cavity filters in high-power paths, and added path attenuation by means of the attenuator (for GPS only).

Validation for isolation (or inversely, coupling) is discussed in detail in Section D.2. The potential impact of coupling was greatest for active devices like signal generators or amplifiers, so the test points were the active device outputs of each signal path. At each test point, the spectrum analyzer detected 1) the forward power of the intended output of the signal path, and 2) reverse power that coupled from all other signal paths.

The isolation between two paths was computed as:

$$\begin{aligned} \text{Isolation (in dB)} = & \text{Forward power at the coupling source test point (dBm)} \\ & - \text{Reverse coupled power at victim test point (dBm)}. \end{aligned} \quad (3.1)$$

The smallest possible isolation through the passive output paths would be 0 dB, if all power from the coupling source were received as reverse power at the victim test point. Larger values indicate more protection of the victim path from the coupling source.

Measured isolation values between paths in the testbed are listed in Table 3.8. The isolation figure between the high-power LTE IB DL and GPS were greater than 130 dB, supporting the idea that the single-antenna transmit system did not introduce problems via coupling.

Symptoms of insufficient isolation can include IMD or even errors in the output level of paths that are victims of coupling (if adaptive leveling control loop is involved). These risks can be by ensuring that the forward power in a given path is greater than the (undesired) reverse power

Table 3.8: Isolation: Forward Power Available From a Coupling Source Relative to Reverse Coupled Power Absorbed in a Victim Test Point

Victim Path	Coupling Source				GPS	
	LTE IB DL	LTE IB UL1	LTE OOB UL	LTE OOB DL		
<b>LTE IB DL</b>	—	—	—	—	—	dB ±2.9 dB
<b>LTE IB UL1</b>	—	—	52.7	—	—	dB ±2.9 dB
<b>LTE OOB UL</b>	91.7	77.0	—	13.5	62.3	dB ±2.9 dB
<b>LTE OOB DL</b>	106.8	87.2	117.9	—	—	dB ±2.9 dB
<b>GPS</b>	132.7	—	70.4	—	—	dB ±2.9 dB

*Coupled signals too weak to measure are denoted by —*

Table 3.9: Coupled power ratio: Coupled Power Relative to Intended Forward Power at the Victim Test Point

Victim Path	Coupling Source				GPS	
	LTE IB DL	LTE IB UL1	LTE OOB UL	LTE OOB DL		
<b>LTE IB DL</b>	—	—	—	—	—	dB ±2.9 dB
<b>LTE IB UL1</b>	—	—	-61.3	—	—	dB ±2.9 dB
<b>LTE OOB UL</b>	-71.3	-68.4	—	-81.6	-102.3	dB ±2.9 dB
<b>LTE OOB DL</b>	-18.3	-10.5	-49.8	—	—	dB ±2.9 dB
<b>GPS</b>	-72.4	—	-30.5	—	—	dB ±2.9 dB

*Coupled signals too weak to measure are denoted by —*

coupled from another paths.

A gauge of the potential risk is the ratio of coupled power to the forward power at the test point, in decibels:

$$\begin{aligned} \text{Coupled power ratio (in dB)} = & \text{Reverse coupled power at victim test point (dBm)} \\ & - \text{Forward power at the victim test point (dBm)} \end{aligned} \quad (3.2)$$

This ratio is less than 0 dB if the coupled power level is smaller than the victim’s forward power level. This is a loose guideline for a “safe” reverse coupled power level.

The coupled power ratio for each combination of coupling paths is listed in Table 3.9. The most concerning case by this measure was LTE IB UL1 coupling into LTE OOB DL, but this coupled level is still smaller than -10 dB (10 dB below the desired forward power). This test point was directly at the signal generator output; the error induced on the forward power if the adaptive leveling loop absorbs this power was approximately 0.4 dB. The largest coupling ratio for any other signal path was -30.5 dB, too small to motivate further validation work.

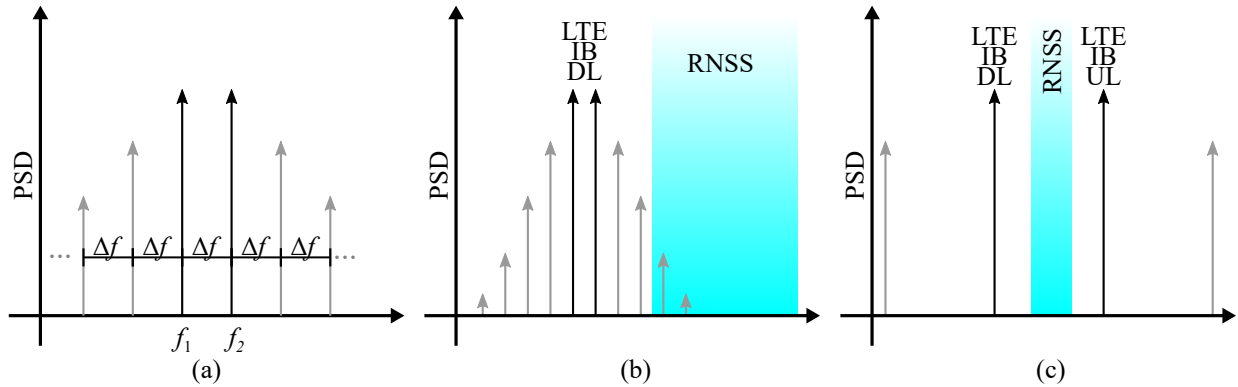


Figure 3.12: Intermodulation products of simple two-tone input signals illustrated (a) in general, (b) at the band edges of LTE IB DL, and (c) at each of LTE IB DL and UL1.

### 3.6.4 LTE Filtering and Spectral Regrowth

Any nonlinear character of a system block causes spectral regrowth: input signals producing signal components at new frequencies. Signals created at these new frequencies are IMD products that risk corrupting the testbed output spectrum. This section is a brief overview of the characterization test efforts detailed in Appendix D.

#### 3.6.4.1 Review of Spectral Regrowth

Active system blocks, like amplifiers, receivers, and signal generators, are known for adding IMD. Passive system blocks (like filters, cables, connectors, and antennas) exhibit a weaker form of IMD known as PIM at junctions between dissimilar or oxidized metals. The impacts of PIM are dramatically (many tens of decibels) weaker compared to those of an active device.

An illustration of the intermodulation phenomenon for a few scenarios is shown in Figure 3.12 for a simple two-tone input signal. The input tone frequencies  $f_1$  and  $f_2$  produce IMD products on either side at same spacing as the input signals,  $\Delta f = f_2 - f_1$  as in Figure 3.12a.

Intermodulation is a problem in this test application if it results in a failure to confine high-power LTE IB signals within the emissions masks in Figure 2.4. For example, the LTE IB paths needs very small OOB output to ensure they are smaller than those of the corresponding LTE OOB paths. Figure 3.12b illustrates this with simple two-tone inputs. Emulating the DL mask requires that the OOB spectral density at 1541 MHz is 107 dB lower than 1531 MHz. Even a filter that effectively eliminates IMD may introduce new PIM products above the prescribed levels.

#### 3.6.4.2 Out-of-Band Outputs of the LTE IB DL Signal Path

Section D.5 details the tests we performed to characterize of intermodulation effects in the testbed output.

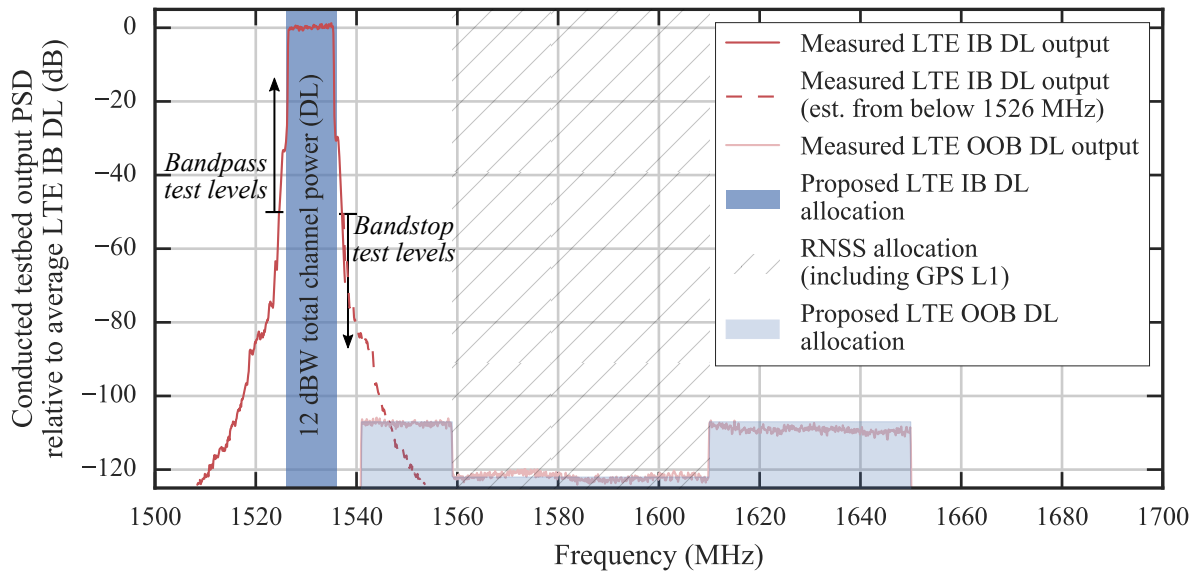


Figure 3.13: High dynamic range measurements of LTE IB DL and LTE DL OOB conducted output signals performed with the downlink test diplexer. Output PSD standard uncertainty varies with relative level:  $\pm 0.5$  dB at 0 dB relative level, and  $\pm 3.1$  dB below -70 dB relative level.

Our use of a measurement diplexer designed for PIM testing extended the dynamic range of the spectrum measurements of LTE IB DL past 120 dB. The measurement result was the power spectral density of the actual LTE IB DL testbed conducted output (Figure 3.13). The IB signal output was stronger than the OOB signal mask across the span 1541 MHz to 1549 MHz. This infraction of the desired mask should be considered when interpreting DUT response at the highest LTE IB DL power levels, though quantifying its effects would require additional testing on each DUT.

### 3.6.4.3 Out-of-Band Outputs of the LTE IB UL Signal Path

No low-PIM test diplexer was available to test uplink bands. As an alternative, we performed a simpler two-tone input test. Results are shown in Figures 3.14 and 3.15. Below the LTE IB UL measurement dynamic range, the two-tone IMD test demonstrated a continued monotonic decrease, suggesting that IMD product components stay weaker than the desired LTE OOB path outputs.

### 3.6.4.4 Intermodulation Between LTE Signal Paths

A different potential IMD impact was mentioned in stakeholder feedback on the test plan: products of different LTE IB signals. The only relevant scenario under test was that of DL+UL1, in which the LTE IB DL and UL1 signals “bookend” the GPS sources.

We studied the IMD products of this scenario (Figure 3.12c). These products for DL and UL1 inputs were centered at 1429.5 MHz and 1734 MHz at -120 dBc. These products were both very

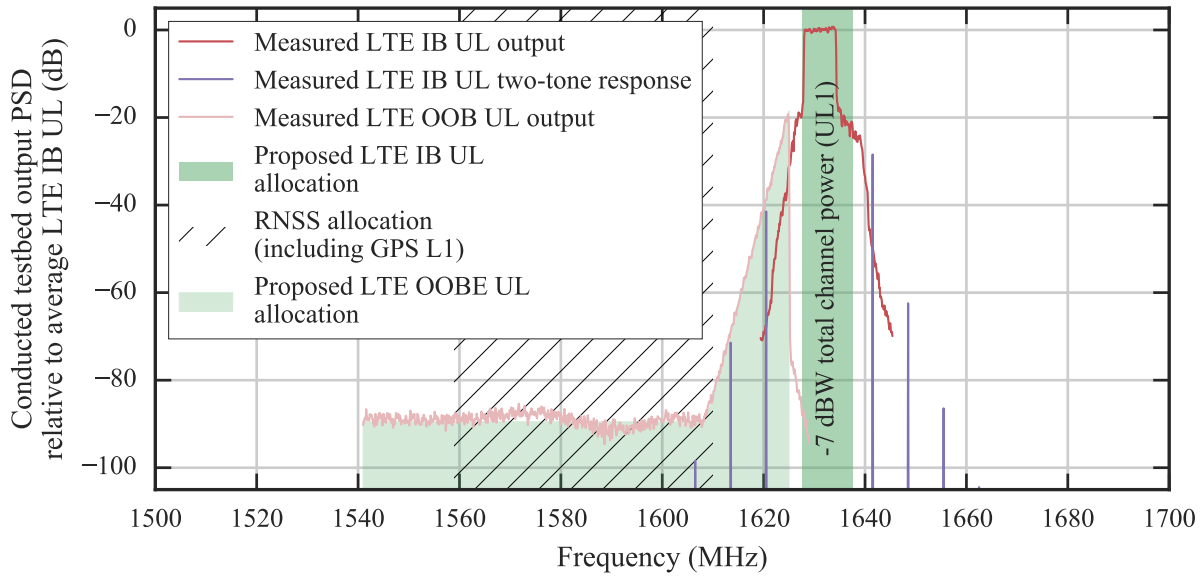


Figure 3.14: Measurements of LTE IB UL1 and LTE UL OOB conducted output spectra. Output PSD standard uncertainty varies with relative level:  $\pm 0.5$  dB at 0 dB relative level, and  $\pm 3.1$  dB at -70 dB relative level.

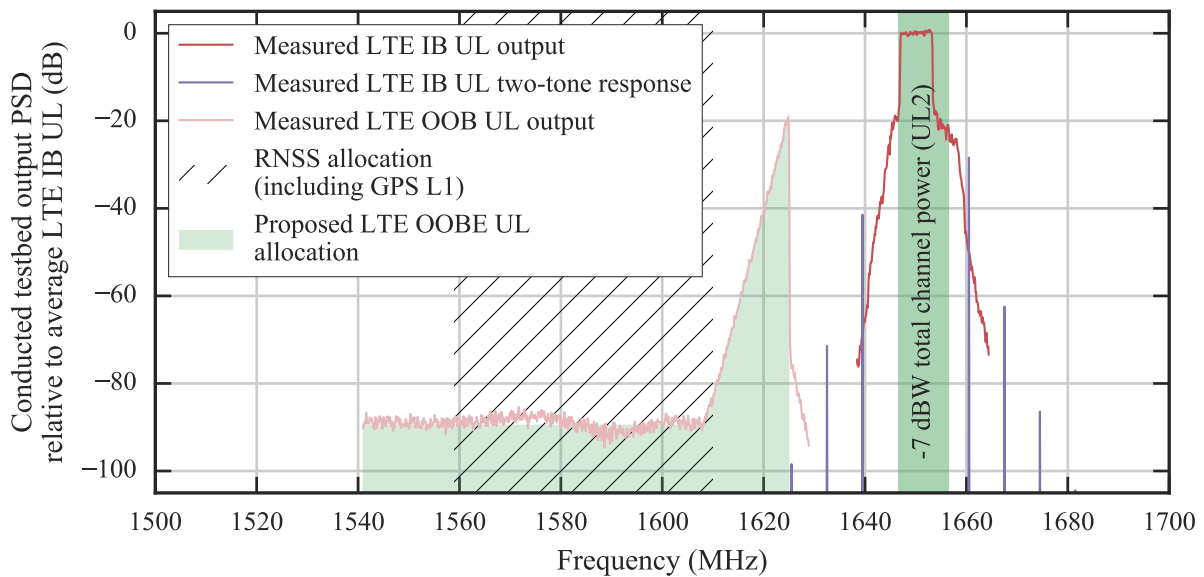


Figure 3.15: Measurements of LTE IB UL2 and LTE UL OOB conducted output spectra. In-band measurements were generated from UL1 data. Output PSD standard uncertainty varies with relative level:  $\pm 0.5$  dB at 0 dB relative level, and  $\pm 3.1$  dB at -70 dB relative level.

weak and far out of band, and therefore not of substantial concern to the test process or its results.

Some concerns may have originated from the physical potential for intermodulation between the proposed 1531 MHz band and another band near 1550 MHz. Though this combination of bands does include intermodulation products inside the RNSS, the band near 1550 MHz is no longer proposed for use in the most recent Federal Communications Commission (FCC) filings [11]. This band was therefore not included in the study and not tested for IMD interactions.

### **3.7 Summary**

The testbed provided the capability to radiate a mixture of GPS, LTE IB DL, LTE IB UL, LTE OOB UL, and LTE OOB UL signals. The power level of each signal component was controllable and EIIP at the plane of the DUT is calibrated with signal parameters applied according to Chapter 2.

The testbed underwent extensive performance validation testing. The results of these tests provided stakeholders with several key characteristics of the DUT test conditions: LTE modulation fidelity, dynamic range, signal path isolation, and measurements of the actual emissions masks output by the testbed.



## 4 GPS Receiver Test Processes

### 4.1 Automation

All test data analyzed in this report (presented Chapter 6) were collected from the global positioning system (GPS) devices via automated test scripts running on a personal computer (PC). The role of the scripted automation was to 1) collect and log data stream(s) from the GPS device under test (DUT) 2) and coordinate the measurement system with the DUT. These capabilities were linked to source code designed to ensure test parameters and processes match those in Chapter 2 and Chapter 4, respectively.

Investment of time and effort into test automation before collecting data can reduce human intervention necessary during tests. The benefits in this test campaign included:

1. Unattended tests ran for several hours or days, overnight or during weekends.
2. Test executions were made less dependent on the staff member operating the testbed.
3. Human error was minimized in repetitive tasks, such as repeated tests at different power levels.
4. Precise repetition of test conditions were made possible.

These benefits tended to become more substantial in tests that 1) required large-scale coordination between many instruments and/or 2) run for extended periods. In this campaign, test parameters and processes required control of up to 15 different test devices, and typical test runs lasting between several hours and several days. The alternative to automation here strains human focus and patience, limiting test output and risks data corruptions by test mistakes.

A few aspects of the test process were not automated. Manual tasks performed by the National Advanced Spectrum and Communications Test Network (NASCTN) technical team during testing included:

1. physically (un)mounting and (dis)connecting DUTs for test, and
2. identifying the range of long-term evolution (LTE) transmit power levels to test for each DUT.

Task 2 is not automated because it required a feedback process with parsed GPS data. Implementation would be burdensome given the wide variety of nuanced behaviors of each DUT.

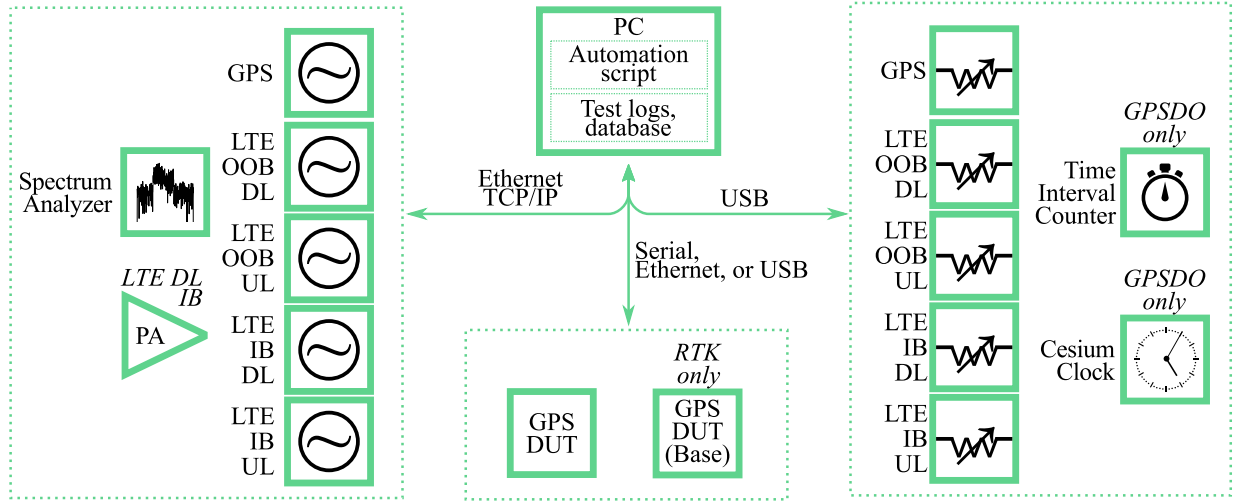


Figure 4.1: Data connections with the PC that executes test automation.

### 4.1.1 Backend

All test control was implemented in the Python programming language. The source code incorporated extensive use of object-oriented concepts for extensibility and maintainability.

The structure of the source code is illustrated by the class diagrams in Figures 4.2-4.4. The DUT and instrument drivers in Figures 4.2 and 4.4, respectively, show the structure of driver implementation, from generic base driver classes (at the top) to application-specific drivers for the DUTs and instruments used in these tests (at the bottom).

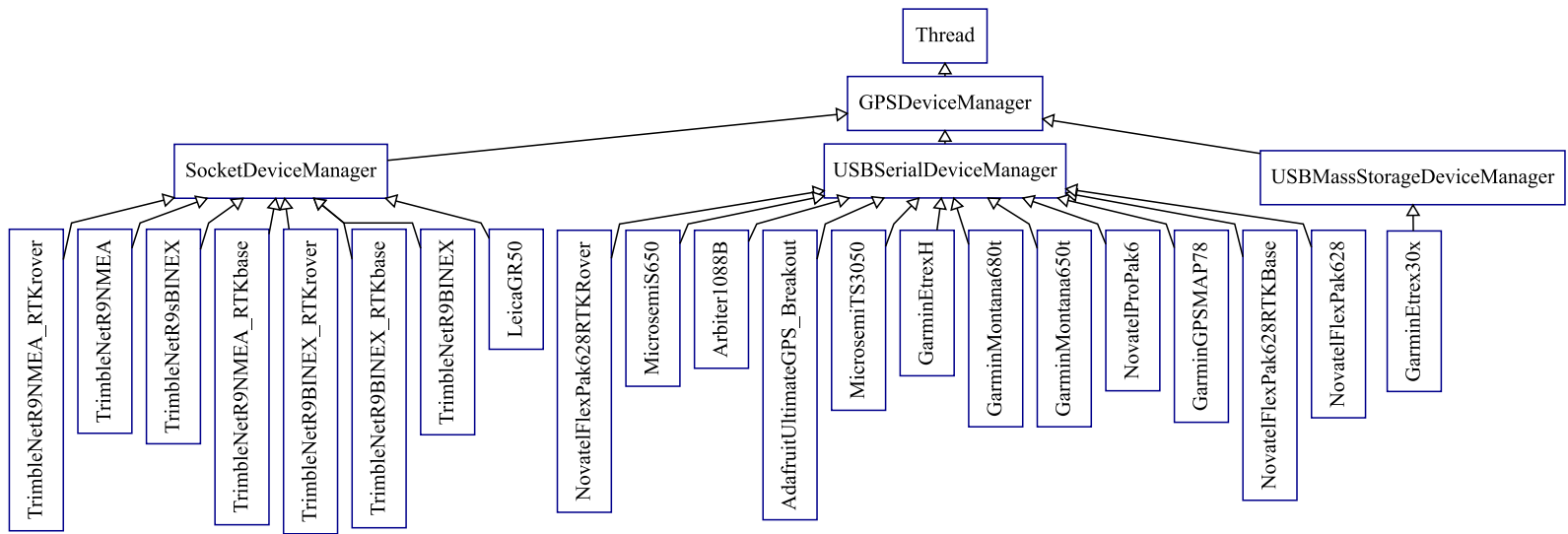


Figure 4.2: Class relationships that define the structure of DUT implementation in test automation software.

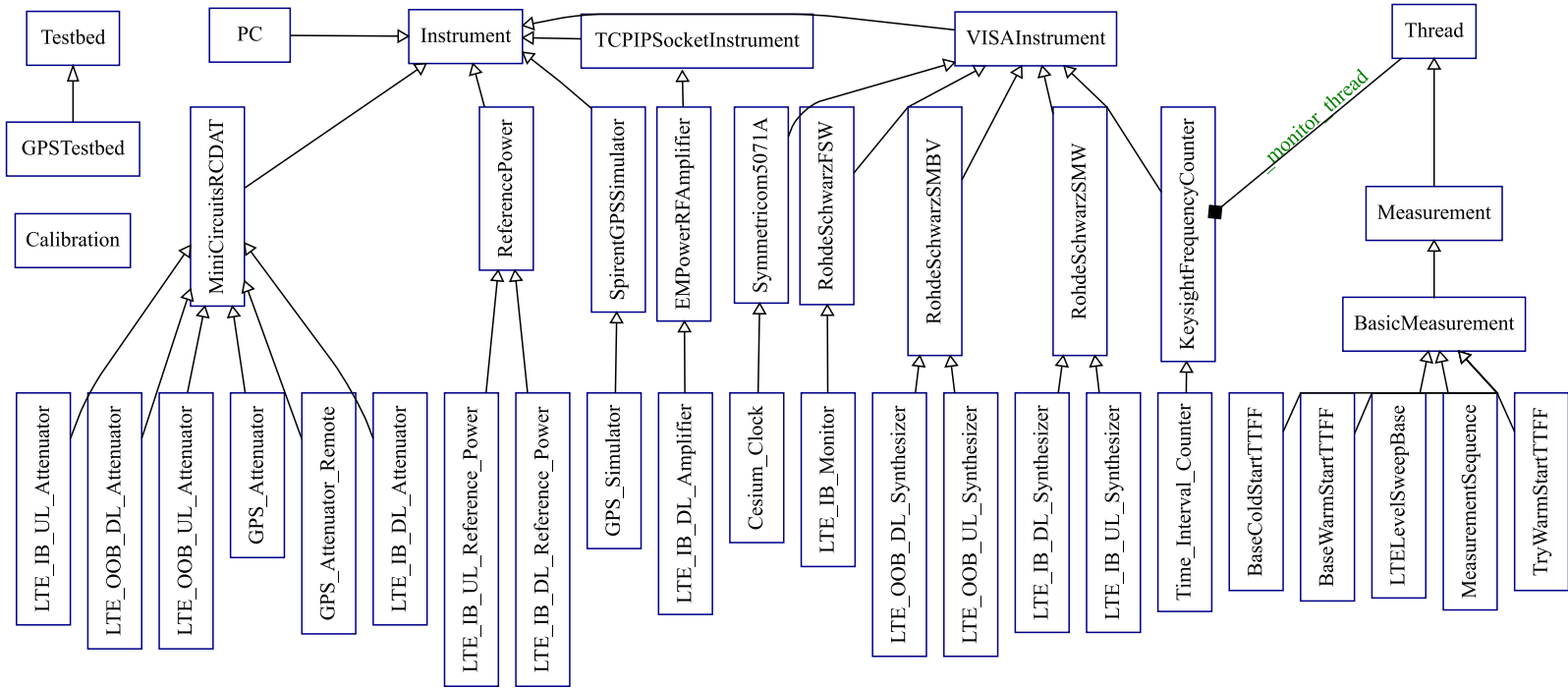


Figure 4.3: Class relationships that define the structure of instrumentation implementation in test automation software.

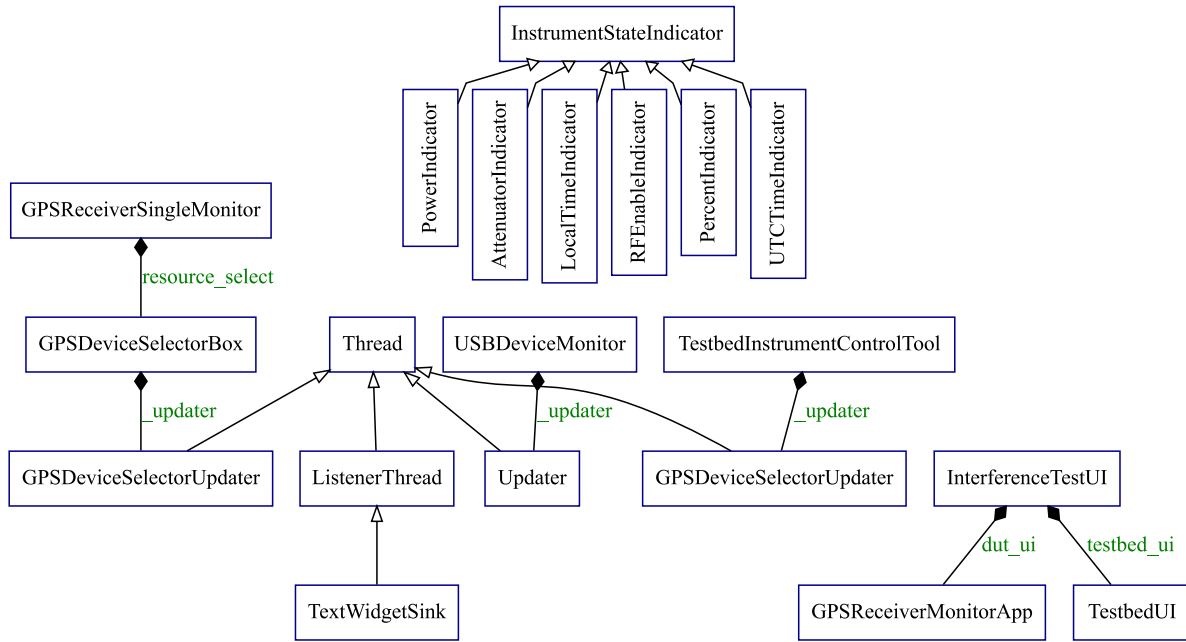


Figure 4.4: Class relationships that define the structure of UI implementation in test automation software.

Many test automation tasks required software user interface (UI) or input/output (I/O) operations through *blocking* function calls. Examples of these operations included loops that fetched DUT data with universal serial bus (USB) serial or transmission control protocol (TCP)/internet protocol (IP) socket connections, or loops that continuously retrieved time interval measurements from the time interval counter (TIC). These operations used few processor cycles, but until they completed (for example with any new DUT data) they prevented the main control script from executing other concurrent operations such as interacting with other instruments in the background, or collecting data from more than one DUT data stream simultaneously.

The solution shown in each class diagram is extensive use of threading. Each class diagram shows use of python’s built-in thread objects. The threading enabled simultaneous and independent collection of data from up to 4 DUT data streams (2 data streams per device connection in some 2-receiver real-time kinematic (RTK) systems).

#### 4.1.2 Frontend

The user interface architecture illustrated by Figure 4.4 provides a user frontend for executing tests. The user interface was accessible (on the local machine only) with a web browser. The implementation of this frontend is illustrated in Figure 4.4.

Various frontend tools gave the test operator control over relevant configuration and state settings of the test equipment, ability to start and stop data collection on one or more DUT data connections, and ability to start a sequence of one or more of the test procedures defined in Section 4.3.

The monitoring and control frontend for instruments and DUTs is shown in Figure 4.5. It allowed interactive instrument control and showed the live state during automated test sequences.

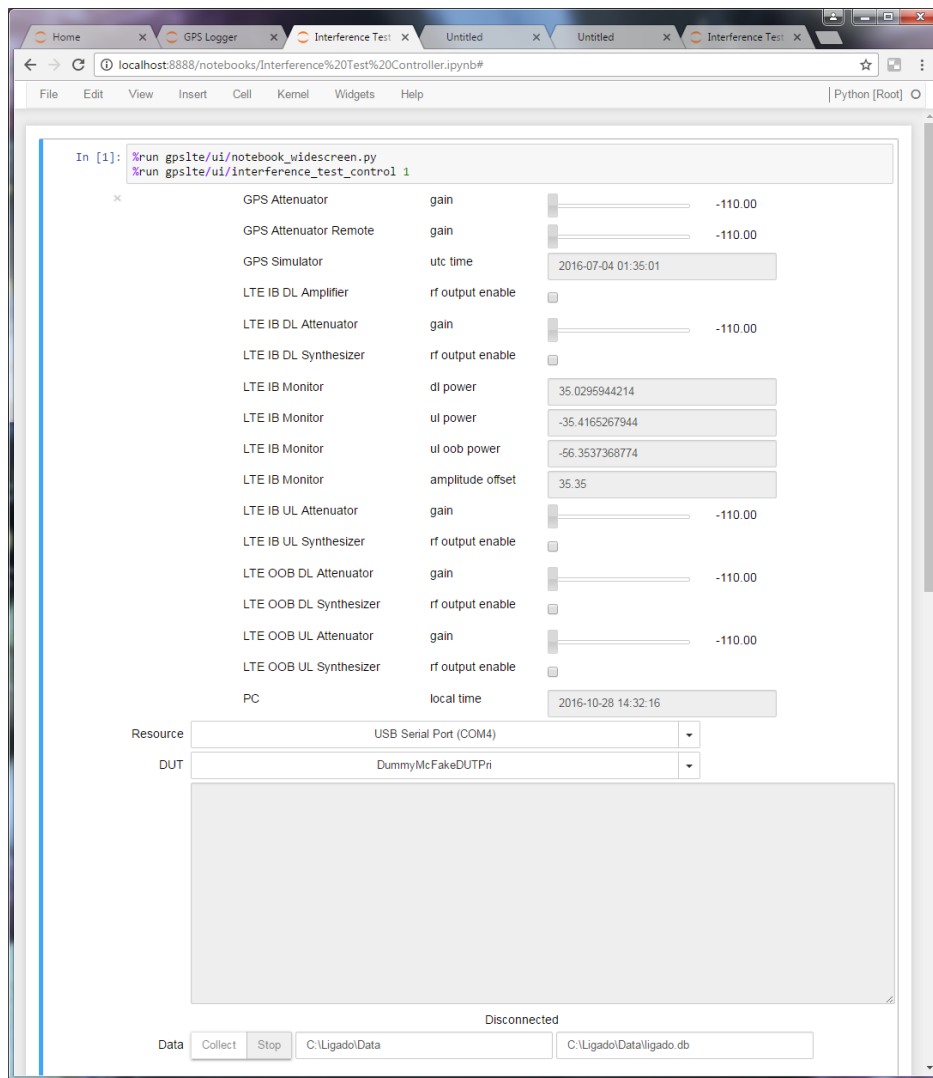


Figure 4.5: Frontend user interface for monitor and control of instruments and DUTs.

The bottom half of the instrument panel frontend provided controls for test operators to customize and execute automated test sequences. An example user interface of this tool is shown in Figure 4.6. Short snippets of python code create classes that can adjust parameters of the basic test procedures that are outlined in Section 4.3.

### 4.1.3 Extension and Customization

This architecture invites future support for additional DUTs. Implementation of a new DUT driver is a subclass of the relevant device manager and incorporates some configuration options. For example, a new device that streams National Marine Electronics Association (NMEA) formatted data

over a serial connection would subclass the USB serial device manager and set a few configuration parameters like baud rate. It is in this sense that the source code is extensible. It is particularly straightforward to add USB serial devices because there are few configuration settings. Here is an example definition that is sufficient to create a simple driver:

```
class ExampleGPSReceiverDevice(USBSerialDeviceManager):
    baud_rate          = 9600
    data_format        = 'nmea'
    usb_serial_id      = primary_usb_serial_id
```

where `baud_rate` is the serial data baud rate, `data_format` hints at the data format (for later use by the parser), and `primary_usb_serial_id` is a resource string that ties the the USB-serial converter device to a unique identifier in the operating system. Configuration attributes (beyond the three shown) are available for devices that require the script to send configuration text in order to enable data output or facilitate cold-start initialization.

Test sweeps are similarly customizable. Figure 4.5 shows examples in use during the test process. For example:

```
class LTE_DL_Levels(campaign.LTELevelSweepBase):
    no_lte_dwell       = 900                # seconds
    lte_dwell          = 1200              # seconds
    gains              = -110, -56, -7.5, -5 # dB (via atten.)
    lte_signal_type    = 'dl'
    lte_ib_dl_gain_mode = 'high'
    gps_scenario_type  = 'limited'
```

Here, an inherited copy of the generic LTE power level sweep class is configured for a 900 s (15 min) soak time without LTE, followed by a 1200 s (20 min) test time with LTE. This process is repeated at the specified LTE downlink gain levels (applied to both in-band and out-of-band at each setting): -110 dB, -56 dB, -7.5 dB, and -5 dB. The GPS simulator scenario is configured for the limited exposure case but supports all scenarios in Section 2.2.



Figure 4.6: Frontend user interface for customizing, selecting, and starting automated measurements.

## 4.2 DUT Placement, Orientation and System Level Checks

Given the large variety in geometrical shape and DUT system types, DUT specific procedures were developed to ensure repeatable measurements. The primary reference point for DUT placement was given by a DUT test stand, located  $3.32 \text{ m} \pm 0.08 \text{ m}$  downrange of the signal source antenna, see Figure 3.7. In general, external antennas were placed boresight with respect to the signal antenna; if a DUT did not have an external antenna, then the DUT's geometric center was aligned as close as possible to the geometric center of the test stand reference plane. It is of note that all power levels were calibrated to the reference plane of the test stand and that actual DUT placement variation with respect to the reference plane was incorporated in the uncertainty estimations.

### 4.2.1 General Location and Navigation Units (GLN)

#### 4.2.1.1 Fixturing

Because they have internal antennas, a general location and navigation (GLN) DUT was placed directly into the chamber, see Figure 3.1. This required that the GLN data link infrastructure (cabling and power supply) for the DUT to also have been attached to the test stand. Great care was given in mitigating the effects of data cables through routing and fixturing along the mast of the test stand. Furthermore, as GLN DUTs are typically battery driven, they were either supplied with a charging mechanism or a battery to AC adapter that allowed the DUT to perform throughout long measurement cycles.

#### 4.2.1.2 System Level Checks

Typically, the GLN devices listed a GPS coverage item in their menu which outlined GPS signal strength. This first order estimate of GPS power coupled into the DUT was used to optimize GLN DUT orientation with respect to the source antenna.

### 4.2.2 High Precision Positioning and Real Time Kinematic Units (HPP & RTK)

#### 4.2.2.1 Fixturing

Antennas belonging to high-performance positioning (HPP) units were attached to the antenna mast through an adapter plate. This allowed for relatively accurate ( $\pm 0.08 \text{ m}$ ) placement of the antenna to boresight with the source antenna. A cable leading from the antenna was of sufficient length to reach the DUT receiver. The DUT was placed outside of the chamber (see Figure 3.2), just below the shielding floor of the chamber. In the case of tests at National Technical Systems (NTS), the receiver was placed in a control room just below the chamber, and at the NIST Broadband Interoperability Testbed (NBIT) facility the receivers were placed in access cubbyholes. These access cubbyholes were covered with a grounded metal plate, and absorber.

#### 4.2.2.2 System Level Checks

The DUT system was checked out by observing the reported  $C/N_0$  values in the presence of the calibrated nominal GPS signal. If the reported signal strength was stable and of similar value across all satellite channels, the setup was deemed ready for testing.

Real time kinematic units had the added complexity of feeding a conducted signal to the base-station. The signal strength provided to the base-station was adjustable by means of a programmable attenuator. The reported signal strength of the base was equal to or slightly higher than the signal strength reported by the rover. RTK testing was conducted in a zero-baseline solution, the RTK base receiver's fixed location was set to the simulator "true" location and the RTK rover was exposed to the same simulated position.

#### 4.2.3 GPS Disciplined Oscillator Units (GPSDO)

##### 4.2.3.1 Fixturing

Antennas for the GPS-disciplined oscillator (GPSDO) units were setup in a similar manner as for HPP and RTK units, that is, boresight with respect to the signal antenna. The GPSDO receiver units were setup outside of the chamber, and collocated with the cesium clock timing reference unit and TIC (see Figure 3.4). Note that the Microsemi TS3050 had the GPS receiver incorporated into the antenna unit with a long cable link to the operating unit. For this DUT, the antenna-GPS receiver element was treated like an antenna and setup boresight with respect to the signal antenna.

##### 4.2.3.2 System Level Checks

As for the HPP and RTK units, the GPSDO systems were checked for  $C/N_0$  levels across all satellites in the presence of the calibrated nominal GPS signal. The unit's 1 pulse-per-second (PPS) signals were compared against the cesium (Cs) clock's output. If the  $C/N_0$  values were stable across all channels and the TIC reading was below 1 second, the setup was deemed ready for testing.

#### 4.3 Test Procedure

##### 4.3.1 Power Level Sweeps

**Selection of Power Levels** GLN DUTs were initialized through a menu driven procedure at the very beginning of a power level sweep. As shown in Figure 4.7 the user had the option of selecting whether the power level sweep should occur with either a nominal or limited satellite exposure. Subsequently, the LTE waveform was selected. In order to arrive at the desired power levels to test, the user performed an initial sweep across a wide band of power levels. This pre-screen was used to train the power levels for the test run. Power levels were selected in ascending order. The total number of power levels per LTE waveform was at a minimum 6 levels, consisting of a baseline test

(no LTE) and 5 LTE power levels.

#### 4.3.1.1 General Location and Navigation (GLN)

**Device Manual Reset Procedure** GLN DUTs followed a menu driven procedure. This procedure constituted the extent of menu driven reset capability and was able to delete stored information.

1. Device was power cycled
2. Select Menu → “SETUP” → “RESET” the following items were initiated:
  - ↳ “Reset Trip Data”
  - ↳ “Delete All Waypoints”
  - ↳ “Clear Current Track”
  - ↳ “Clear Track and Trip Data”
  - ↳ “Reset All Settings”
3. Select Menu → “SETUP” → “SYSTEM” and the following items were initiated:
  - ↳ “GPS → WAAS/EGNOS ”
  - ↳ “Interface” → “NMEA In/OUT”
  - ↳ “NMEA Sentences” → “ON” and the following subcategorized were configured:
    - ↳ “GSA,GSV” → “ON”
    - ↳ “WPL,RTE” → “OFF”
    - ↳ “GARMIN Proprietary” → “ON”
4. Power cycle the device

GLN DUTs were connected to the data acquisition system via a serial port. The baudrate for all GLN DUTs was 4800 baud.

**LTE Test Loop** After the DUT was configured through configuration commands, the first (“Day 1” nominal or limited) GPS-simulation was loaded and started. The DUT was exposed to 15 min of the GPS simulation without the presence of an LTE signal. This allowed the DUT to download new almanac and ephemeris information as well as settle into a position solution. DUT data acquisition coincided with the initialization of the GPS simulation. After the 15 min “soak period”, LTE was introduced at the initial LTE power level (typically a baseline without LTE). The DUT was exposed to the GPS + LTE signal for an additional 20 min. Subsequent to the exposure, data acquisition was terminated and the GPS simulator was stopped. This loop was performed for each LTE power step and constituted a power level run.

For subsequent power levels, the GPS simulation was incremented by 24 hours (e.g., from “Day 1” to “Day 2”) and the test loop was restarted at the initialization phase of the DUT. The test loop continued until all of the specified power levels were tested. For GLN type DUTs, it was essential to advance the GPS simulation by 24 hours at each power level so as to overcome constraints of reversing time and ensure consistent reporting of data. Some of the GLNs were more sensitive to these time constraints than others. The device’s manual reset procedure was performed at the beginning of the power level sweep.

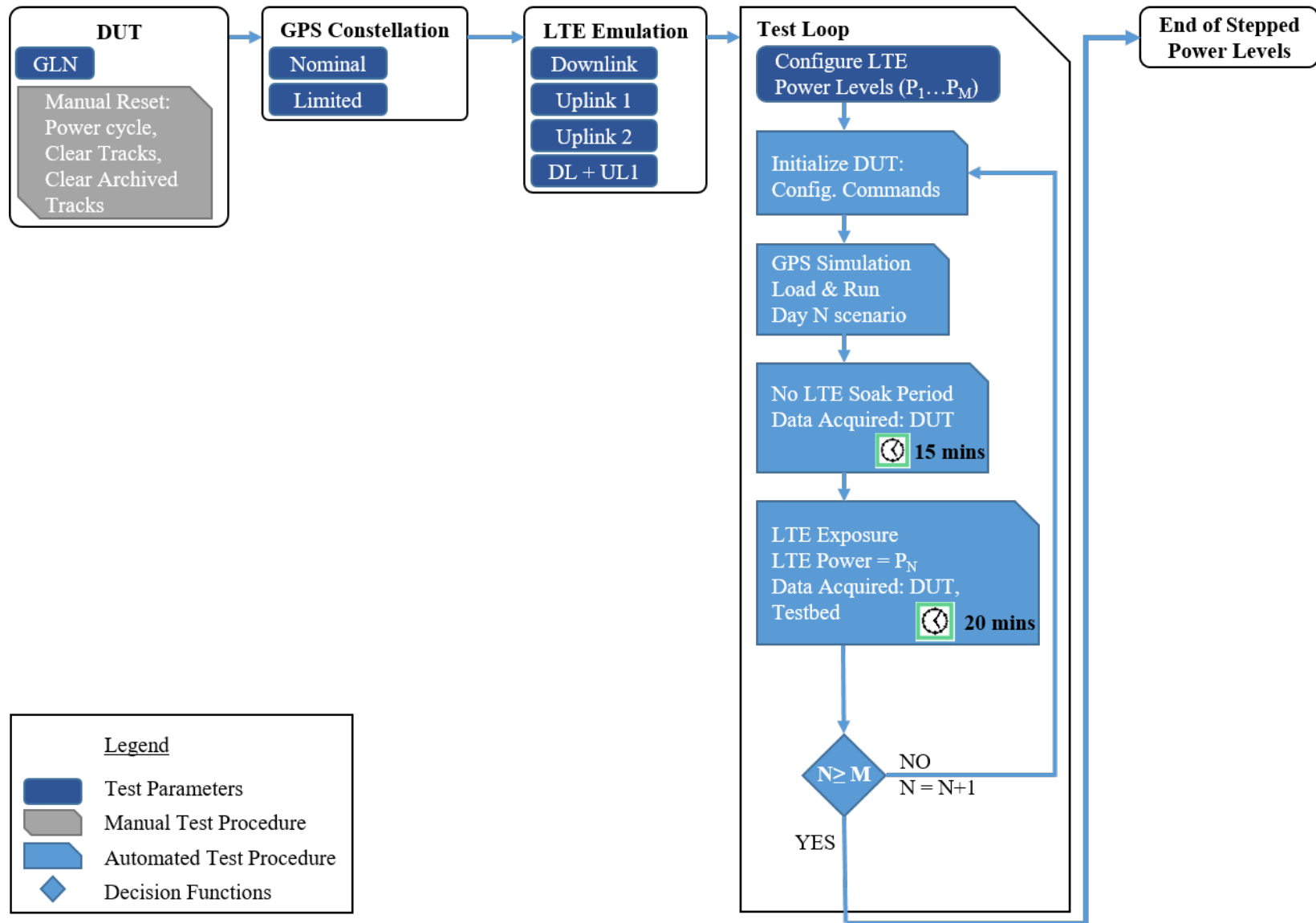


Figure 4.7: Power level sweep procedure for General Location and Navigation devices.

### 4.3.1.2 High Precision Positioning and Real Time Kinematic Units (HPP & RTK)

**DUT Cold Start Reset Procedure** HPP and RTK were initialized with a programmatic cold-start. This cold-start procedure deleted stored almanac data and ephemeris data, reset internal clocking (if necessary), and power cycled the DUT prior to introduction of the GPS and LTE signals. Cold-start command structures varied substantially from manufacturer to manufacturer. In the case of RTK DUTs, both base and rover were cold-started at the same time during the initialization phase. The reset commands (procedure) are outlined in Table 4.1.

Table 4.1: HPP & RTK Configuration Command Structures Configuration Commands for HPP and RTK DUTs

DUT <sup>1</sup>	Type	Interface	Command
Leica <sup>†</sup> GR50	HPP	Ethernet HEX	delete ephemeris and almanac reset time to 00:00:00 power cycle
Novatel FlexPak 628	HPP	Serial ASCII 115200 baud	“FRESET\r\n” “LOG COM1 GPGGA ONTIME 1\r\n” “LOG COM1 GPGSV ONTIME 1\r\n” “LOG COM1 BESTPOSA ONTIME 1\r\n” “LOG COM1 RANGEA ONTIME 1\r\n” “SERIALCONFIG COM1 115200\r\n”
Novatel ProPak 6	HPP	Serial ASCII 115200 baud	“FRESET\r\n” “LOG COM1 GPGGA ONTIME 1\r\n” “LOG COM1 GPGSV ONTIME 1\r\n” “LOG COM1 BESTPOSA ONTIME 1\r\n” “LOG COM1 RANGEA ONTIME 1\r\n” “SERIALCONFIG COM1 115200\r\n”
Novatel FlexPak 628	RTK (base)	Serial ASCII 9600 baud	“FRESET\r\n” “FIX POSITION 31.5982273 -110.2778474 1352.303\r\n” “GENERATERTKCORRECTIONS RTCMV3 COM2\r\n” “LOG COM1 GPGGA ONTIME 1\r\n” “LOG COM1 GPGSV ONTIME 1\r\n” “LOG COM1 BESTPOSA ONTIME 1\r\n” “LOG COM1 RANGEA ONTIME 1\r\n” “SERIALCONFIG COM1 9600\r\n”
Novatel FlexPak 628	RTK (rover)	Serial ASCII 9600 baud	“FRESET\r\n” “INTERFACEMODE COM2 RTCMV3 NONE OFF \r\n” “LOG COM1 GPGGA ONTIME 1\r\n” “LOG COM1 GPGSV ONTIME 1\r\n” “LOG COM1 BESTPOSA ONTIME 1\r\n” “LOG COM1 RANGEA ONTIME 1\r\n”

Table 4.1: HPP & RTK Configuration Command Structures Configuration Commands for HPP and RTK DUTs

DUT <sup>1</sup>	Type	Interface	Command
			“SERIALCONFIG COM1 9600\r\n”
Trimble NetR9	HPP	Ethernet cURL	“show?position” *“set?IoPort&port=TcpPort5017&NmeaGGA=1&NmeaGSV=1&NmeaGNS=1&NmeaGLL=1&NmeaPJK=1&NmeaGRS=1&NmeaGSA=1&NmeaRMC=1&NmeaVTG=1&NmeaDP=1&NmeaVGK=1&NmeaAVR=1&NmeaVHD=1&NmeaPJT=1&NmeaZDA=1&NmeaGGK=1&NmeaGST=1&NmeaBPQ=1” **“set?IoPort&Binex=1,7F05,smoothPhase,smoothRange,slips,metaData:60,stnId,antConfig,antXyz,antOffset,sysState:60,metTilt&port=TcpPort5017” “Reset?GnssData”
Trimble NetR9	RTK (base)	Ethernet cURL	“show?position” *“set?IoPort&port=TcpPort5017&NmeaGGA=1&NmeaGSV=1&NmeaGNS=1&NmeaGLL=1&NmeaPJK=1&NmeaGRS=1&NmeaGSA=1&NmeaRMC=1&NmeaVTG=1&NmeaDP=1&NmeaVGK=1&NmeaAVR=1&NmeaVHD=1&NmeaPJT=1&NmeaZDA=1&NmeaGGK=1&NmeaGST=1&NmeaBPQ=1” **“set?IoPort&Binex=1,7F05,smoothPhase,smoothRange,slips,metaData:60,stnId,antConfig,antXyz,antOffset,sysState:60,metTilt&port=TcpPort5017” “set?RtkControls&motion=static&mode=lowLatency” “set?IoPort&port=TcpPort28001&Cmr=cmrPlus” “Reset?GnssData”
Trimble R9s	RTK (rover)	Ethernet cURL	“show?position” *“set?IoPort&port=TcpPort5017&NmeaGGA=1&NmeaGSV=1&NmeaGNS=1&NmeaGLL=1&NmeaPJK=1&NmeaGRS=1&NmeaGSA=1&NmeaRMC=1&NmeaVTG=1&NmeaDP=1&NmeaVGK=1&NmeaAVR=1&NmeaVHD=1&NmeaPJT=1&NmeaZDA=1&NmeaGGK=1&NmeaGST=1&NmeaBPQ=1” **“set?IoPort&Binex=1,7F05,smoothPhase,smoothRange,slips,metaData:60,stnId,antConfig,antXyz,antOffset,sysState:60,metTilt&port=TcpPort5017” “set?RtkControls&motion=static&mode=lowLatency” “set?IoPort&remotePort=remoteip:remoteport&port=TcpPort28001”

Table 4.1: HPP & RTK Configuration Command Structures Configuration Commands for HPP and RTK DUTs

DUT <sup>1</sup>	Type	Interface	Command
“Reset?GnssData”			

<sup>†</sup> Commands listed for this device are the tasks required for proper initialization rather than the specific command structure.

<sup>1</sup>Certain commercial equipment, instruments, or materials are identified in this report in order to specify the experimental procedure adequately. Such identification is not intended to imply recommendation or endorsement by National Institute of Standards and Technology (NIST) nor is it intended to imply that the materials or equipment identified are necessarily the best available for the purpose.

**LTE Test Loop** With the exception of the ability to programmatically initialize the DUT, the LTE test loop follows the same procedure as discussed for the GLN devices. A flowchart of the overall procedure is outlined in Figure 4.8.

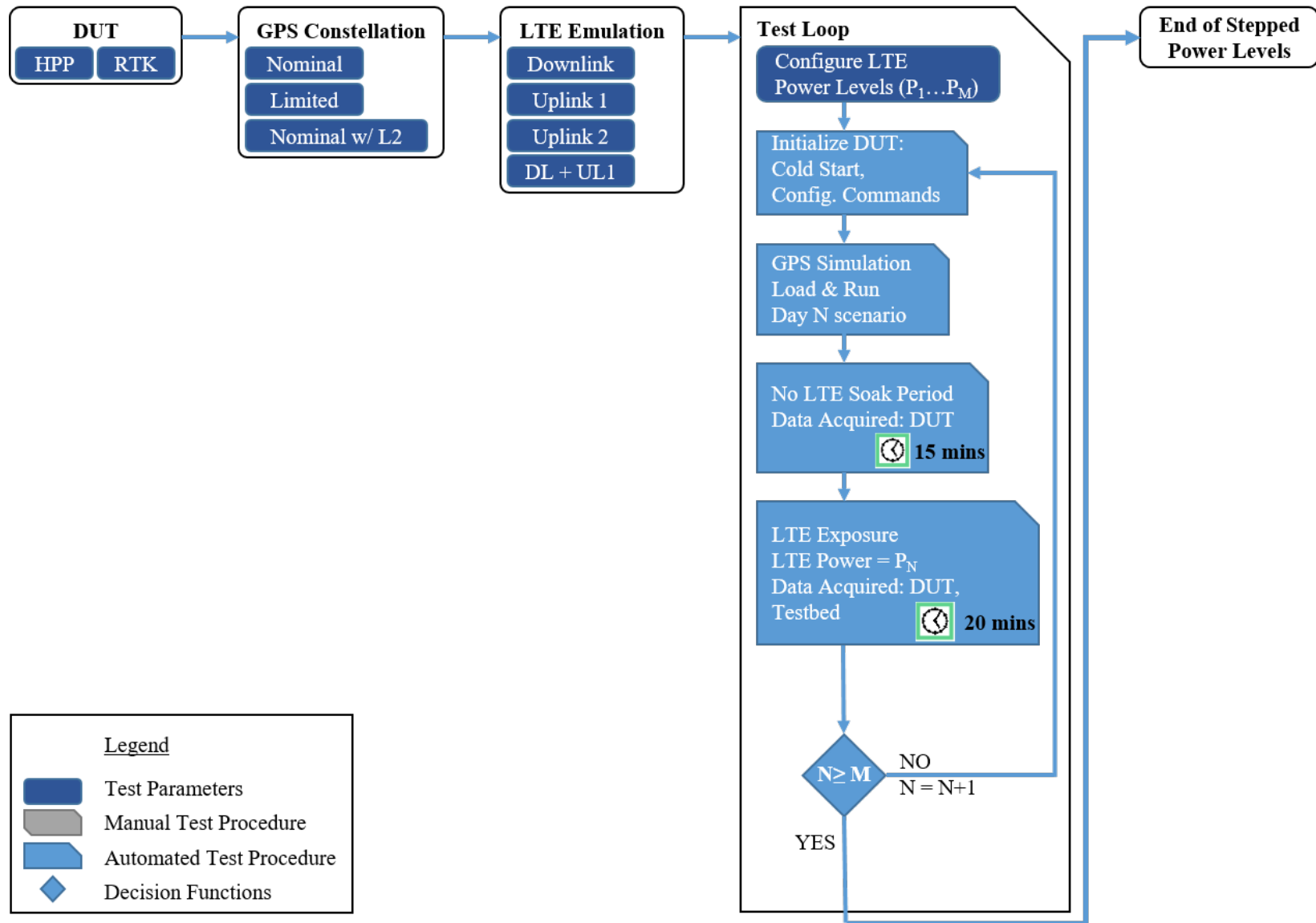


Figure 4.8: Power level sweep procedure for High Precision Positioning and Real Time Kinematic devices.

Table 4.2: Configuration Commands for GPSDO DUTs

DUT <sup>1</sup>	Type	Interface	Command
Arbiter 1088B	GPSDO	Serial ASCII	<i>Manual power cycle</i> “B0\r\n” “0,1B\r\n”
Microsemi SyncServer S650	GPSDO	Serial ASCII	“username\r\n” “password\r\n” “set configuration factory\r\n” “username\r\n” “password\r\n” “show gnss status\r\n”
Microsemi TimeSource TS3050	GPSDO	Serial ASCII	“username\r\n” “password;\r\n” “ACT-USER::TELECOM:101::TS3000!!;\r\n” “INIT-SYS::TS3050:101::1;” “username\r\n” “password;\r\n” “ACT-USER::TELECOM:101::TS3000!!;\r\n” “RTRV-GPS-STAT::GPS:101;\r\n”

<sup>1</sup>Certain commercial equipment, instruments, or materials are identified in this report in order to specify the experimental procedure adequately. Such identification is not intended to imply recommendation or endorsement by NIST nor is it intended to imply that the materials or equipment identified are necessarily the best available for the purpose.

### 4.3.1.3 GPS Disciplined Oscillator Units (GPSDO)

**DUT Reset Procedure** Two of the GPSDO DUTs were programmatically reset through a cold-start procedure. The other DUT was manually power-cycled at the beginning of every LTE power level. The reset command structure is in Table 4.2.

**LTE Test Loop** Unlike GLN, HPP, and RTK units, the GPSDO units were exposed to the LTE waveform during initialization of the test. This forced the GPSDO DUTs to acquire a fix in the presence of the LTE signal. Furthermore, the DUTs were tested for longer periods of 150 min. The extended test time was required to accommodate long settling times as well as capture slow drifts inherent to GPSDO’s internal timing crystals. The test loop procedure is shown in the flowchart in Figure 4.9.

**Time Interval Counter and Cs-clock Reference** The time interval counter was setup to take two reference signals from the Cs-clock reference into account. First, a 10 MHz timing signal, which set the timebase of the TIC to that of the Cs-clock reference. Second, the Cs-clock’s 1 PPS signal to its channel 1 input. The GPSDO’s 1 PPS signal was set to the TIC’s channel 2 input. The TIC then triggered on the rising edge of the channel 1 and channel 2 inputs and recorded the time delta between the trigger events. This time was recorded in nanoseconds. The Cs-clock reference was setup and allowed to stabilize for 24 hours prior to the timing tests. A log file was acquired for each test.

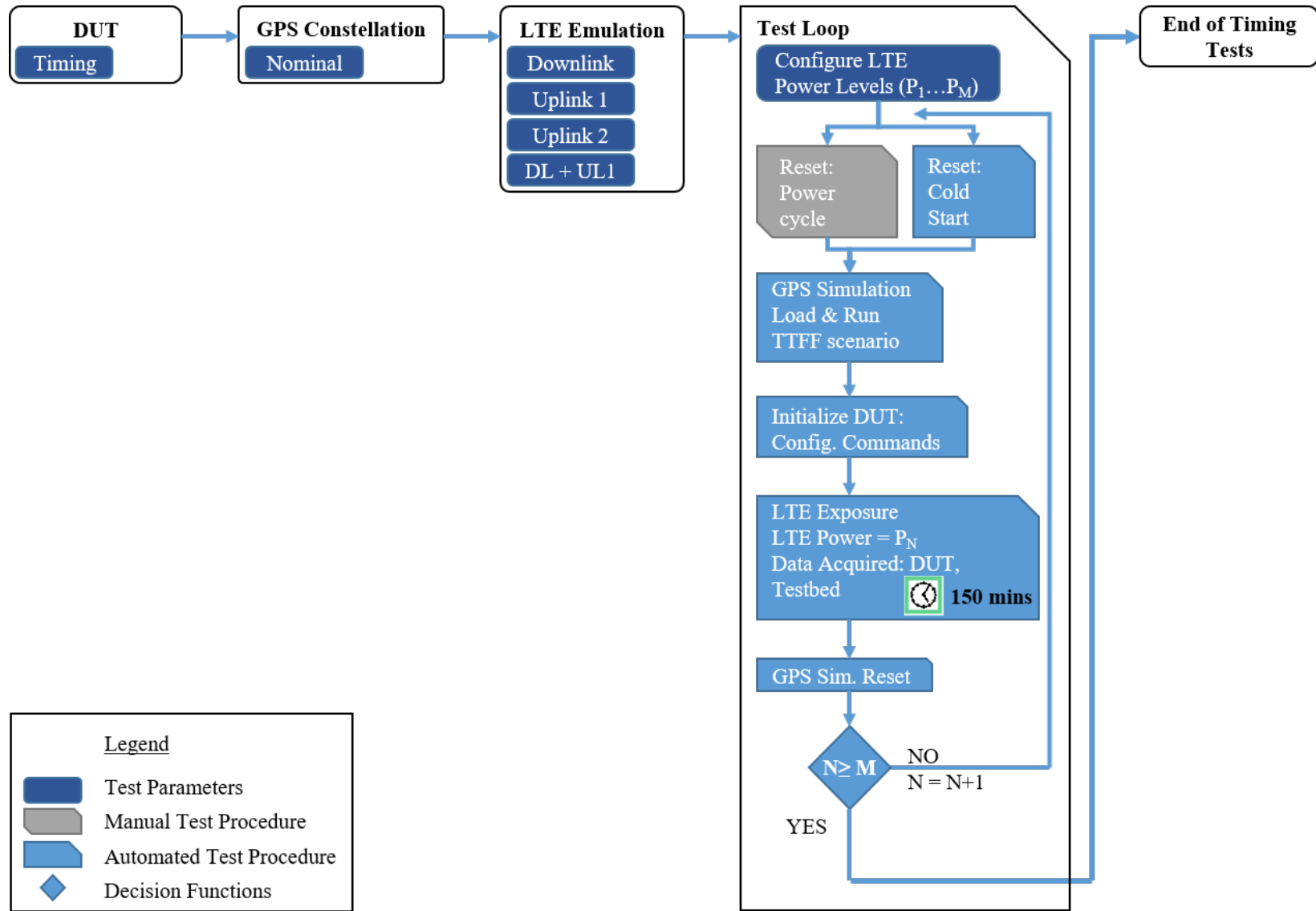


Figure 4.9: Power level sweep procedure for GPS Disciplined Oscillator devices.

### 4.3.2 TTFR Sweeps

As previously described in Section 2.2, time to first reacquisition (TTFR) tests were developed to accommodate DUTs without a programmatic restart capability. The test was devised similar to a tunnel scenario. The DUT was exposed to one location for 2 mins. and then “traveled” through a tunnel (no GPS coverage) for a period of 3 mins. At the end of the tunnel the DUT was exposed to a second location for 2 mins. The time constants were derived from experimental procedure to determine an adequate time without a GPS signal such that the DUT lost fix while preserving a realistic overall test time.

The TTFR was calculated from the timestamp when the DUT was reintroduced to GPS coverage to the time the DUT reports a reacquired fix. The tunnel cycling was carried out for 50 cycles leading to 100 re-acquisitions.

Prior to any TTFR sweep, the DUT was manually reinitialized as outlined in GLN devices manual reset procedure. The LTE power levels were selected through an informed decision derived from GLN nominal power level sweeps. In general the goal was to perform a TTFR sweep for the LTE power levels that were associated with 1 dB, 3 dB, and 6 dB degradation in  $C/N_0$ . After initialization of the DUTs, the GPS-simulation and LTE-signal were started simultaneously such that the DUT attempted reacquisition in the presence of the LTE-signal. The test loop for the TTFR sweeps is graphically represented in Figure 4.10.

### 4.3.3 TTFF Sweeps

The time to first fix (TTFF) sweeps were carried out on DUTs capable of programmatic cold-starts. TTFF procedures were carried out for a stationary location (same location as the power level sweeps) and in the presence of the LTE-signal. That is, the GPS-simulation and LTE-waveform were radiated simultaneously. The TTFF was calculated from the simulator start time (01:35:18 UTC) and the time at which the DUT reported its first fix. For HPP DUTs, the first fix occurred when the first valid position solution was reported, whereas RTK units were timed against their ability to resolve a valid RTK fix. As RTK units had the more challenging task in acquiring a fix and calculating a valid RTK solution, a less stringent cycle time of 5 mins. was used, HPP units were allotted 2 mins. of acquisition time. Each DUT was exposed to 100 TTFF cycles.

As was the case for TTFR sweeps, the LTE power levels chosen for the TTFF tests were informed by prior power sweep tests and priority was given to those LTE power levels that were associated with 1 dB, 3 dB, and 6 dB degradation of  $C/N_0$ . The TTFF sweep flowchart is shown in Figure 4.11.

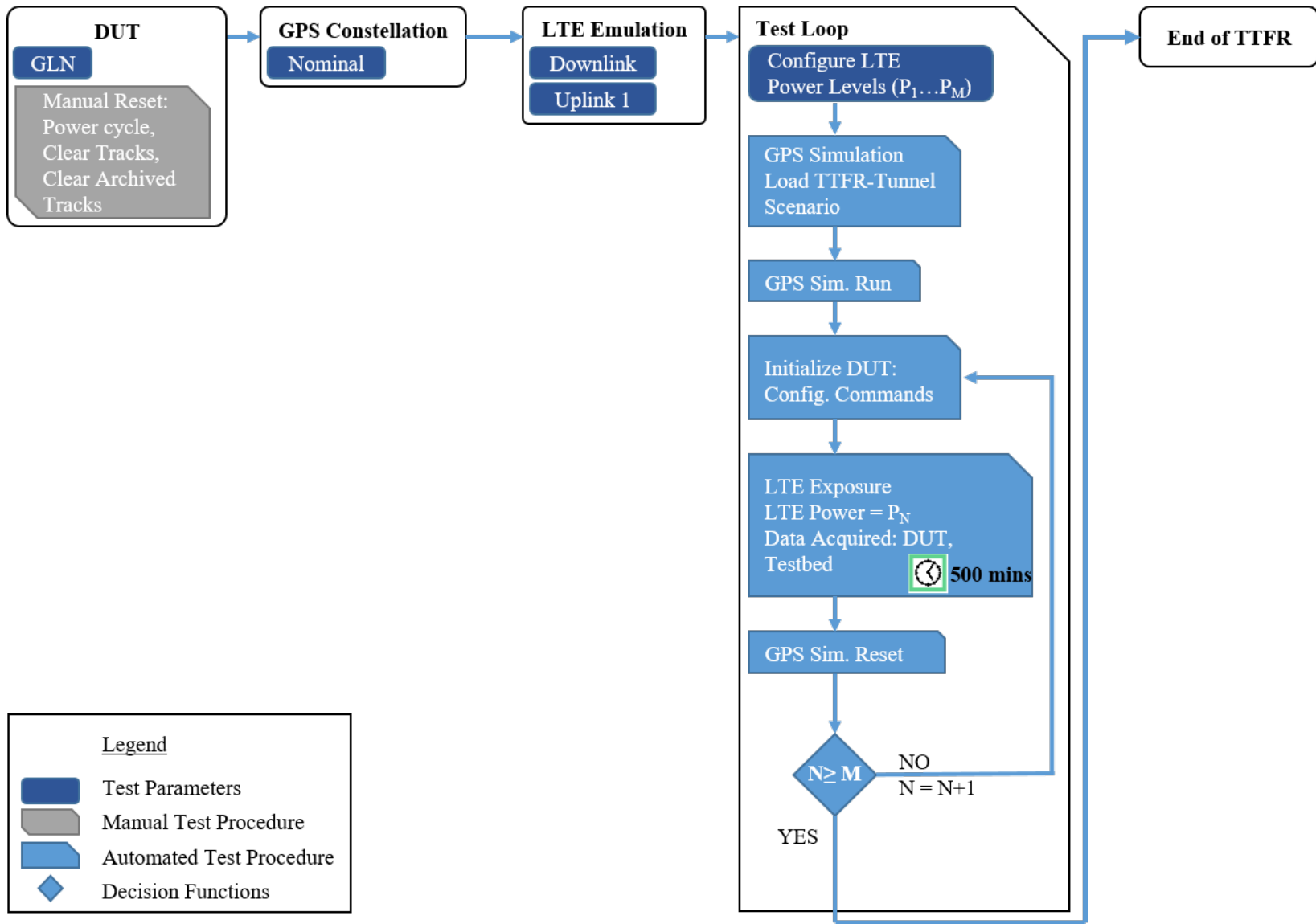


Figure 4.10: Time to first reacquisition procedure for General Location and Navigation devices.

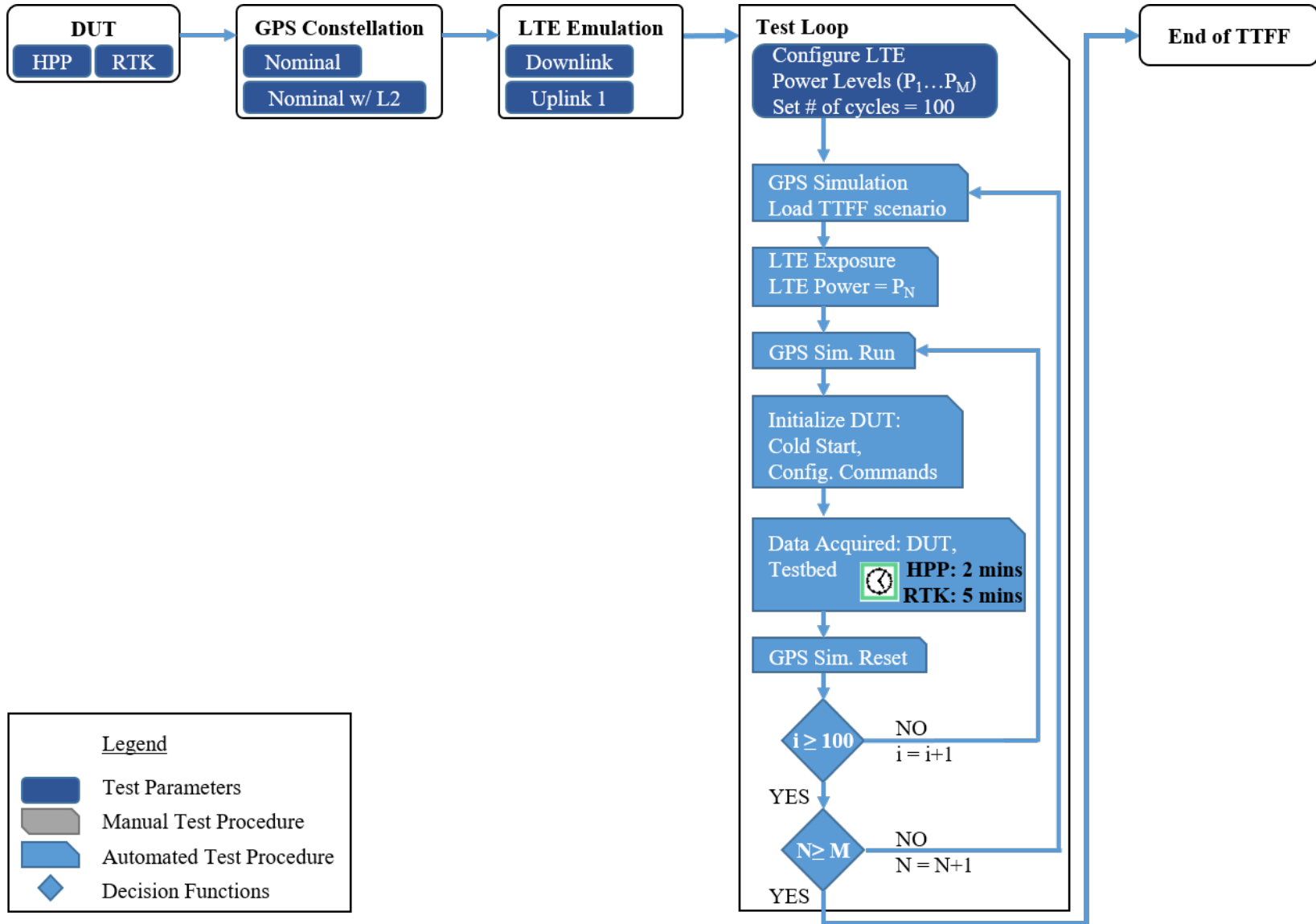


Figure 4.11: Time to first fix procedure for High Precision Positioning and Real Time Kinematic devices.

## 4.4 Data Acquisition

A collection of data files was acquired for each individual power level. The exception is in TTFB tests where a separate set of data was collected for each TTFB cycle. The DUT's data stream was collected throughout the measurement cycle. As the LTE signal was introduced, a testbed state file was acquired which contained metadata information that was associated with the DUT data file for the specific powerlevel. Testbed metadata included:

- Run number
- PC local time at the instance the LTE signal was tested
- GPS simulator time at the instance that the LTE signal was introduced
- GPS attenuator gain (dB)
- GPS attenuator remote gain (dB, for the conducted path to the RTK-base unit)
- LTE in-band (IB) monitor amplitude offset (dB, offset for the spectrum analyzer readings)
- LTE IB downlink band (DL) synthesizer radio frequency (RF) state (on/off)
- LTE IB DL amplifier RF state (on/off)
- LTE IB DL attenuator gain (dB)
- LTE IB DL monitored value (dB, spectrum analyzer reading)
- LTE out-of-band (OOB) DL synthesizer RF state (on/off)
- LTE OOB DL attenuator gain (dB)
- LTE IB uplink bands (UL) synthesizer RF state (on/off)
- LTE IB UL attenuator gain (dB)
- LTE IB UL monitored value (dB, spectrum analyzer reading)
- LTE OOB UL synthesizer RF state (on/off)
- LTE OOB UL attenuator gain (dB)
- LTE OOB UL monitored value (dB, spectrum analyzer reading)

### 4.4.1 General Location and Navigation (GLN)

For GLN devices, the data stream and associated testbed file were recorded on a per power level basis. The actual NMEA data collected for the GLN devices are outlined in Table 4.3. An example 1 sec. capture is in Figure 4.12. GLN DUTs reported new data every 2 secs.

Table 4.3: NMEA Strings Collected for the Various DUTs

Device <sup>1</sup>	Type	Interface	NMEA Strings	Other Data Strings
Garmin eTrex H	GLN	Serial	GPBOD, GPGGA, GPGLL, GPGSA, GPGSV, GPRMB, GPRMC, GPRTE	PGRME, PGRMZ
Garmin eTrex 30x	GLN	Mass storage	—	—
Garmin GPSMAP 78	GLN	Serial	GPBOD, GPBWC, GPGGA, GPGLL, GPGSA, GPGSV, GPRMB, GPRMC, GPVTG, GPXTE	HCHDG, PGRME, PGRMM, PGRMZ
Garmin Montana 650t	GLN	Serial	GPBOD, GPBWC, GPGGA, GPGLL, GPGSA, GPGSV, GPRMB, GPRMC, GPVTG, GPXTE	HCHDG, PGRME, PGRMM, PGRMZ
Garmin Montana 680t	GLN	Serial	GPBOD, GPBWC, GPGGA, GPGLL, GPGSA, GPGSV, GPRMB, GPRMC, GPVTG, GPXTE	HCHDG, PGRME, PGRMM, PGRMZ
Leica GR50	HPP	Ethernet	GNRMC, GPGGA, GPGGK, GPGGQ, GPGLL, GPGNS, GPGSA, GPGSV, GPVTG', GPZDA	PTNL-GGK
Novatel FlexPak 628	HPP	Serial	GPGGA, GPGSV	BESTPOSA, RANGEA
Novatel FlexPak 628	RTK	Serial	GPGGA, GPGSV	BESTPOSA, RANGEA
Novatel ProPak 6	HPP	Serial	GPGGA, GPGSV	BESTPOSA, RANGEA
Trimble NetR9	HPP	Ethernet	GPGGA, GPGLL, GPGNS, GPGRS, GPGSA, GPGST, GPGSV, GPRMC, GPVTG, GPZDA	PFUGDB, PTNL-AVR, PTNL-BPQ, PTNL-GGK, PTNL-PJK, PTNL-PJT, PTNL-VGK, PTNL-VHD
Trimble NetR9	RTK (base)	Ethernet	GPGGA, GPGLL, GPGNS, GPGRS, GPGSA, GPGST, GPGSV, GPRMC, GPVTG, GPZDA	PFUGDB, PTNL-AVR, PTNL-BPQ, PTNL-GGK, PTNL-PJK, PTNL-PJT, PTNL-VGK, PTNL-VHD
Trimble R9s	RTK (rover)	Ethernet	GPGGA, GPGLL, GPGNS, GPGRS, GPGSA, GPGST, GPGSV, GPRMC, GPVTG, GPZDA	PFUGDB, PTNL-AVR, PTNL-BPQ, PTNL-GGK, PTNL-PJK, PTNL-PJT, PTNL-VGK, PTNL-VHD
Arbiter 1088B	GPSDO	Serial	GPGLL	—

<sup>1</sup>Certain commercial equipment, instruments, or materials are identified in this report in order to specify the experimental procedure adequately. Such identification is not intended to imply recommendation or endorsement by NIST nor is it intended to imply that the materials or equipment identified are necessarily the best available for the purpose.

Table 4.4: Non-NMEA Data Formats Collected for the Various DUTs

Device <sup>1</sup>	Type	Interface	Format
Trimble NetR9	HPP	Ethernet	BINEX
Trimble NetR9	RTK (base)	Ethernet	BINEX
Trimble R9s	RTK (rover)	Ethernet	BINEX
Arbiter 1088B	GPSDO	Serial	ASCII <sup>†</sup>
	TIC	USB	ASCII
	Cs Clock	Serial	ASCII
MicroSemi SyncServer S650	GPSDO	Serial	TL1/ASCII <sup>‡</sup>
	TIC	USB	ASCII
	Cs Clock	Serial	ASCII
MicroSemi TimeSource 3050	GPSDO	Serial	TL1/ASCII <sup>‡</sup>
	TIC	USB	ASCII
	Cs Clock	Serial	ASCII

<sup>†</sup> The manufacturer specific ASCII format was read and parsed.

<sup>‡</sup> The manufacturer made use of transaction language 1 (TL1) to provide ASCII type formatted data. The data was not standardized from DUT to DUT and separate parser were written to accommodate device specific formatting.

<sup>1</sup> Certain commercial equipment, instruments, or materials are identified in this report in order to specify the experimental procedure adequately. Such identification is not intended to imply recommendation or endorsement by NIST nor is it intended to imply that the materials or equipment identified are necessarily the best available for the purpose.

#### 4.4.2 High Precision Positioning and Real Time Kinematic Units (HPP & RTK)

HPP and RTK data acquisition formats were streamed. Some of the HPP DUTs and RTK DUTs had, in addition to NMEA data, a binary exchange (BINEX) data stream which contained KPI's such as pseudorange and carrierphase. These BINEX files were stored in a binary format and then subsequently converted to receiver independent exchange (RINEX) (a printout of the RINEX format is in Figure 4.18 and Figure 4.19). The metadata from the testbed state file was associated with all of the data streams. The HPP and RTK data collection formats are outlined in Table 4.3 and Table 4.4 and an example 1 sec. NMEA data capture is shown in Figure 4.13. HPP and RTK DUTs were configured to report new data every second, however, some baudrate limitations on the RTK units caused intermittent reporting of some data strings.

#### 4.4.3 GPS Disciplined Oscillator Units (GPSDO)

In addition to the custom ASCII stream (examples in Figure 4.14, 4.15, and 4.16) and testbed metadata files, the GPSDO's also collected time interval counter data which was stored as a two column \*.csv file with a time stamped data capture of TIC data. The TIC captured the 1 PPS output of the GPSDO and compared it against the standard reference time provided by the cesium clock. This time-interval capture represented the time differential between the GPS true time and the timing signal reported by the DUT. Moreover, the state file of the cesium clock (format shown

in Figure 4.17) was collected via a serial port.

```
$GPRMC,015450,A,3135.8937,N,11016.6708,W,0.0,212.2,180236,10.0,E,D*3A
$GPRMB,A,,,,,,,,,,,,,V,D*19
$GPGGA,015450,3135.8937,N,11016.6708,W,2,12,0.8,1379.5,M,-26.6,M,,*44
$GPGSA,A,3,02,05,12,13,15,18,20,21,25,26,29,51,1.4,0.8,1.2*3A
$GPGSV,3,1,12,02,14,076,42,05,39,043,42,12,13,179,42,13,29,101,42*71
$GPGSV,3,2,12,15,33,142,42,18,30,226,42,20,87,293,42,21,36,294,42*78
$GPGSV,3,3,12,25,34,210,42,26,13,315,42,29,80,030,42,51,53,174,40*7A
$GPGLL,3135.8937,N,11016.6708,W,015450,A,D*5A
$GPBOD,,T,,M,,*47
$GPBWC,015450,,,,,T,,M,,N,,D*7B
$GPVTG,212.2,T,202.2,M,0.0,N,0.0,K,D*27
$GPXTE,A,A,,N,D*54
$PGRME,3.0,M,3.0,M,4.2,M*28
$PGRMZ,4528,F,*13
$PGRMM,WGS 84*06
$HCHDG,268.5,,10.0,E*11
```

Figure 4.12: 1 second capture of the Garmin 680t NMEA data stream.

```
$GPGGA,015647.00,3135.89363545,N,11016.67084153,W,4,11,0.8,1381.903,M,-28.395,M,1.0,0002*4C
$PTNL,GGK,015647.00,070416,3135.89363545,N,11016.67084153,W,3,11,1.4,EHT1353.508,M*5E
$GPVTG,292.70,T,283.07,M,0.01,N,0.03,K,D*24
$GPGST,015647.00,0.000,0.003,0.003,162.7,0.003,0.003,0.006*52
$PTNL,PJK,015647.00,070416,,,,,3,11,1.4,,M*29
$PTNL,PJT,WGS84,NONE*21
$PTNL,VGK,015647.00,070416,-0000.001,-0000.001,-0000.001,3,11,1.4,M*10
$PTNL,VHD,015647.00,070416,227.134,82.636,-25.233,-65.930,0.001,-0.002,3,11,1.4,M*14
$GPGSV,4,1,13,13,30,099,45,20,86,318,44,15,35,141,44,18,32,227,44*71
$GPGSV,4,2,13,5,38,043,45,21,37,296,44,2,13,078,45,29,81,037,44*77
$GPGSV,4,3,13,12,12,179,45,25,33,209,44,26,14,314,44*49
$GPGSV,4,4,13,51,53,174,45,48,46,219,44*7E
$PTNL,AVR,015647.00,+0.0000,Yaw,+0.0000,Tilt,,0.001,3,1.4,11*31
$GPZDA,015647.01,04,07,2016,00,00*60
$GPGSA,A,3,18,5,21,2,29,12,25,13,20,26,15,,1.4,0.8,1.2*3E
$GPRMC,015647.00,A,3135.89363545,N,11016.67084153,W,0.014,292.700,040716,9.6278,E,D*14
$PTNL,BPQ,015633.02,070416,3135.89363590,N,11016.67084096,W,EHT1353.508,M,4*7B
$GPGLL,3135.89363545,N,11016.67084153,W,015647.00,A,D*75
$GPRGS,015647.00,1,0,0,0,0,0,0,0,0,0,0,0,0,0,0,0,0,0,0,0,*61
$PFUGDP,GP,015647.00,3135.89364,N,11016.67084,W,11,9,FN,0.1,0.1,163,0.1*09
$GPGNS,015647.00,3135.89364,N,11016.67084,W,RNNNN,11,0.8,1381.9,-28.4,1.0,2*0D
```

Figure 4.13: 1 second capture of the Trimble R9s NMEA data stream.

```

0,1B
186:01:39:03
$GPGLL,3135.8930,N,11016.6706,W,013903.340,A*38V=10 S=18 T=10 P=OFF E=00
L U=00 S=OFF
S2 P3 F00002 #00001 T2016:186:01:37:54 W110:16:40.238 N31:35:53.581 H+01363.75
I=03:00 X=ff:ff

```

Figure 4.14: 1 sec. capture of the Arbiter 1088B ASCII data stream.

```

-----
SyncServer> [[m
SyncServer> [[mshow gnss status

Gnss Status

Latitude           : 31 35 53.615 N
Longitude          : 110 16 40.250 W
HGT Val Ellipsoid  : 1350.4 m
HDOP               : 0.770000
PDOP               : 1.430000
Fix Quality        : 2
Used Satellites    : 11
Receiver Status    : Tracking
Operation Mode     : Survey
Antenna Status     : OK

Current GNSS Satellite View:

-----
|Index|GnssID|SatID|SNR|Azimuth|Elev|PrRes|
-----|-----|-----|-----|-----|-----|-----|
| 1   |GPS   | 2   |42 | 75    | 15 | 0    |
| 2   |GPS   | 5   |42 | 43    | 42 | 0    |
| 3   |GPS   |12   |42 |180    | 15 |-3    |
| 4   |GPS   |13   |42 |103    | 28 | 2    |
| 5   |GPS   |15   |42 |144    | 32 |-1    |
| 6   |GPS   |18   |42 |224    | 28 |-8    |
| 7   |GPS   |20   |42 |255    | 86 | 7    |
| 8   |GPS   |21   |42 |292    | 35 |-4    |
| 9   |GPS   |25   |42 |212    | 36 |-5    |
|10   |GPS   |26   |42 |317    | 12 |-6    |
|11   |GPS   |29   |42 | 18    | 78 | 5    |
-----

```

Figure 4.15: 1 sec. capture of the MicroSemi SyncServer S650 ASCII data stream.

```

TS3050 16-07-04 02:32:51
M 101 COMPLD
"GPS:LAT=31 35.893N, LONG=110 16.670W, ALT=1380.50, UTC=2-32-51,
MODE=AUTO, MERIT=1024NS, SUCCESS=32%
SAT-29, USE=Y, CNO=47, ELEV=74, AZ=130, LOCK=1677,
SAT-20, USE=Y, CNO=47, ELEV=71, AZ=21, LOCK=459,
SAT-15, USE=N, CNO=46, ELEV=47, AZ=124, LOCK=0,
SAT-21, USE=Y, CNO=46, ELEV=46, AZ=312, LOCK=131,
SAT-18, USE=Y, CNO=46, ELEV=45, AZ=239, LOCK=20,
SAT-13, USE=Y, CNO=46, ELEV=34, AZ=80, LOCK=138,
SAT-5, USE=Y, CNO=46, ELEV=24, AZ=45, LOCK=560,
SAT-25, USE=Y, CNO=46, ELEV=19, AZ=200, LOCK=205,
SAT-26, USE=Y, CNO=47, ELEV=19, AZ=300, LOCK=20,
SAT-10, USE=N, CNO=46, ELEV=10, AZ=231, LOCK=0,
"
/* LINK: 3, CMD: RTRV-GPS-STAT::GPS:101 */
;RTRV-GPS-STAT::GPS:101;

```

Figure 4.16: 1 sec. capture of the MicroSemi TimeSource 3050 ASCII data stream.

```

MJD 57603 20:38:55
CBT ID: US50120381(H)
Status summary: Operating normally
Power source: AC
Log status: 28 entries

Freq Offset:      0e-15  Osc. control:    -9.68 %
RF amplitude 1:   26.5 %  RF amplitude 2:   24.8 %
Zeeman Freq:     39949 Hz  C-field curr:    12.160 mA
E-multiplier:    1920 V   Signal Gain:     14.4 %

CBT Oven:        8.1 V   CBT Oven Err:    0.00 C
Osc. Oven:       -9.0 V   Ion Pump:        0.4 uA
HW Ionizer:      1.0 V   Mass spec:       11.3 V
SAW Tuning:      0.0 V   DRO Tuning:      1.4 V
87MHz PLL:       1.5 V   uP Clock PLL:    2.1 V
+12V supply:     12.2 V  -12V supply:    -12.2 V
+5V supply:      5.4 V   Thermometer:     45.8 C

```

Figure 4.17: ASCII state file of the timing reference cesium clock.

```

16 7 5 2 1 24.0000000 0 11G20G05G18G21G29G02G12G25G13G15G26
104980966.084 7 19977213.641
44.900
116994172.377 7 22263257.781
44.800
118062674.195 7 22466577.586
44.300
120281742.053 7 22888853.859
44.700
105425694.642 7 20061843.992
44.300
127754322.590 7 24310839.469
43.900
129922863.467 7 24723501.578
44.600
120168115.232 7 22867241.336
44.900
119646993.118 7 22768064.828
45.000
116610144.382 7 22190181.102
44.900
128058864.061 7 24368795.508
45.000

```

Figure 4.18: 1 sec. capture of RINEX v2.11 converted from BINEX, acquired during standalone mode with L1 frequency only.

16	7	12	1	57	15.000000	0	11G20G13G15G18G05G21G02G29G12G25G26		
104952190.300	7				81780961.00844		19971738.227		19971745.9804
					43.800		25.6004		
119984455.818	7				93494422.13544		22832282.391		22832291.0474
					43.200		26.2004		
117247236.261	7				91361553.13144		22311414.359		22311422.9694
					44.500		26.0004		
118674772.413	7				92473888.21044		22583056.508		22583065.3874
					44.000		26.6004		
116281670.847	7				90609180.03044		22127677.180		22127685.5984
					44.000		26.2004		
120625970.135	7				93994302.81444		22954358.281		22954366.8554
					44.100		25.0004		
127252607.861	7				99157915.60244		24215366.836		24215376.2114
					43.900		25.9004		
105478562.485	7				82191159.20544		20071911.891		20071920.0314
					43.700		25.8004		
129030062.009	7				100542955.53844		24553607.227		24553617.5864
					43.900		26.4004		
119420196.379	7				93054756.02444		22724912.594		22724921.6994
					44.000		25.2004		
128519828.357	7				100145393.33844		24456516.609		24456526.4224
					43.700		26.1004		

Figure 4.19: 1 sec. capture of RINEX v2.11 converted from BINEX, acquired during RTK mode with L1 and L2 frequencies.



## 5 Data Processing and Analysis Methods

Automated processing methods were required to reliably parse, sort, and analyze over 38,000 raw data and testbed files. The processing had to confront two significant challenges. First, for each device under test (DUT) and test condition, data were collected in a variety of formats that had to be parsed, homogenized, and organized. In particular, the development of robust parsing software demanded a sizable effort due to DUT-dependent variations in the raw data. Second, the processing had to handle the diverse set of test conditions described in Chapter 2 and Chapter 4, with tests often spread over multiple days. To address the above challenges, we developed software for data parsing, database creation, data wrangling, and data analysis. Each of these topics is covered by a section below. A collection of data files containing test results is provided along with this report. The last section of this chapter summarizes the contents of these files.

### 5.1 Data Parsing

Raw data were collected in a variety of formats that depended on the DUT according to Table 4.3 and Table 4.4. For example, American standard code for information interchange (ASCII) data formats included sentences specified by the National Marine Electronics Association (NMEA)-0183 standard [12, 13], vendor-specific sentences, and device-specific data streams. Binary data in the binary exchange (BINEX) [14] format were also acquired when it could be collected robustly.

To deal with the diversity of raw data, we developed a “master-parser” program, which operated according to the flowchart in Figure 5.1. The master-parser program started by using the path and testbed variables to determine the type of test (LTE Power Sweep, GPS-disciplined oscillator (GPSDO), time to first fix (TTFF), or time to first reacquisition (TTFR)), DUT, and data format. Next, the raw data was directed to the appropriate data parsing/conversion program. Lastly, a database record was created; Section 5.2 describes the database. A summary of the data parsing capabilities is shown in Table 5.1. Details on the parsers for each data format are given in the following subsections.

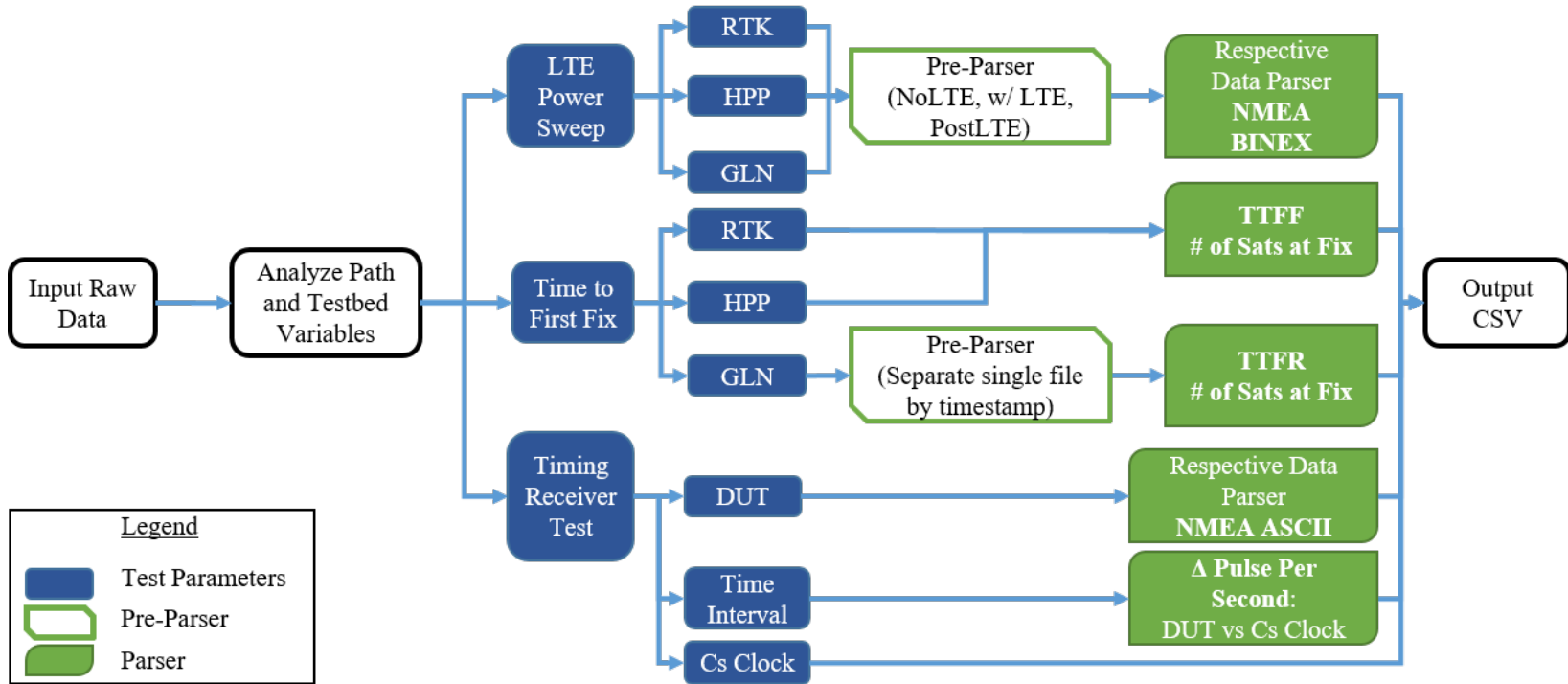


Figure 5.1: Flowchart for raw data parsing.

Table 5.1: Data Parsing Capability by Message in Supported Formats. Not All Supported Messages in Each Format are Output by Every DUT.

	NMEA <sup>1</sup>	BINEX	ASCII <sup>2</sup>	ASCII <sup>3</sup>
<b>Device Status Messages</b>				
Receiver status message	☑	—	☑	☑
Operation mode code	☑	—	☑	—
Clock status	—	—	—	☑
<b>Signal Lock Information</b>				
Signal locked?	☑	—	☑	☑
Fix quality code	☑	—	☑	—
Fraction of time with lock	—	—	—	☑
Lock loss period	—	—	—	☑
Out of lock delay	—	—	—	☑
<b>Time and Date</b>				
UTC time	☑	—	☑	☑
GPS time	—	☑	—	—
Time of week	☑	—	—	—
<b>Position</b>				
Latitude	☑	—	☑	☑
Longitude	☑	—	☑	☑
Height/altitude	☑	—	☑	☑
<b>Constellation Geometry Metrics</b>				
HDOP	☑	—	☑	—
PDOP	☑	—	☑	—
TDOP	—	—	—	☑
Satellites in view	☑	—	☑	☑
Geometrical axis information	☑	—	☑	☑
<b>Data per Satellite by PRN:</b>				
C/N <sub>0</sub>	☑	☑	☑	—
Relative signal strength	—	—	—	☑
Azimuth	☑	—	☑	—
Elevation	☑	—	☑	—
Applied to solution?	☑	—	☑	—
Satellite lock	☑	—	☑	—
Pseudorange	☑	☑	—	—
carrier phase	☑	☑	—	—

<sup>1</sup> NMEA category includes standard NMEA 0183 and manufacturer specific sentences.

<sup>2</sup> Custom ASCII format through transaction language 1 (TL1) interface.

<sup>3</sup> Custom ASCII format from Arbiter 1088B interface.

## 5.1.1 NMEA

Most devices under test supported a streaming ASCII data format defined in the NMEA 0183 standard [12, 13]. Though the NMEA organization is involved in other activities, and their standard 0183 also defines other parameters (such as electrical signaling, timing, etc.), we use the shorthand term NMEA to refer exclusively to the ASCII data format and the full range of variants implemented among the population of DUTs.

### 5.1.1.1 NMEA Preprocessor

To properly assess DUT response to long-term evolution (LTE) power during a power sweep, the portion of the data stream corresponding to applied LTE power had to be separated from the portion without LTE power. The NMEA preprocessor separated NMEA data into four bins defined by the known state of GPS and LTE signals in the testbed. This binning required valid timestamp information from the NMEA sentence. If a timestamp was unavailable, a No-Timestamp flag was assigned.

The NMEA preprocessor program started by determining the LTE activation and deactivation times. The activation time was retrieved from the testbed logs output by the automated testbed program. For the power sweep tests, LTE deactivation time was always set to 02:10:01. The portion of a power level test with LTE was 1200 seconds long, however the NMEA preprocessor truncated the data by 17 seconds at the beginning and end of the capture to account for variations in the number of leap-seconds reported by the DUTs. A leap-second accounting on a DUT basis is found in Table 5.2. A complete data capture (DUT initialization period, No-LTE soak period, and LTE exposure period) was separated into four bins as follows:

1. **No Timestamp:** NMEA output from a DUT often started devoid of date, time, or position immediately after the device initialization. These sentences lacked data that could be correlated with the state of the testbed.
2. **No LTE:** NMEA lines containing a timestamp and collected before the LTE activation time.
3. **With LTE:** NMEA sentences collected during the time when the LTE signal was active. These lines contained the data that was fed into subsequent processing and analysis.
4. **Post LTE:** NMEA sentences collected after the LTE power was turned off.

Table 5.2: Fix Flag Indicators, Leap Second Accounting, and Source of the Timestamp for Each DUT.

DUT <sup>1</sup>	Type	Reset Time	Leap Seconds	Fix Quality	Data	Fix Indicator
DUT 1	GLN	3 min interval	+17	“GPS fix”	GPGGA	1
DUT 2	GLN	3 min interval	+17	“GPS fix”	GPGGA	1
DUT 3	GLN	3 min interval	+17	“GPS fix”	GPGGA	1
DUT 4	GLN	—	—	—	—	—
DUT 5	GLN	—	—	—	—	—
DUT 6	GLN	—	—	—	—	—
DUT 7	HPP	1904 92118 TOW	+0	“GPS fix”	BESTPOSA	“SOL_COMPUTED,SINGLE”
DUT 8	HPP	1904 92118 TOW	+0	“GPS fix”	BESTPOSA	“SOL_COMPUTED,SINGLE”
DUT 9	HPP	01:35:18 UTC	+0	“GPS fix”	GPGGA	1
DUT 10	HPP	01:35:01 UTC	+17	“GPS fix”	GPGGA	1
DUT 11	RTK	1904 92118 TOW	+0	“RTK Float”	BESTPOSA	“SOL_COMPUTED,L1_FLOAT”
DUT 12	RTK	01:35:01 UTC	+17	“RTK Fixed Integer”	GPGGA	4
DUT 13	GPSDO	—	—	—	—	—
DUT 14	GPSDO	—	—	—	—	—
DUT 15	GPSDO	—	—	—	—	—

### 5.1.1.2 NMEA to Output CSV Conversion

The NMEA parser loaded every NMEA sentence binned in the *With LTE* category. Table 5.3 lists the sentence types that were supported by the parser, which included standard NMEA and manufacturer-specific sentences. While each of these sentence types was supplied by at least one DUT, only sentences listed in the first column were analyzed.

Table 5.3: List of Parsed NMEA Sentences.

Analyzed	Not Analyzed
GPGGA	GPBWC
GPGSV	GPGGA
BESTPOSA	GPGLL
BESTPOSA	GPGSA
RANGEA	GPRMB
PTNL-VGK	GPRMC
PTNL-VHD	GPVTG
PFUGDP	GPZDA

Timestamp information was necessary in order to map DUT outputs to the testbed state. However, sentences that did not include timestamp information were indexed with an extrapolated “harmonized” timestamp. The extrapolation was implemented as a simple feed-forward technique: the most recently output time and date was combined to form the timestamp index.

Although different sentence types contained different types of position information, no indexing over the data was necessary for positioning data. Therefore, in the absence of any driving need or motivation, no harmonization or feed-forward strategy was applied to position data.

Satellite-specific information, such as DUT estimates of  $C/N_0$  for each satellite, was provided by GPGSV or vendor-specific sentences. These data are typically formatted as a list of satellites with the associated key performance indicator (KPI) information that were observed. In order to streamline post-processing, the output comma-separated values (CSV) files provided the data for all satellites reported during the entirety of the NMEA file, organized in order of pseudo-random noise (PRN) code number. The data reported for each satellite was therefore tracked across the entire run.

The different KPIs that were collected, e.g., position, and  $C/N_0$ , were not included in every NMEA sentence. Therefore, blank entries in the output CSV files were common. The output CSV files had DUT independent header information, which maintained the anonymity of output results within any one class of receivers.

### 5.1.2 BINEX

Data in the BINEX format was acquired from some of the high-performance positioning (HPP) and real-time kinematic (RTK) devices. The BINEX parsing started by converting the binary data to ASCII receiver independent exchange (RINEX) format v2.11 [15] using the UNAVCO freeware program called TEQC [16], which offered advantages of quality control and log output among other features. The RINEX files were organized such that for each timestamp, there was a list of satellite PRN numbers with corresponding L1 or L2 pseudorange, carrier phase, and  $C/N_0$ . For this test, only PRN's tagged with a "G" were generated as the global positioning system (GPS) emulator only simulated GPS satellites and not global navigation satellite system (GLONASS), geostationary signal payloads, or Galileo satellites. Example RINEX v2.11 is shown in Figures 4.18 and 4.19.

The satellite-specific measurands in the RINEX files were parsed from ASCII to CSV by associating the PRN number in the satellite list to the corresponding measurand in the data list after the timestamp line (see Figure 4.18 to see the RINEX data format). The BINEX CSV files were formatted in a similar manner to the NMEA CSV files, with the timestamp in the first column followed by the measurands by PRN in subsequent columns. If a satellite-specific measurand was missing at a given timestamp, corresponding cells were left empty.

### 5.1.3 GPSDO Formats

The GPSDO devices provided data in DUT-specific ASCII formats. Specifically, the Arbiter 1088B supplied data in a graphical ASCII table format, and the MicroSemi DUTs delivered data in different formats through a TL1 interface. A custom parser was written for each of these ASCII-based formats. The parsers relied on identifying character patterns that separated periodic entries. The measurand values were then extracted from each entry by looking for character patterns known to be adjacent to relevant data. The relevant values were populated into variables, and these variables were concatenated into an output string, one per entry, with the values separated by commas. After all entries were parsed, the lines were written to a CSV file that could be easily read for subsequent processing.

### 5.1.4 TTFF and TTFR

The TTFF was calculated as the difference between the time the DUT was initialized and the time the DUT reported a valid fix. The fix validity was dependent on the operating mode of the DUT. For HPP units, the fix validity was taken as the first position solution without regard to fix quality. For RTK, units the fix validity was taken as the highest RTK fix (RTK float or RTK integer solution). For the TTFF sweeps, the DUT was reset at the start of the GPS simulation at a coordinated universal time (UTC) time of 01:35:18. Many of the devices did not report leap seconds in their time reporting; the leap second offset and fix flag indicator for each of the DUTs is outlined in Table 5.2.

For TTFR, the DUTs time to lock was calculated as the time difference between the reintroduction of the GPS signal and the reported time at which GPS fix was reacquired. The DUTs were reintroduced to a GPS signal every 3 min.

### 5.1.5 Time Interval Data and Cesium Clock Log File

The time interval counter reported data in a two-column CSV format. The first column corresponded to personal computer (PC) local time and the second column to the time interval in seconds. No special parser was implemented prior to data analysis.

The Cs-clock log file was not parsed for data analysis, but the ASCII files were inspected manually. These Log files pertain information to confirming Cs-clock “health” and no abnormalities or errors were found.

## 5.2 Database Creation

A database was implemented to facilitate efficient access to a large variety of data for analysis. The database encompassed over 38,000 raw data and testbed files, and more than 19,000 parsed data files. To manage the files, an SQLite [17] relational database acted as a local database, providing test result access by filters and queries.

The master-parser software added a database record for each DUT, test with test conditions, raw data file, and parsed data file. For each raw data file under consideration, meta-data about the DUT, type of test, test conditions, and data formats were stored in memory until the raw data was parsed. At that time, structured query language (SQL) queries inserted the data into their respective tables. Figure 5.2 shows table layout with their respective column names. The small column right of the column name indicates data type: “t” for text, “#” for float or integer, and “d” for datetime-timestamps. The arrows between tables indicate the relationship between the column name in the originating table and the receiving table ID by foreign key mapping. Many test conditions produced more than one type of data file (logs, multiple data formats, etc.); to avoid duplicate entries of test conditions, a check for an existing test was executed on analysis of the raw data file.

The data analysis software interfaced with the database by dynamically accessing parsed data based on the test criteria. For example, a query of the database to get all of the tests for an uplink test on DUT 1 was:

```
select * from Test where testtype=0 and DUT=1
```

The result was a table of all parameters in the test table matching these conditions. To retrieve the related parsed data, the query was (inputting the test ID’s):

```
select * from parsedData where test in (the queried Test id’s)
```

A more refined query to find a baseline Uplink 2 test for a high precision device (DUT 7) could

look like:

```
select * from Test where testtype=29 and DUT=7 and  
LTE_IB_DL_Attenuator_gain=-110 and LTE_IB_UL_Attenuator_gain=-110  
ORDER BY created_at ASC LIMIT 1
```

Data analysis required quick access to the data given a set of test conditions, regardless of the file type. The ability to easily add new data files to the database expedited the analysis necessary to digest the test data.

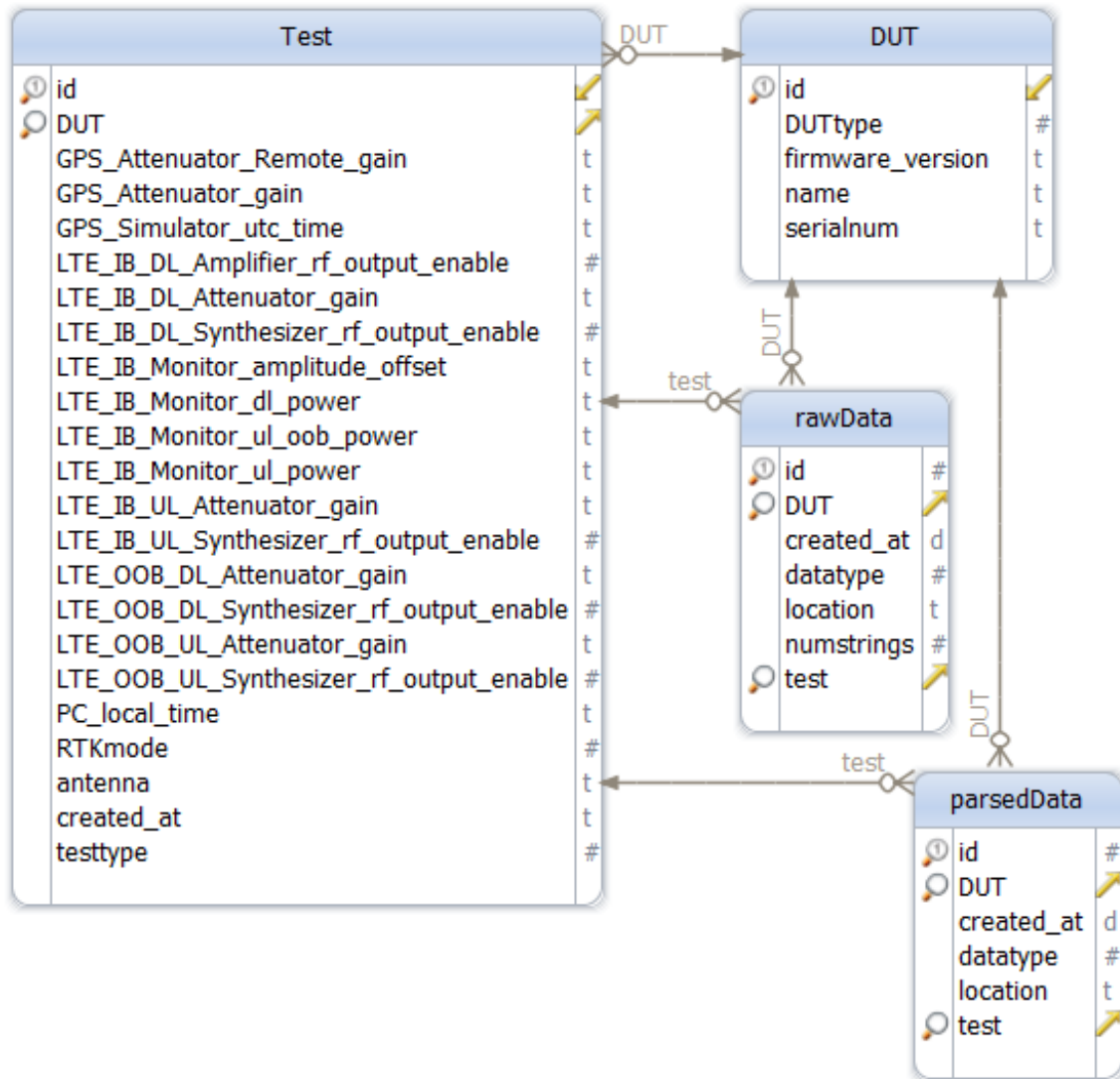


Figure 5.2: Relational database layout with table names, column names, and data types. Also shown is the relational foreign key mapping.

## 5.3 Data Wrangling

Data wrangling is the process of cleaning, unifying, and converting complex data sets for further analysis. This section describes the wrangling steps after the raw data was parsed and the database was formed.

### 5.3.1 Aggregation, Sorting, and Cleaning

For a given test type and device class (e.g., uplink band 1 (low) (UL1) LTE power sweep tests for HPP devices), the database was queried for a list of test results. The database entry for each test included the DUT name, testbed information, e.g., attenuator values, as well as the path to each associated raw and parsed datafile. After the LTE power level was determined from the testbed information, measurands were extracted from each parsed datafile. Namely, for most devices, the UTC time, position, fix, and number of satellites-in-view were read from either parsed “GGA” or parsed “BESTPOS” NMEA files. Likewise, carrier-to-noise-density ratio ( $C/N_0$ ) for each GPS satellite was read from either parsed “GSV”, “RANGE”, or “BINEX” files, depending on the DUT. When available, pseudorange and carrier phase for each satellite were read from parsed “RANGE” or “BINEX” files.

Practical aspects of the data acquisition required sorting and aggregation steps. Namely, test scheduling logistics often required non-sequential data acquisition for a given test type and DUT. Moreover, for some test-types (such as combination UL/DL power sweeps, TTFF, and timing tests), a baseline test was not reacquired if one had been acquired previously for that DUT. Therefore, for each test-type and DUT, we aggregated all test results and then sorted them by LTE power level. If a baseline test was missing for a given test-type, the software found a baseline test for that DUT and combined it with the results.

For each LTE power level, the ability of the DUT to sustain GPS lock was checked. A sustained GPS lock was determined if the following conditions were met: 1) lock for at least 80% of the test interval (i.e., lock for at least 16 out of 20 minutes for LTE power sweep tests), 2) no gaps in lock of more than 1 minute, and 3) DUT time not frozen for more than 50 seconds. If any of these conditions was violated, a loss of sustained lock was recorded, and the data for that power level was not processed further. The above criteria for a sustained GPS-lock were empirically motivated by the range of DUT behaviors observed during our testing.

For satellite-specific measurands ( $C/N_0$ , pseudorange, and carrier phase), some DUTs reported data for the simulated wide-area augmentation system (WAAS) signal, or for satellites that were not in the simulated GPS constellation. A further cleaning step addressed this problem by limiting processing and analysis to data corresponding to L1 signals from the constellation of simulated GPS satellites.

### 5.3.2 Position Error Calculation

For the LTE sweep tests, position data in the form of latitude, longitude, and altitude were obtained from DUTs in the GLN, HPP, and RTK classes. Also, the true DUT position was known, since it was given to the GPS simulator. To compute 3D position error (3DPE), the latitude, longitude, and altitude coordinates were transformed into the cartesian earth-centered earth-fixed (ECEF) coordinate system [18], and then the Euclidean distance between the true and reported position was calculated from the ECEF coordinates. Coordinate conversions started by transforming the “height above geoid” altitude (an approximation to mean sea-level) into the height above the World Geodetic System 1984 (WGS84) ellipsoid [18], given the distance offset between the geoid and ellipsoid provided by the DUT.

## 5.4 Statistical Analysis Methods

This section describes the analysis methods that were applied to the data from each test. In particular, it focuses on the methods used to estimate summary statistics and their associated uncertainties. Data visualization is covered subsequently in Section 5.5.

### 5.4.1 LTE Power Sweep Tests

For the LTE power sweep tests on GLN, HPP, and RTK devices, the 3D position error and  $C/N_0$  were analyzed, as discussed below. The number of satellites in view data were plotted as described in Section 5.5, but not analyzed further. Some HPP and RTK DUTs provided pseudorange and carrier phase for each satellite in view; these measurands are included in the CSV datafiles described in Section 5.6 that accompany this report. Analyses of pseudorange and carrier phase were not attempted due to the heavy dependence of these measurands on satellite movements, and due to the complicated choices that need to be made in their processing.

The  $C/N_0$  data collected for each GPS satellite in view were first reduced to a scalar time series by finding the median across all GPS satellites for each time point. The choice to use the median instead of a different statistic, such as the mean, was motivated by the fact that, unlike the mean, the median is robust to outliers. Therefore, because  $C/N_0$  values are typically lower for GPS satellites near the horizon, the median  $C/N_0$  across GPS satellites is less sensitive to satellite movements toward the horizon.

To enable comparison of DUT performance at different LTE power levels, the time series for 3DPE and median  $C/N_0$  were analyzed by estimating the median of the steady-state portion of the time series. The underlying assumption of this analysis is that the DUT reached a steady-state condition during the measurement period. Recall from Chapter 4 that for each LTE power level, the DUT was first given 15 minutes without LTE before LTE was applied for 20 minutes. The analysis of each time series consisted of two main steps, warm-up time estimation and steady-state median estimation, which are described next.

### 5.4.1.1 Warm-up Time Estimation

Non-steady-state DUT performance was expected immediately after the application of LTE power. The aim of the warm-up time estimation step was to estimate, in an automated fashion, how much of the time series needed to be discarded prior to steady-state median estimation. To accomplish this task, the marginal standard error rule-5 (MSER-5) method was chosen, since it was found to offer superior performance in a comparison-study of warmup-up estimation algorithms by Hoad et al. [19]. The MSER-5 method finds the point in the time series where the standard deviation of batched-averages of length 5 is minimized when the data before that point are deleted. Details on this method can be found in [19, 20].

Two examples of warm-up time estimates for time series from our testing are shown in Figure 5.3. In both cases, it can be seen that the estimated warm-up time captures the transient behavior of the time series.

### 5.4.1.2 Steady-state Median Estimation

After discarding data from the estimated warm-up period, point and confidence interval estimates of the steady-state median were obtained from each warmed-up time series. Note that because GPS time series of GPS measurands exhibit strong correlations, classical estimators of confidence intervals for quantiles are unsuitable, since they are designed for independent samples. For this reason, we applied the averaged group quantile method of Heidelberger and Lewis [21], which is designed for quantile estimation from statistically dependent sequences. Note that the Heidelberger and Lewis method does not make any distributional assumptions about the data, i.e., it is nonparametric.

Note that for  $C/N_0$ , if the data were extracted from parsed “RANGEA” NMEA sentences or BINEX data, then they were reported with a resolution of 0.1 dB. However, if  $C/N_0$  data were extracted from “GSV” NMEA sentences, then they were reported with a resolution of 1 dB. The coarse quantization of  $C/N_0$  from “GSV” sentences therefore implied that the minimum uncertainty in median  $C/N_0$  was  $\pm 0.5$  dB. Thus, when derived from “GSV” data, the confidence intervals for median  $C/N_0$  were required to have a length of at least 1 dB.

Confidence intervals estimated with the above method assess sampling variability due to changing experimental conditions and device performance. However, for  $C/N_0$ , there is another component of variability due to the unknown choice of  $C/N_0$  estimation algorithm implemented by the DUT. To draw conclusions about  $C/N_0$  for a group of DUTs, it is necessary to understand this component. A preliminary investigation into variability due to the choice of  $C/N_0$  estimation algorithm is presented in Appendix B.

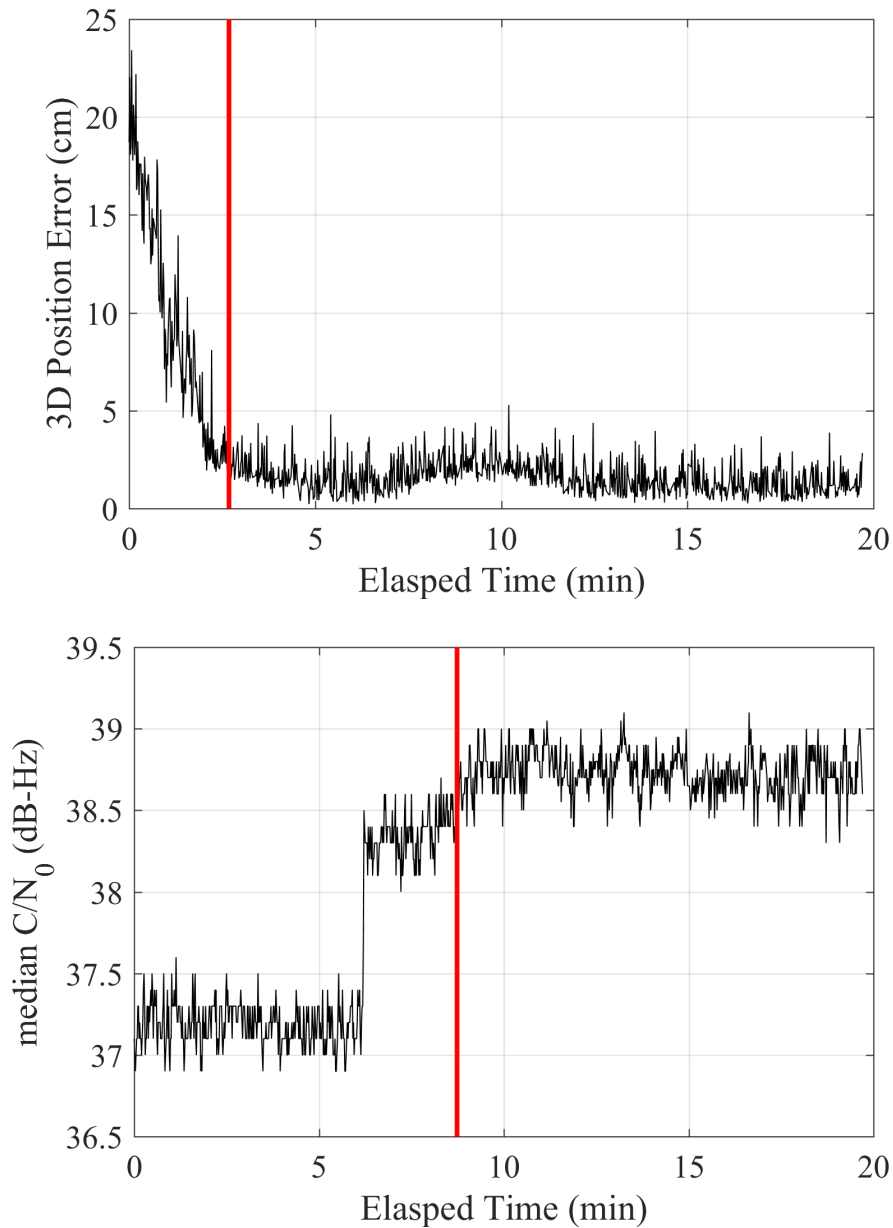


Figure 5.3: Examples of warm-up time estimates. The estimated warm-up time is indicated by the red vertical line. Top: A 3DPE time series for DUT 11, Antenna B in the limited exposure scenario for an UL1 test with an LTE power level (EIIP) of  $-49.7 \text{ dBm} \pm 2.7 \text{ dB}$ . Bottom: A median  $C/N_0$  time series for DUT 9, Antenna C for a combination UL1/DL test with an LTE power level (EIIP) of  $-50.0 \text{ dBm} \pm 2.7 \text{ dB}$ .

## 5.4.2 TTFF and TTFR Tests

The TTFF and TTFR tests were analyzed by estimating the empirical cumulative distribution function (CDF) at each LTE power level. Recall that these tests consisted of a series of repeated trials (roughly 100), where each trial collected fix data for a specified time, e.g., 120 s for HPP devices or 300 s for RTK. If a fix was not acquired in the specified measurement time, then the TTFF/TTFR is known to be greater than the measurement time by an unknown amount. In statistics terminology, such data are said to be “right-censored.” To handle the presence of censored data, the Kaplan-Meier estimator [22] for the empirical CDF was used. In addition, pointwise 95% confidence bands for the empirical CDF were estimated with Greenwood’s formula [23, 24].

## 5.4.3 Timing Tests

Measurands for timing tests of GPSDO receivers included time interval counter (TIC) data, fix, the number of satellites in view, and for some devices,  $C/N_0$ . The testing for each LTE power level lasted 150 min. To allow for DUT conditioning, data collected from the first half of testing (75 min) was not used for analysis. The decision to use a conditioning-time of 75 min was based on the observation that the TIC data from all DUTs appeared to settle after that period.

The second 75 min of TIC data were processed as follows. First, a warm-up time was estimated using the method of Section 5.4.1.1. Second, the portion of the TIC time series following the estimated warm-up period was adjusted by subtracting its mean. The resulting time series, the “warmed-up TIC output,” was plotted for each power level. The warmed-up TIC output was also analyzed by calculating Allan time deviation (TDEV), a recommended metric for characterizing the error of a time source [25, p. 18]. Essentially, TDEV characterizes the standard deviation in time error for different averaging times. Pointwise 95% confidence bands for TDEV were estimated using the “simple” method given in [25, p. 37].

Time series for the number of satellites in view were plotted for each LTE power level, but were not analyzed further. When  $C/N_0$  data were available, they were analyzed in the same manner as described in Subsection 5.4.1 for the LTE power sweep tests.

## 5.5 Data Visualization

This section introduces the different types of plots that are used to present the test results.

### 5.5.1 LTE Power Sweep Tests

Figure 5.4 contains examples of the plots for 3D position error. Note that in both plots, the label “BL” is used to indicate a baseline test without LTE. The top plot is a scatter plot that shows points for data collected over the full 20 minutes of LTE exposure. To help visualize the data and to also communicate the uncertainty in the LTE power, data in the scatter plot are randomly dithered in the

horizontal direction. Namely, for each power level, the horizontal coordinate is randomly generated from a normal distribution with mean given by the estimated LTE power and standard deviation corresponding to the uncertainty in LTE power as given in Section C.4. The scatter plot is used to communicate the full range of data collected for each power level in a compact, easy-to-read format. However, when interpreting the scatter plot, note that the data for each power level is actually a time series, and consequently, the time-dependent, correlated nature of the data is not conveyed.

The bottom plot in Figure 5.4 presents estimates for the median of the steady-state 3DPE time series at each power level. Namely, for each power level, a 95% confidence region for the median is shown as a box, with a circular marker indicating a point estimate. Each 95% confidence region is constructed by finding a 97.5% confidence interval for the median 3DPE in the vertical direction and a 97.5% confidence interval for the LTE power in the horizontal direction. By the Bonferroni inequality, it follows that the region has at least 95% coverage.<sup>1</sup> To aid comparison with the baseline result, a lightly-shaded box is shown extending from the baseline confidence region.

The 95% confidence regions can be interpreted as follows. Suppose that the experiment for a given power level is repeated a large number of times (e.g., 10,000), and that from each trial, a 95% confidence region is estimated. (Note that the confidence region varies randomly with the trial.) Then the proportion of trials for which the confidence region covers the population steady-state median will be approximately 0.95. In other words, the confidence region covers the population steady-state median with a probability of approximately 95%.

Figure 5.5 contains examples of the plots for  $C/N_0$  under the nominal satellite condition. The top plot is a scatter plot that shows  $C/N_0$  data for all GPS satellites collected over the full 20 minutes of LTE exposure. Like the 3DPE scatter plot, the data are randomly dithered in the horizontal direction to aid visualization and to communicate LTE power uncertainty. Likewise, the horizontal coordinate is randomly generated from a normal distribution with mean given by the estimated LTE power and standard deviation corresponding to the uncertainty in LTE power.

The bottom plot in Figure 5.5 shows estimates for the steady-state median of the median  $C/N_0$  time series, as explained in Subsection 5.4.1. Like the 3DPE median plot, the 95% confidence regions are constructed by finding a 97.5% confidence interval for the median  $C/N_0$  in the vertical direction and a 97.5% confidence interval for the LTE power in the horizontal direction. To aid comparison with the baseline result, a lightly-shaded box is shown extending from the baseline confidence region.

Recall from Section 5.3.1 that conditions for a sustained GPS lock were checked at each LTE power level. When a DUT failed to maintain sustained GPS lock for a test, the lowest power level with no sustained lock is recorded on the plot with a red annotation, as shown in Figure 5.5.

Figure 5.6 contains examples of the plots for  $C/N_0$  under the limited satellite condition. Compared

<sup>1</sup>For two events,  $E_1$  and  $E_2$ , the Bonferroni inequality [26, p. 13] takes the form  $P(E_1 \cap E_2) \geq P(E_1) + P(E_2) - 1$ . Plugging in  $P(E_1) = P(E_2) = 0.975$  yields  $P(E_1 \cap E_2) \geq 0.95$ .

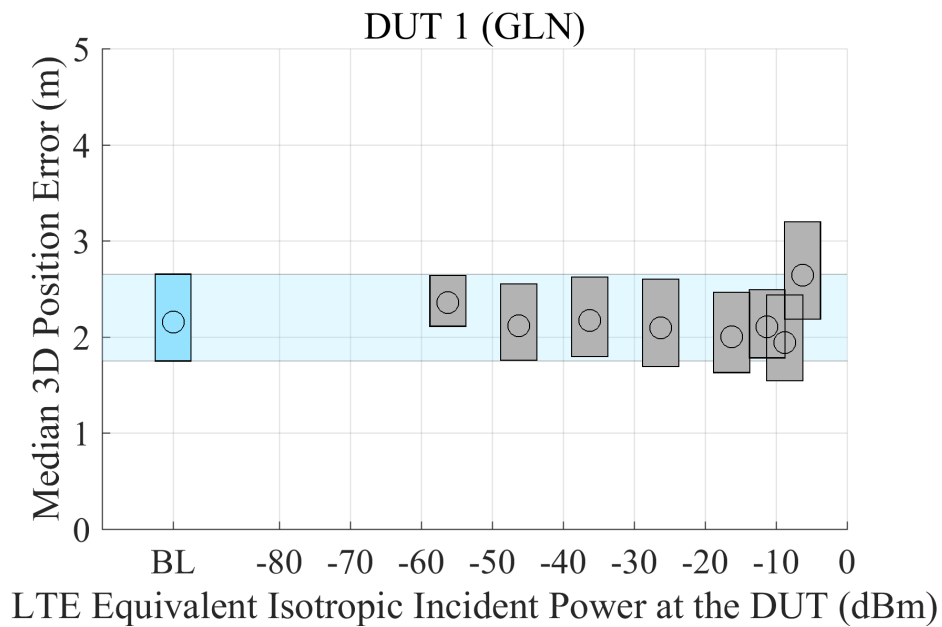
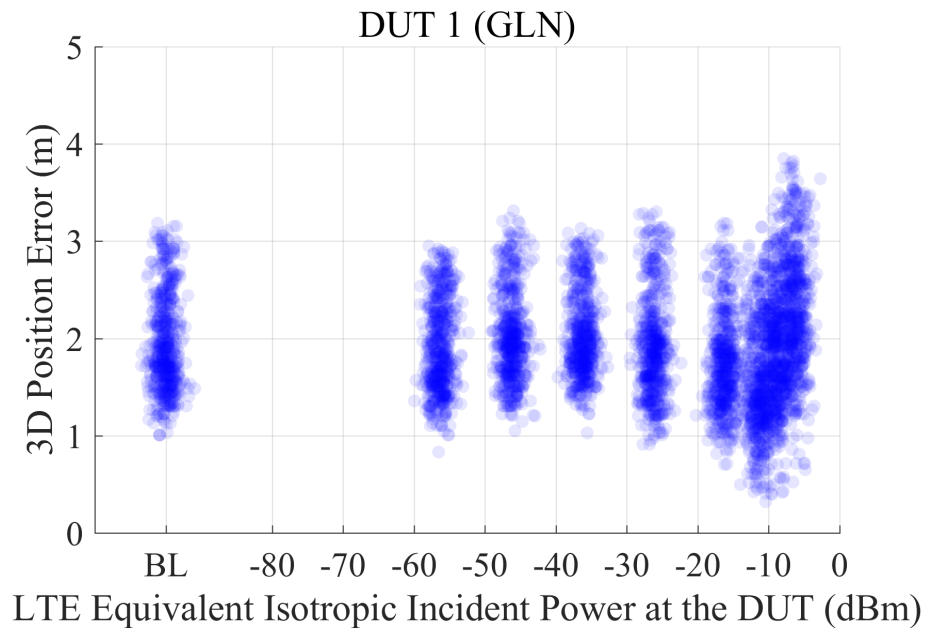


Figure 5.4: Example 3D position error plots for an LTE power sweep test. Top: scatter plot. Bottom: steady-state median plot. In the median plot, the boxes are 95% confidence regions, and the circular marker inside each box indicates a point estimate.

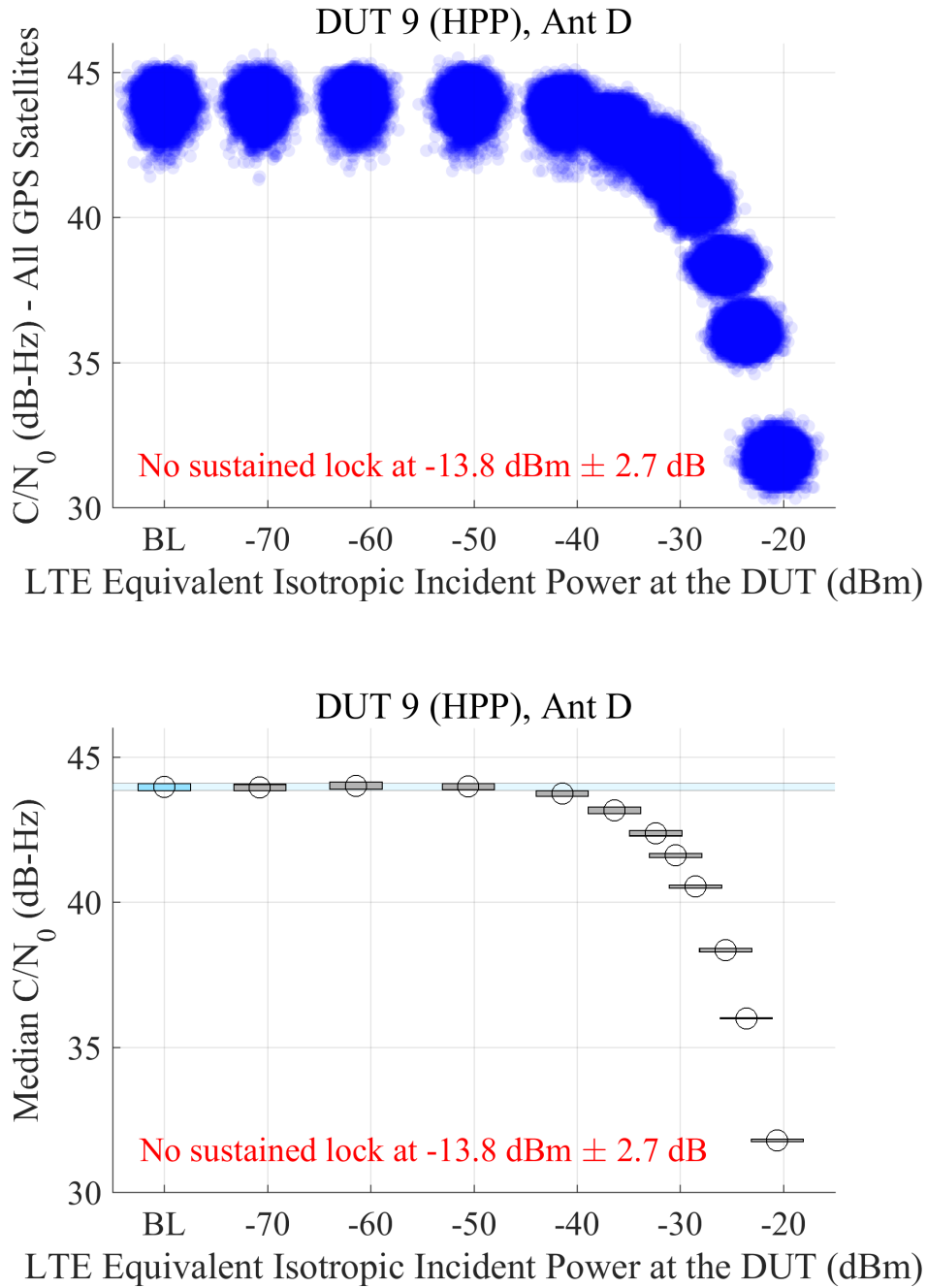


Figure 5.5: Example  $C/N_0$  plots for an LTE power sweep test under the nominal satellite condition. Top: scatter plot. Bottom: steady-state median plot. In the median plot, the boxes are 95% confidence regions, and the circular markers indicate point estimates.

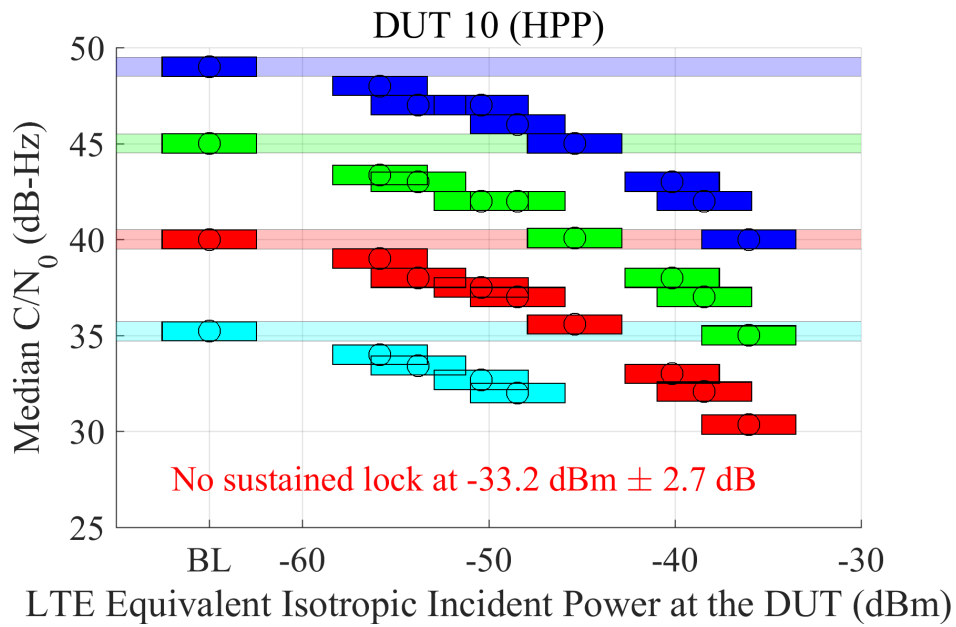
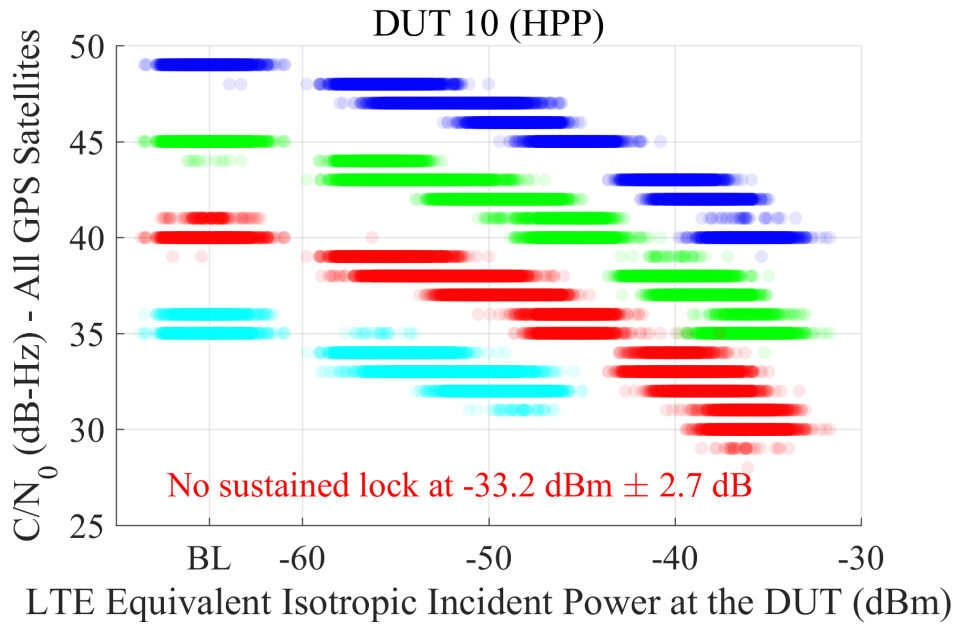


Figure 5.6: Example  $C/N_0$  plots for an LTE power sweep test under the limited satellite condition. Top: scatter plot. Bottom: plot of 95% confidence regions for the steady-state median of each satellite pair.

to the plots for the nominal satellite condition, the only difference is that a distinct color is used for each pair of GPS satellites with the same effective isotropic incident power (EIIP) at the DUT. Specifically, blue is used for satellites at  $-128.5 \text{ dBm} \pm 2.7 \text{ dB}$ , green is used for satellites at  $-133.5 \text{ dBm} \pm 2.7 \text{ dB}$ , red is used for satellites at  $-138.5 \text{ dBm} \pm 2.7 \text{ dB}$ , and cyan is for satellites at  $-143.5 \text{ dBm} \pm 2.7 \text{ dB}$ . Note that when a DUT does not report data for a given pair of satellites, that color is not shown on the plot.

Lastly, Figure 5.7 shows an example scatterplot for the number of satellites in view. Like the previously-described scatter plots, the data for each power level are shown for the full 20 minute collection period and the points are horizontally dithered.

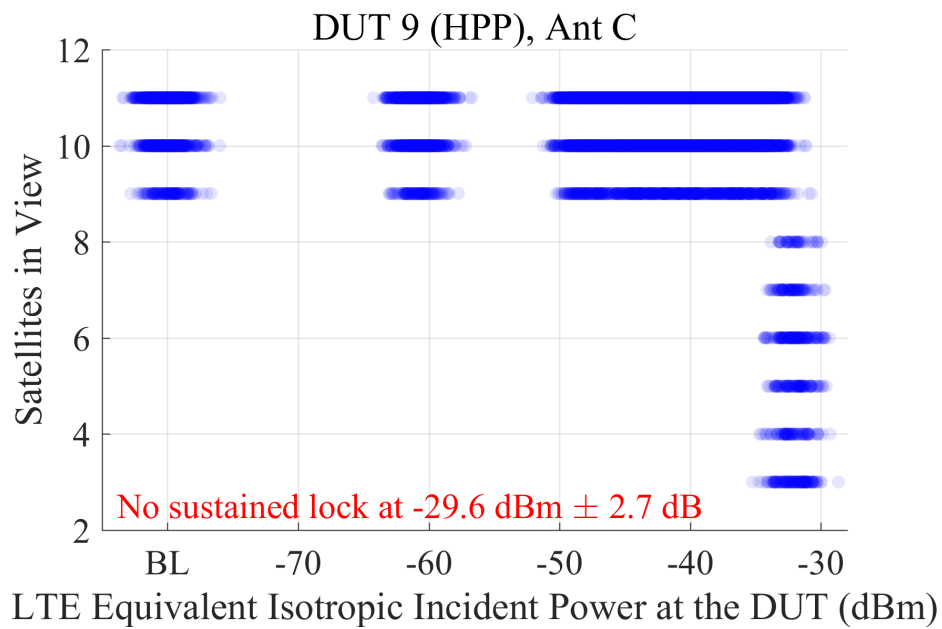


Figure 5.7: Example scatter plot for the number of satellites in view.

### 5.5.2 TTFF and TTFR Tests

Example plots for the TTFF and TTFR tests are shown in Figure 5.8. The top plot is a scatterplot of the TTFF at each power level. Like the LTE sweep plots, the data points are randomly dithered in the horizontal direction to aid visualization and to communicate LTE power uncertainty. Points representing TTFF trials for which no fix was acquired are placed at the “>120” tick mark.

The bottom plot in Figure 5.8 shows the empirical CDFs for TTFF at each power level. The solid lines indicate the CDF estimate and the dashed lines indicate pointwise 95% confidence bands. The color used for each CDF corresponds to the LTE power indicated by the colorbar on the right side.

In the LTE power colorbar, note that black indicates a baseline (BL) test with no LTE power. The remaining colors are divided into eight 10 dB intervals, centered at 0 dBm, -10 dBm, -20 dBm, etc. Each 10 dB interval is further subdivided into four 2.5 dB pieces, as indicated by the color gradations.

Although it is not shown on the example plots, note that if a fix was acquired for less than 20% of the TTFF or TTFR tests at a given LTE power level, then the power level is recorded with a red annotation at the top of the plots. For example, if the observation time was 120 s, and no fixes were acquired at -30 dBm, then an annotation of the form “Fix > 120 s at -30 dBm  $\pm$  2.7 dB” is written on the plot.

### 5.5.3 Timing Tests

Figures 5.9, 5.10, and 5.11 contain example plots for the timing tests. The color of each line-plot corresponds to the power level given by the colorbar on the right side, which is the same as that used for the TTFF CDF plots. Figure 5.9 is a plot of the warmed-up TIC time-series for each LTE power level. Figure 5.10 contains example plots for TDEV. The top plot shows TDEV for averaging times from 1 to 1024 seconds. Because the confidence bands for TDEV are too small to be visible, they are not shown in this plot. Therefore, to communicate the relative size of the pointwise 95% confidence bands, additional zoom plots of TDEV are provided for each DUT, as shown in Figure 5.10.

Figure 5.11 contains an example plot for the number of satellites in view. Note that the number of satellites in view data are plotted as a time series for each power level rather than a scatter plot. The choice to use time series plots for the number of satellites in view was motivated by the fact that the number of satellites in the simulated GPS constellation changed over the course of the timing tests, which was not the case for the LTE power sweep tests of GLN, HPP, and RTK devices.

When  $C/N_0$  data was available, which was the case for most GPSDO DUTs, it was plotted as described above for the LTE power sweep tests.

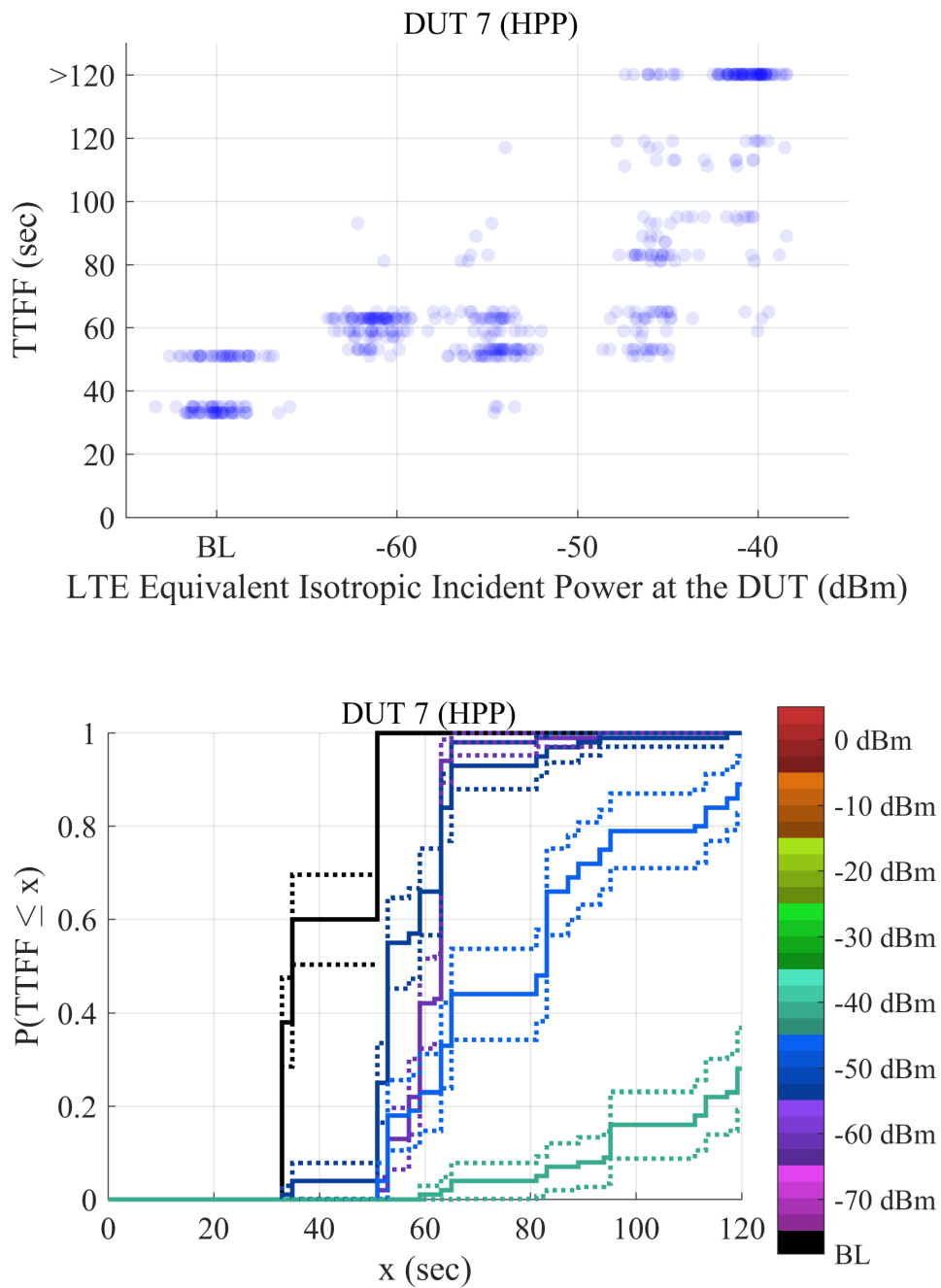


Figure 5.8: Example plots for TTF and TTFR tests. Top: Scatter plot. Bottom: Empirical CDF plot.

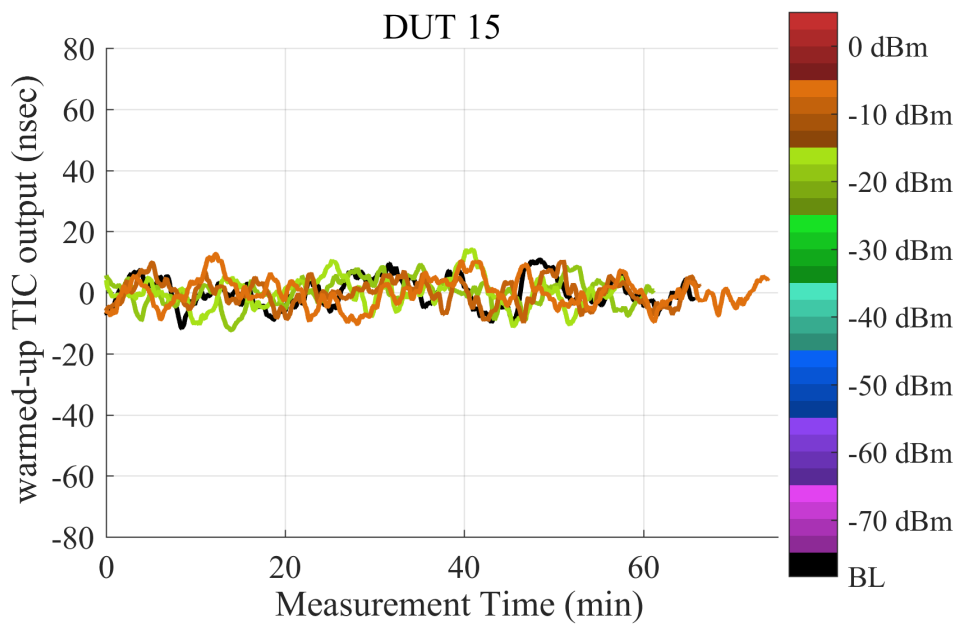


Figure 5.9: Example plot of warmed-up TIC output for a timing test.

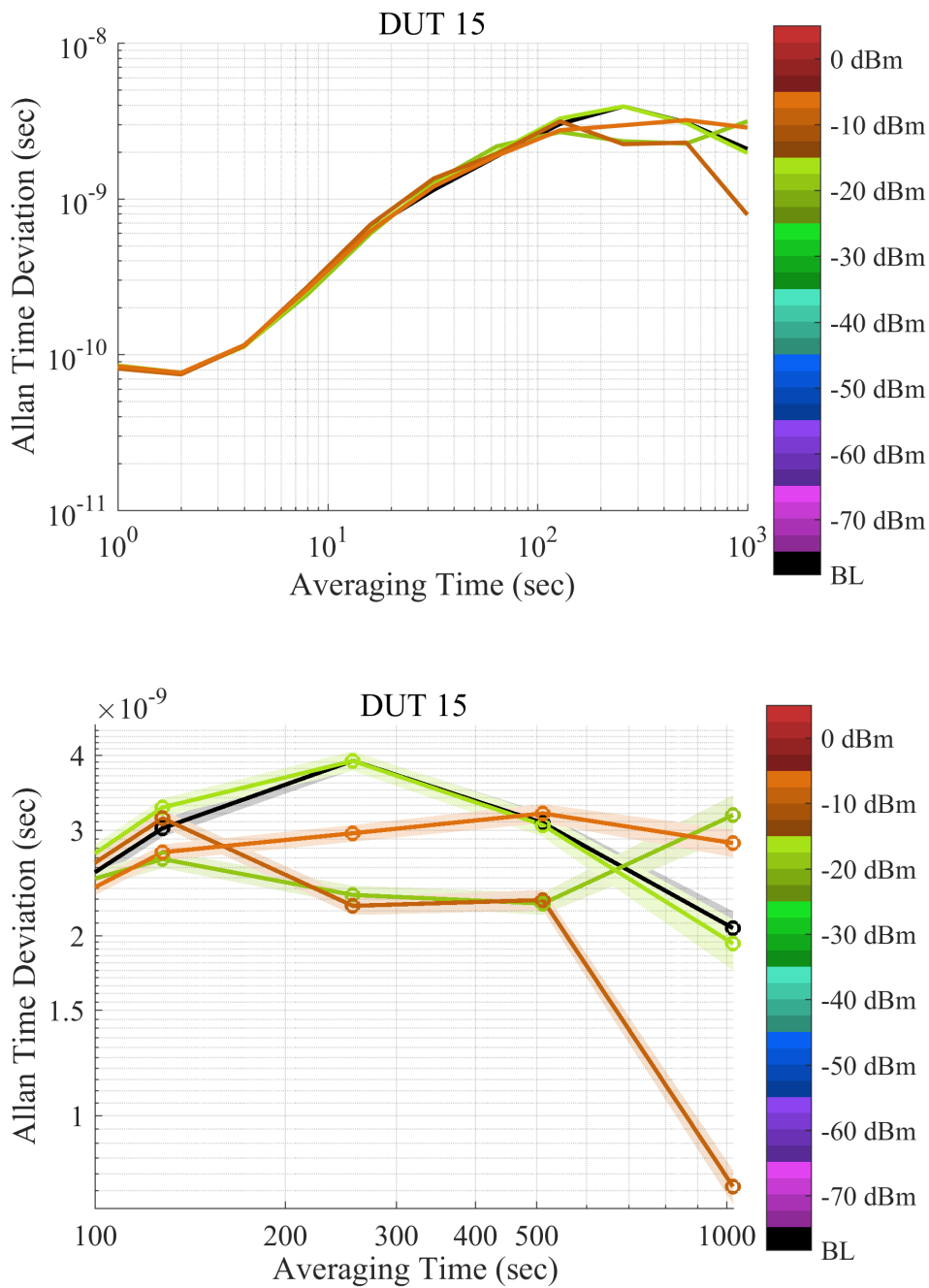


Figure 5.10: Example plots of Allan time deviation (TDEV) for a timing test. Top: TDEV plotted versus averaging time. Bottom: Zoom plot of TDEV, with shaded regions indicating pointwise 95% confidence bands.

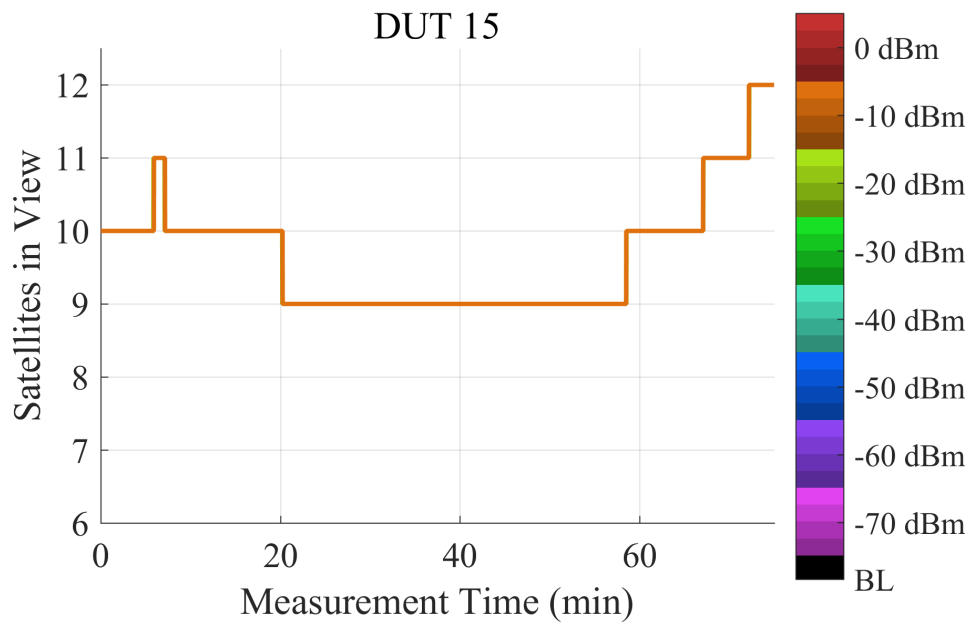


Figure 5.11: Example plot of Number of Satellites in View for a timing test.

## 5.6 Data Files Accompanying This Report

A set of over 3,800 CSV files (780 MB) comprising our test data after the parsing and wrangling steps is available along with this report. A list of the (DUT-dependent) measurands is given in Table 5.4.

The files are organized in a nested directory structure, where the directory levels correspond to test type, device class & LTE type, and DUT number, respectively. For the LTE power sweep tests, the data files are separated by LTE power level. By contrast, for TTFF and TTFR tests, the data for all LTE power levels for a given DUT and LTE type are listed in a single file. A detailed description of the file headers is included with the data files.

Table 5.4: Measurands (Subject to Availability) Provided in Data Files.

Parameter	Format	Source	Notes
UTC date/time	YY-MM-DD HH:MM:SS.ff	DUT	When missing: forward-filled with most recent previous timestamp
Latitude	Float	DUT	Degrees, negative value: South
Longitude	Float	DUT	Degrees, negative value: West
Altitude	Float	DUT	Meters, WGS84 model
3D Position Error	Float	DUT GPS simulator	Meters, Euclidean distance from simulator truth
Fix indicator	Boolean 0 or 1	DUT	0: no-fix or 1: fix <sup>1</sup>
$C/N_0$	Integer/Float <sup>2</sup>	DUT	dB-Hz, by satellite PRN
Pseudorange	Float	DUT	Meters, L1 only, by satellite PRN
Pseudorange Error	Float	DUT GPS simulator	Meters, L1 only, by satellite PRN difference with simulator truth
Carrier phase	Float	DUT	Cycles, L1 only, by satellite PRN
raw TIC measurement	Float	TIC, DUT GPS simulator	Seconds, 1 PPS difference, last 75 minutes of test
processed TIC measurement	Float	TIC, DUT GPS simulator	Nanoseconds, warm-up period excluded and mean subtracted
TTFF	Integer	DUT	Seconds
TTFR	Integer	DUT	Seconds

<sup>1</sup>Fix quality necessary to preserve functionality of the system. e.g. An RTK unit that drops its fix quality below its threshold for providing RTK solutions may still provide valid non-RTK GPS solutions. However, as it is no longer functioning as a RTK unit, the fix indicator is set to zero.

<sup>2</sup> Integer rounded format from standard NMEA strings, floating-point precision from manufacturer-specific strings. The CSV file reports the highest precision  $C/N_0$  available.

## 6 Test Results

### 6.1 Summary

This chapter presents plots summarizing the test results for each test condition and device class. Details on the types of plots presented in this chapter can be found in Section 5.5. A brief summary of the types of plots for each test type is given below.

- Long-term evolution (LTE) power level sweeps for general location and navigation (GLN), high-performance positioning (HPP), and real-time kinematic (RTK) devices:
  - Scatter plots versus LTE power for 3D position error (3DPE), carrier-to-noise-density ratio ( $C/N_0$ ), and the number of satellites in view
  - Plots of 95% confidence regions for the median versus LTE power for 3DPE and  $C/N_0$
- LTE power level sweeps for GPS-disciplined oscillator (GPSDO) devices:
  - Time-series plots of warmed-up time interval counter (TIC) output
  - Plots of Allan Time Deviation (TDEV) for the warmed-up TIC data
  - Time-series plots of the number of satellites in view
  - $C/N_0$  Scatter plots and 95% confidence regions for median versus LTE power (When  $C/N_0$  is available from DUT)
- Time to first fix (TTFF) and time to first reacquisition (TTFR) tests
  - Scatter plots of TTFF or TTFR versus LTE power
  - Plots of empirical cumulative distribution function (CDF) for time to first fix (TTFF) and TTFR at each tested power level. Solid lines indicate the CDF estimate and dashed line indicate pointwise 95% confidence bands.

The plot types listed above are presented in sections Section 6.3 - Section 6.5. First, Section 6.2 presents measurements of the frequency response for each external antenna.

## 6.2 Frequency Response of DUT Antennas

The antenna response was measured for the antennas listed in Table 2.4. The test was performed with the device under test (DUT) receive antenna and right-hand circularly-polarized (RHCP) global positioning system (GPS) source antenna in the test configuration outlined in Figure 3.7. The response was measured with a vector network analyzer (VNA). As the majority of antennas were active, a bias-tee (Minicircuits ZFBT-282-1.5A) was connected in line to drive the active antennas with a direct current (DC) voltage source. Applied voltage depended on the antenna specification. Antenna names have been anonymized but correspond to antenna names called out in testing of DUTs (e.g., Ant C in Figure 6.1 is the same antenna as called out in DUT 9 (HPP), Ant C).

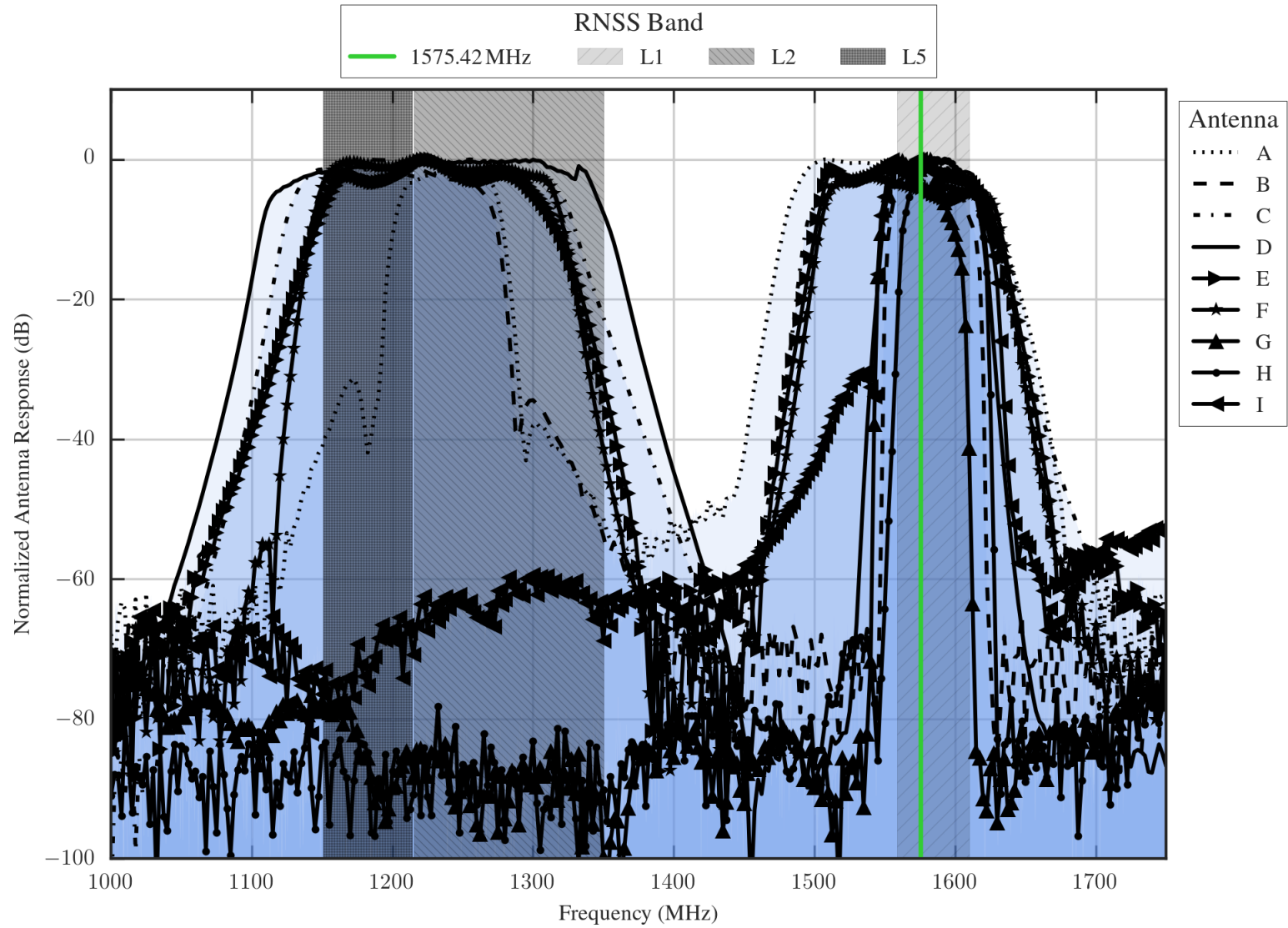


Figure 6.1: Normalized  $S_{21}$  S-parameter responses of external DUT antennas.

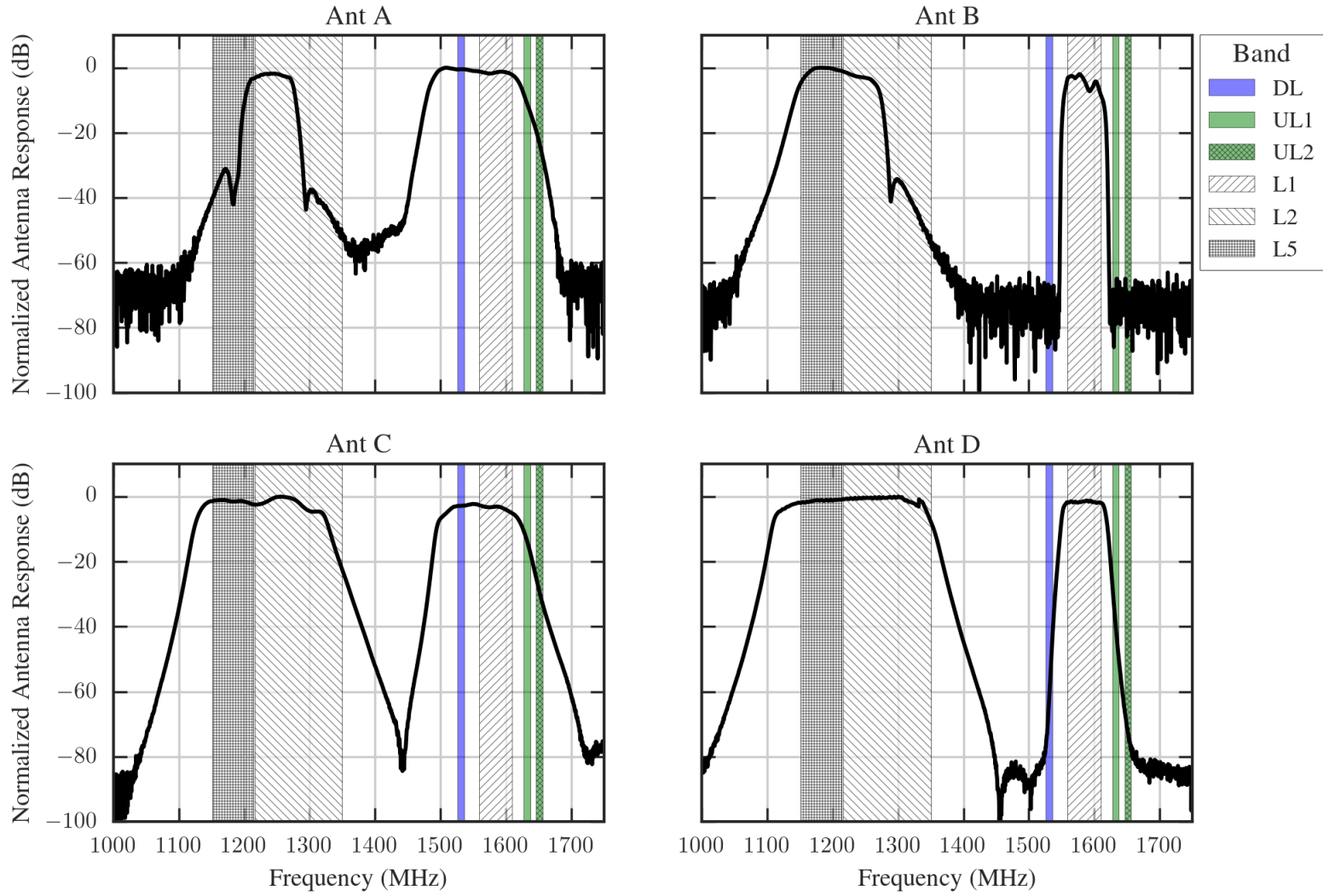


Figure 6.2: Normalized  $S_{21}$  S-parameter responses of external DUT antennas.

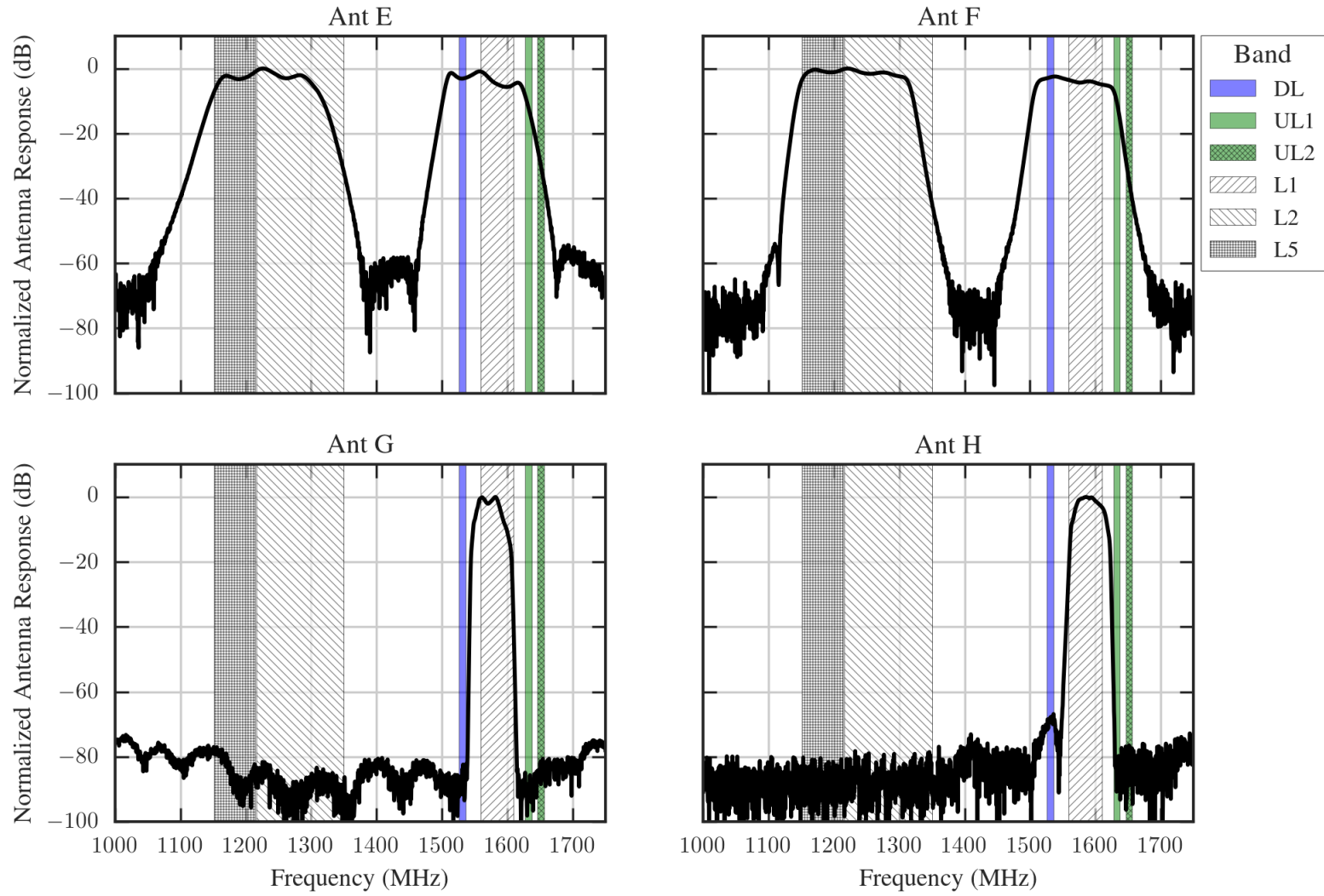


Figure 6.3: Normalized  $S_{21}$  S-parameter responses of external DUT antennas.

### 6.3 LTE Power Level Sweeps for Nominal GPS Power Exposure

Previous parts of this report address the definition and execution of these tests:

- The GPS receivers under test are listed in Subsection 2.1.1.
- The incident power condition, effective isotropic incident power (EIIP), is defined in Subsection 2.1.4.
- The simulated GPS signal parameters are listed in Section 2.2.
- The simulated GPS constellation parameters in the nominal power scenario are listed in Subsubsection 2.2.2.1.
- The radiated LTE waveforms are listed in Section 2.3.
- Parameters for the LTE power sweep tests are given in Subsection 2.4.1.
- The tests executed for each DUT are listed in Table 2.8.
- The transmission system that creates the test conditions is detailed in Chapter 3.
- Each DUT under test is positioned according to Section 4.2.
- The test procedure for LTE power level sweeps is detailed by Subsection 4.3.1.
- Data acquisition from each DUT is described by Section 4.4.
- Data processing and analysis are described in Chapter 5.
- LTE equivalent isotropic incident power at the DUT (dBm) for the GPSDO tests can be found in Table 6.1.

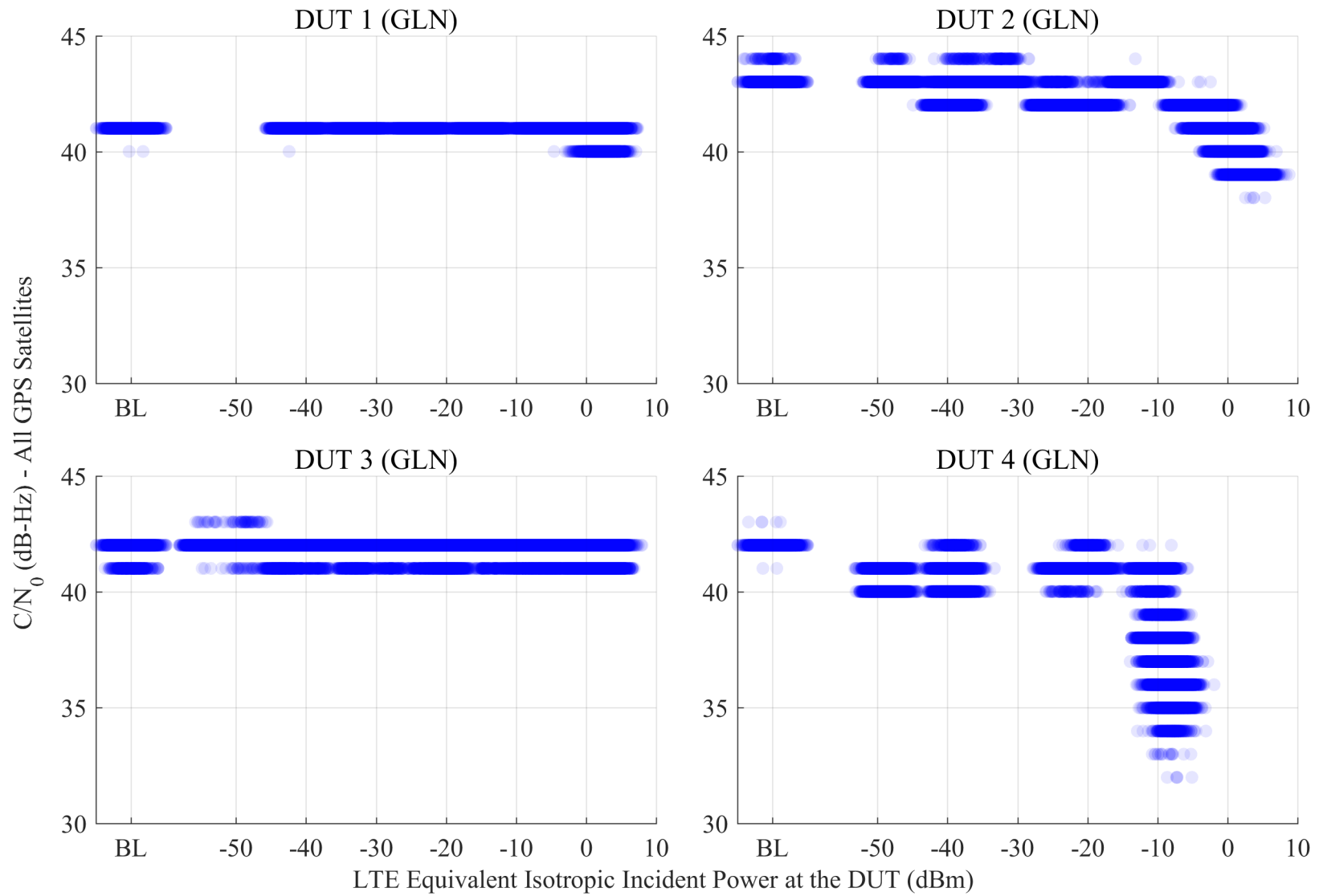


Figure 6.4: Scatterplots of reported  $C/N_0$  from GLN receivers, swept with LTE power level. The GPS scenario is nominal, and the type of incident LTE is DL.

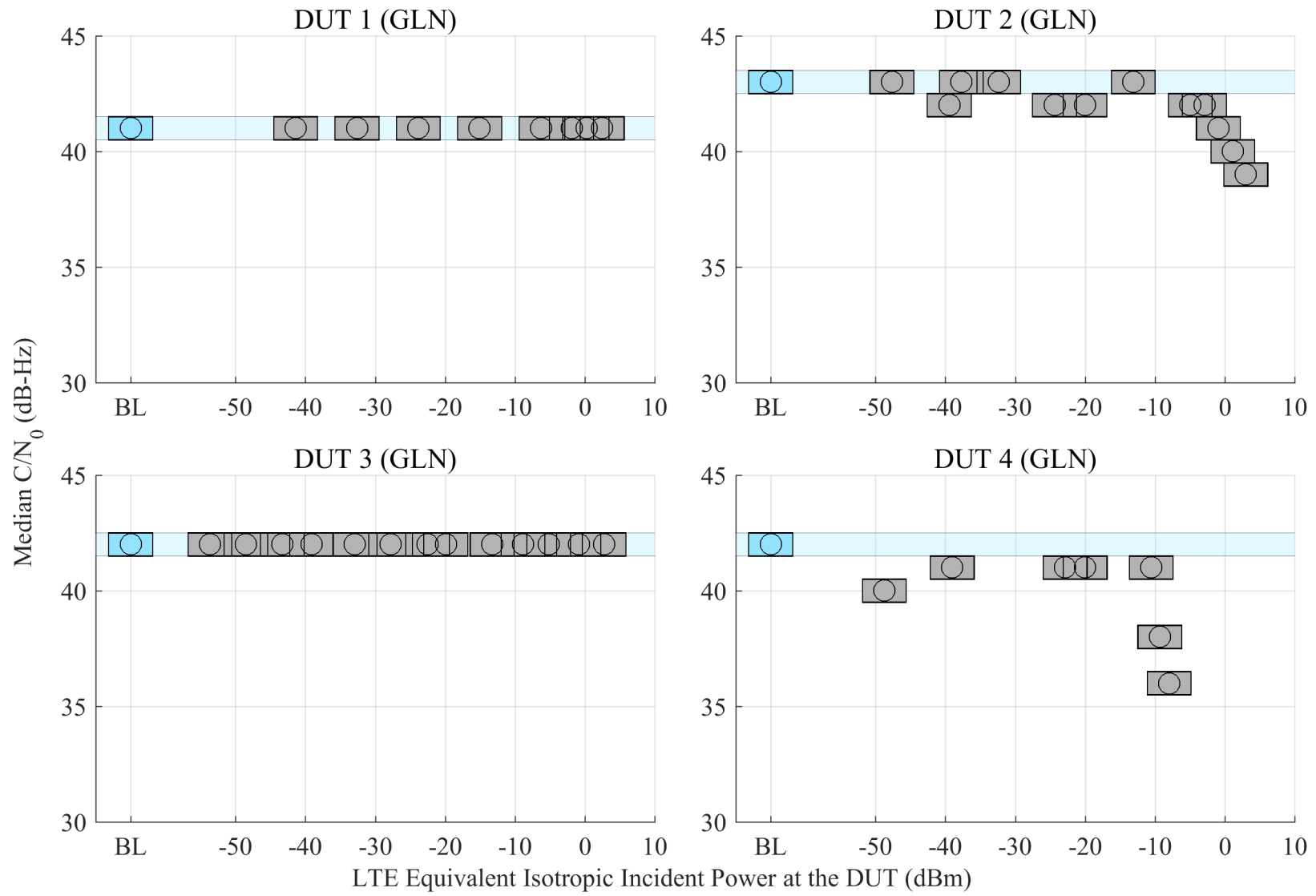


Figure 6.5: Estimated 95% confidence regions of the median of reported  $C/N_0$  from GLN receivers, swept with LTE power level. The GPS scenario is nominal, and the type of incident LTE is DL.

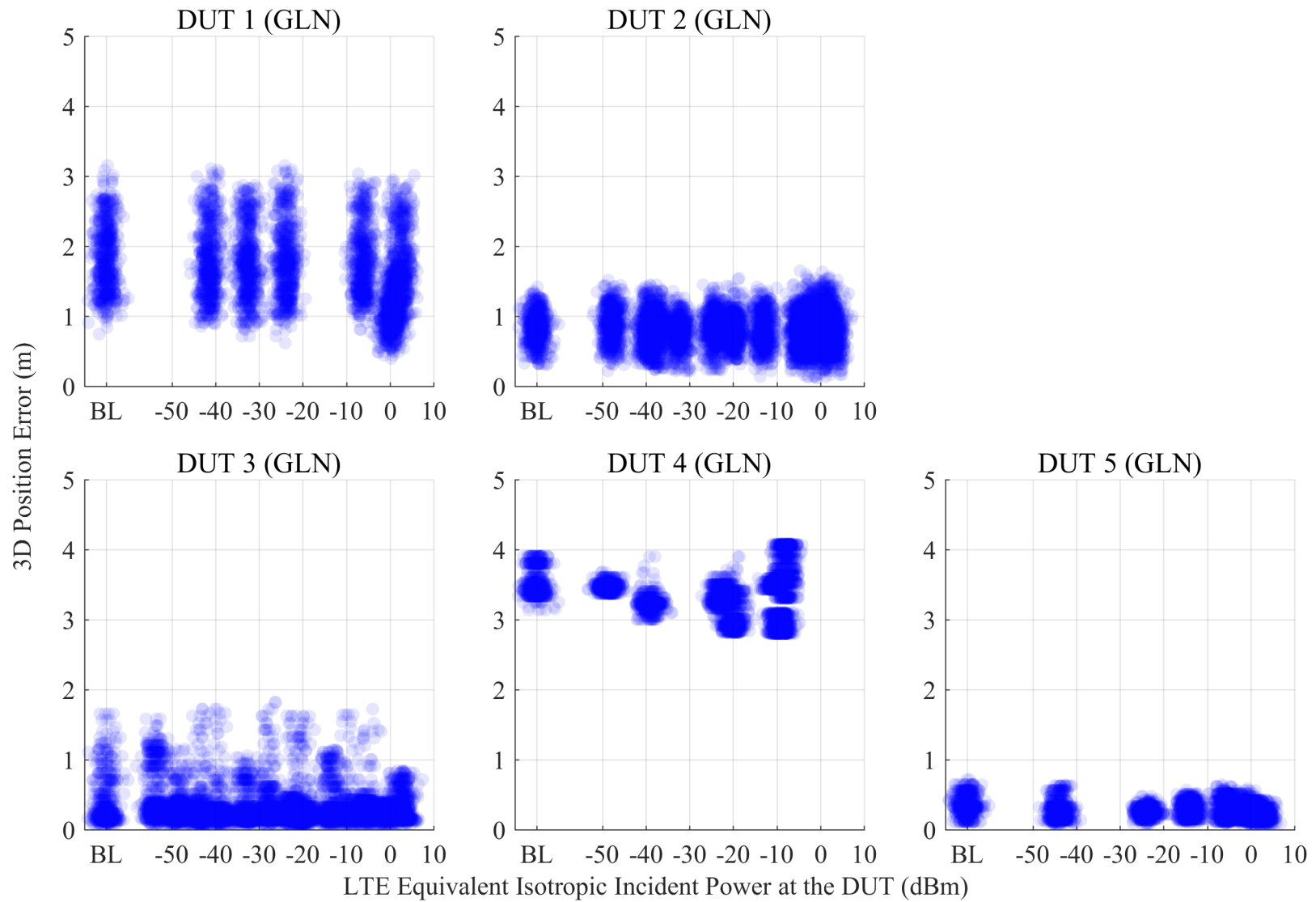


Figure 6.6: Scatterplots of error in reported 3-D position compared to simulator truth from GLN receivers, swept with LTE power level. The GPS scenario is nominal, and the type of incident LTE is DL.

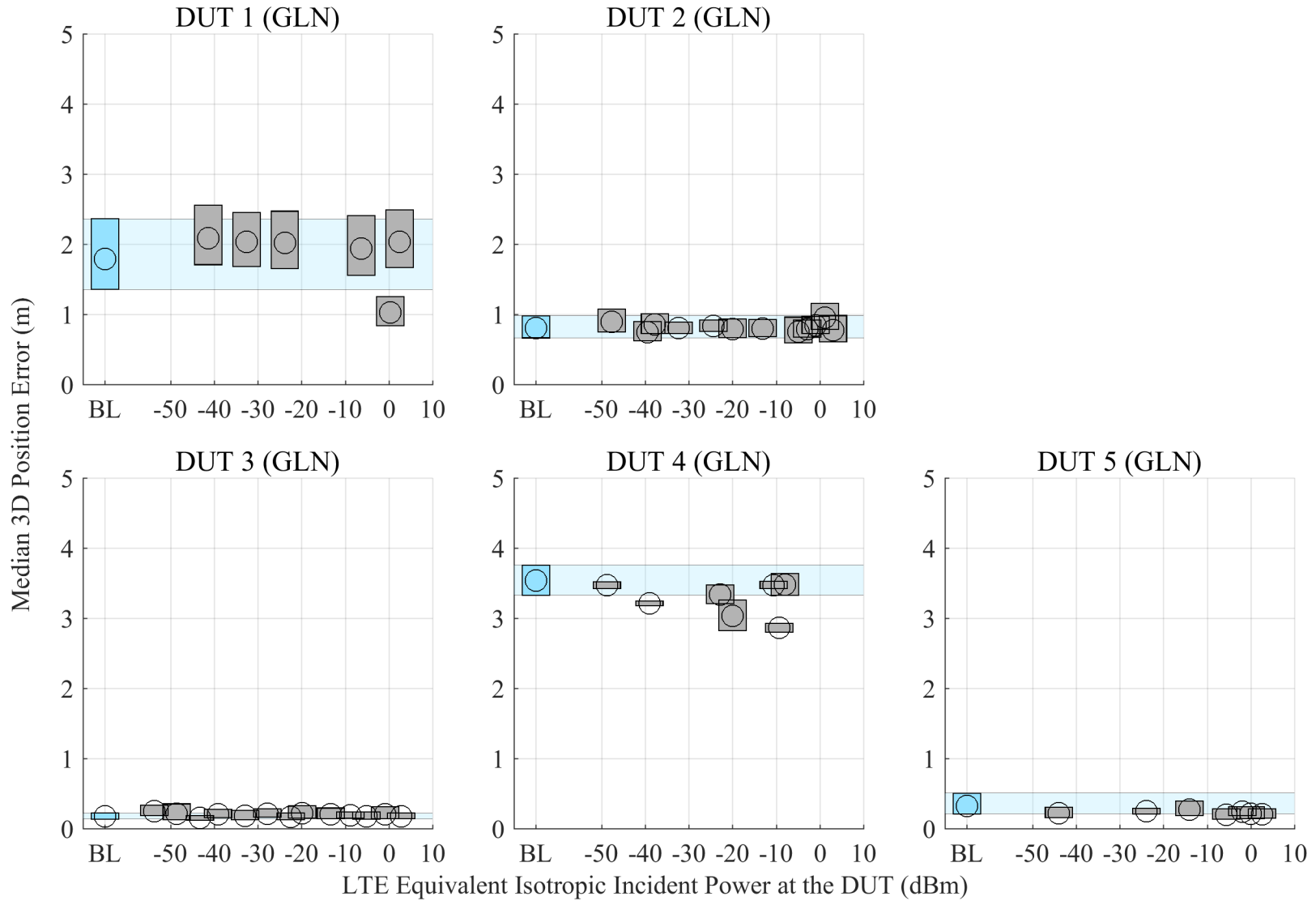


Figure 6.7: Estimated 95% confidence regions of the median error in reported 3-D position from GLN receivers, swept with LTE power level. The GPS scenario is nominal, and the type of incident LTE is DL.

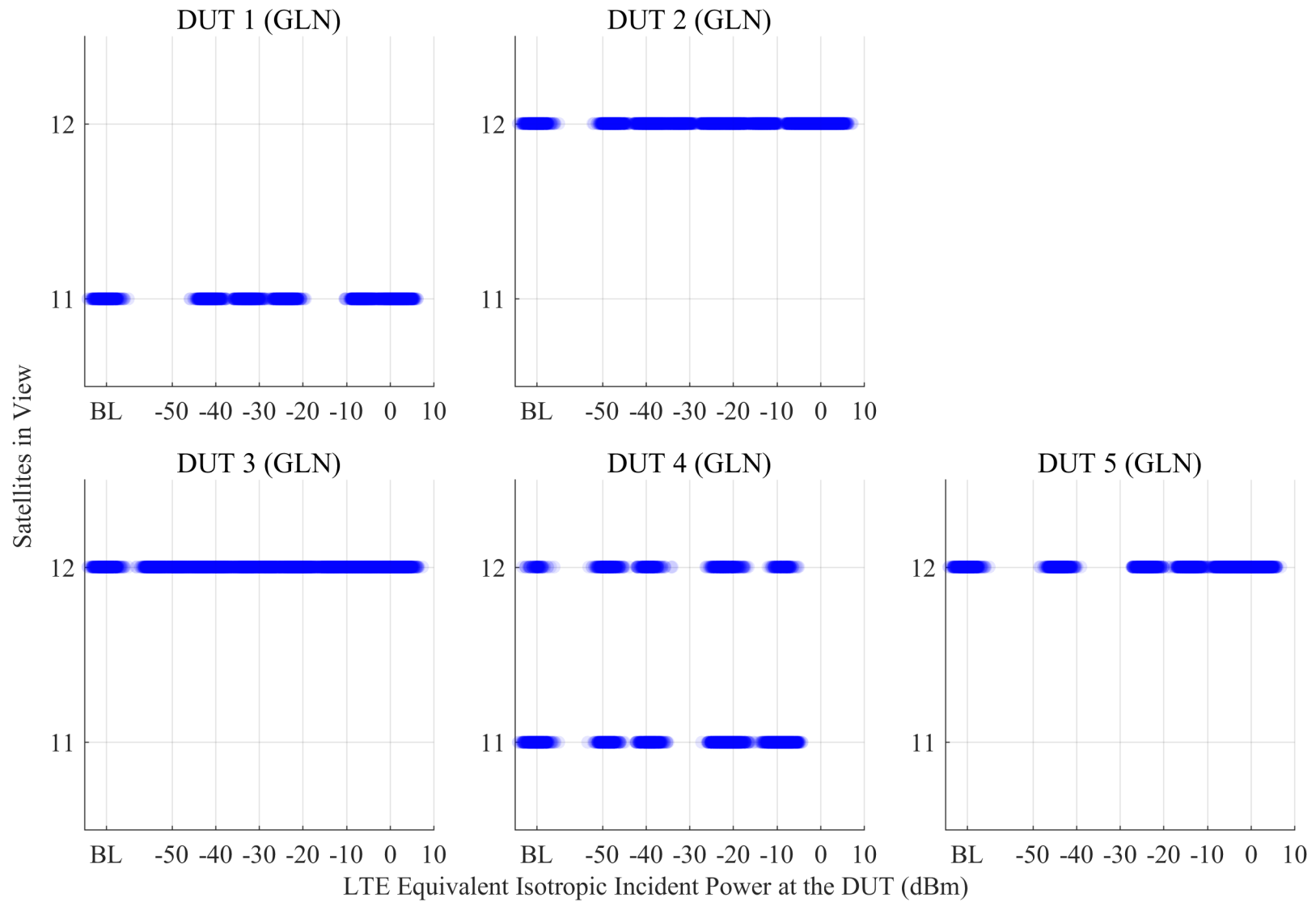


Figure 6.8: Scatterplots of the number of satellites in view from GLN receivers, swept with LTE power level. The GPS scenario is nominal, and the type of incident LTE is DL.

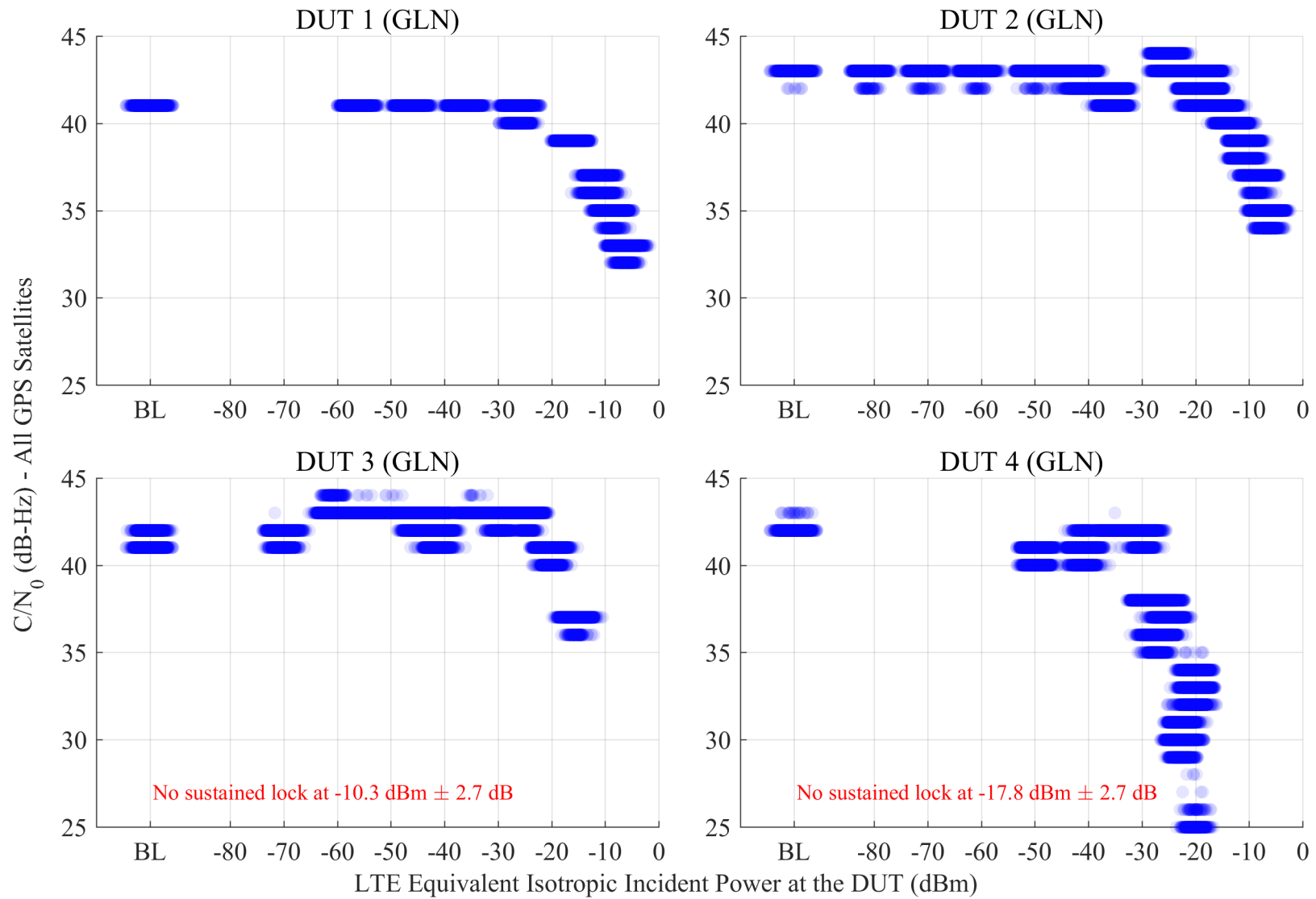


Figure 6.9: Scatterplots of reported  $C/N_0$  from GLN receivers, swept with LTE power level. The GPS scenario is nominal, and the type of incident LTE is UL1.

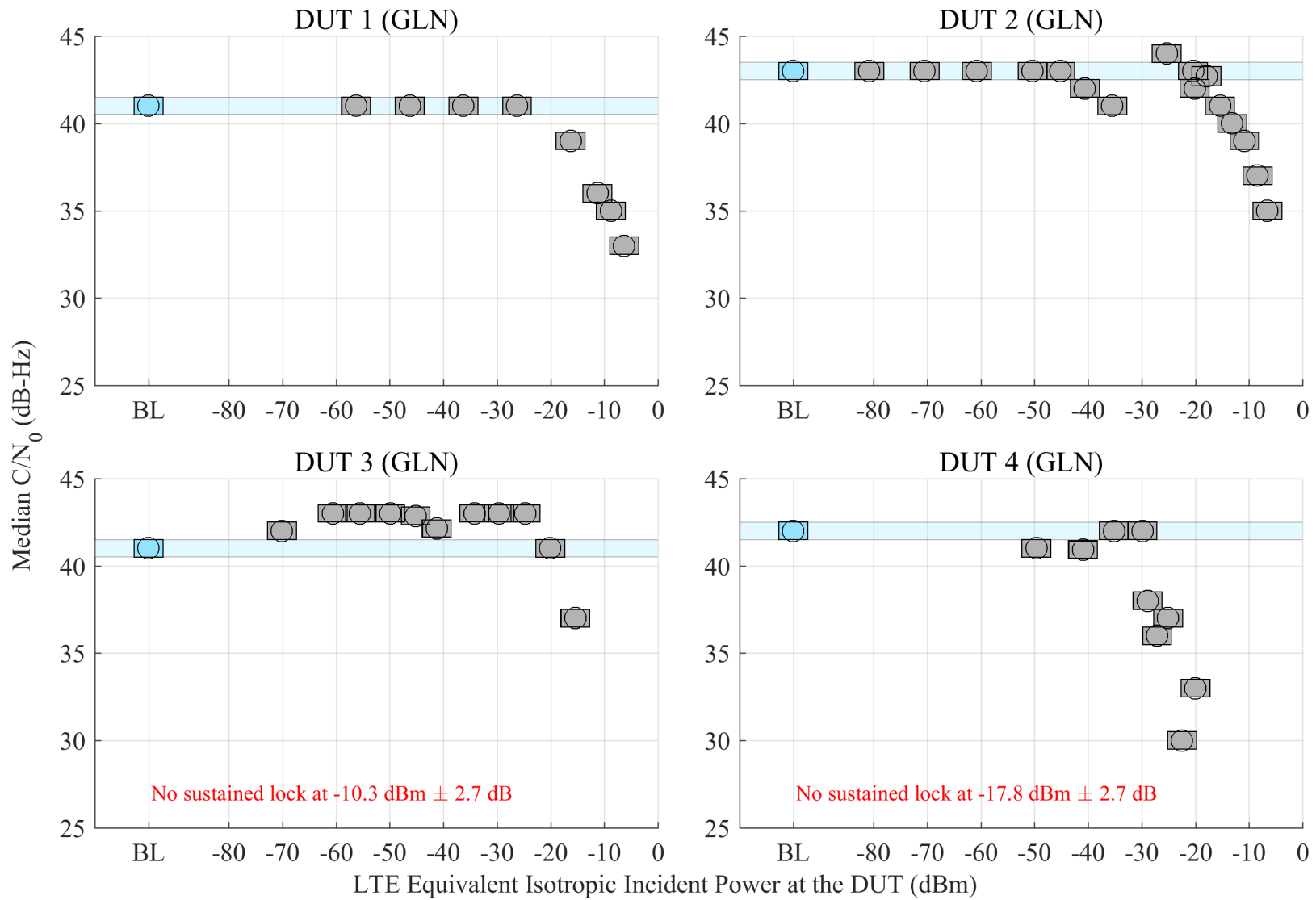


Figure 6.10: Estimated 95% confidence regions of the median of reported  $C/N_0$  from GLN receivers, swept with LTE power level. The GPS scenario is nominal, and the type of incident LTE is UL1.

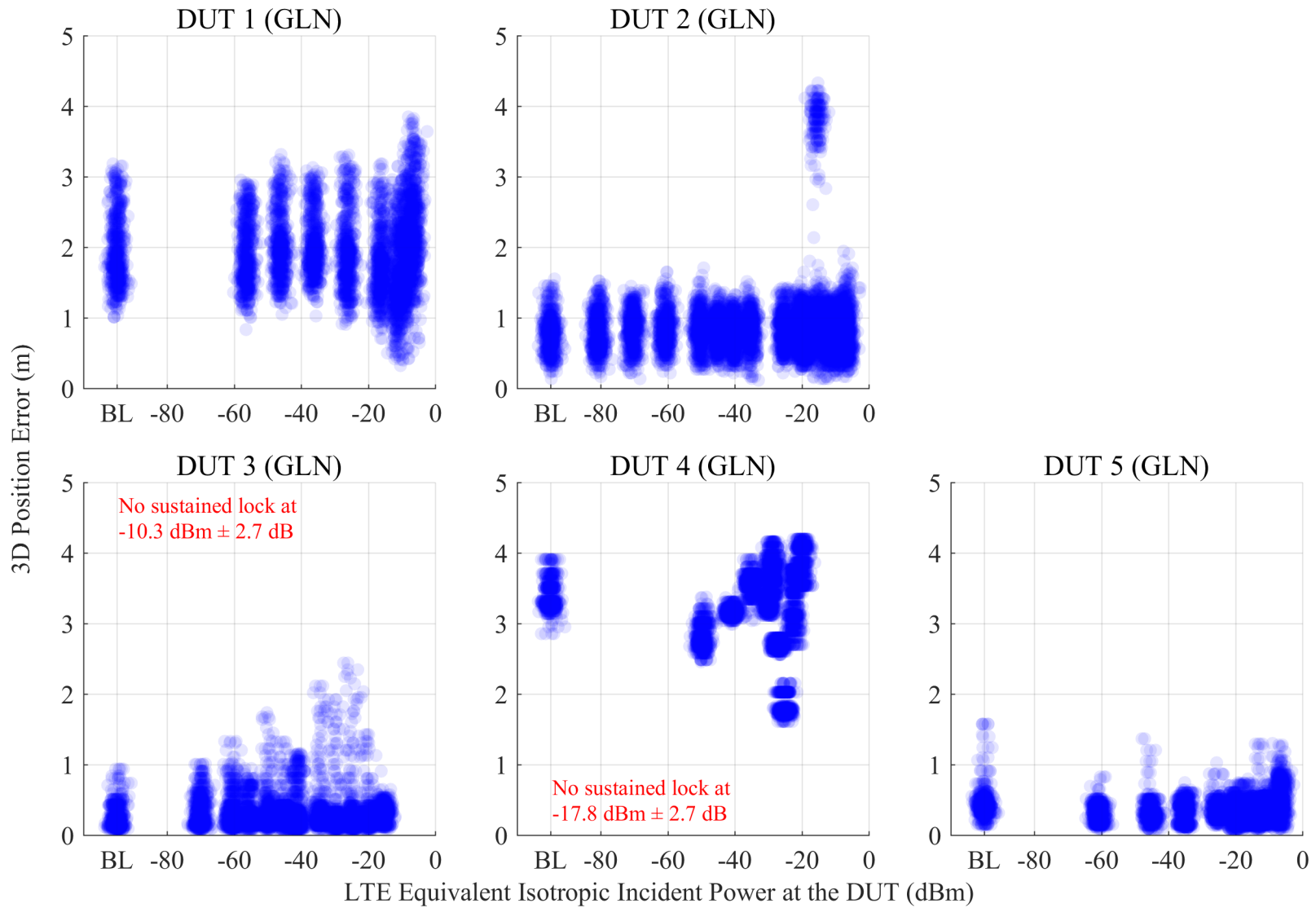


Figure 6.11: Scatterplots of error in reported 3-D position compared to simulator truth from GLN receivers, swept with LTE power level. The GPS scenario is nominal, and the type of incident LTE is UL1.

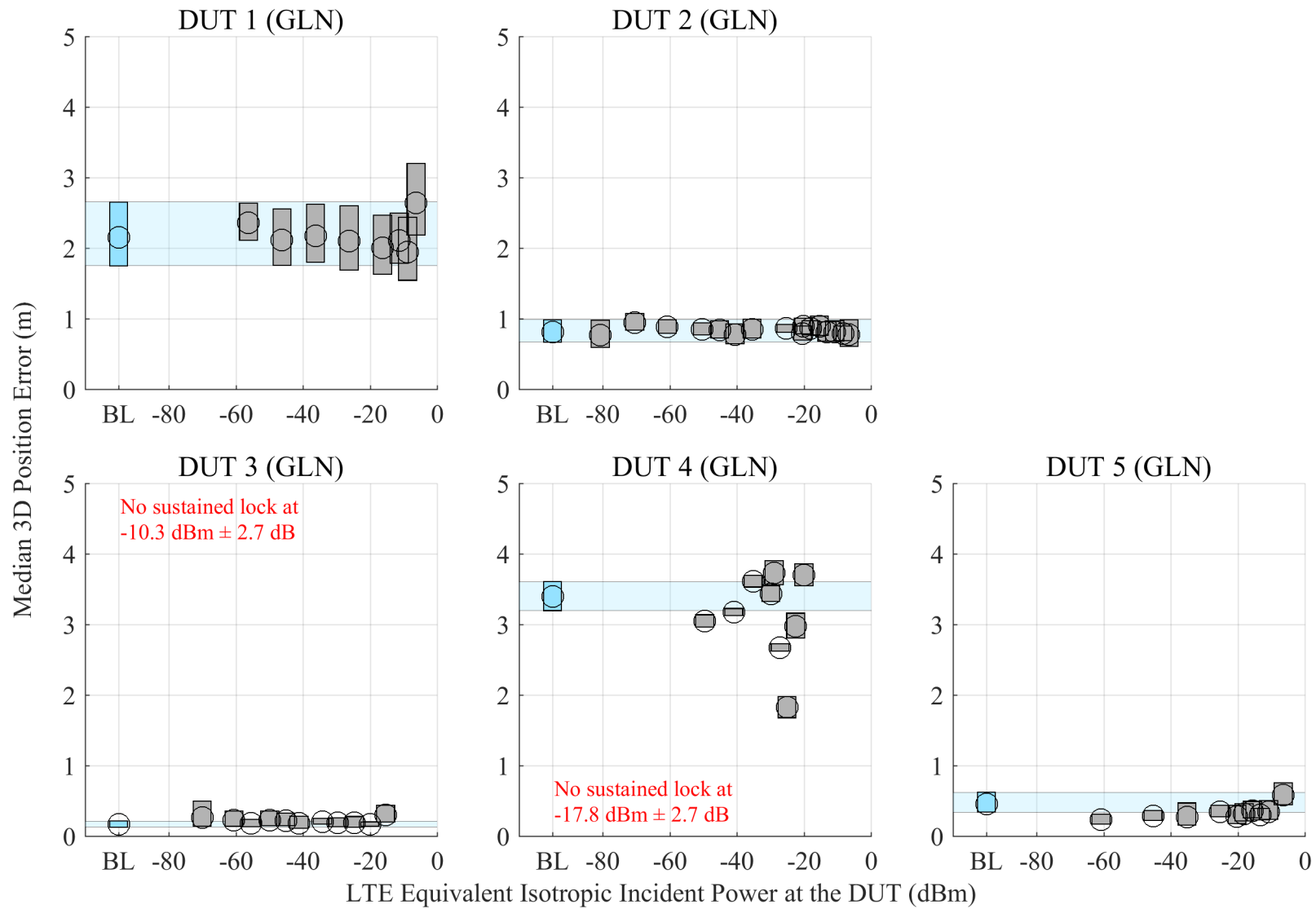


Figure 6.12: Estimated 95% confidence regions of the median error in reported 3-D position from GLN receivers, swept with LTE power level. The GPS scenario is nominal, and the type of incident LTE is UL1.

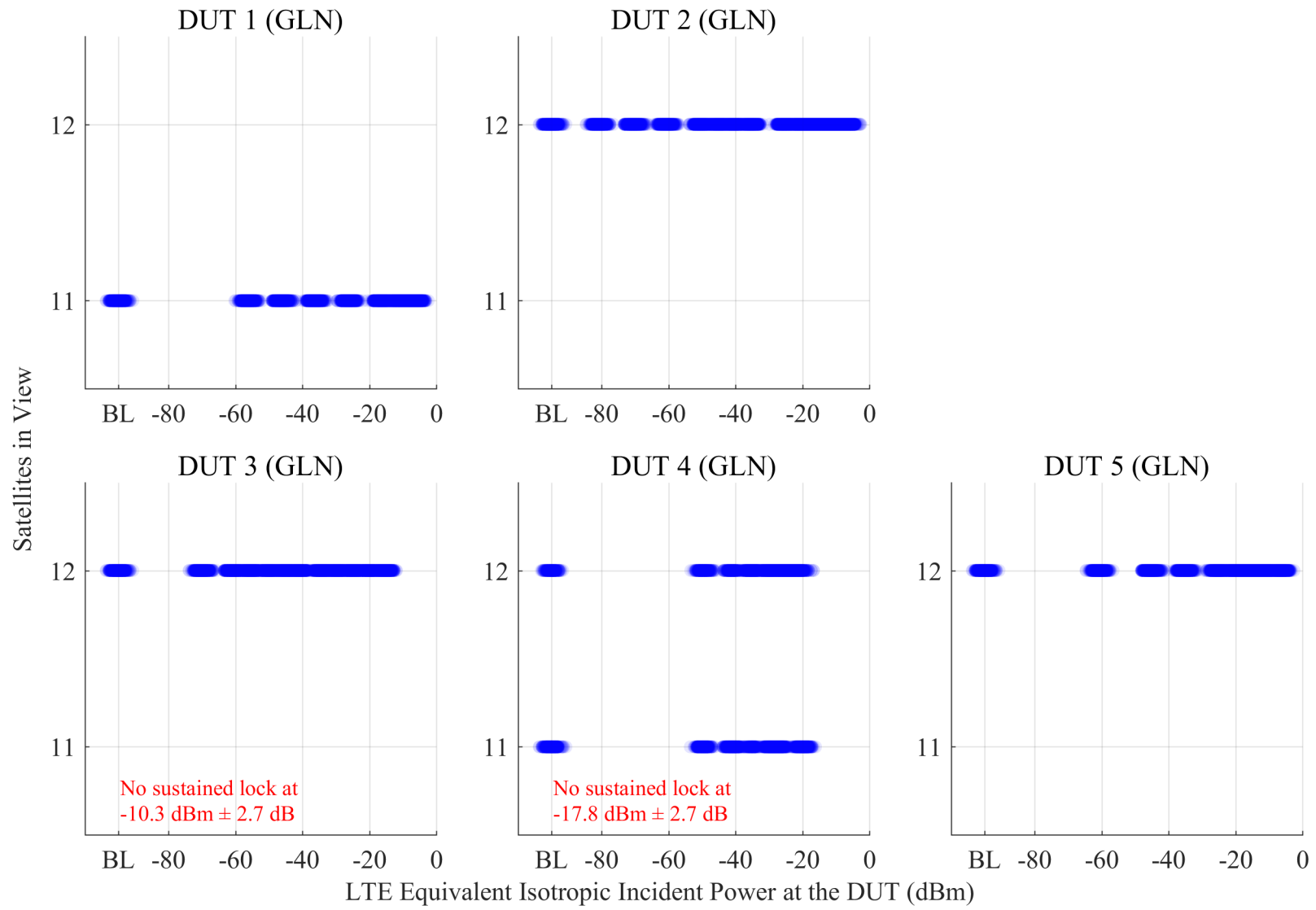


Figure 6.13: Scatterplots of the number of satellites in view from GLN receivers, swept with LTE power level. The GPS scenario is nominal, and the type of incident LTE is UL1.

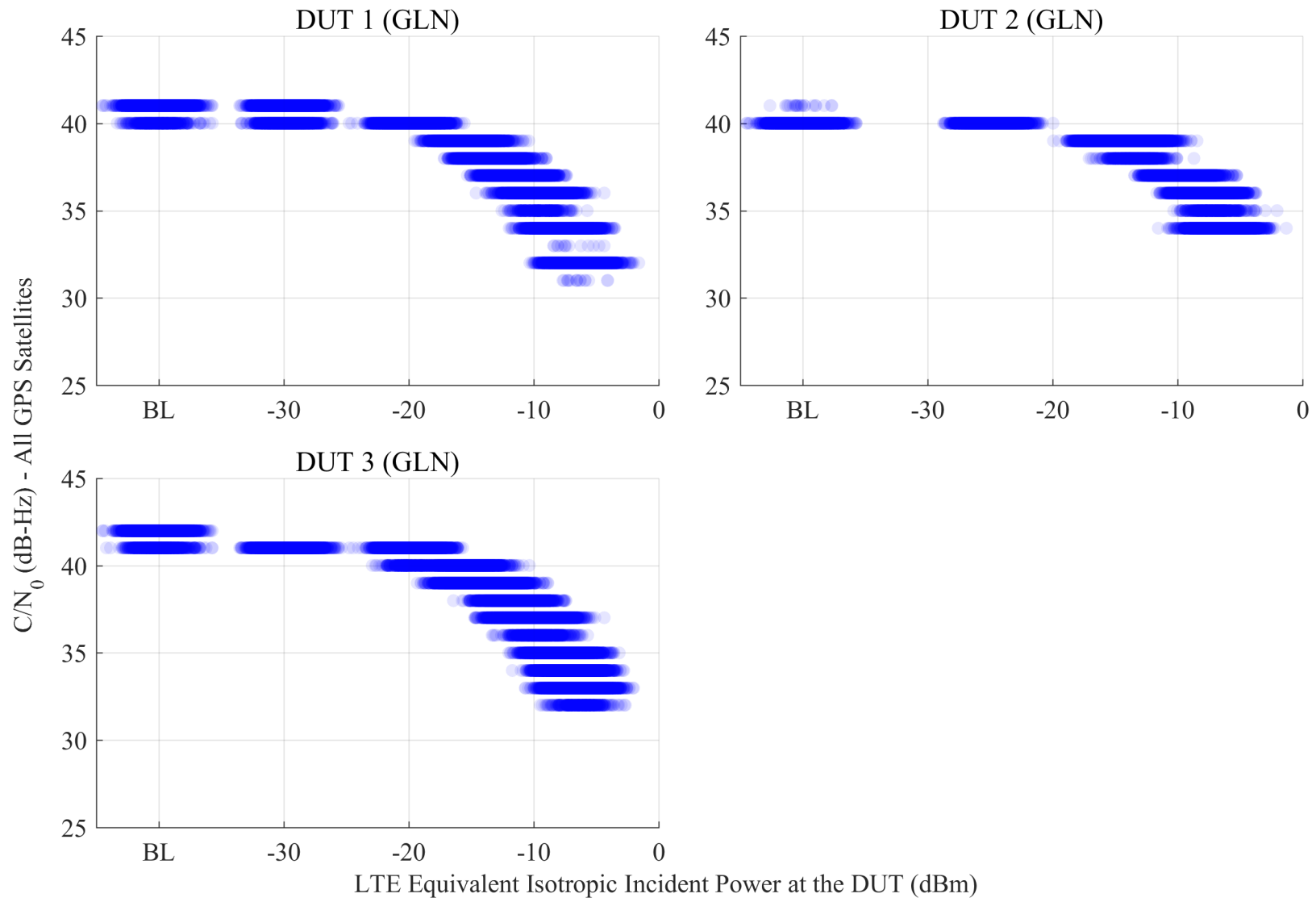


Figure 6.14: Scatterplots of reported  $C/N_0$  from GLN receivers, swept with LTE power level. The GPS scenario is nominal, and the type of incident LTE is UL2.

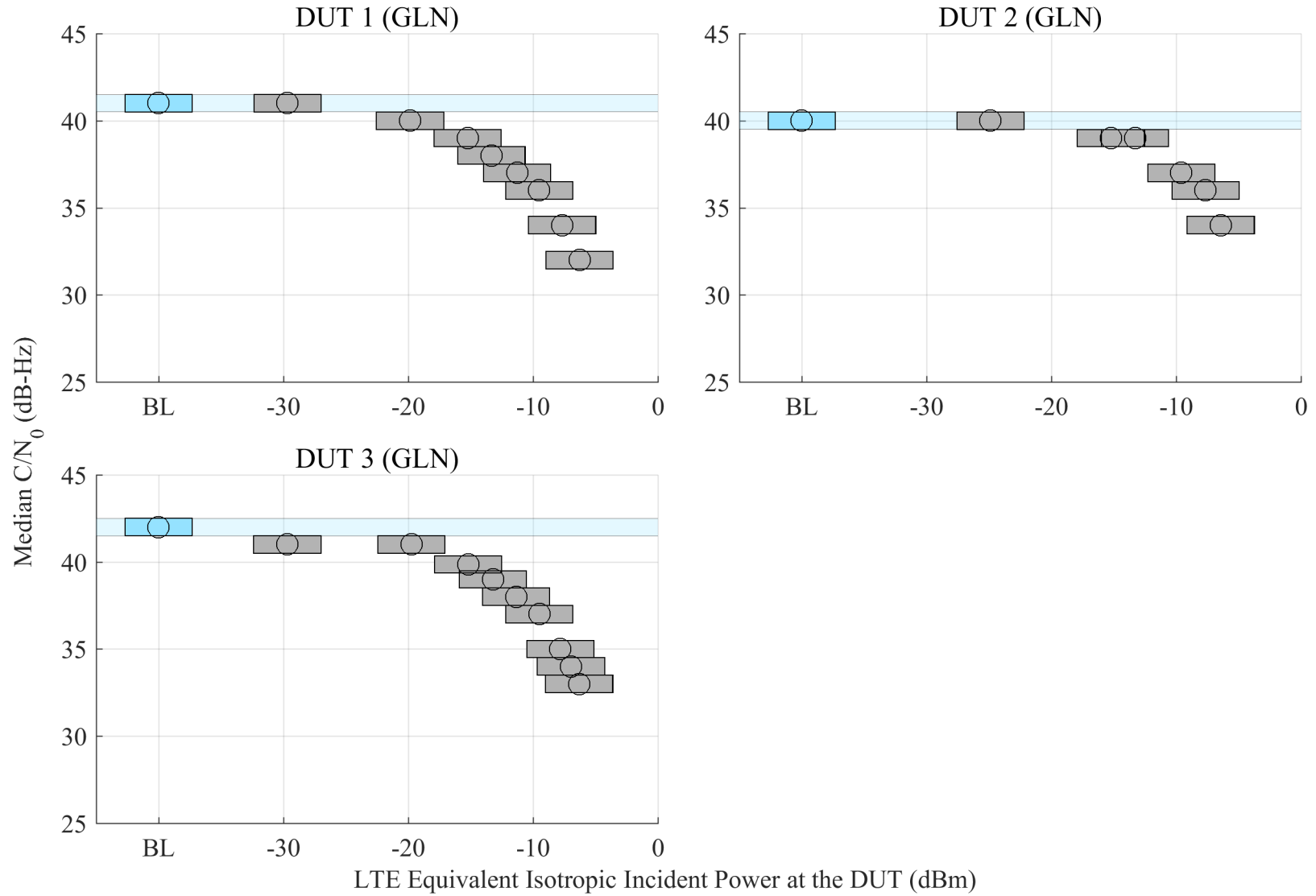


Figure 6.15: Estimated 95% confidence regions of the median of reported  $C/N_0$  from GLN receivers, swept with LTE power level. The GPS scenario is nominal, and the type of incident LTE is UL2.

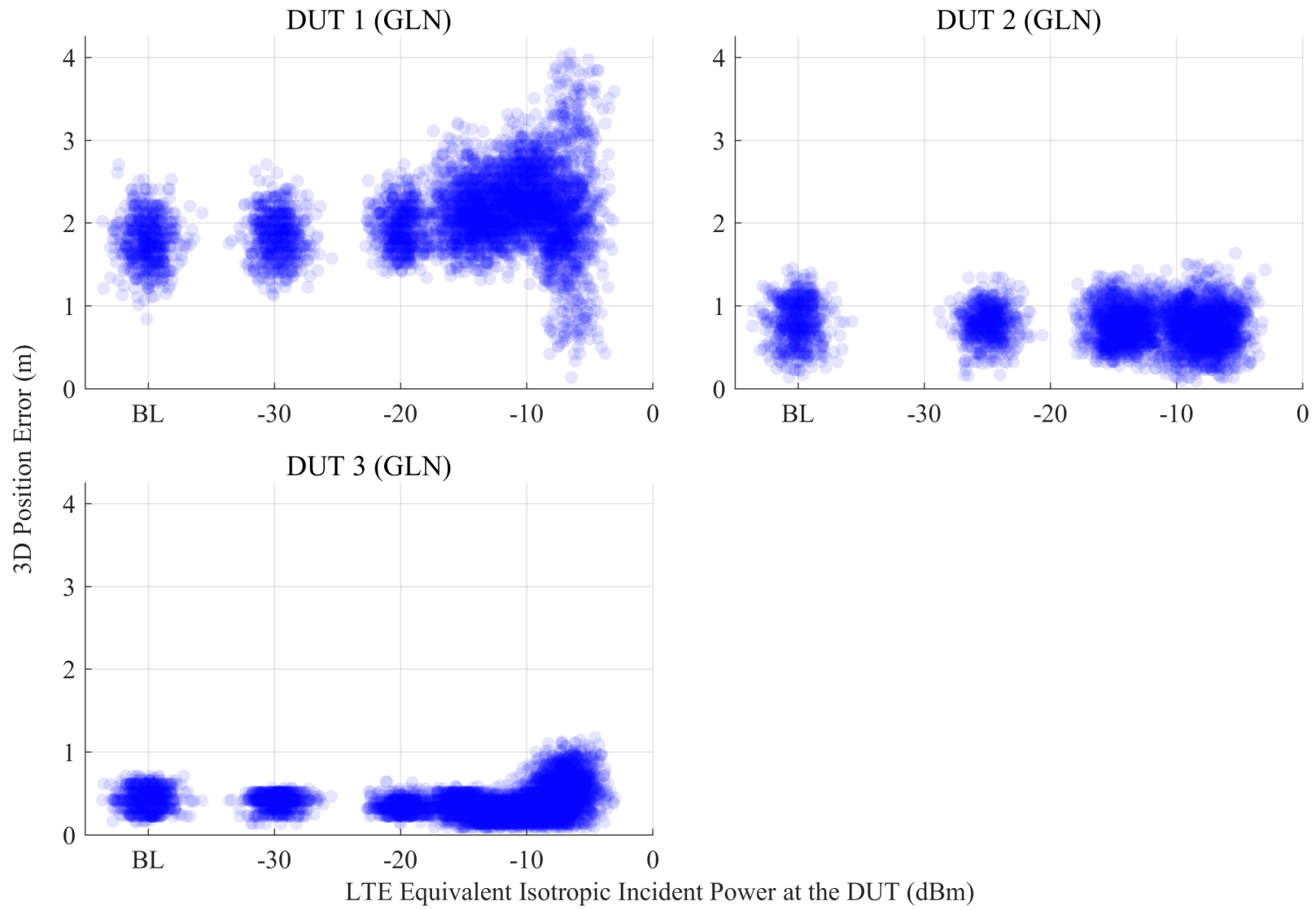


Figure 6.16: Scatterplots of error in reported 3-D position compared to simulator truth from GLN receivers, swept with LTE power level. The GPS scenario is nominal, and the type of incident LTE is UL2.

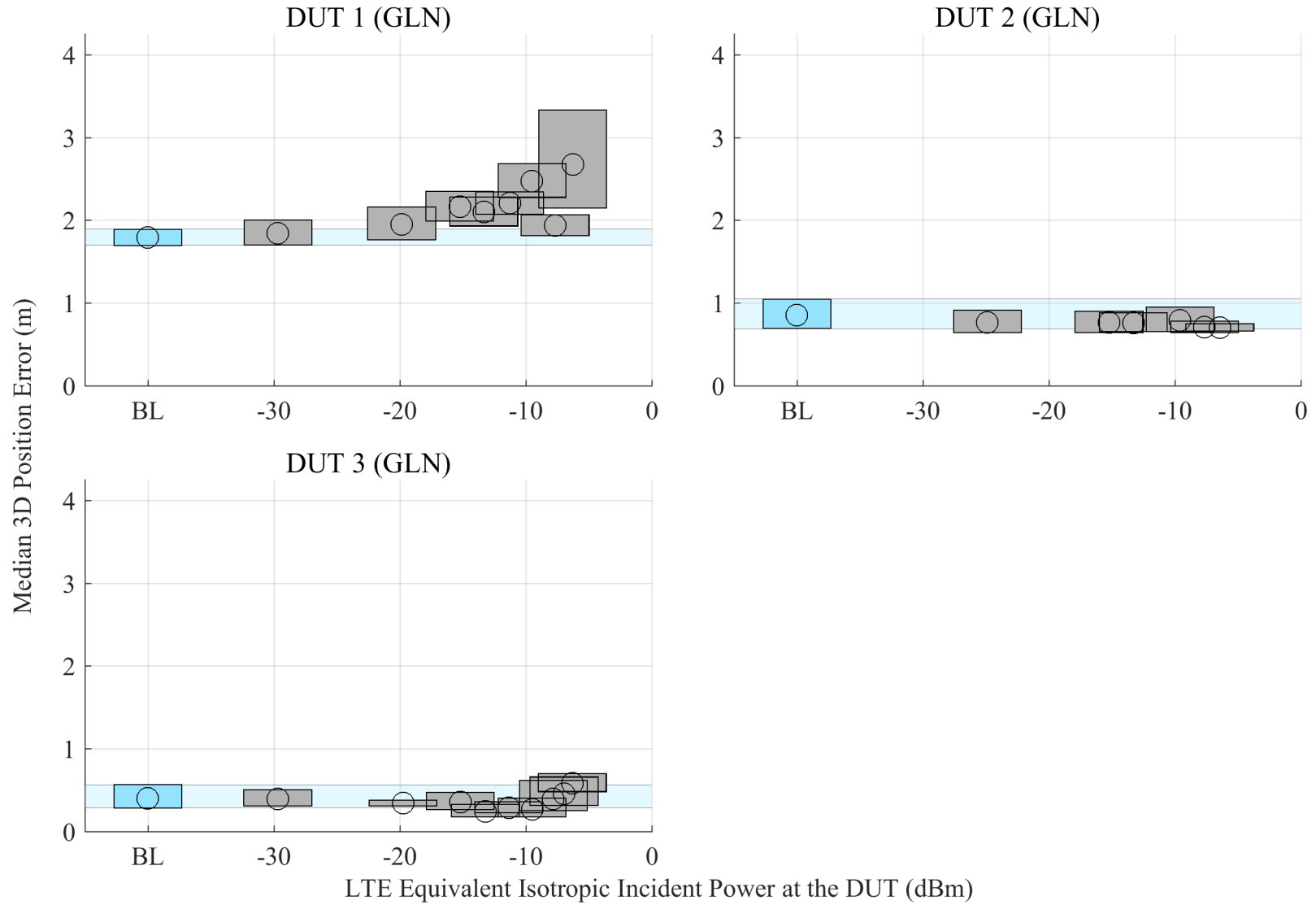


Figure 6.17: Estimated 95% confidence regions of the median error in reported 3-D position from GLN receivers, swept with LTE power level. The GPS scenario is nominal, and the type of incident LTE is UL2.

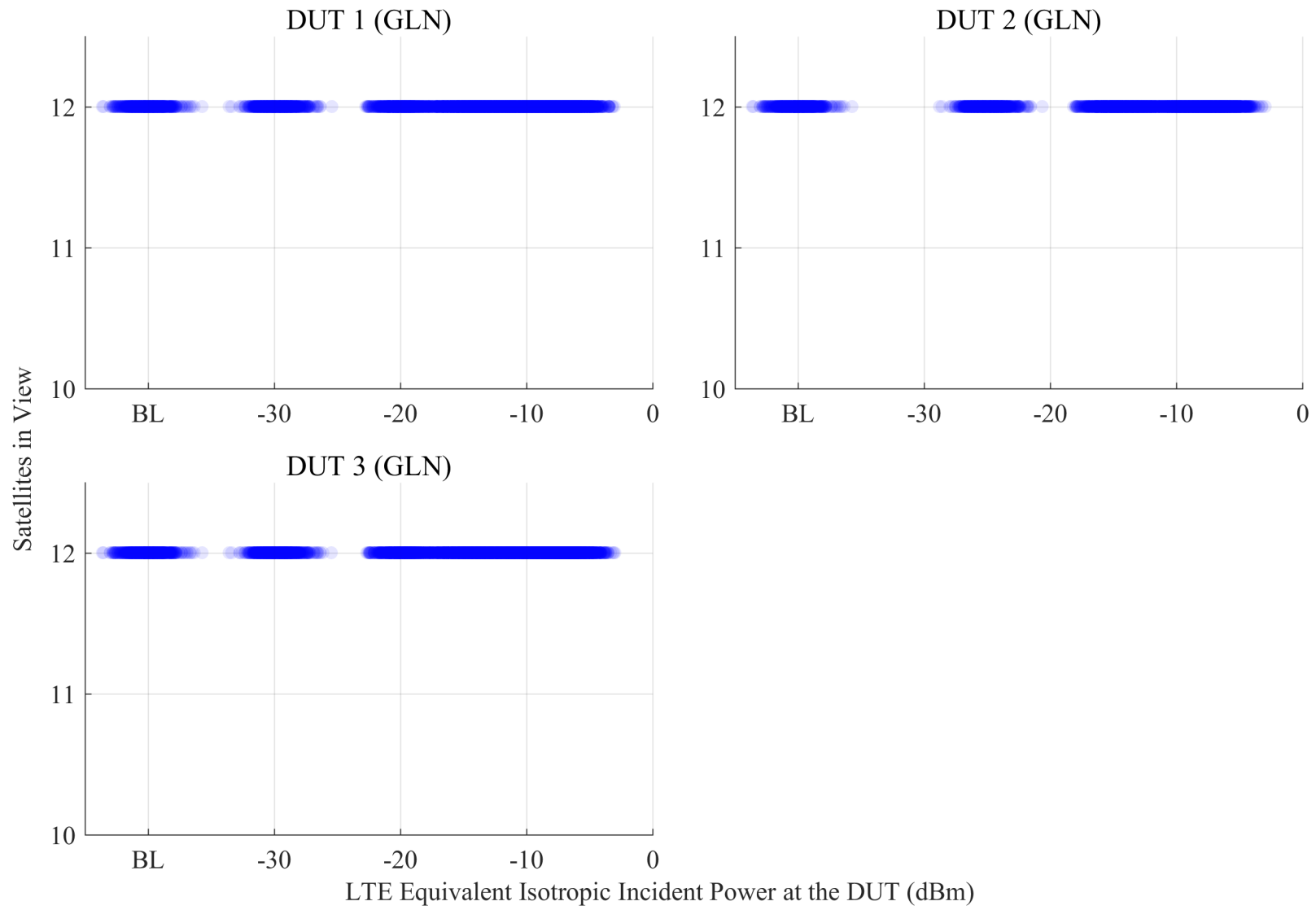


Figure 6.18: Scatterplots of the number of satellites in view from GLN receivers, swept with LTE power level. The GPS scenario is nominal, and the type of incident LTE is UL2.

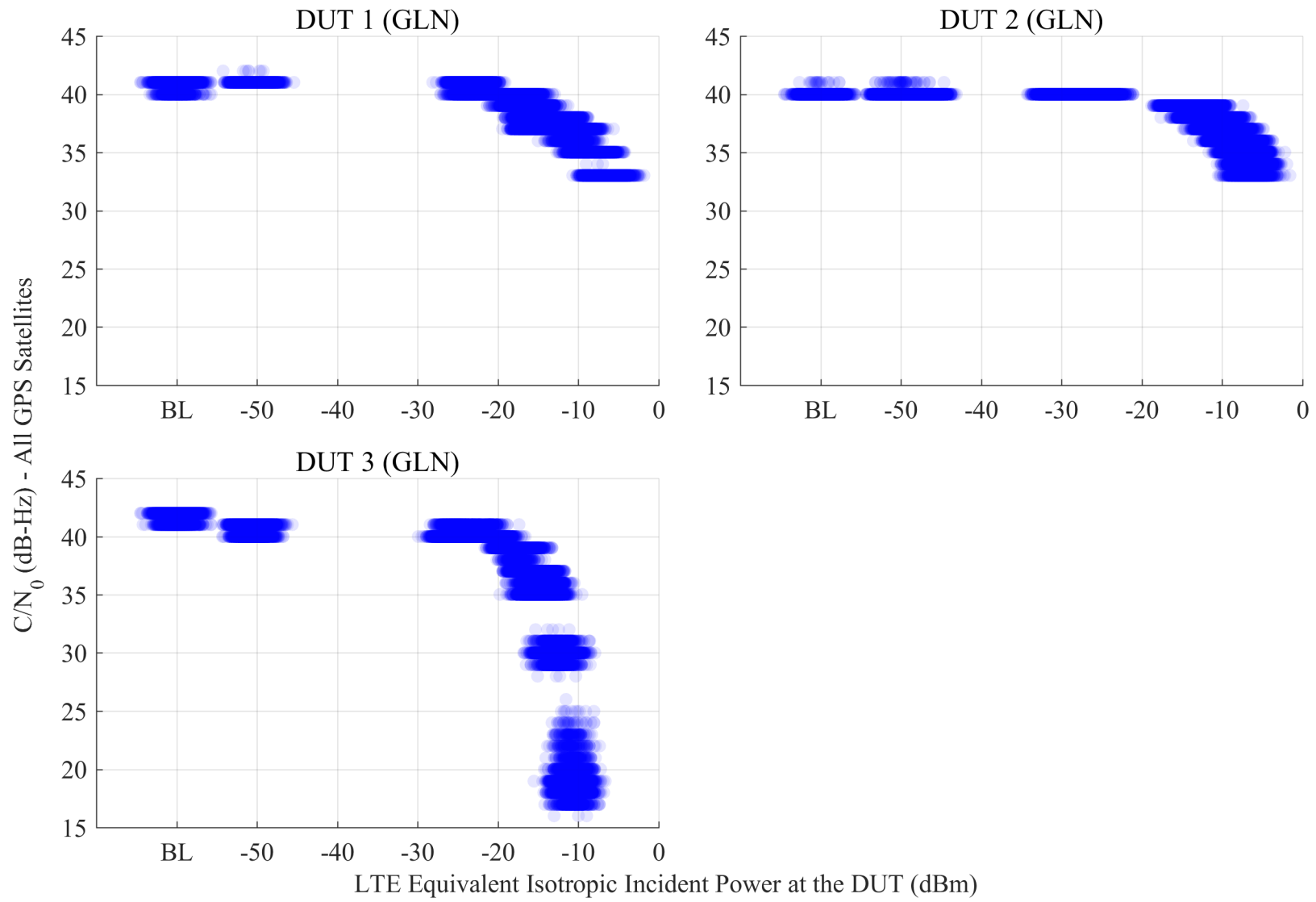


Figure 6.19: Scatterplots of reported  $C/N_0$  from GLN receivers, swept with LTE power level. The GPS scenario is nominal, and the type of incident LTE is Combination DL + UL1. The UL level was swept, and the DL level was fixed at -50 dBm EIIP unless otherwise annotated. The horizontal axis reports the linear sum of DL and UL power.

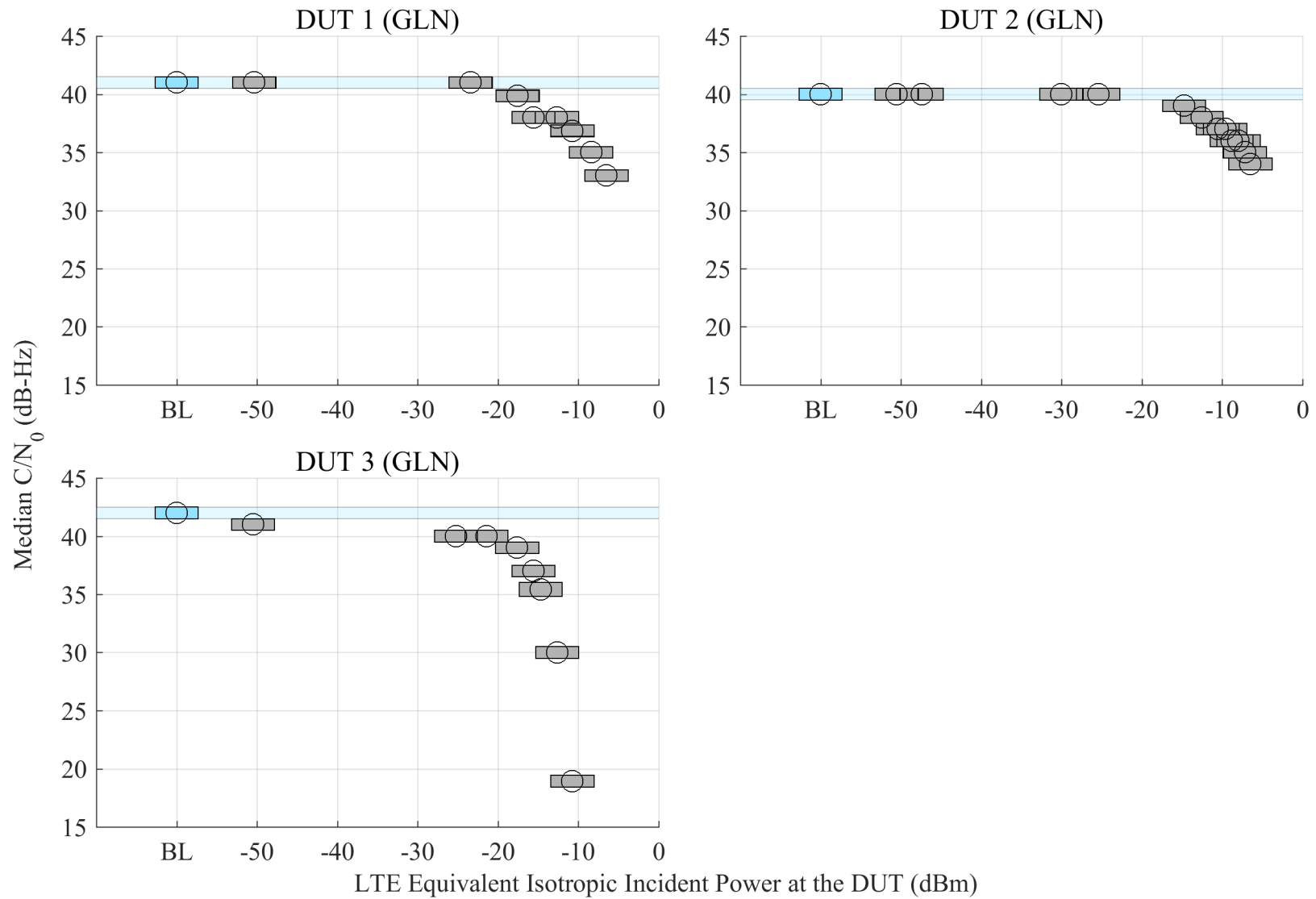


Figure 6.20: Estimated 95% confidence regions of the median of reported  $C/N_0$  from GLN receivers, swept with LTE power level. The GPS scenario is nominal, and the type of incident LTE is Combination DL + UL1. The UL level was swept, and the DL level was fixed at -50 dBm EIIP unless otherwise annotated. The horizontal axis reports the linear sum of DL and UL power.

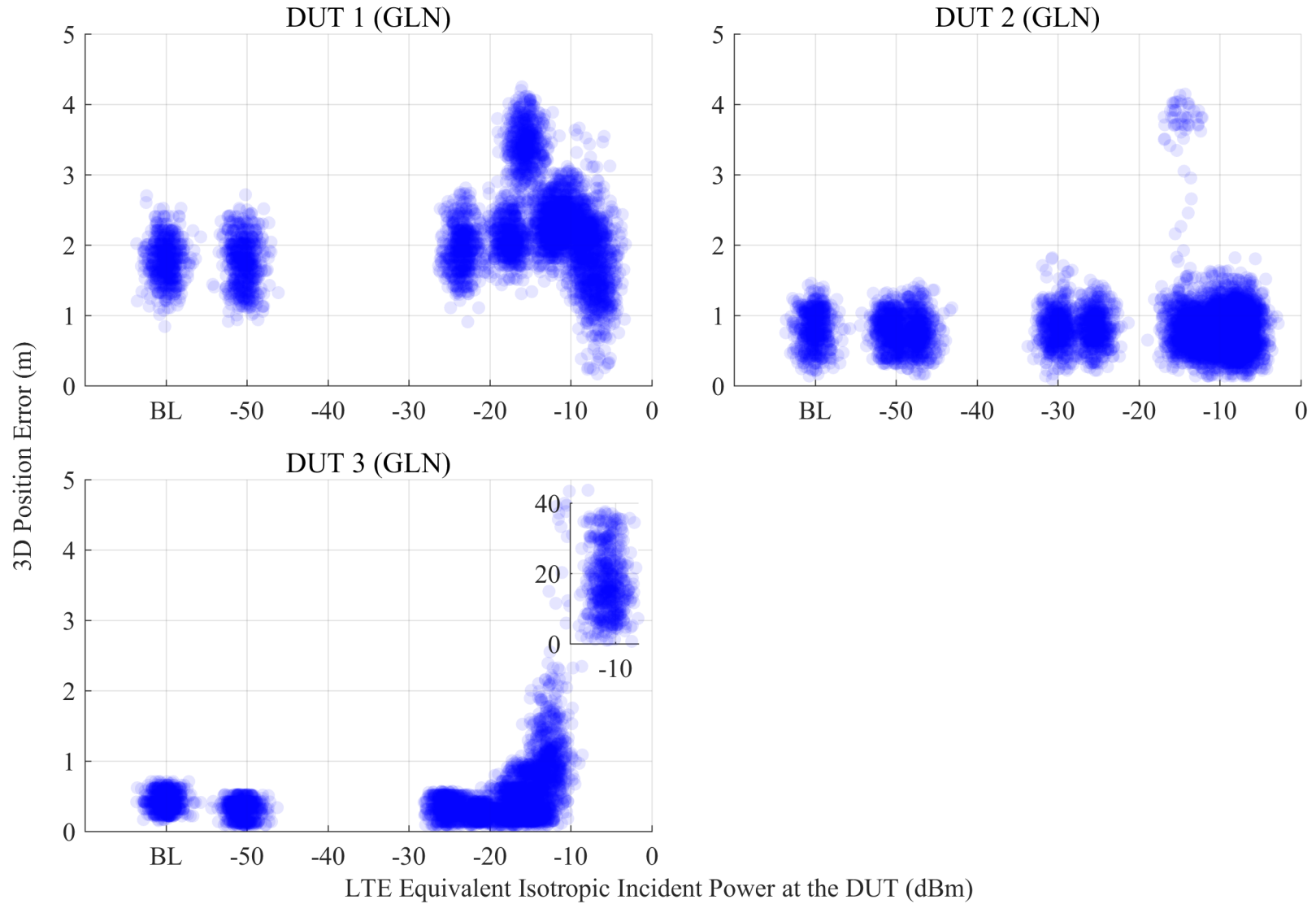


Figure 6.21: Scatterplots of error in reported 3-D position compared to simulator truth from GLN receivers, swept with LTE power level. The GPS scenario is nominal, and the type of incident LTE is Combination DL + UL1. The UL level was swept, and the DL level was fixed at -50 dBm EIIIP unless otherwise annotated. The horizontal axis reports the linear sum of DL and UL power.

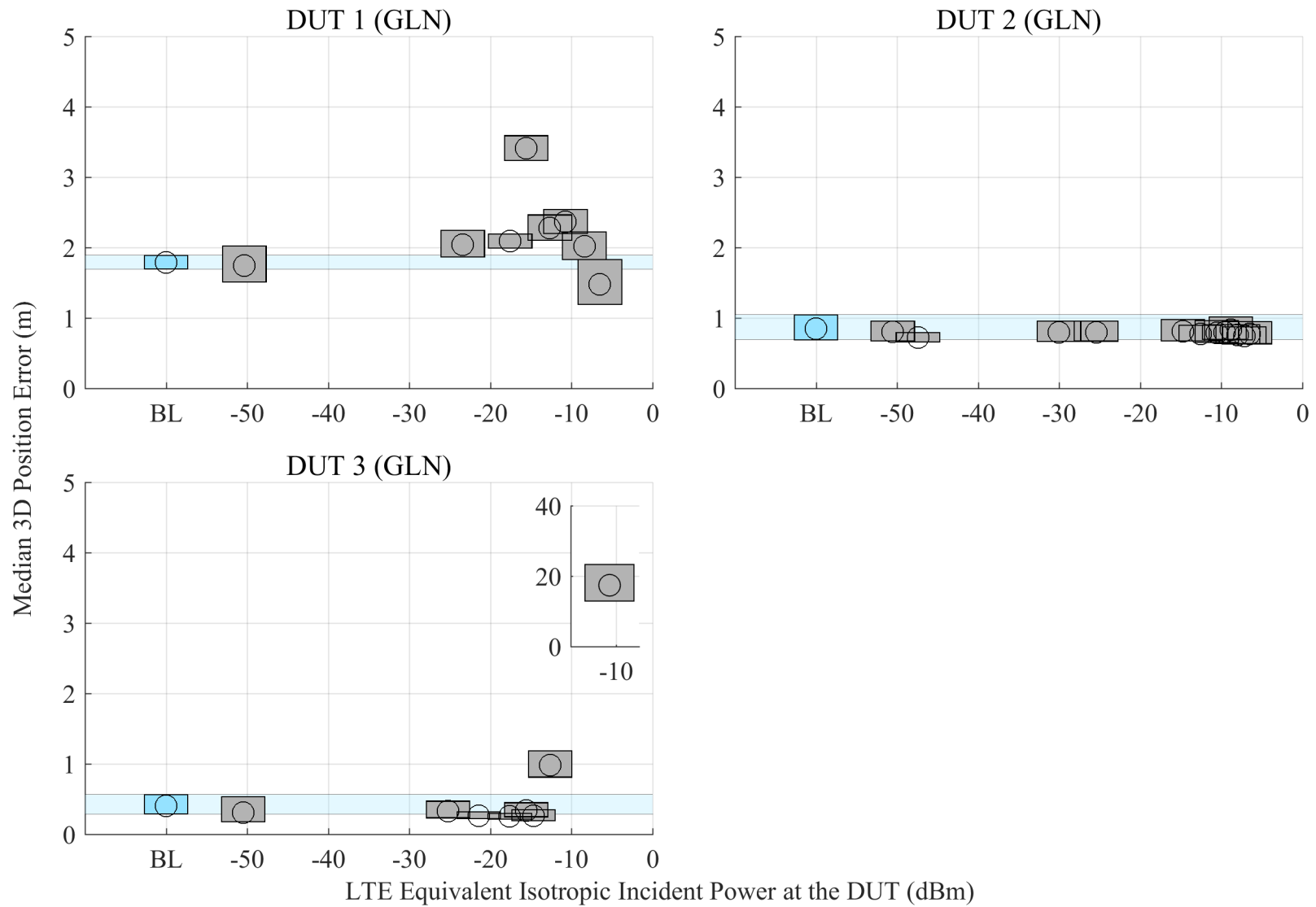


Figure 6.22: Estimated 95% confidence regions of the median error in reported 3-D position from GLN receivers, swept with LTE power level. The GPS scenario is nominal, and the type of incident LTE is Combination DL + UL1. The UL level was swept, and the DL level was fixed at -50 dBm EIIP unless otherwise annotated. The horizontal axis reports the linear sum of DL and UL power.

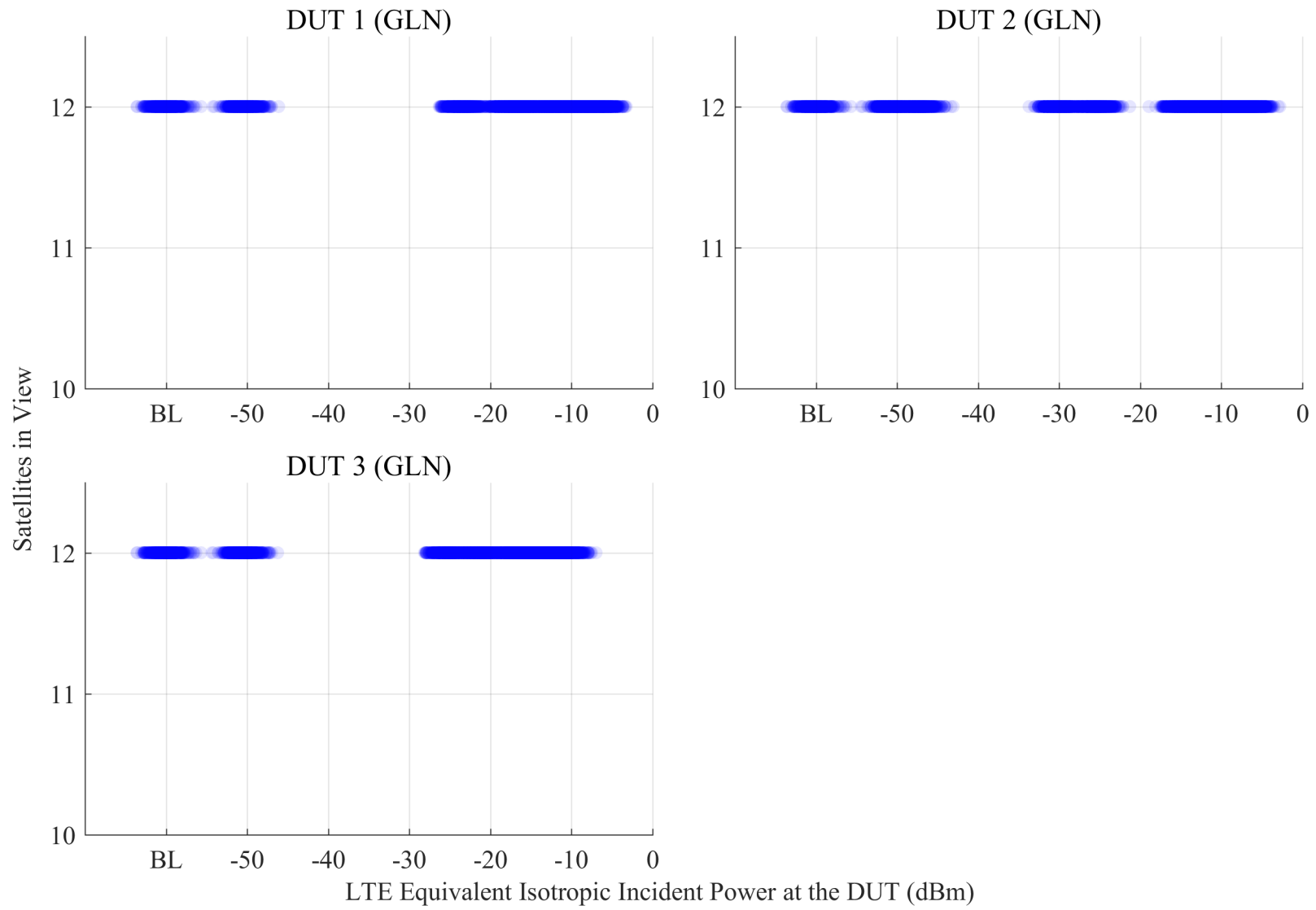


Figure 6.23: Scatterplots of the number of satellites in view from GLN receivers, swept with LTE power level. The GPS scenario is nominal, and the type of incident LTE is Combination DL + UL1. The UL level was swept, and the DL level was fixed at -50 dBm EIIP unless otherwise annotated. The horizontal axis reports the linear sum of DL and UL power.

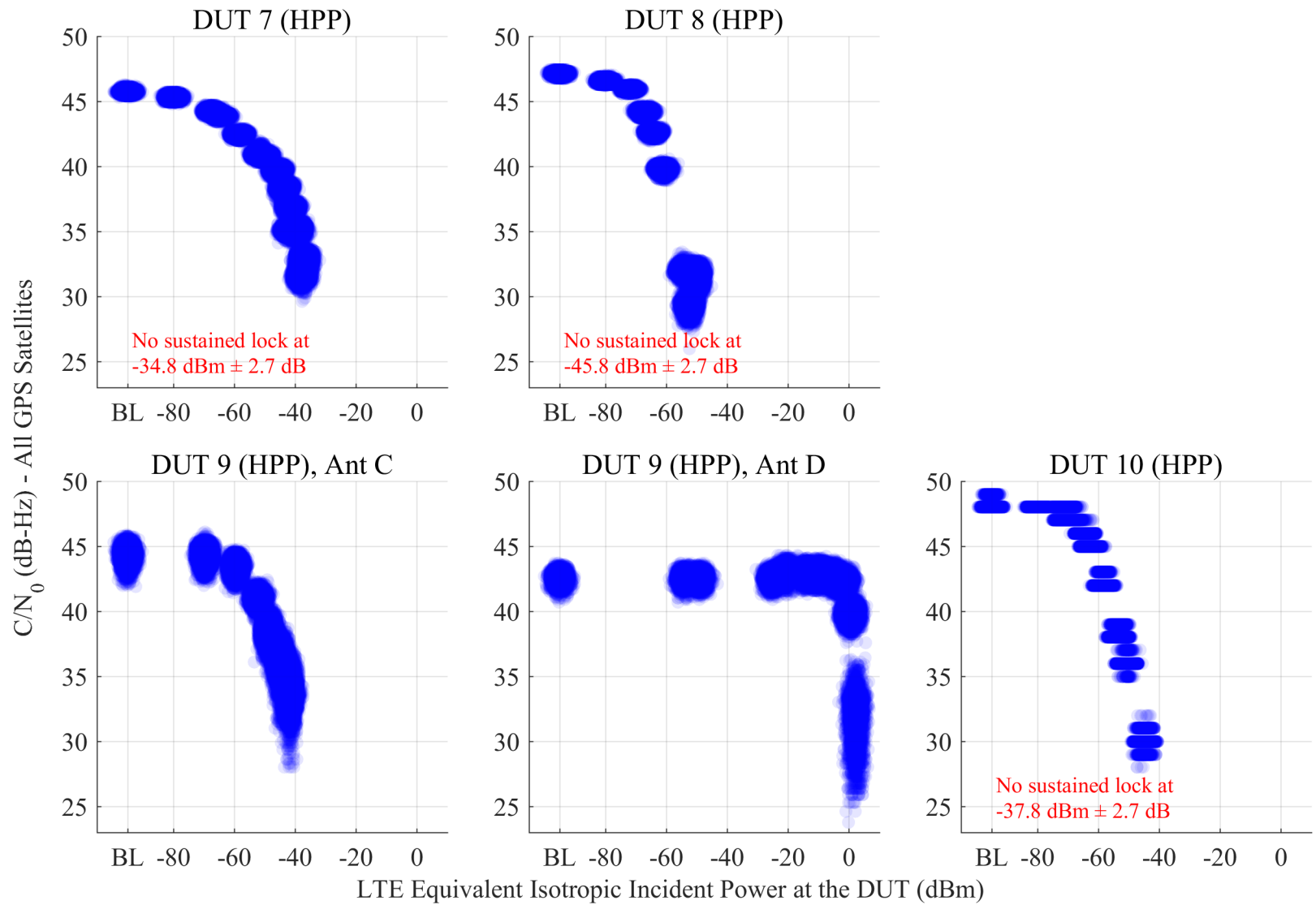


Figure 6.24: Scatterplots of reported  $C/N_0$  from HPP receivers, swept with LTE power level. The GPS scenario is nominal, and the type of incident LTE is DL.

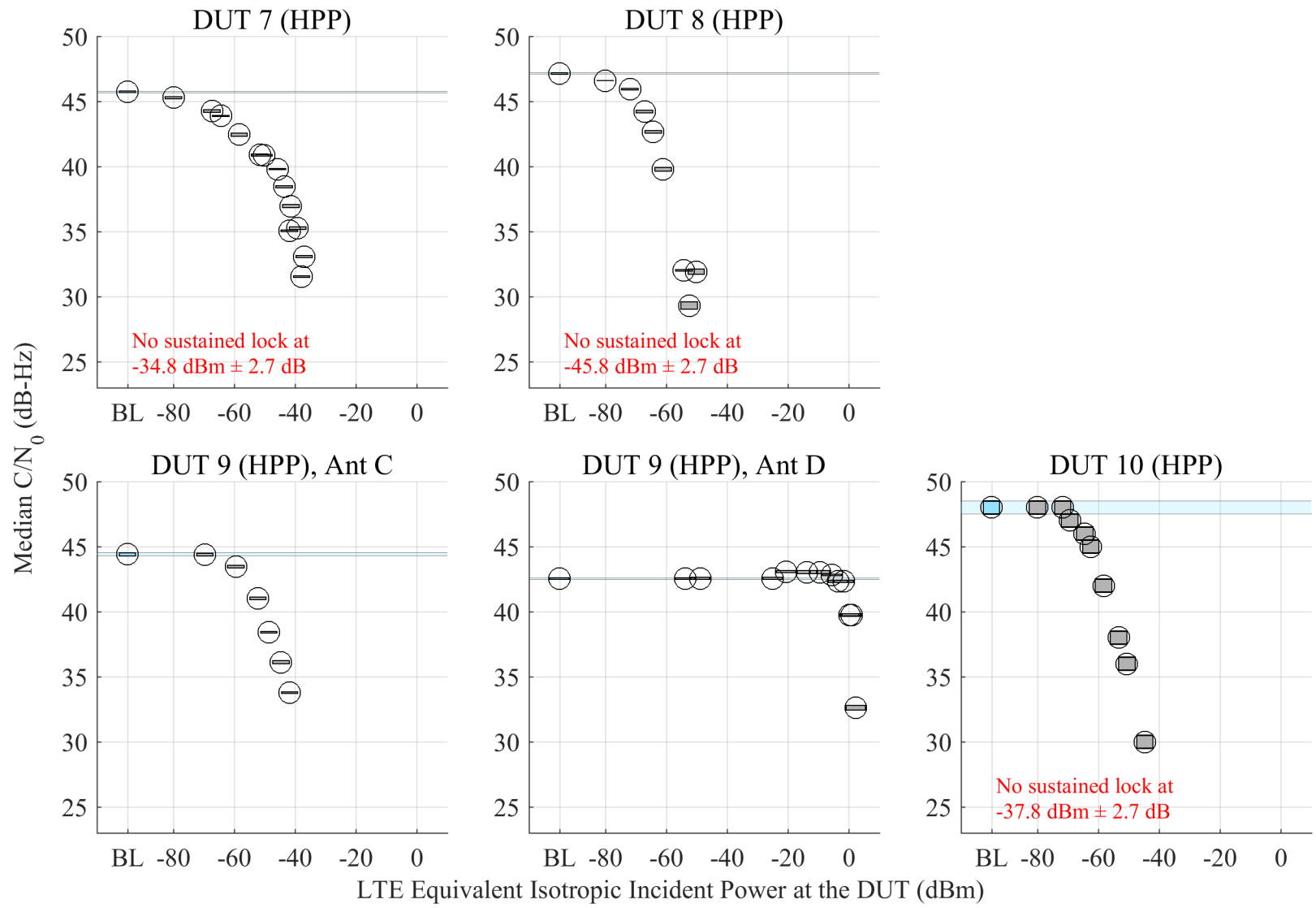


Figure 6.25: Estimated 95% confidence regions of the median of reported  $C/N_0$  from HPP receivers, swept with LTE power level. The GPS scenario is nominal, and the type of incident LTE is DL.

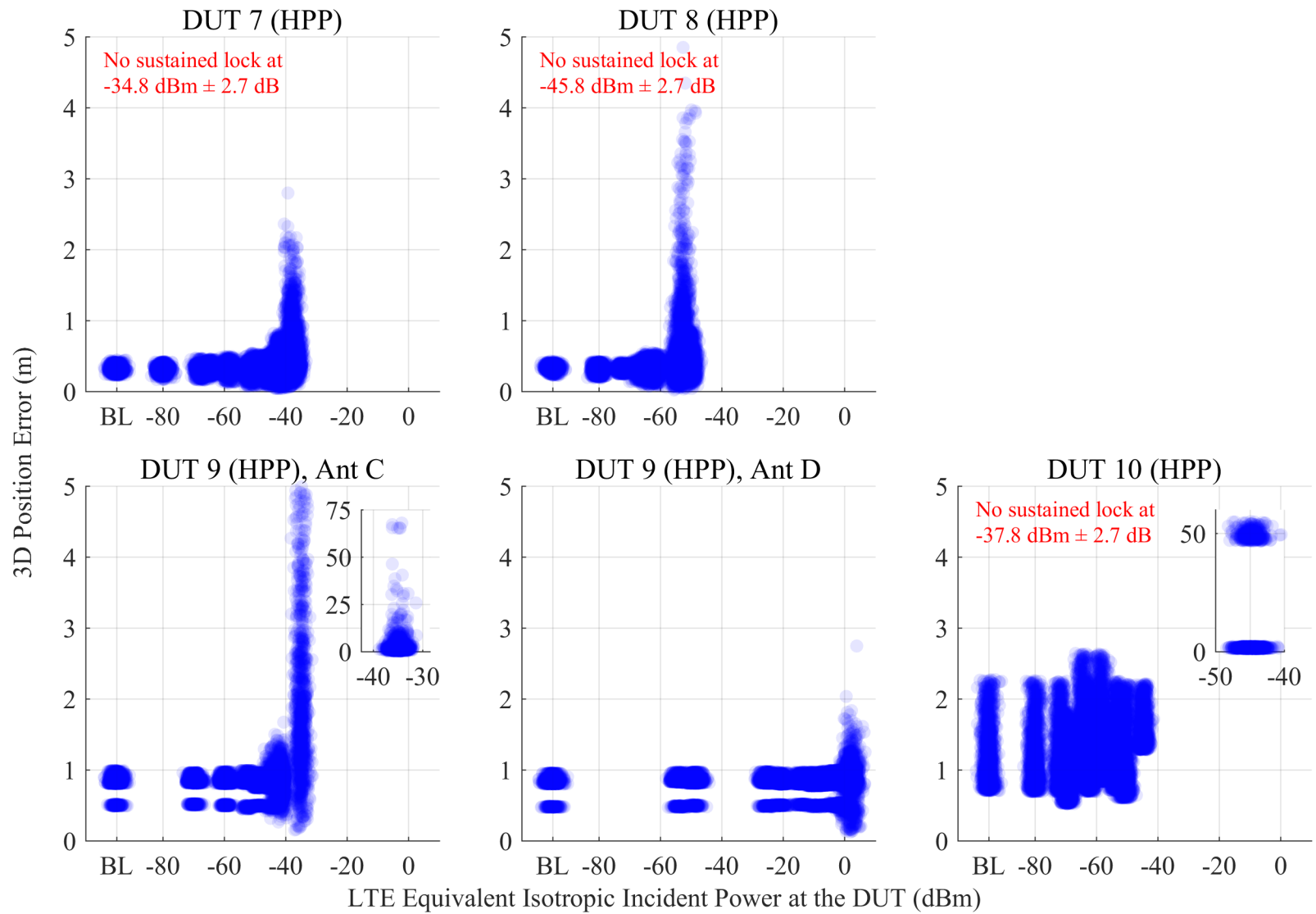


Figure 6.26: Scatterplots of error in reported 3-D position compared to simulator truth from HPP receivers, swept with LTE power level. The GPS scenario is nominal, and the type of incident LTE is DL.

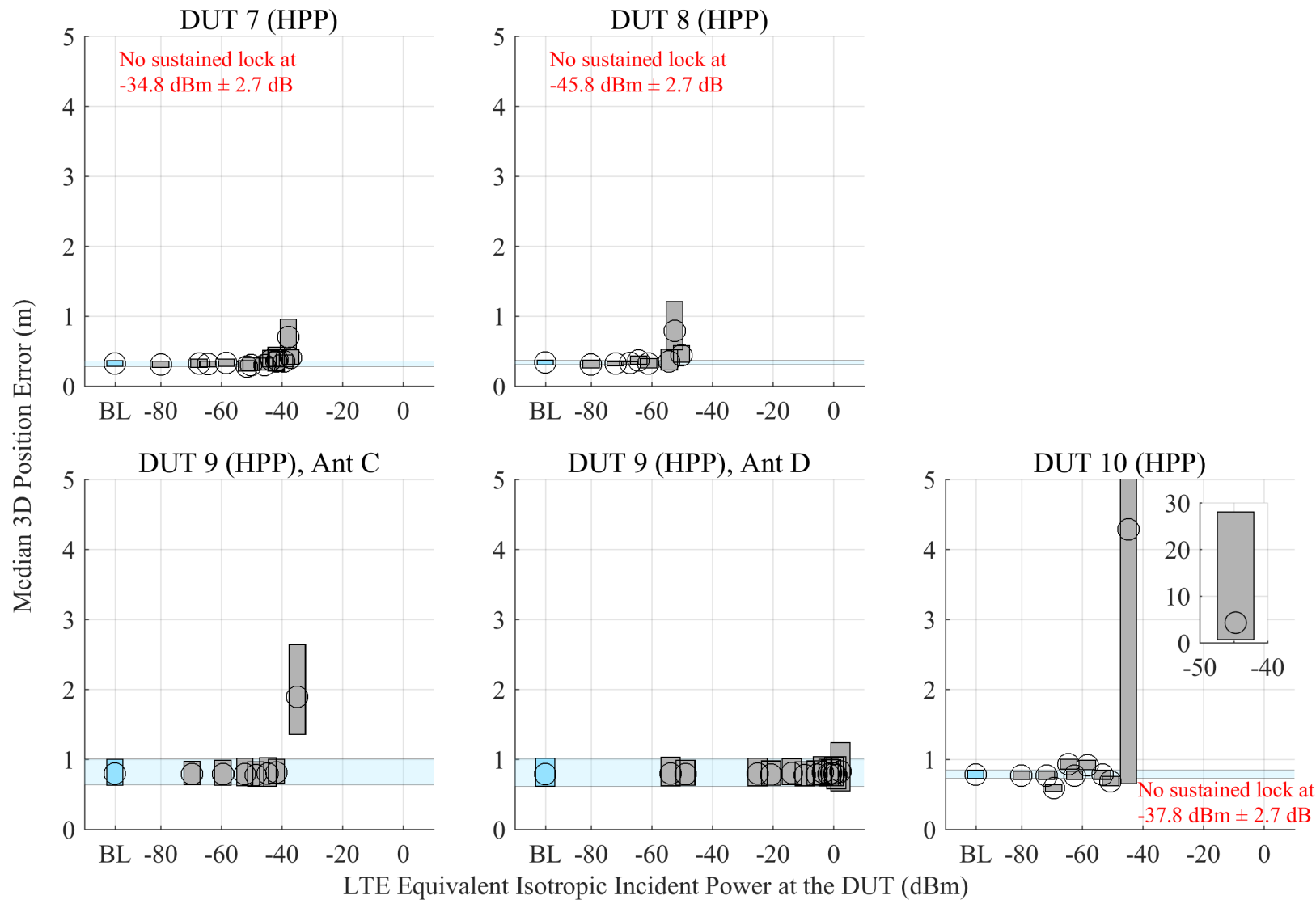


Figure 6.27: Estimated 95% confidence regions of the median error in reported 3-D position from HPP receivers, swept with LTE power level. The GPS scenario is nominal, and the type of incident LTE is DL.

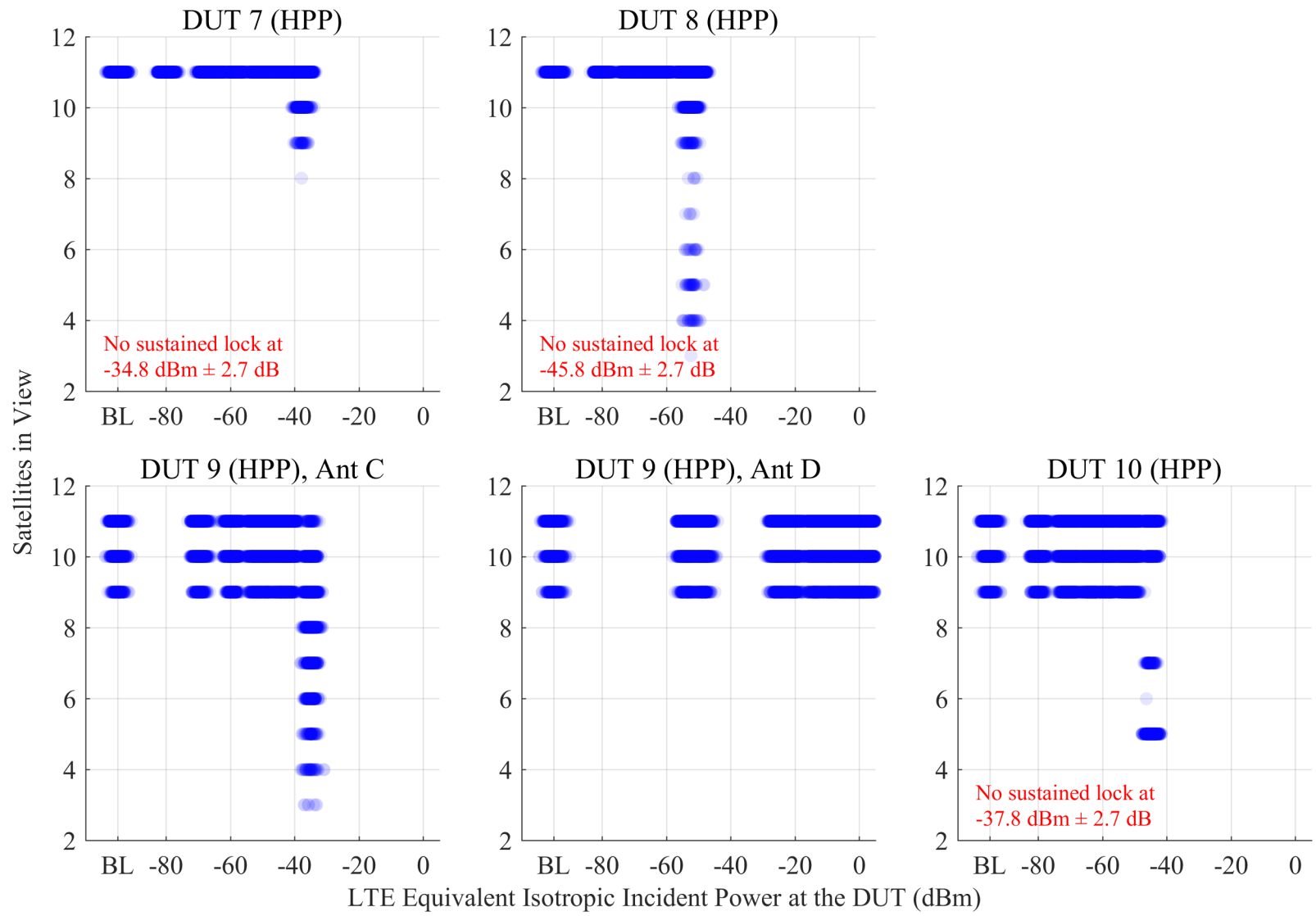


Figure 6.28: Scatterplots of the number of satellites in view from HPP receivers, swept with LTE power level. The GPS scenario is nominal, and the type of incident LTE is DL.

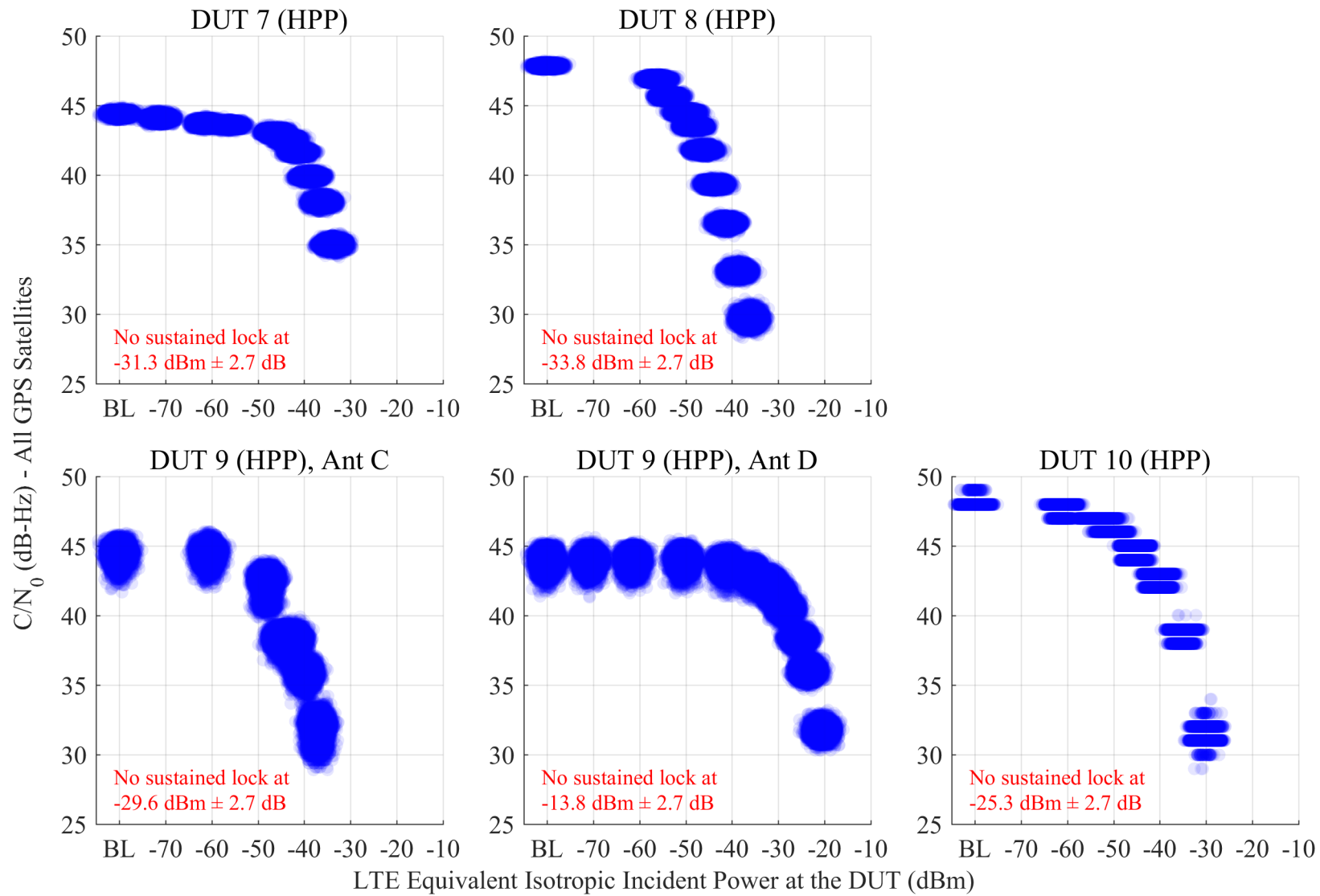


Figure 6.29: Scatterplots of reported  $C/N_0$  from HPP receivers, swept with LTE power level. The GPS scenario is nominal, and the type of incident LTE is UL1.

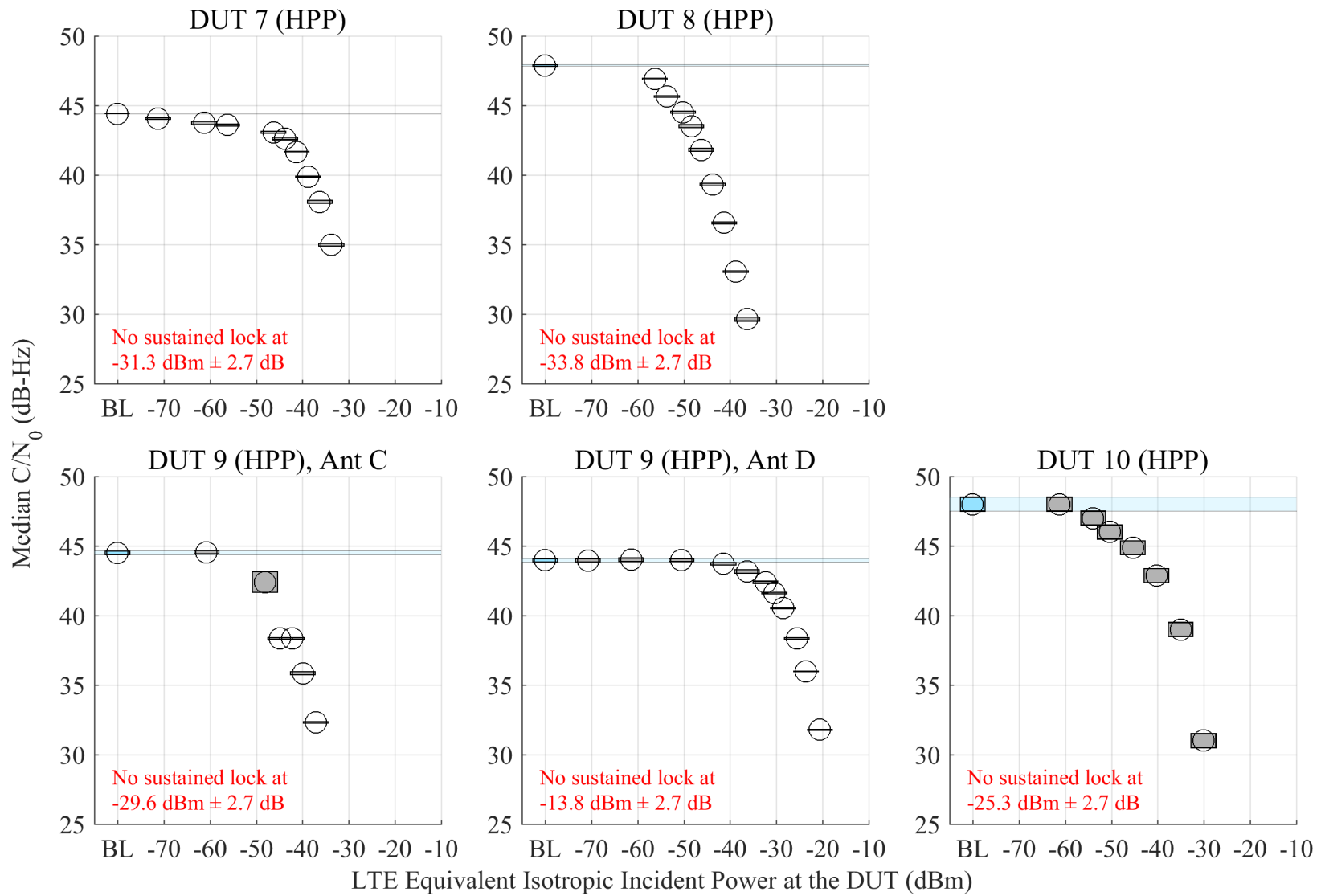


Figure 6.30: Estimated 95% confidence regions of the median of reported  $C/N_0$  from HPP receivers, swept with LTE power level. The GPS scenario is nominal, and the type of incident LTE is UL1.

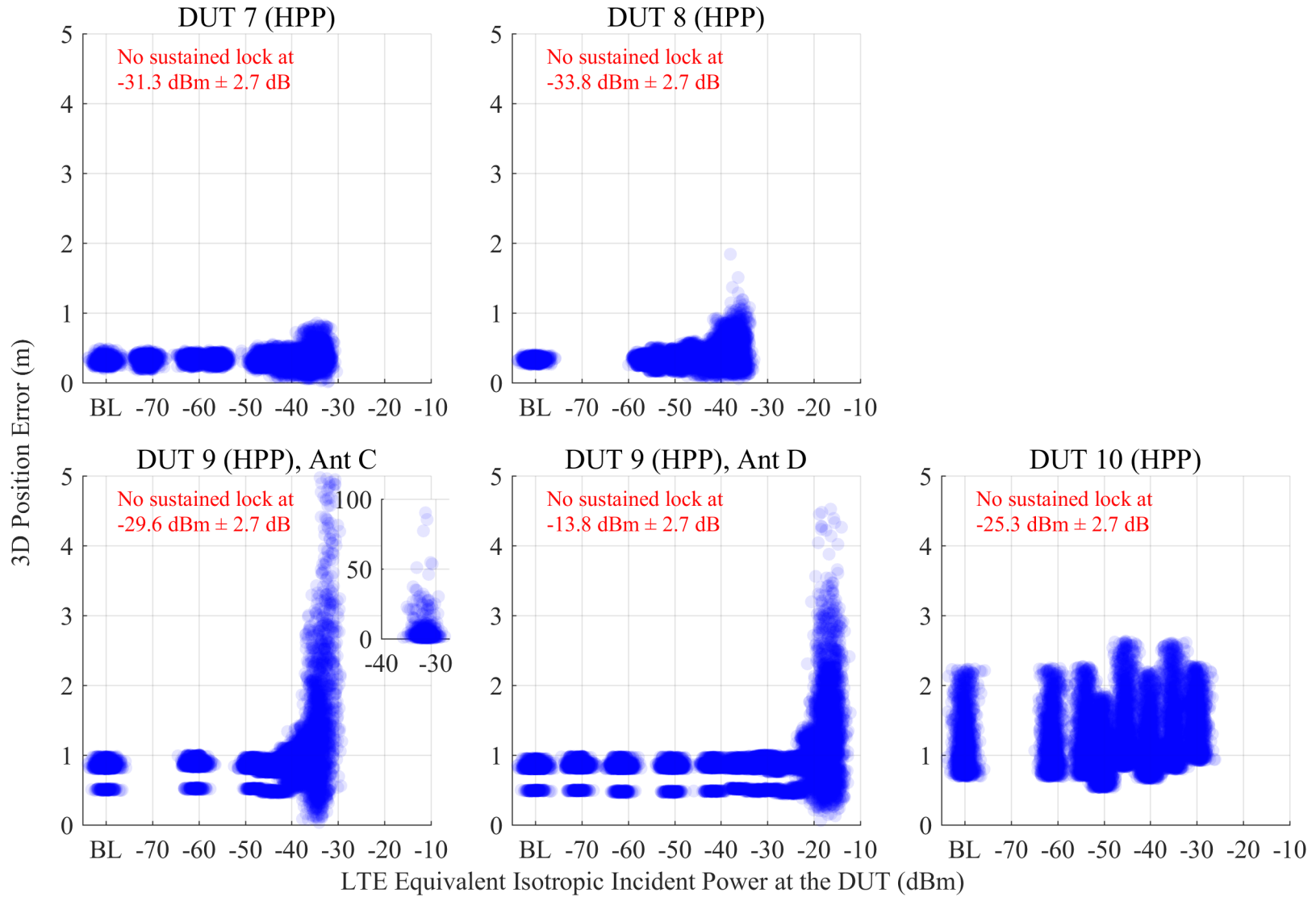


Figure 6.31: Scatterplots of error in reported 3-D position compared to simulator truth from HPP receivers, swept with LTE power level. The GPS scenario is nominal, and the type of incident LTE is UL1.

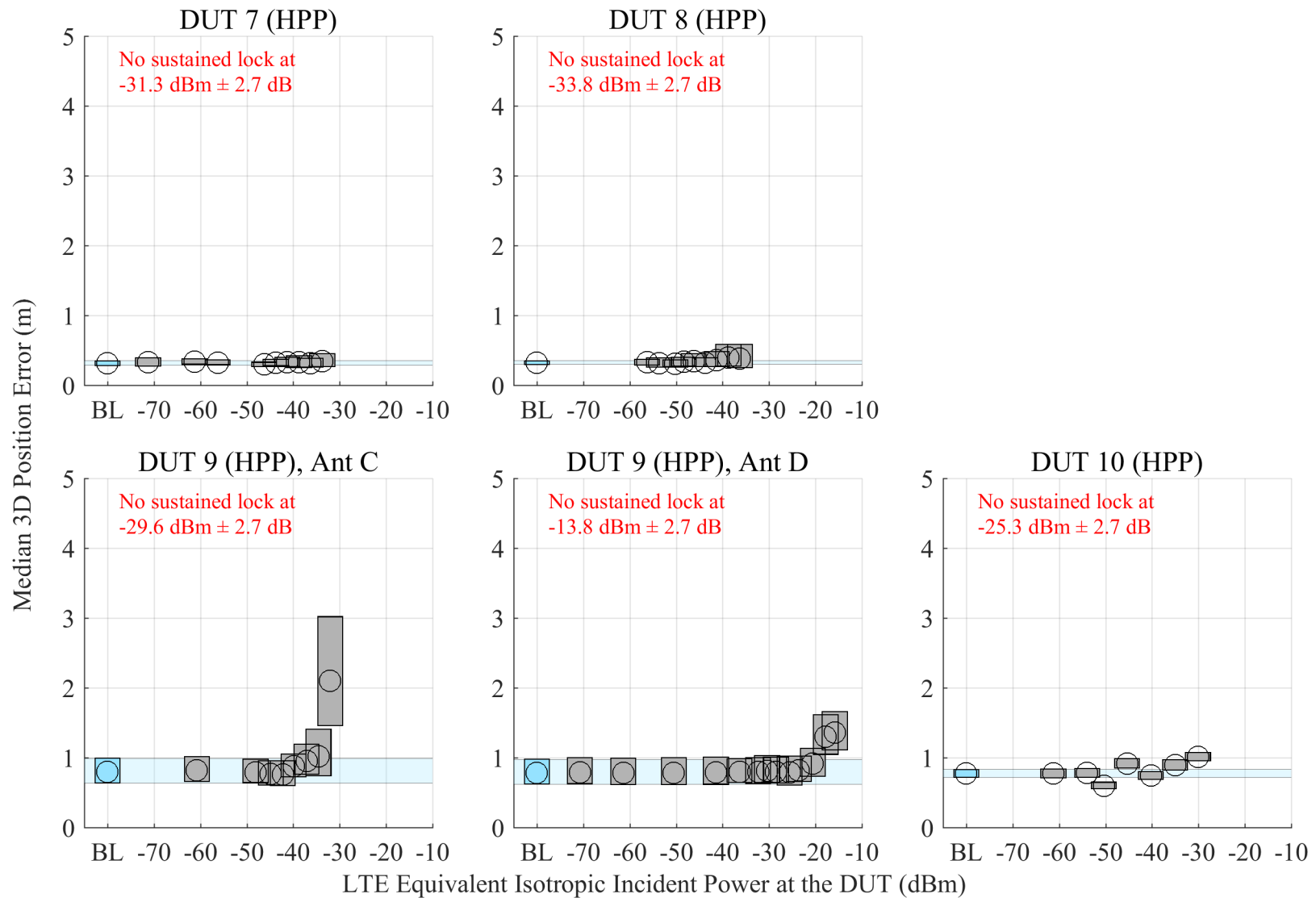


Figure 6.32: Estimated 95% confidence regions of the median error in reported 3-D position from HPP receivers, swept with LTE power level. The GPS scenario is nominal, and the type of incident LTE is UL1.

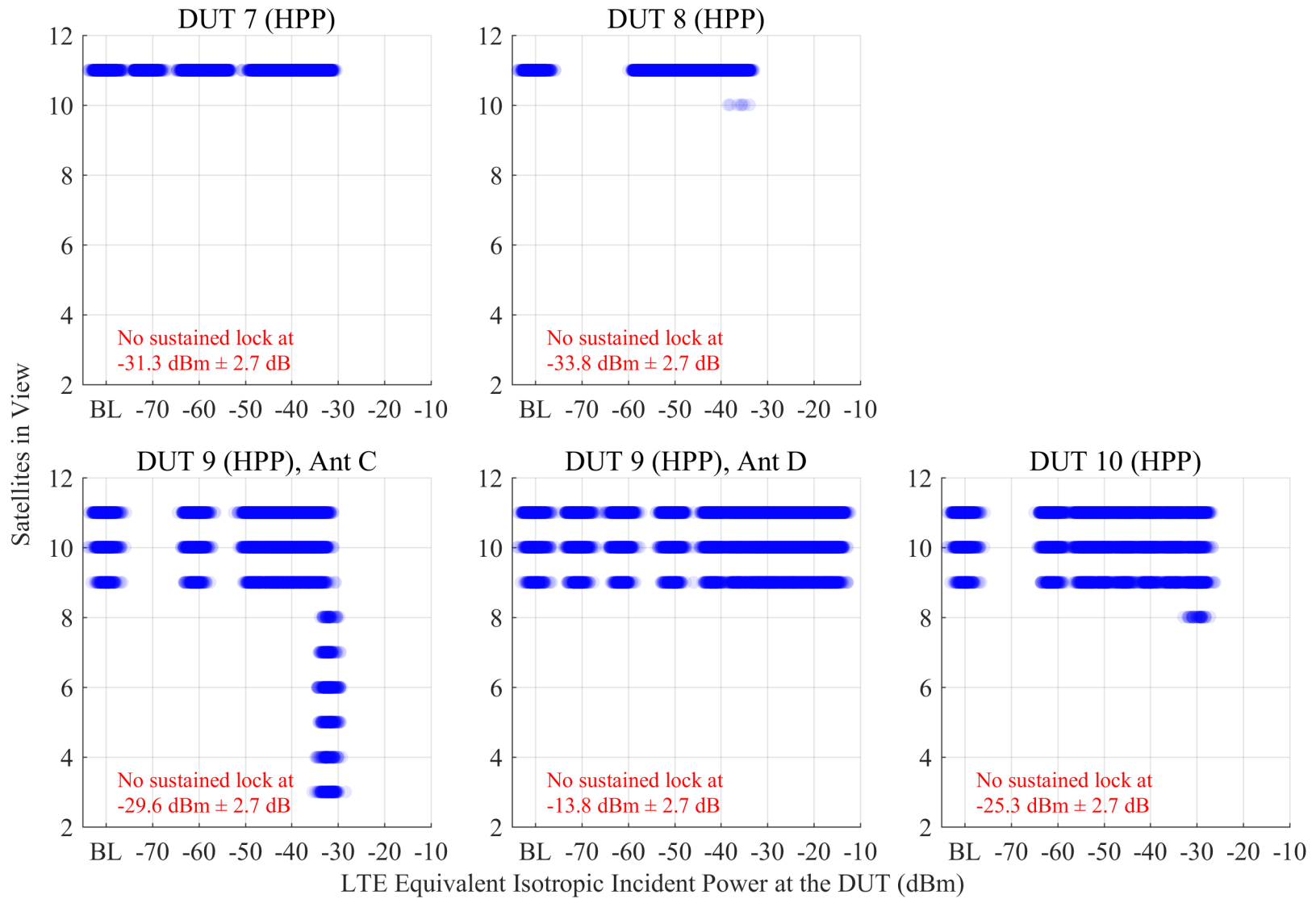


Figure 6.33: Scatterplots of the number of satellites in view from HPP receivers, swept with LTE power level. The GPS scenario is nominal, and the type of incident LTE is UL1.

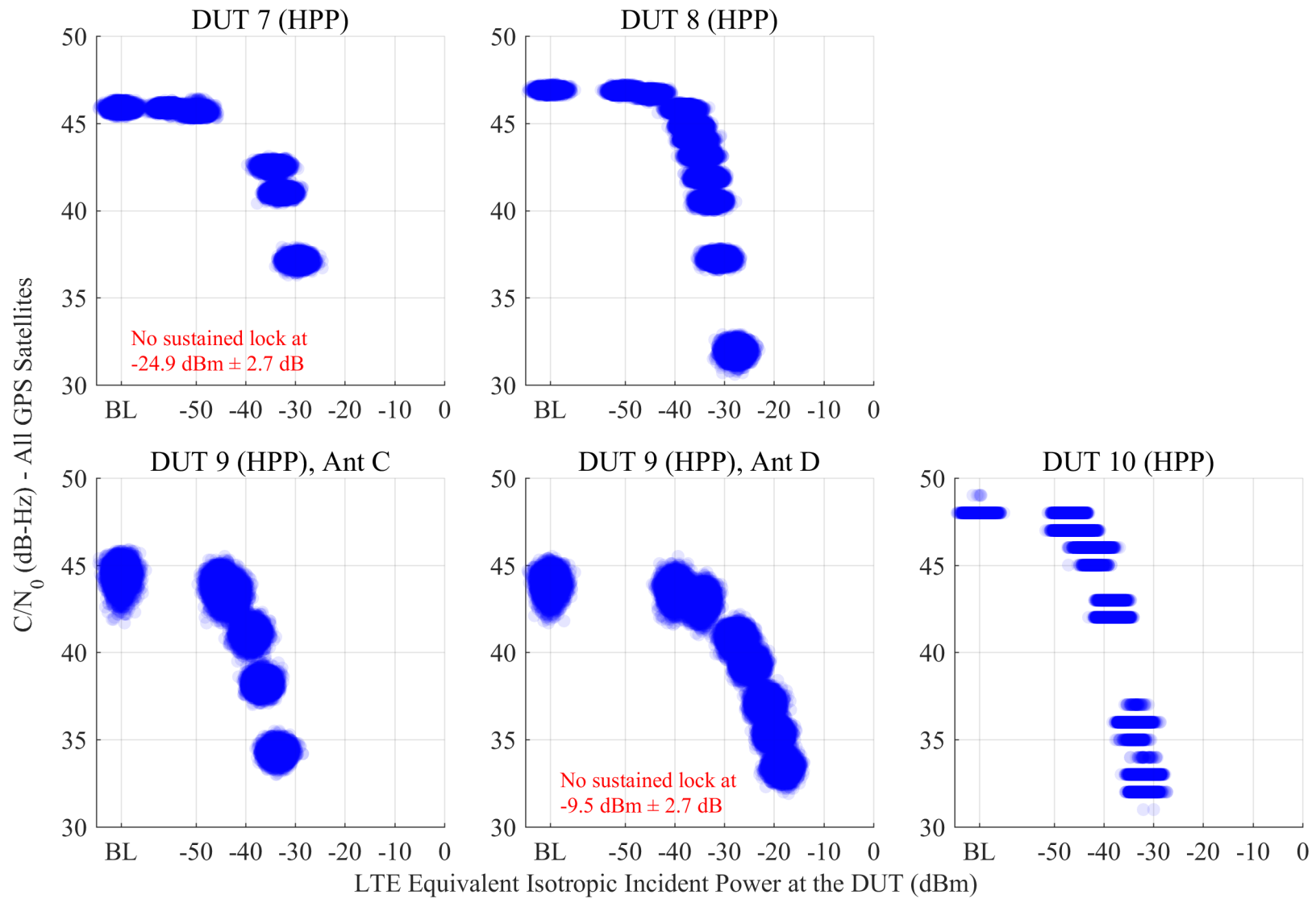


Figure 6.34: Scatterplots of reported  $C/N_0$  from HPP receivers, swept with LTE power level. The GPS scenario is nominal, and the type of incident LTE is UL2.

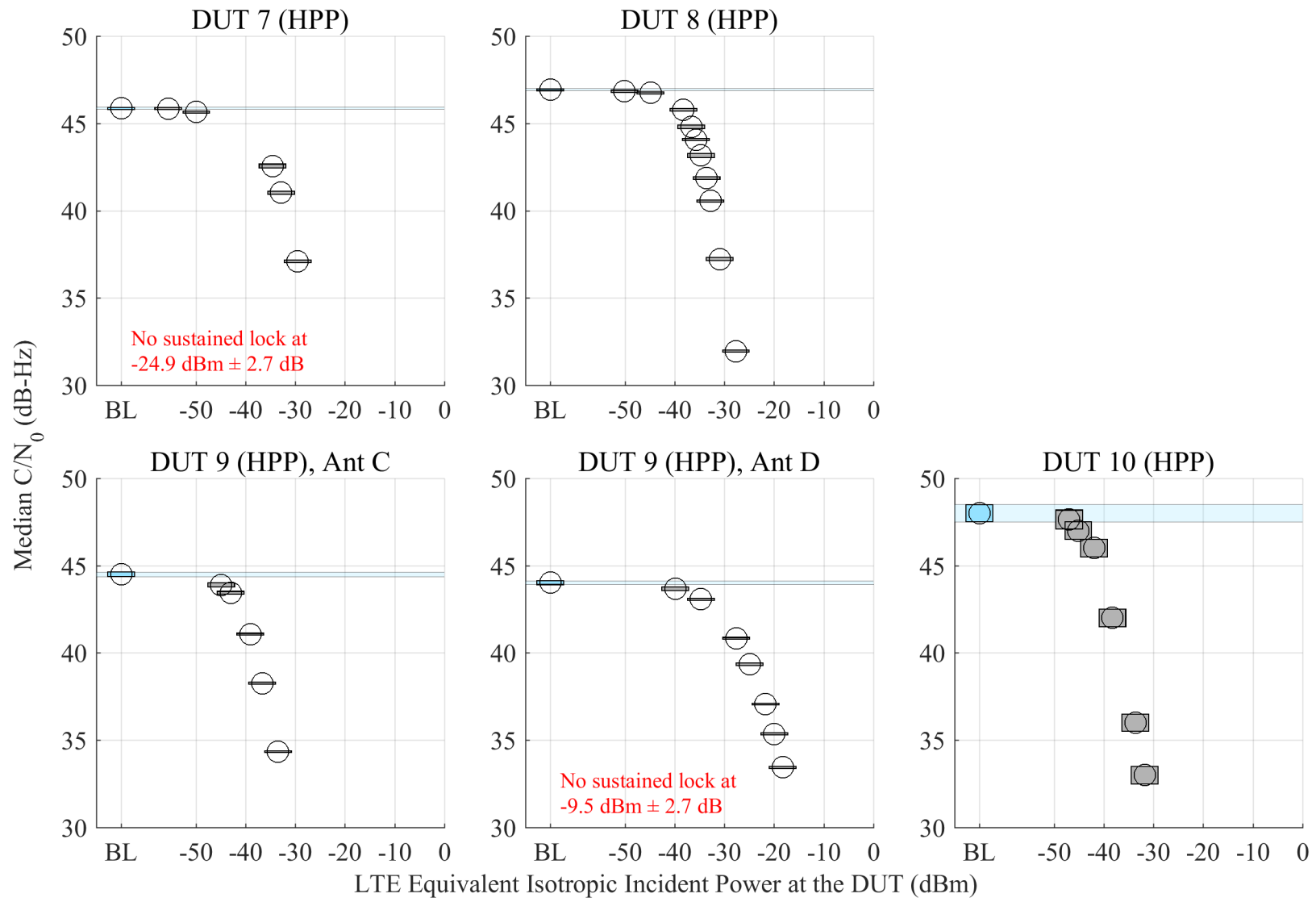


Figure 6.35: Estimated 95% confidence regions of the median of reported  $C/N_0$  from HPP receivers, swept with LTE power level. The GPS scenario is nominal, and the type of incident LTE is UL2.

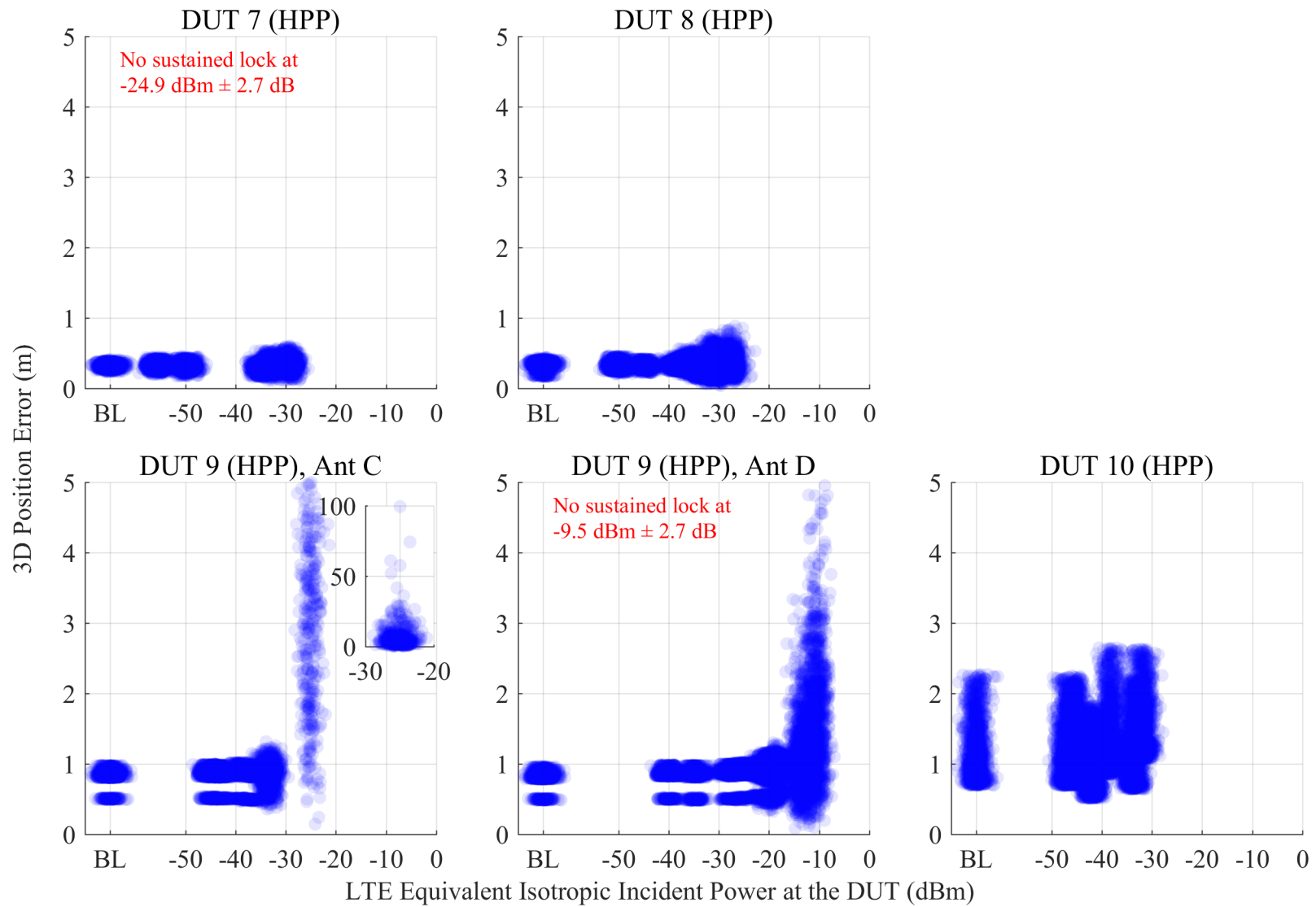


Figure 6.36: Scatterplots of error in reported 3-D position compared to simulator truth from HPP receivers, swept with LTE power level. The GPS scenario is nominal, and the type of incident LTE is UL2.

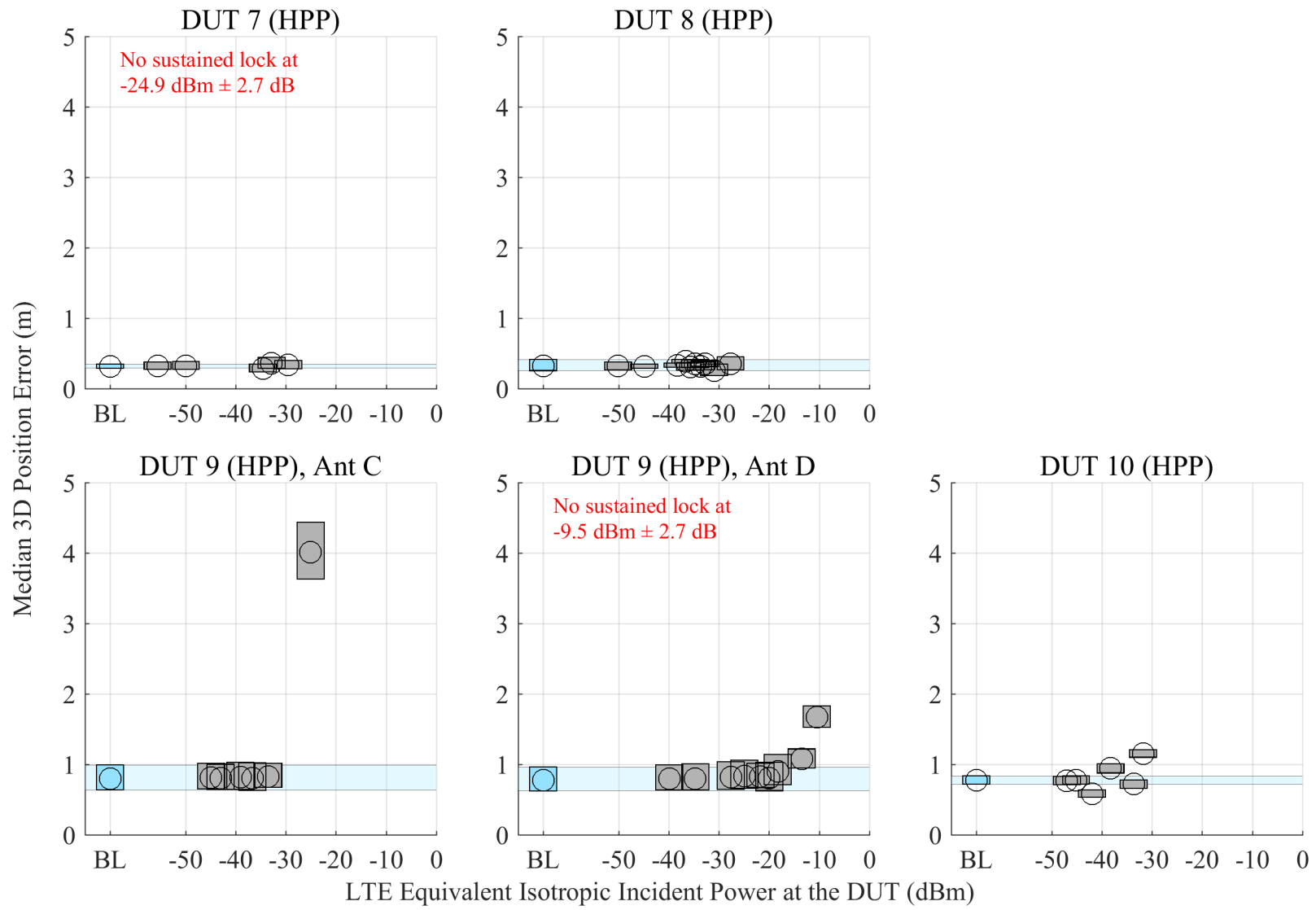


Figure 6.37: Estimated 95% confidence regions of the median error in reported 3-D position from HPP receivers, swept with LTE power level. The GPS scenario is nominal, and the type of incident LTE is UL2.

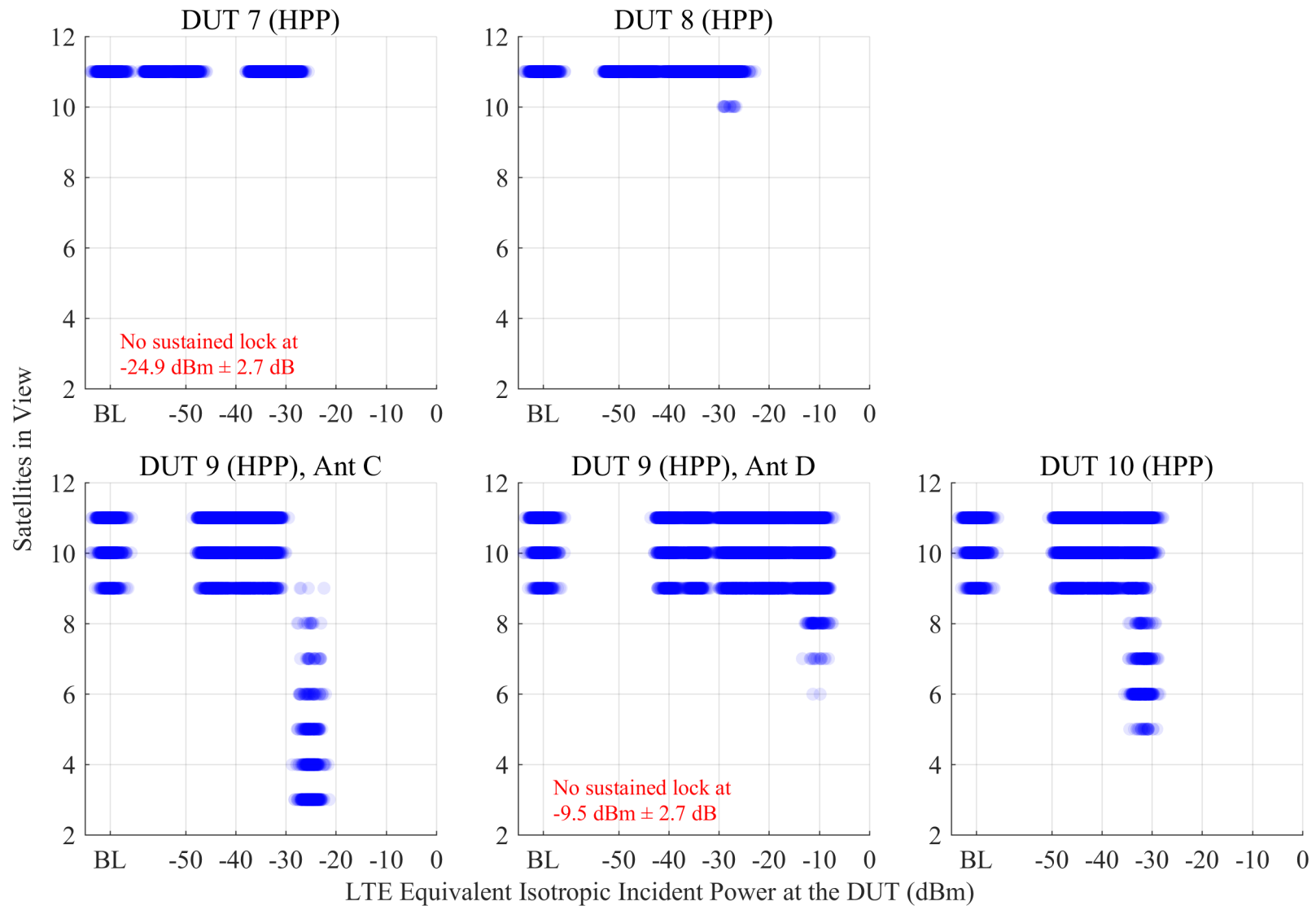


Figure 6.38: Scatterplots of the number of satellites in view from HPP receivers, swept with LTE power level. The GPS scenario is nominal, and the type of incident LTE is UL2.

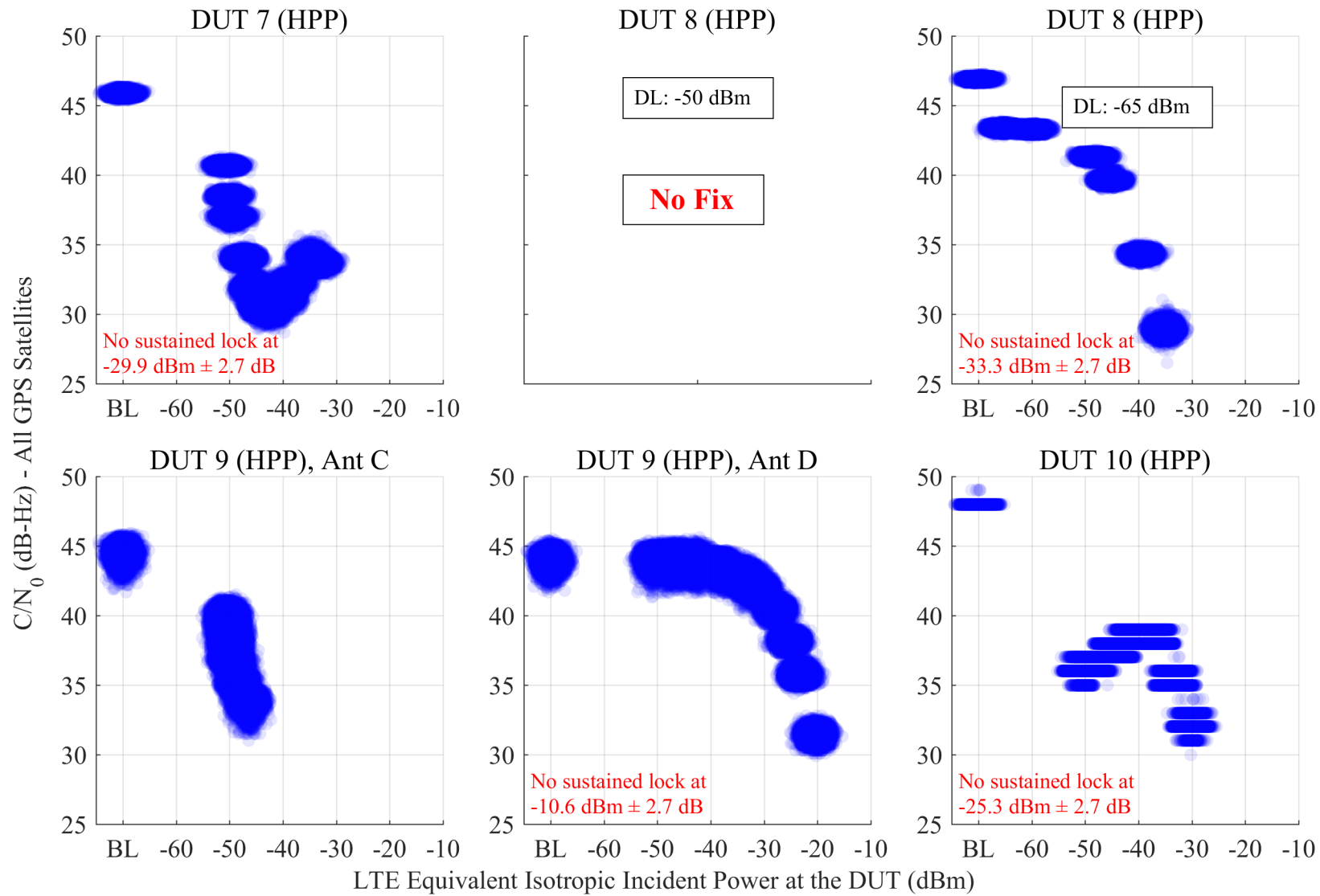


Figure 6.39: Scatterplots of reported  $C/N_0$  from HPP receivers, swept with LTE power level. The GPS scenario is nominal, and the type of incident LTE is DL + UL1. The UL level was swept, and the DL level was fixed at -50 dBm EIIP unless otherwise annotated. The horizontal axis reports the linear sum of DL and UL power.

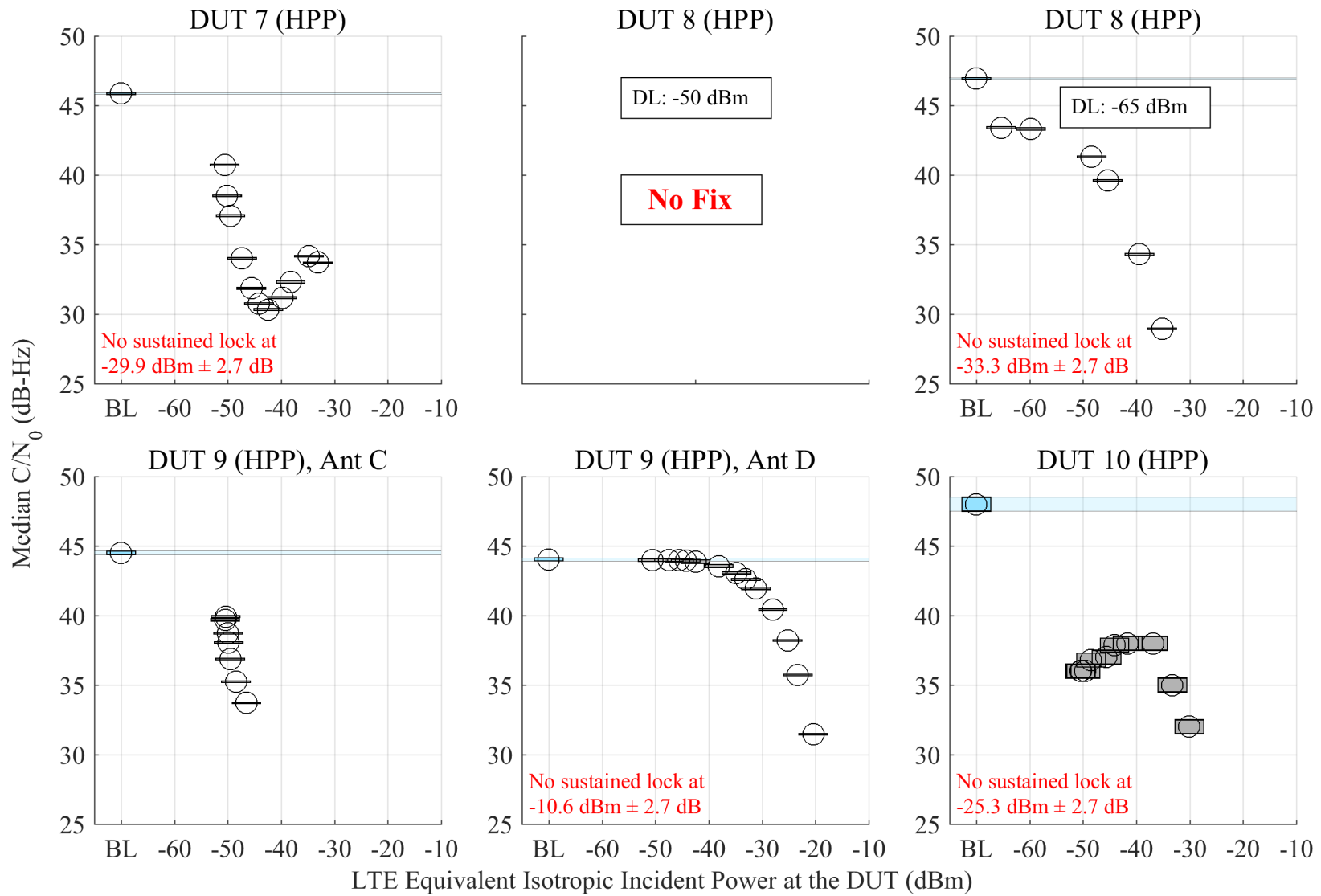


Figure 6.40: Estimated 95% confidence regions of the median of reported  $C/N_0$  from HPP receivers, swept with LTE power level. The GPS scenario is nominal, and the type of incident LTE is DL + UL1. The UL level was swept, and the DL level was fixed at -50 dBm EIIIP unless otherwise annotated. The horizontal axis reports the linear sum of DL and UL power.

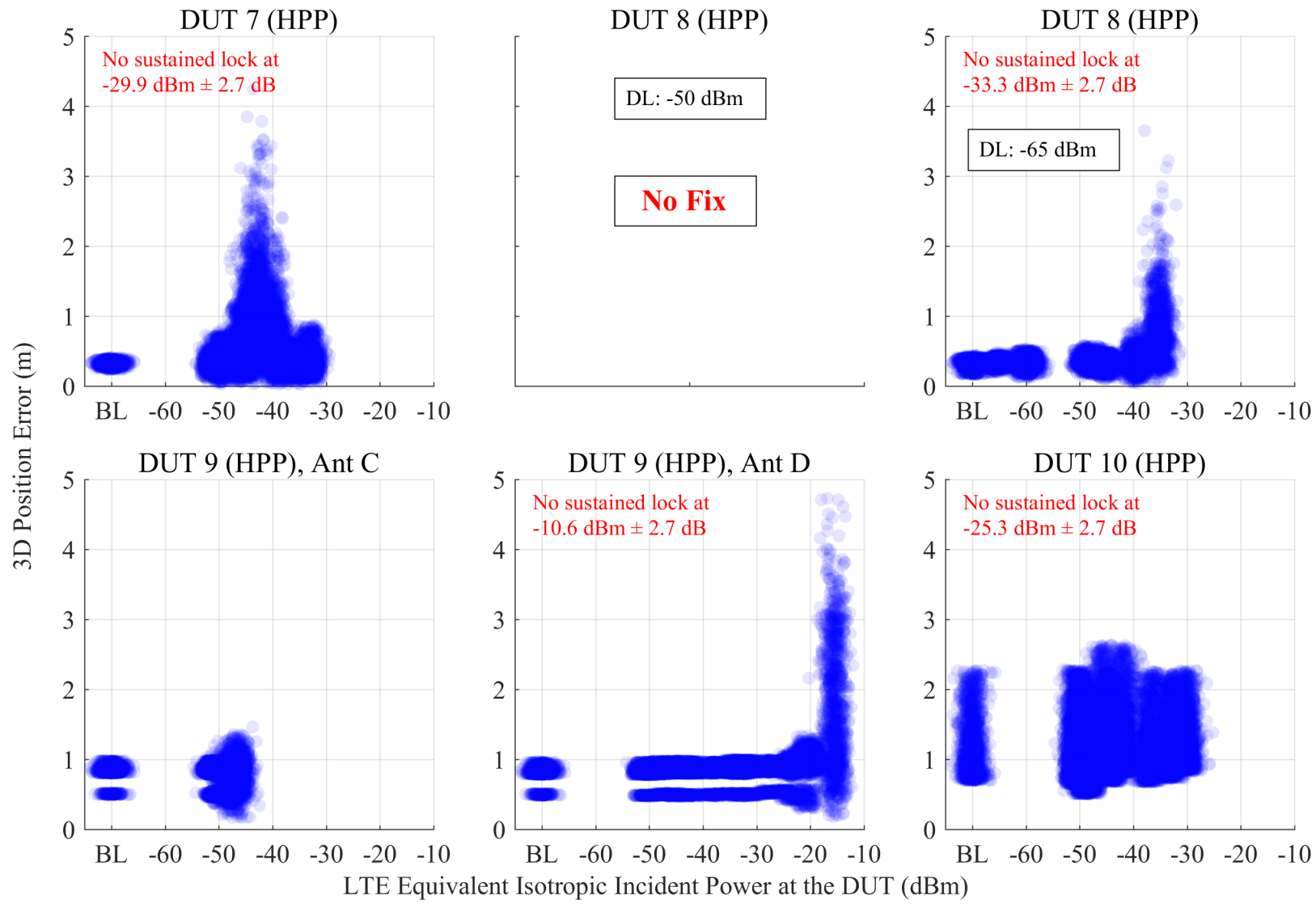


Figure 6.41: Scatterplots of error in reported 3-D position compared to simulator truth from HPP receivers, swept with LTE power level. The GPS scenario is nominal, and the type of incident LTE is DL + UL1. The UL level was swept, and the DL level was fixed at -50 dBm EIPP unless otherwise annotated. The horizontal axis reports the linear sum of DL and UL power.

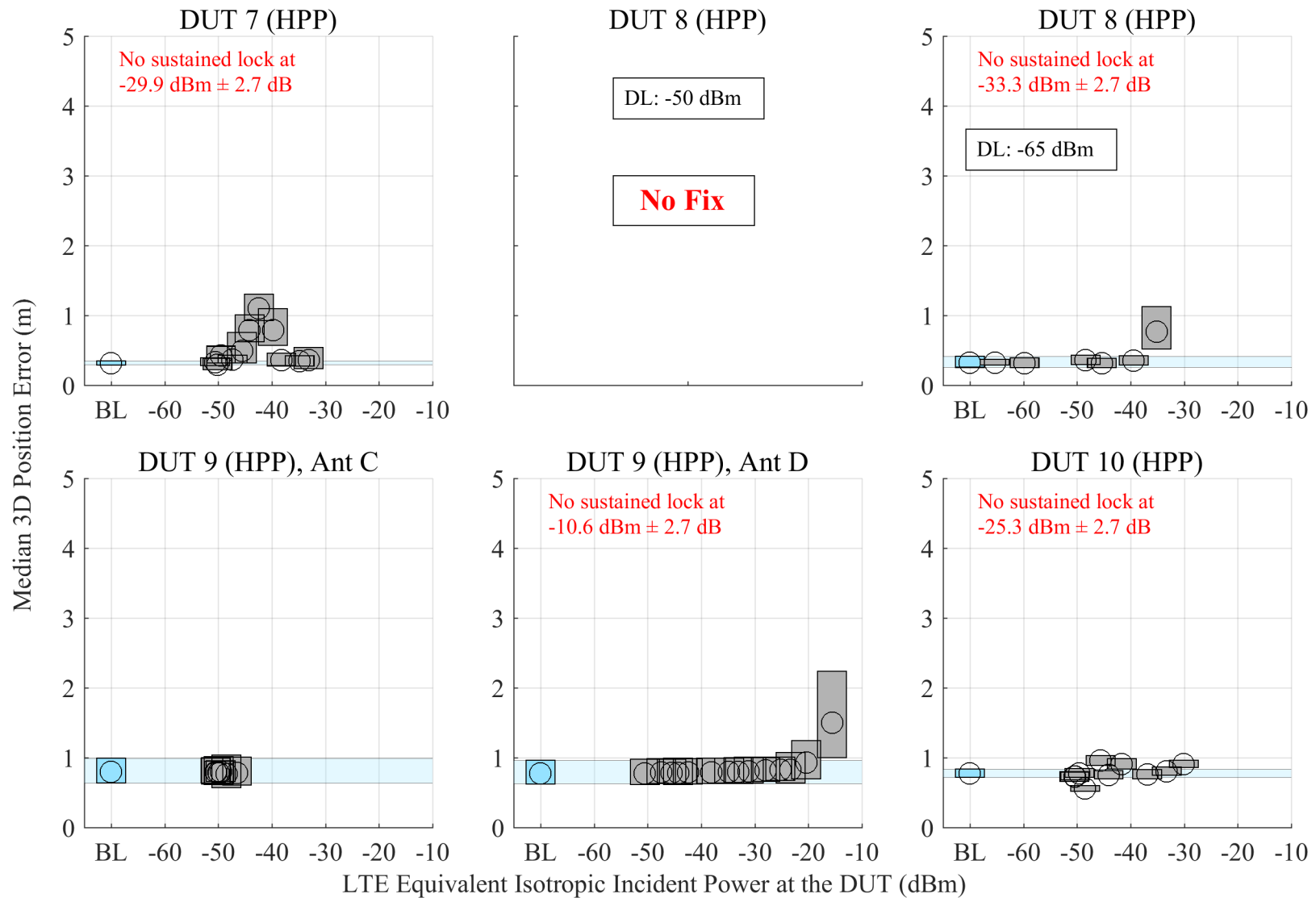


Figure 6.42: Estimated 95% confidence regions of the median error in reported 3-D position from HPP receivers, swept with LTE power level. The GPS scenario is nominal, and the type of incident LTE is DL + UL1. The UL level was swept, and the DL level was fixed at -50 dBm EIIIP unless otherwise annotated. The horizontal axis reports the linear sum of DL and UL power.

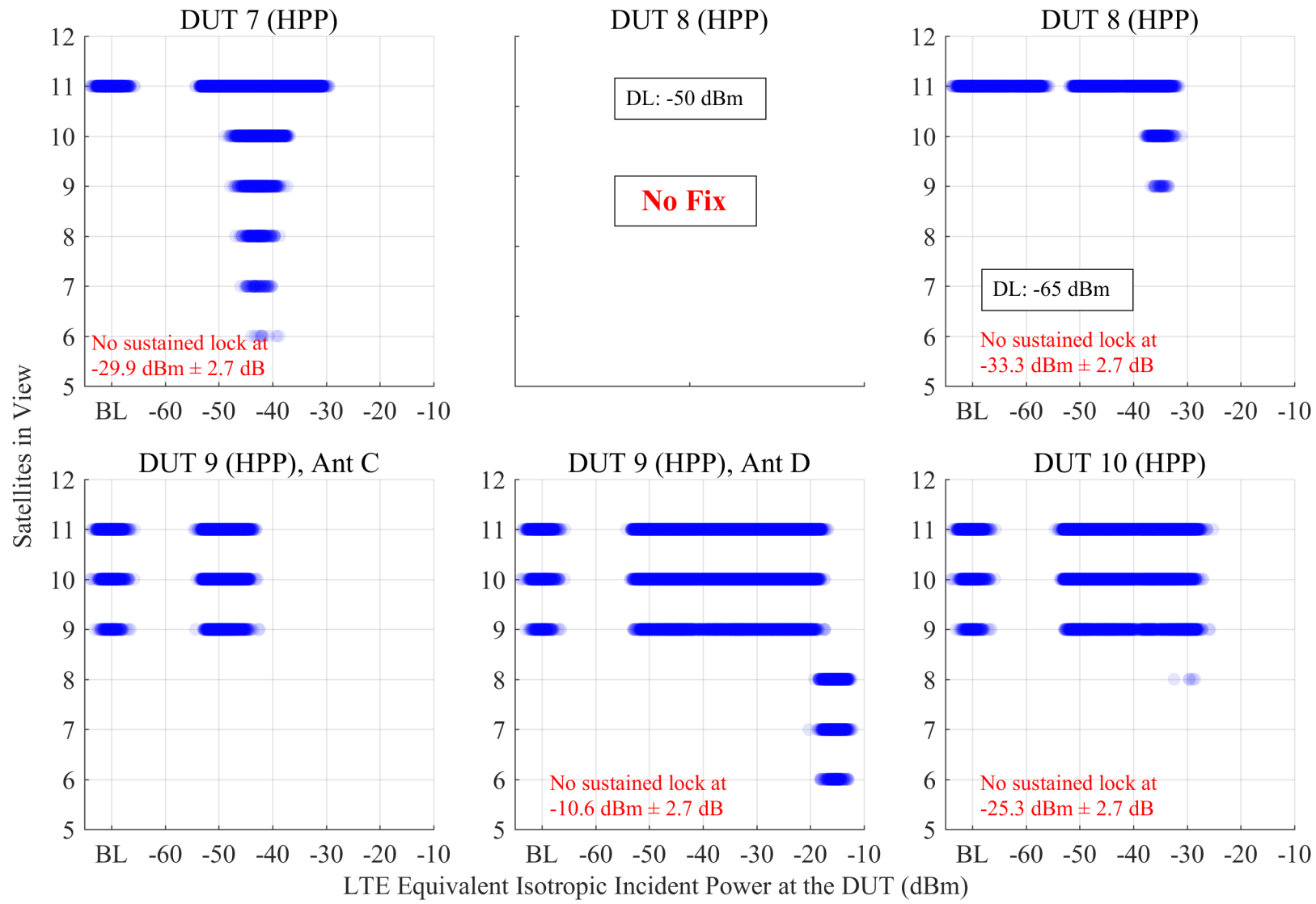


Figure 6.43: Scatterplots of the number of satellites in view from HPP receivers, swept with LTE power level. The GPS scenario is nominal, and the type of incident LTE is DL + UL1. The UL level was swept, and the DL level was fixed at -50 dBm EIIP unless otherwise annotated. The horizontal axis reports the linear sum of DL and UL power.

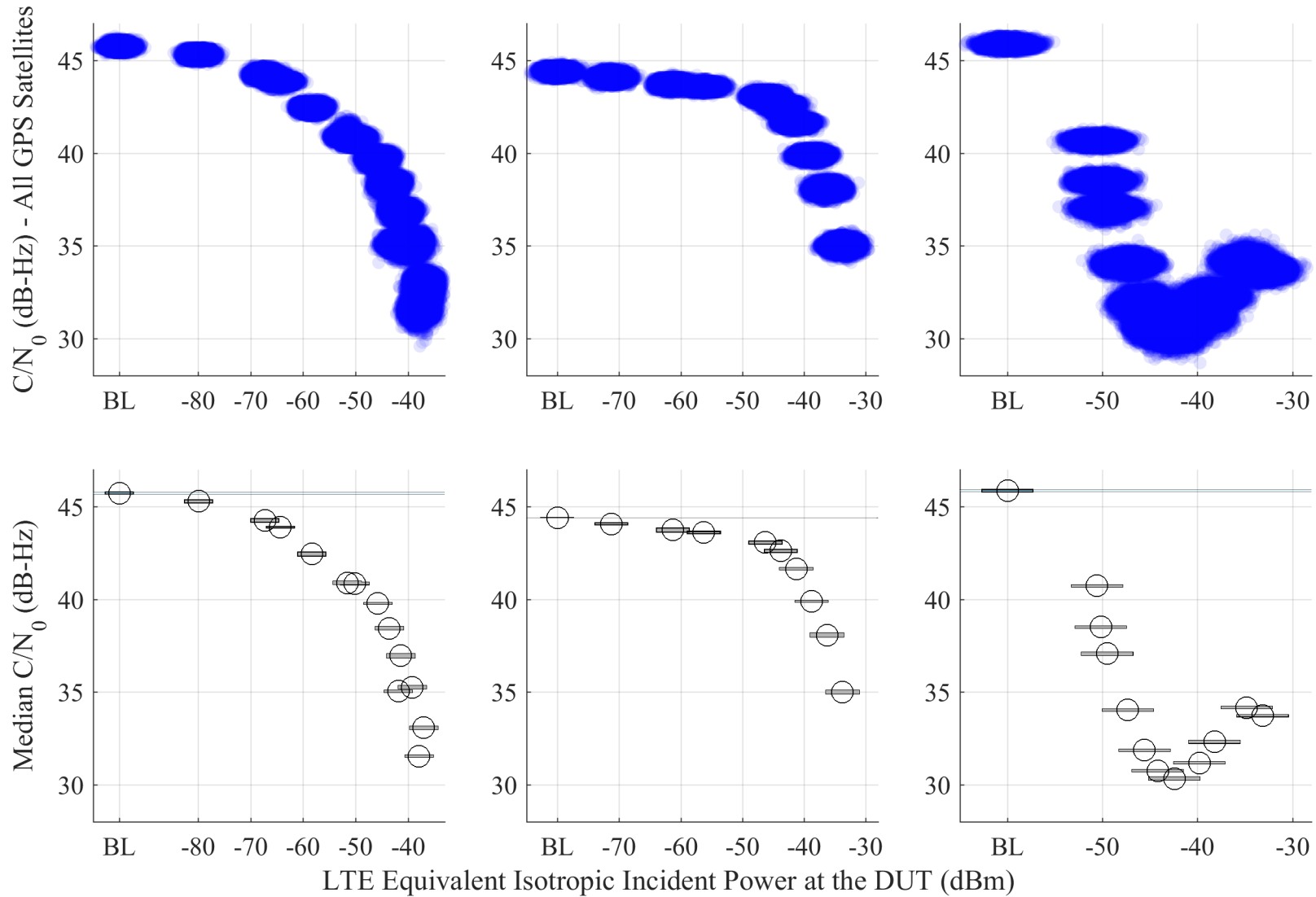


Figure 6.44:  $C/N_0$  response from DUT 7 (HPP), swept with LTE power, for the combination DL + UL1 LTE scenario. Top row are the scatterplots and the bottom row is that of the estimated 95% confidence regions of the median. Left column: Downlink LTE signal, middle column: Uplink 1, right column: Combination DL + UL1. The UL level was swept, and the DL level was fixed at -50 dBm EIIP unless otherwise annotated. The horizontal axis reports the linear sum of DL and UL power.

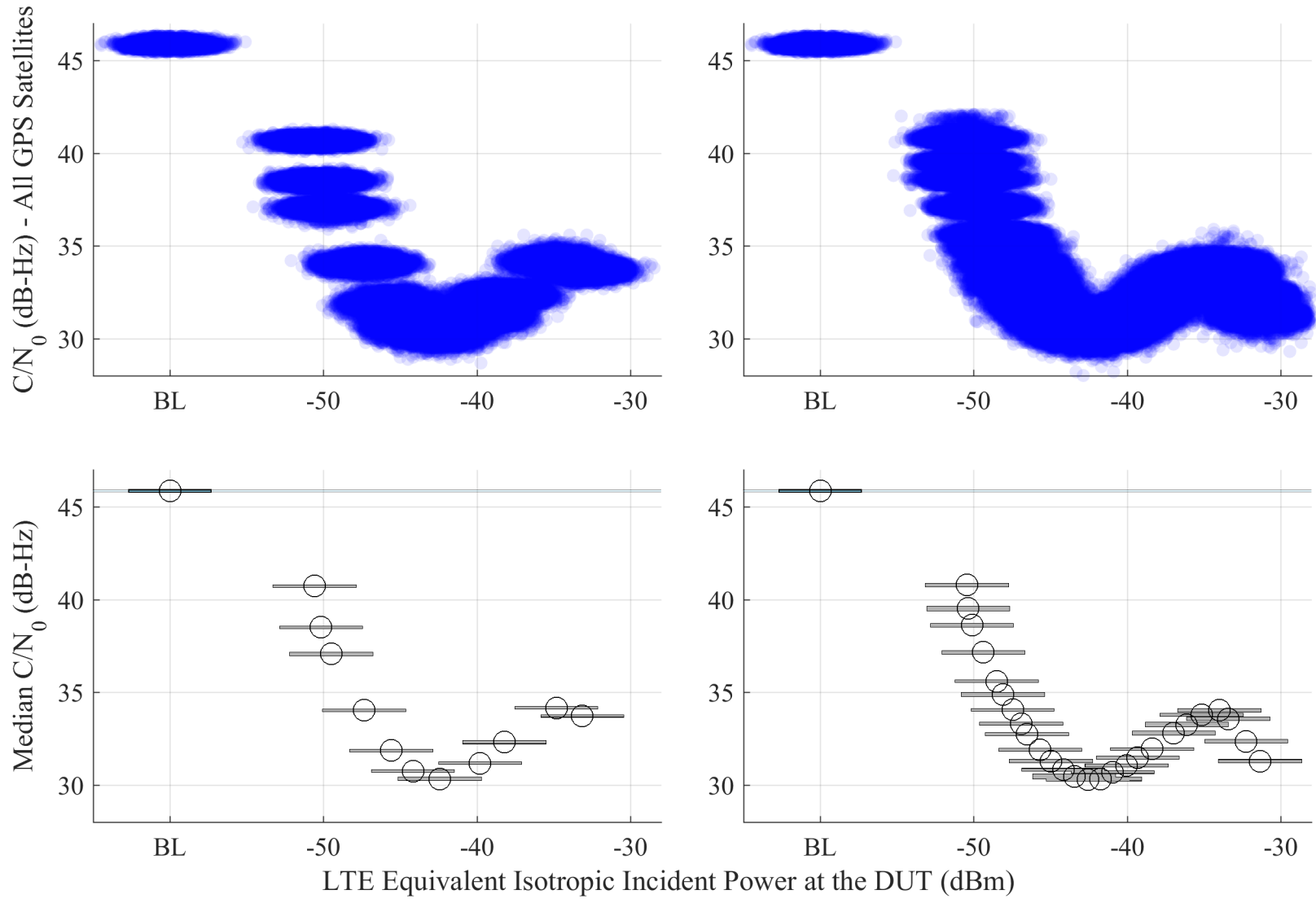


Figure 6.45: Repeat test of  $C/N_0$  from DUT 7 (HPP), swept with LTE power, for the combination DL + UL1 LTE scenario. The repeat was after several days and tests of other DUTs. The trend of the  $C/N_0$  response of the repeated measurement (right column) follows the initial (left column) measurement closely. The UL level was swept, and the DL level was fixed at -50 dBm EIIP unless otherwise annotated. The horizontal axis reports the linear sum of DL and UL power.

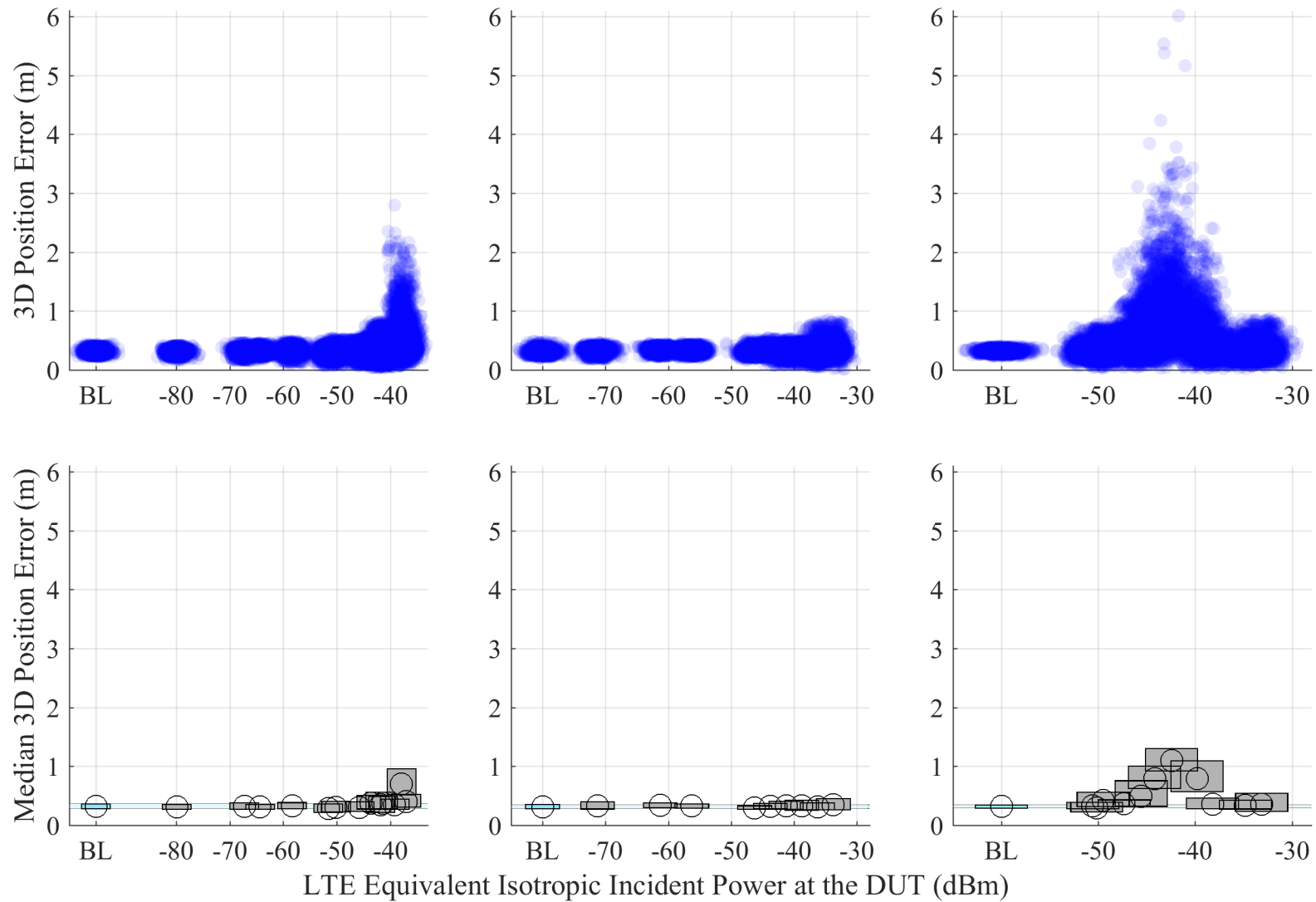


Figure 6.46: Error in reported 3-D position from DUT 7 (HPP), swept with LTE power, for the combination DL + UL1 LTE scenario. Top row are the scatterplots and the bottom row is that of the estimated 95% confidence regions of the median error in reported 3-D position. Left column: Downlink LTE signal, middle column: Uplink 1, right column: Combination DL + UL1. The UL level was swept, and the DL level was fixed at -50 dBm EIP unless otherwise annotated. The horizontal axis reports the linear sum of DL and UL power.

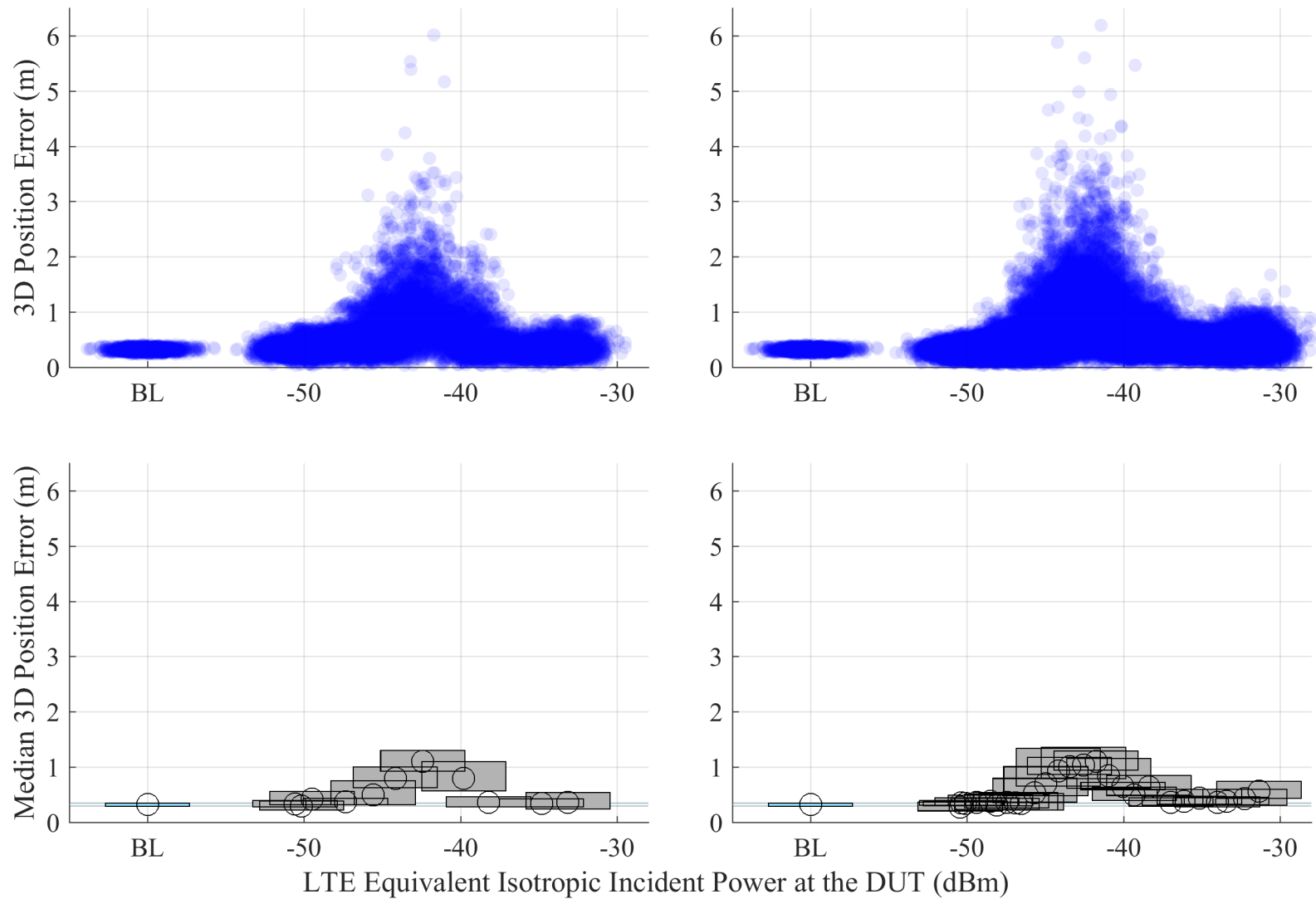


Figure 6.47: Repeat test of error in reported 3-D position from DUT 7 (HPP), swept with LTE power, for the combination DL + UL1 LTE scenario. The repeat was after several days and tests of other DUTs. The trend of the repeated measurement result (right column) follows the initial (left column) measurement closely. The UL level was swept, and the DL level was fixed at -50 dBm EIIP unless otherwise annotated. The horizontal axis reports the linear sum of DL and UL power.

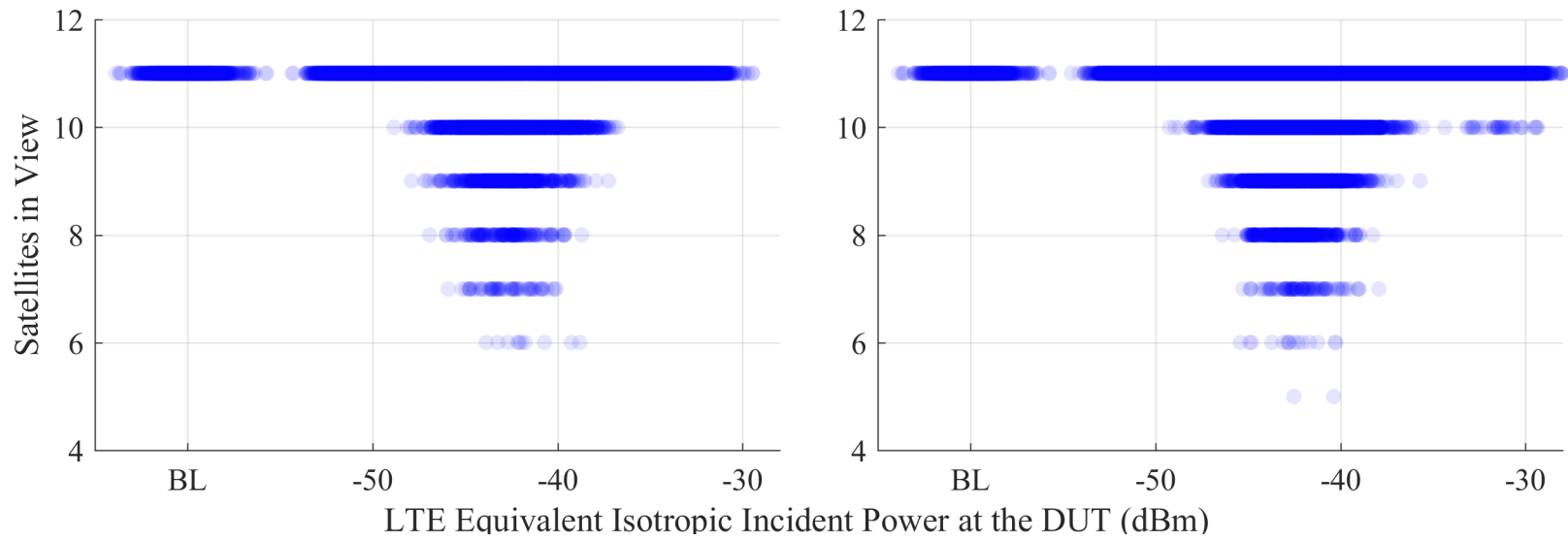


Figure 6.48: Repeat test the number of satellites in view to from DUT 7 (HPP), swept with LTE power, for the combination DL + UL1 LTE scenario. The repeat was after several days and tests of other DUTs. The trend of the repeated measurement result (right column) follows the initial (left column) measurement closely. The UL level was swept, and the DL level was fixed at -50 dBm EIIP unless otherwise annotated. The horizontal axis reports the linear sum of DL and UL power.

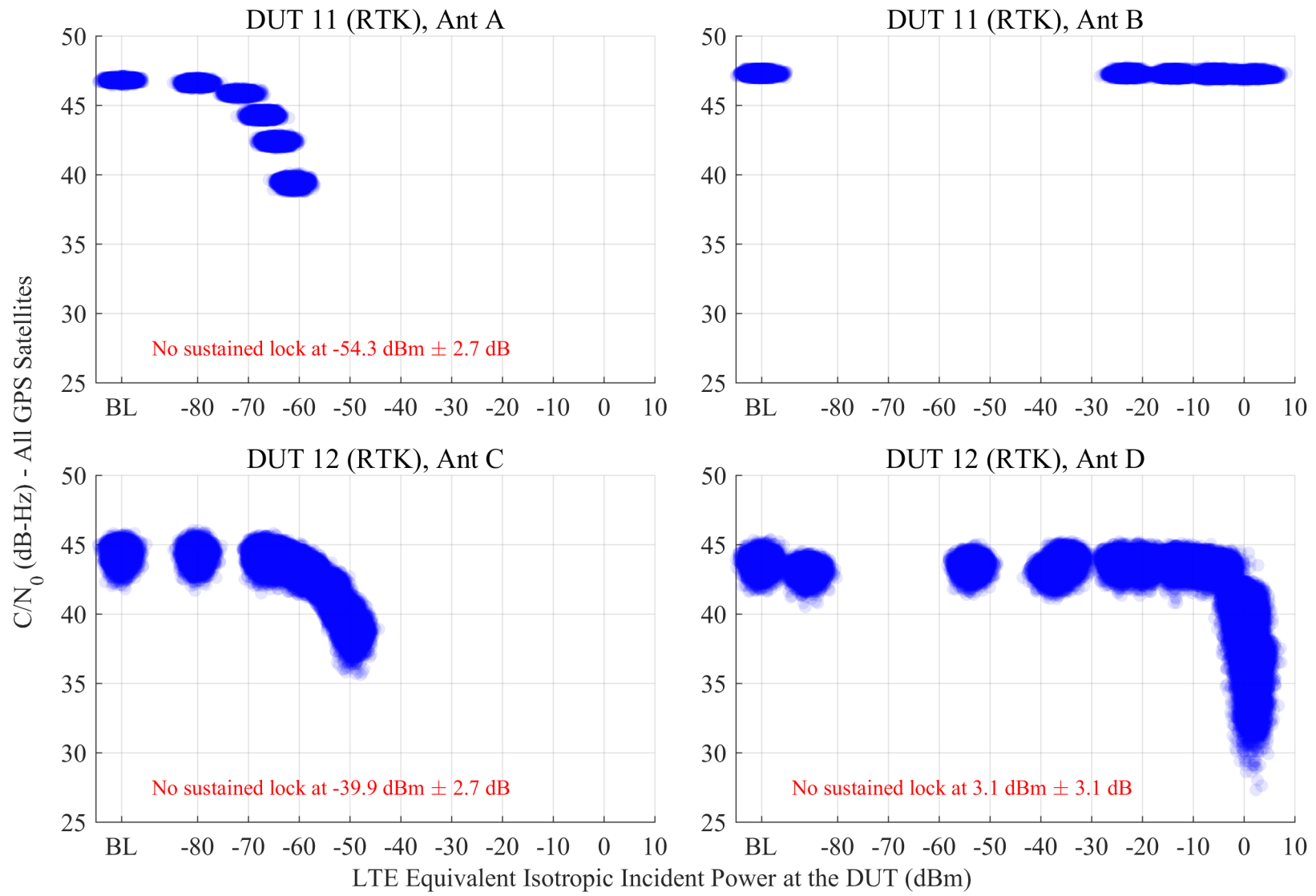


Figure 6.49: Scatterplots of reported  $C/N_0$  from RTK receivers, swept with LTE power level. The GPS scenario is nominal, and the type of incident LTE is DL.

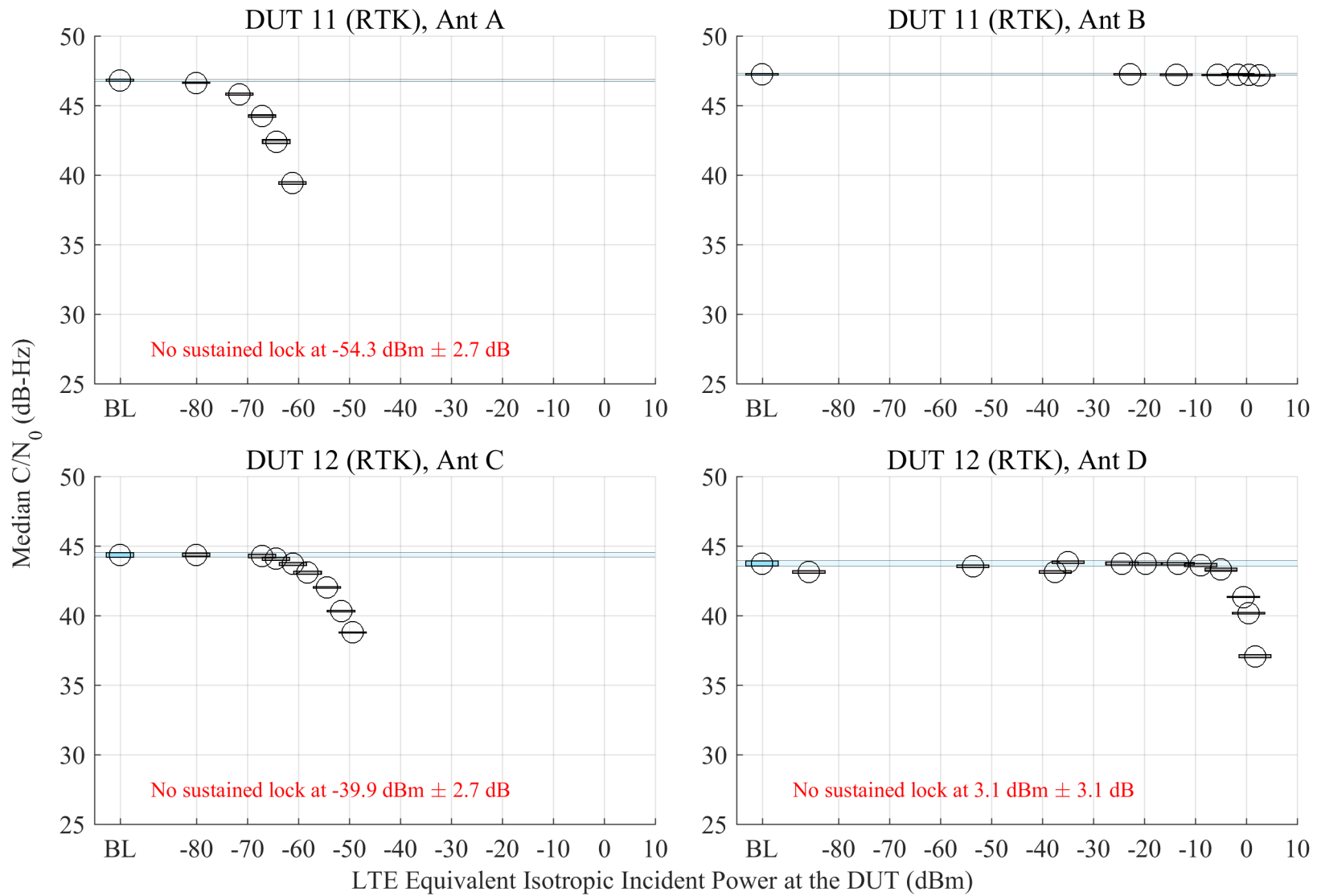


Figure 6.50: Estimated 95% confidence regions of the median of reported  $C/N_0$  from RTK receivers, swept with LTE power level. The GPS scenario is nominal, and the type of incident LTE is DL.

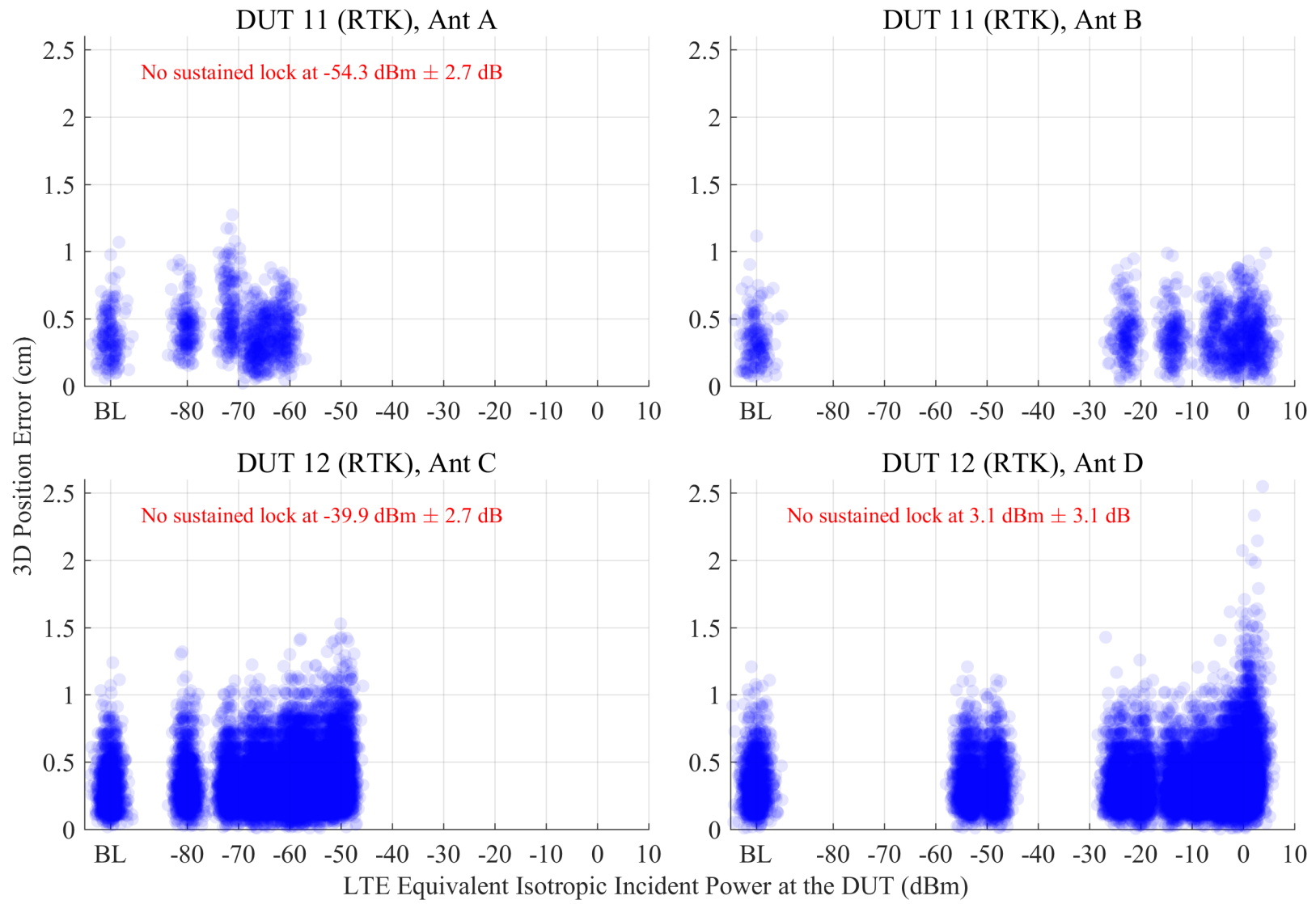


Figure 6.51: Scatterplots of error in reported 3-D position compared to simulator truth from RTK receivers, swept with LTE power level. The GPS scenario is nominal, and the type of incident LTE is DL.

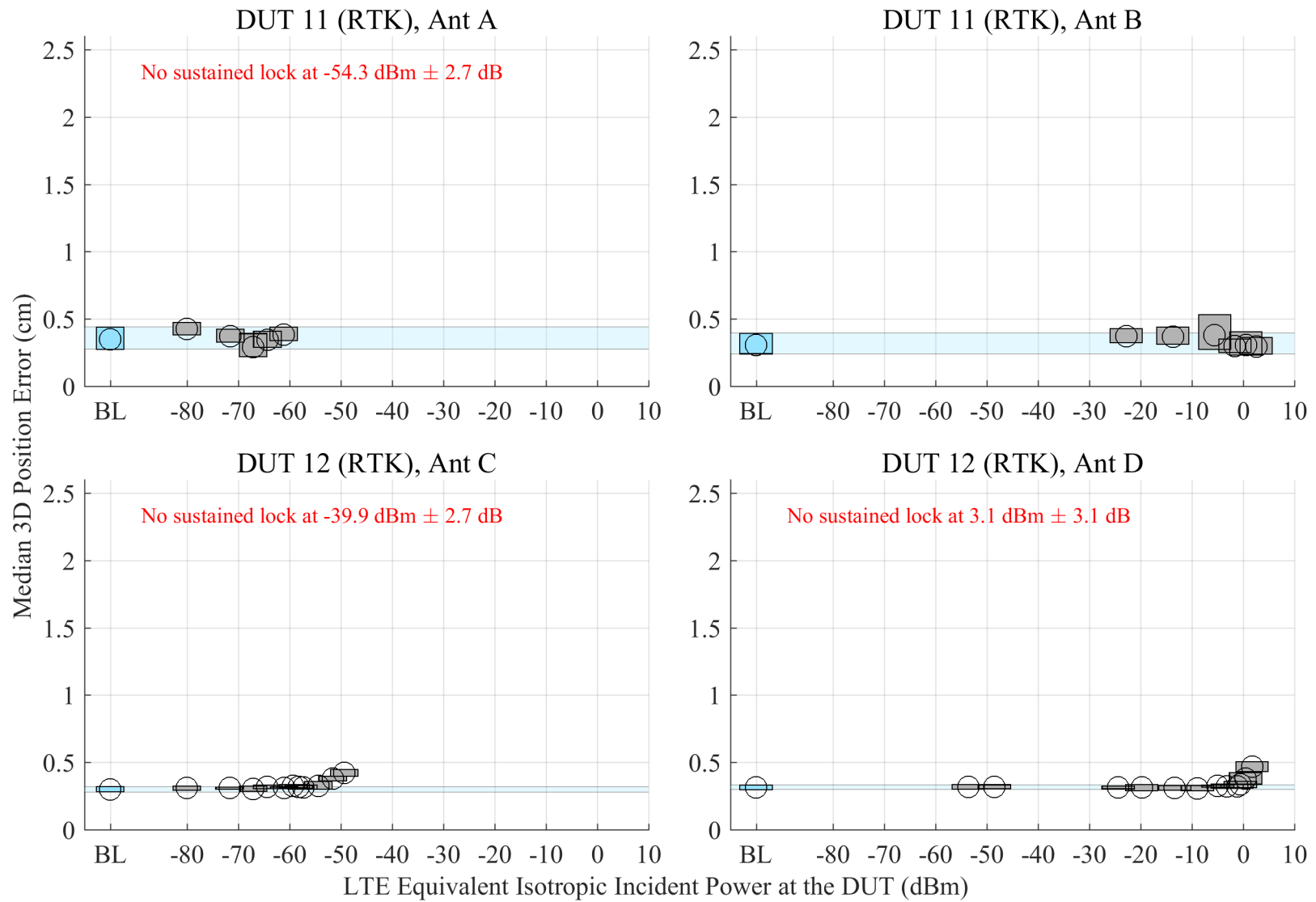


Figure 6.52: Estimated 95% confidence regions of the median error in reported 3-D position from RTK receivers, swept with LTE power level. The GPS scenario is nominal, and the type of incident LTE is DL.

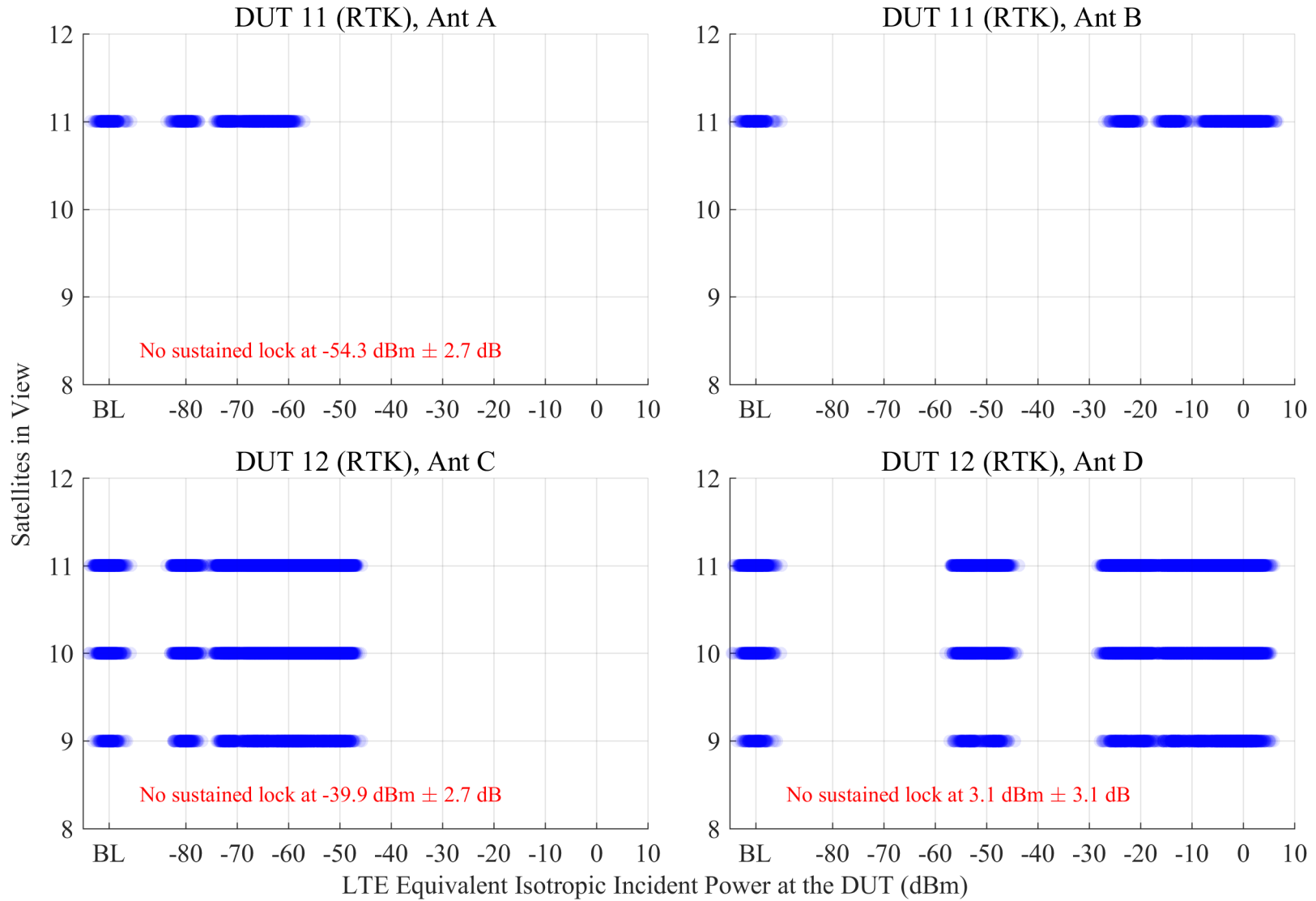


Figure 6.53: Scatterplots of the number of satellites in view from RTK receivers, swept with LTE power level. The GPS scenario is nominal, and the type of incident LTE is DL.

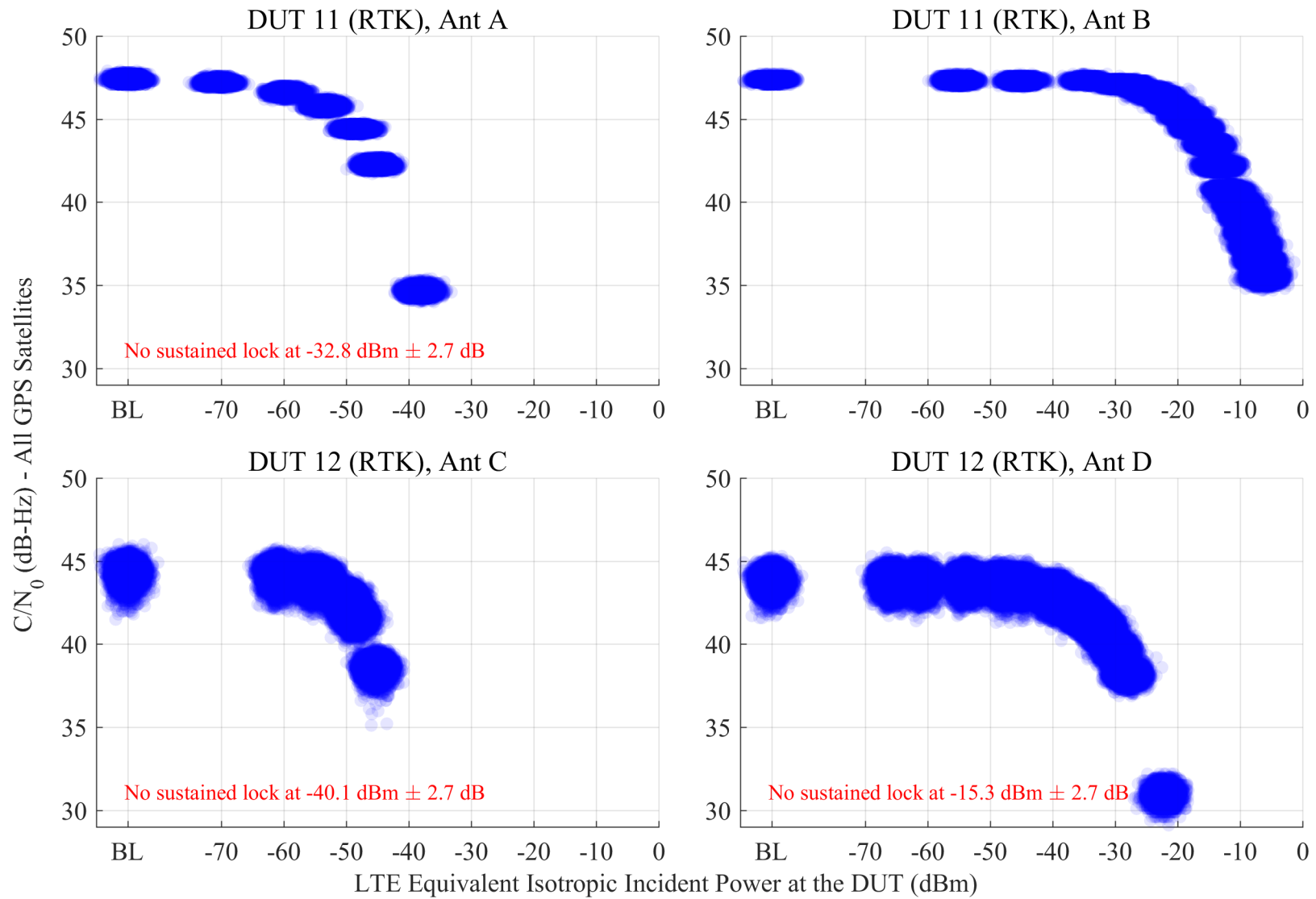


Figure 6.54: Scatterplots of reported  $C/N_0$  from RTK receivers, swept with LTE power level. The GPS scenario is nominal, and the type of incident LTE is UL1.

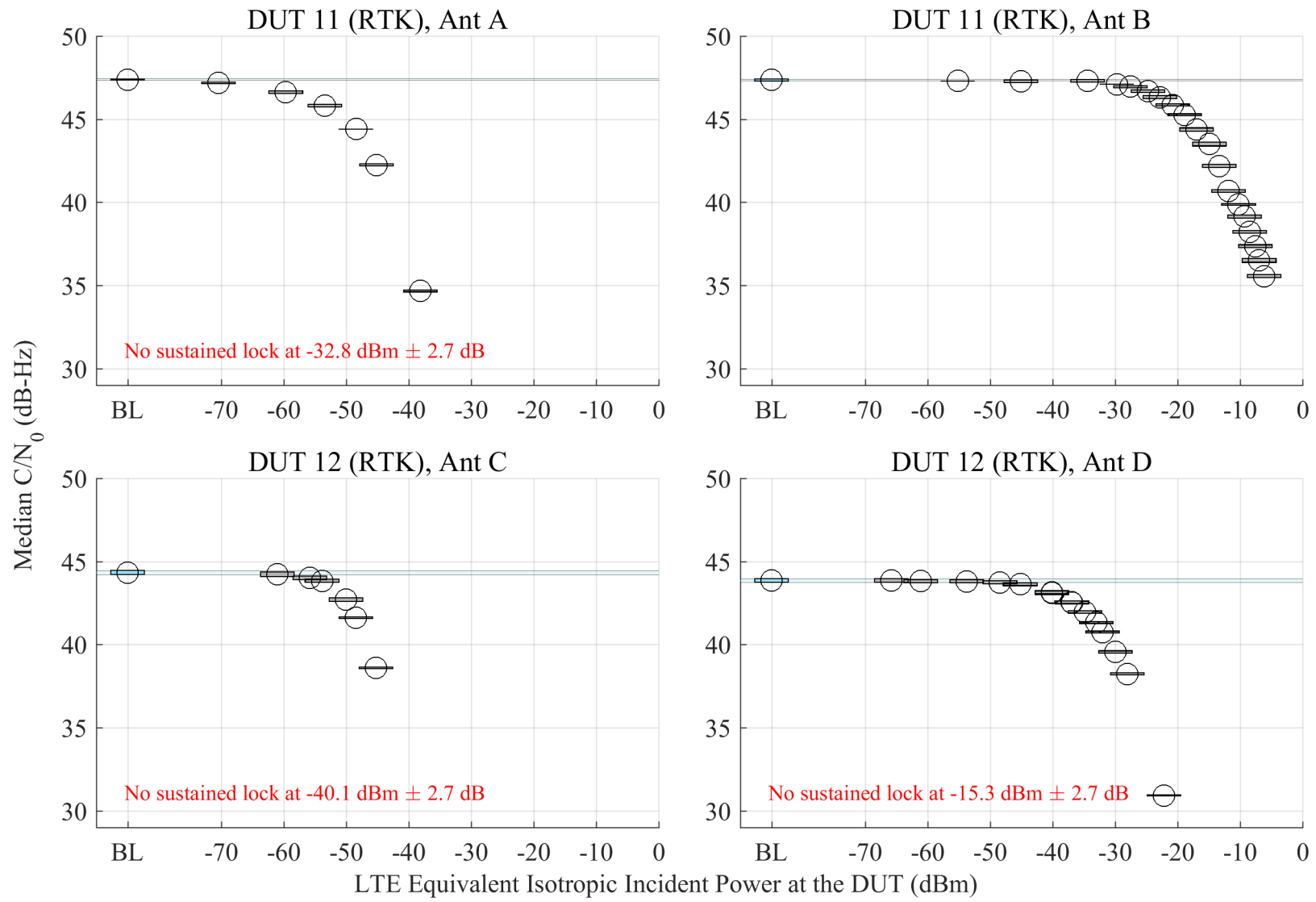


Figure 6.55: Estimated 95% confidence regions of the median of reported  $C/N_0$  from RTK receivers, swept with LTE power level. The GPS scenario is nominal, and the type of incident LTE is UL1.

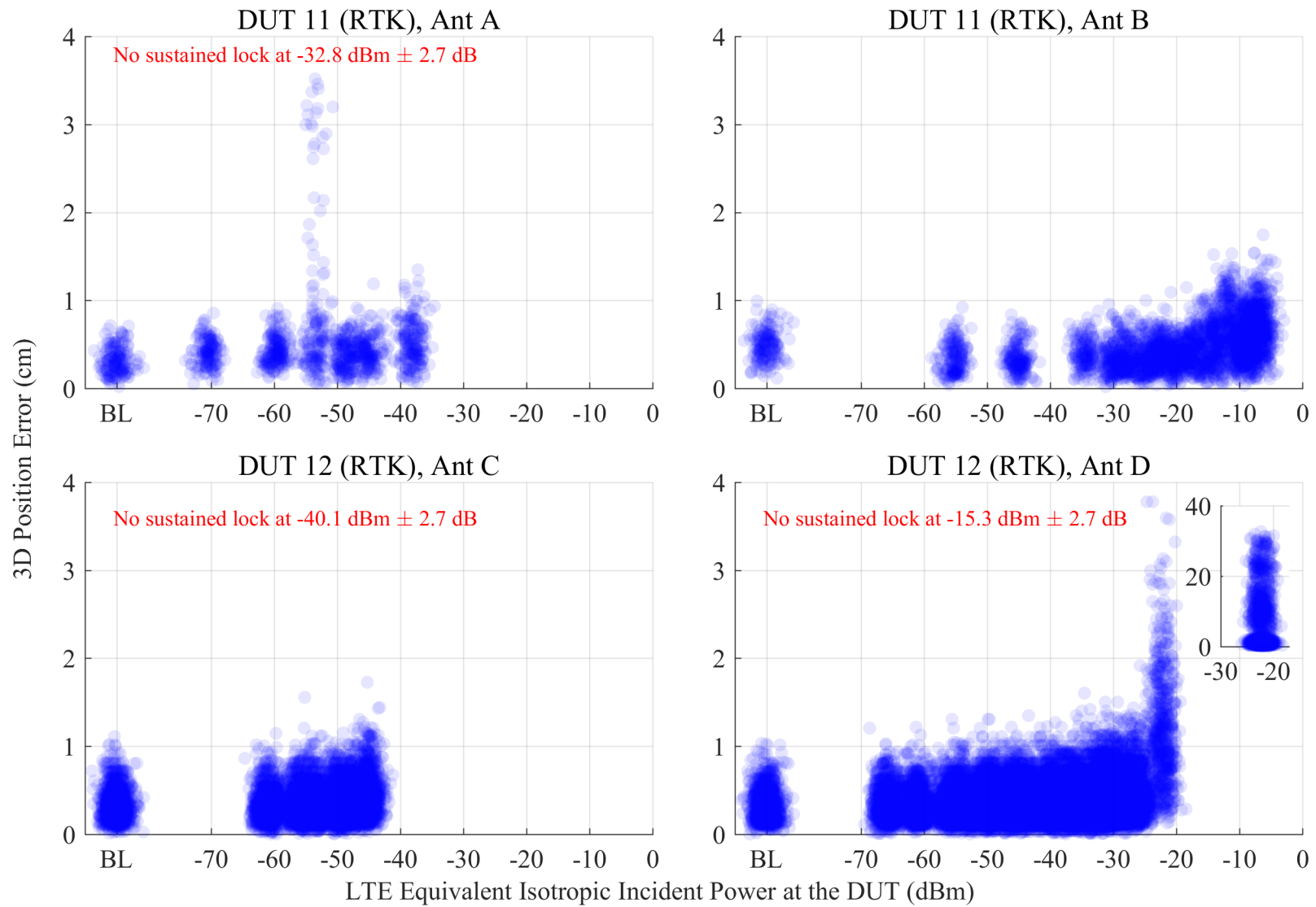


Figure 6.56: Scatterplots of error in reported 3-D position compared to simulator truth from RTK receivers, swept with LTE power level. The GPS scenario is nominal, and the type of incident LTE is UL1.

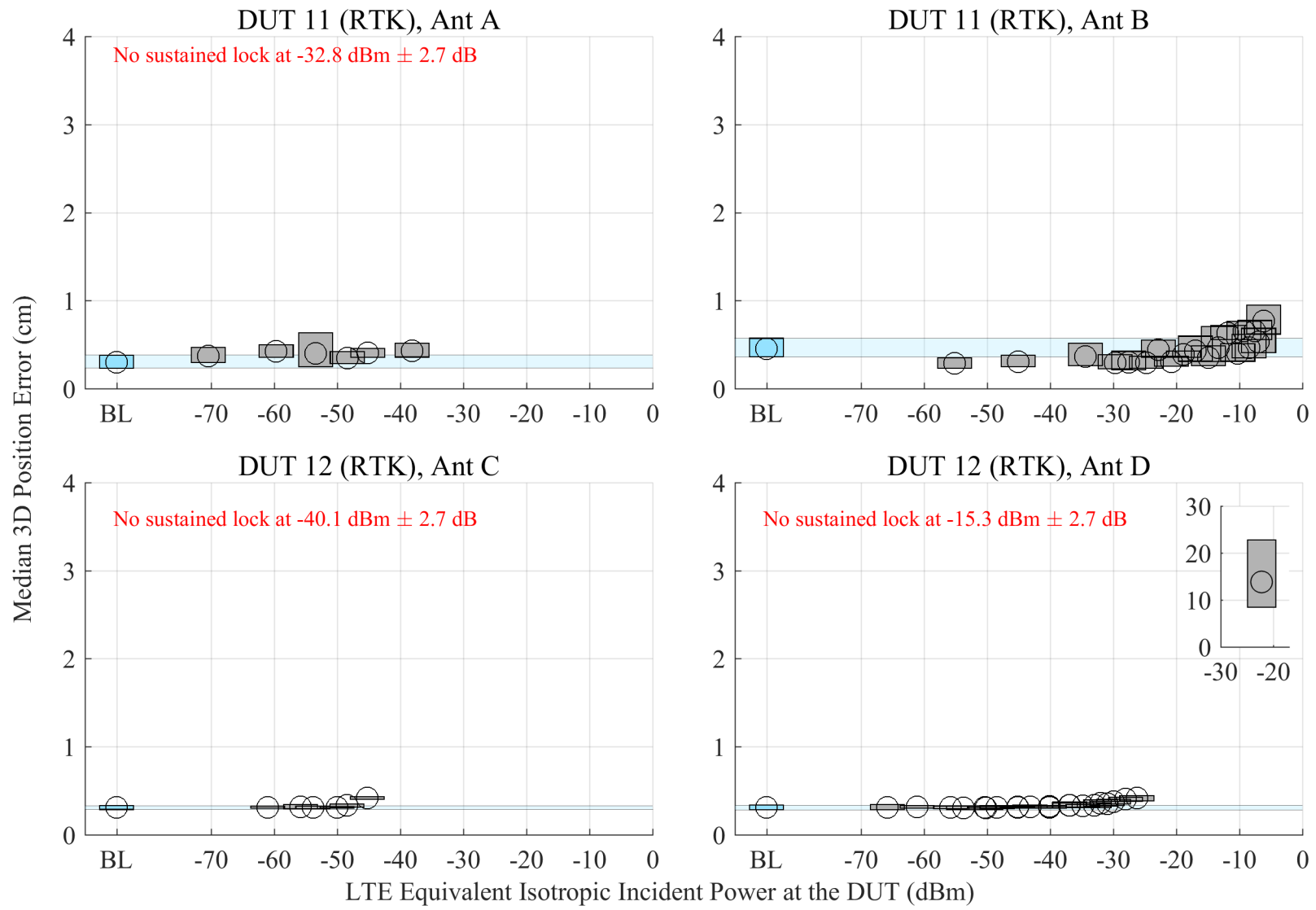


Figure 6.57: Estimated 95% confidence regions of the median error in reported 3-D position from RTK receivers, swept with LTE power level. The GPS scenario is nominal, and the type of incident LTE is UL1.

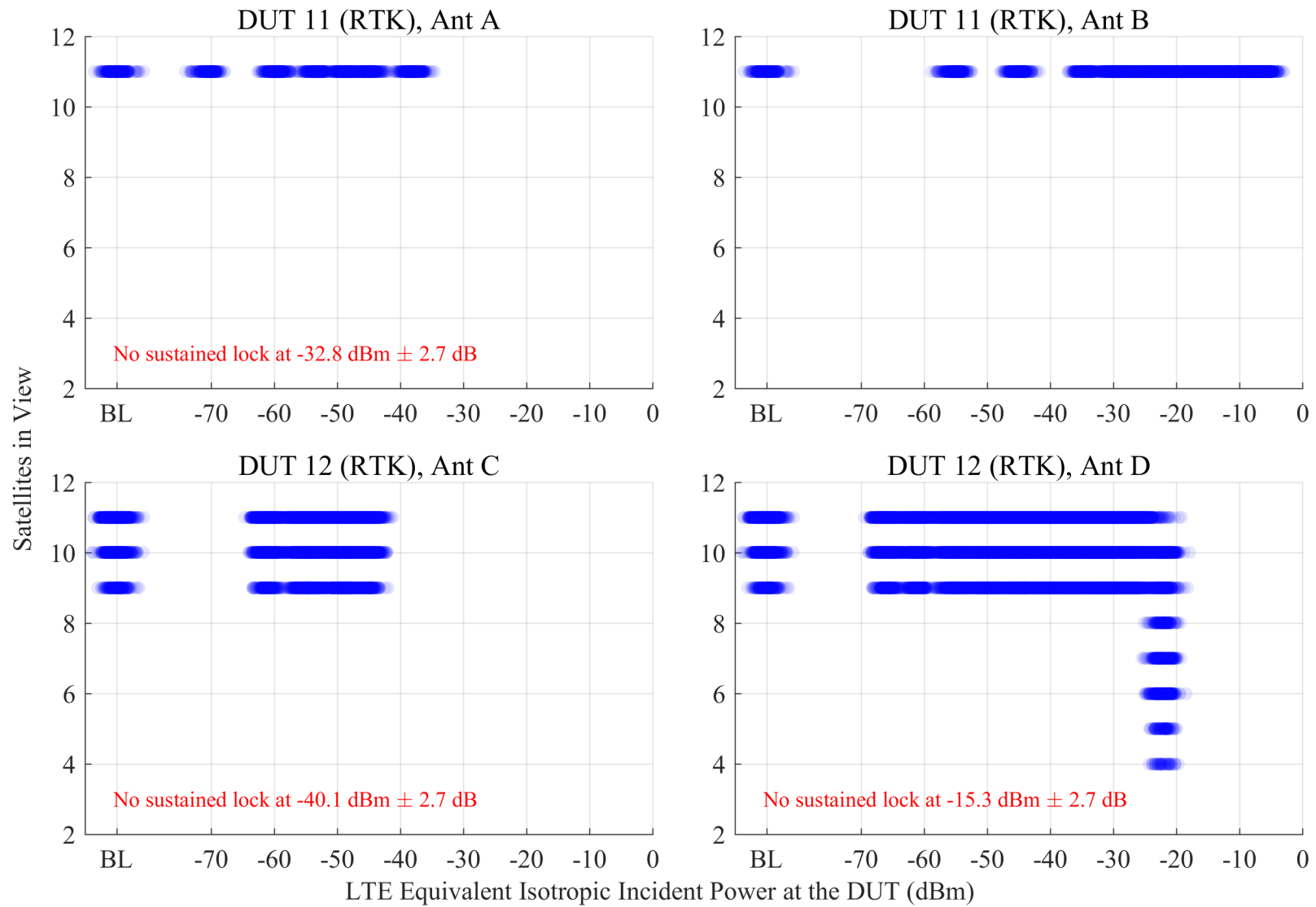


Figure 6.58: Scatterplots of the number of satellites in view from RTK receivers, swept with LTE power level. The GPS scenario is nominal, and the type of incident LTE is UL1.

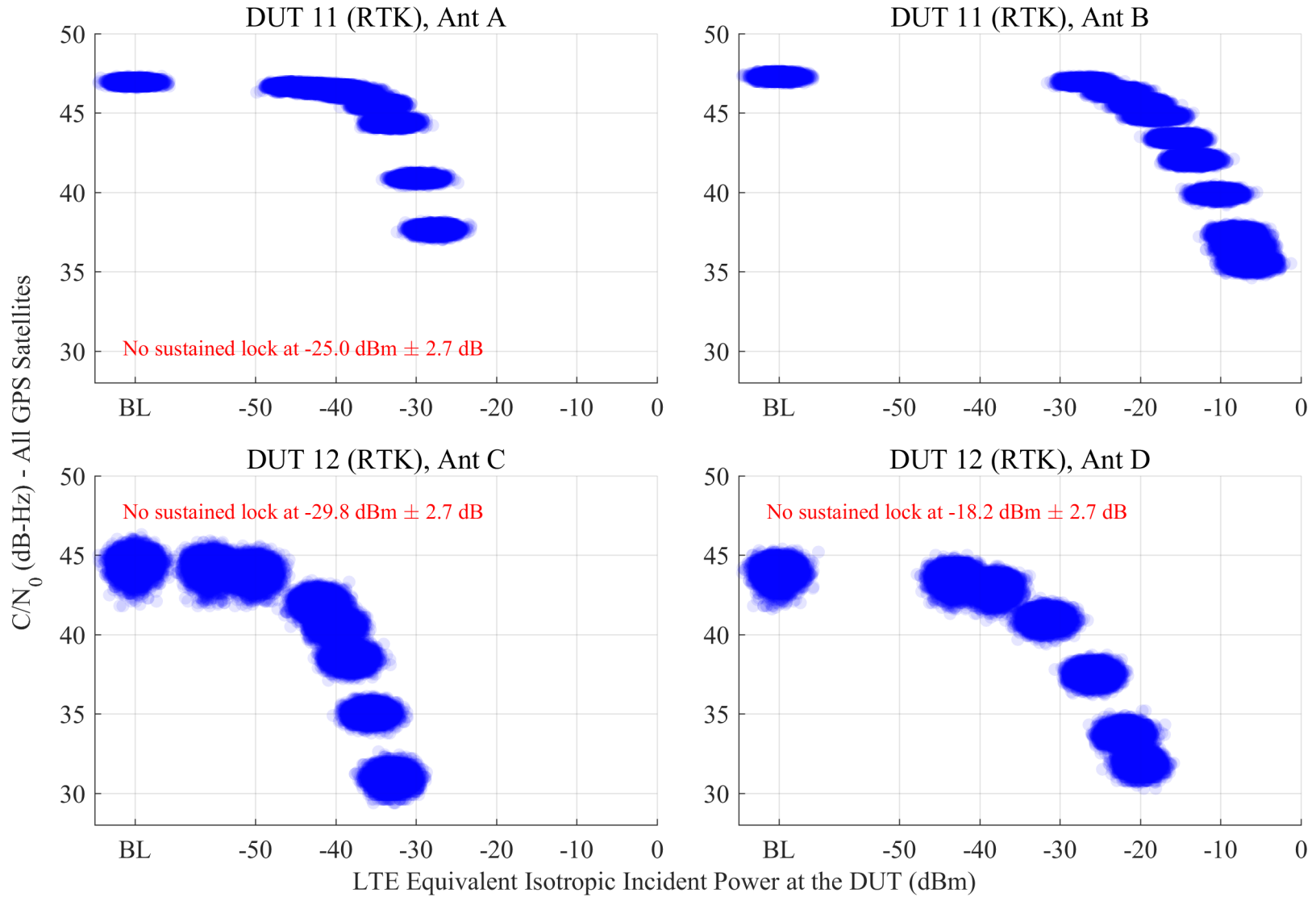


Figure 6.59: Scatterplots of reported  $C/N_0$  from RTK receivers, swept with LTE power level. The GPS scenario is nominal, and the type of incident LTE is UL2.

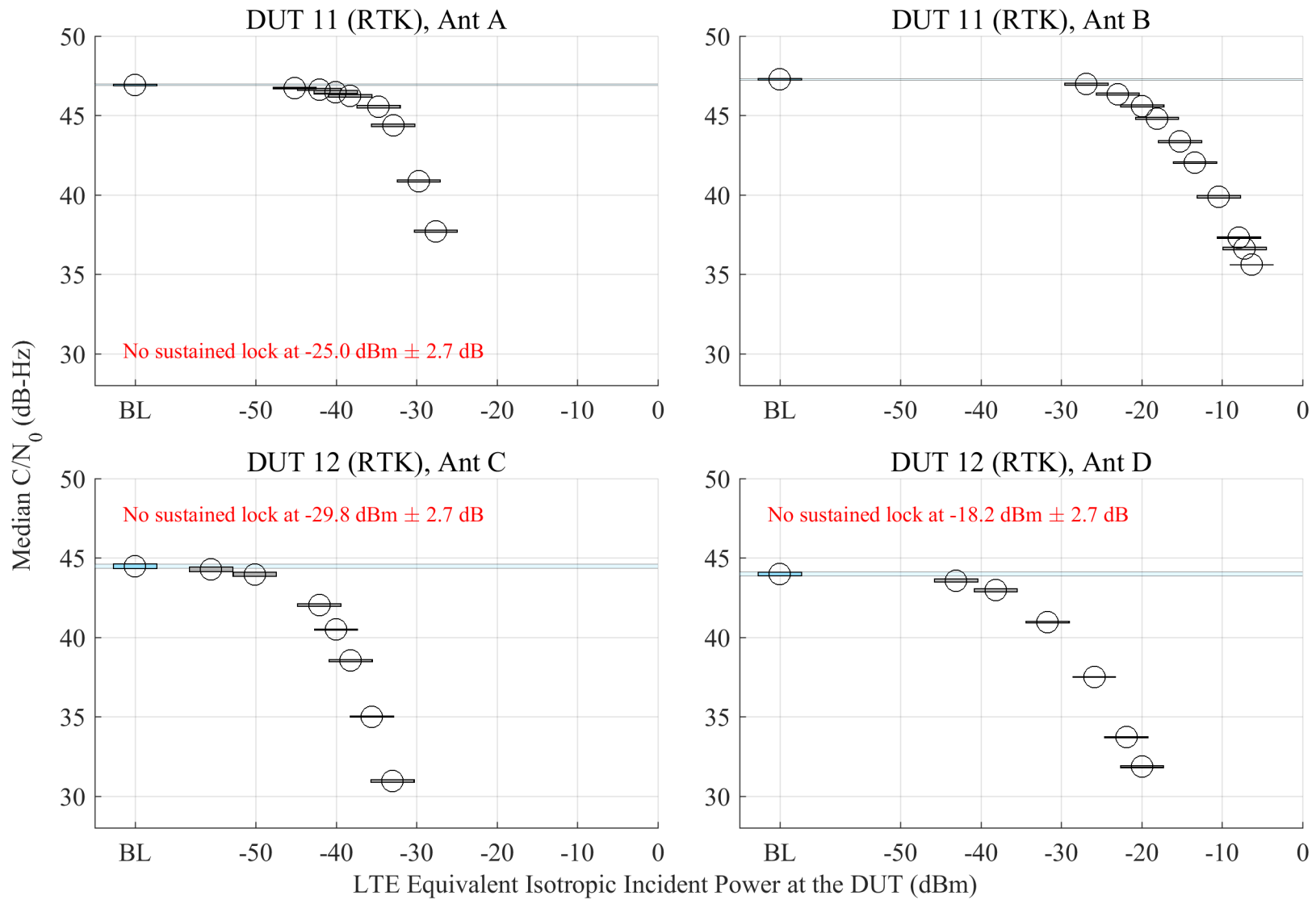


Figure 6.60: Estimated 95% confidence regions of the median of reported  $C/N_0$  from RTK receivers, swept with LTE power level. The GPS scenario is nominal, and the type of incident LTE is UL2.

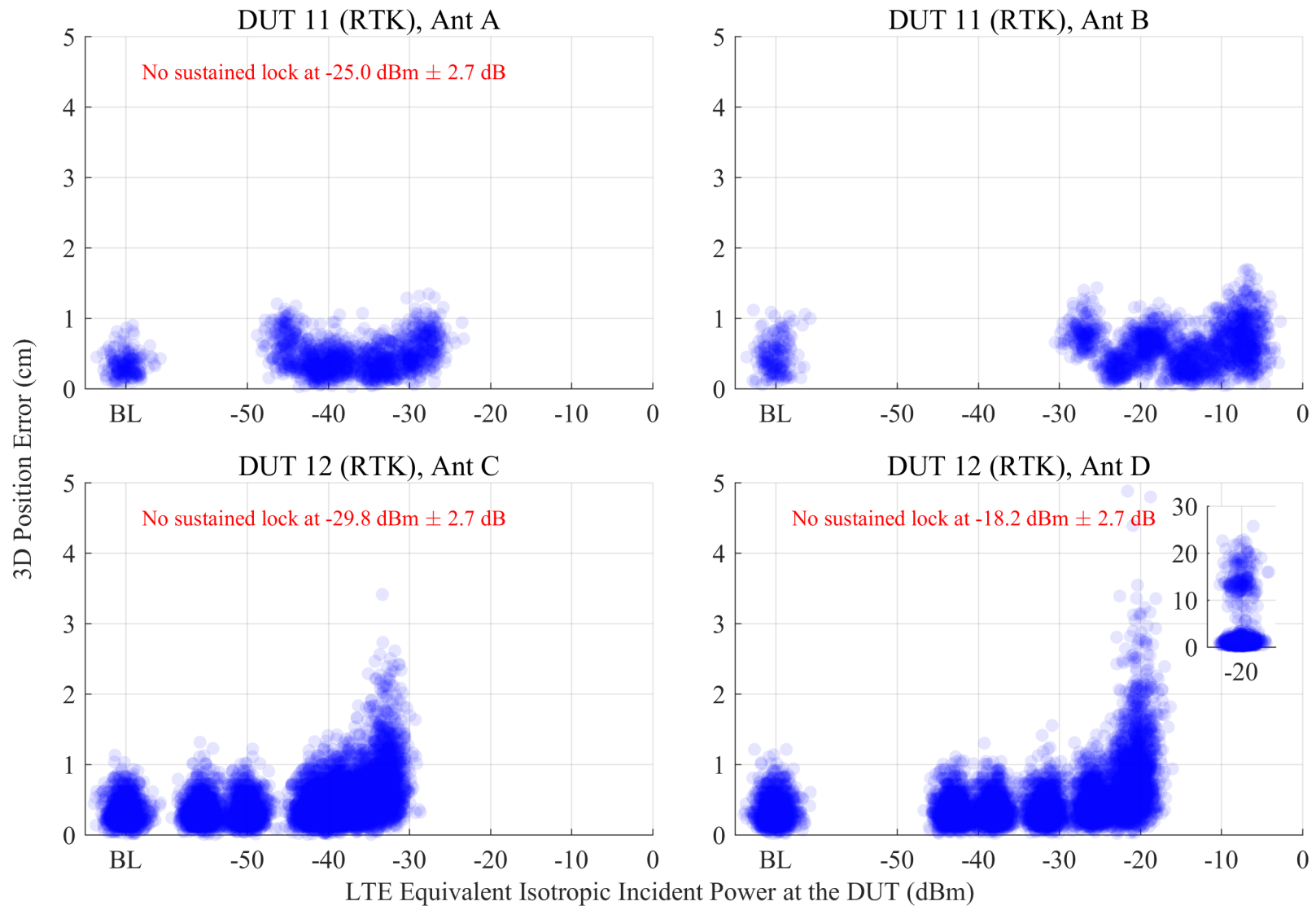


Figure 6.61: Scatterplots of error in reported 3-D position compared to simulator truth from RTK receivers, swept with LTE power level. The GPS scenario is nominal, and the type of incident LTE is UL2.

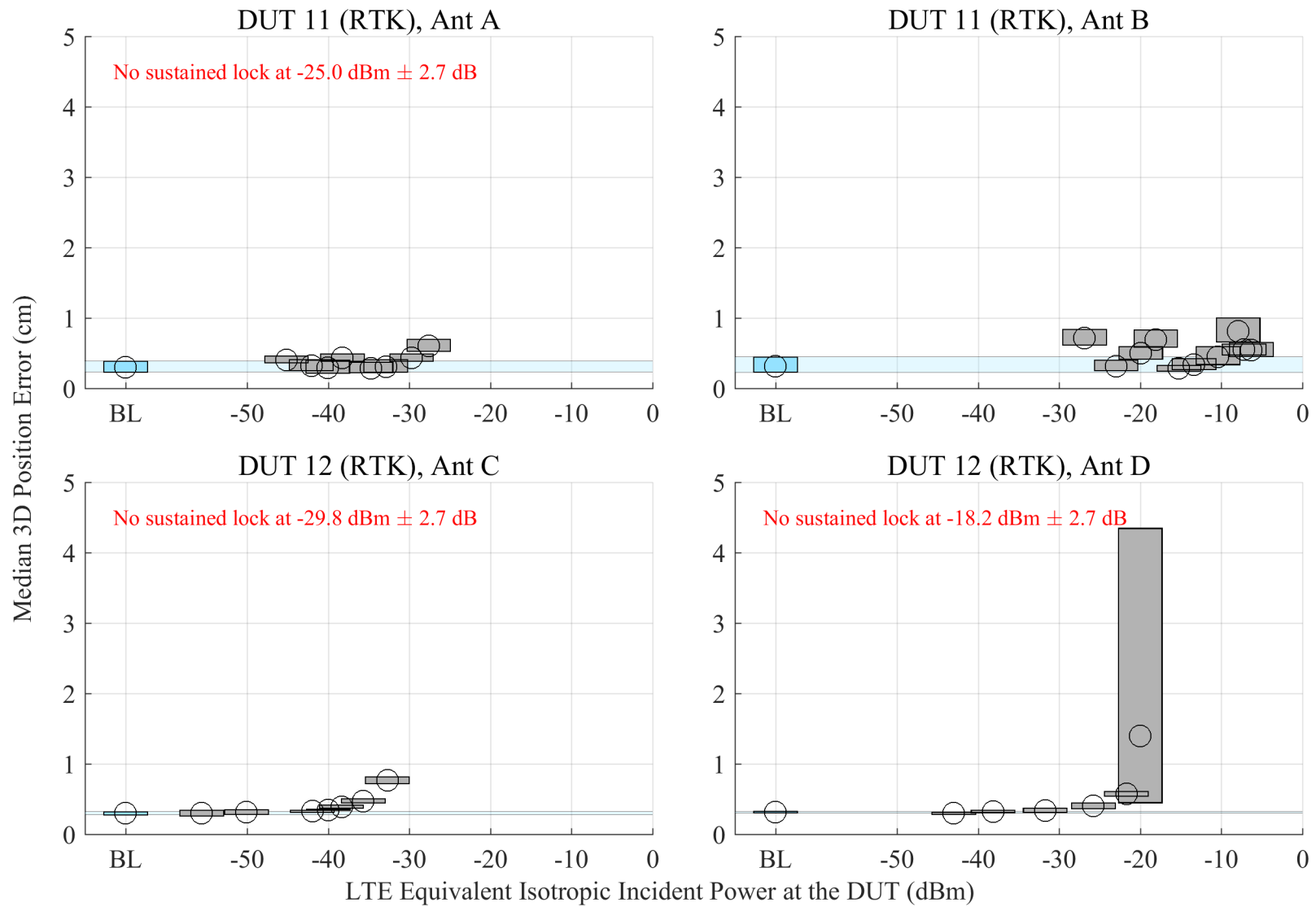


Figure 6.62: Estimated 95% confidence regions of the median error in reported 3-D position from RTK receivers, swept with LTE power level. The GPS scenario is nominal, and the type of incident LTE is UL2.

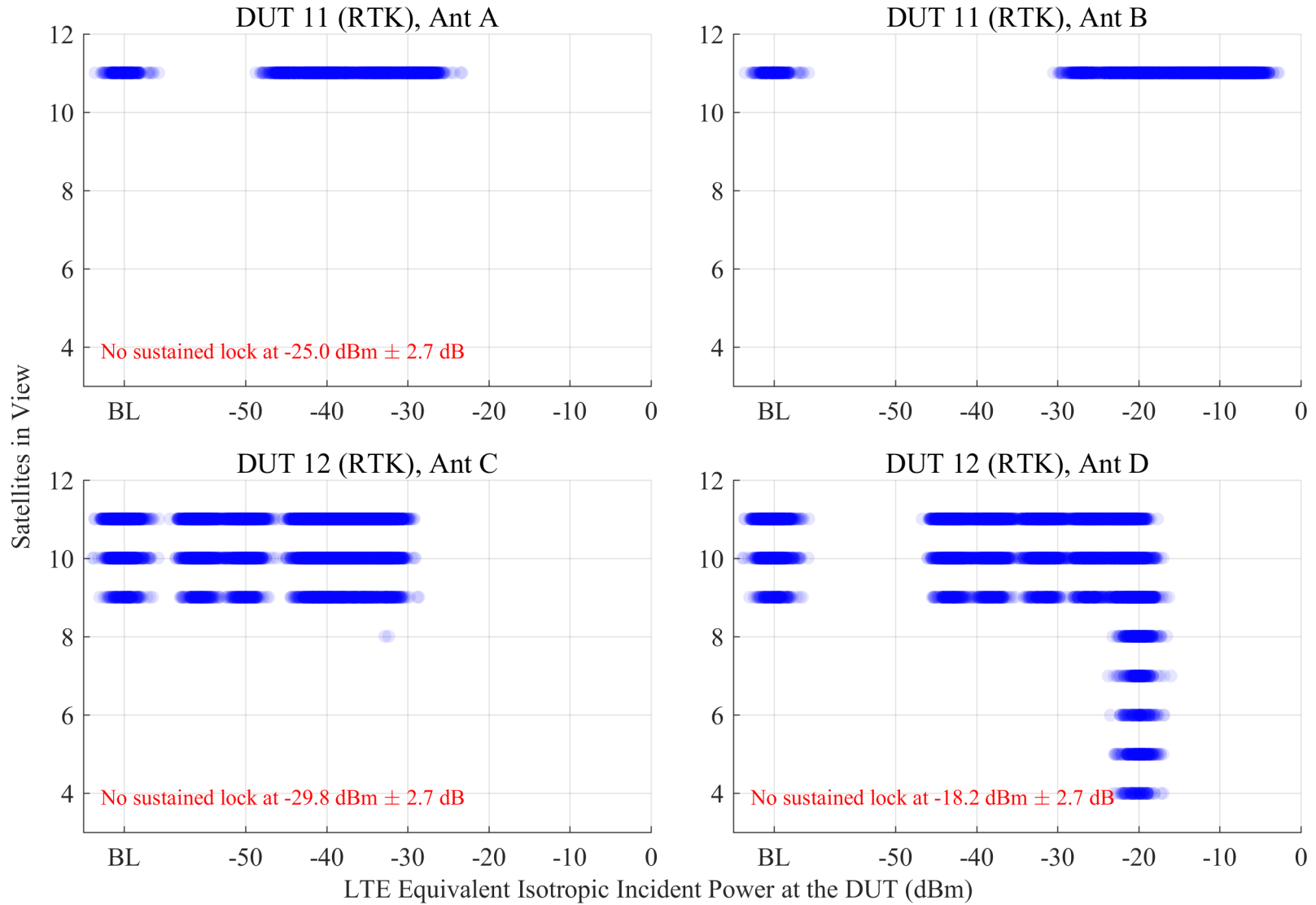


Figure 6.63: Scatterplots of the number of satellites in view from RTK receivers, swept with LTE power level. The GPS scenario is nominal, and the type of incident LTE is UL2.

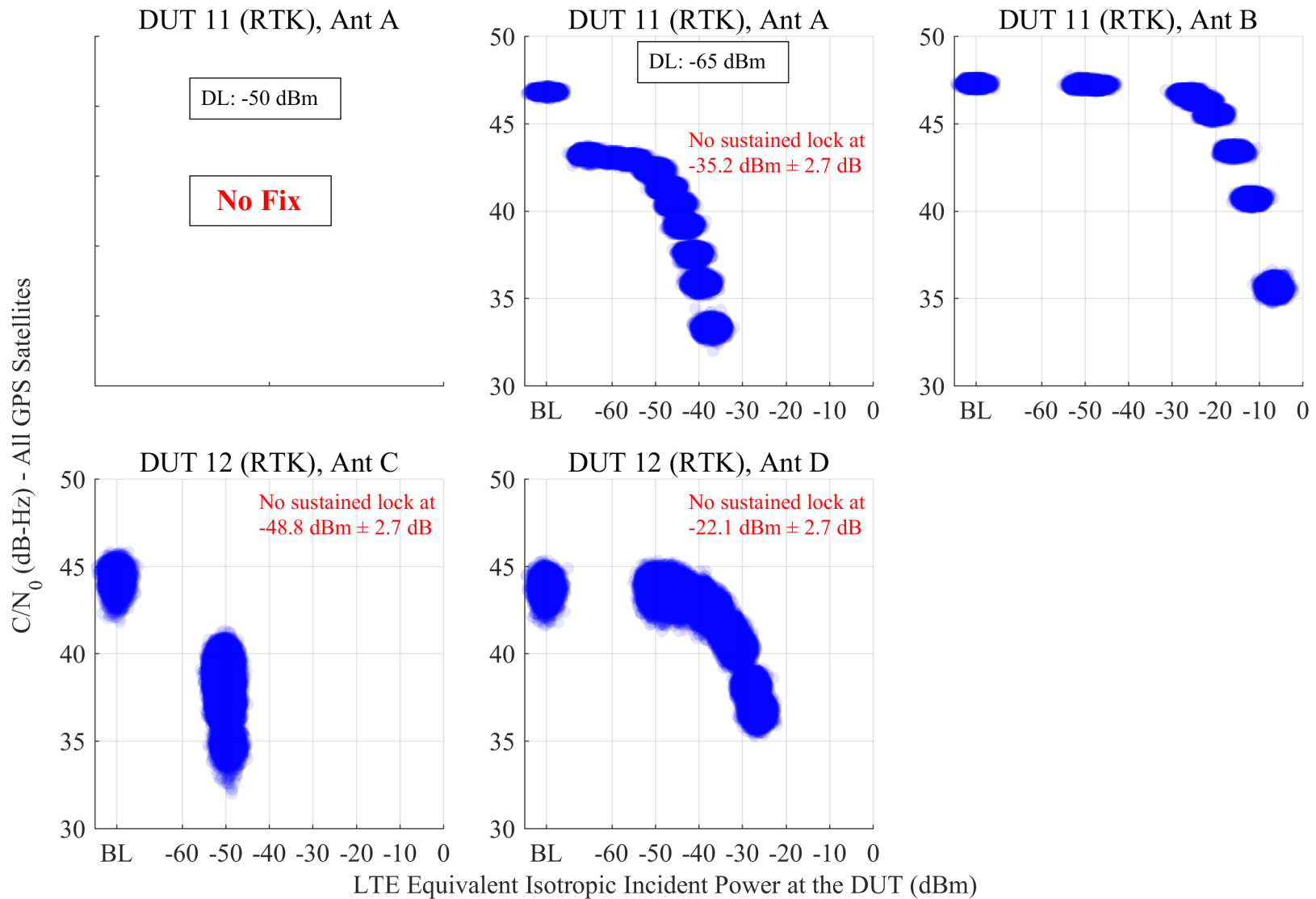


Figure 6.64: Scatterplots of reported  $C/N_0$  from RTK receivers, swept with LTE power level. The GPS scenario is nominal, and the type of incident LTE is Combination DL + UL1. The UL level was swept, and the DL level was fixed at -50 dBm EIPP unless otherwise annotated. The horizontal axis reports the linear sum of DL and UL power.

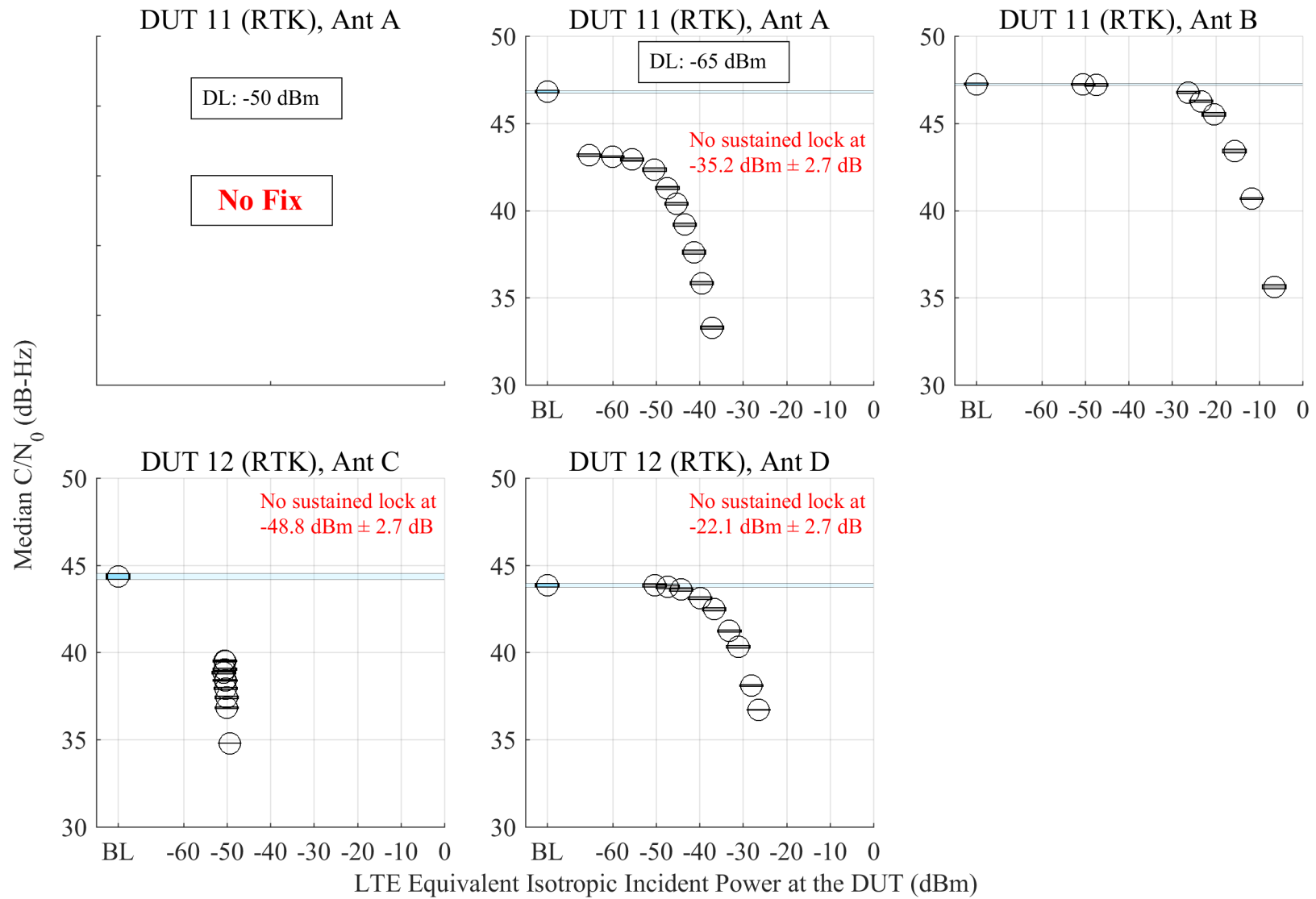


Figure 6.65: Estimated 95% confidence regions of the median of reported  $C/N_0$  from RTK receivers, swept with LTE power level. The GPS scenario is nominal, and the type of incident LTE is Combination DL + UL1. The UL level was swept, and the DL level was fixed at -50 dBm EIPP unless otherwise annotated. The horizontal axis reports the linear sum of DL and UL power.

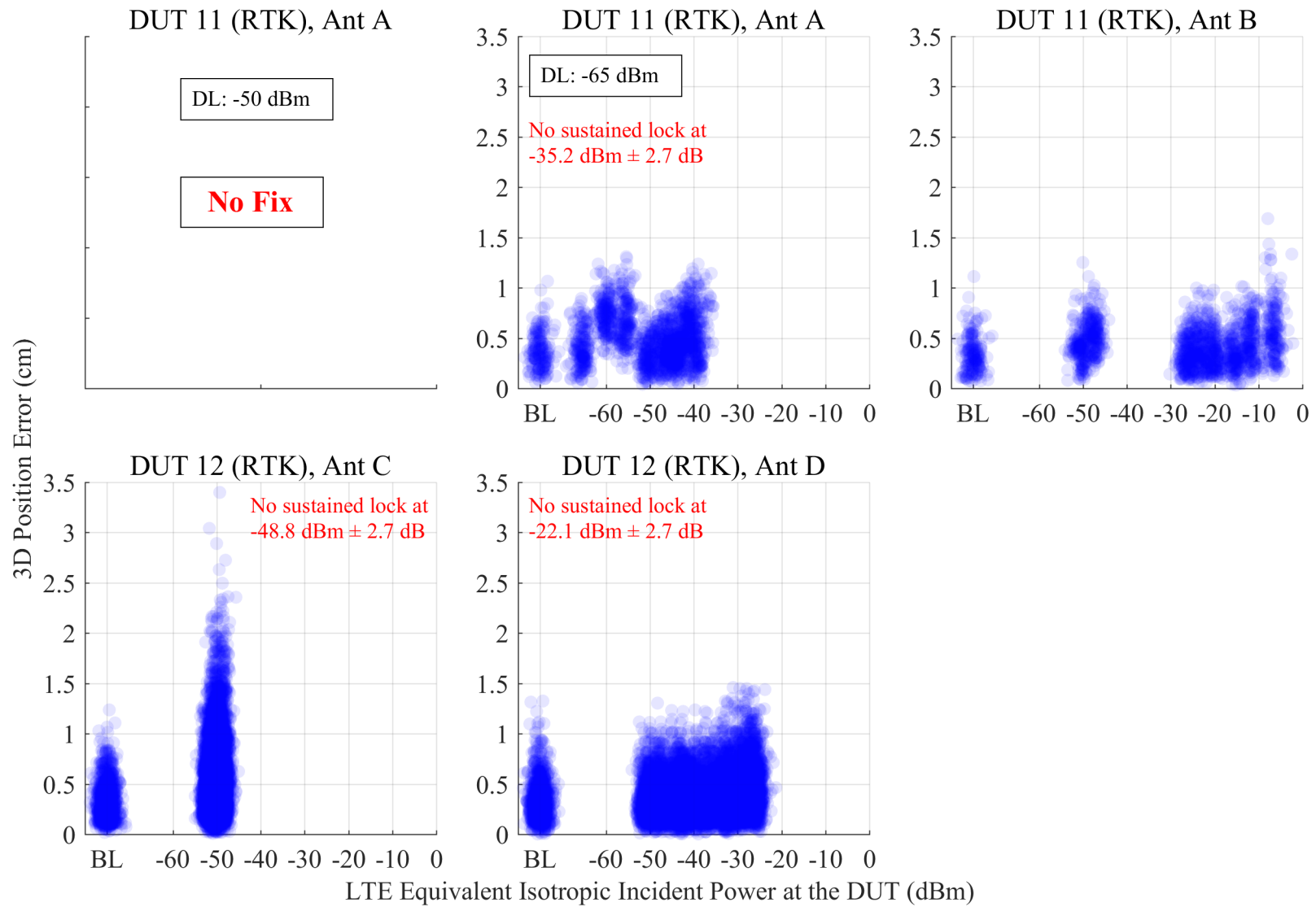


Figure 6.66: Scatterplots of error in reported 3-D position compared to simulator truth from RTK receivers, swept with LTE power level. The GPS scenario is nominal, and the type of incident LTE is Combination DL + UL1. The UL level was swept, and the DL level was fixed at -50 dBm EIIIP unless otherwise annotated. The horizontal axis reports the linear sum of DL and UL power.

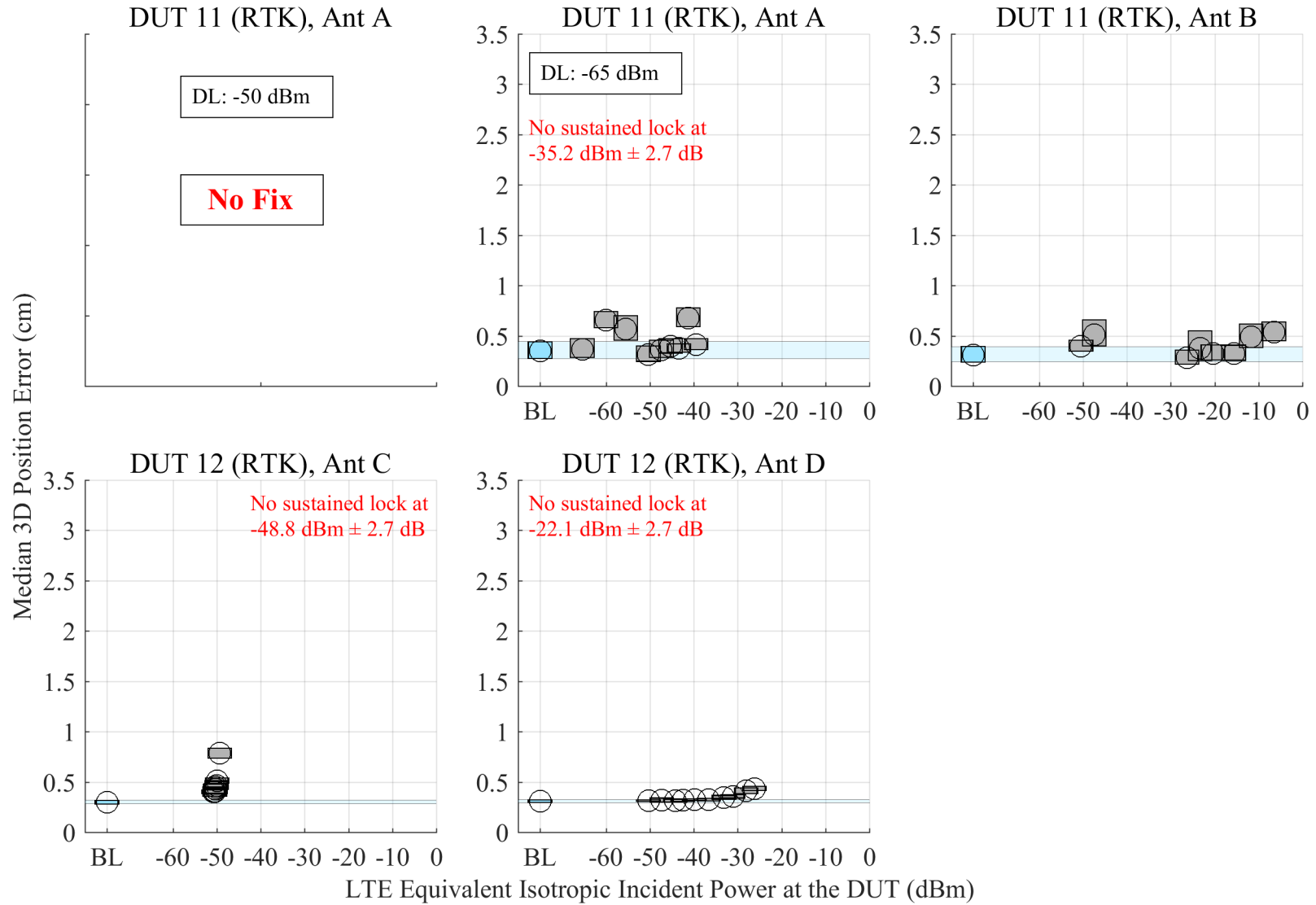


Figure 6.67: Estimated 95% confidence regions of the median error in reported 3-D position from RTK receivers, swept with LTE power level. The GPS scenario is nominal, and the type of incident LTE is Combination DL + UL1. The UL level was swept, and the DL level was fixed at -50 dBm EIPP unless otherwise annotated. The horizontal axis reports the linear sum of DL and UL power.

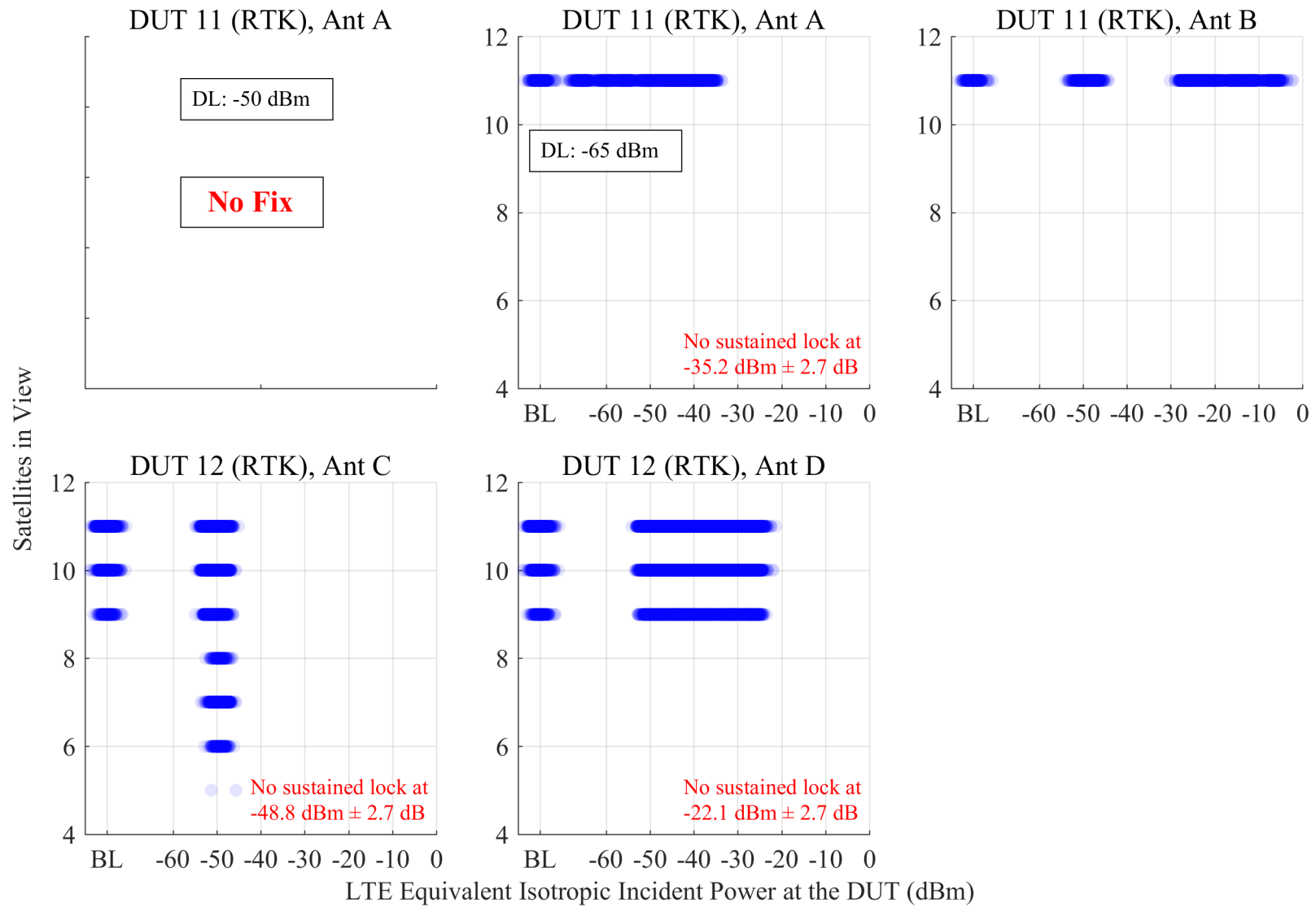


Figure 6.68: Scatterplots of the number of satellites in view from RTK receivers, swept with LTE power level. The GPS scenario is nominal, and the type of incident LTE is Combination DL + UL1. The UL level was swept, and the DL level was fixed at -50 dBm EIIP unless otherwise annotated. The horizontal axis reports the linear sum of DL and UL power.

Table 6.1: LTE Powers by DUT for the Timing Test. The Uncertainty Corresponds to the 95% Confidence Interval.

<b>Device</b>	<b>UL 1 (dBm)</b>	<b>DL (dBm)</b>	<b>DL + UL 1 (dBm)</b>	<b>UL 2 (dBm)</b>
DUT 13	-20.5 ±2.7 dB	-2.3 ±3.1 dB	-20.5 ±2.7 dB	-20.2 ±2.7 dB
	-15.8 ±2.7 dB	3 ±3.1 dB	-15.7 ±2.7 dB	-15.3 ±2.7 dB
	-10.9 ±2.7 dB	—	-10.7 ±2.7 dB	-10.6 ±2.7 dB
	—	—	-6.6 ±2.7 dB	—
DUT 14	-19.9 ±2.7 dB	-19.8 ±3.1 dB	-20.4 ±2.7 dB	-20 ±2.7 dB
	-15.2 ±2.7 dB	-9.9 ±3.1 dB	-15.6 ±2.7 dB	-15.5 ±2.7 dB
	-10.3 ±2.7 dB	-2.1 ±3.1 dB	-10.8 ±2.7 dB	-10.5 ±2.7 dB
	-8 ±2.7 dB	-0.5 ±3.1 dB	-6.5 ±2.7 dB	-6.3 ±2.7 dB
	-6.2 ±2.7 dB	1.5 ±3.1 dB	—	—
DUT 15	-19 ±2.7 dB	-20 ±3.1 dB	-20.4 ±2.7 dB	-20.1 ±2.7 dB
	-15.2 ±2.7 dB	-10.6 ±3.1 dB	-14.8 ±2.7 dB	-15.2 ±2.7 dB
	-9.4 ±2.7 dB	-2.5 ±3.1 dB	-10.8 ±2.7 dB	-10.4 ±2.7 dB
	-6.2 ±2.7 dB	1.4 ±3.1 dB	-6.5 ±2.7 dB	-6.4 ±2.7 dB

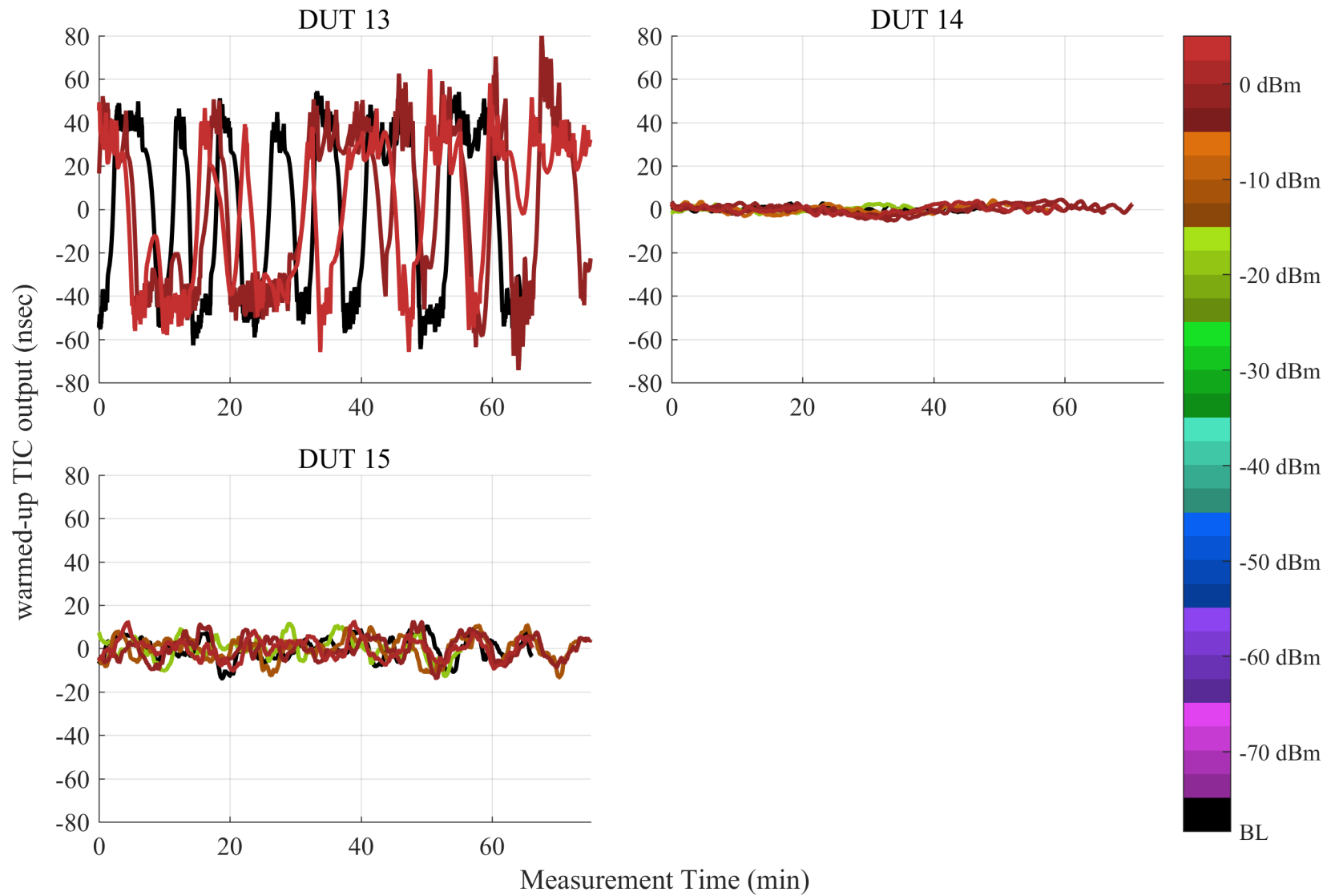


Figure 6.69: Plots of stability of 1 PPS output of a GPSDO receiver measured against that of the GPS simulator from GPSDO receivers, swept with LTE power level. The GPS scenario is timing, and the type of incident LTE is DL.

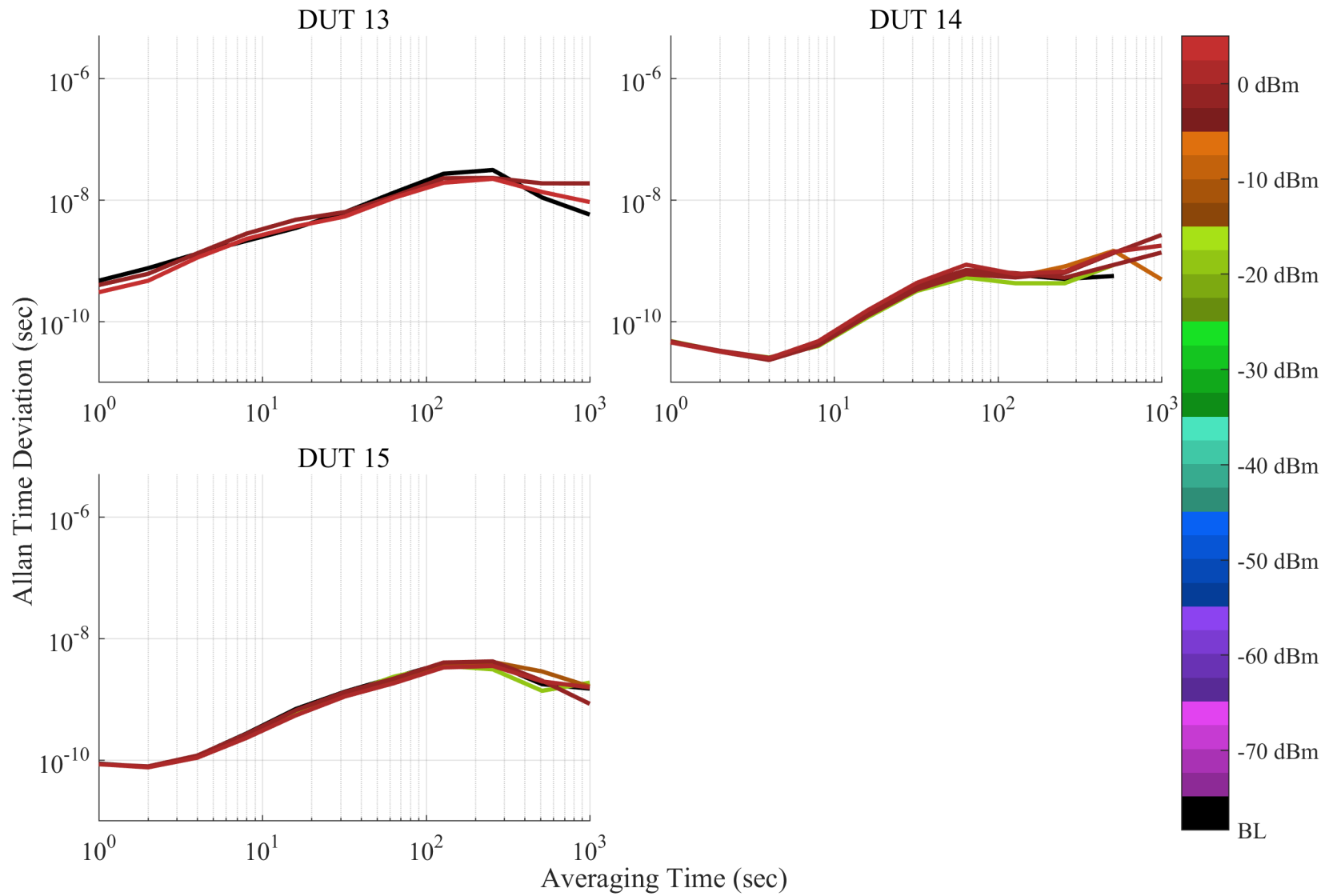


Figure 6.70: Allan time deviation plots from GPSDO receivers, swept with LTE power level. The GPS scenario is timing, and the type of incident LTE is DL.

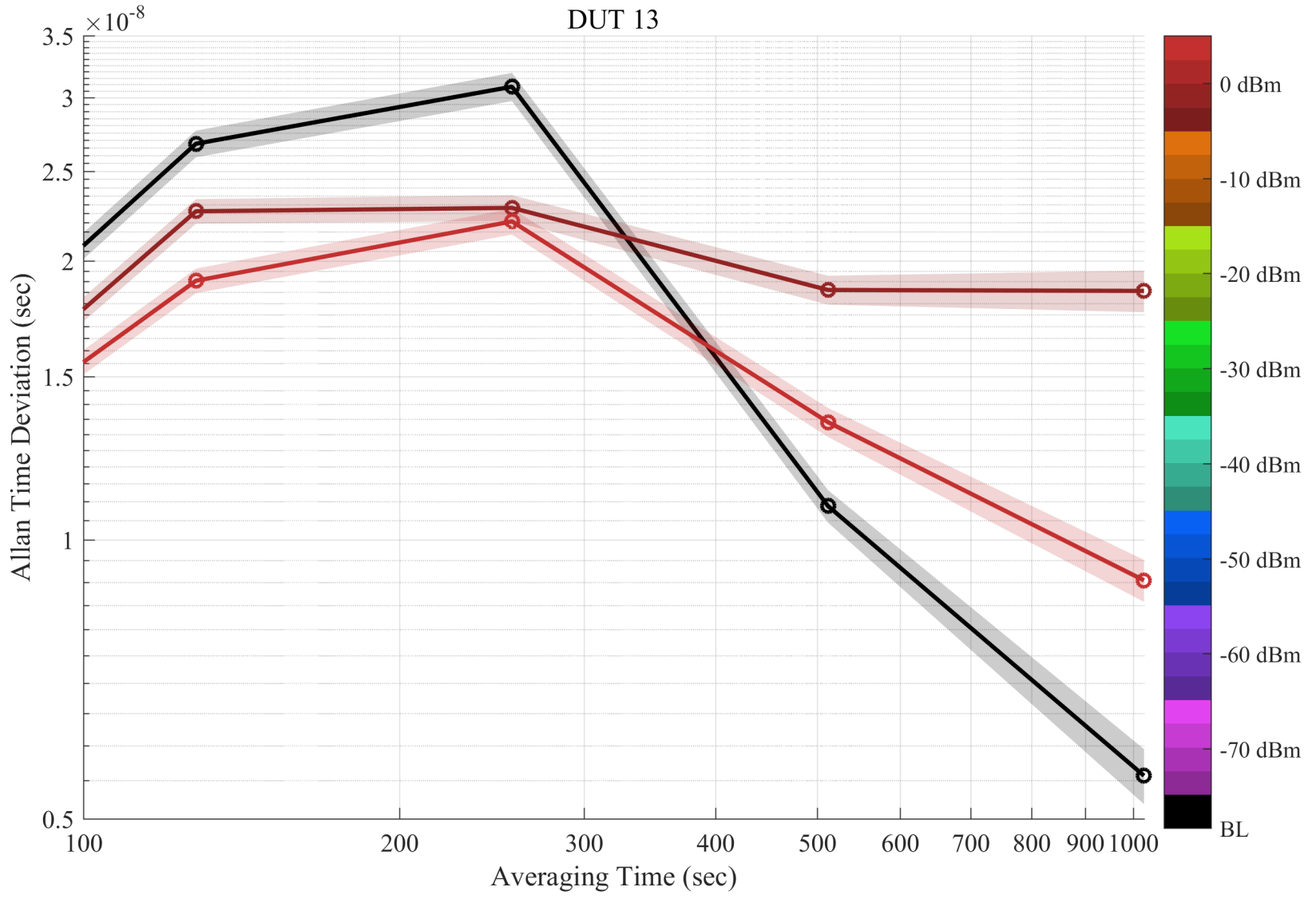


Figure 6.71: Zoom of Allan time deviation for DUT 13. Shaded regions indicate pointwise 95% confidence bands. Each curve corresponds to a tested LTE power level. The GPS scenario is timing, and the type of incident LTE is DL.

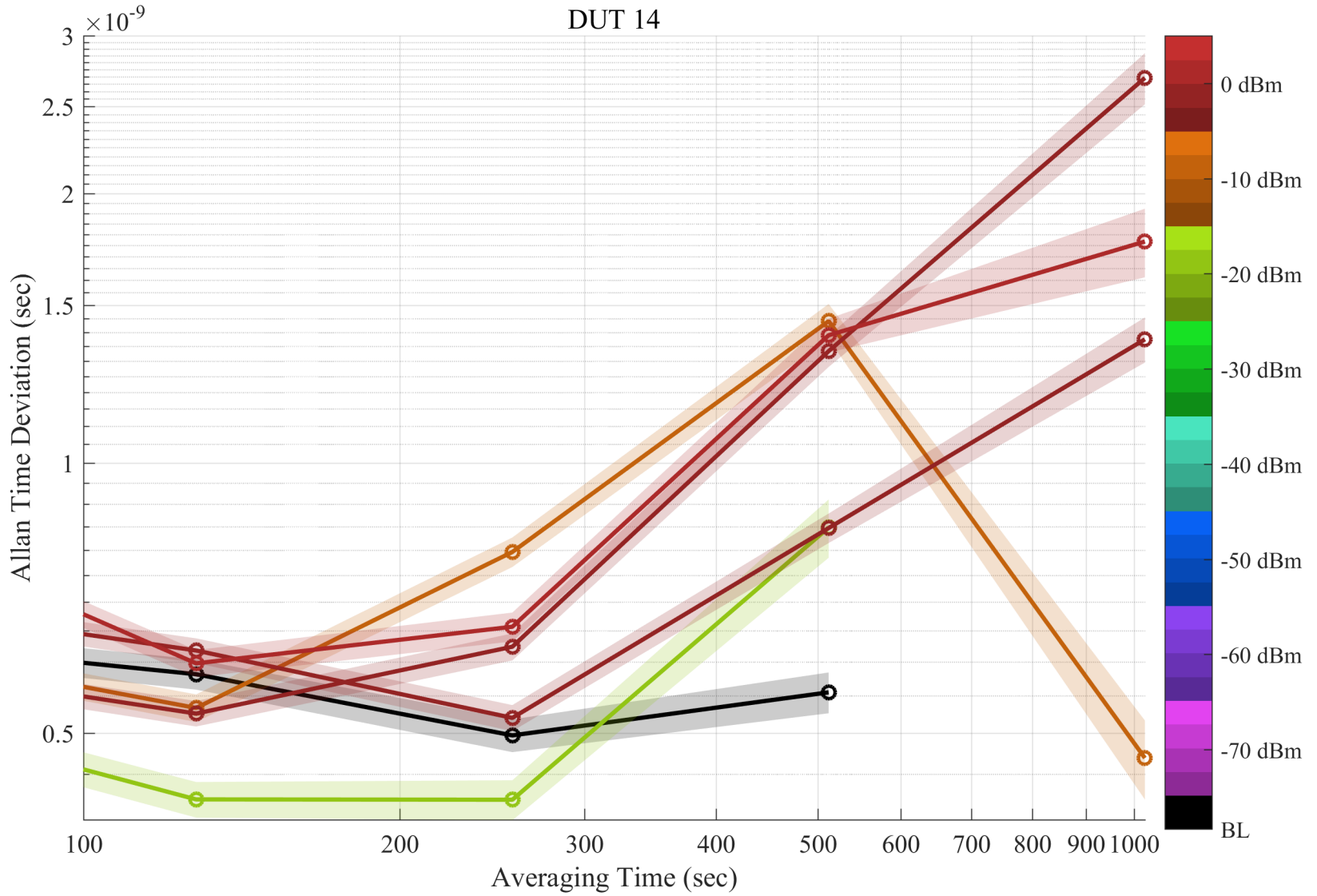


Figure 6.72: Zoom of Allan time deviation for DUT 14. Shaded regions indicate pointwise 95% confidence bands. Each curve corresponds to a tested LTE power level. The GPS scenario is timing, and the type of incident LTE is DL.

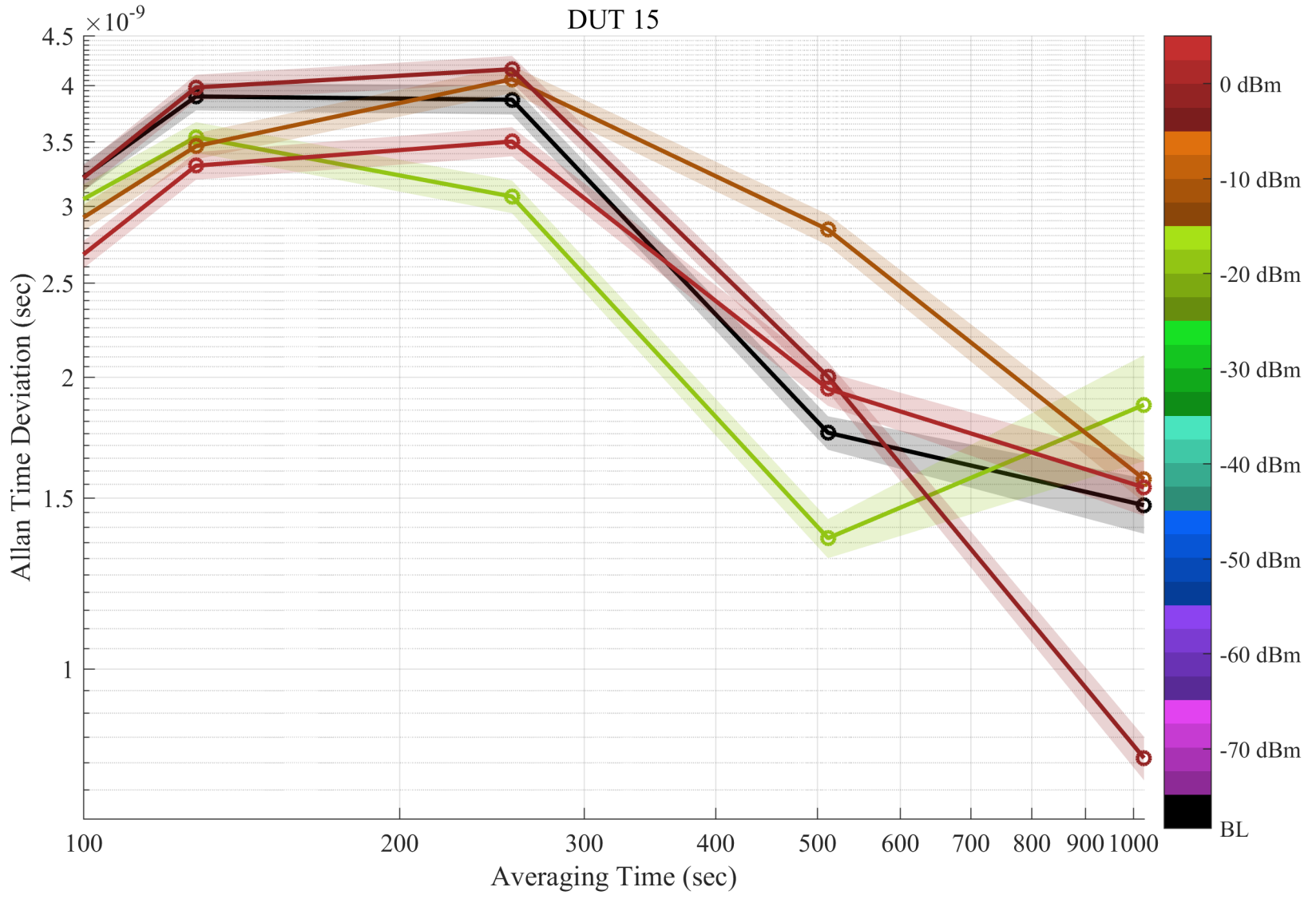


Figure 6.73: Zoom of Allan time deviation for DUT 15. Shaded regions indicate pointwise 95% confidence bands. Each curve corresponds to a tested LTE power level. The GPS scenario is timing, and the type of incident LTE is DL.

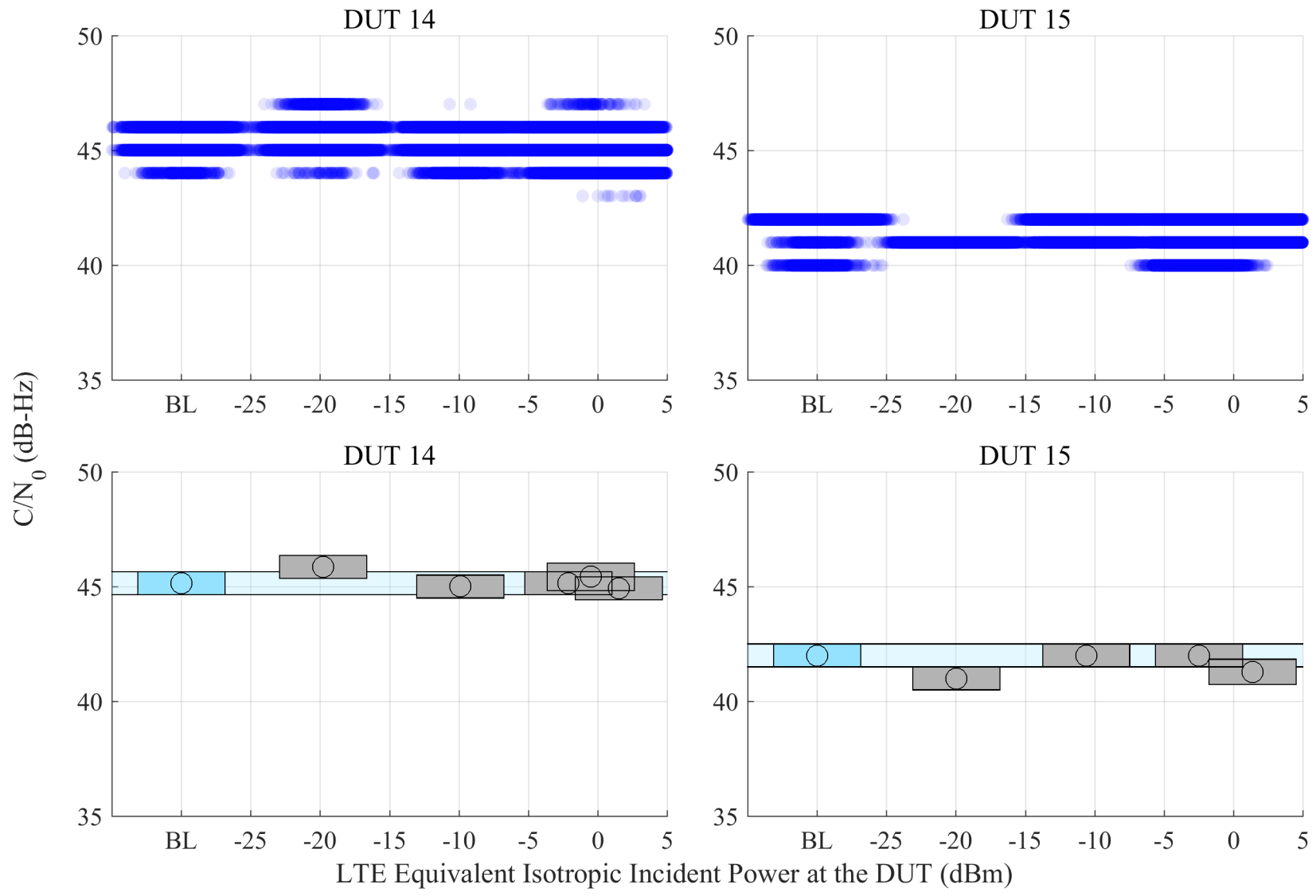


Figure 6.74:  $C/N_0$  scatter plots and median, with estimated 95% confidence region of the median from GPSDO receivers, swept with LTE power level. The GPS scenario is timing, and the type of incident LTE is DL.

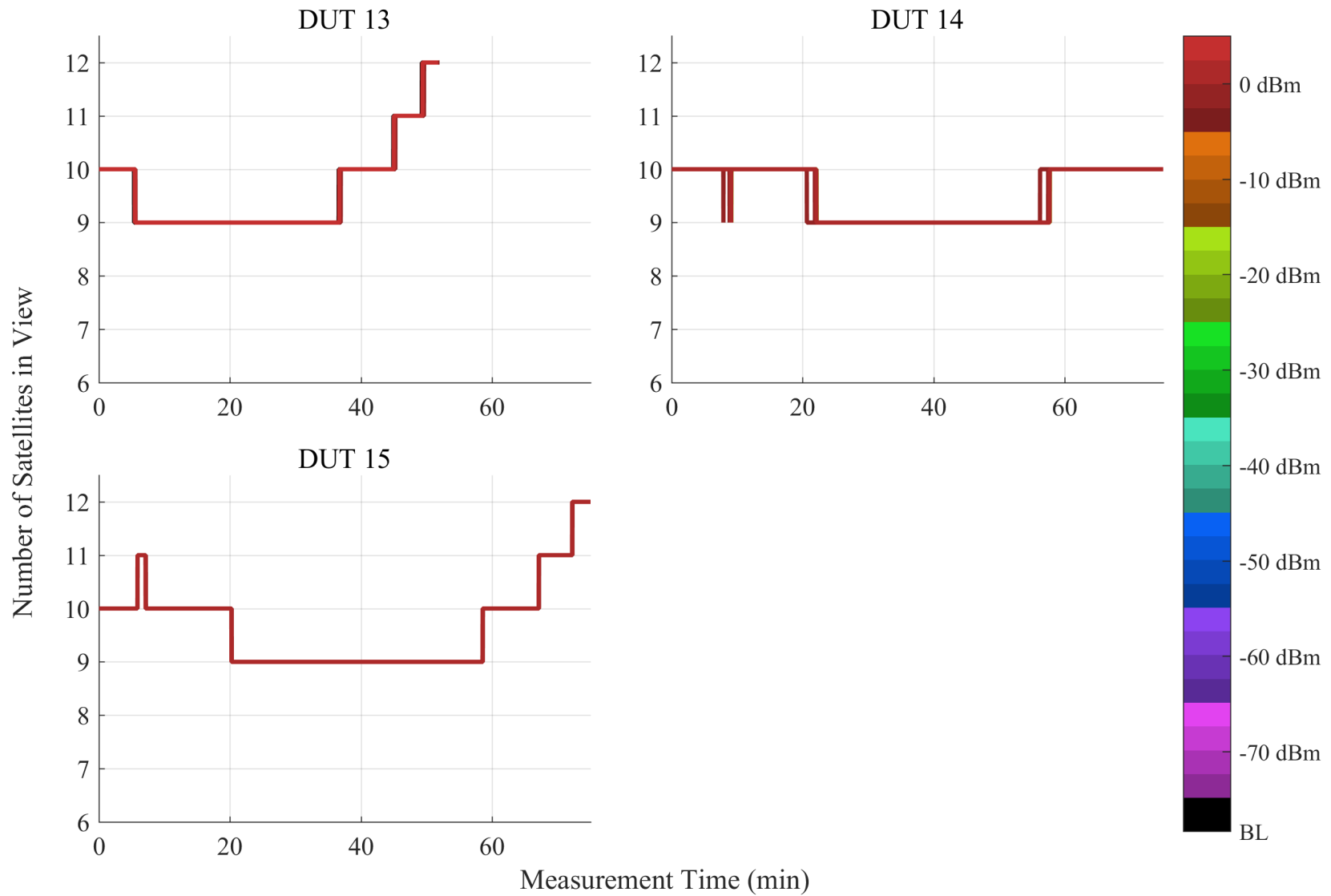


Figure 6.75: Number of satellites in view from GPSDO receivers, swept with LTE power level. The GPS scenario is timing, and the type of incident LTE is DL.

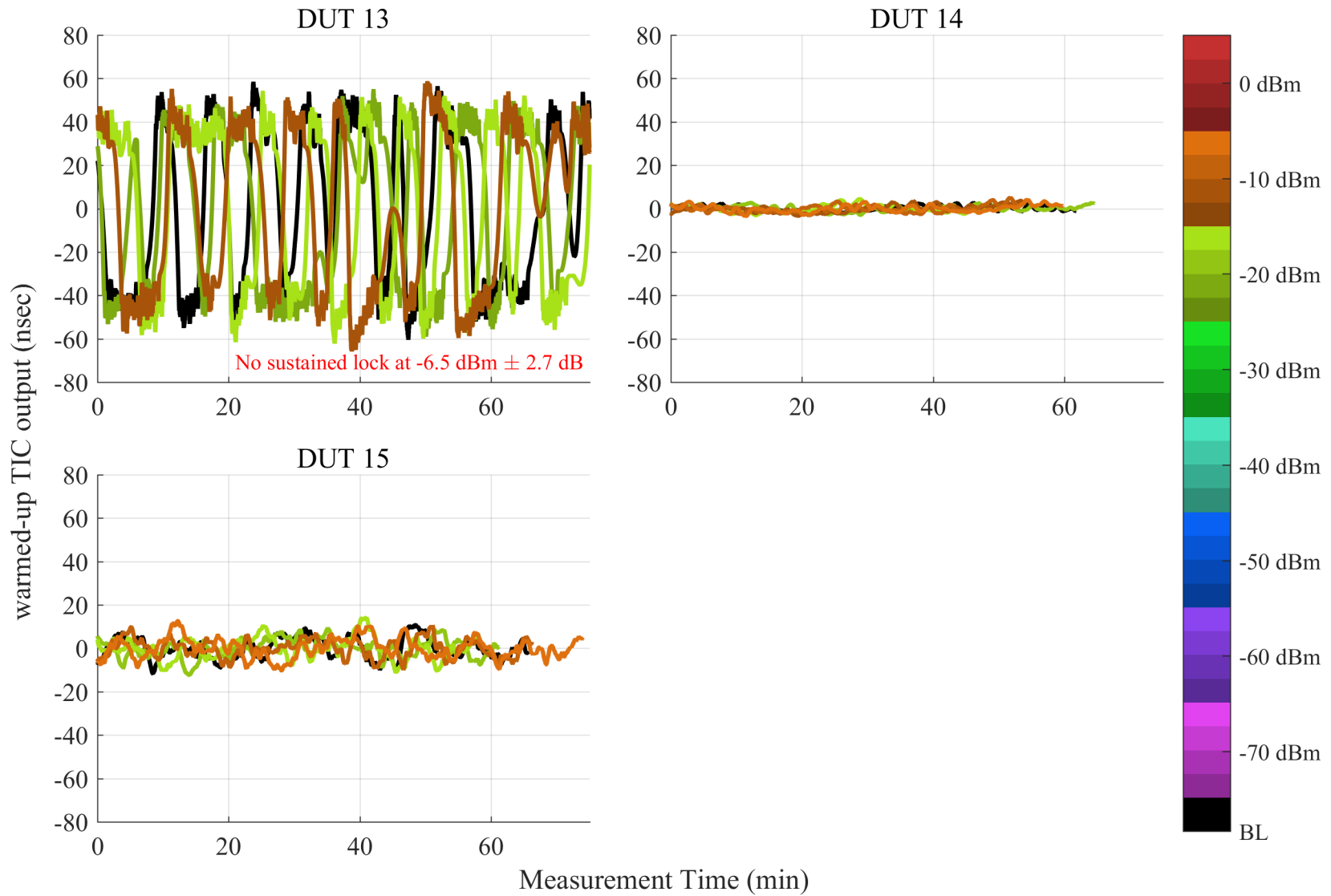


Figure 6.76: Plots of stability of 1 PPS output of a GPSDO receiver measured against that of the GPS simulator from GPSDO receivers, swept with LTE power level. The GPS scenario is timing, and the type of incident LTE is UL1.

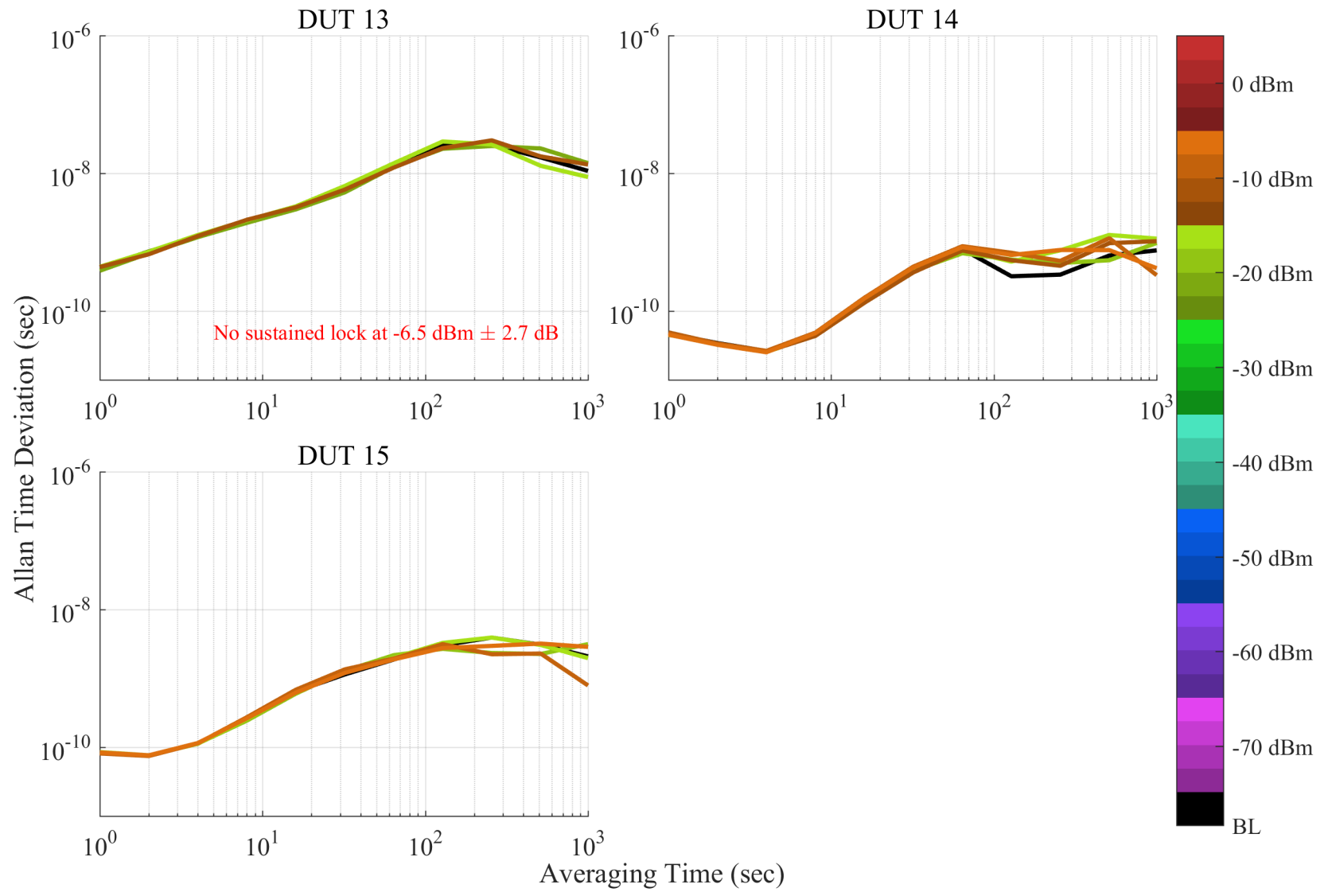


Figure 6.77: Allan time deviation plots from GPSDO receivers, swept with LTE power level. The GPS scenario is timing, and the type of incident LTE is UL1.

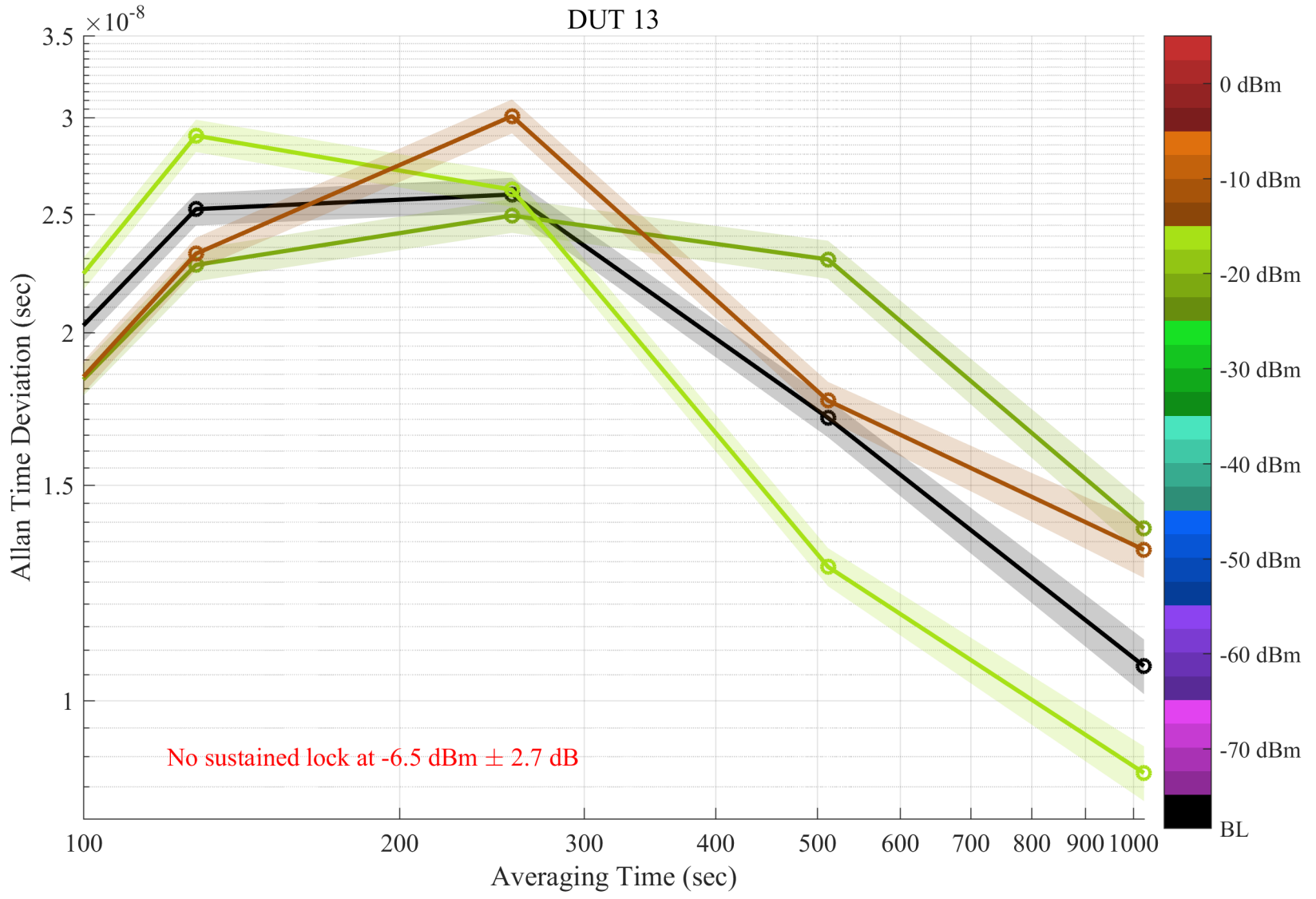


Figure 6.78: Zoom of Allan time deviation for DUT 13. Shaded regions indicate pointwise 95% confidence bands. Each curve corresponds to a tested LTE power level. The GPS scenario is timing, and the type of incident LTE is UL1.

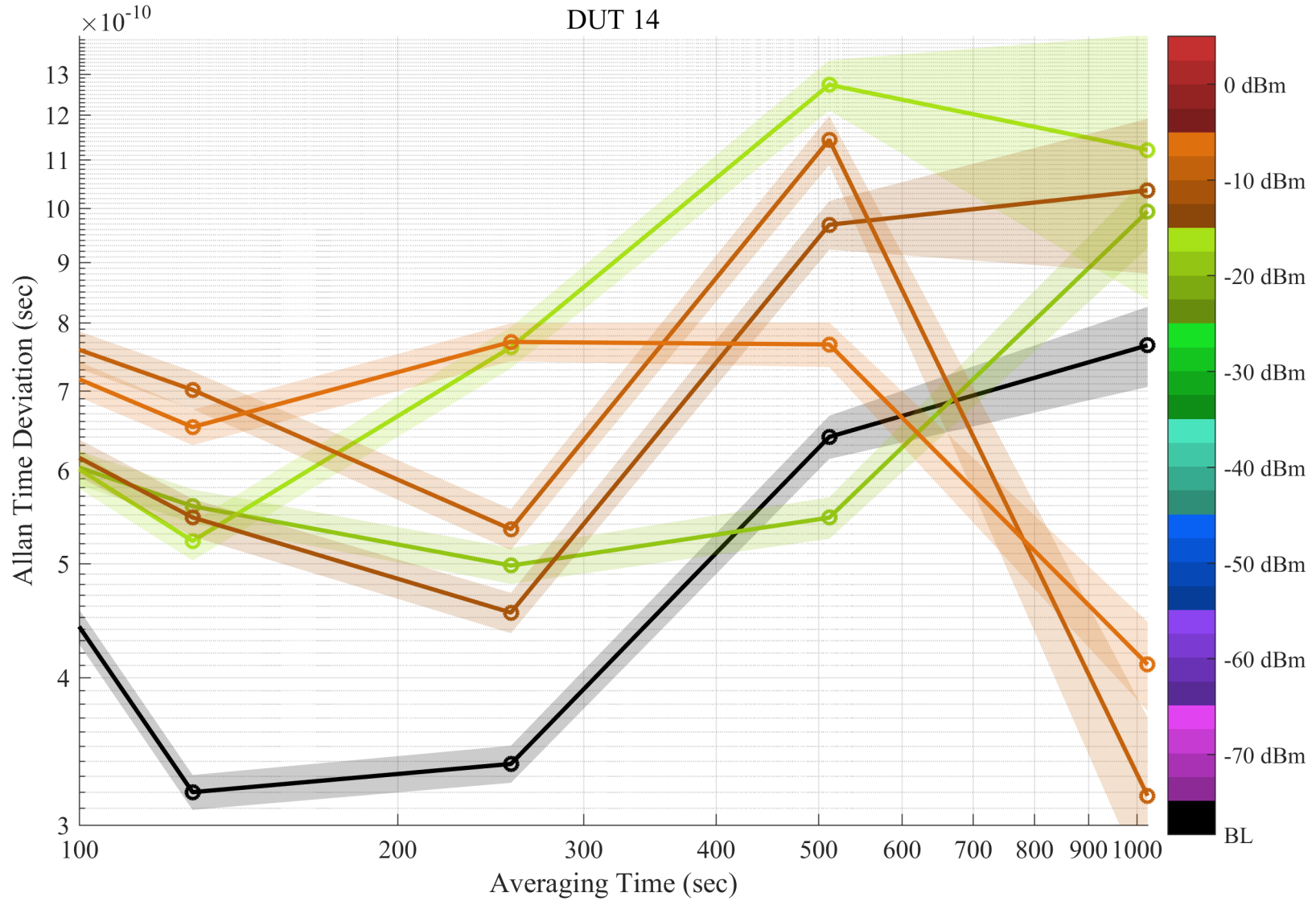


Figure 6.79: Zoom of Allan time deviation for DUT 14. Shaded regions indicate pointwise 95% confidence bands. Each curve corresponds to a tested LTE power level. The GPS scenario is timing, and the type of incident LTE is UL1.

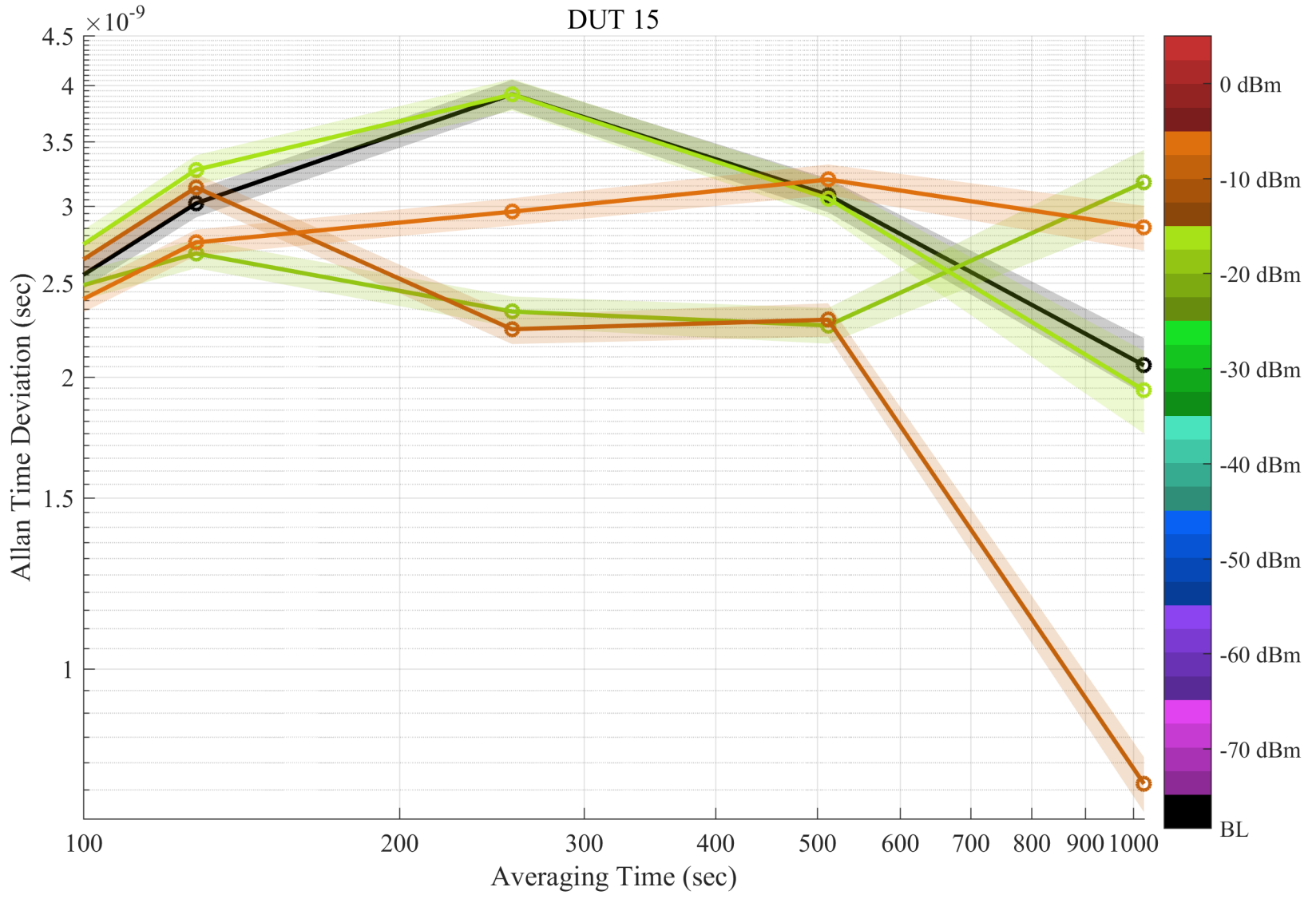


Figure 6.80: Zoom of Allan time deviation for DUT 15. Shaded regions indicate pointwise 95% confidence bands. Each curve corresponds to a tested LTE power level. The GPS scenario is timing, and the type of incident LTE is UL1.

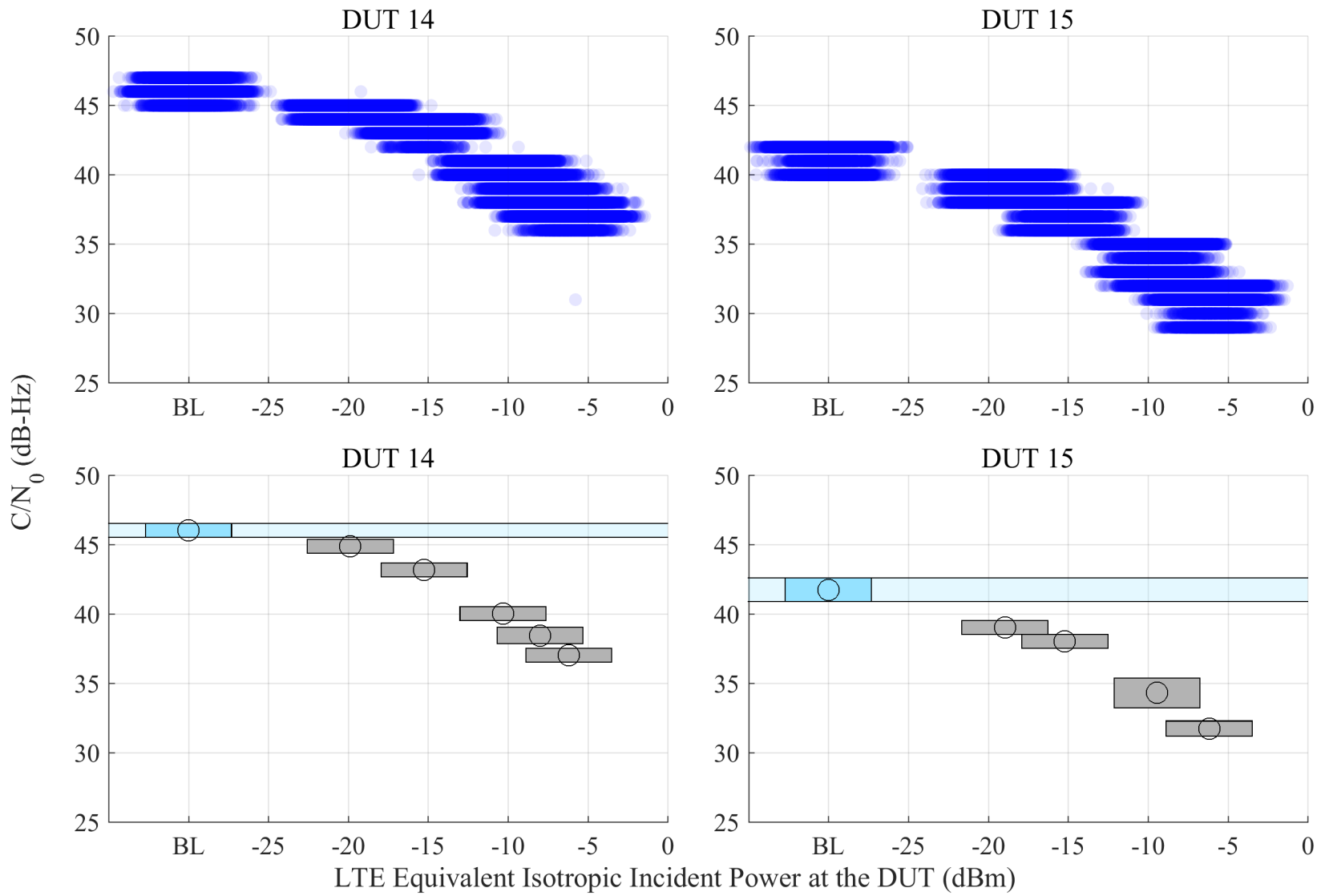


Figure 6.81:  $C/N_0$  scatter plots and median, with estimated 95% confidence region of the median from GPSDO receivers, swept with LTE power level. The GPS scenario is timing, and the type of incident LTE is UL1.

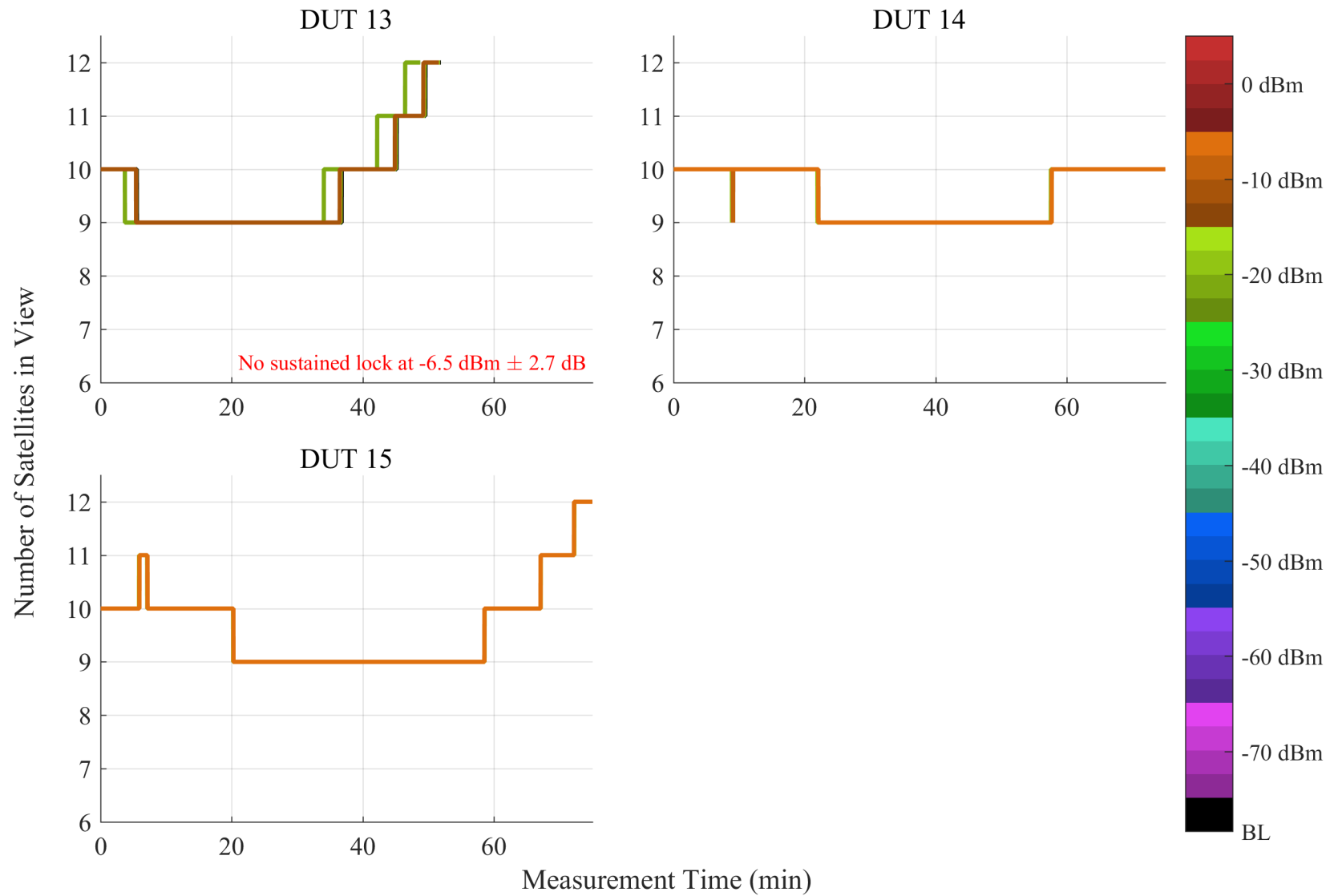


Figure 6.82: Number of satellites in view from GPSDO receivers, swept with LTE power level. The GPS scenario is timing, and the type of incident LTE is UL1.

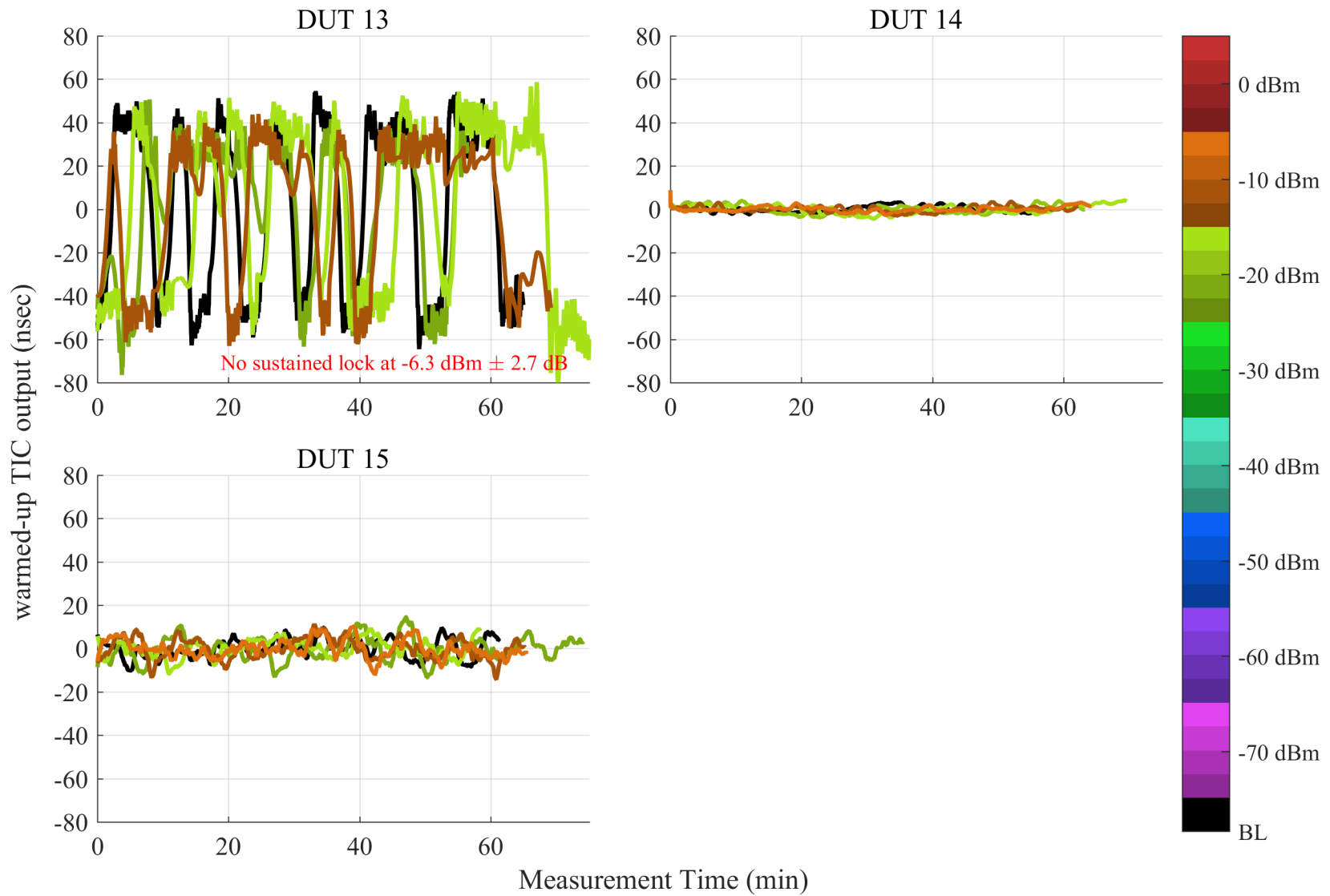


Figure 6.83: Plots of stability of 1 PPS output of a GPSDO receiver measured against that of the GPS simulator from GPSDO receivers, swept with LTE power level. The GPS scenario is timing, and the type of incident LTE is UL2.

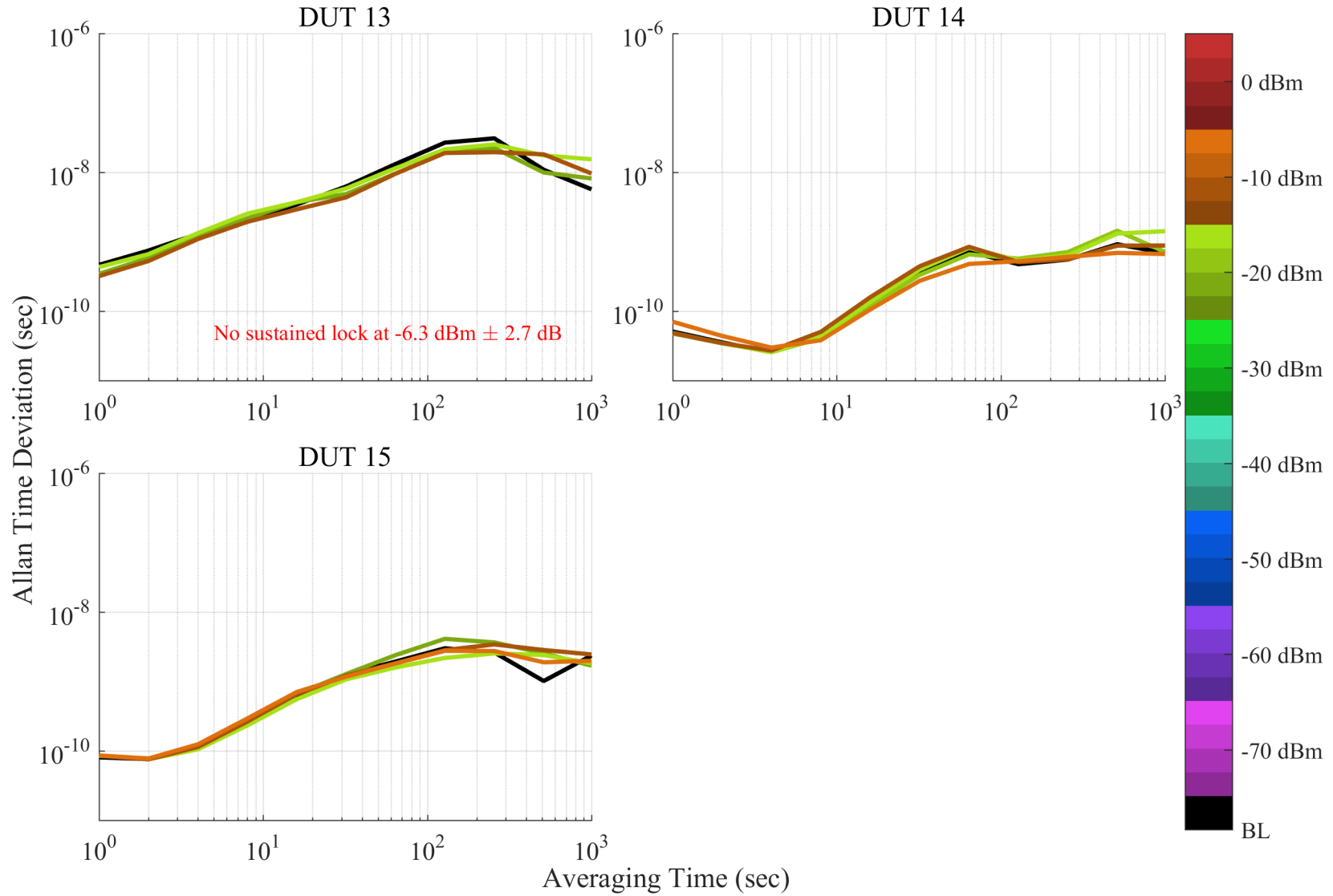


Figure 6.84: Allan time deviation plots from GPSDO receivers, swept with LTE power level. The GPS scenario is timing, and the type of incident LTE is UL2.

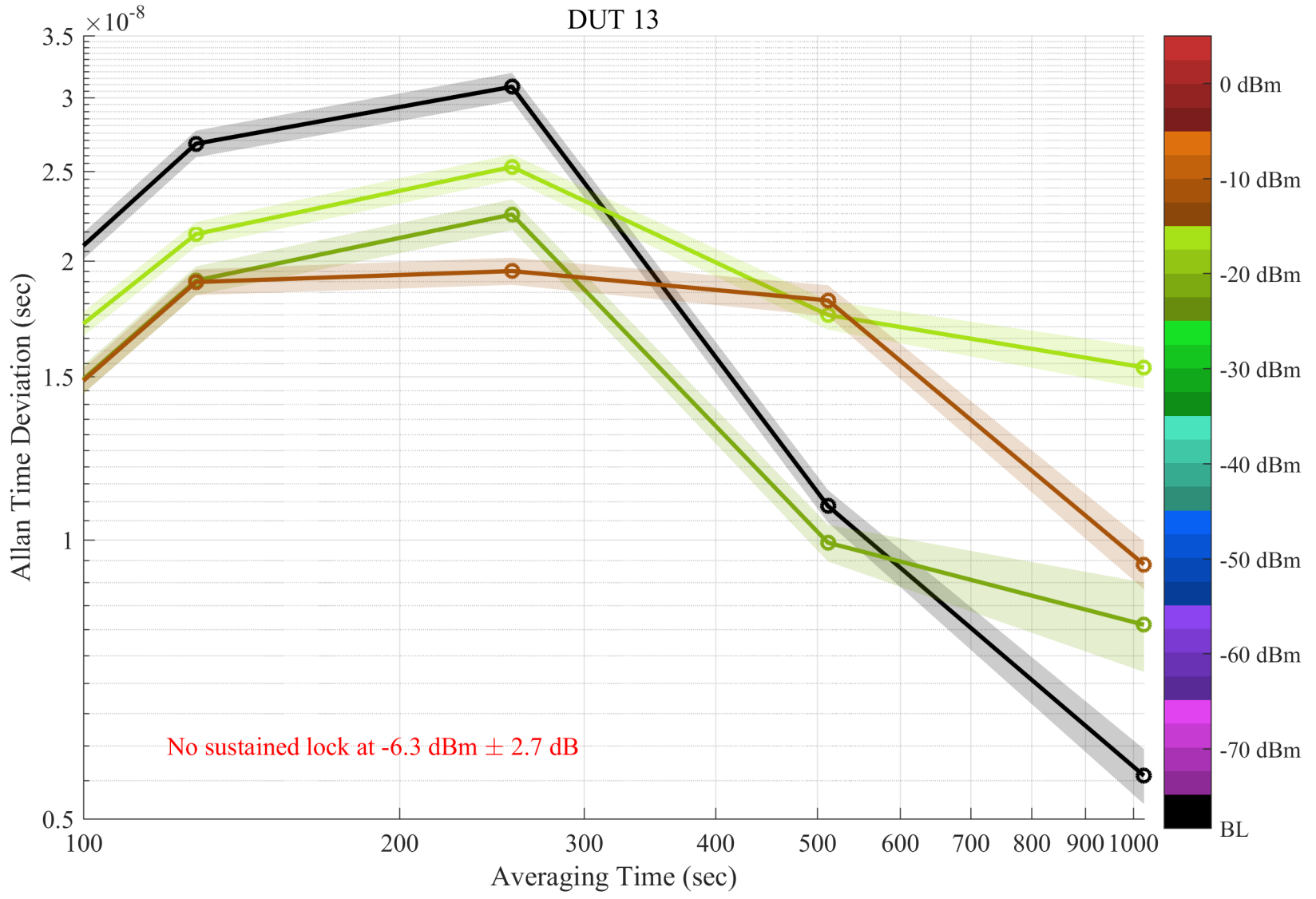


Figure 6.85: Zoom of Allan time deviation for DUT 13. Shaded regions indicate pointwise 95% confidence bands. Each curve corresponds to a tested LTE power level. The GPS scenario is timing, and the type of incident LTE is UL2.

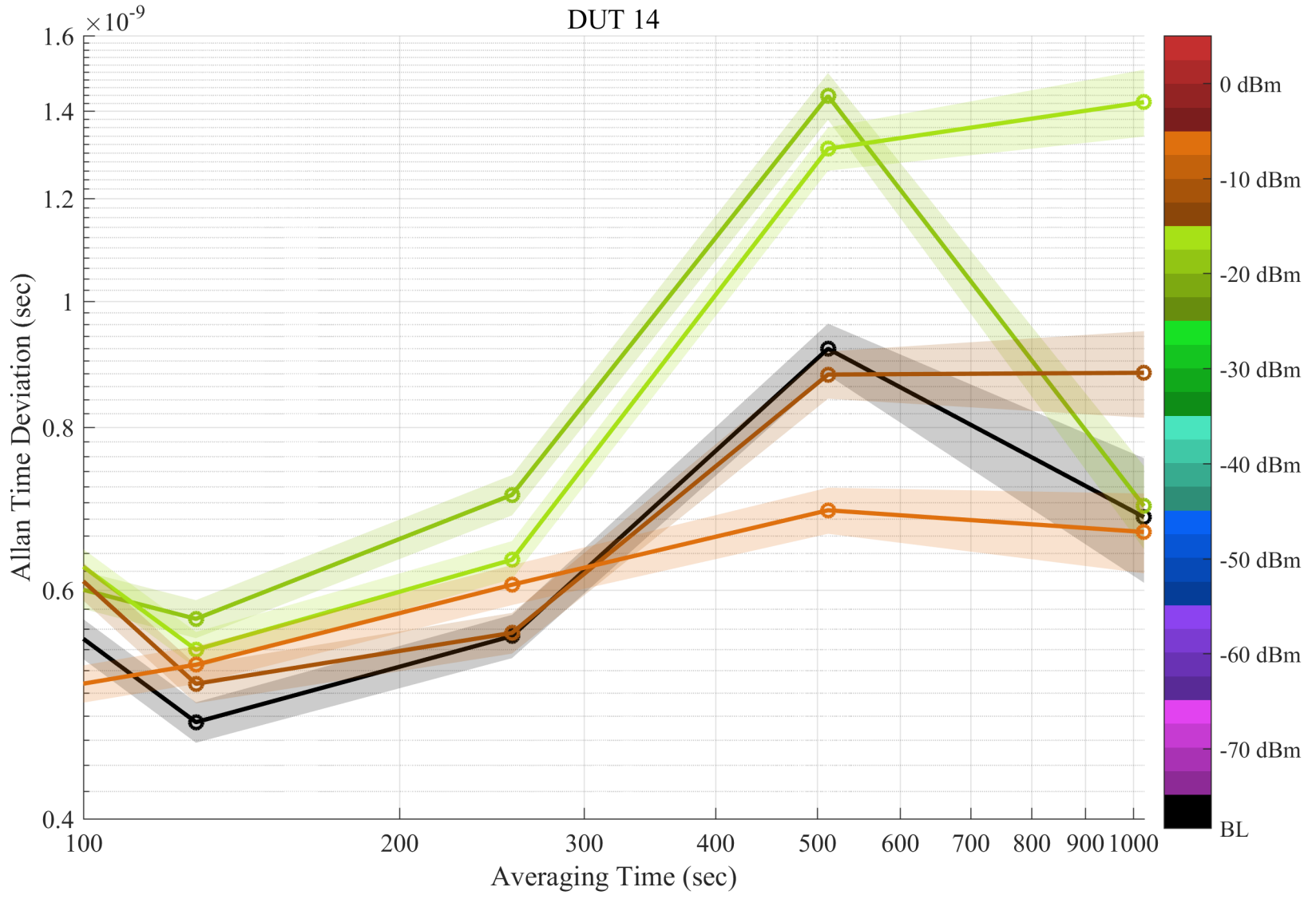


Figure 6.86: Zoom of Allan time deviation for DUT 14. Shaded regions indicate pointwise 95% confidence bands. Each curve corresponds to a tested LTE power level. The GPS scenario is timing, and the type of incident LTE is UL2.

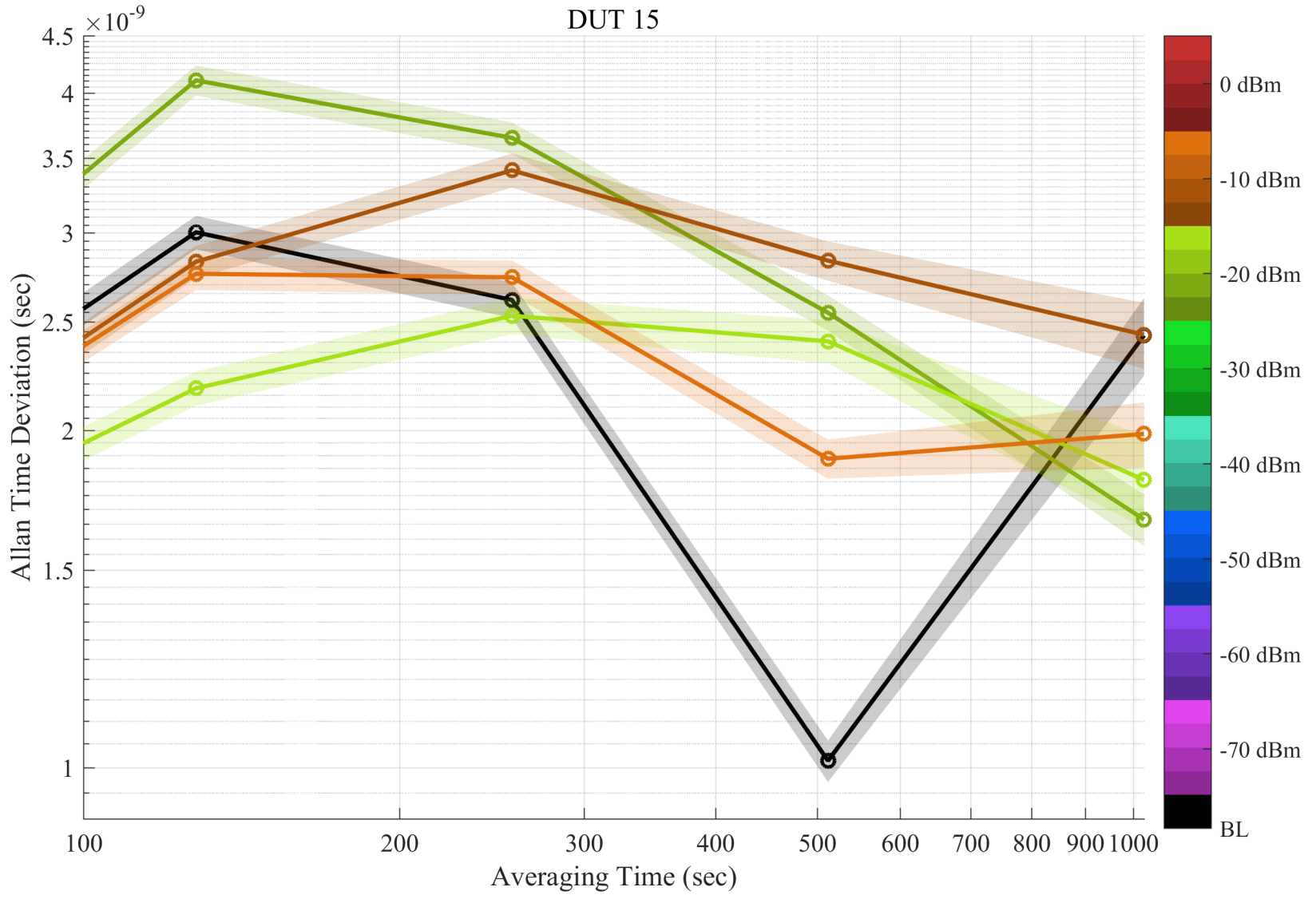


Figure 6.87: Zoom of Allan time deviation for DUT 15. Shaded regions indicate pointwise 95% confidence bands. Each curve corresponds to a tested LTE power level. The GPS scenario is timing, and the type of incident LTE is UL2.

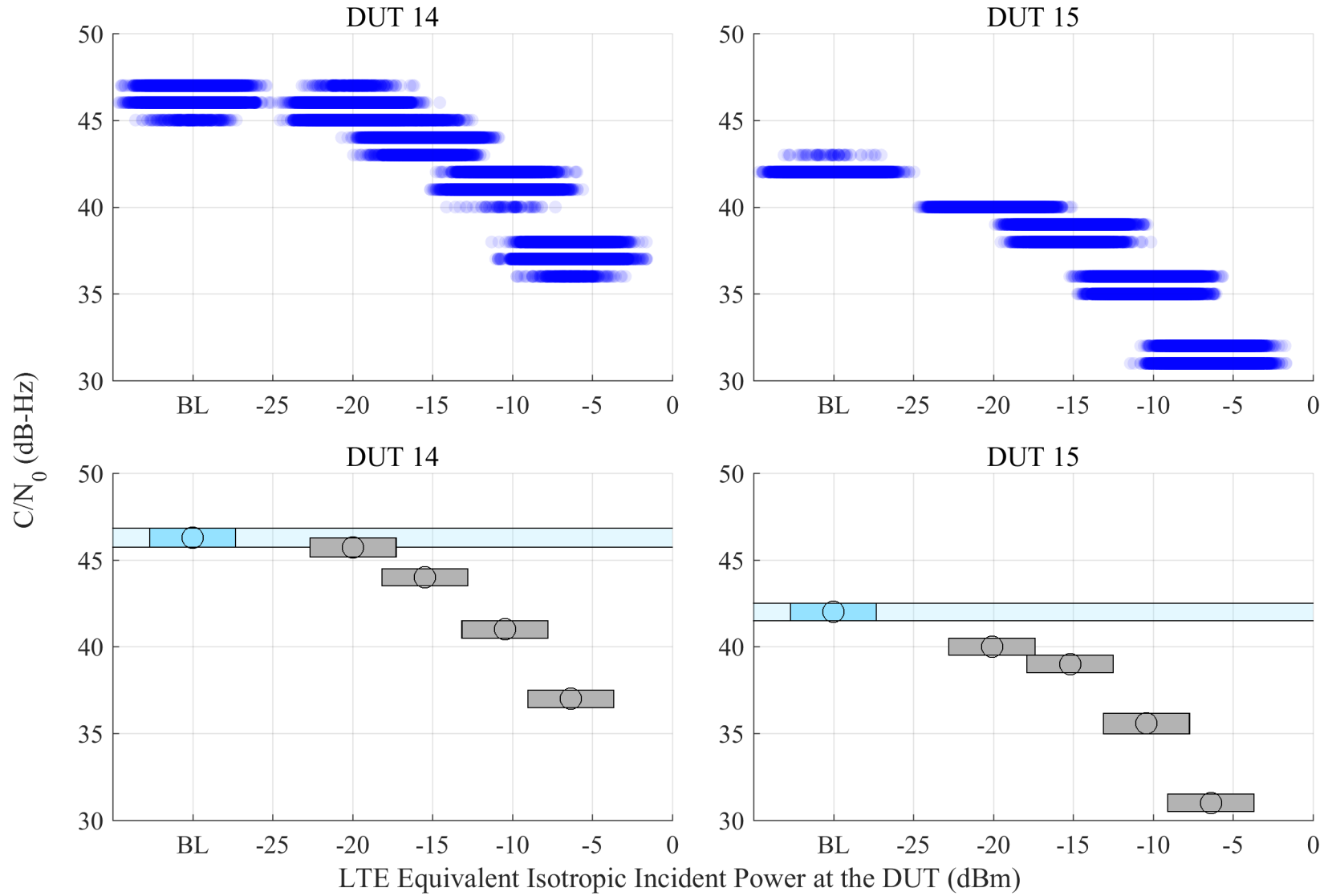


Figure 6.88:  $C/N_0$  scatter plots and median, with estimated 95% confidence region of the median from GPSDO receivers, swept with LTE power level. The GPS scenario is timing, and the type of incident LTE is UL2.

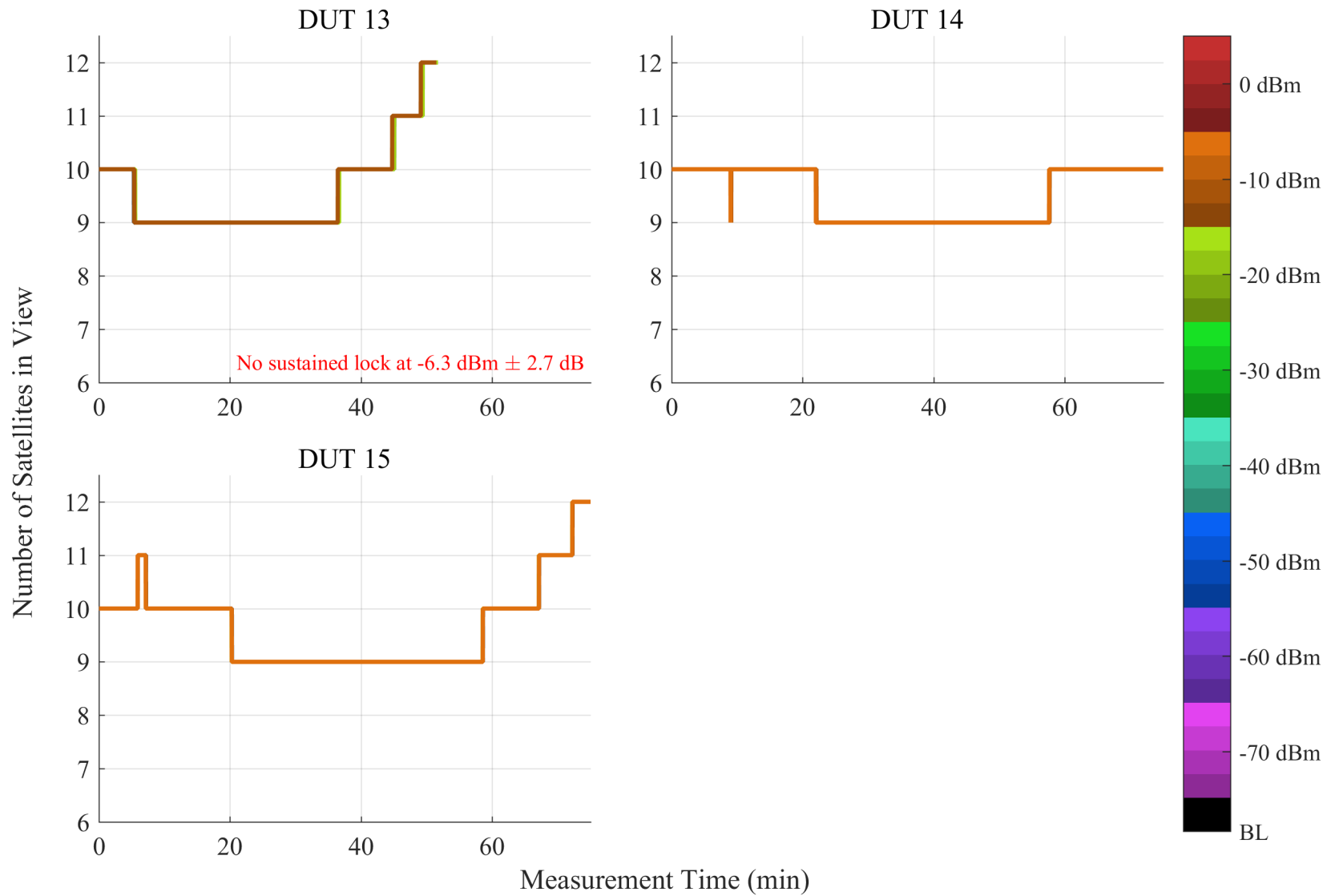


Figure 6.89: Number of satellites in view from GPSDO receivers, swept with LTE power level. The GPS scenario is timing, and the type of incident LTE is UL2.

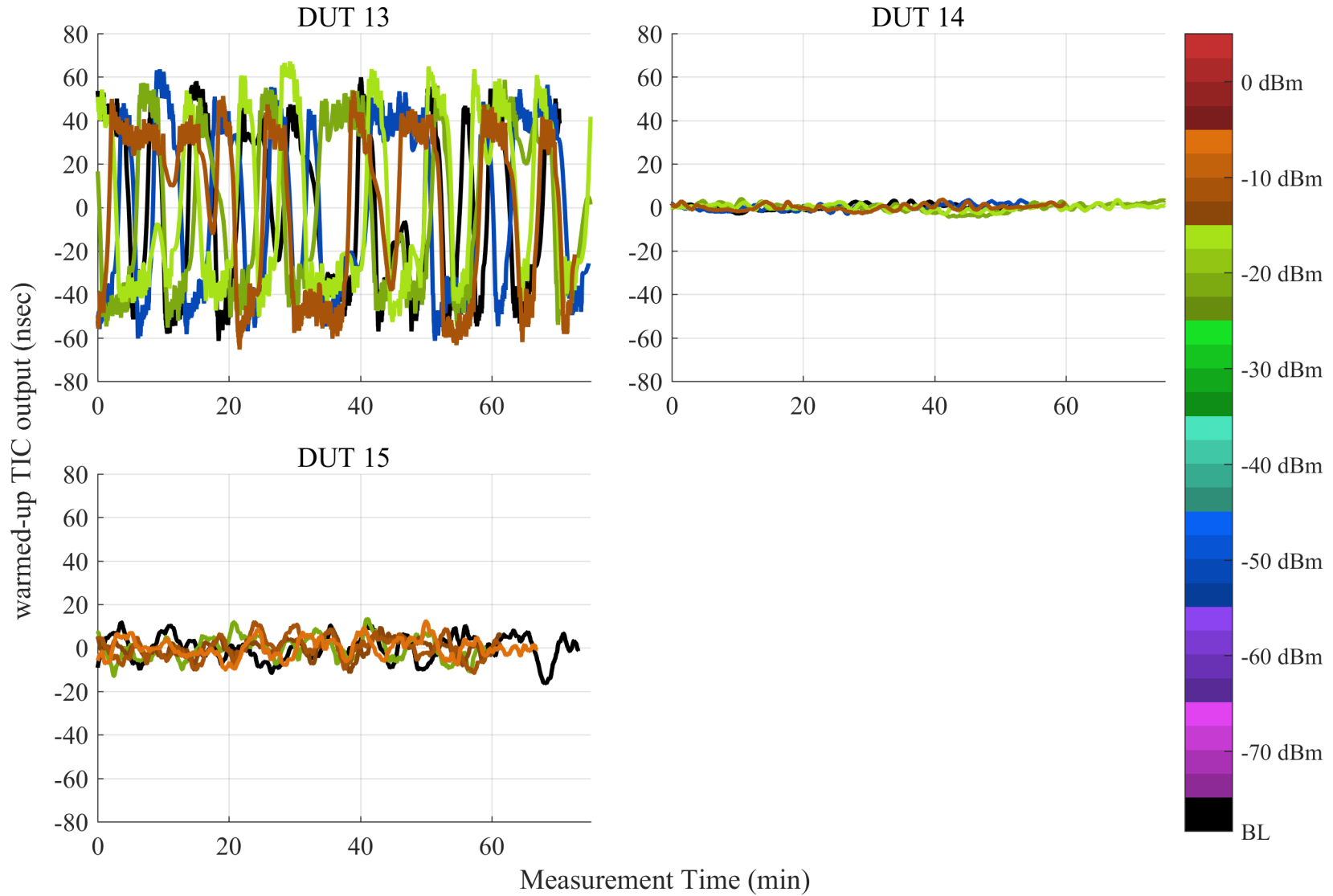


Figure 6.90: Plots of stability of 1 PPS output of a GPSDO receiver measured against that of the GPS simulator from GPSDO receivers, swept with LTE power level. The GPS scenario is timing, and the type of incident LTE is DL + UL1. The UL level was swept, and the DL level was fixed at -50 dBm EIIP unless otherwise annotated. The colorbar reports the linear sum of DL and UL power.

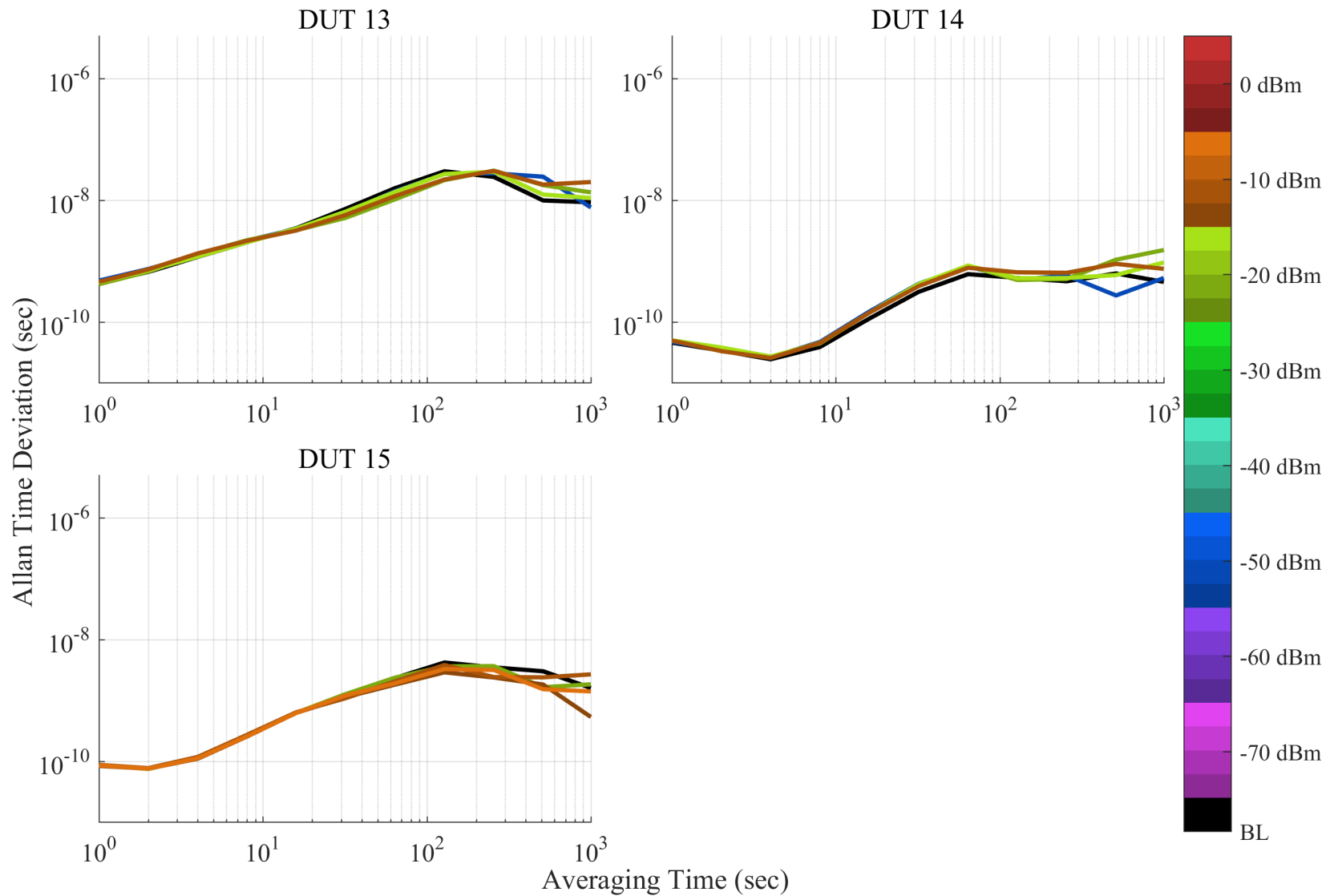


Figure 6.91: Allan time deviation plots from GPSDO receivers, swept with LTE power level. The GPS scenario is timing, and the type of incident LTE is DL + UL1. The UL level was swept, and the DL level was fixed at -50 dBm EIRP unless otherwise annotated. The colorbar reports the linear sum of DL and UL power.

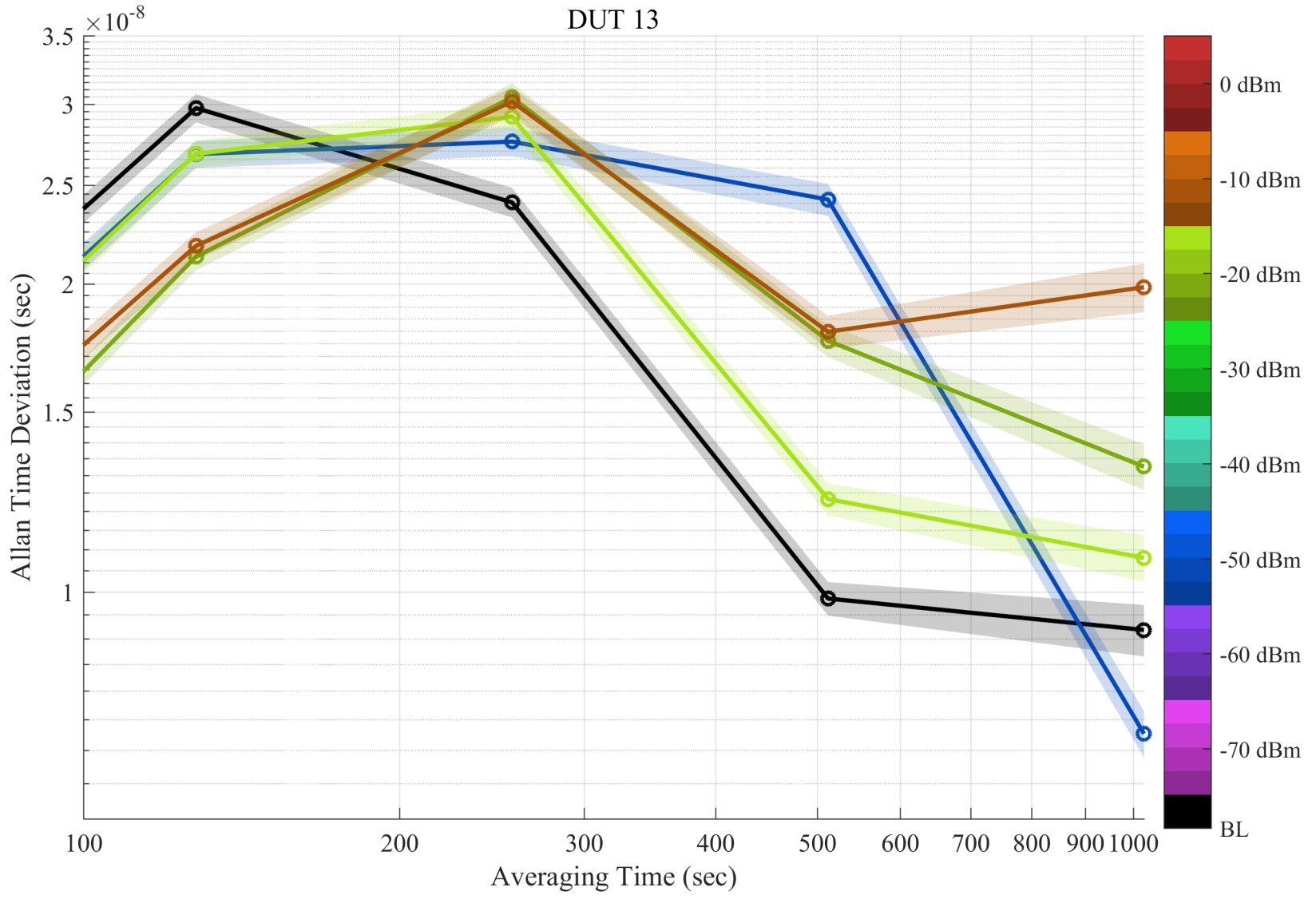


Figure 6.92: Zoom of Allan time deviation for DUT 13. Shaded regions indicate pointwise 95% confidence bands. Each curve corresponds to a tested LTE power level. The GPS scenario is timing, and the type of incident LTE is DL + UL1. The UL level was swept, and the DL level was fixed at -50 dBm EIIP unless otherwise annotated. The colorbar reports the linear sum of DL and UL power.

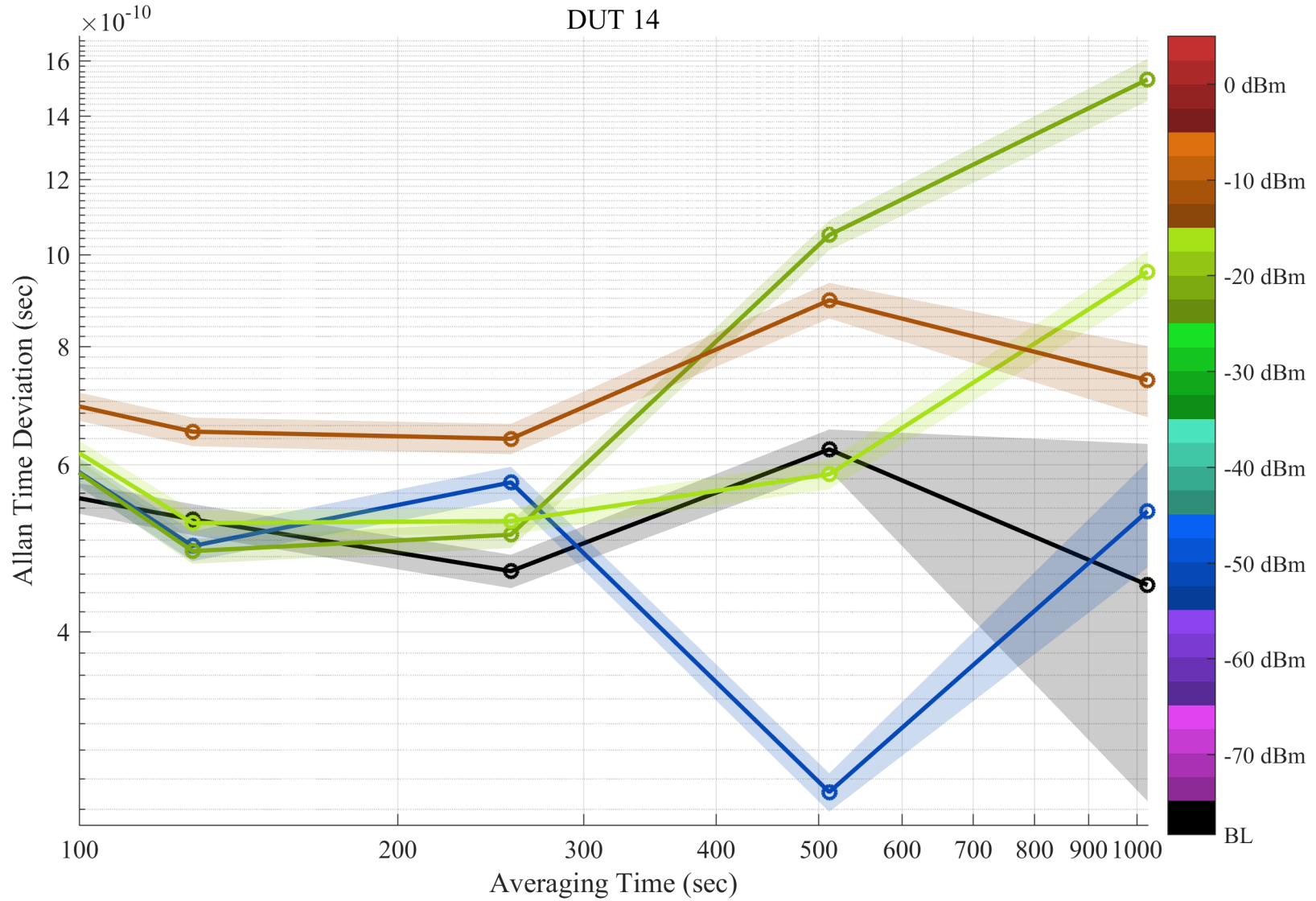


Figure 6.93: Zoom of Allan time deviation for DUT 14. Shaded regions indicate pointwise 95% confidence bands. Each curve corresponds to a tested LTE power level. The GPS scenario is timing, and the type of incident LTE is DL + UL1. The UL level was swept, and the DL level was fixed at -50 dBm EIIP unless otherwise annotated. The colorbar reports the linear sum of DL and UL power.

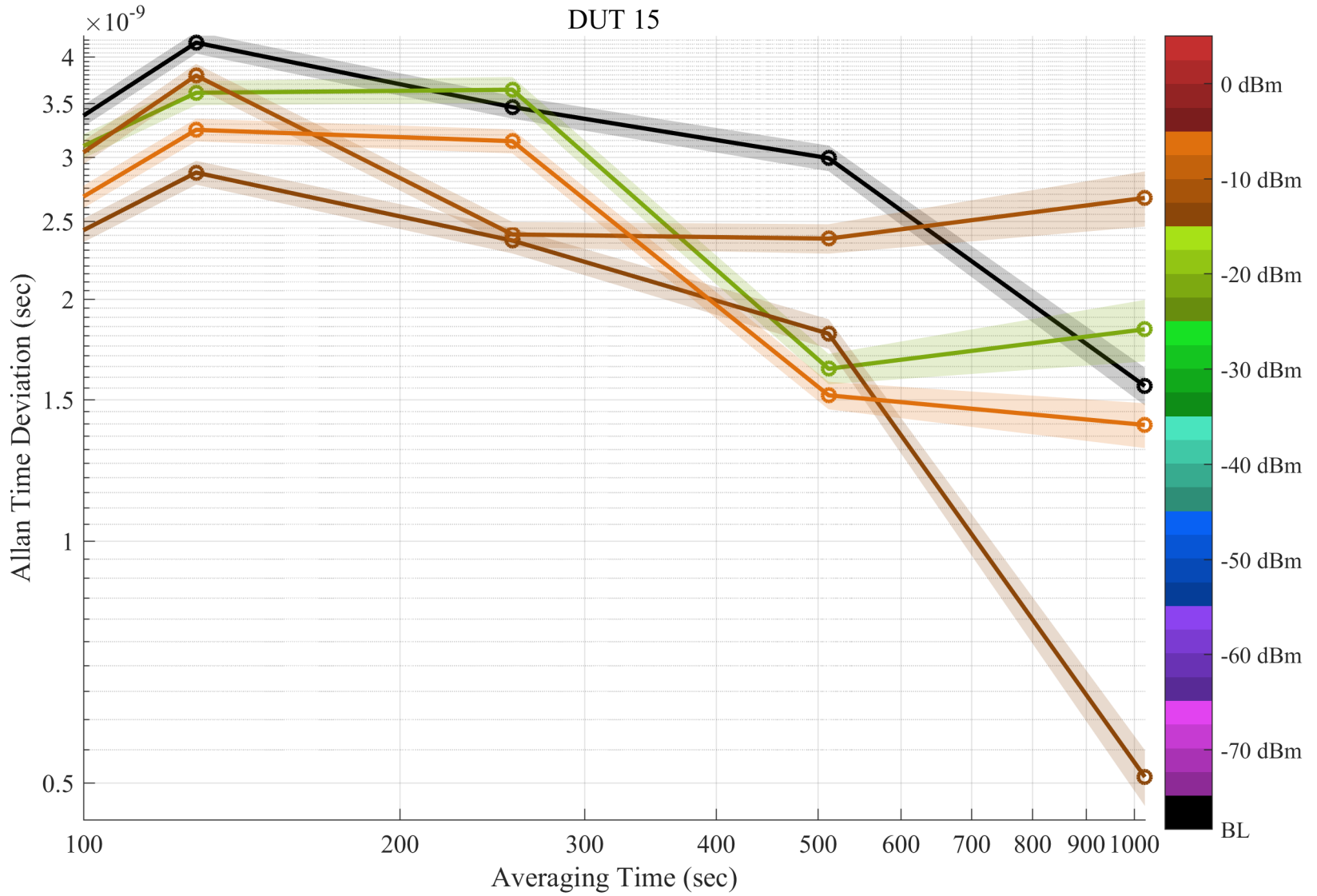


Figure 6.94: Zoom of Allan time deviation for DUT 15. Shaded regions indicate pointwise 95% confidence bands. Each curve corresponds to a tested LTE power level. The GPS scenario is timing, and the type of incident LTE is DL + UL1. The UL level was swept, and the DL level was fixed at -50 dBm EIIP unless otherwise annotated. The colorbar reports the linear sum of DL and UL power.

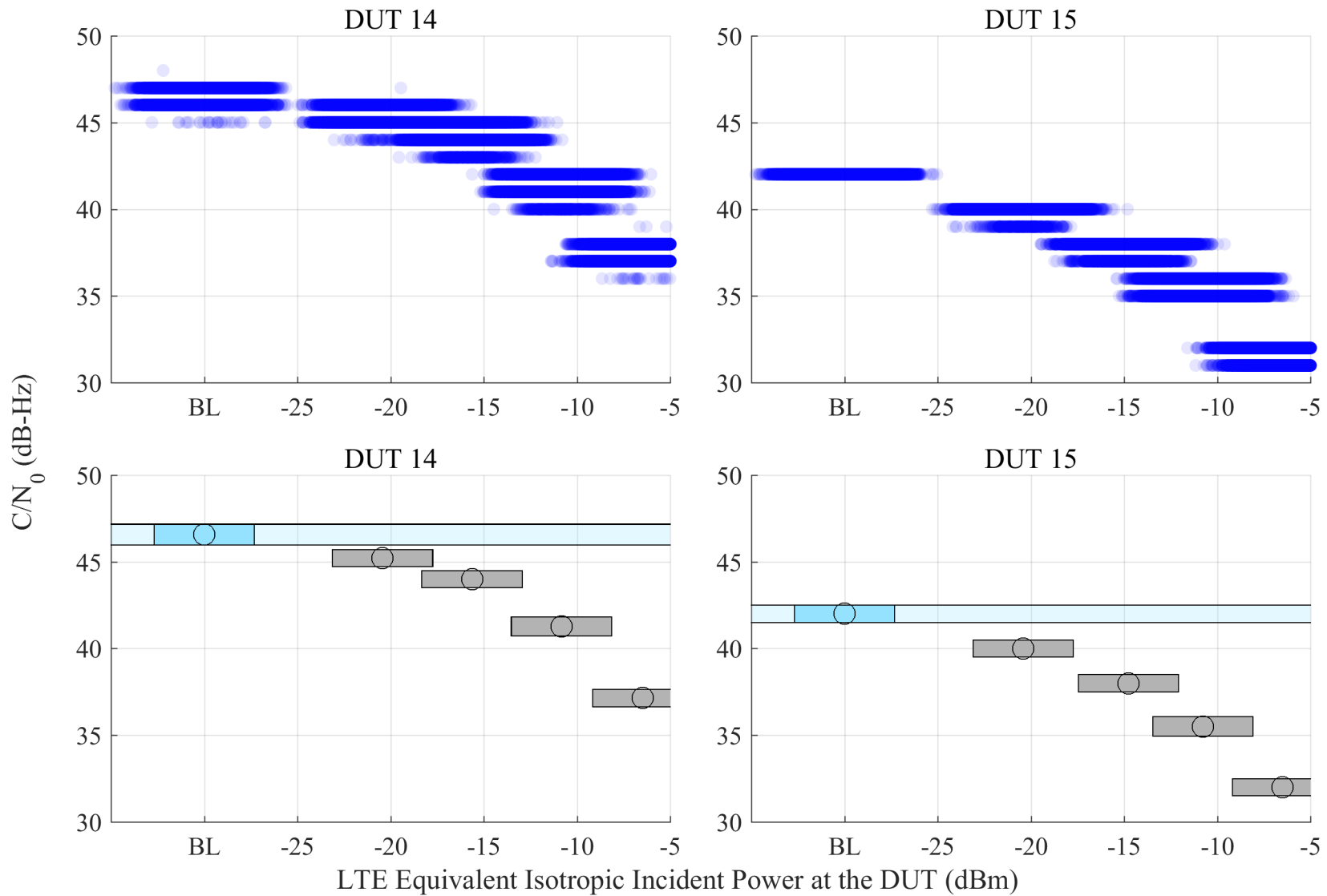


Figure 6.95:  $C/N_0$  scatter plots and median, with estimated 95% confidence region of the median from GPSDO receivers, swept with LTE power level. The GPS scenario is timing, and the type of incident LTE is DL + UL1. The UL level was swept, and the DL level was fixed at -50 dBm EIIP unless otherwise annotated. The horizontal axis reports the linear sum of DL and UL power.

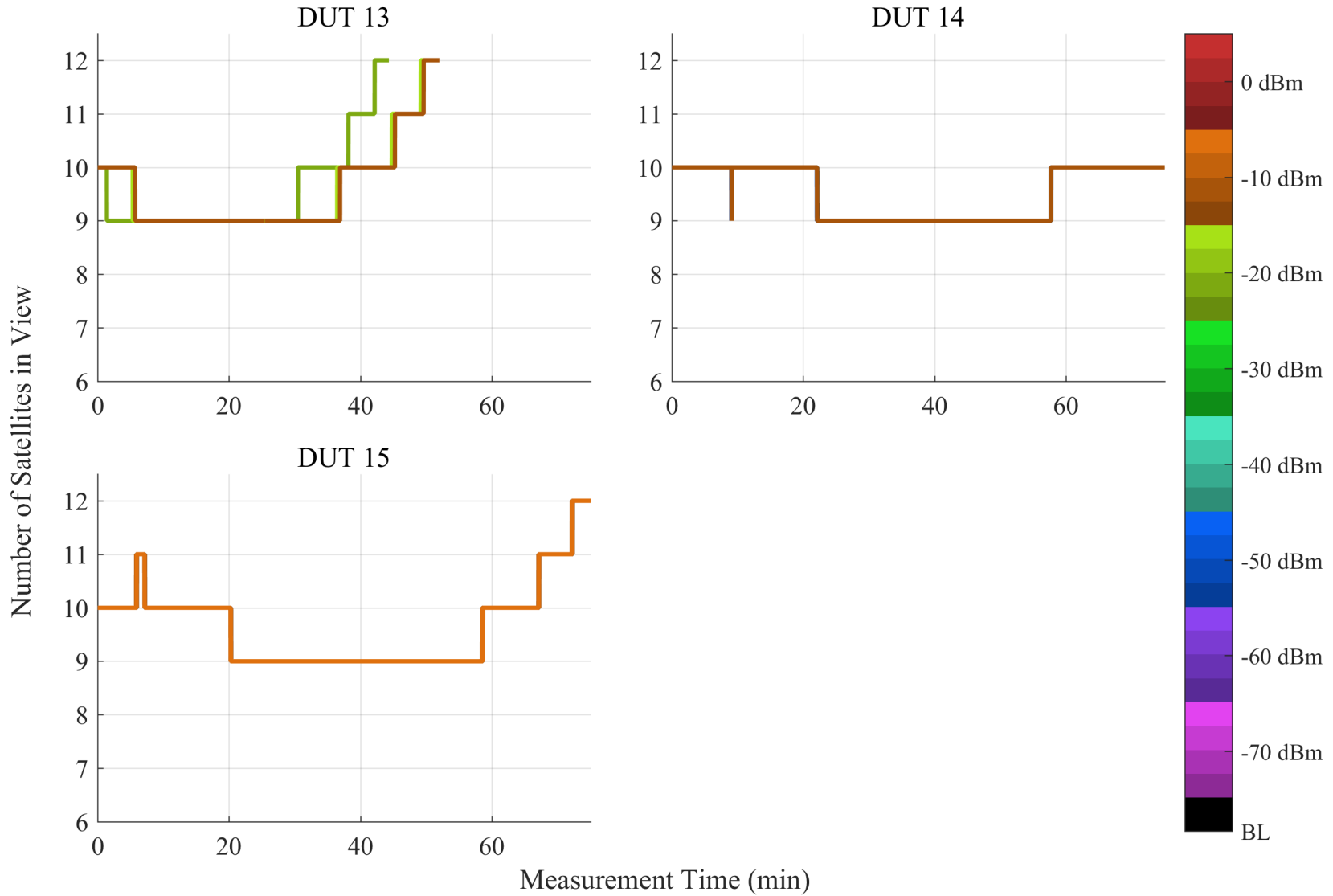


Figure 6.96: Number of satellites in view from GPSDO receivers, swept with LTE power level. The GPS scenario is timing, and the type of incident LTE is DL + UL1. The UL level was swept, and the DL level was fixed at -50 dBm EIRP unless otherwise annotated. The colorbar reports the linear sum of DL and UL power.

## 6.4 TTFF and TTFR Tests

Previous parts of this report address the definition and execution of these tests:

- The GPS receivers under test are listed in Subsection 2.1.1.
- The incident power condition, EIIP, is defined in Subsection 2.1.4.
- The simulated GPS signal parameters are listed in Section 2.2.
- The simulated GPS constellation parameters are listed in Subsubsection 2.2.2.1.
- The radiated LTE waveforms are listed in Section 2.3.
- Parameters for the TTFF and TTFR tests are given in Subsection 2.4.2.
- The tests executed for each DUT are listed in Table 2.9.
- The transmission system that creates the test conditions is detailed in Chapter 3.
- Each DUT under test is positioned according to Section 4.2.
- The test procedure for TTFR and TTFF power level sweeps are detailed by Subsection 4.3.2 and Subsection 4.3.3.
- Data acquisition from each DUT is described by Section 4.4.
- Data processing and analysis are described in Chapter 5.
- LTE equivalent isotropic incident power at the DUT (dBm) for the TTFF and TTFR test can be found in Table 6.2.

Table 6.2: LTE Power by DUT for the Time-to-First Fix Test. The Uncertainty Corresponds to the 95% Confidence Interval.

<b>Device</b>	<b>Type</b>	<b>UL 1 (dBm)</b>	<b>DL (dBm)</b>
DUT 1	GLN	-12.7 ±2.7 dB	2.4 ±3.1 dB
DUT 2	GLN	-12.9 ±2.7 dB	0.8 ±3.1 dB
DUT 3	GLN	-15.3 ±2.7 dB	2.8 ±3.1 dB
DUT 7	HPP	-46.3 ±2.7 dB	-61.2 ±2.7 dB
		-41.3 ±2.7 dB	-54.5 ±2.7 dB
		-35.8 ±2.7 dB	-45.8 ±2.7 dB
		-33.8 ±2.7 dB	-40.5 ±2.7 dB
DUT 8	HPP	-51.3 ±2.7 dB	-63.4 ±2.7 dB
		-50.2 ±2.7 dB	-62.3 ±2.7 dB
		-46.3 ±2.7 dB	—
DUT 9, Ant C	HPP	-50.0 ±2.7 dB	-52.3 ±2.7 dB
		-45.9 ±2.7 dB	—
		-42.9 ±2.7 dB	—
DUT 9, Ant D	HPP	-33.8 ±2.7 dB	-1.5 ±3.1 dB
		-27.5 ±2.7 dB	0.4 ±3.1 dB
DUT 10	HPP	-47.2 ±2.7 dB	-62.5 ±2.7 dB
DUT 11, Ant A	RTK	-59.7 ±2.7 dB	-67.0 ±2.7 dB
		-45.3 ±2.7 dB	—
		-43.9 ±2.7 dB	—
DUT 11, Ant B	RTK	-15.4 ±2.7 dB	-24.6 ±3.1 dB
		-12.5 ±2.7 dB	-7.2 ±3.1 dB
		—	1.9 ±3.1 dB
DUT 12, Ant C	RTK	-48.5 ±2.7 dB	-54.3 ±3.1 dB
DUT 12, Ant D	RTK	-33.4 ±2.7 dB	-1.3 ±3.1 dB
		-31.0 ±2.7 dB	—

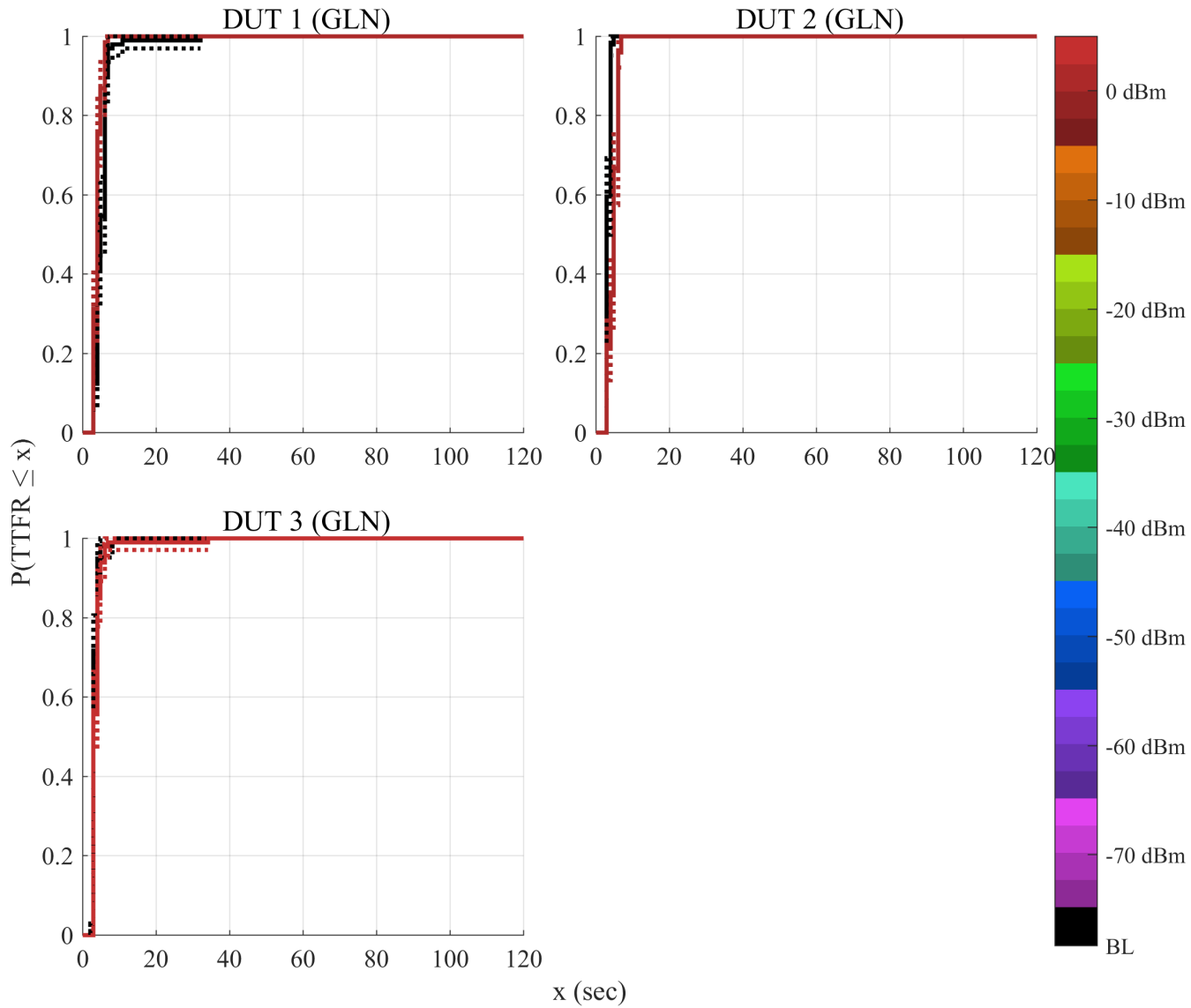


Figure 6.97: CDF plots of TTFR from lock acquisition reported by GLN receivers at different LTE power levels. The GPS scenario is TTFR, and the type of incident LTE is DL.

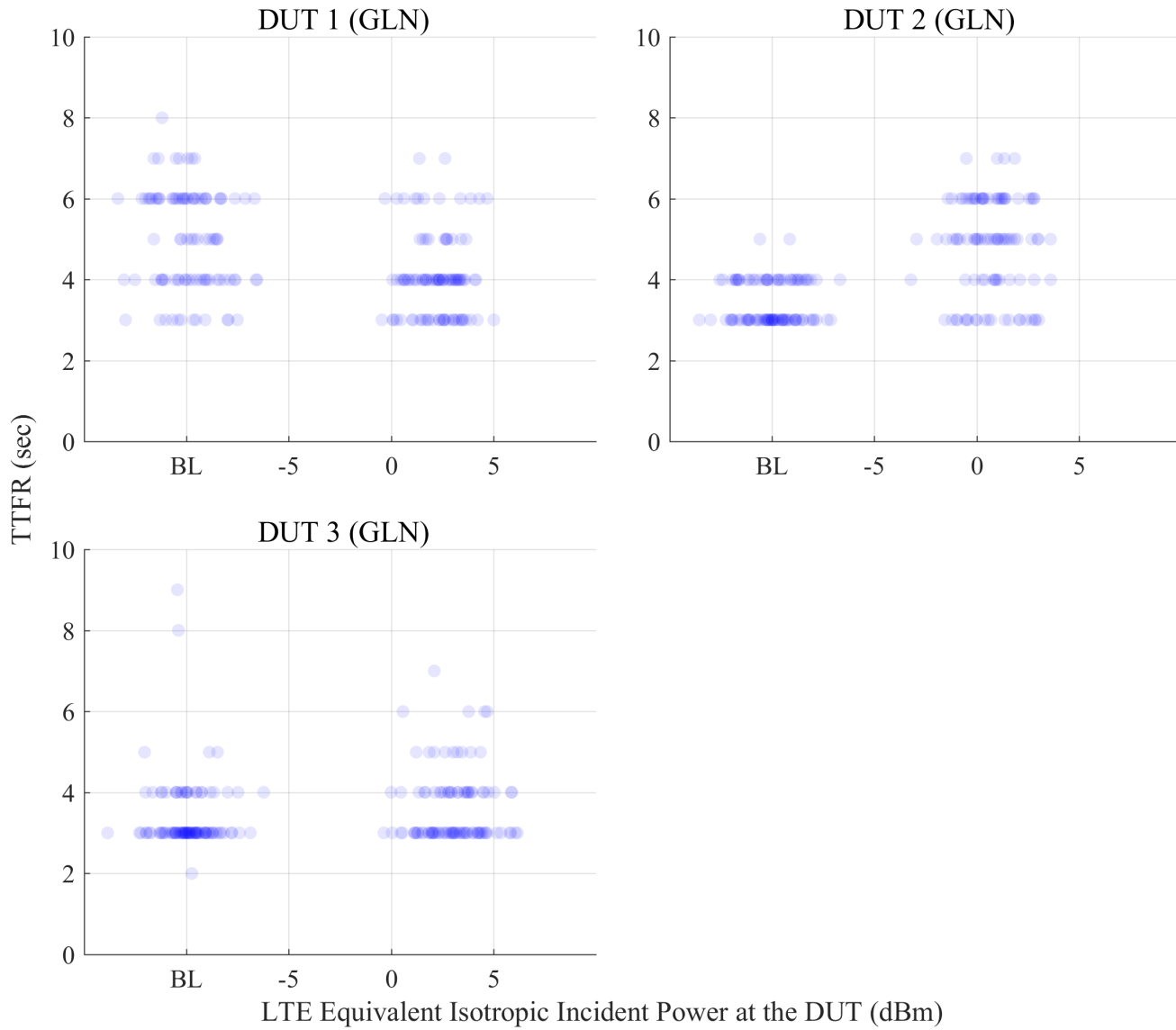


Figure 6.98: Scatterplots of TTFR from lock acquisition reported by GLN receivers at different LTE power levels. The GPS scenario is TTFR, and the type of incident LTE is DL.

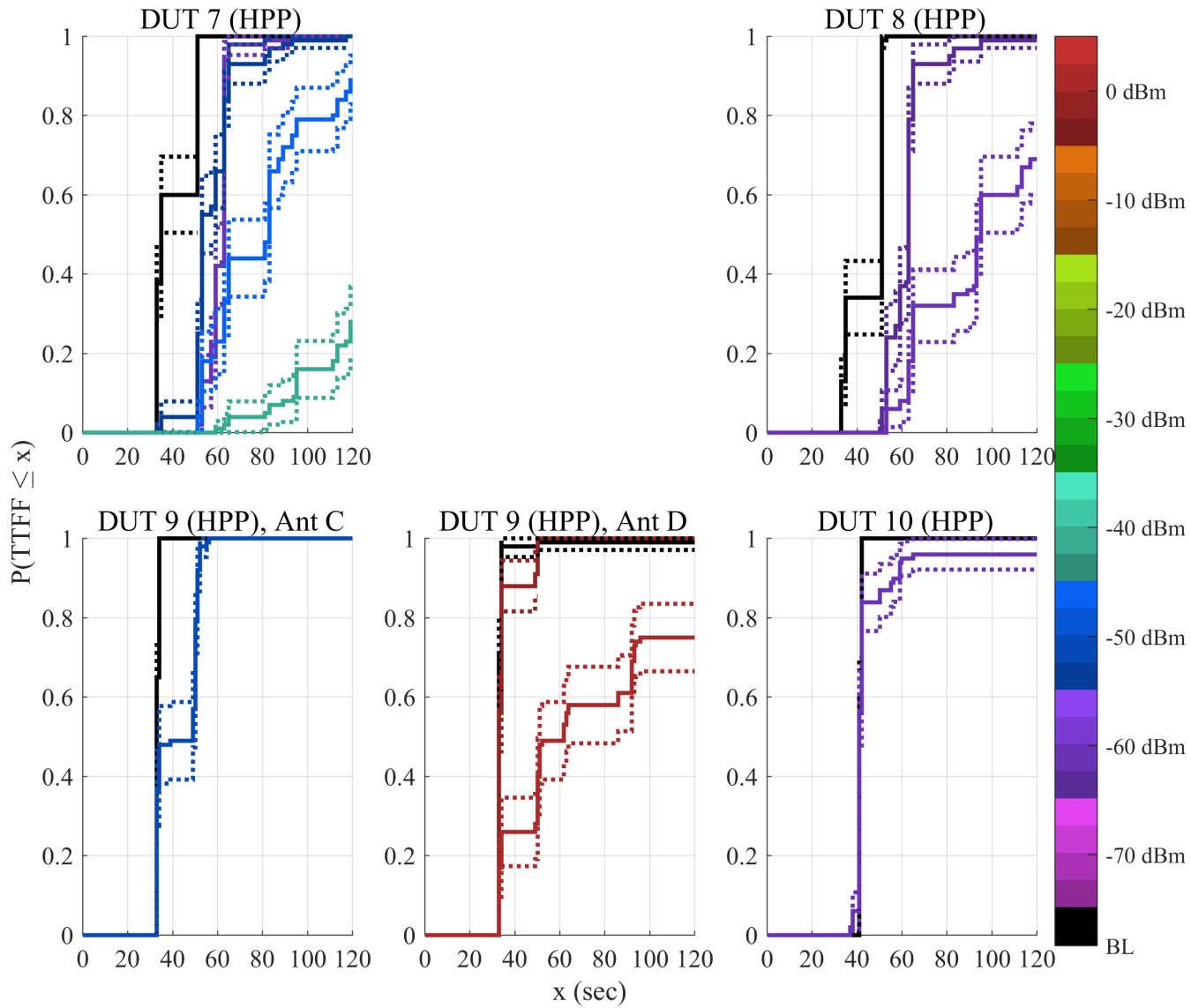


Figure 6.99: CDF plots of TTFR from lock acquisition reported by GLN receivers at different LTE power levels. The GPS scenario is TTFR, and the type of incident LTE is UL1.

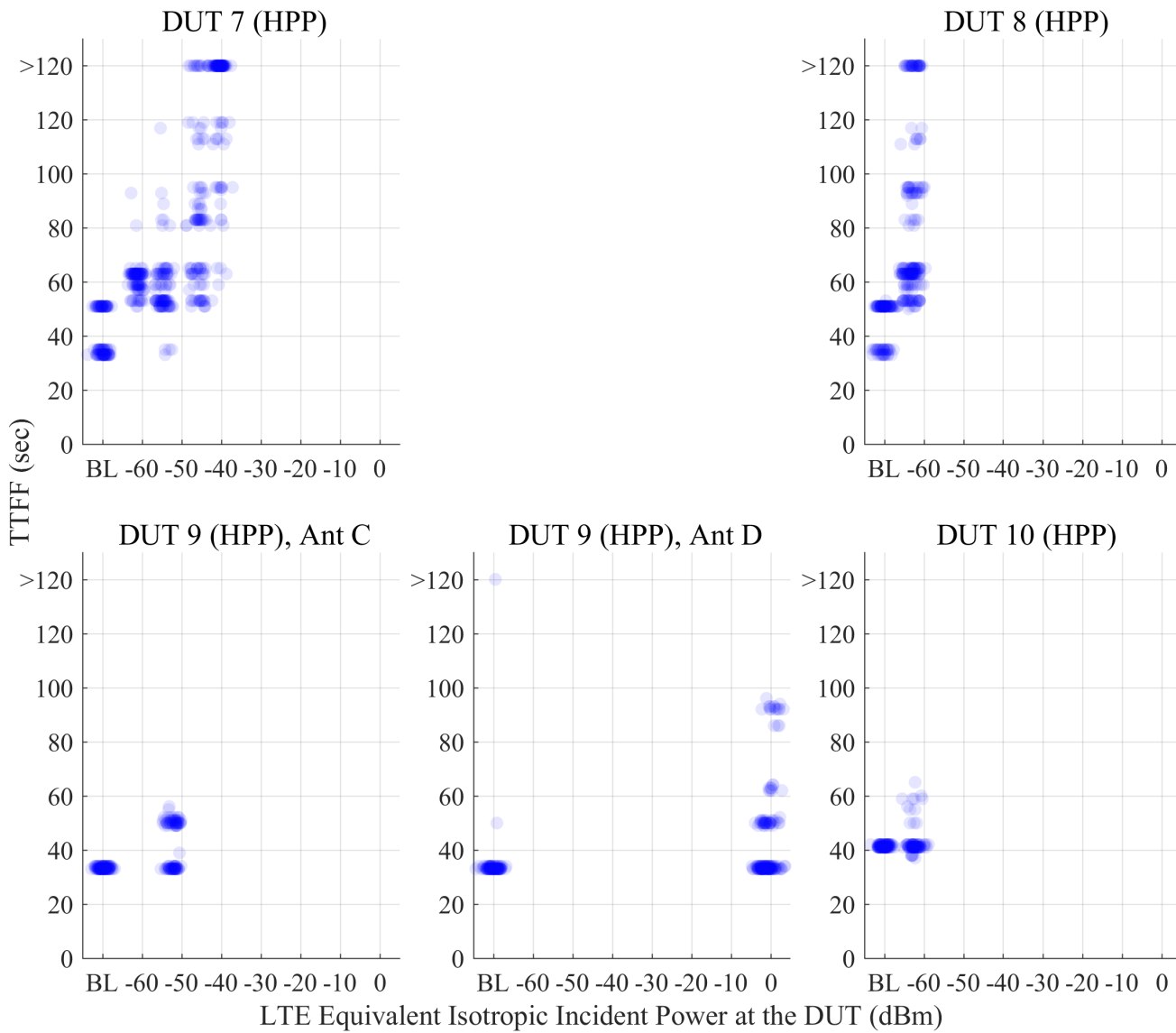


Figure 6.100: Scatterplots of TTFR from lock acquisition reported by GLN receivers at different LTE power levels. The GPS scenario is TTFR, and the type of incident LTE is UL1.

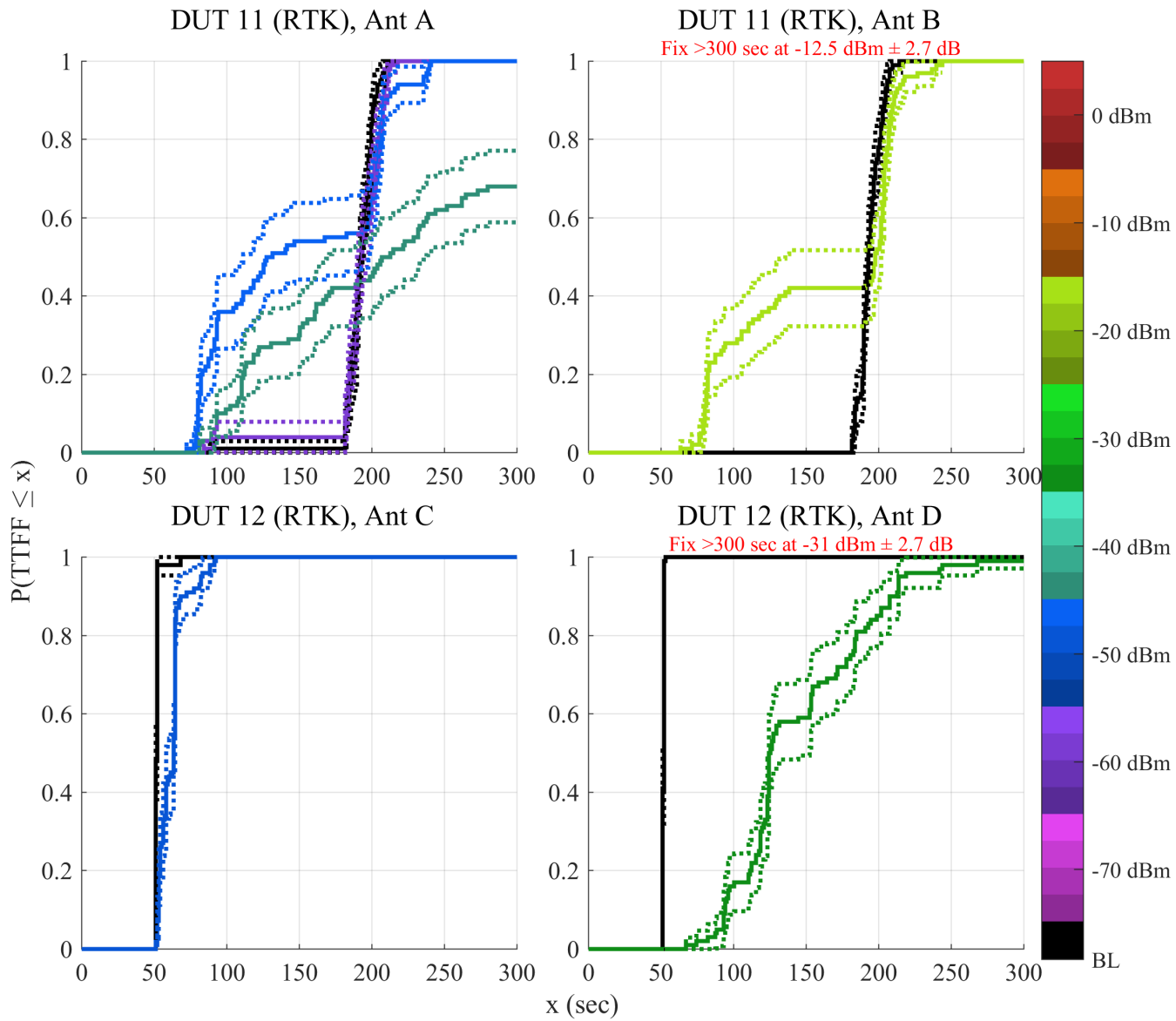


Figure 6.101: CDF plots of TTF from lock acquisition reported by HPP receivers at different LTE power levels. The GPS scenario is TTFF, and the type of incident LTE is DL.

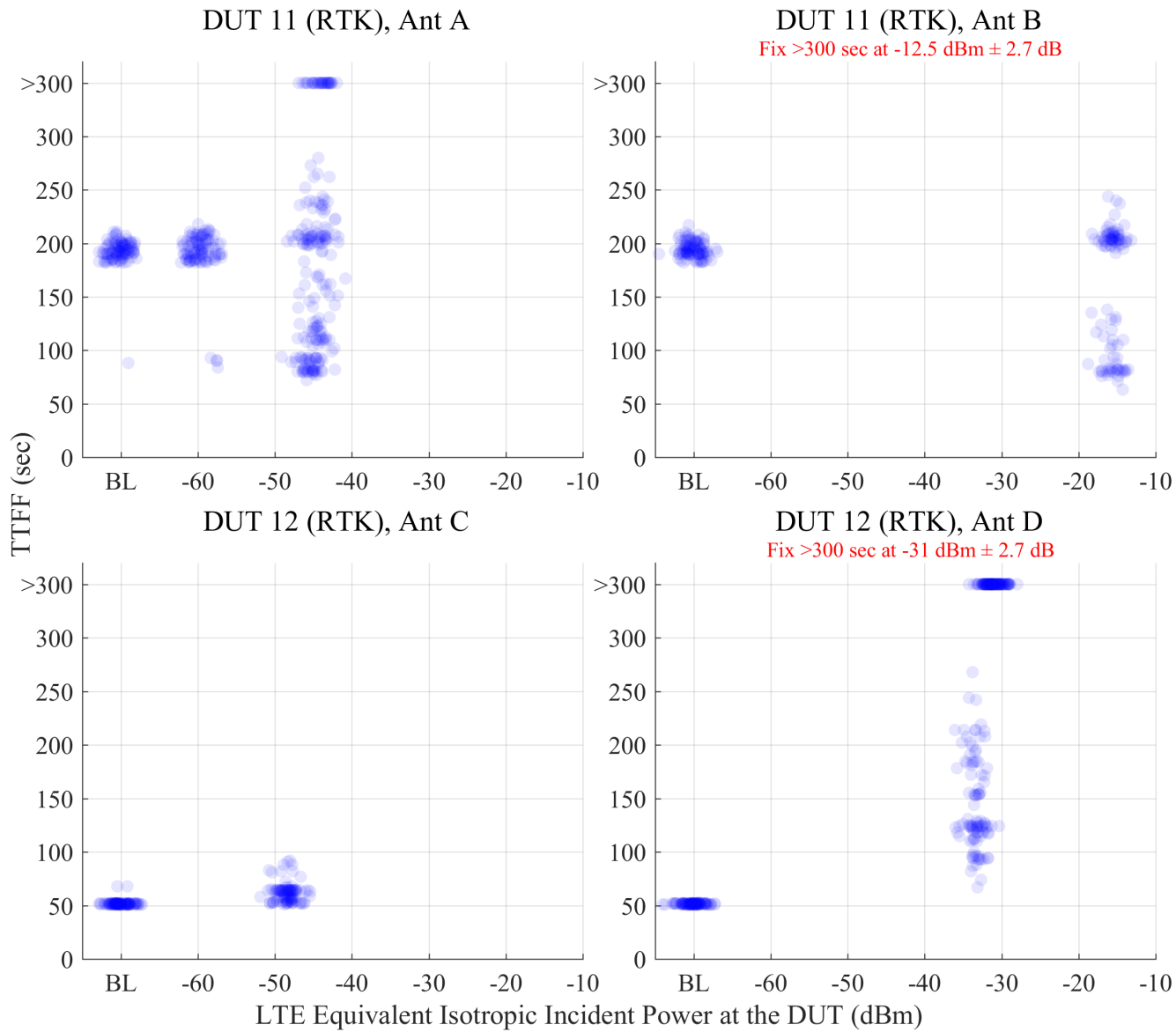


Figure 6.102: Scatterplots of TTF from lock acquisition reported by HPP receivers at different LTE power levels. The GPS scenario is TTF, and the type of incident LTE is DL.

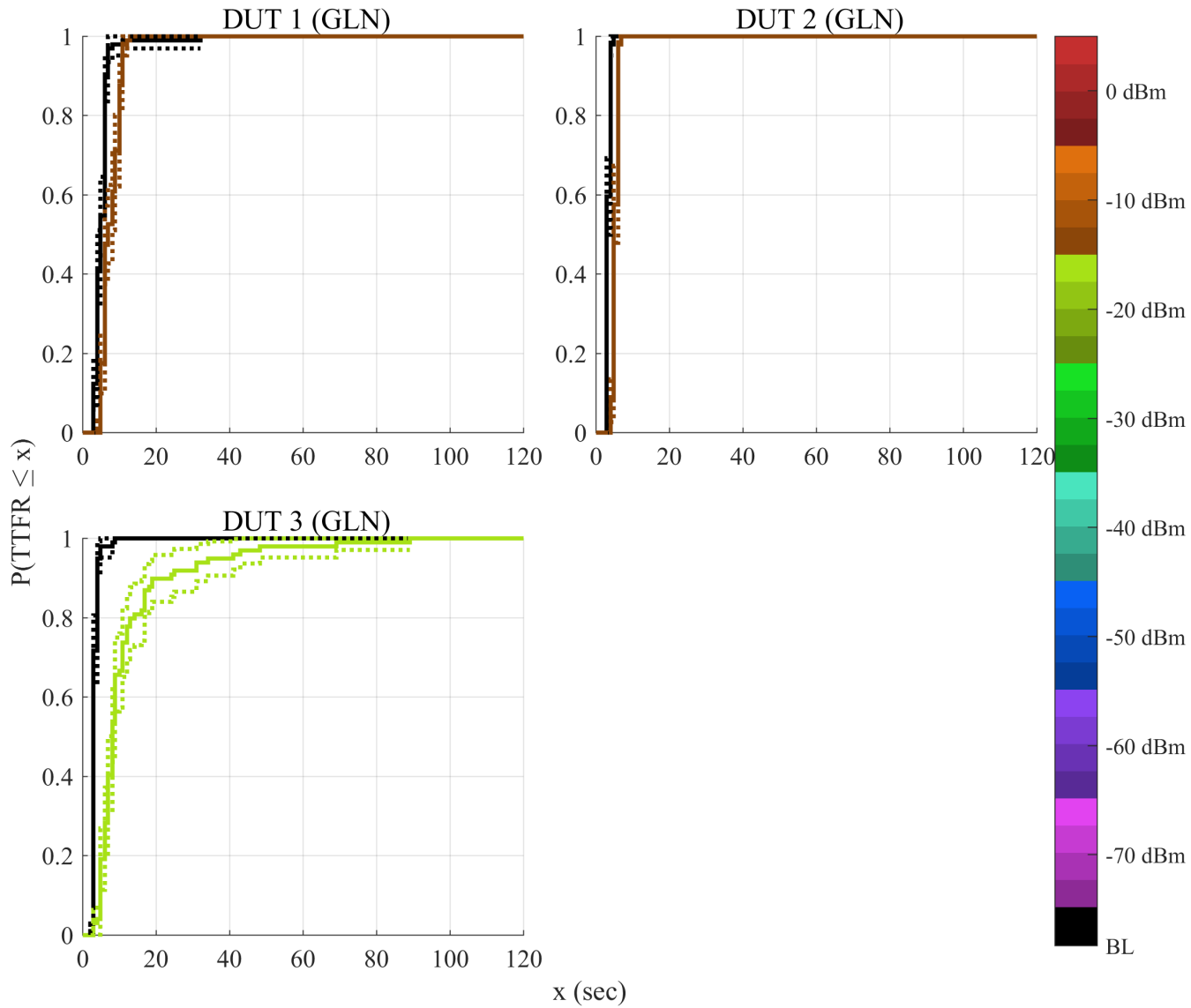


Figure 6.103: CDF plots of TTFF from lock acquisition reported by HPP receivers at different LTE power levels. The GPS scenario is TTFF, and the type of incident LTE is UL1.

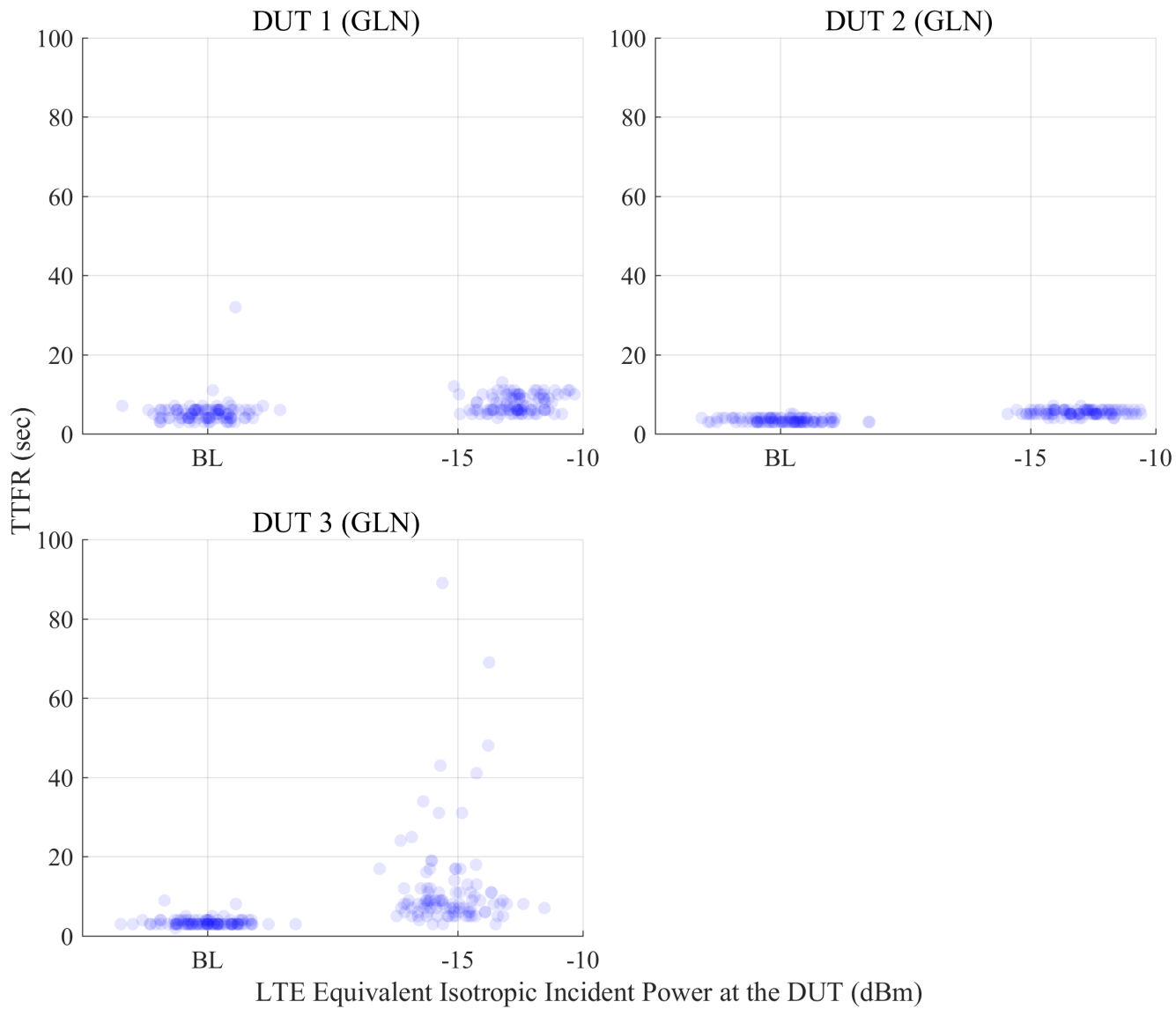


Figure 6.104: Scatterplots of TTFR from lock acquisition reported by HPP receivers at different LTE power levels. The GPS scenario is TTFR, and the type of incident LTE is UL1.

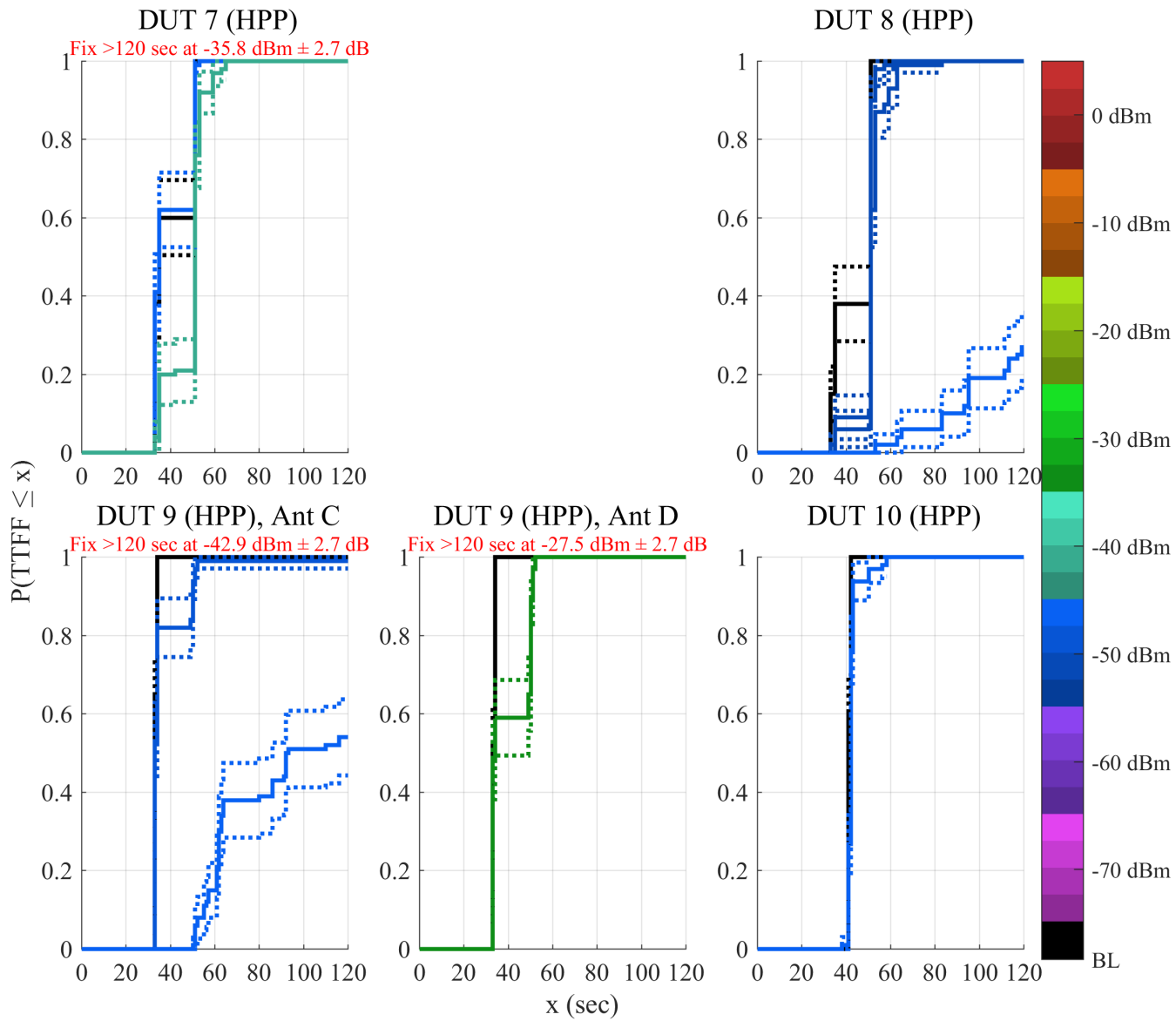


Figure 6.105: CDF plots of TTF from lock acquisition reported by RTK receivers at different LTE power levels. The GPS scenario is TTFF, and the type of incident LTE is DL.

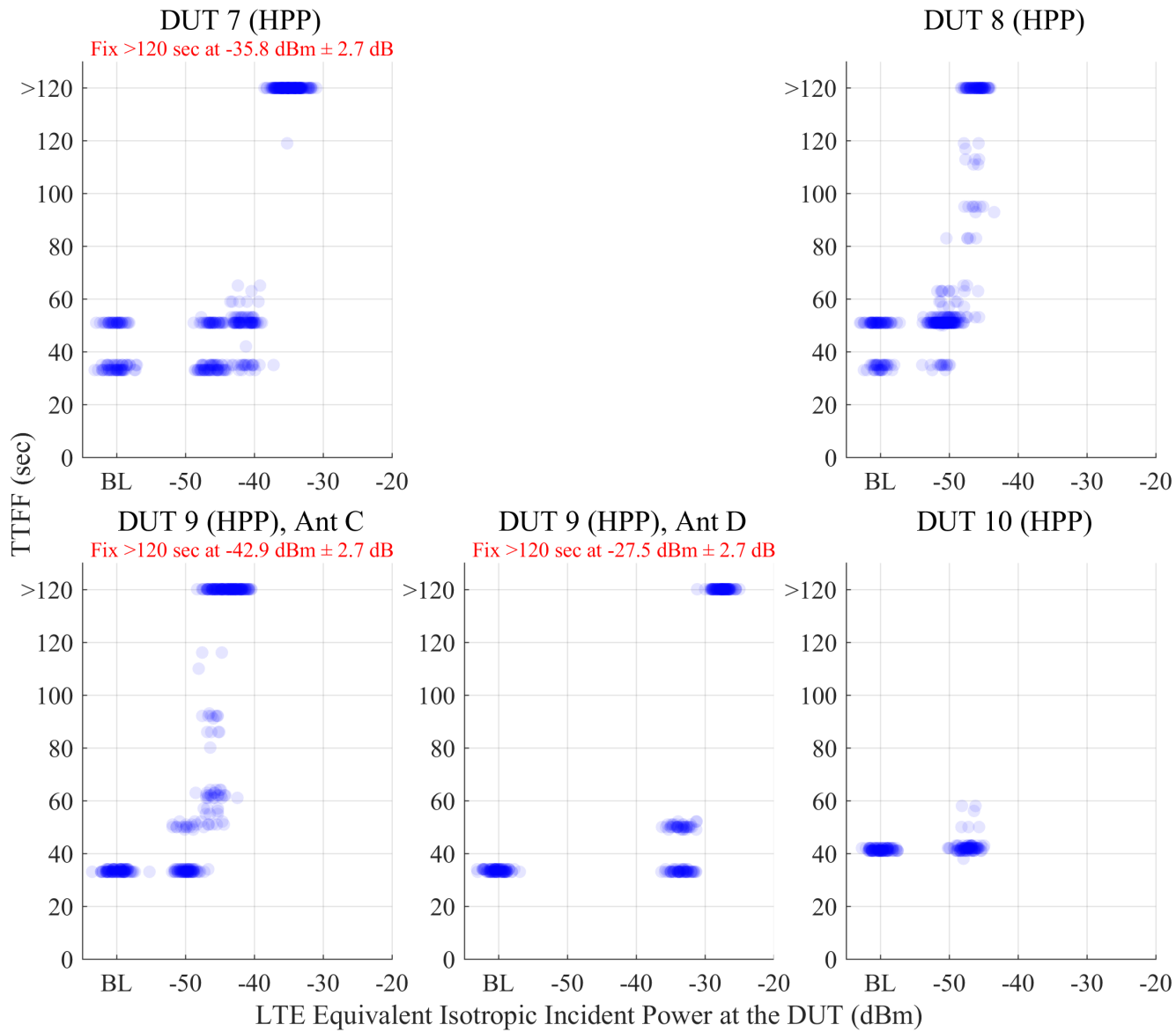


Figure 6.106: Scatterplots of TTF from lock acquisition reported by RTK receivers at different LTE power levels. The GPS scenario is TTF, and the type of incident LTE is DL.

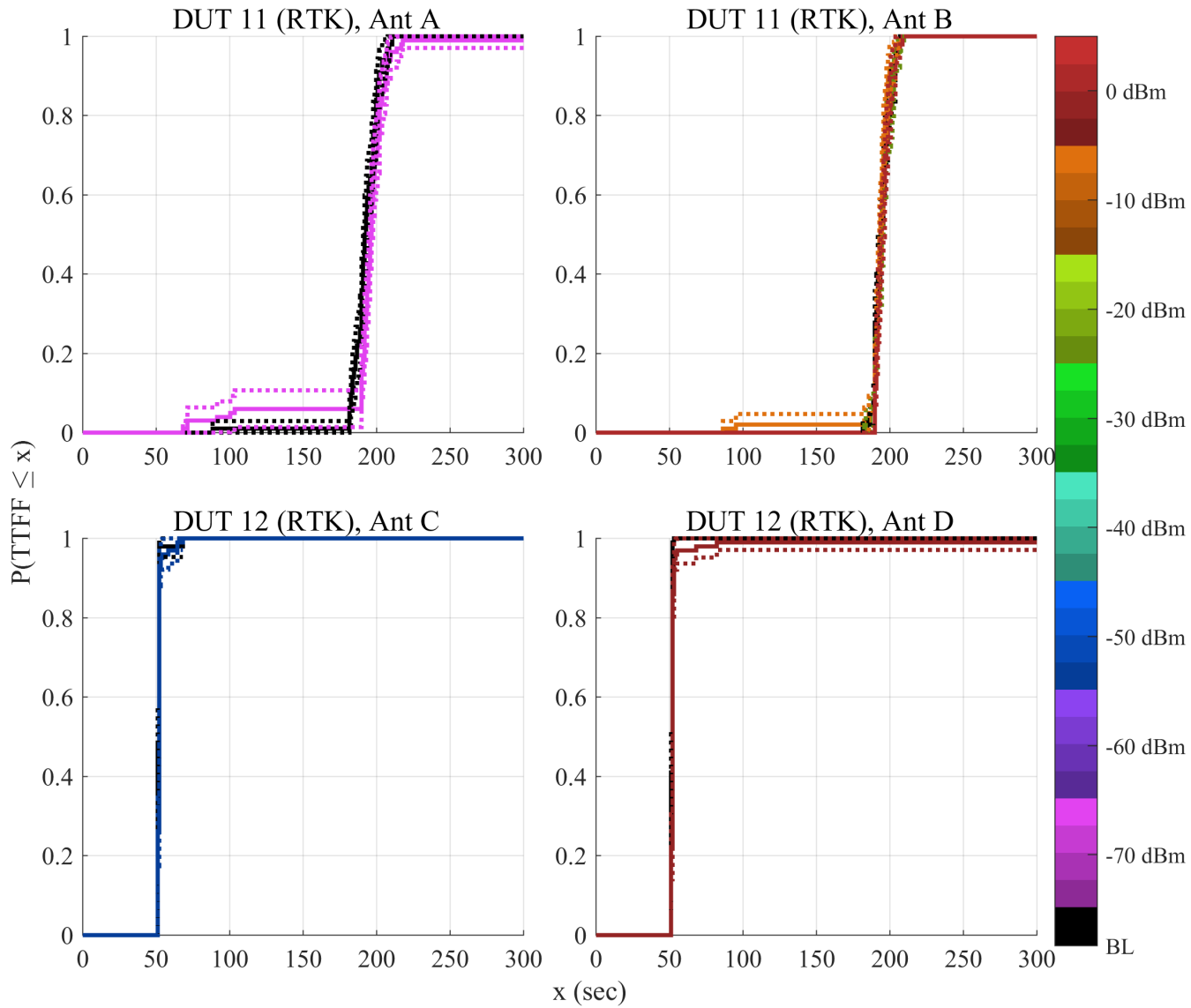


Figure 6.107: CDF plots of TTF from lock acquisition reported by RTK receivers at different LTE power levels. The GPS scenario is TTF, and the type of incident LTE is UL1.

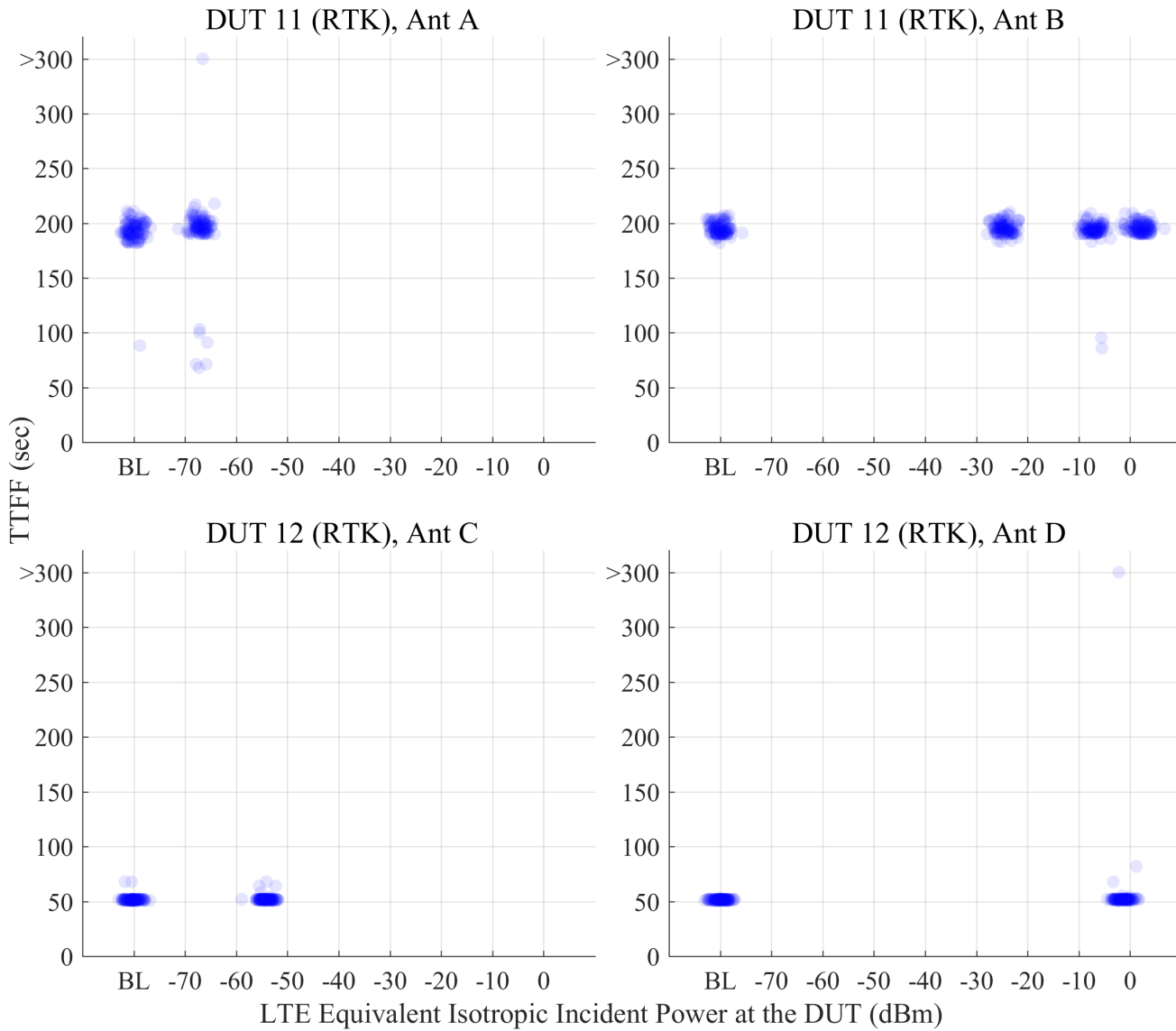


Figure 6.108: Scatterplots of TTF from lock acquisition reported by RTK receivers at different LTE power levels. The GPS scenario is TTF, and the type of incident LTE is UL1.

## 6.5 LTE Power Level Sweeps for Limited GPS Power Exposure

Previous parts of this report address the definition and execution of these tests:

- The GPS receivers under test are listed in Subsection 2.1.1.
- The incident power condition, EIIP, is defined in Subsection 2.1.4.
- The simulated GPS signal parameters are listed in Section 2.2.
- The simulated GPS constellation parameters in the limited scenario are listed in Subsubsection 2.2.2.2.
- The radiated LTE waveforms are listed in Section 2.3.
- Parameters for the LTE power sweep tests are given in Subsection 2.4.1.
- The tests executed for each DUT are listed in Table 2.10.
- The transmission system that creates the test conditions is detailed in Chapter 3.
- Each DUT under test is positioned according to Section 4.2.
- The test procedure for LTE power level sweeps is detailed by Subsection 4.3.1.
- Data acquisition from each DUT is described by Section 4.4.
- Data processing and analysis are described in Chapter 5.

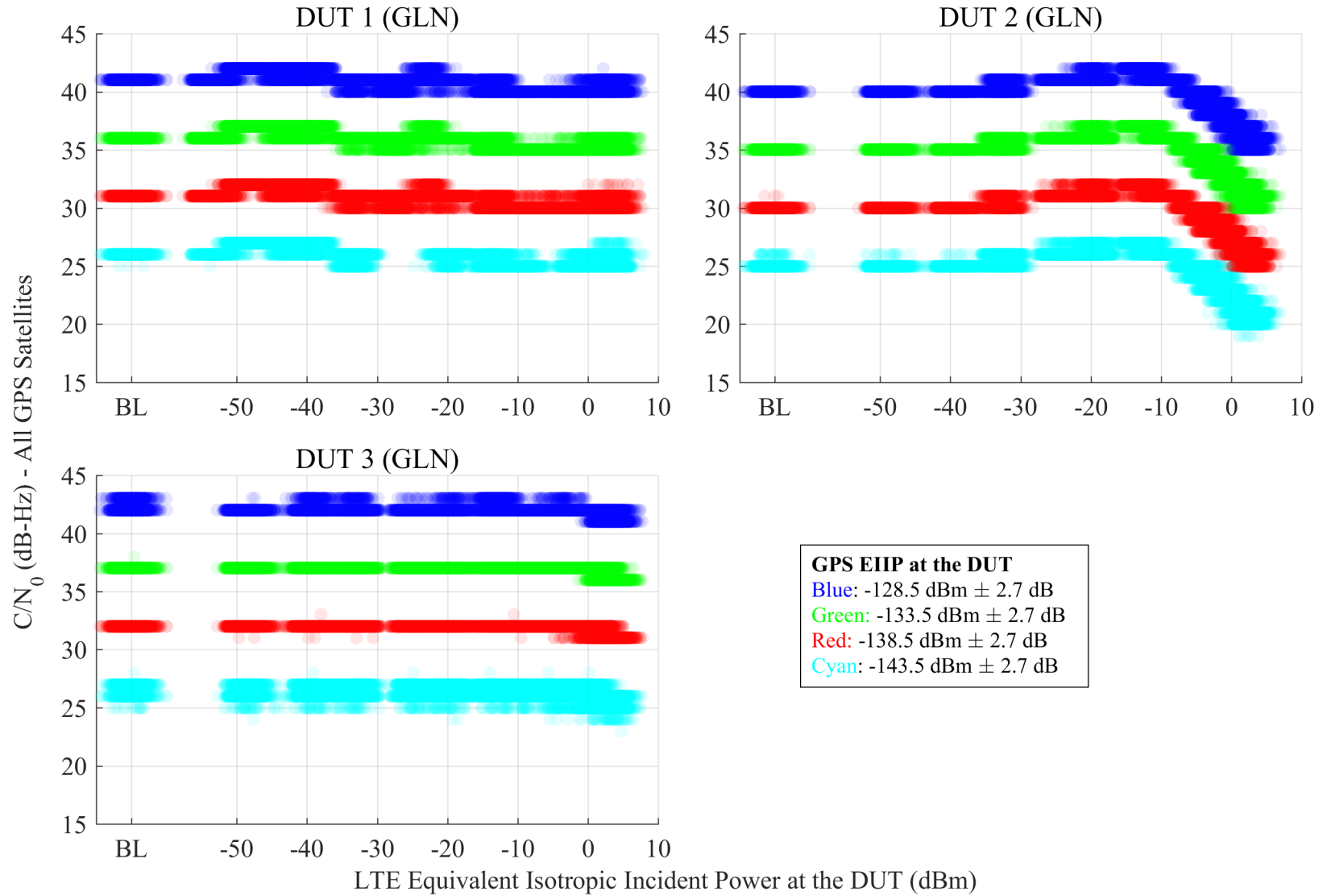


Figure 6.109: Scatterplots of reported  $C/N_0$  from GLN receivers, swept with LTE power level. The GPS scenario is limited, and the type of incident LTE is DL.

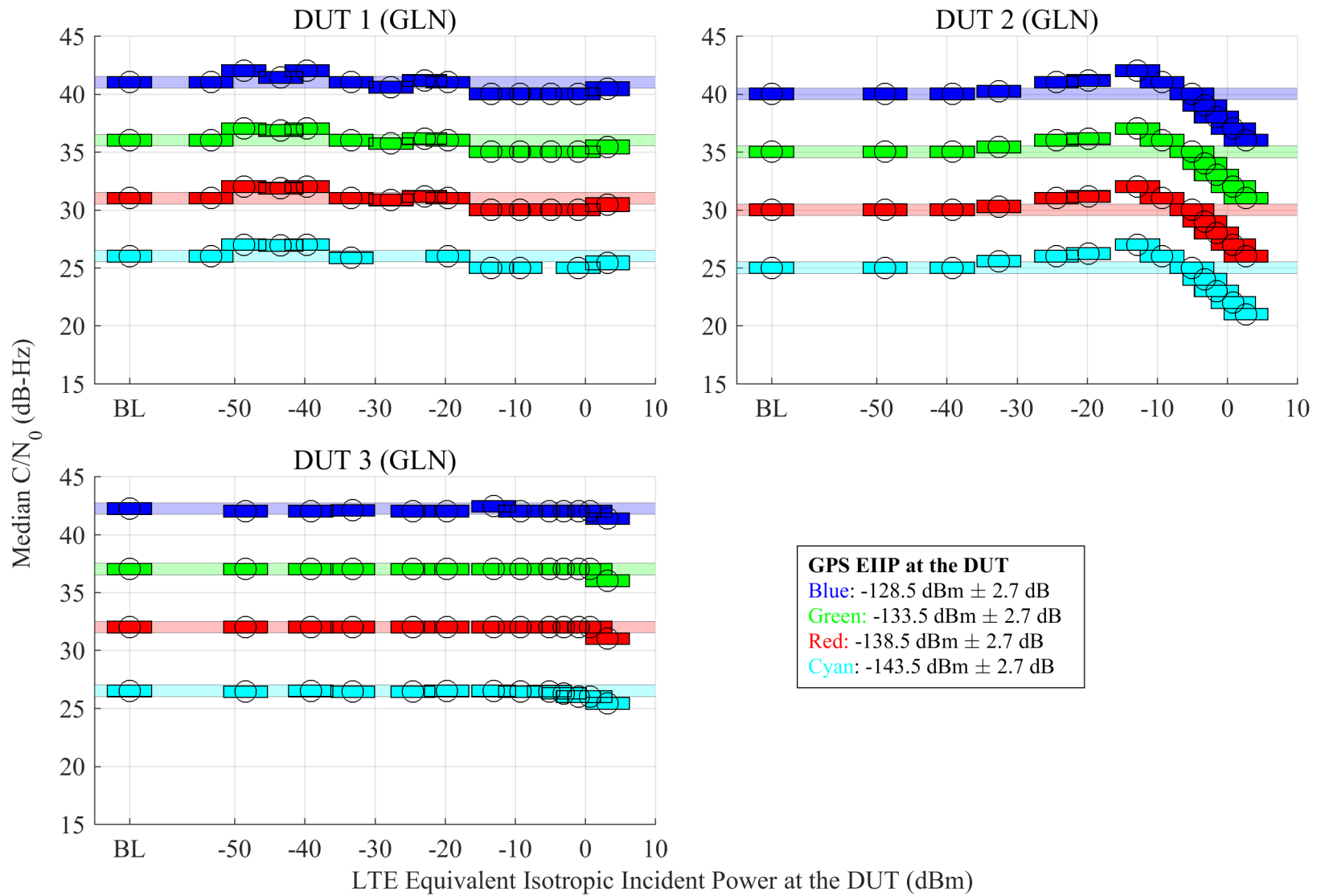


Figure 6.110: Estimated 95% confidence regions of the median of reported  $C/N_0$  from GLN receivers, swept with LTE power level. The GPS scenario is limited, and the type of incident LTE is DL.

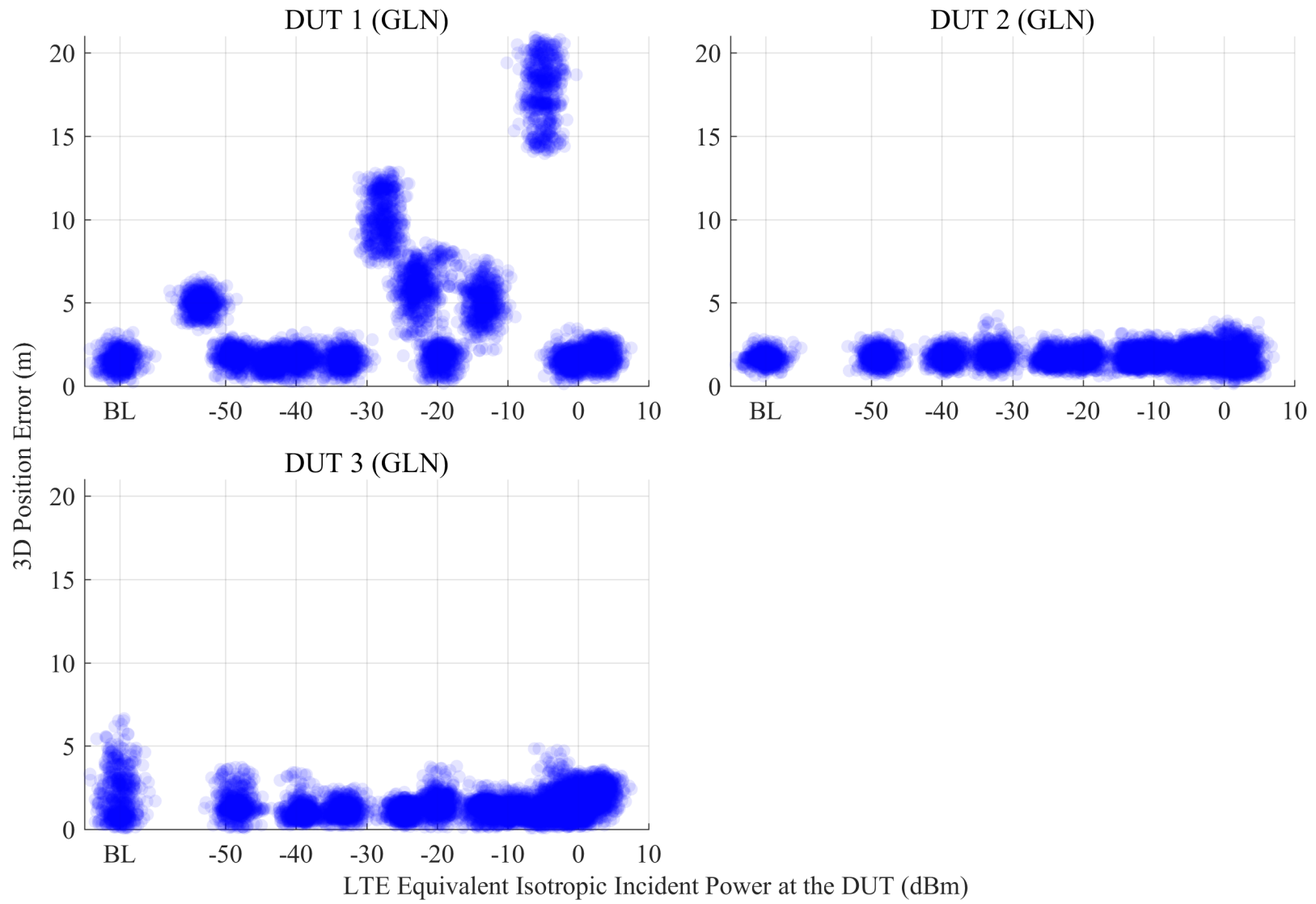


Figure 6.111: Scatterplots of error in reported 3-D position compared to simulator truth from GLN receivers, swept with LTE power level. The GPS scenario is limited, and the type of incident LTE is DL.

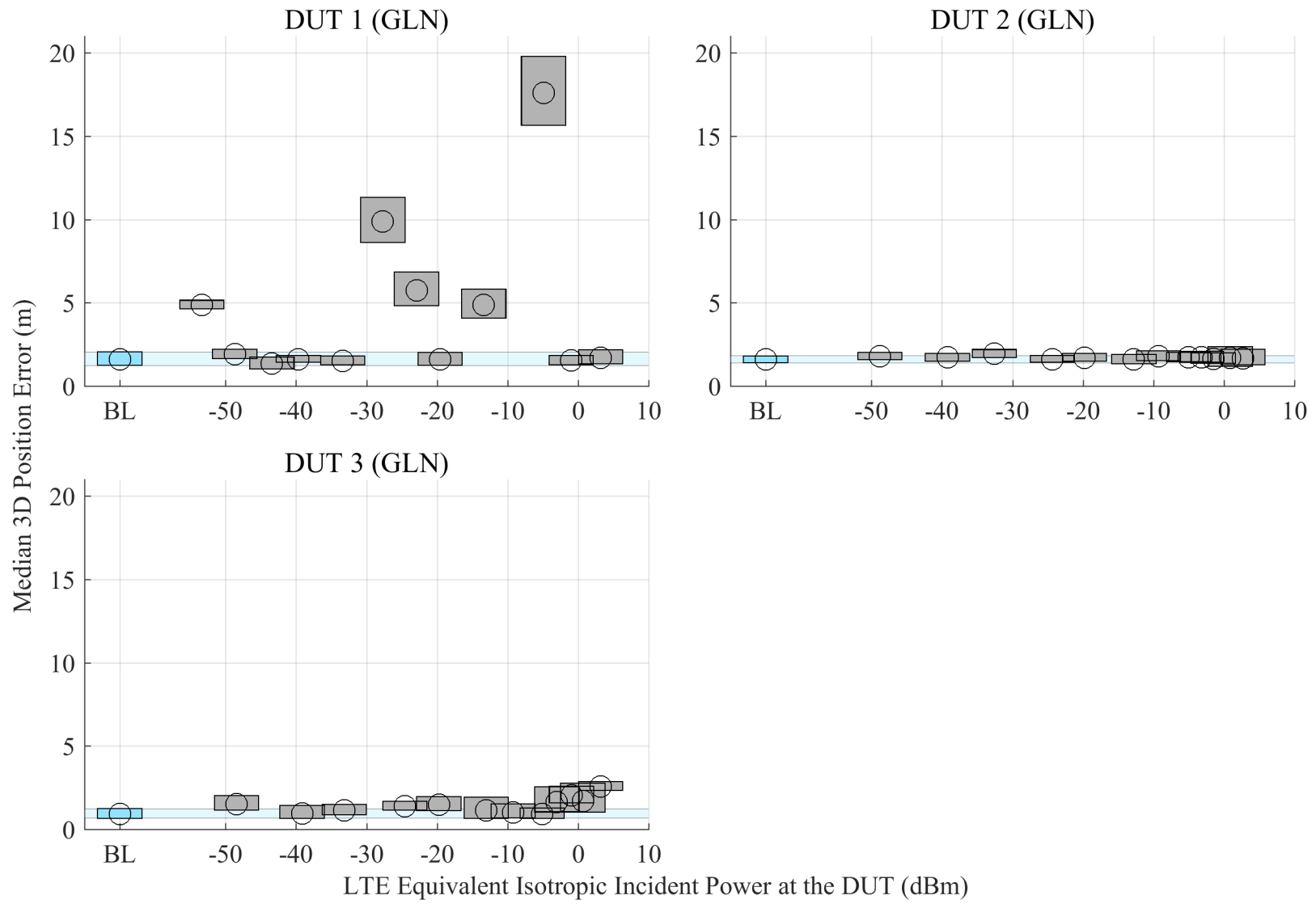


Figure 6.112: Estimated 95% confidence regions of the median error in reported 3-D position from GLN receivers, swept with LTE power level. The GPS scenario is limited, and the type of incident LTE is DL.

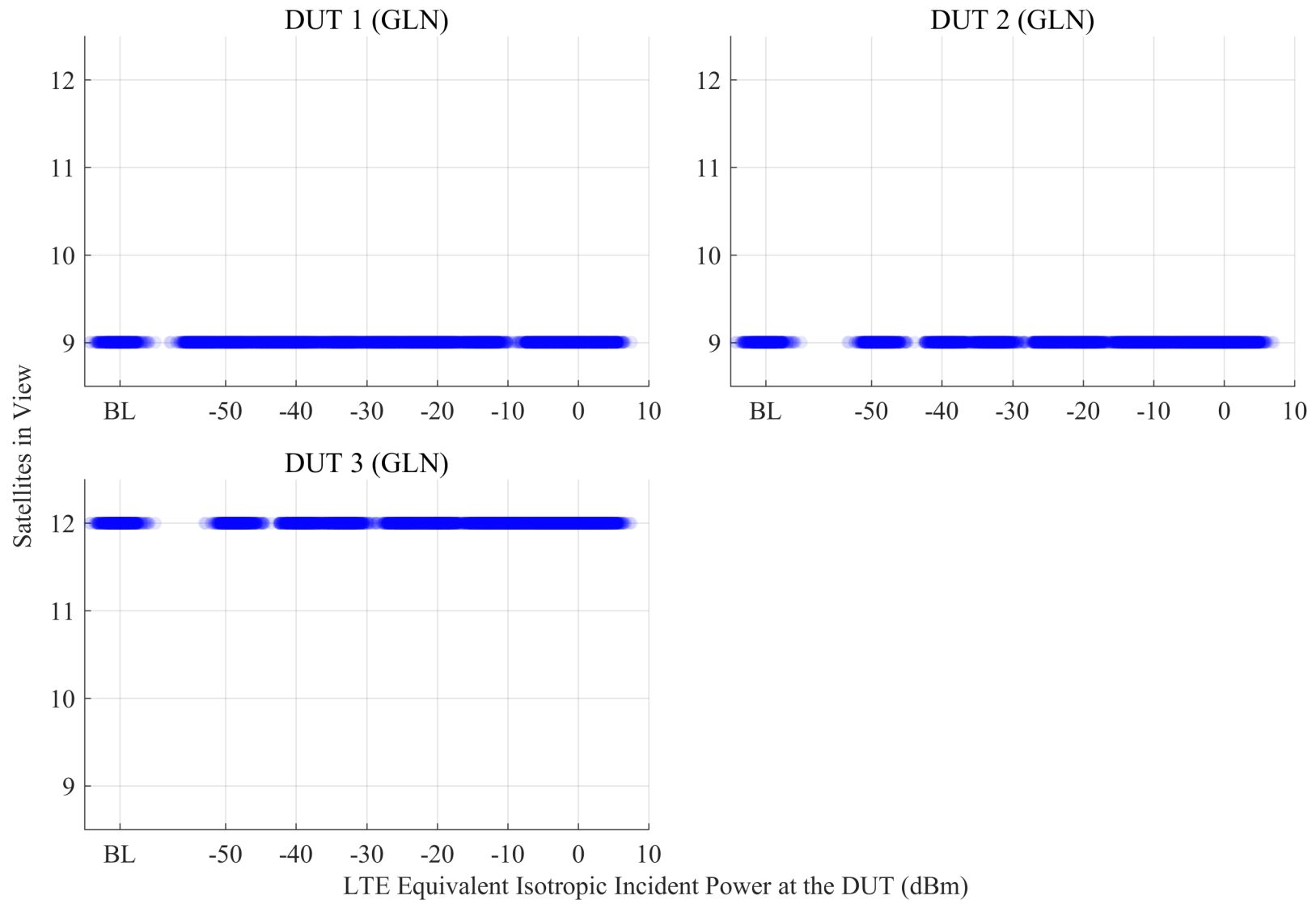


Figure 6.113: Scatterplots of the number of satellites in view from GLN receivers, swept with LTE power level. The GPS scenario is limited, and the type of incident LTE is DL.

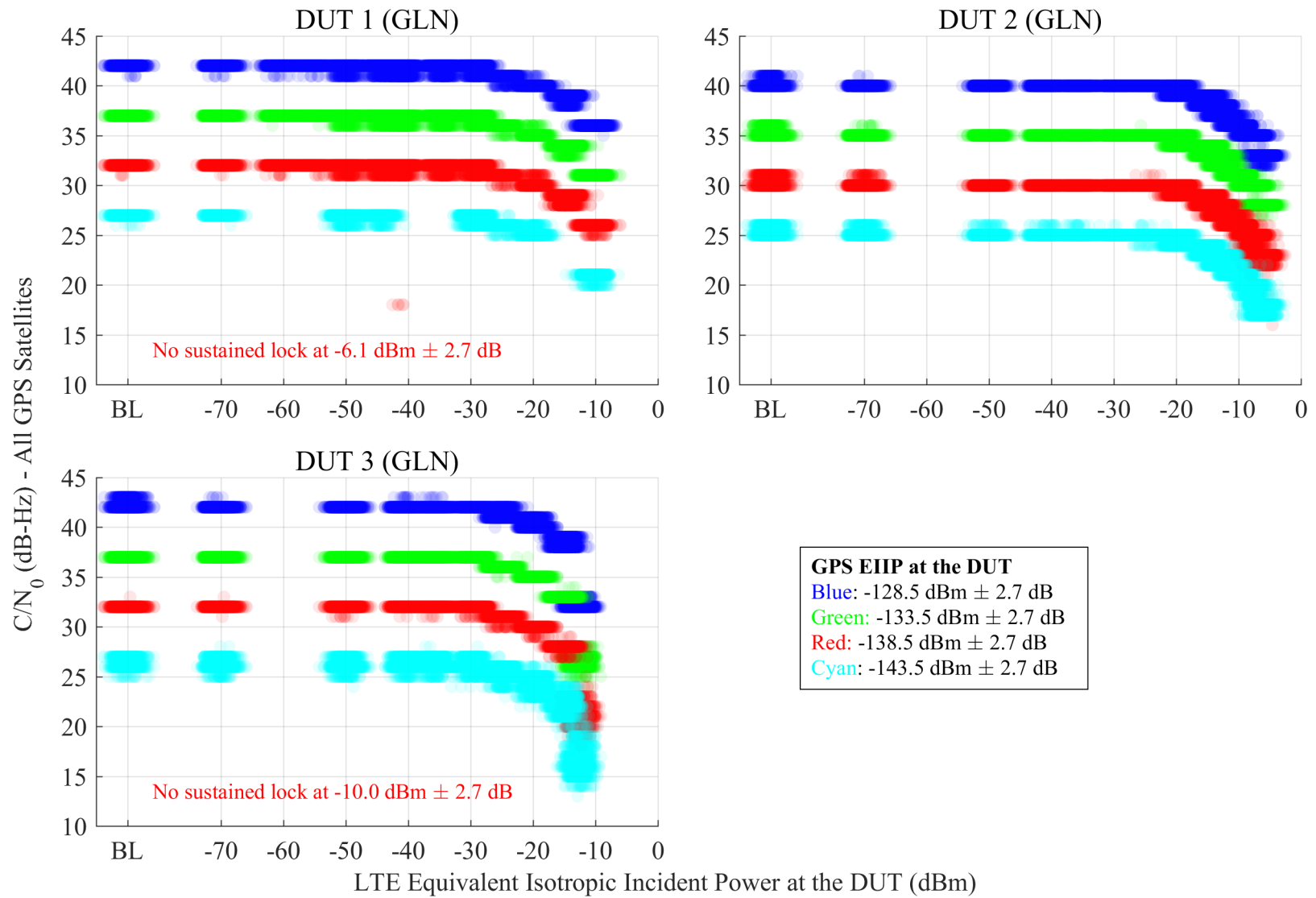


Figure 6.114: Scatterplots of reported  $C/N_0$  from GLN receivers, swept with LTE power level. The GPS scenario is limited, and the type of incident LTE is UL1.

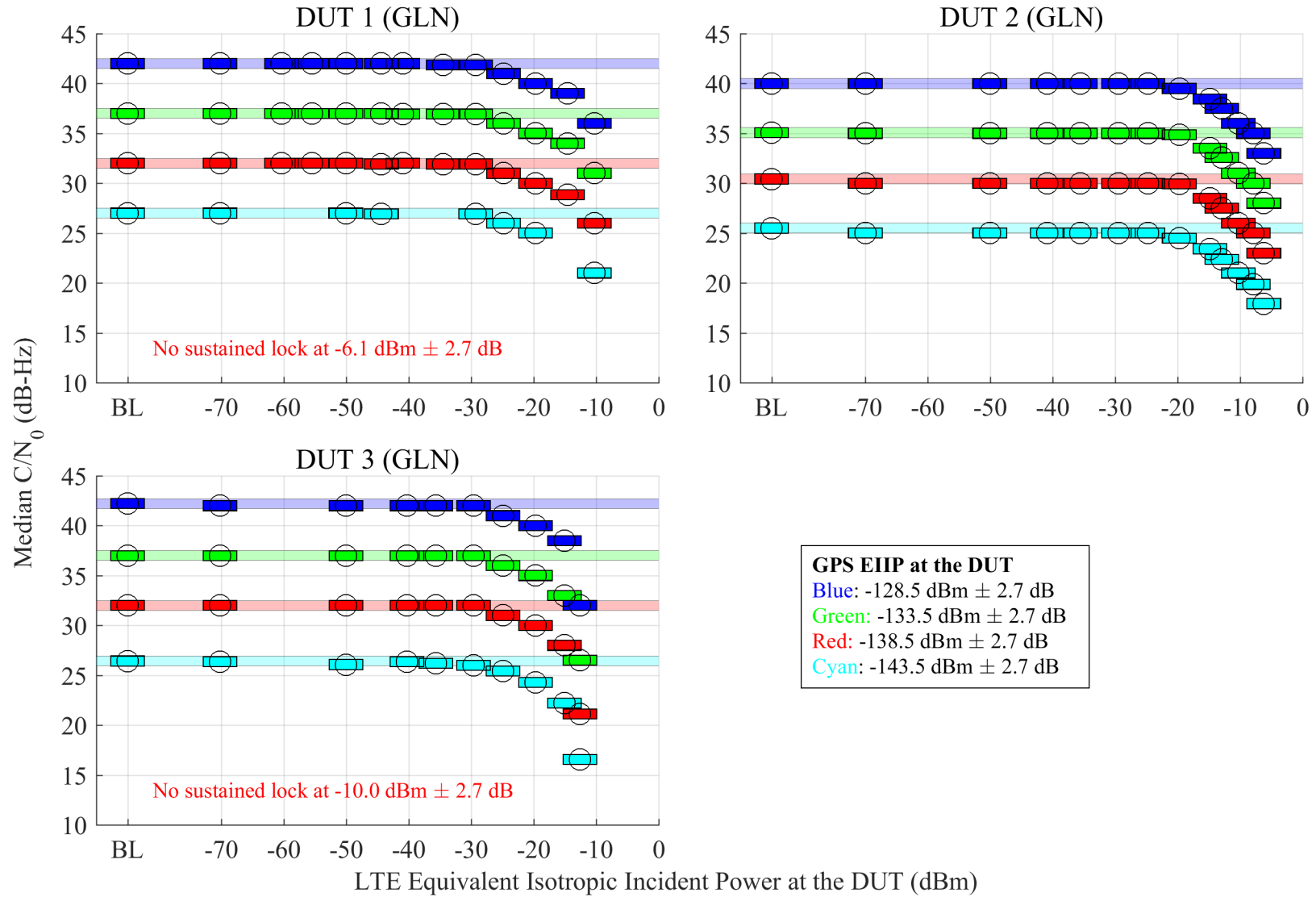


Figure 6.115: Estimated 95% confidence regions of the median of reported  $C/N_0$  from GLN receivers, swept with LTE power level. The GPS scenario is limited, and the type of incident LTE is UL1.

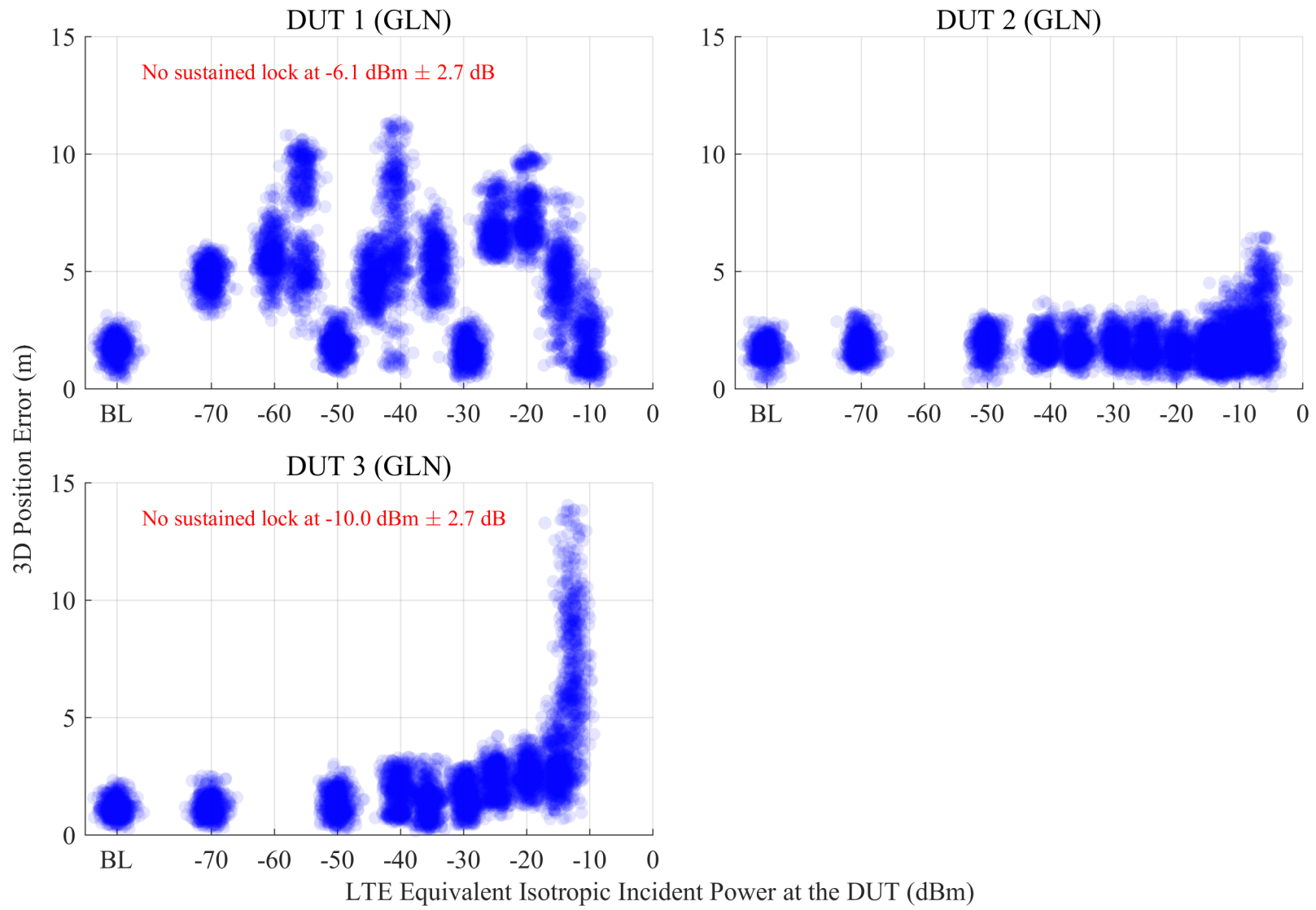


Figure 6.116: Scatterplots of error in reported 3-D position compared to simulator truth from GLN receivers, swept with LTE power level. The GPS scenario is limited, and the type of incident LTE is UL1.

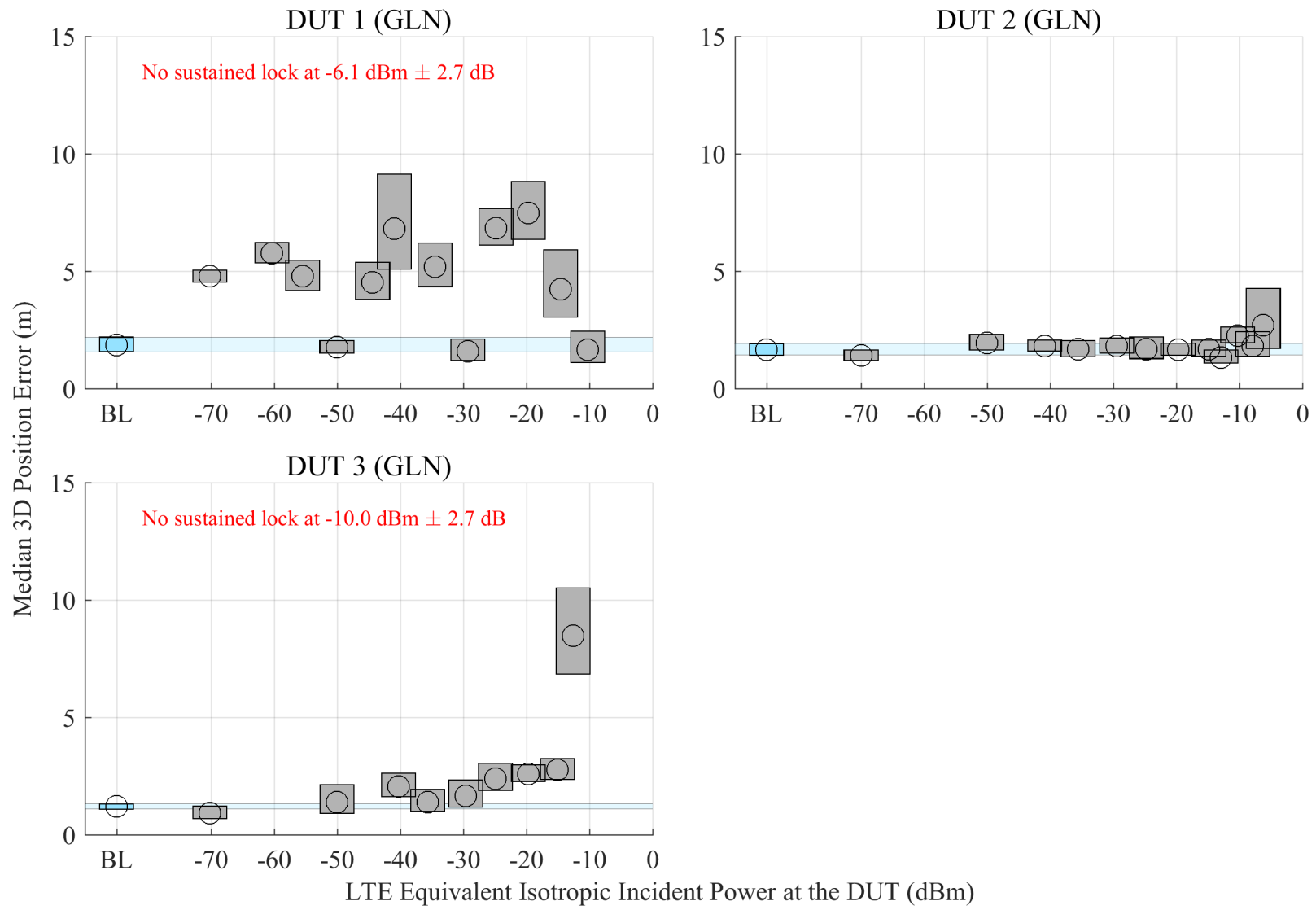


Figure 6.117: Estimated 95% confidence regions of the median error in reported 3-D position from GLN receivers, swept with LTE power level. The GPS scenario is limited, and the type of incident LTE is UL1.

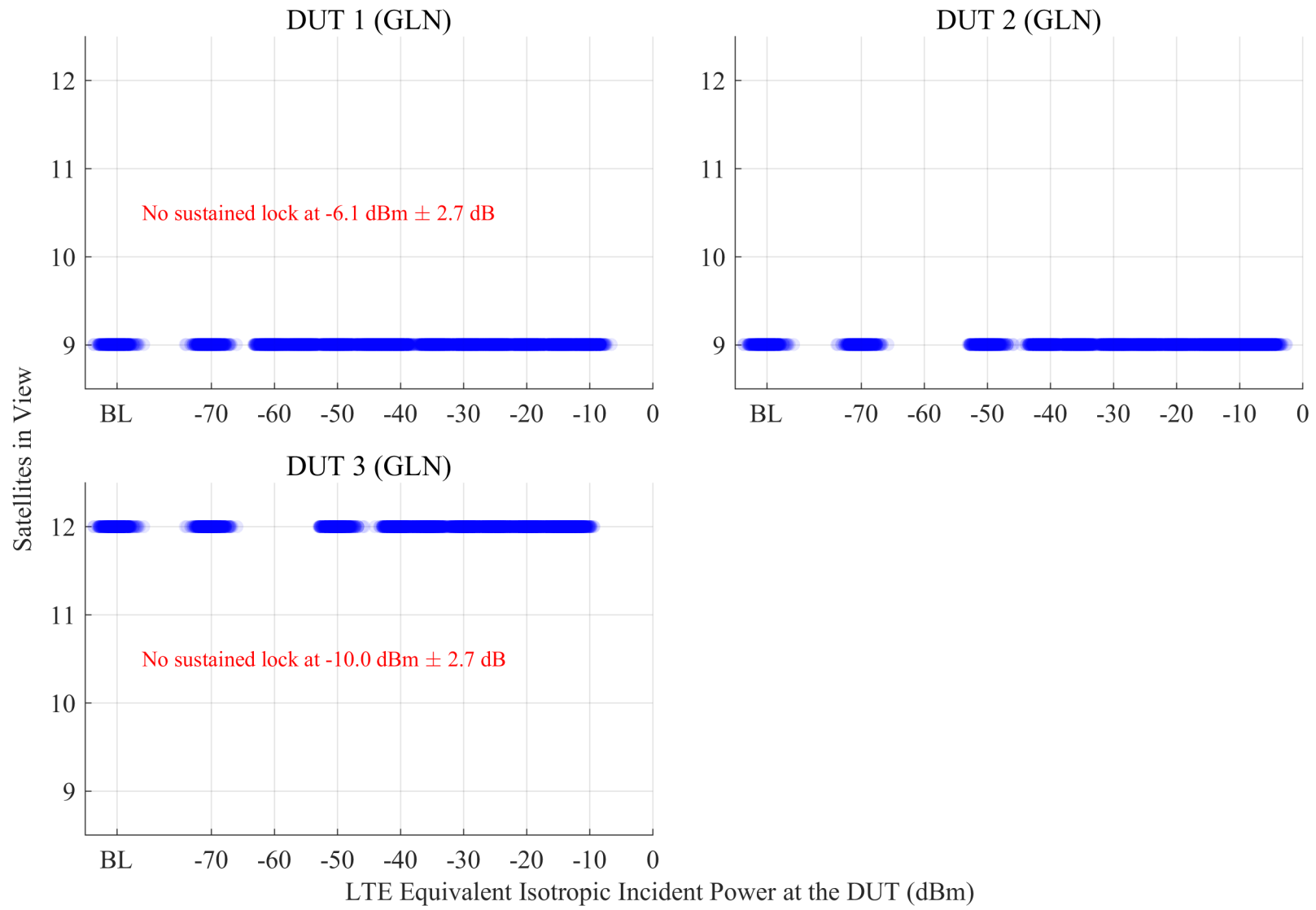


Figure 6.118: Scatterplots of the number of satellites in view from GLN receivers, swept with LTE power level. The GPS scenario is limited, and the type of incident LTE is UL1.

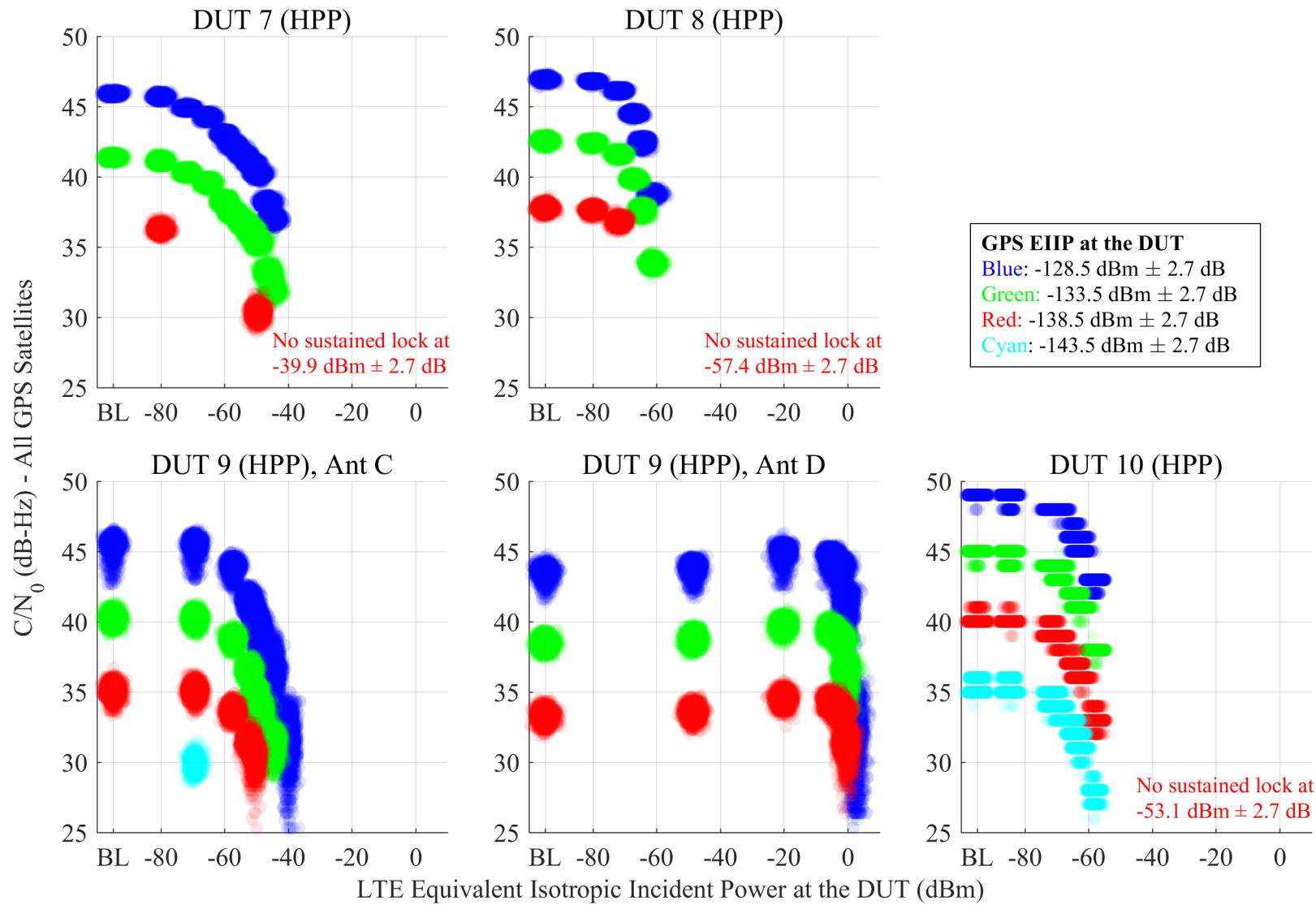


Figure 6.119: Scatterplots of reported  $C/N_0$  from HPP receivers, swept with LTE power level. The GPS scenario is limited, and the type of incident LTE is DL.

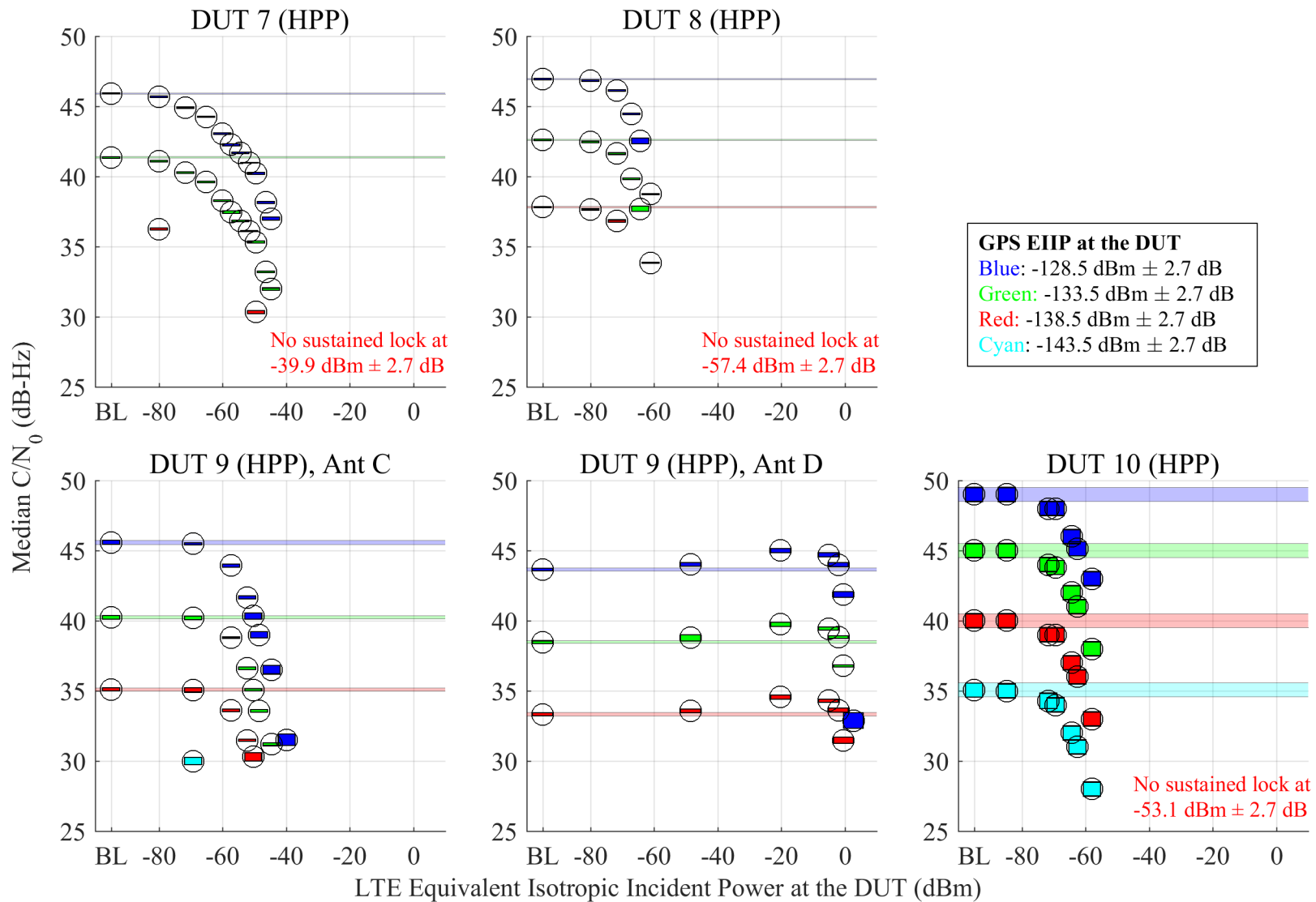


Figure 6.120: Estimated 95% confidence regions of the median of reported  $C/N_0$  from HPP receivers, swept with LTE power level. The GPS scenario is limited, and the type of incident LTE is DL.

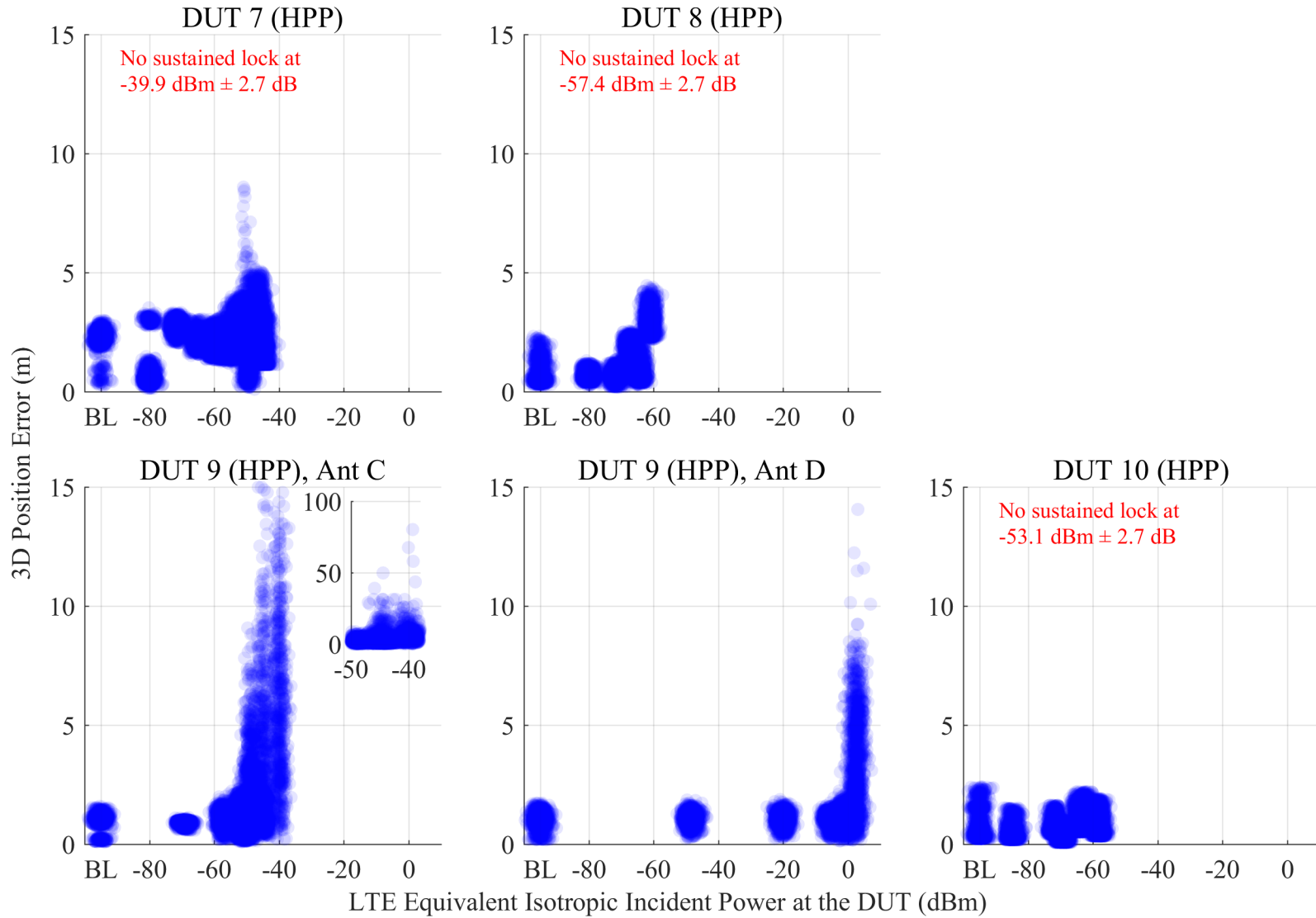


Figure 6.121: Scatterplots of error in reported 3-D position compared to simulator truth from HPP receivers, swept with LTE power level. The GPS scenario is limited, and the type of incident LTE is DL.

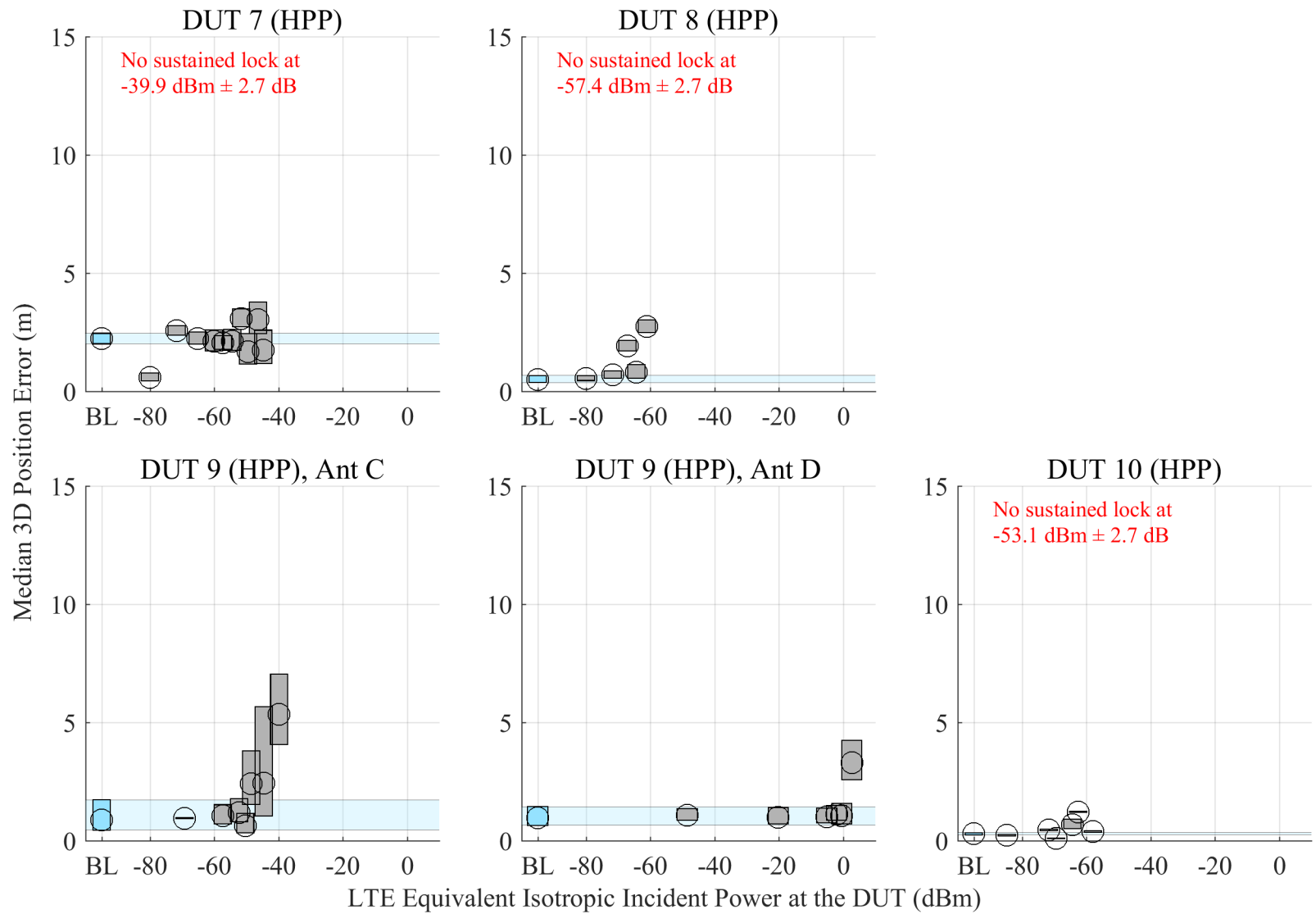


Figure 6.122: Estimated 95% confidence regions of the median error in reported 3-D position from HPP receivers, swept with LTE power level. The GPS scenario is limited, and the type of incident LTE is DL.

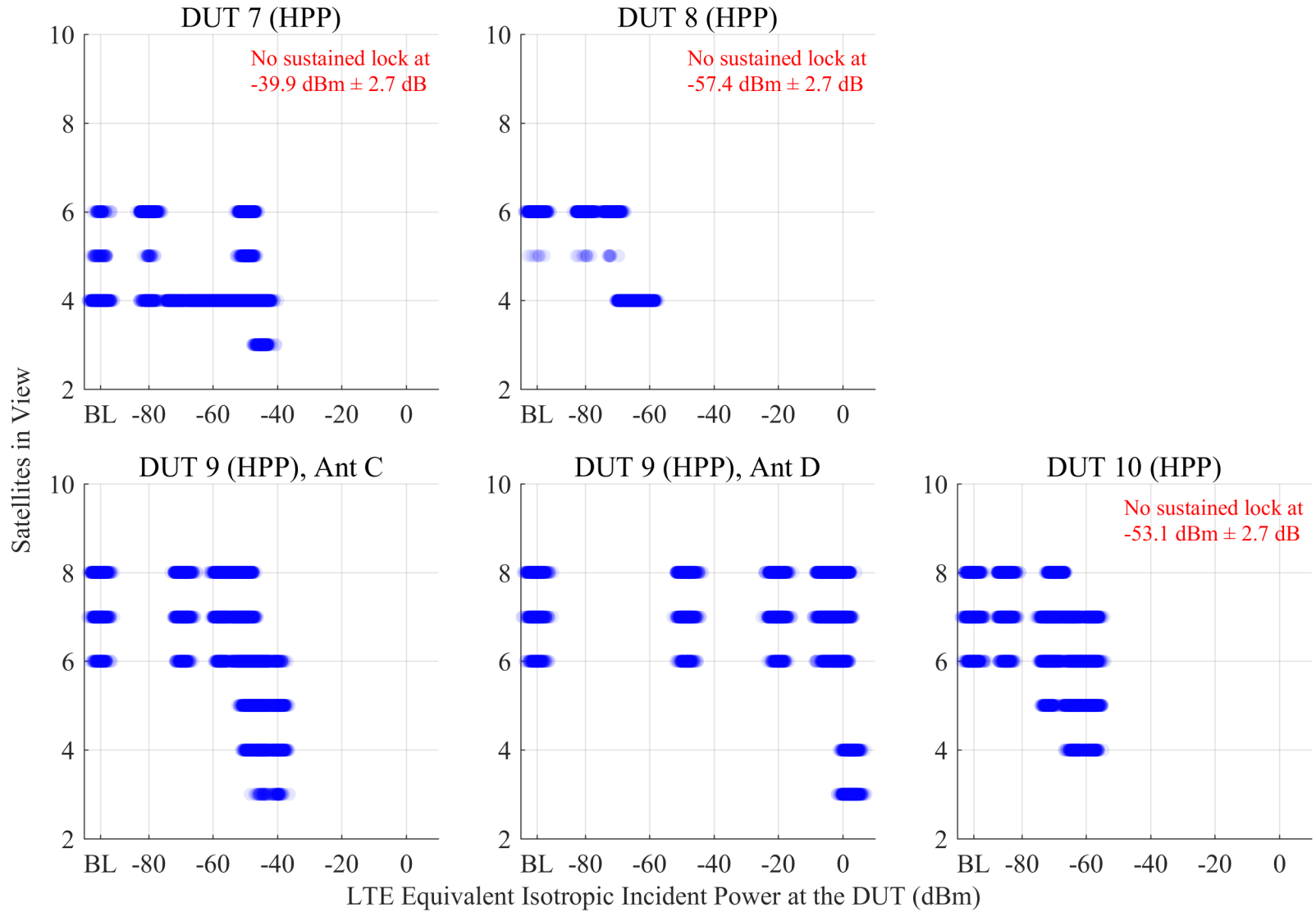


Figure 6.123: Scatterplots of the number of satellites in view from HPP receivers, swept with LTE power level. The GPS scenario is limited, and the type of incident LTE is DL.

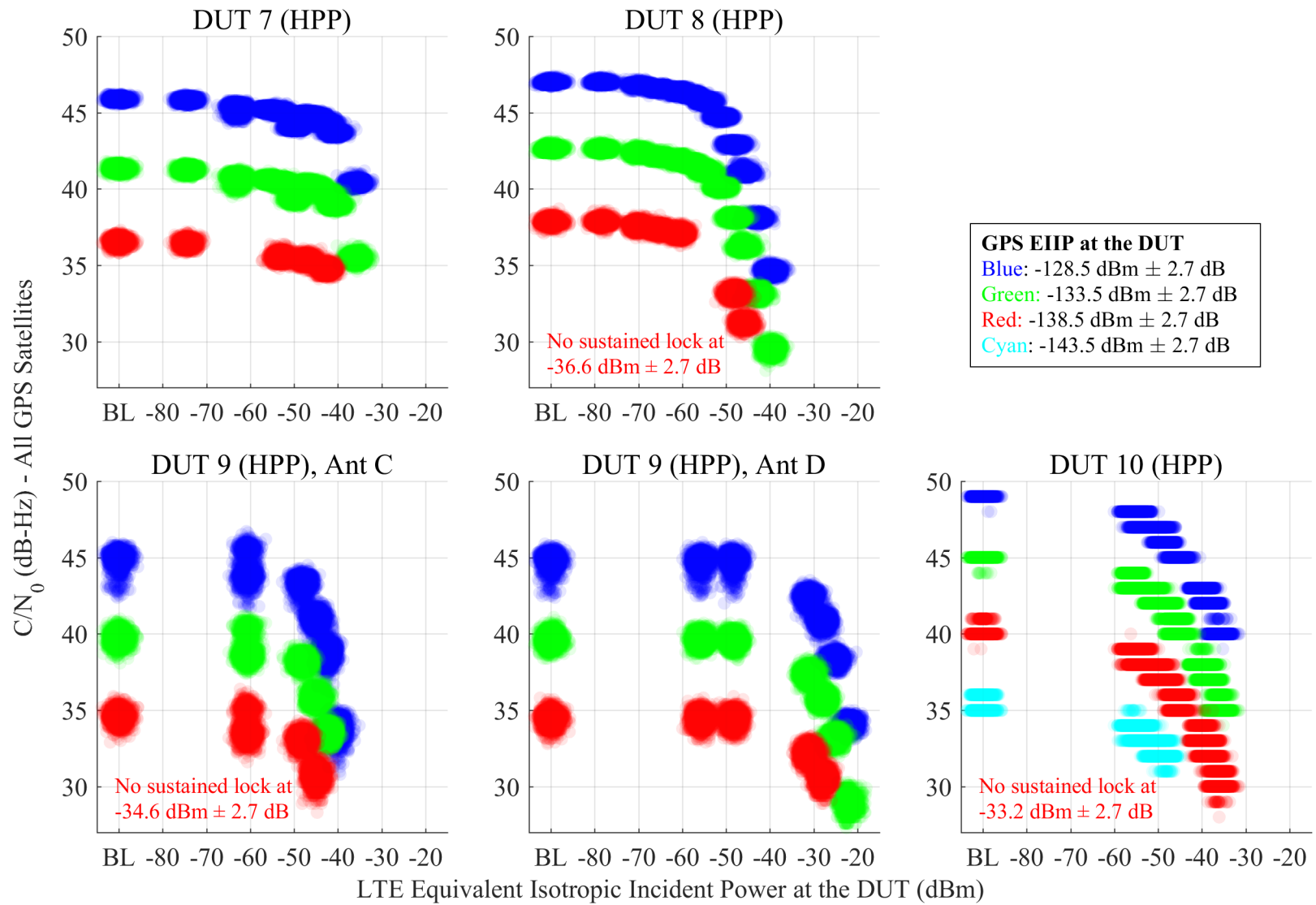


Figure 6.124: Scatterplots of reported  $C/N_0$  from HPP receivers, swept with LTE power level. The GPS scenario is limited, and the type of incident LTE is UL1.

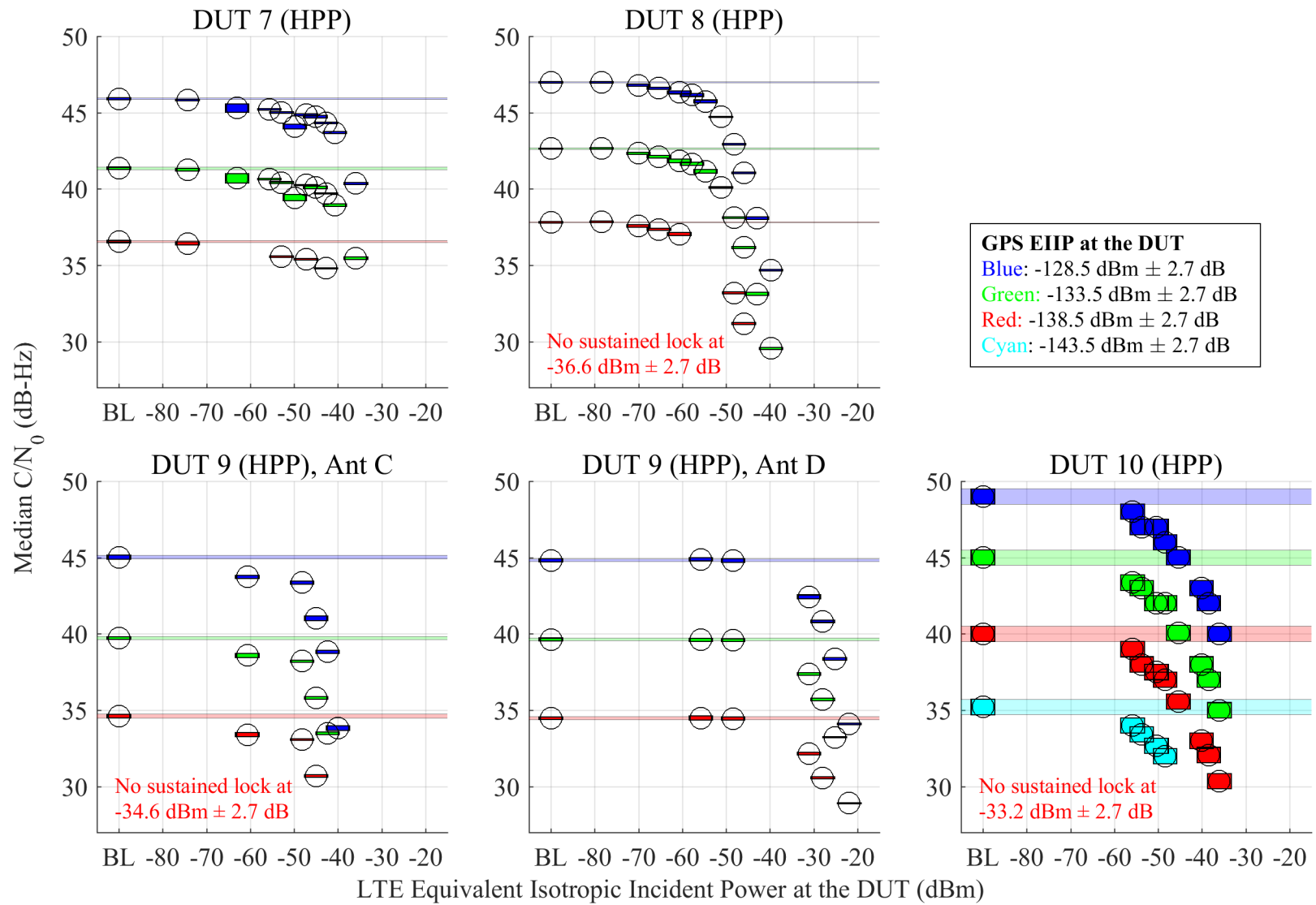


Figure 6.125: Estimated 95% confidence regions of the median of reported  $C/N_0$  from HPP receivers, swept with LTE power level. The GPS scenario is limited, and the type of incident LTE is UL1.

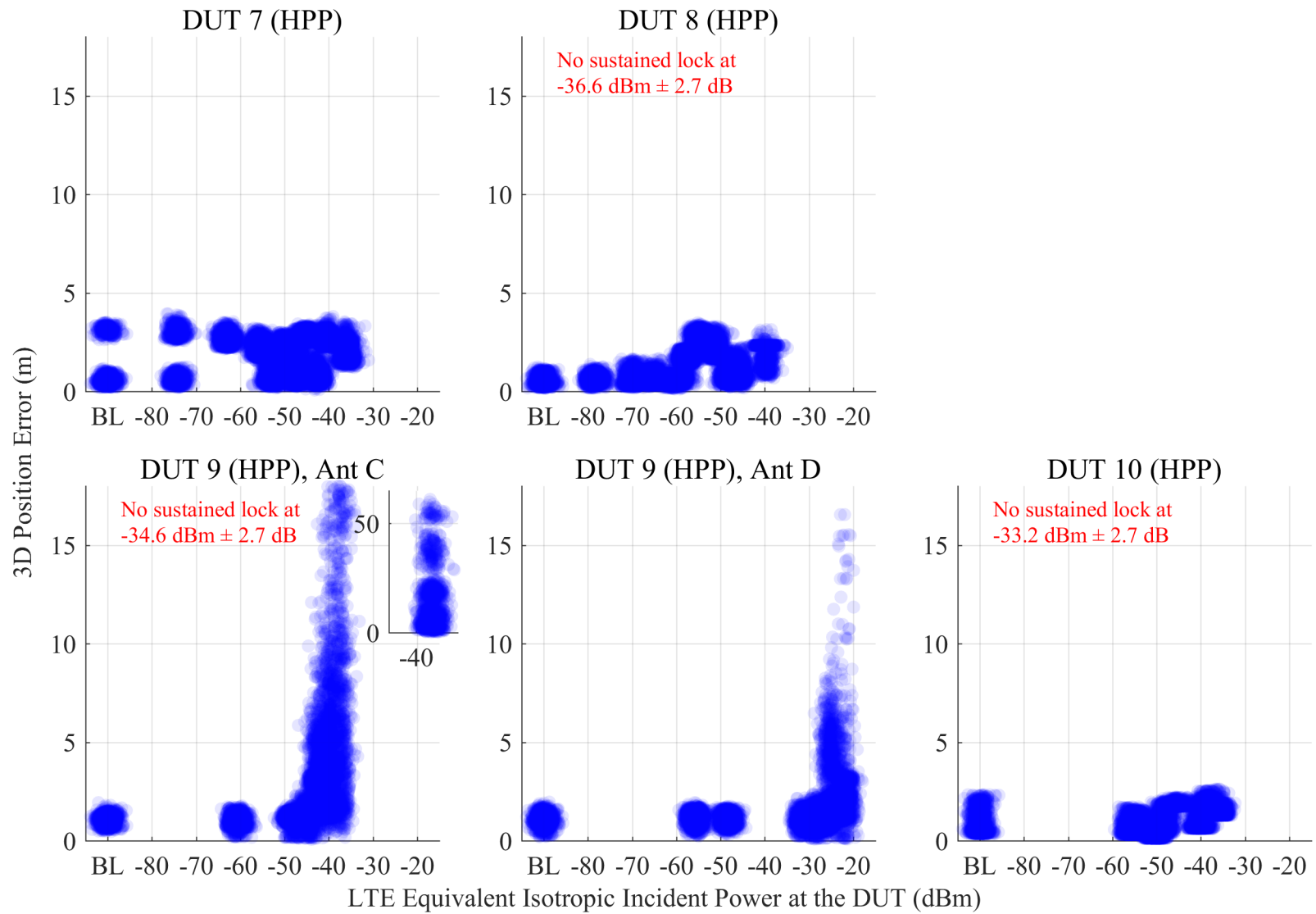


Figure 6.126: Scatterplots of error in reported 3-D position compared to simulator truth from HPP receivers, swept with LTE power level. The GPS scenario is limited, and the type of incident LTE is UL1.

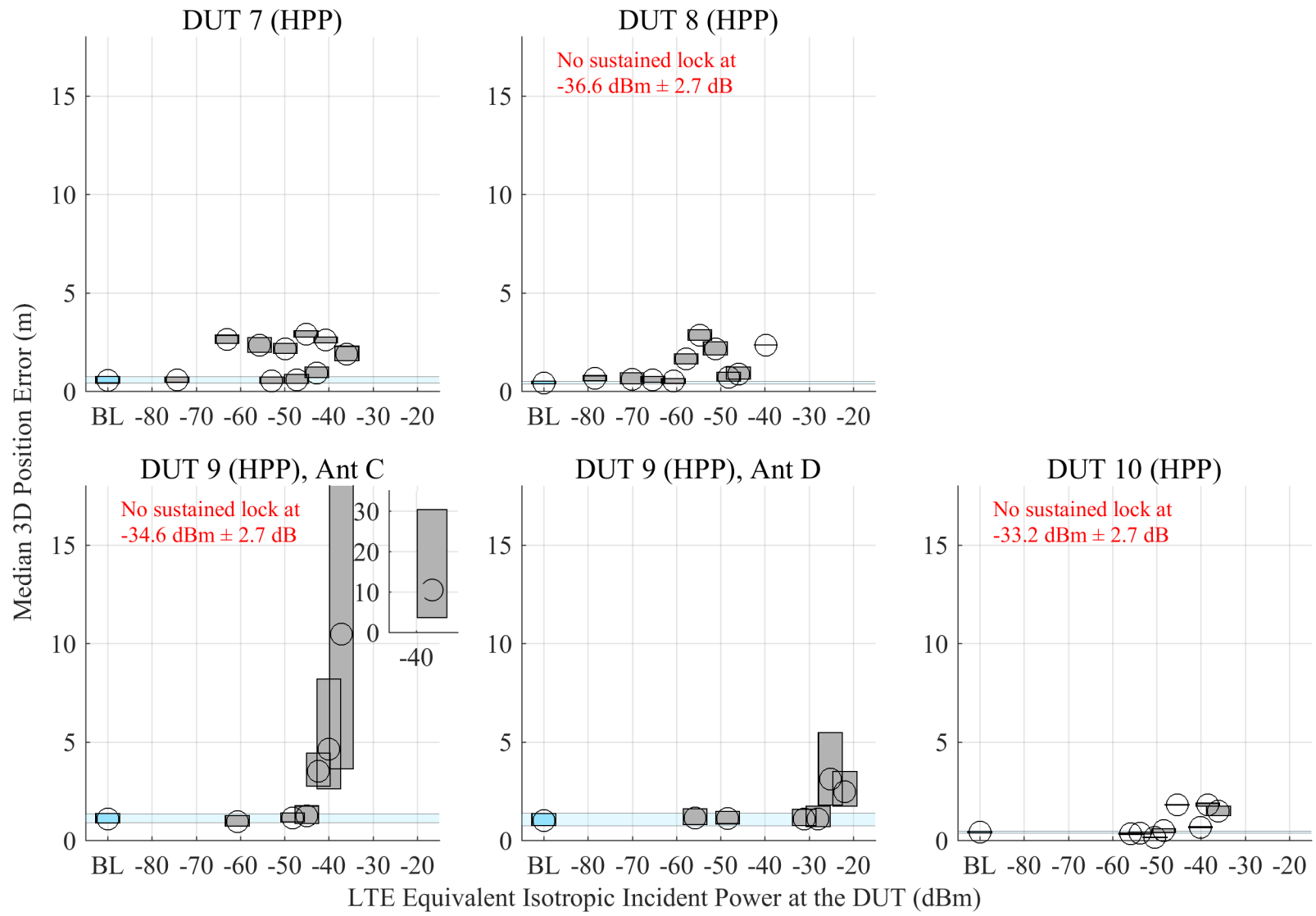


Figure 6.127: Estimated 95% confidence regions of the median error in reported 3-D position from HPP receivers, swept with LTE power level. The GPS scenario is limited, and the type of incident LTE is UL1.

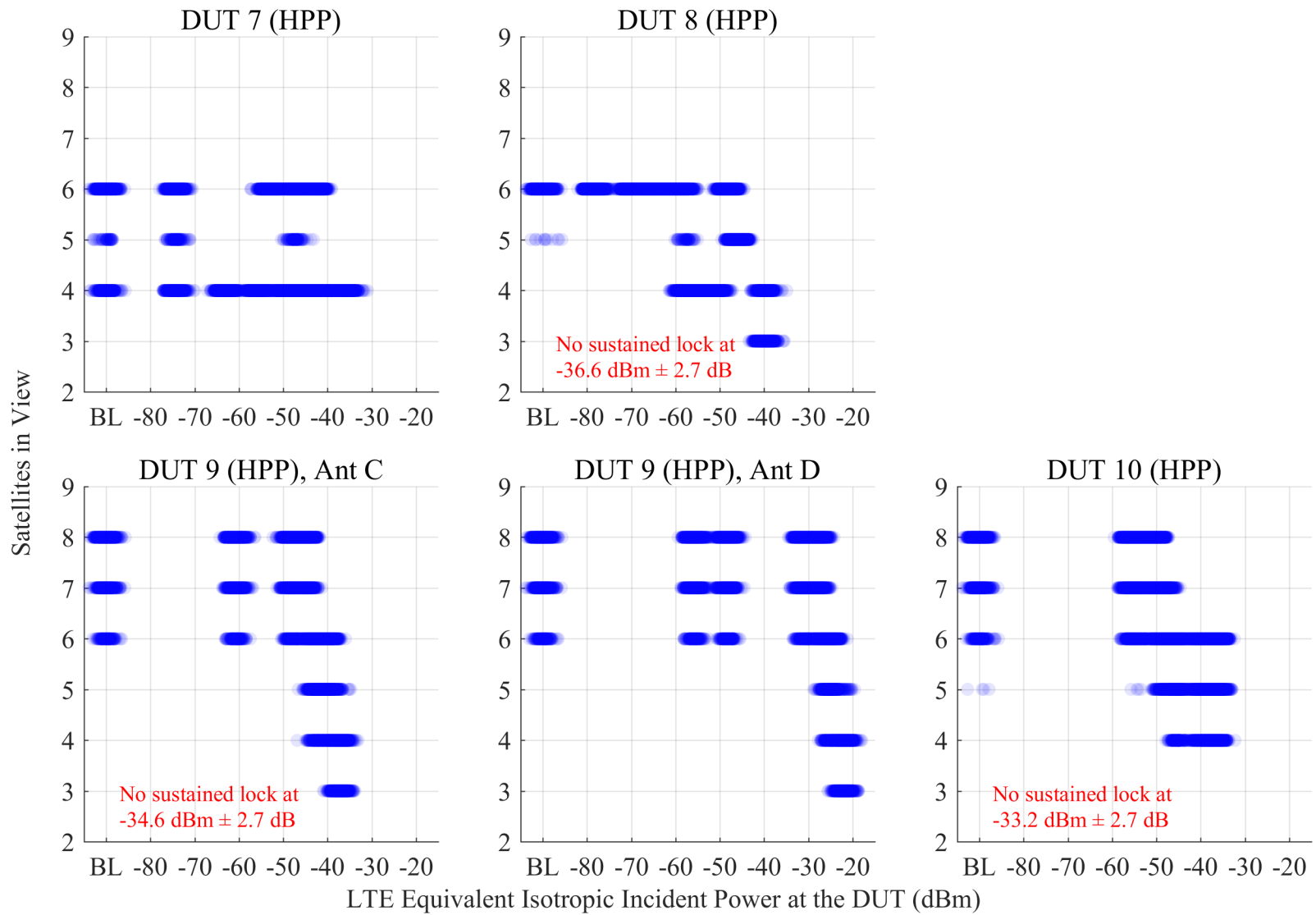


Figure 6.128: Scatterplots of the number of satellites in view from HPP receivers, swept with LTE power level. The GPS scenario is limited, and the type of incident LTE is UL1.

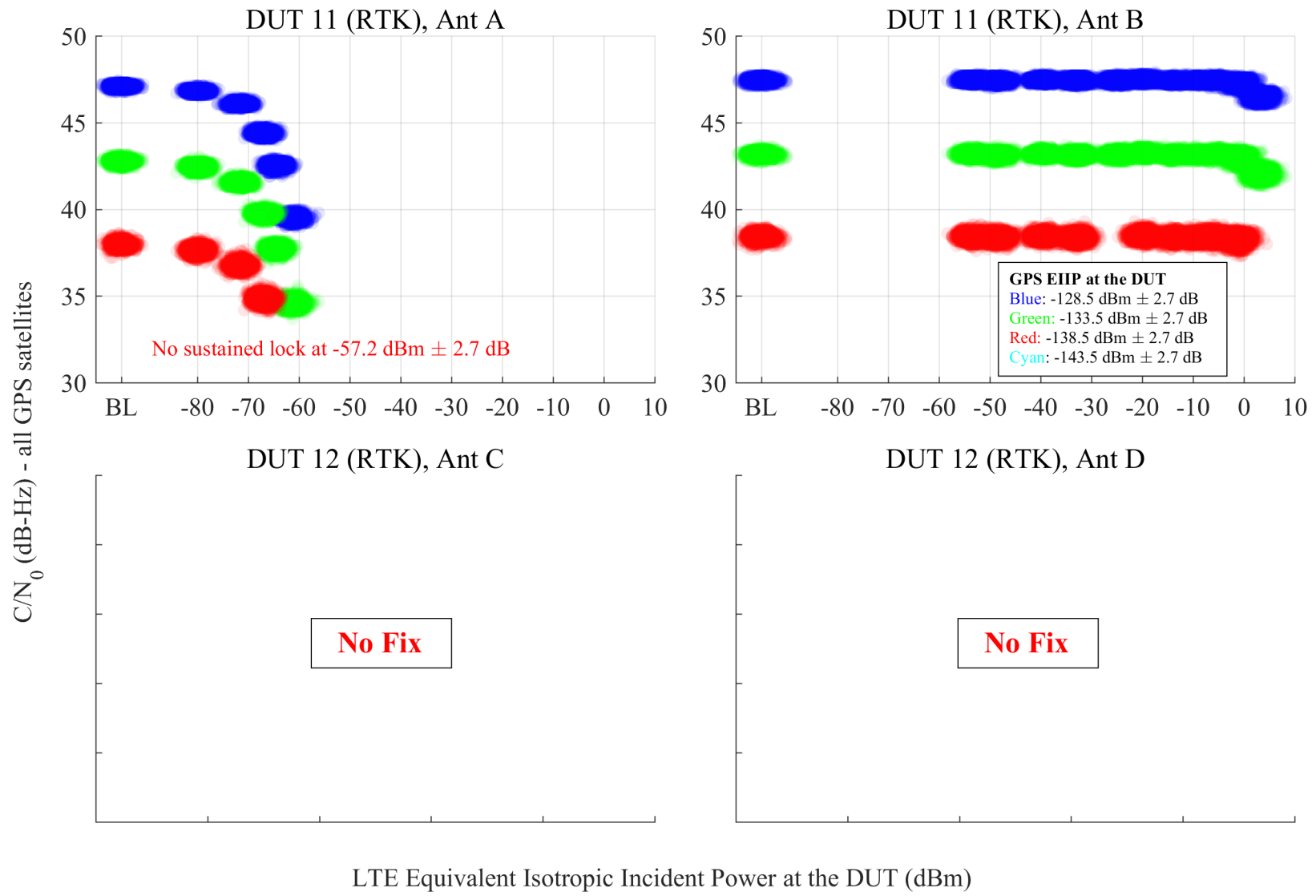


Figure 6.129: Scatterplots of reported  $C/N_0$  from RTK receivers, swept with LTE power level. The GPS scenario is limited, and the type of incident LTE is DL.

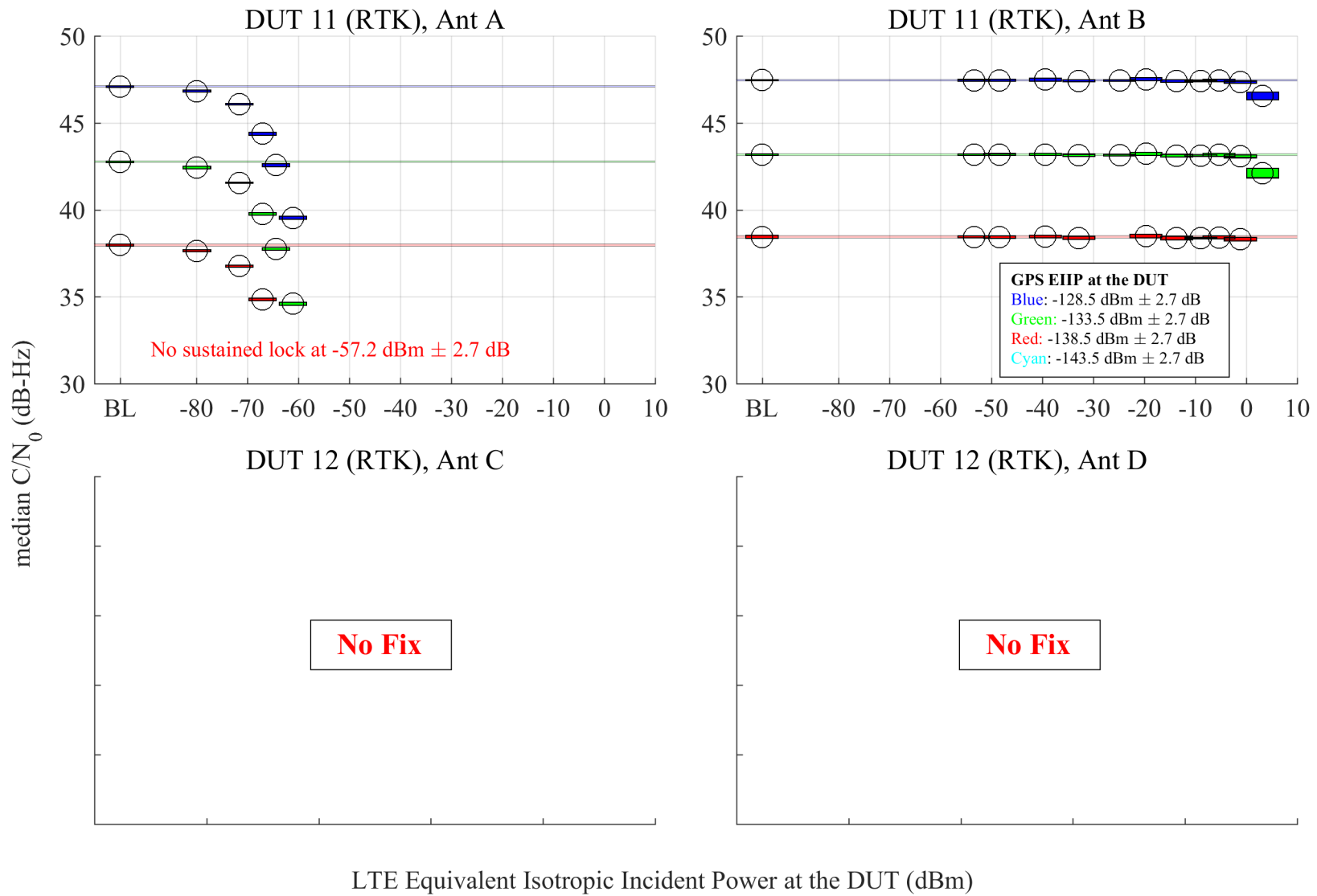


Figure 6.130: Estimated 95% confidence regions of the median of reported  $C/N_0$  from RTK receivers, swept with LTE power level. The GPS scenario is limited, and the type of incident LTE is DL.

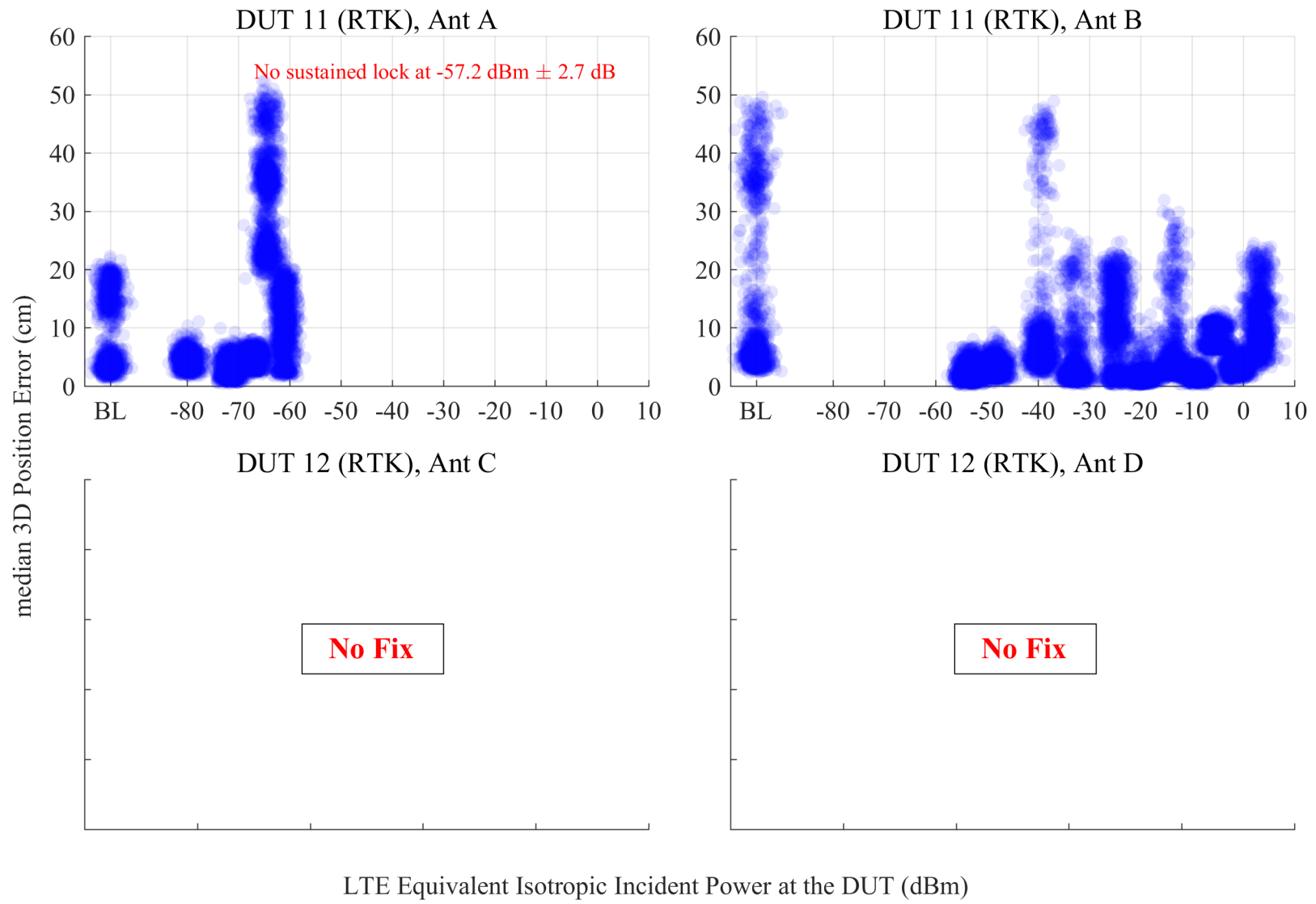


Figure 6.131: Scatterplots of error in reported 3-D position compared to simulator truth from RTK receivers, swept with LTE power level. The GPS scenario is limited, and the type of incident LTE is DL.

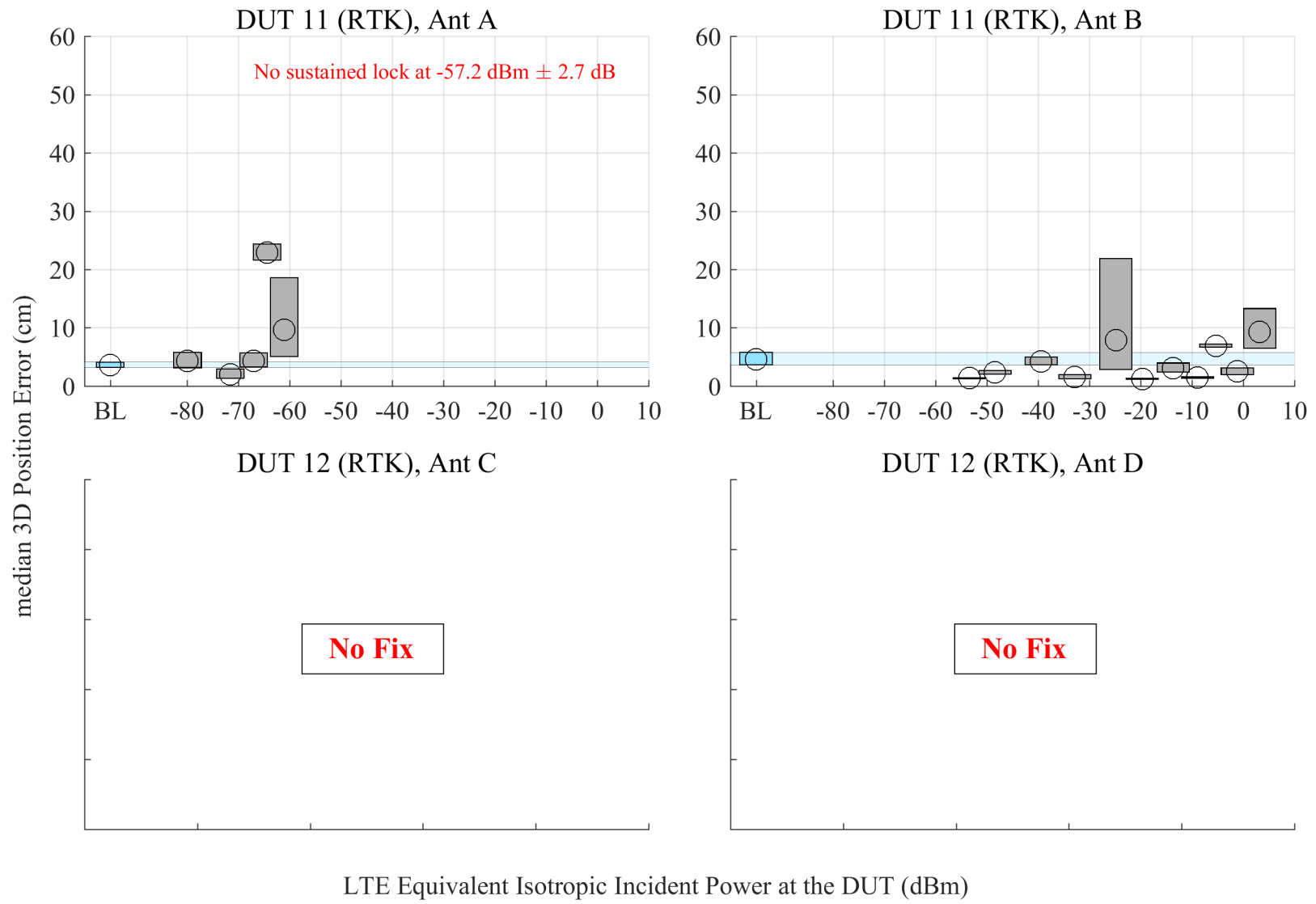


Figure 6.132: Estimated 95% confidence regions of the median error in reported 3-D position from RTK receivers, swept with LTE power level. The GPS scenario is limited, and the type of incident LTE is DL.

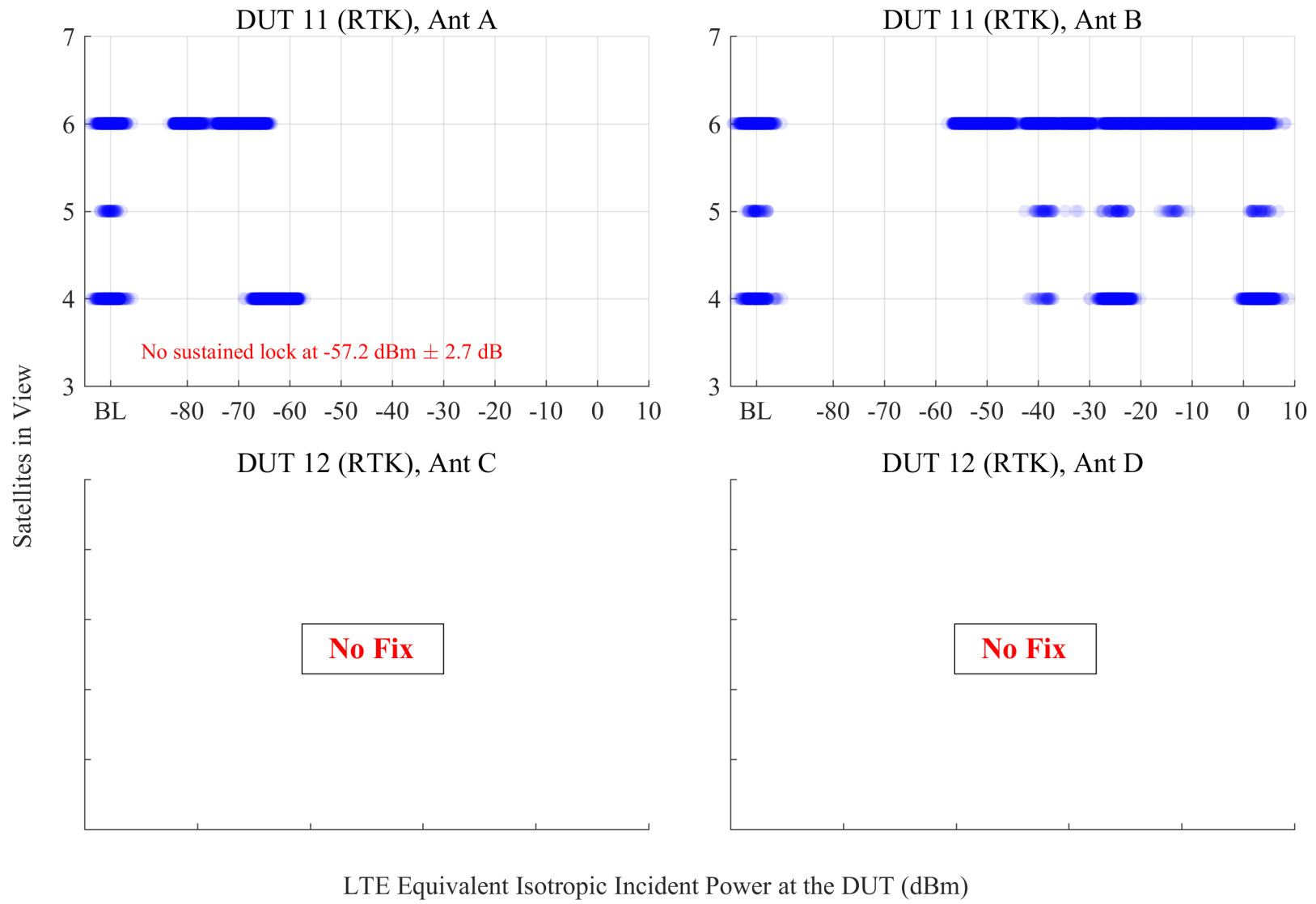


Figure 6.133: Scatterplots of the number of satellites in view from RTK receivers, swept with LTE power level. The GPS scenario is limited, and the type of incident LTE is DL.

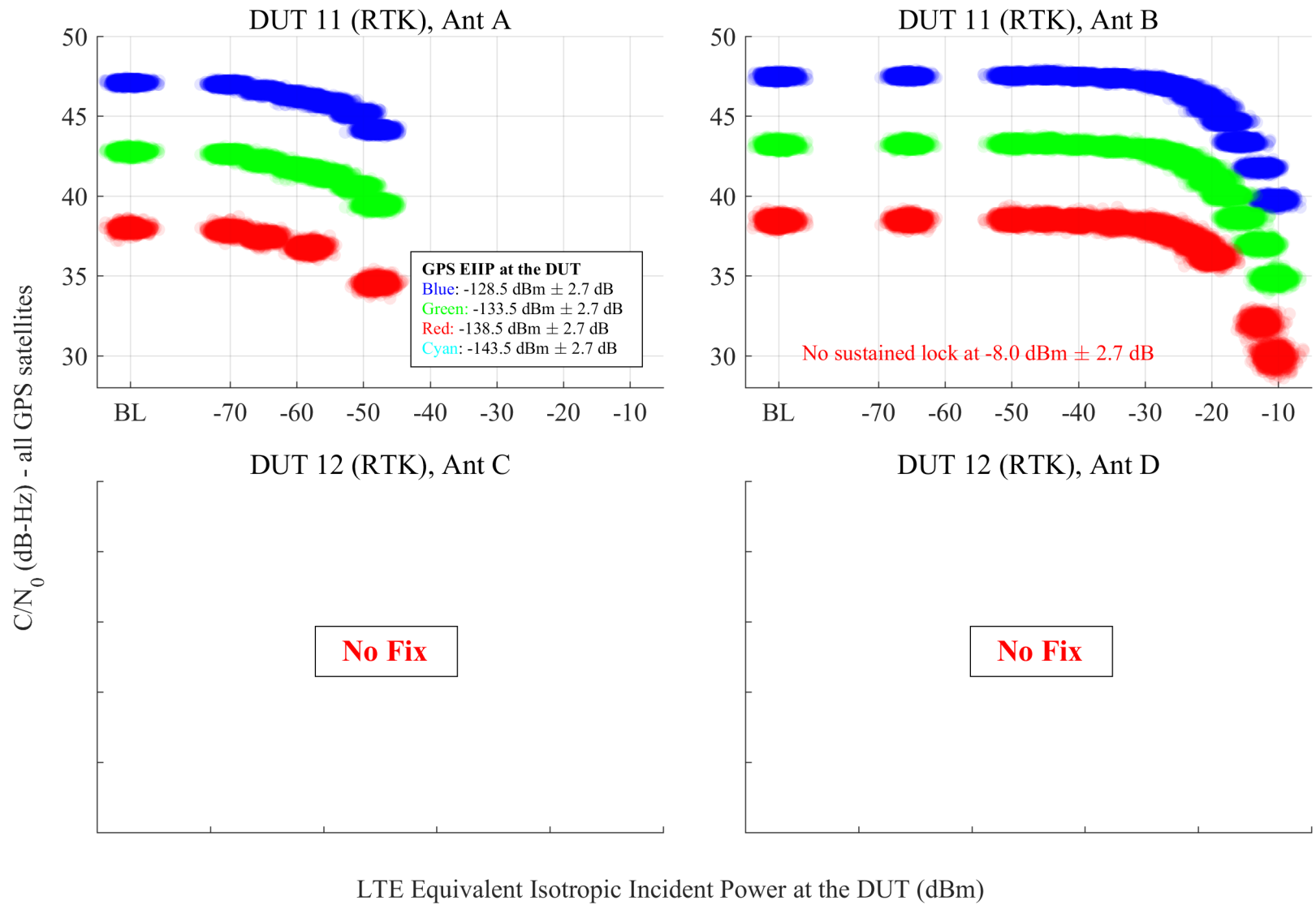


Figure 6.134: Scatterplots of reported  $C/N_0$  from RTK receivers, swept with LTE power level. The GPS scenario is limited, and the type of incident LTE is UL1.

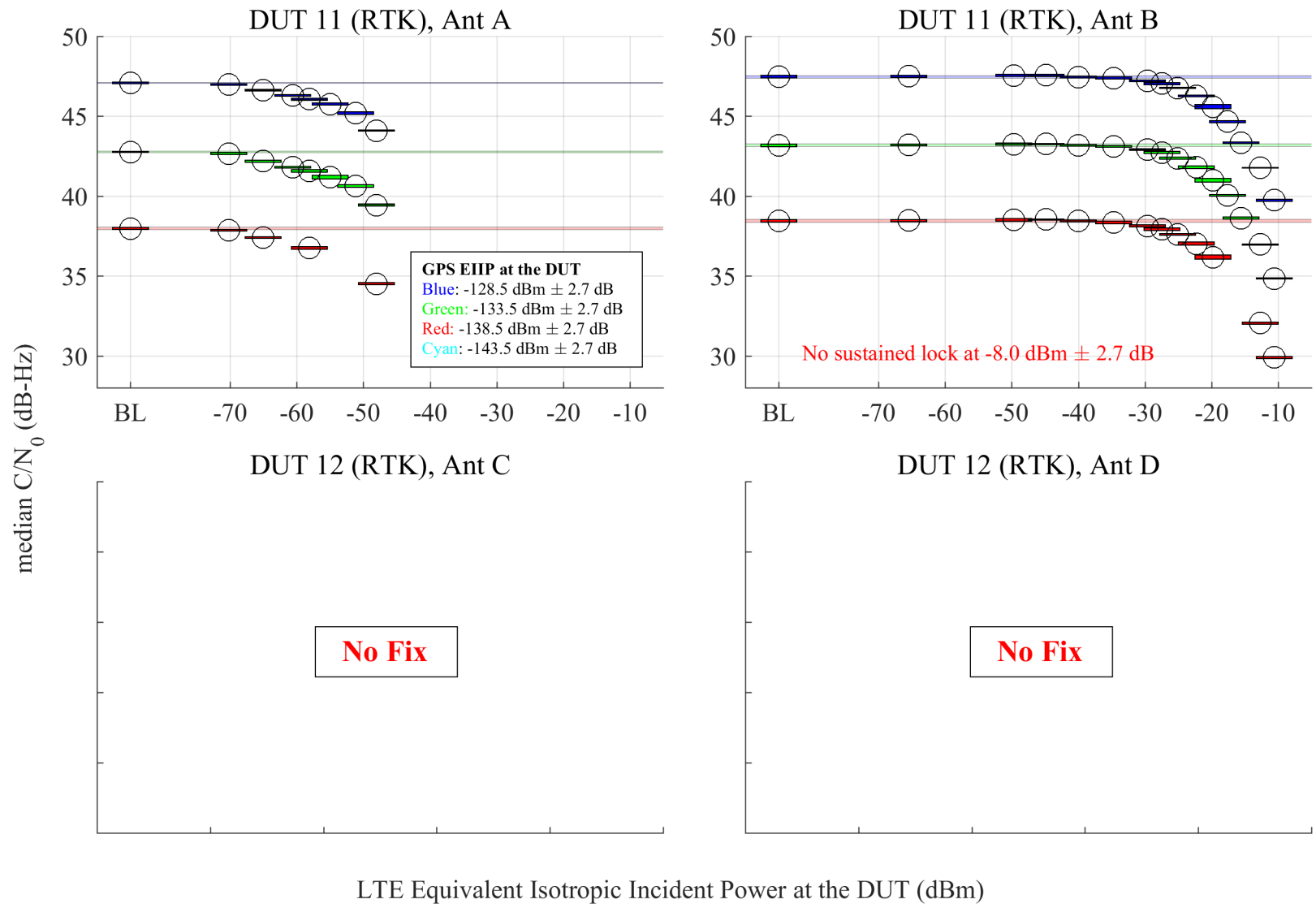


Figure 6.135: Estimated 95% confidence regions of the median of reported  $C/N_0$  from RTK receivers, swept with LTE power level. The GPS scenario is limited, and the type of incident LTE is UL1.

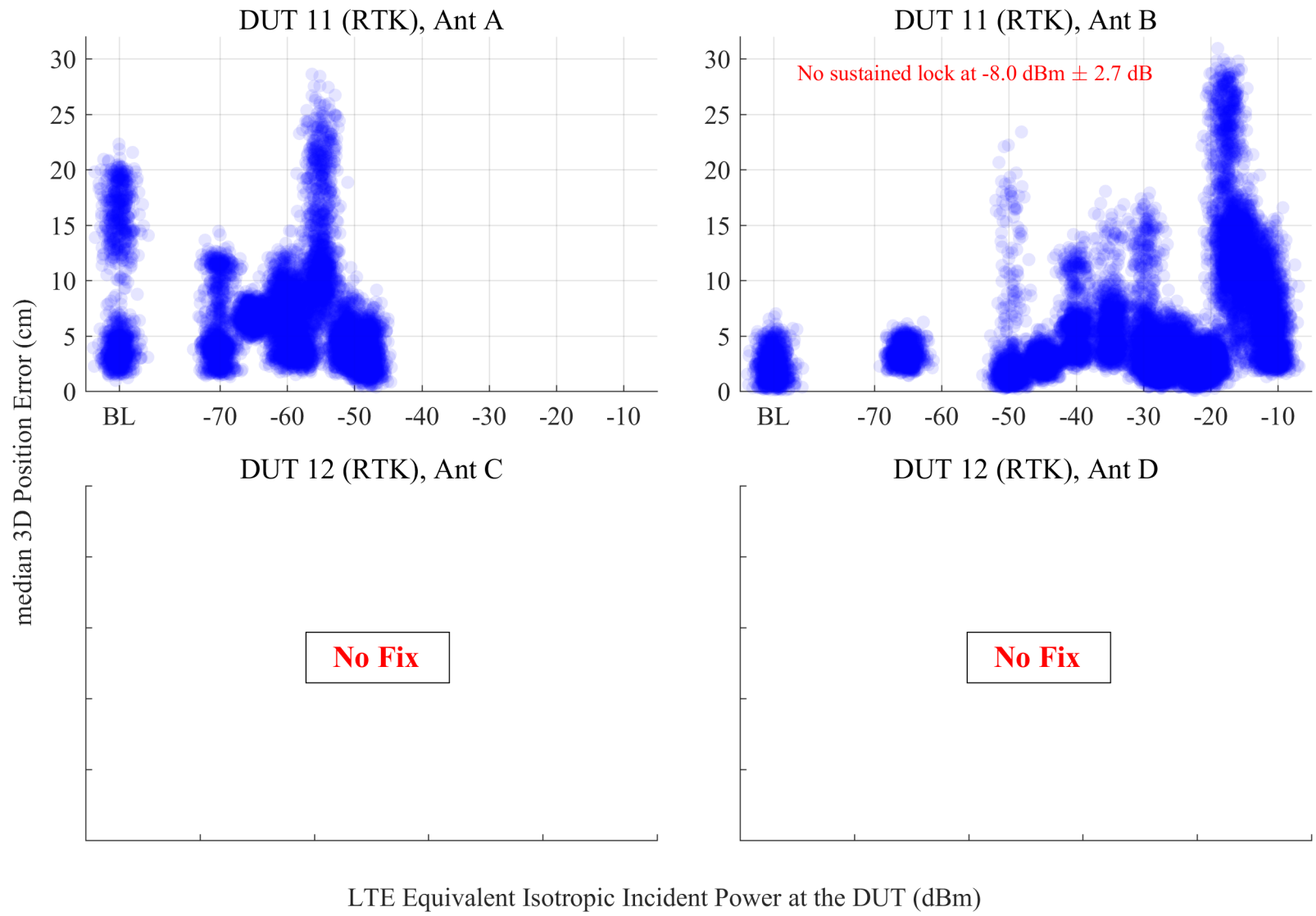


Figure 6.136: Scatterplots of error in reported 3-D position compared to simulator truth from RTK receivers, swept with LTE power level. The GPS scenario is limited, and the type of incident LTE is UL1.

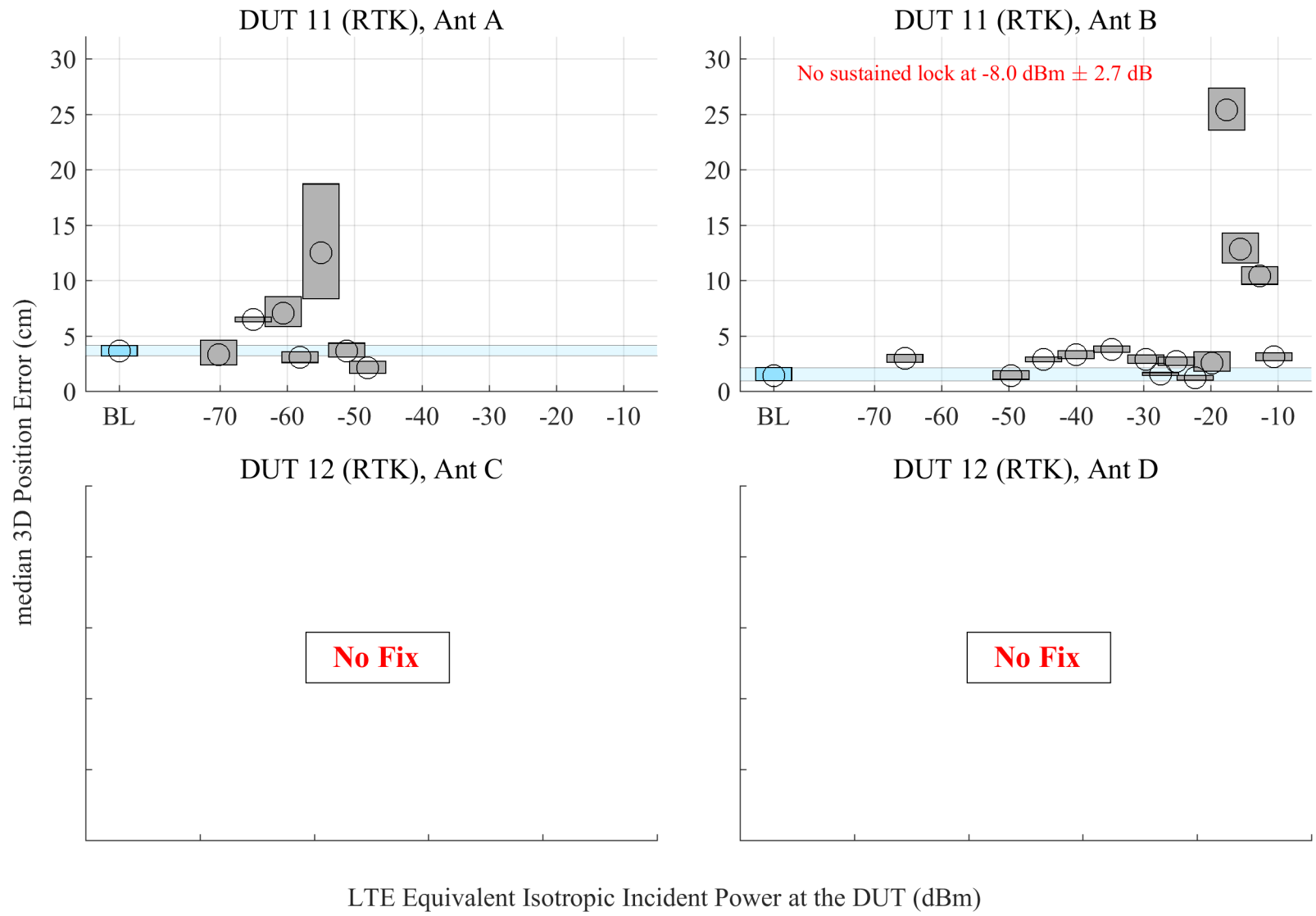


Figure 6.137: Estimated 95% confidence regions of the median error in reported 3-D position from RTK receivers, swept with LTE power level. The GPS scenario is limited, and the type of incident LTE is UL1.

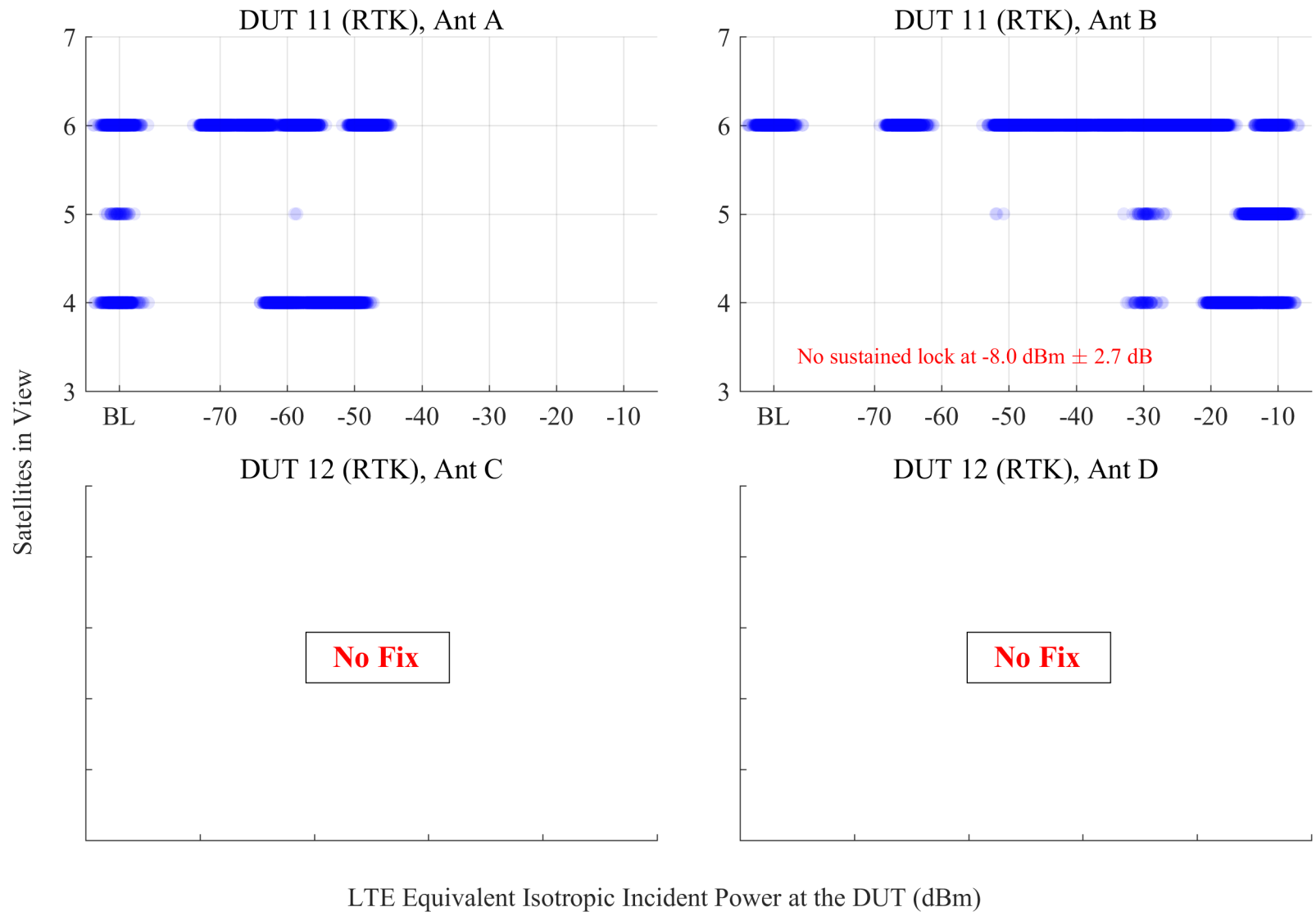


Figure 6.138: Scatterplots of the number of satellites in view from RTK receivers, swept with LTE power level. The GPS scenario is limited, and the type of incident LTE is UL1.



## 7 Conclusions

The two primary goals of this report were to document a test methodology that allows the measurement on the impact to global positioning system (GPS) receivers from adjacent band long-term evolution (LTE) waveforms and to provide data from a set of GPS receivers subject to the test methodology. Data was presented without defining or use of pass/fail criteria as the establishment of those criteria was not part of this project.

The various chapters in the report contained details on specific aspects of the test method, test setup, calibration, uncertainty analysis, testbed automation, and data handling that, accompanied with the data plots, illustrate the important features of the test method and the quality of the resulting data. In addition, in the process of developing and executing the test methodology, several important insights were observed.

First, well integrated automation in testing and data acquisition was imperative to not only reduce human errors but also to optimize testing and provide reproducible data. To this end, maintaining persistent test states through reiterative measurements was achieved by:

- controlling a known, repeatable and appropriate radio frequency (RF) signaling chain,
- synchronizing test equipment and conditions with the data collection from the device,
- defining incident LTE and GPS signal strength explicitly in terms of equivalent isotropic incident power at the plane of the device under test (DUT),
- transmitting the LTE power and the GPS signal via the same antenna to eliminate ambiguity,
- initializing devices to a known state prior to sweeps which in some cases was a “cold start” or a “warm start,”
- presenting the same satellite constellation to the devices for each test cycle,
- fixturing of source antenna and DUT antenna, and
- processing and reviewing the data during the measurement campaign to verify proper operation.

This led to well controlled and sustained testing with multiple tests in this project exceeding 30 hours without the need of human interaction, all while providing DUT response data that was tightly correlated relative to LTE waveforms. The automation made it possible to perform 100 time to first reacquisition (TTFR) and time to first fix (TTFF) tests on DUTs in a practical manner.

Second, many factors needed to be considered in the calibration of the RF signaling chain. In

a measurement effort such as this one, uncertainty in the RF conditions presented to the DUT influence the conclusions one can draw with respect to the quantified impact. The calibration process and uncertainty analysis were critical to establishing the bounds of both the test conditions and reported DUT responses.

Third, the DUT data reporting capabilities had a significant impact on the required test time and the uncertainties associated with the data sets used in the final analysis stage. In order to interpret the data correctly, multiple processing steps were typically necessary, which often required knowledge of manufacturer specific reporting formats and features. In addition, GPS devices were found to be not always standardized even within a manufacturer's own set of devices, which impacted the ability to run the same test protocol across all GPS platforms within a class.

Fourth, out-of-band emissions (OOBEs) were important when trying to quantify the impacts of adjacent band activity to a weak signal, in this case, the adjacent band LTE impacts on the received GPS signal. The interaction with the DUT may occur outside of the fundamental bands of operation for either the DUT or the transmitted signal.

Fifth, the device settling time and strong time-correlations between data samples had to be considered in both the test processes and the data analysis. For testing, this implied that test times needed to be sufficiently long so that GPS receivers were able to time adapt to test conditions. Furthermore, enough time series data needed to be collected to facilitate statistically meaningful data analysis. This implies that efforts must be made to assess warm-up time and to choose analysis methods that account for strong data correlations.

## 7.1 Future Considerations

As with any project of this complexity, we learned valuable lessons and discovered new areas of technical opportunity.

The initial screening and test plan development focused on the test methodology and the data analysis to answer the main question of LTE impacts on GPS. However, the data requirements (including storage, data parsing, data cleaning, file management, and dissemination) should be addressed as early as possible, and developed and considered at a similar level of importance in future proposal screening and testing efforts.

Future tests will also need to continue to ensure buy-in from the manufacturers of DUTs to support access to any required automated data streaming or device state control.

## A Radiated Signal Levels: Test and Application to Practical Scenarios

A recurring question in the area of RF interference-effects measurements is whether such measurements can be better performed via radiation in propagation scenarios designed to be “realistic” versus measurands that seek to isolate and minimize uncontrolled propagation effects. This problem is examined and supports extrapolating measurements to real-world deployments.

The goal of RF interference-effects measurements on victim receivers is helpful to understand the circumstances under which interference between two or more radio systems will occur in real-world environments and conditional scenarios. Measurements typically do not completely answer this question, but measurements can (and do) provide definitive data points which can be integrated into models, simulations, and analysis for validation or prediction.

### A.1 Definition of Power Incident Upon DUTs

Meaningful and repeatable tests of DUT response require clearly defined parameters that quantify the RF test conditions applied to each DUT.

The fundamental physical parameter that applies to the GPS and LTE radiation incident upon a DUT is the incident (electric or magnetic) field strength (or closely related plane wave power density). This is the convention in electromagnetic compatibility (EMC) [27, 28][29, p. 467] and historical work in communications [30–34]. It has also applied in previous publications by some authors of this work [35–37]. Fields are the basic quantity in Maxwell’s equations, the basis of the classical electromagnetism underpinning antenna and propagation theory, RF and microwave circuits, and commercial electromagnetic simulation tools. Field strength is also a fundamentally measurable measurement quantity supported by metrology instruments and test standards. Therefore, calibrated measurements of RF radiation levels should to be closely related with (and traceable to) field strength.

Modern communications standards increasingly use an unnamed alternative to incident field strength: the *equivalent* power that would be received by an impedance-matched receive antenna with 0 dBi gain. The emphasis on “equivalent” here underscores that this is not a description of power that is actually *received* by the DUT; it is only a description of the incident field strength as it would be observed with an idealized isotropic antenna receive antenna. This type of quantity is already in use within 3rd-generation partnership project (3GPP) test standards [7, 9] and academic literature [38–40]. We call it effective isotropic incident power (EIIP) because it is the complement

to effective isotropic radiated power (EIRP), applied to the receive antenna.

We are not aware of any standardized mathematical definition of EIIP. We use the following for the purposes of this report:

$$\text{EIIP} = \text{“Power at the plane of the DUT”} = \frac{P_r}{G_r e_p}, \quad (\text{A.1})$$

where  $P_r$  is receive power available from the receive antenna,  $G_r$  is the partial gain [41] of the receive antenna, and  $e_p$  is the polarization efficiency between the transmit and receive antennas. This definition of EIIP makes it possible to characterize the incident field input of a DUT without specifying polarization behavior, much like the quantity of *total* electric field (which simplifies reporting and interpretation of measurements).

Its complement, EIRP, is defined as

$$\text{EIRP} = P_t G_t, \quad (\text{A.2})$$

with transmit power delivered into the transmit antenna  $P_t$  and transmit antenna partial gain  $G_t$ . In free space propagation, these parameters are related through an “effective isotropic” version of the Friis equation,

$$\text{EIIP} = \text{“Power at the plane of the DUT”} = P_t G_t \left( \frac{\lambda_0}{4\pi d} \right)^2 = \text{EIRP} \left( \frac{\lambda_0}{4\pi d} \right)^2, \quad (\text{A.3})$$

where  $d$  is the separation distance between antennas.

The relationship between EIIP and incident *total* field strength at the DUT,  $|E_r|$ , is

$$\text{EIIP} = \text{“Power at the plane of the DUT”} = \frac{|E_r|^2 \lambda_0^2}{\eta_0 4\pi}, \quad (\text{A.4})$$

where  $\eta_0 \approx 377 \Omega$  and  $\lambda_0 = c_0 f$  is the wavelength at the center frequency in free space. The EIIP parameters discussed in this report are therefore directly convertible to physical values of electric field strength.

## A.2 Single-Antenna Test Technique for Controlling Signal-to-Interference Ratio

Consider the propagation losses implied by the single-antenna test scenario. The transmit signals share the same propagation loss ( $L_{pol,s} - L_{pol,i} = 0$ ), polarization loss ( $L_{rs} - L_{ri} = 0$ ), and victim receive antenna gain ( $G_{rs} - G_{ri} = 0$ ). The resulting signal-to-interference ratio (SIR) ratio inside of the DUT,  $\text{SIR}_{\text{test}}$ , is simply

$$\text{SIR}_{\text{test}} = P_{rs} - P_{ri} = (\text{EIRP}_s - \text{EIRP}_i) + L_{\text{filt}}, \quad (\text{A.5})$$

notated as follows:

$P_{ri}$  = LTE power absorbed by the GPS receiver after filtering (in dBm),

$EIRP_i$  = LTE effective isotropic radiated power from the transmit antenna toward of the GPS receiver (in dBm),

$EIRP_s$  = GPS effective isotropic radiated power from the transmit antenna toward of the GPS receiver (in dBm), and

$L_{filt}$  = Losses introduced by interference out-of-band rejection filtering (in dBm), also known as the Off-Frequency Rejection (OFR) component of the Frequency-Dependent Rejection (FDR) term.

The equation is exact only when sharing a single transmit antenna.

The SIR, when controlled this way, is dominated by the signal radiated by the testbed and the DUT out-of-band filtering characteristics. The SIR is independent of propagation variables as long as the propagation coherence bandwidth is wide enough to include both the GPS and LTE signals under test. This characteristic is expected of the anechoic or semi-anechoic test environments used in this study.

These simplifications help to achieve a tractable test scope. Application-specific estimation tools may use propagation models and assumptions about device antenna patterns to estimate signal, interference, and noise power levels. This type of simulation may then use measured GPS device response data like that found in this report to model more realistic interference scenarios.



## B Variability due to Choice $C/N_0$ Estimator: A simulation study

### B.1 Introduction

Variability in carrier-to-noise-density ratio ( $C/N_0$ ) estimates from each DUT can be grouped into two components. The first component captures variations in the performance of a given DUT that arise from its intrinsic variability and from changing experimental conditions (e.g., variations in radiated signal strength). This variability component enables inferences about a single DUT; it was evaluated by the data analysis described in Section 5.4.

Second, because each DUT was a “black-box” device, with an unknown  $C/N_0$  estimation algorithm, there is variability attributable to the choice of  $C/N_0$  estimation algorithm implemented by the DUT. This component of variability was not included in our previous analyses. Because it concerns inter-DUT variations, this variability component is needed to make inferences about a population of DUTs.

To shed light on the variability in  $C/N_0$  estimates due to the choice of estimation algorithm, we conducted a limited simulation study, described here. As a starting point, we built upon the work of Falletti et al. [42], which compared the estimation bias of five  $C/N_0$  estimators. Our work went beyond that of Falletti et al. in three ways. First, we modeled the effect of an adjacent LTE uplink (UL1) signal and associated OOB, with the parameters described in Chapter 2. Second, we investigated the effect of a Rician fading model for the GPS signal channel. Lastly, instead of only evaluating estimation bias, as done in [42], our work evaluated the inter-algorithm variability of different  $C/N_0$  estimators by comparing their distributions.

### B.2 Methods

Following [42], the discrete-time signal at the correlator output of a GPS receiver can be modeled as

$$r_C[n] = \sqrt{P_d}D[n] + \sqrt{P_n}\eta[n], \quad (\text{B.1})$$

where  $D[n]$  is the binary phase-shift keying (BPSK) navigation signal,  $P_d$  is a function of the carrier power (see [42] for details),  $\eta[n]$  is noise (modeled as additive complex white Gaussian noise) and  $P_n$  is the noise power. Adding the effect of an adjacent-band LTE signal, we obtain the modified model

$$r_C[n] = \sqrt{P_d}D[n] + \sqrt{P_n}\eta[n] + \sqrt{P_I}\xi[n], \quad (\text{B.2})$$

where  $\xi[n]$  is a term due to the adjacent-band LTE signal, and  $P_I$  is the LTE interference power. As explained in [42], due to the linearity of the GPS receiver correlator, the  $C/N_0$  ratio associated to the signal entering the GPS receiver can be expressed as

$$\frac{C}{N_o} = \frac{P_d}{P_n} B_{\text{eqn}}, \quad (\text{B.3})$$

where  $B_{\text{eqn}}$  is normalized equivalent noise bandwidth.

The five  $C/N_0$  estimation algorithms studied in [42] were evaluated. These algorithms include

- Beaulieu’s method
- signal-to-noise variance (SNV)
- moments method (MM)
- real signal-complex noise (RSCN)
- narrowband-wideband power ratio (NWPR) method

In general, these algorithms use  $r_C[n]$  values to estimate  $C/N_0$ ; see [42] for details. The  $C/N_0$  performance results in [42] were obtained for the additive white Gaussian noise (AWGN) channel with no interference. This case, however, may not be practical. Therefore, we extended the performance evaluation from AWGN to two more practical scenarios.

- Non-fading GPS signal plus AWGN + LTE OOB, and
- GPS signal with Rician fading plus AWGN + LTE OOB.

Rician fading is a typical scenario in a real GPS environment, where there are both line-of-sight (LOS) and non-line-of-sight (NLOS) components. Two parameters of the Rician fading channel model are the Rician K-factor and the maximum Doppler shift in Hz. The K-factor is the power ratio between LOS and NLOS components.

For the scenarios with LTE OOB, the LTE OOB interference was estimated by using the GPS receiver mask and LTE power spectral density (PSD) as well as the carrier frequency separation between GPS and LTE systems. The correlation output between the GPS mask and LTE PSD in the frequency domain indicated the overlapping area, which represented interference from LTE falling into the GPS receiver. The overlapping area is a function of carrier frequency separation. If the carrier frequencies are the same, the overlapping area is at its maximum and results in co-channel interference. If the carrier frequencies are separated by a certain value, the overlapping area is reduced from the maximum overlapping area. We call the ratio between LTE OOB interference power at the given frequency separation and the original interference power the “rejection factor.”

Mathematically, it takes the form

$$F_{\text{rejection}}(f) = 10 \log \left\{ \frac{\int_{-\infty}^{\infty} S(\tau - f)C(\tau)d\tau}{\int_{-\infty}^{\infty} S(\tau - f_0)C(\tau)d\tau} \right\}, \quad (\text{B.4})$$

where  $S(f)$  and  $C(f)$  are the power spectral densities of the LTE UL1 signal and GPS receiver mask, respectively, and  $f_0$  is the carrier frequency of the GPS receiver. We assumed a GPS receiver mask with a passband from 1559-1610 MHz, corresponding to the L1 band. Combining this receiver model with the UL1 OOB mask, we calculated the rejection factor to be 49.6 dB.

The LTE OOB interference was correlated with a randomly selected coarse/acquisition (C/A) pseudo-random noise (PRN) code. The resulting correlator samples due to LTE OOB interference were then added to the navigation bit samples as shown in Eq. (B.2). Values of carrier-to-interference-density ratio ( $C/I_0$ ) at the correlator output with LTE uplink interference were calculated using the following relationship

$$\frac{C}{I_0} = C - (\text{EIRP}_{\text{LTE}} - P_L + G_{\text{gps}} + F_{\text{rejection}}) + PG + 10 \log B, \quad (\text{B.5})$$

where  $C$  is the received carrier power in the GPS L1 C/A signal for each satellite,  $\text{EIRP}_{\text{LTE}}$  is the LTE UL power,  $P_L$  is the path loss,  $G_{\text{gps}}$  is the GPS receiver antenna gain,  $PG$  is the processing gain, and  $B$  is the LTE signal bandwidth. Our simulations used the values given in Table B.1.

Table B.1: Parameters used for Eq. (B.5).

Parameter	Value
$C$	-128.5 dBm
$\text{EIRP}_{\text{LTE}}$	23 dBm
$P_L$	46.25 dBm
$G_{\text{gps}}$	3.1 dBi
$PG$	$10 \log(1023)$ dB
$B$	10 Mhz

The navigation signal,  $D[n]$ , was taken to be  $a_n e^{j\theta_n}$ , where  $a_n = \pm 1$  for BPSK data modulation, and  $\theta_n$  is the residual carrier phase error due to imperfect carrier tracking. We also modeled the error due to imperfect maximum Doppler shift frequency estimation of the Rician fading channel. The residual carrier phase error,  $\theta_n$ , due to imperfect carrier tracking loop was assumed to have a uniform distribution over the interval  $[-\sqrt{3}\sigma_\theta, \sqrt{3}\sigma_\theta]$ , where  $\sigma_\theta = 1$  radian. For the Rician fading channel, the K-factor and max Doppler shift frequency were taken to be 20 dB and 1 Hz, respectively.

We simulated 2000 Monte Carlo trials for each scenario and then made histograms to summarize the results.

### B.3 Results

Figures B.1 and B.2 contain histograms for the five  $C/N_0$  estimators under AWGN and Rician GPS channels, respectively.

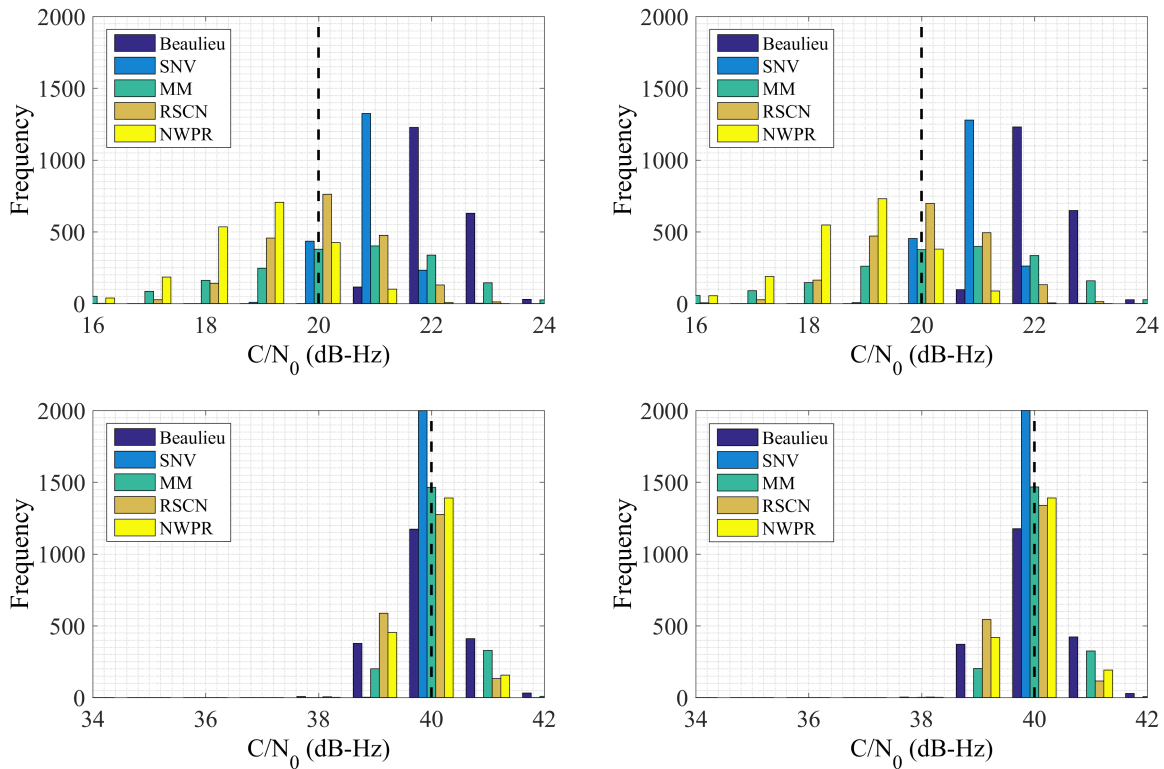


Figure B.1: Histograms of  $C/N_0$  estimates with an AWGN GPS channel. Top: true  $C/N_0 = 20$  dB-Hz, Bottom: true  $C/N_0 = 40$  dB-Hz. The LTE power at the plane of DUT is -20 dBm (Left) and -40 dBm (Right). The vertical dashed line indicates the true  $C/N_0$  value.

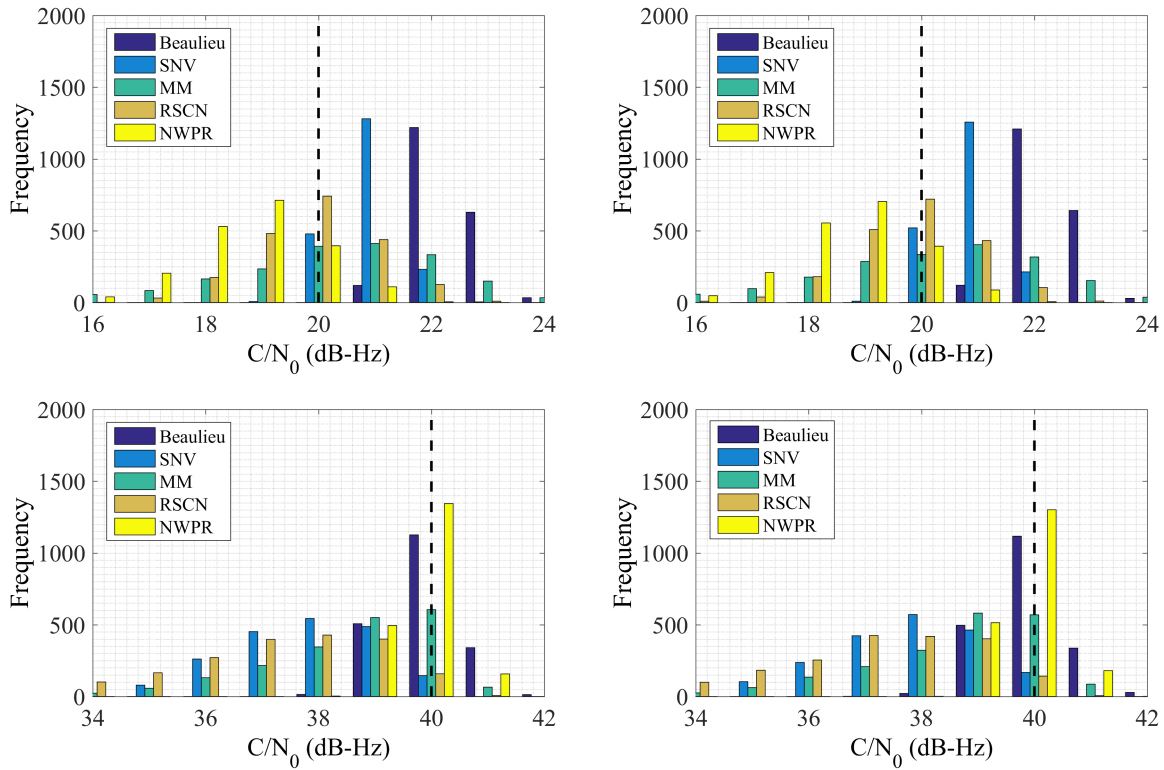


Figure B.2: Histograms of  $C/N_0$  estimates with a Rician GPS channel. Top: true  $C/N_0 = 20$  dB-Hz, Bottom: true  $C/N_0 = 40$  dB-Hz. The LTE power at the plane of DUT is  $-20$  dBm (Left) and  $-40$  dBm (Right). The vertical dashed line indicates the true  $C/N_0$  value.

#### B.4 Summary

The limited results presented here indicate that under some conditions, there may be differences between distributions of  $C/N_0$  estimators. Such differences would indicate variations that could be expected due to the choice of an  $C/N_0$  estimation algorithm. However, note that the results shown here are preliminary, and do not warrant strong conclusions, which would require a more thorough investigation. This evaluation of  $C/N_0$  estimation algorithms included some features that may be important to consider in future investigations, such as

- a fading GPS channel,
- modeling the effect of in-band and out-of-band LTE signals,
- computing the impact of LTE on the GPS receiver correlator using actual C/A PRN codes, and
- imperfect carrier tracking loop and Doppler shift estimation.



## C Testbed Configuration and Calibration

### C.1 Test Instrument Configuration

#### C.1.1 GPS Simulation

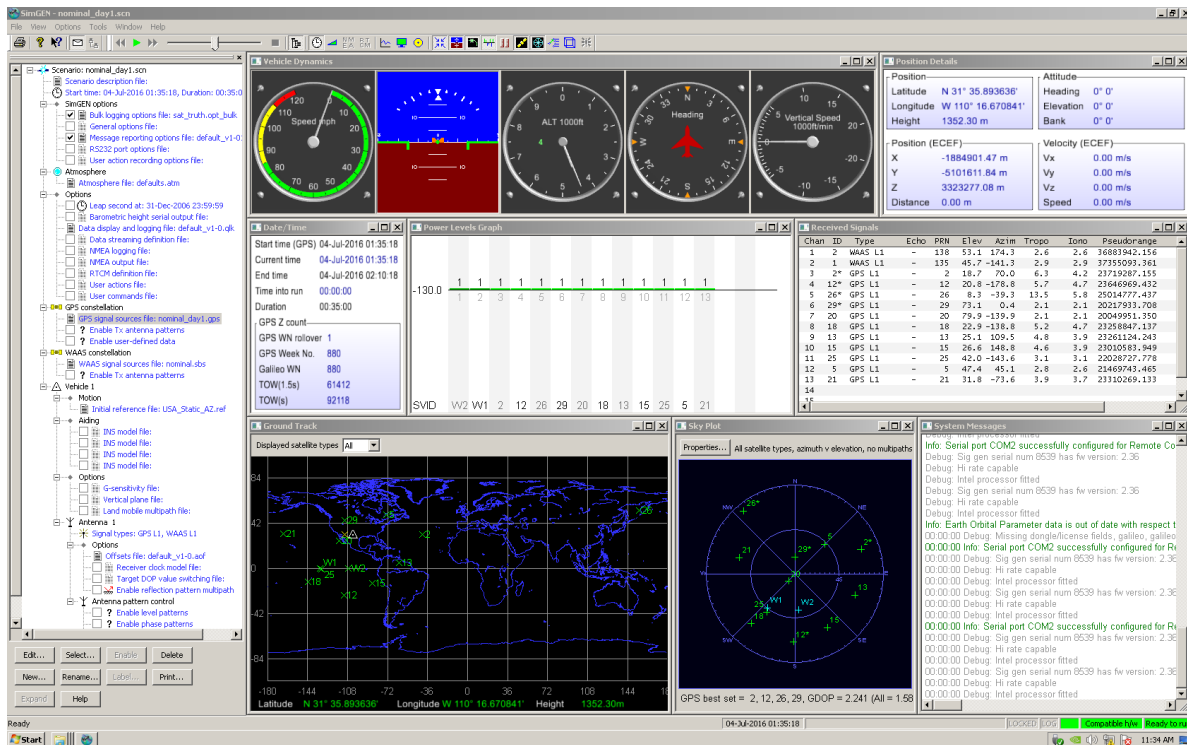


Figure C.1: General User Interface of the GPS Simulator. The Setup shows the configuration for “Day 1” of the nominal GPS scenario.

#### C.1.1.1 Almanac Modification

In order to keep the same GPS satellite constellation between days, all scenarios must have the same static position or the same dynamic profile. Additionally, a modified almanac must be used for every simulation scenario. To achieve this:

1. The almanac of the initial scenario was used as a template for almanacs of subsequent days. This file was obtained from the United States Coast Guard Navigation Center.
2. The Spirent Positioning Application (PosApp) requires almanacs to be in YUMA, SEM or

receiver independent exchange (RINEX) format. The YUMA format was used since it is a hand-editable American standard code for information interchange (ASCII) text file.

3. In the almanac file, there are 3 fields for every satellite that require modification: “Time of Applicability (sec GPS time)”, “Right Ascension at Week” and “Week (week number GPS time)”.
  - (a) The “Time of Applicability” needs to be shifted to the GPS week time corresponding to the start time of when the modified scenario was set to start. Every 24 hours the GPS week time increments by 86400 sec, whereas a whole week consists of 604800 sec.
  - (b) The “Right Ascension at Week” is recalculated by using the following functions:  
 $rot_{rate} = 0.000072921151467$  (rotation rate of earth [rad/s])  
 $RA$  (“Right Ascension”)  
 $TA$  (“Time of Applicability”)  
 $Ro = RA + (rot_{rate} * TA)$   
 $Ro_{int} = integer(Ro / (2 * \pi))$   
 $Ro_{new} = Ro - Ro_{int} * (2 * \pi)$   
 $Ro_{new}$  is the modified “Right Ascension” at Week, if the  $Ro_{new}$  is greater than  $\pi$  it will need to be projected onto a semicircle:  
 $Ro_{new} = ((2 * \pi) - Ro_{new}) * -1$
  - (c) The week needs to be adjusted to the GPS week number of the date of applicability. (In epoch format, 0 to 1023)
4. After the almanac is modified, the text file was saved with the \*.alm file name extension.
5. To apply the modified constellation to the scenario:
  - (a) In PosApp, access the GPS Signal Sources under the Constellation tree (see Figure C.1).
  - (b) Navigate to the “Motion tree” and expand the “Orbits tree”.
  - (c) On the orbits window click the “Load Orbits from file”.
  - (d) A pop-up window will appear prompting the user to select an almanac and specify the format.

If the steps above are completed, every scenario will have an identical initial constellation (save for minor rounding errors). This allows the user to have a test scenario with the same constellation and satellite tracks in future nearby dates. Thus DUTs will experience the same satellite configuration for each LTE power level sweep step, even though the date advances by 24 hrs.

### C.1.2 LTE IB DL Signal Generator

The LTE IB DL signal generator is configured to the save state preset listed in Table C.1. These are mostly default settings for an LTE DL configuration, but are listed here for completeness.

Table C.1: Testbed LTE IB DL Signal Generator Configuration

<b>Parameter</b>	<b>Value</b>
Center (LO) frequency	1531 MHz
Duplexing	FDD
PAR	10.38 dB
Link direction	Downlink (OFDMA)
Channel BW	10 MHz
FFT size	1024
RB per slot	50
Behavior in Unsch RB	Dummy data
Modulation	QPSK
Data source	PN9
Power	0 dB

### C.1.3 LTE IB UL Signal Generator

Table C.2: Testbed LTE IB UL Signal Generator Configuration

<b>Parameter</b>	<b>Value</b>
Center (LO) frequency	1632.5 MHz (UL1) or 1651.5 MHz (UL2)
Duplexing	FDD
PAR	6.67 dB
Link direction	Uplink (SC-FDMA)
Channel BW	10 MHz
FFT size	1024
RB per slot	50
Number of UEs	1
Set 1 No. RB	35
Set 1 Offset VRB	0
3GPP Release	8/9
Modulation	QPSK
Power	0 dB

The LTE IB UL signal generator is configured to the save state preset listed in Table C.2. These are mostly default settings for an LTE DL configuration, but are listed here for completeness. The primary difference is that, although the channel is set up for 50 resource block (RB) per slot, only 35 are used for communication, and these blocks are the 35 lowest-frequency blocks (Offset VRB 0)in the channel, to concentrate energy as close as possible to the GPS L1 band.

Table C.3: Testbed LTE OOB DL Signal Generator Configuration

Parameter	Value
Center (LO) frequency	1595 MHz
Baseband (IF) sample rate	195 MHz
PAR	13.47 dB
AWG file duration	100 ms
Duty cycle	100%
Output power level	Calibration dependent near -35 dBm (Section C.3)

Table C.4: Testbed LTE OOB UL Signal Generator Configuration

Parameter	Value
Center (local oscillator (LO)) frequency	1620 MHz
Baseband (intermediate frequency (IF)) sample rate	195 MHz
PAR	11.8 dB
AWG file duration	100 ms
Duty cycle	100%
Output power level	Calibration dependent near +4 dBm (Section C.3)

#### C.1.4 LTE OOB DL Signal Generator

The LTE OOB DL signal generator is configured to the save state preset listed in Table C.3. The peak-to-average ratio (PAR) values, determined by the structure of the OOB waveform input as a custom arbitrary waveform generation (AWG) file, are lower than some other noise (and noise-like LTE IB) because significant energy is concentrated near 1625 MHz.

#### C.1.5 LTE OOB UL Signal Generator

The LTE OOB UL signal generator is configured to the save state preset listed in Table C.4. The PAR values, determined by the structure of the OOB waveform input as a custom AWG file, are lower than some other noise (and noise-like LTE IB) because significant energy is concentrated near 1625 MHz.

#### C.1.6 Spectrum Analyzer

The spectrum analyzer is configured to the save state preset listed in Table C.5.

Table C.5: Testbed Spectrum Analyzer Configuration

Parameter	Value
Frequency sweep start	1500 MHz
Frequency sweep stop	1700 MHz
Resolution bandwidth	100 kHz
Video bandwidth	1 MHz
Number of points	2001
Reference level	(Autolevel)
Input attenuation	(Autolevel)
Trace averaging	50 traces (linear power mean)
Triggering	Single mode, software trigger (initiated from testbed software)
Reference power offset	Calibration dependent +35 dB to +36 dB (Section C.3)

## C.2 Procedures

The calibration procedures here apply to the leveling circuitry of Figure 3.9 when connected to the LTE signal generators and GPS simulator.

### C.2.1 Amplifier Signal Level Limits

The processes for these preliminary calibrations are included here for completeness. The results do not factor into the measurement uncertainty of the testbed, so they are not included in the calibration records listed in Section C.3.

#### C.2.1.1 LTE IB DL

The maximum LTE IB DL operating output power is limited by the power handling capability of the hybrid couplers. We compute the safe amplifier output level as follows:

$$\begin{aligned}
 \text{LTE IB DL amplifier output limit (dBm)} &= 54 \text{ dBm (hybrid coupler input maximum)} \\
 &\quad -1 \text{ dB (Margin)} \\
 &= 53 \text{ dBm (200 W)} \tag{C.1}
 \end{aligned}$$

This output level includes some losses through connector adapters and the LTE IB DL filter, so the actual output of the amplifier is slightly higher. A procedure for establishing safe levels for any supported signal generator output is listed in Table C.6.

Table C.6: Conducted Level Calibration Procedure: Limit LTE IB DL Maximum Output Levels

Action	Value
1 Disable LTE IB DL amplifier	
2 Substitute power attenuation at LTE IB DL filter output	50 dB
3 Connect power sensor at 50 dB attenuation output	
4 Set power sensor offset	50 dB
5 Set LTE IB DL attenuator gain	-110 dB
6 Set LTE IB DL signal generator output power	Max. leveled output
7 Enable LTE IB DL signal generator LTE modulation	
8 Slowly increase attenuation until power sensor displays target	53 dBm <sup>1</sup> (200 W)
9 Record LTE IB DL attenuation level	<b>Min. attenuation (dB)</b>
10 Disable LTE IB DL amplifier	
11 Insert fixed attenuation at LTE IB DL generator output	<b>Min. attenuation (dB)</b> (or slightly more)
12 Save instrument state	

<sup>1</sup>LTE IB DL amplifier output limit from Equation C.1

### C.2.1.2 LTE IB UL

The maximum safe level at the LTE IB UL amplifier input is limited by the manufacturer-specified input compression level. We aim to keep the input *peak* power below this level to maintain signal fidelity, so we back off signal levels by the input signal PAR, and a small additional margin:

$$\begin{aligned}
 \text{LTE IB UL input limit (dBm)} &= -25 \text{ dBm (LTE IB UL input P1dB)} \\
 &\quad - 8 \text{ dB (LTE IB UL signal PAR)} \\
 &\quad - 2 \text{ dB (Margin)} \\
 &= -35 \text{ dBm.} \tag{C.2}
 \end{aligned}$$

We used the procedure in Table C.7 to ensure that the LTE IB UL amplifier input signal stays below this limit.

### C.2.1.3 LTE OOB UL

The maximum safe level at the LTE OOB UL amplifier input is also limited by the manufacturer-specified input compression level. The calculation is similar to Equation C.2:

$$\begin{aligned}
 \text{LTE OOB UL input limit (dBm)} &= 10.0 \text{ dBm (LTE OOB UL input P1dB)} \\
 &\quad - 11.8 \text{ dB (LTE OOB UL signal PAR)} \\
 &\quad - 5 \text{ dB (Margin)} \\
 &= -6.8 \text{ dBm.} \tag{C.3}
 \end{aligned}$$

Table C.7: Conducted Level Calibration Procedure: Limit LTE IB UL Maximum Input Level

Action	Value
1 Disable LTE IB DL amplifier	
2 Set LTE IB DL attenuator gain at	-110 dB
3 Set LTE IB UL signal generator output power	Max. leveled output
4 Substitute power sensor for LTE IB UL amplifier	
5 Measure RMS power at cable output	<b>Ref LTE IB UL (dBm)</b>
6 Insert fixed attenuation at LTE IB UL generator output	<b>Ref LTE IB UL (dBm)</b> -(-35 dBm <sup>1</sup> )
7 Disconnect power sensor	
8 Reconnect LTE IB UL amplifier	
9 Save instrument state	

<sup>1</sup>LTE IB UL input limit from Equation C.2

Table C.8: Conducted Level Calibration Procedure: Limit LTE OOB UL Maximum Input Level

Action	Value
1 Disable LTE OOB UL amplifier	
2 Set LTE OOB UL attenuator gain at	-110 dB
3 Set LTE OOB UL signal generator output power	0 dBm
4 Substitute power sensor for LTE OOB UL amplifier	
5 Measure RMS power at cable output	<b>Ref LTE OOB UL (dBm)</b>
6 Set safe LTE OOB UL generator level (dBm)	7 dBm -6.8 dBm <sup>1</sup> <b>+Ref LTE OOB UL (dBm)</b>
8 Disconnect power sensor	
9 Reconnect LTE OOB UL amplifier	
10 Save instrument state	

<sup>1</sup>LTE OOB UL input limit from Equation C.3

This input level limit was achieved according to the procedure in Table C.8.

### C.2.2 Conducted Testbed Output Levels

All measurements of testbed output power need to be traceable to physical power standards. The tool that most directly accomplishes this is the power sensor (viewed with power meter when appropriate).

The power sensor should be an *average* or *root mean square (RMS)* power sensor instead of a continuous-wave (CW) power sensor, because the signals are modulated. We need to measure directly at the testbed output, because power sensors are not in general sensitive enough to measure the aggregate output power of the emulated GPS signal at the coupled output.

Table C.9: Conducted Level Calibration Procedure: GPS Output Power

Action	Value
1 <input type="checkbox"/> Determine GPS software reference level	GPS software reference level (dBm)
2 <input type="checkbox"/> Determine GPS scenario output setting	GPS emulator output setting (dBm)
3 <input type="checkbox"/> Calculate GPS emulator output offset (dB)	GPS software reference level (dBm) – GPS emulator output setting (dBm)
4 <input type="checkbox"/> Find calibrated reference level in manufacturer cal. certificate	Ref. single C/A at emulator output (dBm)
5 <input type="checkbox"/> Start nominal L1 scenario on GPS emulator	
6 <input type="checkbox"/> Connect power sensor to GPS emulator CAL L1 out	
7 <input type="checkbox"/> Record output power reading	<b>GPS aggregate at emulator output (dBm)</b>
8 <input type="checkbox"/> Compute GPS aggregate to single C/A correction (dB)	Ref. single C/A at emulator output (dBm) +GPS emulator output offset (dB) – <b>GPS emulator aggregate (dBm)</b>
8 <input type="checkbox"/> Reconnect GPS emulator to testbed	
9 <input type="checkbox"/> Restart the same GPS emulator scenario	
10 <input type="checkbox"/> Disable all LTE amplifiers and outputs	
11 <input type="checkbox"/> Set GPS attenuator	0 dB
12 <input type="checkbox"/> Replace testbed antenna with power sensor	
13 <input type="checkbox"/> Measure testbed maximum GPS output	<b>Max aggregate GPS at output (dBm)</b>
14 <input type="checkbox"/> Compute Max conducted single C/A GPS at output (dBm)	<b>Max aggregate GPS at output (dBm)</b> + GPS aggregate to single C/A correction (dB)
15 <input type="checkbox"/> Reconnect transmit antenna to conducted testbed output for spectrum analyzer calibration	

### C.2.2.1 GPS

The procedure for calibrating GPS output power levels is listed in Table C.9.

The output of the GPS simulator is the aggregate of satellites that each put out some of L1 C/A, L1 Y, and (for some tests) L2, plus two wide-area augmentation system (WAAS) signals. The target “nominal” EIIP at the DUT is -128.5 dBm. This is the power level corresponding to the L1 C/A output of *one* satellite. This distinction needs careful attention throughout the calibration process.

The scenarios that were run by the GPS simulator use the deliberately artificial test condition that EIIP from each satellite at the DUT is constant with respect both to time and satellite position in the sky. This was necessary to ensure stable levels to collect strong enough results to apply meaningful uncertainty bounds.

A correction factor needs to be determined to convert the aggregate constellation signal power measured at the testbed output to the desired per-satellite output power. The per-satellite output power of the GPS simulator is calibrated by the manufacturer, so we determined the conversion from aggregate power by measuring the aggregate power output directly from the GPS simulator. The difference between known calibrated output power and measured power is the correction factor.

The calibrated output level of the GPS emulator is valid for output levels configured at the reference level -130 dBm. The nominal operating level of these tests is -128.5 dBm, so the following correction

Table C.10: Conducted Level Calibration Procedure: Spectrum Analyzer

Action	Value
1 <input type="checkbox"/> Disable all amplifiers and generators	
2 <input type="checkbox"/> Set LTE OOB DL generator output	10 dBm at 1575.42 MHz
3 <input type="checkbox"/> Set LTE OOB DL attenuator	0 dB
4 <input type="checkbox"/> Enable LTE OOB DL generator output	
5 <input type="checkbox"/> Set spectrum analyzer ref. level for low noise within max IF level	
6 <input type="checkbox"/> Measure band power, 1575.42 ± 0.5 MHz	<b>Ref. at spectrum analyzer (dBm)</b>
7 <input type="checkbox"/> Measure testbed output power with power sensor	<b>Ref. at output (dBm)</b>
8 <input type="checkbox"/> Set calibrated spectrum analyzer level offset	<b>Ref. at output (dBm)</b> <b>-Ref. at spectrum analyzer (dBm)</b>
9 <input type="checkbox"/> Save instrument state as preset	

is necessary:

$$\begin{aligned}
 \text{GPS reference level offset (dB)} &= -128.5 \text{ dBm (GPS emulator output setting)} \\
 &\quad - -130 \text{ dBm (GPS emulator reference level)} \\
 &= +1.5 \text{ dBm.} \tag{C.4}
 \end{aligned}$$

### C.2.2.2 Spectrum Analyzer

Calibrating the level offset on the spectrum analyzer corrects spectrum measurements to the forward power at the testbed output, instead of those at the coupler output (where the analyzer is connected).

The calibration is performed at a single frequency, 1575.42 MHz. This was chosen because it is relatively close to the center frequency of the full variety of GPS and LTE signals under study.

The test signal at this frequency is excited with the LTE OOB DL signal generator in order to avoid the use of amplifiers that add additional noise. The calibrated offset level is determined relative to the physical testbed output power, which is determined by power sensor. Details are listed in Table C.10.

### C.2.3 Relative OOBE Levels

#### C.2.3.1 LTE OOB DL

The relative OOBE signal levels are the OOBE signal PSD of Figure 2.4 normalized against the corresponding total IB power. Though normalization produces strange scaling units of dB(MHz), the result is independent of the in-band LTE signal parameters (like the fraction of loaded resource blocks) or power level.

Table C.11: Conducted Level Calibration Procedure: LTE OOB DL Relative to LTE IB DL

Action	Value
1 <input type="checkbox"/> Disable LTE IB DL amplifier	
2 <input type="checkbox"/> Set LTE OOB DL attenuator	0 dB
3 <input type="checkbox"/> Set LTE OOB DL signal generator to reference level	0 dBm
4 <input type="checkbox"/> Record total band power 1549.5 MHz — 1551.5 MHz	<b>Ref LTE OOB DL at output (dBm/MHz)</b>
5 <input type="checkbox"/> Disable LTE OOB DL signal generator	
6 <input type="checkbox"/> Enable LTE IB DL signal generator output	
7 <input type="checkbox"/> Set LTE IB DL attenuator	0 dB
8 <input type="checkbox"/> Enable LTE IB DL amplifier	
9 <input type="checkbox"/> Record total band power 1526 MHz — 1536 MHz	<b>Max. LTE IB DL at output (dBm)</b>
10 <input type="checkbox"/> Set calibrated LTE OOB DL generator level (dBm)	0 dBm <b>+Ref LTE OOB DL at output (dBm/MHz)</b> <b>–Max. LTE IB DL at output (dBm)</b> <b>–117 dB(MHz)<sup>1</sup></b>
11 <input type="checkbox"/> Save instrument state	

<sup>1</sup>LTE IB DL OOBE offset from Equation C.5

The relative level scaling is computed as follows for LTE OOB DL calibration:

$$\begin{aligned}
 \text{LTE OOB DL relative level (dB(MHz) at 1550 MHz)} &= -85 \text{ dBW/MHz (1550 MHz)} \\
 &\quad -32.0 \text{ dBW (LTE IB DL band power)} \\
 &= -117 \text{ dB(MHz)}. \tag{C.5}
 \end{aligned}$$

Like the LTE OOB UL relative calibration, while this calibration is taken at a single test frequency (1550 MHz), it applies across the entire LTE OOB DL bandwidth, with the exception of various errors in radiated frequency flatness (and slight variation in  $\lambda$  in free space calculations).

Relative LTE OOB DL levels are established according to the calibration process listed in Table C.11. The intent of the calibration is to ensure that LTE OOB UL levels match the emissions mask relative to LTE IB DL *if the attenuators in both paths are set to the same value*. Signal outputs are referenced to the LTE OOB UL peak near 1625 MHz to maximize the signal-to-noise ratio (SNR) of the calibration measurement.

### C.2.3.2 LTE OOB UL

The relative level scaling is computed as follows for LTE OOB UL calibration:

$$\begin{aligned}
 \text{LTE OOB UL relative level (dB(MHz))} &= -34 \text{ dBW/MHz (LTE OOB UL max PSD)} \\
 &\quad -(-7.0 \text{ dBW (LTE IB UL band power)}) \\
 &= -27 \text{ dB(MHz)}. \tag{C.6}
 \end{aligned}$$

where PSD measurements are taken at 1625 MHz.

Table C.12: Conducted Level Calibration Procedure: LTE OOB UL Relative to LTE IB UL

Action	Value
1 <input type="checkbox"/> Disable LTE IB UL amplifier	
2 <input type="checkbox"/> Set LTE OOB UL attenuator	0 dB
3 <input type="checkbox"/> Set LTE OOB UL signal generator output power (from Table C.8)	<b>Max LTE OOB UL at source (dBm)</b>
4 <input type="checkbox"/> Measure PSD at 1624.7 MHz with spectrum analyzer	<b>Max LTE OOB UL at output (dBm/100 kHz)</b>
5 <input type="checkbox"/> Disable LTE OOB UL signal generator	
6 <input type="checkbox"/> Enable LTE IB UL signal generator output	
7 <input type="checkbox"/> Set LTE IB UL attenuator	0 dB
8 <input type="checkbox"/> Enable LTE IB UL amplifier	
9 <input type="checkbox"/> Record total band power with the spectrum analyzer across 1627.5 MHz — 1637.5 MHz (for UL1), or across 1646 MHz — 1656 MHz (for UL2)	<b>Max. LTE IB UL at output (dBm)</b>
10 <input type="checkbox"/> Set calibrated LTE OOB UL generator level (dBm)	<b>Max LTE OOB UL input (dBm)</b> <b>+Max LTE OOB UL at output (dBm/100 kHz)</b> <b>–Max. LTE IB UL at output (dBm)</b> <b>–27 dB(MHz)<sup>1</sup></b> <b>–10 dB(MHz/100 kHz)</b>
11 <input type="checkbox"/> Save instrument state	

<sup>1</sup>LTE IB UL OOBE offset from Equation C.6

Resolution bandwidth of 100 kHz was chosen on spectrum analyzer measurements to resolve the sharp peak in the LTE OOB UL spectrum. Conversion between dB(MHz) (from the emissions mask under study) and dB(kHz) (from the spectrum analyzer) is a simple 10 dB offset.

## C.2.4 Radiated Levels

### C.2.4.1 Radiated correction to the plane of the DUT

The Friis equation is the basis of converting from forward power available to the antenna to EIIP (“power at the plane of the DUT”). The conversion equation, based on Equation A.3, is

$$\begin{aligned} \text{Conducted power correction to EIIP at DUT} &= \text{EIIP (dBm)} - P_t \text{ (dBm)} & (C.7) \\ &= G_t \text{ (dBi)} - e_p \text{ (dB)} + 20 \log_{10} \left( \frac{\lambda_0}{4\pi d} \right). \end{aligned}$$

This EIIP carries a defined reference polarization which can be different from the right-hand circularly-polarized (RHCP) testbed transmit polarization. The polarization efficiency  $e_p$  enables this distinction.

We define LTE EIIP as linearly-polarized, which has  $e_p = -3$  dB relative to the RHCP testbed transmission, making the EIIP with linearly-polarized (LP) reference polarization 3 dB larger than that of the EIIP matching the RHCP physical polarization. The polarization adjustment can be interpreted as follows: “the testbed RHCP excites RHCP field components that are 3 dB stronger than any LP field component. Therefore, the total field strength of an incident LP wave needs to be

Table C.13: Corrections from Conducted Power to Radiated EIIP at the Plane of the DUT

	GPS	LTE			
		IB DL	IB UL1	IB UL2	
Separation distance, $d$	3.491	3.491	3.491	3.491	m
Transmit antenna gain, $G_t$	4.1	4.1	4.1	4.1	dBi
Center frequency	1575.42	1531	1632.5	1646	MHz
Wavelength at center frequency, $\lambda_0$	0.1903	0.1958	0.1836	0.1815	m
EIIP reference polarization	RHCP	LP	LP	LP	
Reference to RHCP polarization eff., $e_p$	0	-3	-3	-3	dB
Conducted power correction to EIIP at DUT <sup>1</sup>	-43.15	-39.91	-40.46	-40.56	dB

<sup>1</sup>By Equation C.7

Table C.14: Conducted Level Calibration Procedure: LTE OOB UL Relative to LTE IB UL

Action	Value
1 <input type="checkbox"/> Compute calibrated GPS attenuator setting (in dB)	Max conducted single C/A GPS at output <sup>1</sup> +Conducted power correction to EIIP at DUT <sup>2</sup> -GPS EIIP specification for single C/A signal <sup>3</sup>
2 <input type="checkbox"/> Use the attenuator setting in the testbed automation scripts	

<sup>1</sup>The result of the conducted GPS power calibration in Table C.9

<sup>2</sup>From the GPS column in Table C.13

<sup>3</sup>According to the -128.5 dBm nominal level defined in Subsection 2.2.2

3 dB stronger to excite the effect seen from an RHCP testbed.”

Table C.13 lists of corrections from conducted power to EIIP for GPS and each LTE IB signal. These are used in all conversions from conducted quantities calibrated according to the procedures in the previous subsections.

### C.2.4.2 Nominal GPS output level

The GPS signal path, unlike the LTE paths, is calibrated by determining a calibrated nominal attenuation setting. The test parameters in Chapter 2 define GPS levels in terms of EIIP at the DUT. The level setting of the GPS attenuator therefore depends on the radiated level, via calibrated conducted power and the corresponding correction to GPS EIIP.

## C.3 Calibration Records

We recorded measurements and correction offsets for each calibration procedure in Section C.2. The results of these calibrations through the test campaign are listed in Table C.15. Each calibration applies from date provided until the next calibration date (or the end of the test campaign in early November).

Events that trigger new calibration runs are as follows:

1. The start of the measurement campaign,
2. After moves between test sites,
3. After changes between LTE IB uplink band 1 (low) (UL1) and LTE IB uplink band 2 (high) (UL2) operation, and
4. After changes between LTE IB DL high and medium power amplifiers.

After the first change from LTE IB UL1 to LTE IB UL2, however, calibration results changed by less than 0.25 dB, and no further calibration was performed in switching between uplink bands.

Table C.15: Power Level Calibration Data Taken During the Course of the Test Campaign. Underline Indicates Reuse of Previous Calibration Runs, and **Bold** Values are Measurement Results.

		<b>Aug. 1</b>	<b>Aug. 19</b>	<b>Sep. 19</b>	<b>Oct. 18</b>	
		<b>NTS</b>	<b>NBIT</b>	<b>NBIT</b>	<b>NBIT</b>	
GPS (Conducted)	<b>GPS aggregate at emulator output</b>	-63.80	-62.00	<u>-62.00</u>	<u>-62.00</u>	dBm
<i>Follows Table C.9</i>	Ref. single C/A at emulator output	-79.23	-79.23	<u>-79.23</u>	<u>-79.23</u>	dBm
	GPS emulator output offset	+0.70	+0.70	<u>+0.70</u>	<u>+0.70</u>	dB
	GPS aggregate to single C/A correction	-14.73	-16.53	<u>-16.53</u>	<u>-16.53</u>	dB
	<b>Max aggregate GPS at output</b>	-36.30	-31.40	<u>-31.40</u>	<u>-31.40</u>	dBm
	Max conducted single C/A GPS at output	-51.03	-47.93	<u>-47.93</u>	<u>-47.93</u>	dBm
GPS (Radiated)	Conducted power correction to EIIP at the DUT	-43.72 <sup>1</sup>	<u>-43.72<sup>1</sup></u>	<u>-43.72<sup>1</sup></u>	<u>-43.72<sup>1</sup></u>	dB
<i>Follows Table C.14</i>	GPS EIIP specification for single C/A signal	-128.50	-128.50	<u>-128.50</u>	<u>-128.50</u>	dBm
	Calibrated GPS attenuator setting	33.75	36.85	<u>36.85</u>	<u>36.85</u>	dB
	Calibrated GPS attenuator setting (0.25 dB res.)	33.75	36.75	<u>36.75</u>	<u>36.75</u>	dB
Spectrum Analyzer	<b>Ref. at output</b>	-10.20	-12.65	<u>-12.65</u>	<u>-12.65</u>	dBm
<i>Follows Table C.10</i>	<b>Ref. at spectrum analyzer</b>	-45.10	-48.00	<u>-48.00</u>	<u>-48.00</u>	dBm
	Calibrated spectrum analyzer level offset	34.90	35.35	<u>35.35</u>	<u>35.35</u>	dB
LTE OOB DL	<b>Max. LTE IB DL at output</b>	42.30	42.30	<u>42.30</u>	<u>42.30</u>	dBm
High power LTE IB DL	<b>Ref. LTE OOB DL at output</b>	-39.94	-40.40	<u>-40.40</u>	<u>-40.40</u>	dBm/MHz
<i>Follows Table C.11</i>	Calibrated LTE OOBE DL generator level setting	-34.76	-34.30	<u>-34.30</u>	<u>-34.30</u>	dBm
LTE OOB DL	<b>Max. LTE IB DL at output</b>	—	—	10.07	<u>10.07</u>	dBm
Med. power LTE IB DL	<b>Ref. LTE OOB DL at output</b>	—	—	-40.40	<u>-40.40</u>	dBm/MHz
<i>Follows Table C.11</i>	Calibrated LTE OOBE DL generator level setting	—	—	-66.53	<u>-66.53</u>	dBm
LTE OOB UL	<b>Max. LTE IB UL at source</b>	34.17	<u>34.17</u>	<u>34.17</u>	<u>34.17</u>	dBm
<i>Follows Table C.12</i>	<b>Max. LTE OOB UL at output</b>	-2.9	<u>-2.9</u>	<u>-2.9</u>	<u>-2.9</u>	dBm/100 kHz
	Calibrated LTE OOBE UL generator setting	-2.83	<u>-2.83</u>	<u>-2.83</u>	<u>-2.83</u>	dBm

<sup>1</sup>These original EIIP correction values were revised upward by 0.56 dB to the values listed in Table C.13 at the completion of test. The impact of this correction is well within the GPS EIIP uncertainty interval.

## C.4 Power Level Uncertainty Estimation

The principal output of testbed is the EIIP of the RF signals, namely, the GPS signal, the IB DL LTE signal, the IB UL LTE signal, the OOB DL LTE signal, and the OOB UL LTE signal. Grouping the measured and calculated terms into a single equation helps identify sources of uncertainty and the relationship between terms. A summary equation for EIIP is

$$\text{EIIP (dBm)} = P_{\text{SA}} \text{ (dBm)} + C_{\text{Inc}} \text{ (dB)} - C_{\text{Through}} \text{ (dB)} + G_t \text{ (dBi)} - 20 \log_{10} \left( \frac{4\pi d_{\text{setup}}}{\lambda_0} \right) \quad (\text{C.8})$$

where:

$P_{\text{SA}}$  = Power measured at the Spectrum Analyzer;

$C_{\text{Inc}}$  = Coupling between input of the directional coupler to the input of the Spectrum Analyzer;

$C_{\text{Through}}$  = Coupling between input of the directional coupler to the input of the transmitting antenna;

$G_t$  = Gain of the transmitting antenna;

$\lambda_0 = c_0/f$  is the wavelength at the center frequency in free space.

$d_{\text{setup}}$  = is the separation distance between the source antenna and the plane of the DUT.

### C.4.1 Antenna Gain

For generating and verifying the radiated signals, we used a matched pair of conical log-spiral antennas. These antennas were placed in our NIST Broadband Interoperability Testbed (NBIT) chamber with a tip-to-tip separation distance of 3 m. The antennas were calibrated in 250 MHz steps by the manufacturer per SAE ARP958 [43] with a tip-to-tip separation distance of 1 m. This calibration was not sufficient for our needs for three main reasons. As pointed out in [44], antennas calibrated at 1 m should be used with a separation distance close to 1 m. In addition, such a calibration does not account for the shifting phase center of the antenna, which means that the radiating section of the antenna is behind the tip of the antenna by several cm, resulting in an underestimation of the gain, and therefore an underestimation of the EIIP at the DUT. Finally, the sparse frequency spacing results in only a single calibration point on each end of our frequency spectrum. As a result, gain values between the sample points (which covers all of our measurements) are unknown. For all of these reasons, we chose to perform our own calibration, using methods we would expect most test labs to be able to employ.

Calibrations are based on the Friis transmission formula [10] which states that, for a transmitting antenna with a transmitted power  $P_t$  and gain  $G_t$  and a receiving antenna with gain  $G_r$ , separated

by a distance  $d$ , the received power  $P_r$  will be given by

$$P_r = P_t G_t G_r \left( \frac{\lambda_0}{4\pi d} \right)^2. \quad (\text{C.9})$$

If we assume that the two antennas are identical,  $G_t = G_r$ , and we can solve for  $G_t$  as

$$G_t \approx \sqrt{\frac{P_r}{P_t}} \left( \frac{4\pi d}{\lambda_0} \right). \quad (\text{C.10})$$

For both the manufacturer calibration and our calibration, there was a nominal value  $d_{nom}$  for  $d$  (a tip-to-tip separation of 1 m for the manufacturer, and 3 m separation for our calibration), and an additional term  $d_{cent}$  to account for variable location of the antenna phase center. Since the phase center offset should be the same for both the transmitting and receiving antennas,  $G_t$  is

$$G_t \approx \sqrt{\frac{P_r}{P_t}} \left( \frac{4\pi (d_{nom} + 2d_{cent})}{\lambda_0} \right) = |S_{21_{cal}}| \left( \frac{4\pi (d_{nom} + 2d_{cent})}{\lambda_0} \right) \quad (\text{C.11})$$

where  $S_{21_{cal}}$  is the measured transmission coefficient between the input of the transmitting antenna and the output of the receiving antenna.

According to [45], the active region of a conical log spiral antenna at a given frequency occurs approximately where the circumference of the cone is equal to one wavelength. At 1.5 GHz and 1.75 GHz (these frequencies are chosen because we have manufacturer calibration data), the wavelengths are 20 cm and 17.1 cm, respectively, and this implies that  $d_{cent}$  is approximately 16 cm to 18 cm from the tip. From (C.11), this implies that the gain calibrations provided by the manufacturer need a correction of 1.4 dB at 1.5 GHz and 1.2 dB at 1.75 GHz. For our calibration with  $d_{nom} = 3$  m, the correction is 0.5 dB at 1.5 GHz and 0.4 dB at 1.75 GHz.

To estimate the gain of the transmitting antenna and its associated uncertainty, we measured  $S_{21_{cal}}$  over 30 times, moving the receiving antenna left, right, up, and down, in order to characterize the region of the receiving antenna and also determine possible variability in the measurements. We also moved the receiving antenna towards and away from the transmitting antenna, adjusting for the change in  $d_{nom}$ . These results were then averaged to give our best estimate of  $S_{21_{cal}}$ , which was then used to estimate  $G_t$ . Rather than attempt to keep track of the estimated gain at each frequency, we assumed a constant gain of 4.1 dBi over our measurement span, with variations accounted for in the uncertainty analysis. Our estimated gain, simplified constant approximation, along with the corrected manufacturer calibration with the  $\pm 0.8$  dB uncertainty (coverage factor  $k = 2$ ) is given in Figure C.2. The two estimates of gain agree well at the two points where they overlap.

The phase center term affects more than just the calibration of the gain. In (C.8), if we set  $d_{setup} = d_{DUT} + d_{cent}$  where  $d_{DUT}$  is the distance from the tip of the source antenna to the plane of the DUT, it is apparent that the phase center offset also increases the distance between the source antenna and the plane of the DUT. To illustrate the effect, (C.11) is substituted into (C.8), along

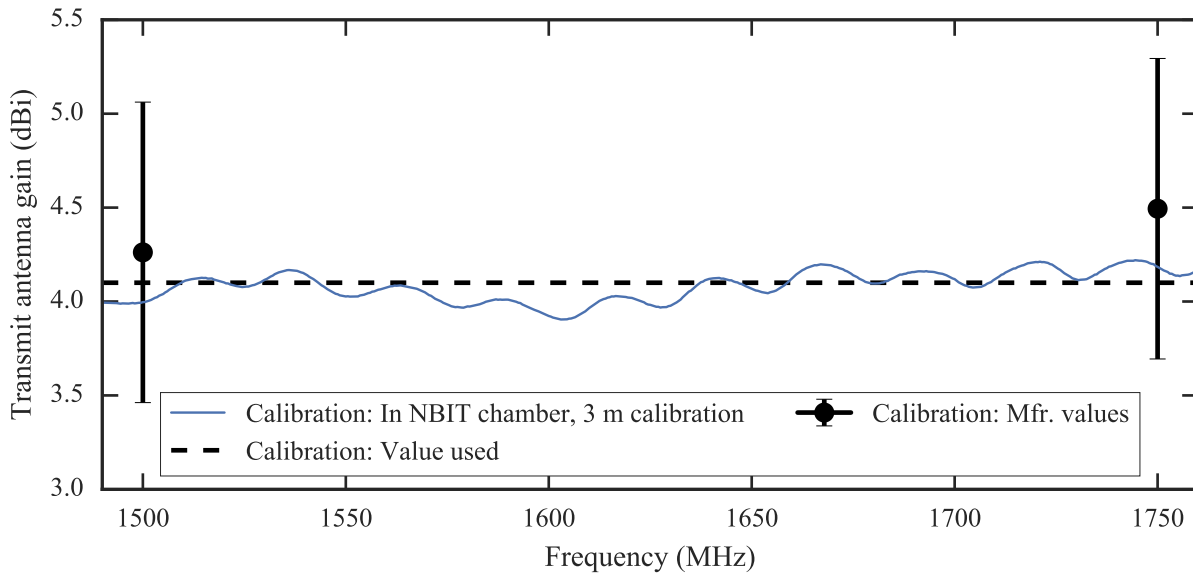


Figure C.2: Antenna gain checks performed by the two-antenna method to 1) compare measured gain values with those reported by the manufacturer, and 2) estimate uncertainty introduced by assuming a constant gain over frequency.

with the expansion of  $d_{setup}$  as

$$\begin{aligned}
 \text{EIP (dBm)} \approx & P_{SA} \text{ (dBm)} \\
 & + C_{Inc} \text{ (dB)} \\
 & - C_{Through} \text{ (dB)} \\
 & + 10 \log_{10} \left( |S_{21_{cal}}| \left( \frac{4\pi}{\lambda_0} (d_{nom} + 2d_{cent}) \right) \right) \\
 & - 20 \log_{10} \left( \frac{4\pi}{\lambda_0} (d_{DUT} + d_{cent}) \right). \tag{C.12}
 \end{aligned}$$

We can now work our way through Equation C.12 term by term to discuss uncertainties.

#### C.4.2 Spectrum Analyzer Power Measurement Uncertainty Components

Based on specifications given by the manufacturer [46], the standard uncertainty of a power measurement is 0.3 dB. However, they recommend that this be increased by 0.2 dB if measurements are taken over a long time period without aligning the system (this was sometimes required for some of our measurements). Therefore, we give a standard uncertainty of 0.5 dB for measurements of power using the spectrum analyzer.

In addition to uncertainty due to the spectrum analyzer, there was additional uncertainty due to source signal variations over time.

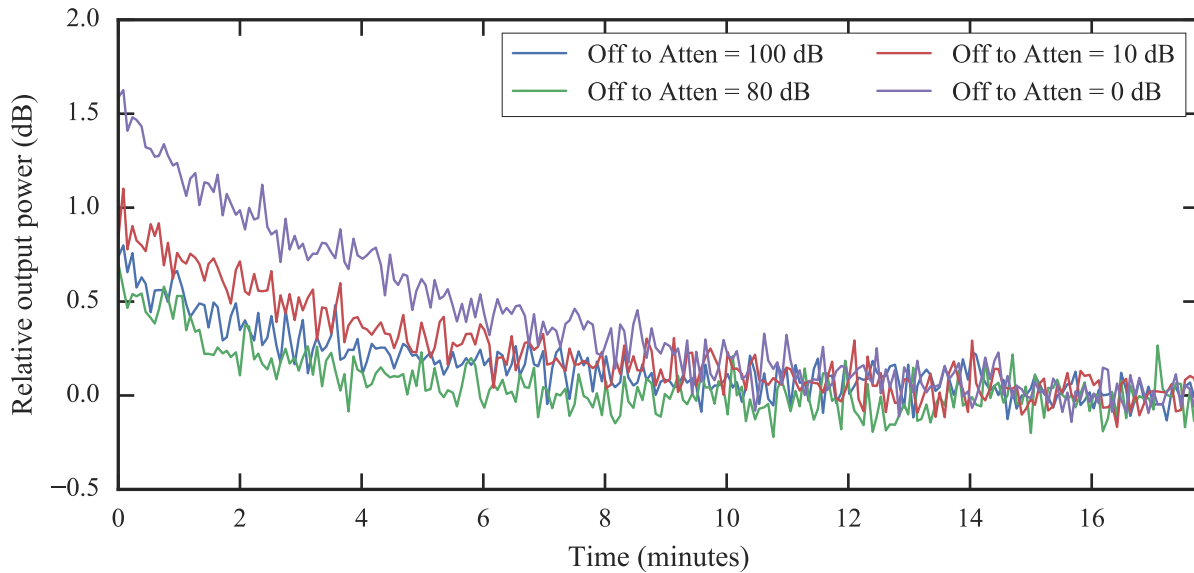


Figure C.3: Output power relative to the average final power. Typical drift in the output of the high-power amplifier after the output is enabled and an LTE downlink signal applied. Results show that the worst drift occurs when the amplifier is set to maximum output power, but is still significant even if the LTE signal is 100 dB below maximum.

### C.4.3 Power Level Time Stability Uncertainty Components

While performing some of the tests, we noted that the output power from the high-power downlink amplifier drifted in time. Specifically, the output power reached a maximum immediately after the amplifier output was enabled and a signal was applied, and gradually decreased. To document these effects, we performed a number of measurements in which the amplifier output was enabled and the output power changed in various combinations. We found that if the output was always enabled, the drift was greatly reduced. However, the high noise floor of the amplifier did not allow us to use this approach since, occasionally, the output noise from the amplifier was sufficient to degrade the performance of a DUT. Given that our tests were always performed by enabling the amplifier and setting the test power level, our only option was to characterize the drift during typical operating conditions. For these tests, the amplifier was disabled for approximately 20 minutes, and then the amplifier was enabled and the external variable was set to a desired level and held constant for another 20 minutes. This was repeated at several different attenuation levels. We present sample results for attenuator values of 0 dB, 10 dB, 80 dB, and 100 dB. The worst-case drift is approximately 1.6 dB for an attenuator setting of 0 dB, and the amplifier takes approximately 15 minutes to reach steady state. To account for this drift, we assign a standard uncertainty of 0.75 dB to the component related to high power downlink amplifier drift. Since coverage factors of  $k = 2$  are commonly applied to the standard uncertainty, the expanded uncertainty of 1.5 dB is sufficient for almost all of the expected drift cases.

We note that only the high-power downlink amplifier showed this behavior. The uplink amplifier and the low power downlink amplifier showed no appreciable drift but we assigned a standard uncertainty of 0.1 dB to all other amplifiers. However, the same tests could also be used to determine the long-term variability of the measurements, and these results could be applied to the appropriate signals. We observed a variability with a standard deviation of 0.2 dB on the low-power in-band downlink, 0.1 dB on the in-band uplink, and 0.6 dB on the out-of-band uplink. The high variability in the out-of-band uplink was due to the shape of the signal, the noise-like characteristic, and the fact that the measurement was based on power at a single frequency rather than averaged over a band. The power of the out-of-band downlink was too low to measure.

#### **C.4.4 Coupled Output Power Calibration Uncertainty Components**

Any variations in the testbed before the directional coupler should be observable as changes in power detected by the spectrum analyzer, so the RF path needed calibrations (the directional coupler, and the cables from the incident sidearm to the spectrum analyzer and to the transmitting antenna). Rather than measure the coupler and cables separately (which increases uncertainty), we calibrated the coupler and cables as a system. The uncertainty in these calibrations is given by a spreadsheet provided by the manufacturer of the network analyzer. (Note: the original spreadsheet downloaded from the the manufacturer's website was non-functional, so we were provided an older version by technical support. The spreadsheet we used was Revision 3.0.0, with dynamic link library (DLL) Revision 4, 9, 6, 31). The spreadsheet gave a standard uncertainty of the transmission coefficient for our test conditions of less than 0.1 dB. Since we calculate the difference between two calibrations, we combine the two uncertainty terms as 0.14 dB.

#### **C.4.5 Antenna Gain Uncertainty Components**

The calibration of the transmitting antenna has several potential sources of error. The two dominant sources relate to imperfections in the manufacture of the antennas themselves: errors can arise if the antennas are not identical or if polarization of the antennas is not perfectly circular. The calibration procedure depends on the antennas being identical, or at least having identical gains. The antennas we used were the same make and model, and the serial numbers were sequential. In addition, we measured the reflection coefficient  $S_{11}$  of each antenna and compared the values of  $1 - |S_{11}|^2$  in the NBIT chamber to ensure similar mismatch characteristics. Differences were less than 0.2 dB indicating that the cables, connectors, and passive components inside the antennas are acceptably similar. Based on our experience with antenna measurements, we assign a standard uncertainty of 0.5 dB to possible differences in the antennas. Similarly, based on [44], 0.5 dB is a typical value to account for departures from circularity.

Chamber imperfections can also affect the accuracy of the estimated gain. Based on our measurements at multiple locations around the position of the DUTs, the standard deviation over all measurements was less than 0.3 dB. To be conservative and to allow for other systematic biases, we increase the standard uncertainty to 0.5 dB.

Overall, the estimated gain presented in Figure C.2 is well approximated by a constant value of 4.1 dB. To account for the variability, we include a standard uncertainty of 0.2 dB.

We estimate that we were able to determine the distance between antennas, including possible variation in phase center, to within 14 cm. This corresponds to a standard uncertainty in the gain of 0.2 dB.

Finally, as mentioned earlier, the calibration of the network analyzer has a standard uncertainty of 0.1 dB.

#### **C.4.6 Programmable Attenuators**

The GPS and LTE OOB DL paths require calibrated attenuation data as the output levels are too weak to be measured directly during tests. These paths' output levels are instead calibrated in advance by characterizing the path response at 0 dB attenuation, then applying the calibrated attenuation level during testbed operation. In this way the testbed output level of each signal is taken to be known even though it is not directly measured in real time during tests.

Measured attenuation errors are shown at 3 frequencies in Figures C.4-C.6. The mapping between the serial number of each attenuator and its corresponding signal chain is given in Table C.16. Measurements were performed on a network analyzer at each attenuation setting down to 70 dB (where the network analyzer measurements became too noisy to give accurate results). As a conservative estimate, we give a standard uncertainty of 0.5 dB for attenuation values of the variable attenuators.

The curve fit shown for each attenuator is the linear regressions between the attenuation setting (horizontal axis) and measured transmission ( $|S_{21}|^2$  in dB, vertical axis). The ideal curve fit response here would be -1 dB in  $|S_{21}|^2$  for each +1 dB in attenuator setting (i.e., a slope of -1). The regression slope of each line is within 1% of this ideal goal. The intercept at the 0 dB attenuation setting indicates the minimum "baseline" attenuation of each device.

Below each curve fit plot is the residual error from the curve fit. The maximum error was approximately 0.7 dB. Each attenuator was similar, so these curves could have been used to generate a correction table for attenuation values; we did not introduce this complexity to the testbed because the magnitude of the error did not dominate the overall uncertainty of GPS or LTE OOB DL EIIP at the DUT.

#### **C.4.7 Uncertainty Budgets**

To summarize the uncertainty, we give tables for the uncertainty budgets of the EIIP for the various RF signals in Tables C.17–C.21.

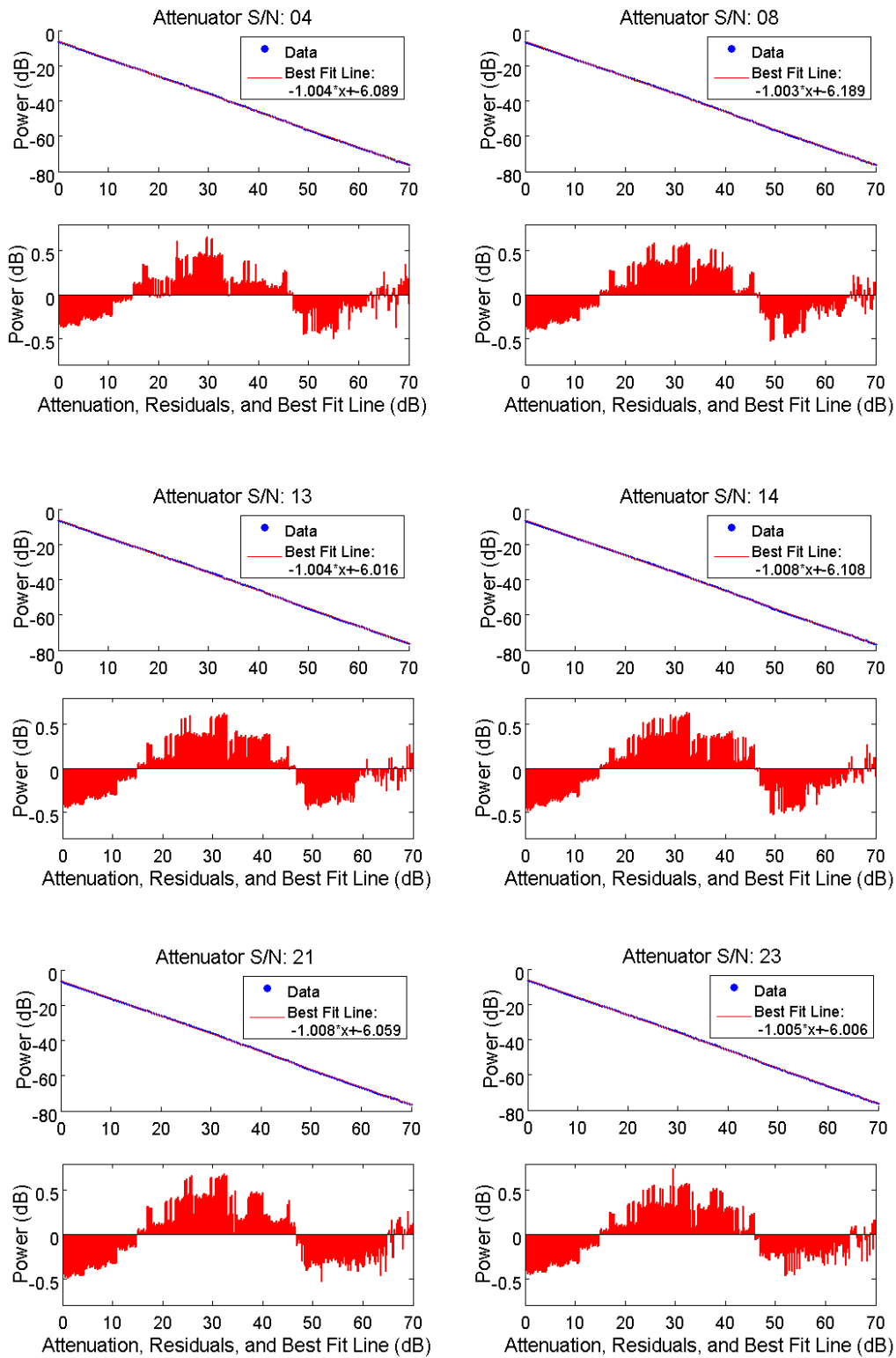


Figure C.4: Testbed programmable attenuator validation measurements, 1540 MHz (near LTE DL).

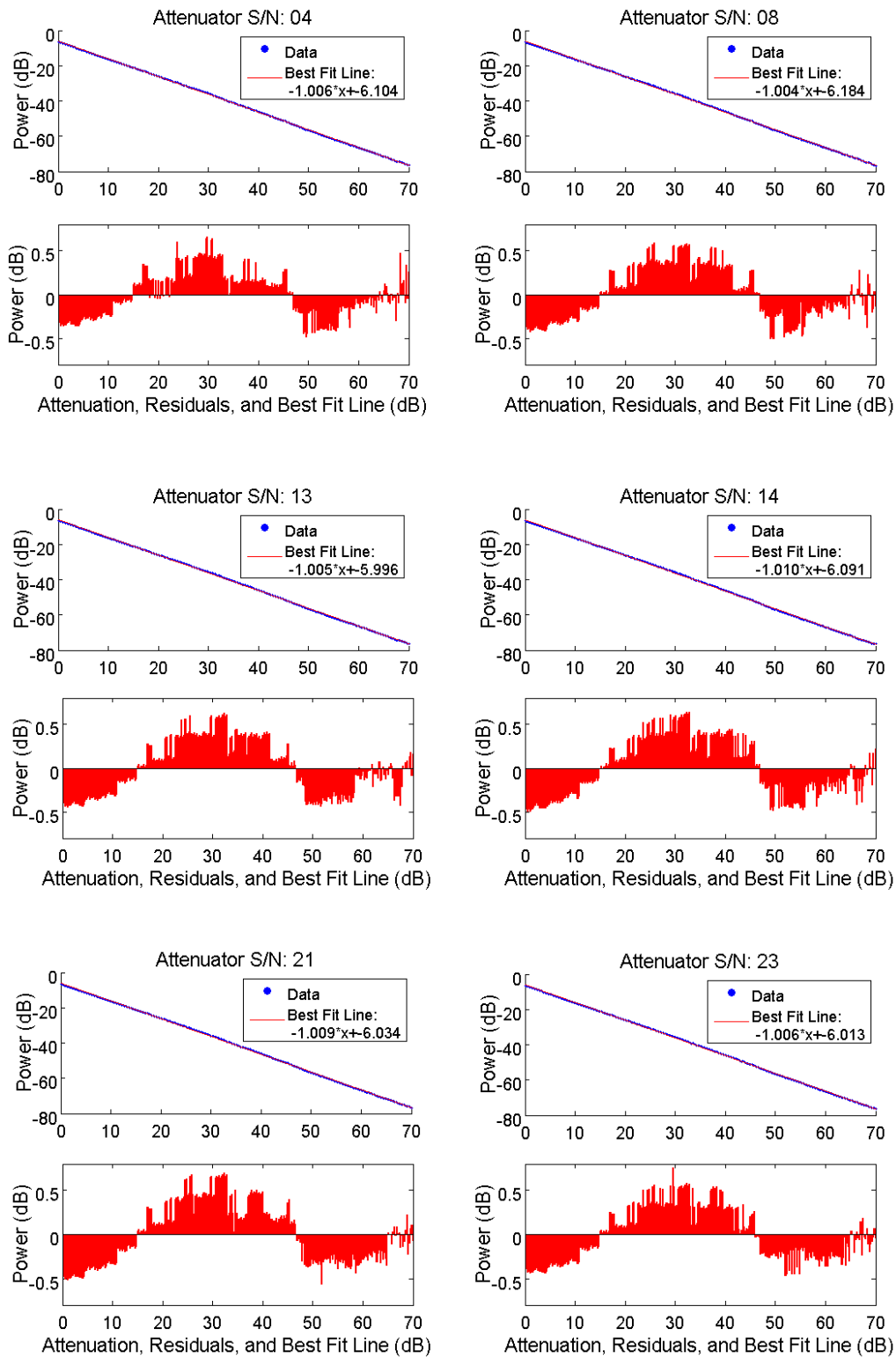


Figure C.5: Testbed programmable attenuator validation measurements, 1580 MHz (near GPS L1 band center).

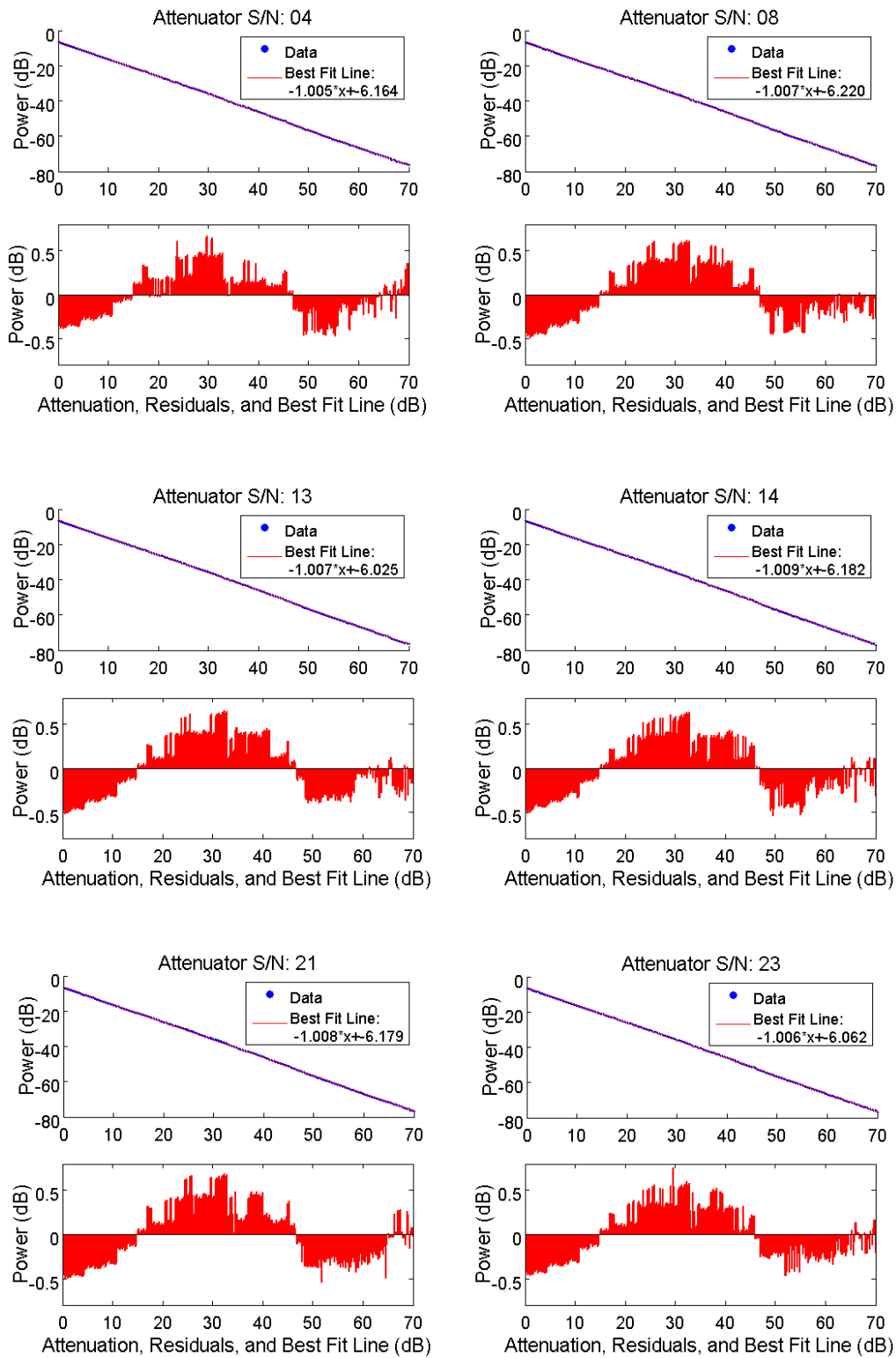


Figure C.6: Testbed programmable attenuator validation measurements, 1640 MHz (near LTE UL1 and LTE UL2).

Table C.16: Serial Number of the Programmable Attenuator Used in Each Signal Path

<b>Serial Number</b>	<b>Signal Path</b>
11604210004	GPS tap (to RTK base)
11604210008	LTE IB DL
11604210013	LTE OOB UL
11604210014	LTE IB UL
11604210021	GPS
11604210023	LTE OOB DL

Table C.17: Uncertainty Budget of the High Power LTE IB DL EIIP.

<b>Uncertainty Classification</b>	<b>Factor</b>	<b>Probability Distribution</b>	<b>Evaluation Type</b>	<b>Designator</b>	<b>Uncertainty</b>	<b>Correction for Distribution</b>	<b>Standard Uncertainty</b>
Antenna Calibration	Non-ideal antennas	Normal	B	U1	0.5 dB	1	0.5 dB
	Spatial variations	Normal	A	U2	0.5 dB	1	0.5 dB
	Network analyzer calibration	Normal	B	U3	0.1 dB	1	0.1 dB
	Frequency flatness	Normal	A	U4	0.2 dB	1	0.2 dB
	Non-circularity of polarization	Normal	B	U5	0.5 dB	1	0.5 dB
	Separation distance	Normal	B	U6	0.2 dB	1	0.2 dB
Instrumentation	Spectrum analyzer	Normal	B	U7	0.5 dB	1	0.5 dB
	Long-term stability	Normal	B	U8	0.1 dB	1	0.1 dB
Testbed	Calibration	Normal	B	U9	0.14 dB	1	0.14 dB
	Amplifier drift	Normal	A	U10	0.75 dB	1	0.75 dB
	Antenna mismatch	U-shaped	B	U11	0.1 dB	0.5	0.05 dB
	Antenna Connection repeatability	Normal	A	U12	0.1 dB	1	0.1 dB
	Separation distance	Normal	A	U10	0.2 dB	1	0.2 dB
	Chamber uniformity	Normal	A	U10	0.5 dB	1	0.5 dB
<b>Combined standard uncertainty:</b>							<b>1.4 dB</b>
<b>Expanded uncertainty (k=2):</b>							<b>2.8 dB</b>

Table C.18: Uncertainty Budget of the Low Power LTE IB DL EIIP.

Uncertainty Classification	Factor	Probability Distribution	Evaluation Type	Designator	Uncertainty	Correction for Distribution	Standard Uncertainty
Antenna Calibration	Non-ideal antennas	Normal	B	U1	0.5 dB	1	0.5 dB
	Spatial variations	Normal	A	U2	0.5 dB	1	0.5 dB
	Network analyzer calibration	Normal	B	U3	0.1 dB	1	0.1 dB
	Frequency flatness	Normal	A	U4	0.2 dB	1	0.2 dB
	Non-circularity of polarization	Normal	B	U5	0.5 dB	1	0.5 dB
	Separation distance	Normal	B	U6	0.2 dB	1	0.2 dB
Instrumentation	Spectrum analyzer	Normal	B	U7	0.5 dB	1	0.5 dB
	Long-term stability	Normal	B	U8	0.2 dB	1	0.2 dB
Testbed	Calibration	Normal	B	U9	0.14 dB	1	0.14 dB
	Amplifier drift	Normal	A	U10	0.1 dB	1	0.1 dB
	Antenna mismatch	U-shaped	B	U11	0.1 dB	0.5	0.05 dB
	Antenna connection Repeatability	Normal	A	U12	0.1 dB	1	0.1 dB
	Separation distance	Normal	A	U10	0.2 dB	1	0.2 dB
	Chamber uniformity	Normal	A	U10	0.5 dB	1	0.5 dB
<b>Combined standard uncertainty:</b>							<b>1.2 dB</b>
<b>Expanded uncertainty (k=2):</b>							<b>2.4 dB</b>

Table C.19: Uncertainty Budget of the LTE IB UL EIIP.

<b>Uncertainty Classification</b>	<b>Factor</b>	<b>Probability Distribution</b>	<b>Evaluation Type</b>	<b>Designator</b>	<b>Uncertainty</b>	<b>Correction for Distribution</b>	<b>Standard Uncertainty</b>
Antenna Calibration	Non-ideal antennas	Normal	B	U1	0.5 dB	1	0.5 dB
	Spatial variations	Normal	A	U2	0.5 dB	1	0.5 dB
	Network analyzer calibration	Normal	B	U3	0.1 dB	1	0.1 dB
	Frequency flatness	Normal	A	U4	0.2 dB	1	0.2 dB
	Non-circularity of polarization	Normal	B	U5	0.5 dB	1	0.5 dB
	Separation distance	Normal	B	U6	0.2 dB	1	0.2 dB
Instrumentation	Spectrum Analyzer	Normal	B	U7	0.5 dB	1	0.5 dB
	Long-term stability	Normal	B	U8	0.1 dB	1	0.1 dB
Testbed	Calibration	Normal	B	U9	0.14 dB	1	0.14 dB
	Amplifier drift	Normal	A	U10	0.1 dB	1	0.1 dB
	Antenna mismatch	U-shaped	B	U11	0.1 dB	0.5	0.05 dB
	Antenna connection repeatability	Normal	A	U12	0.1 dB	1	0.1 dB
	Separation distance	Normal	A	U10	0.2 dB	1	0.2 dB
	Chamber uniformity	Normal	A	U10	0.5 dB	1	0.5 dB
<b>Combined standard uncertainty:</b>							<b>1.2 dB</b>
<b>Expanded uncertainty (k=2):</b>							<b>2.4 dB</b>

Table C.20: Uncertainty Budget of the LTE OOB UL EIIP.

<b>Uncertainty Classification</b>	<b>Factor</b>	<b>Probability Distribution</b>	<b>Evaluation Type</b>	<b>Designator</b>	<b>Uncertainty</b>	<b>Correction for Distribution</b>	<b>Standard Uncertainty</b>
Antenna Calibration	Non-ideal antennas	Normal	B	U1	0.5 dB	1	0.5 dB
	Spatial variations	Normal	A	U2	0.5 dB	1	0.5 dB
	Network analyzer calibration	Normal	B	U3	0.1 dB	1	0.1 dB
	Frequency flatness	Normal	A	U4	0.2 dB	1	0.2 dB
	Non-circularity of polarization	Normal	B	U5	0.5 dB	1	0.5 dB
	Separation distance	Normal	B	U6	0.2 dB	1	0.2 dB
Instrumentation	Spectrum analyzer	Normal	B	U7	0.5 dB	1	0.5 dB
	Long-term stability	Normal	B	U8	0.6 dB	1	0.6 dB
Testbed	Calibration	Normal	B	U9	0.14 dB	1	0.14 dB
	Amplifier drift	Normal	A	U10	0.1 dB	1	0.1 dB
	Antenna mismatch	U-shaped	B	U11	0.1 dB	0.5	0.05 dB
	Antenna connection repeatability	Normal	A	U12	0.1 dB	1	0.1 dB
	Separation distance	Normal	A	U10	0.2 dB	1	0.2 dB
	Chamber uniformity	Normal	A	U10	0.5 dB	1	0.5 dB
<b>Combined standard uncertainty:</b>							<b>1.3 dB</b>
<b>Expanded uncertainty (k=2):</b>							<b>2.7 dB</b>

Table C.21: Uncertainty Budget of the GPS EIIP.

Uncertainty Classification	Factor	Probability Distribution	Evaluation Type	Designator	Uncertainty	Correction for Distribution	Standard Uncertainty
Antenna Calibration	Non-ideal antennas	Normal	B	U1	0.5 dB	1	0.5 dB
	Spatial variations	Normal	A	U2	0.5 dB	1	0.5 dB
	Network analyzer calibration	Normal	B	U3	0.1 dB	1	0.1 dB
	Frequency flatness	Normal	A	U4	0.2 dB	1	0.2 dB
	Non-circularity of polarization	Normal	B	U5	0.5 dB	1	0.5 dB
	Separation distance	Normal	B	U6	0.2 dB	1	0.2 dB
Instrumentation	Spectrum analyzer	Normal	B	U7	0.5 dB	1	0.5 dB
	Long-term stability	Normal	B	U8	0.1 dB	1	0.1 dB
Testbed	Calibration	Normal	B	U9	0.14 dB	1	0.14 dB
	Amplifier drift	Normal	A	U10	0.1 dB	1	0.1 dB
	Antenna mismatch	U-shaped	B	U11	0.1 dB	0.5	0.05 dB
	Antenna connection repeatability	Normal	A	U12	0.1 dB	1	0.1 dB
	Separation distance	Normal	A	U10	0.2 dB	1	0.2 dB
	Chamber uniformity	Normal	A	U10	0.5 dB	1	0.5 dB
<b>Combined standard uncertainty:</b>							<b>1.2 dB</b>
<b>Expanded uncertainty (k=2):</b>							<b>2.4 dB</b>



## D Validation of Conducted Transmitter Performance

The goal of tests in this appendix is to detail checks for substantial performance concerns in physical layer behavior of the testbed. Unlike *calibration* quantities and procedures, the validation results are not used in any measurement equations for GPS receiver input conditions.

### D.1 Validation Test Uncertainties

Uncertainty estimates of validation measurements are provided in this appendix, as they are in Chapter 3 via Appendix C.

The calculation process for uncertainty of the validation quantities are not provided here in detail. Generally, the basis for the uncertainty estimates was:

- tools or guidelines for instrument measurement uncertainty, as provided by the manufacturer of the instruments, and
- the law of propagation of uncertainty [6] applied according to the measurement equations that are applied to test data.

### D.2 Isolation Between Signal Paths

The goal of isolation testing here is to determine the coupled power leaking between signal paths. This effect manifests as reverse power traveling from one signal path backward into the generator or amplifier in another signal path.

#### D.2.1 Overview

The test configuration for determining coupled power into one signal path from all of the other signal paths is illustrated in Figure D.1. Each test is performed at the output of the amplifier or generator that is furthest downstream in each signal path. The choice of this reference plane helps to ensure that isolation levels are studied where they have the most significant potential impact on the system.

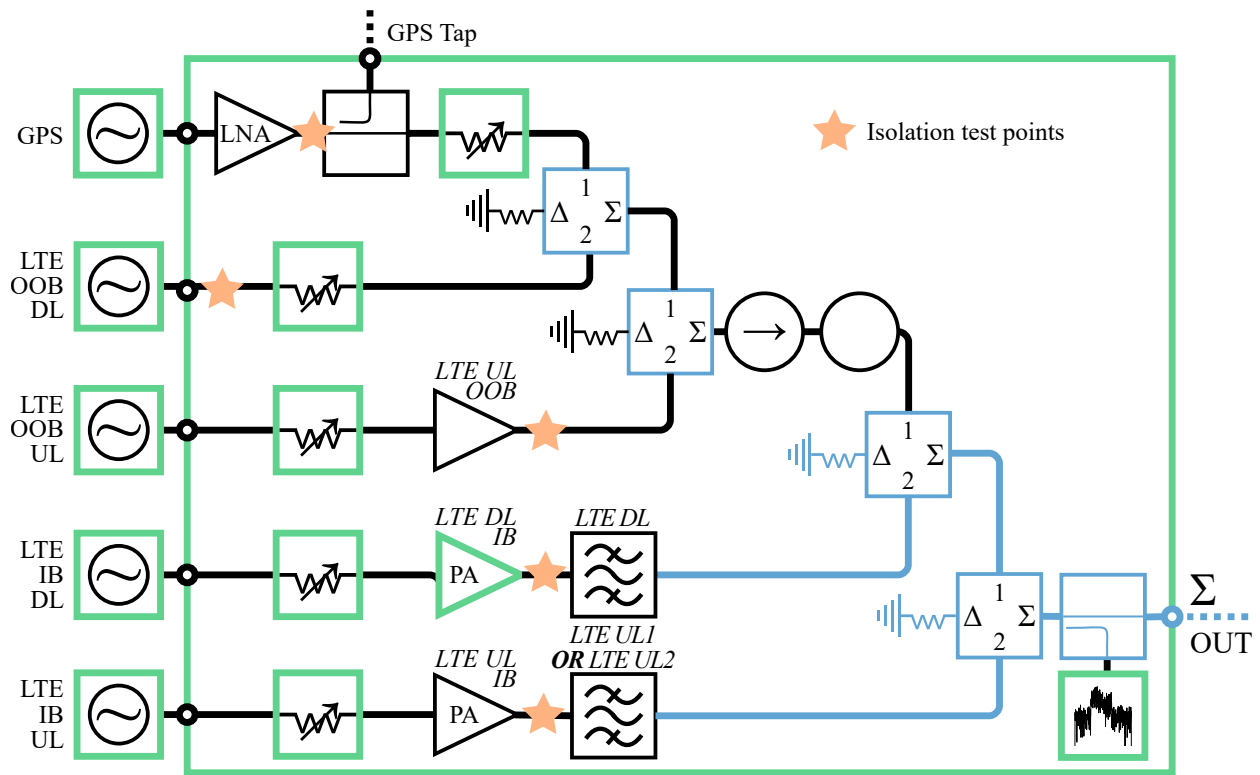


Figure D.1: Test points probed in tests of isolation between signal paths.

Table D.1: Reverse Power Across Signal Paths

Test Point	Source Path					
	LTE IB DL	LTE IB UL1	LTE OOB UL	LTE OOB DL	GPS	
LTE IB DL	—	—	—	—	—	dBm
LTE IB UL1	—	—	-20.7	—	—	dBm
LTE OOB UL	-39.3	-36.4	—	-49.6	-70.2	dBm
LTE OOB DL	-54.4	-46.6	-85.9	—	—	dBm
GPS	-80.3	—	-38.4	—	—	dBm

*All power levels are total power output across the full signal bandwidth  
 Signals that were too weak to detect are denoted by —*

Table D.2: Forward Power at each Signal Test Point

Test Point	Source Path				
	LTE IB DL	LTE IB UL1	LTE OOB UL	LTE OOB DL	GPS
LTE IB DL	52.4				
LTE IB UL1		40.6			
LTE OOB UL			32.0		
LTE OOB DL				-36.1	
GPS					-7.9

*All power levels are total power output across the full signal bandwidth*

Table D.3: Offset Corrections from Signal PSD to Total Signal Power

Signal	Valid PSD Frequencies	Offset
GPS	1575.42 MHz	15.6 dB(Hz)
LTE OOB DL	1541 MHz — 1559 MHz, 1610 MHz — 1650 MHz	27.6 dB(Hz)
LTE OOB UL	1624.6 MHz	10.4 dB(Hz)

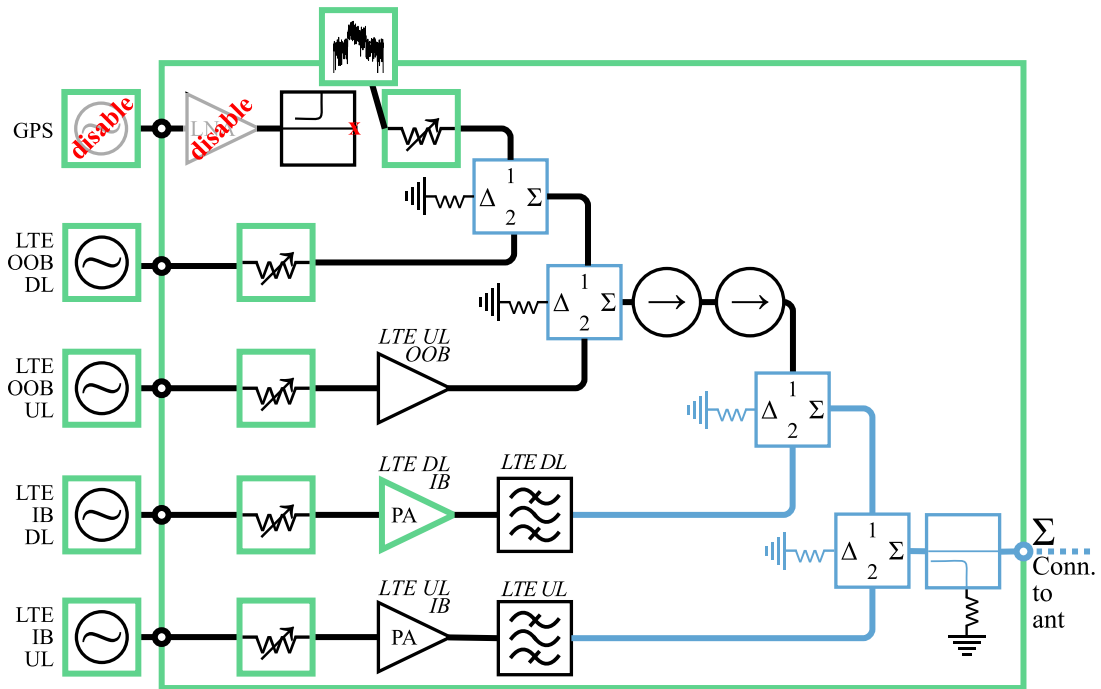
## D.2.2 Measurements at Each Test Point

Test methods and spectrum analyzer captures are shown here for forward and reverse power in each test point (and for both UL1 and UL2 filters).

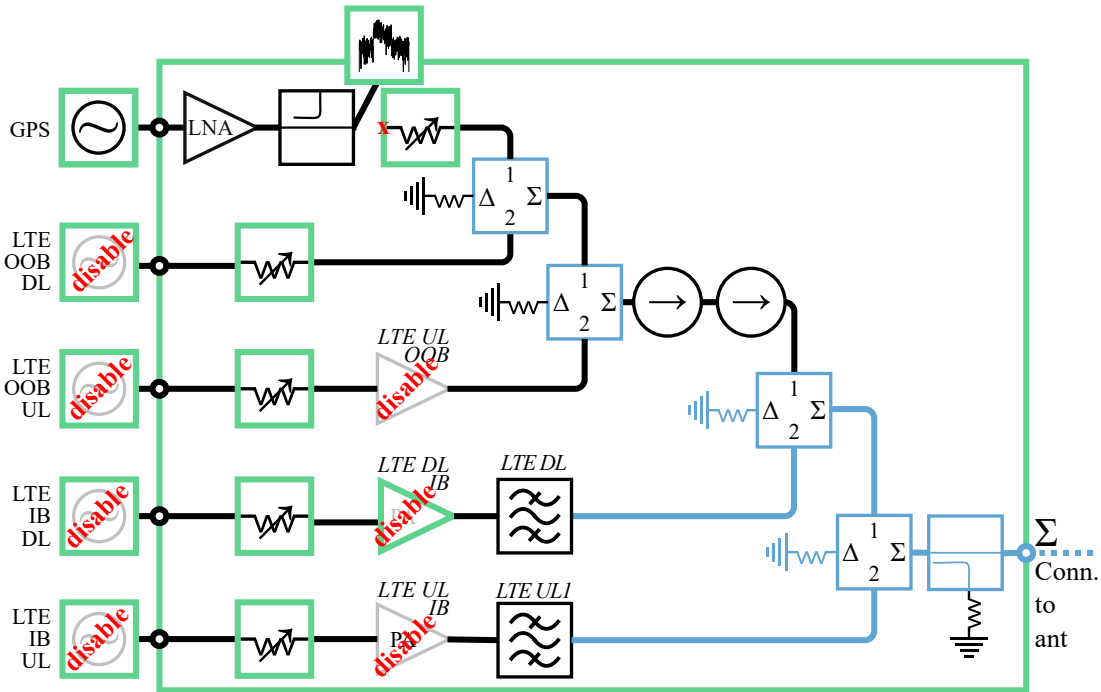
A substitution method is employed at each test point. When forward power is large, power attenuators were inserted inline between the signal source and the spectrum analyzer, and the attenuation (in positive decibels) were set as the amplitude offset in the spectrum analyzer. The specified output VSWR of the amplifier (and in-band impedances of the components impedances) are all smaller than 2:1, so the error added to the validation result should be small.

Each variable attenuator is set at the minimum attenuation (i.e., maximum transmission) condition used in tests. All LTE attenuators are set to 0 dB, and the GPS attenuator was set at its calibrated operating value of approximately 35-40 dB.

Measurements of coupled power at each test point were performed by turning on all other signal paths to reduce the amount of data collected. Some of these coupled signals contained overlapping frequency components. Table D.3 lists corrections that convert between displayed PSD and total output power in the path. The result is valid for each signal's characteristic PSD averaged a large number of times.

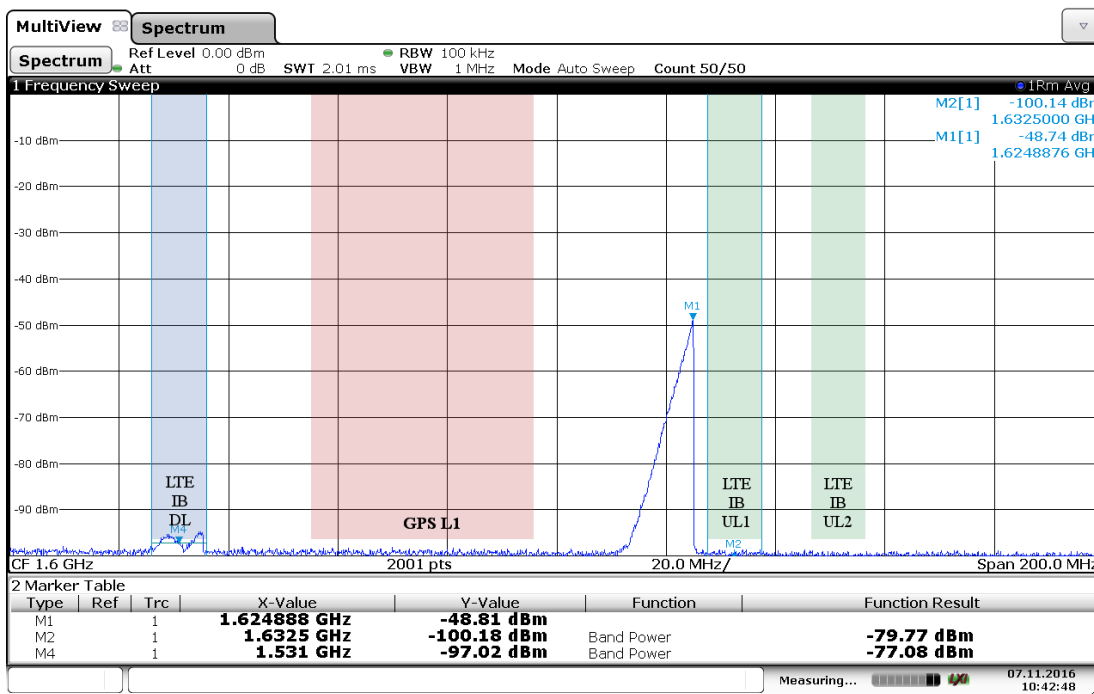


(a) Reverse coupled power



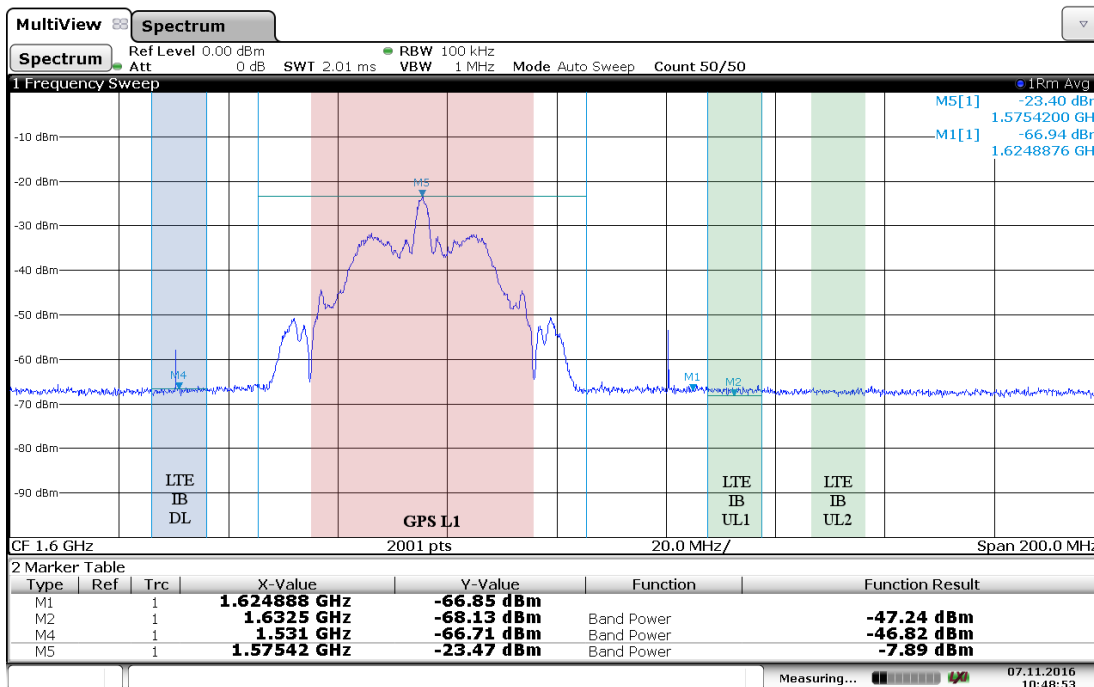
(b) Forward power

Figure D.2: GPS isolation tests: Test circuit for comparing reverse coupled power against forward power



Date: 7.NOV.2016 10:42:48

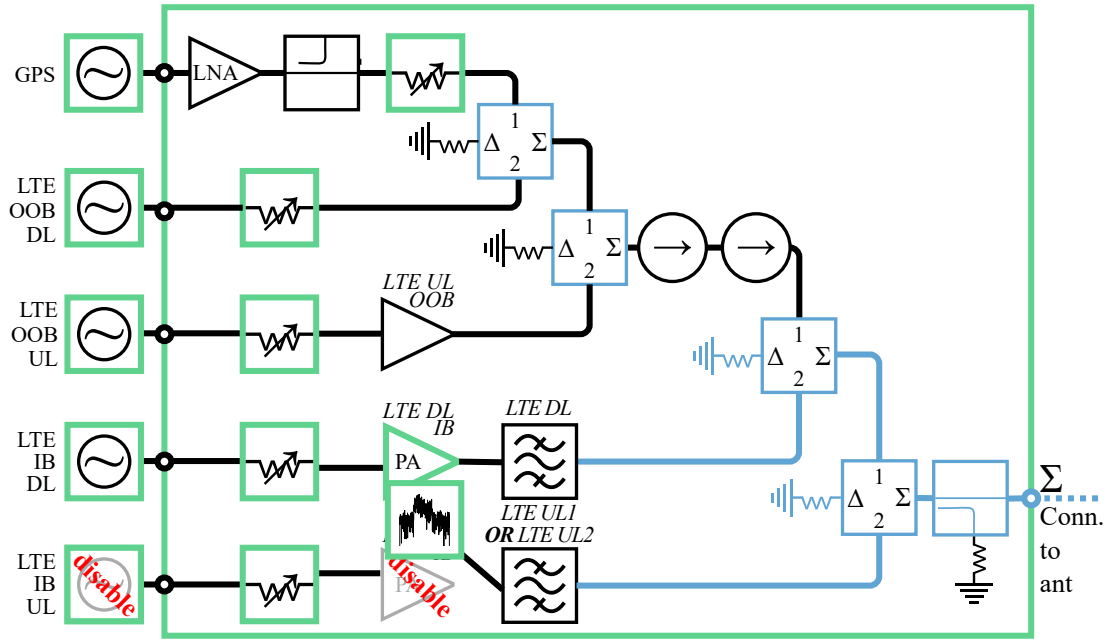
(a) Reverse coupled power at GPS amplifier output, with all LTE signals at maximum



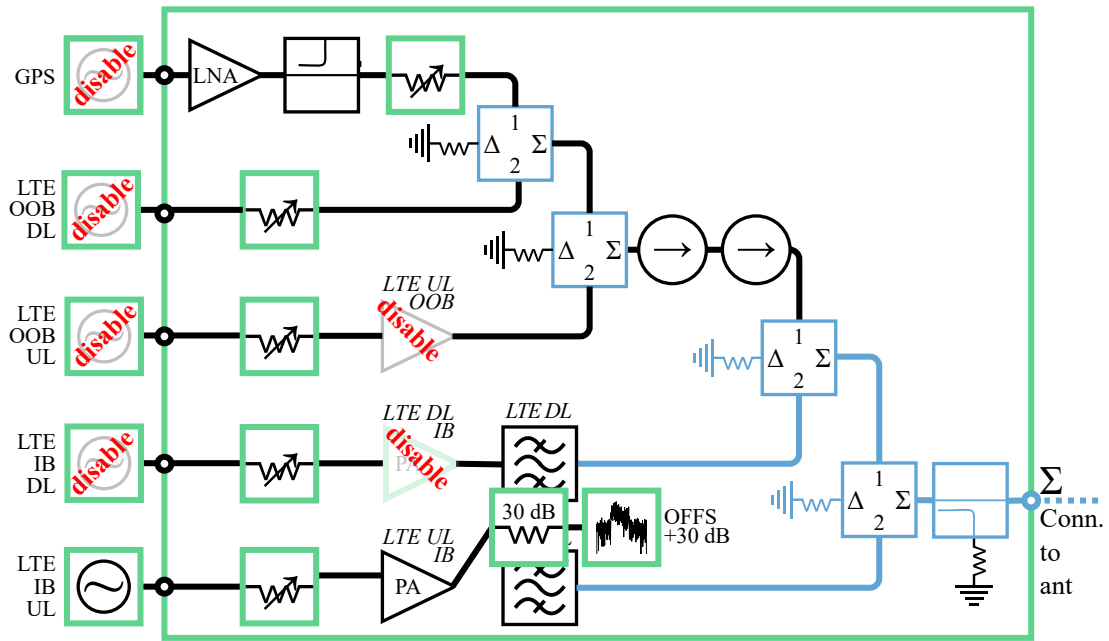
Date: 7.NOV.2016 10:48:53

(b) Forward power at GPS amplifier output

Figure D.3: GPS isolation tests: Comparison of reverse and forward power spectra

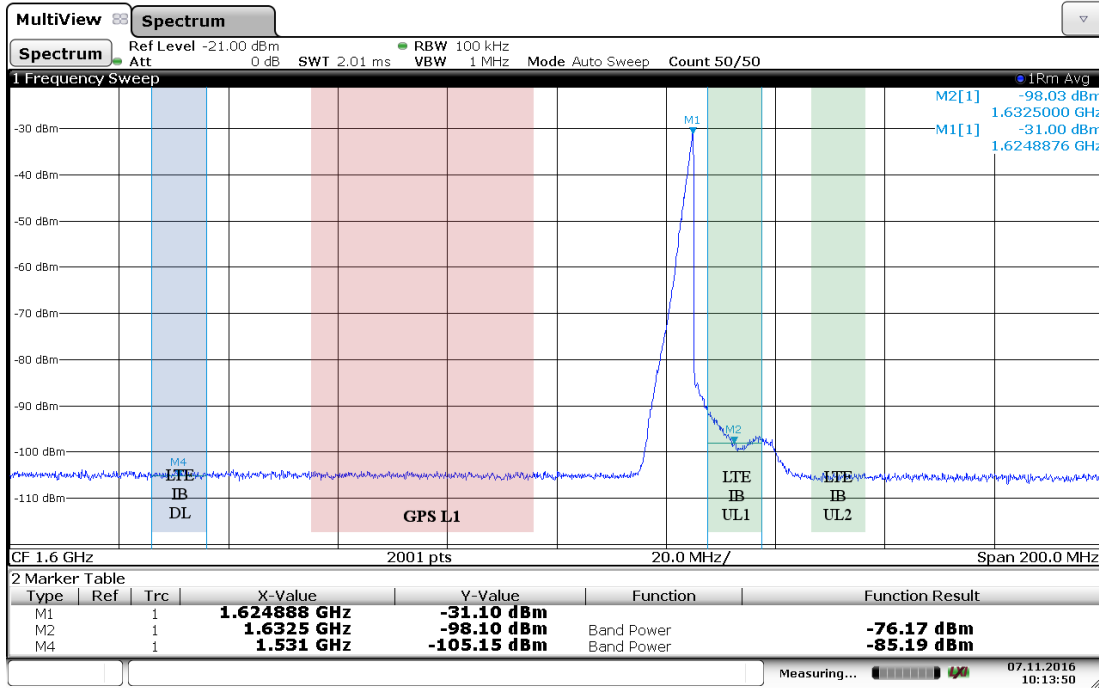


(a) Reverse coupled power



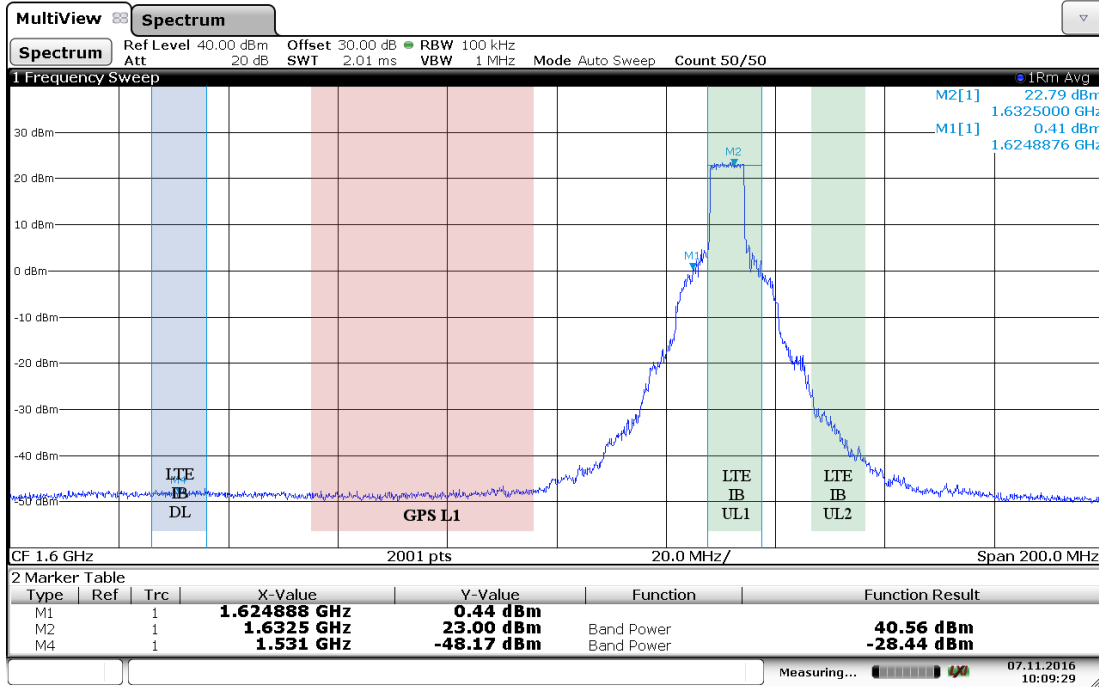
(b) Forward power

Figure D.4: LTE IB UL1 and UL2 isolation tests: Test circuit for comparing reverse coupled power against forward power. Switching between tests of bands UL1 and UL2 is achieved by substituting the indicated cavity filter block.



Date: 7.NOV.2016 10:13:50

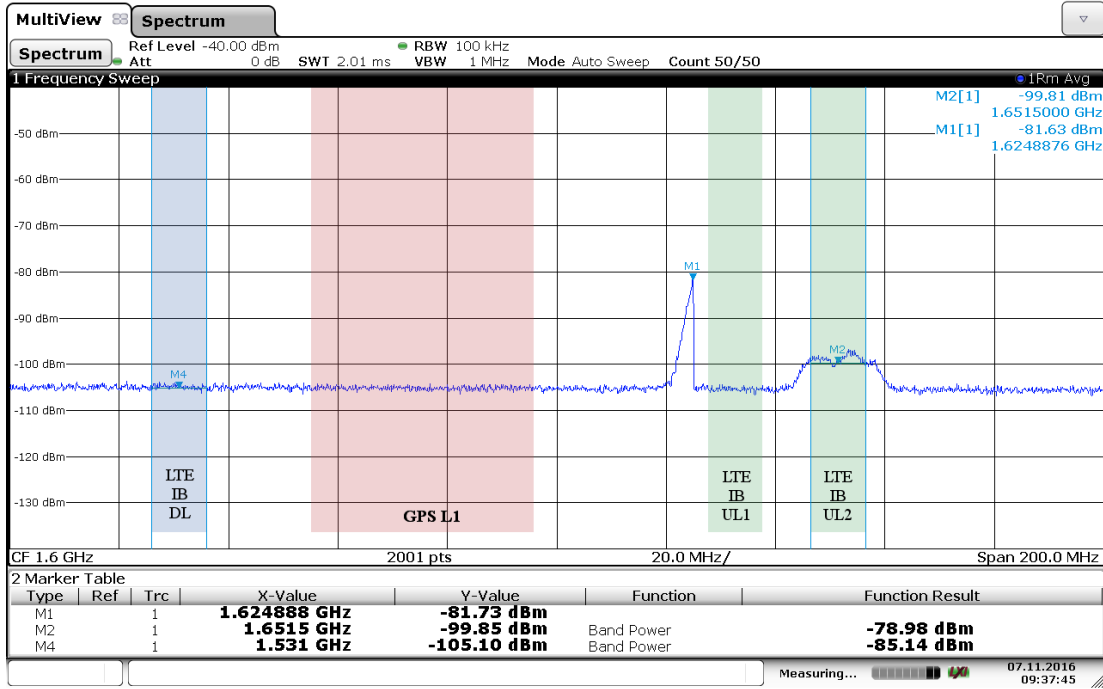
(a) Reverse coupled power at LTE IB UL amplifier output; all other LTE signals at maximum



Date: 7.NOV.2016 10:09:29

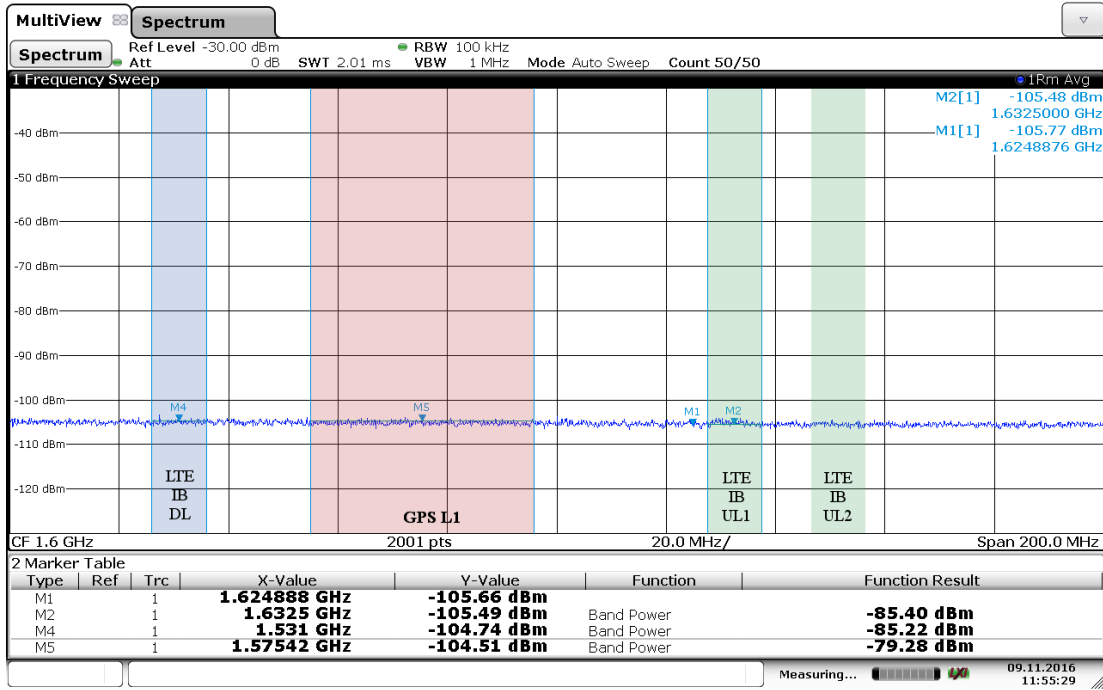
(b) Forward power at LTE IB UL amplifier output

Figure D.5: LTE IB UL1 isolation tests: Comparison of forward and reverse power spectra



Date: 7.NOV.2016 09:37:46

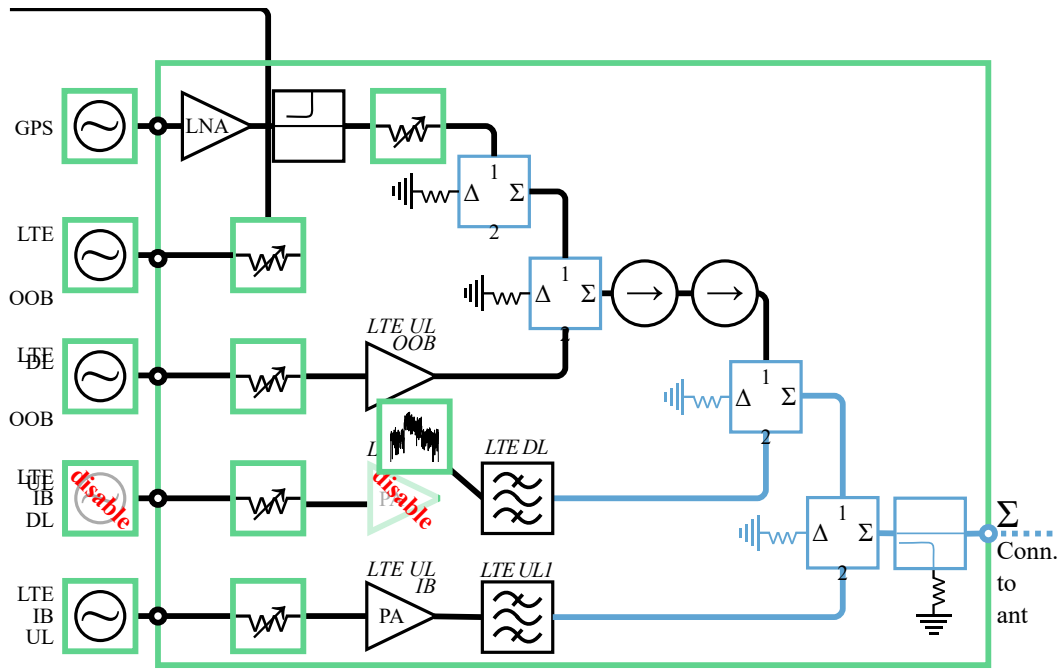
(a) Reverse coupled power at LTE IB UL amplifier output, all other LTE signals at maximum



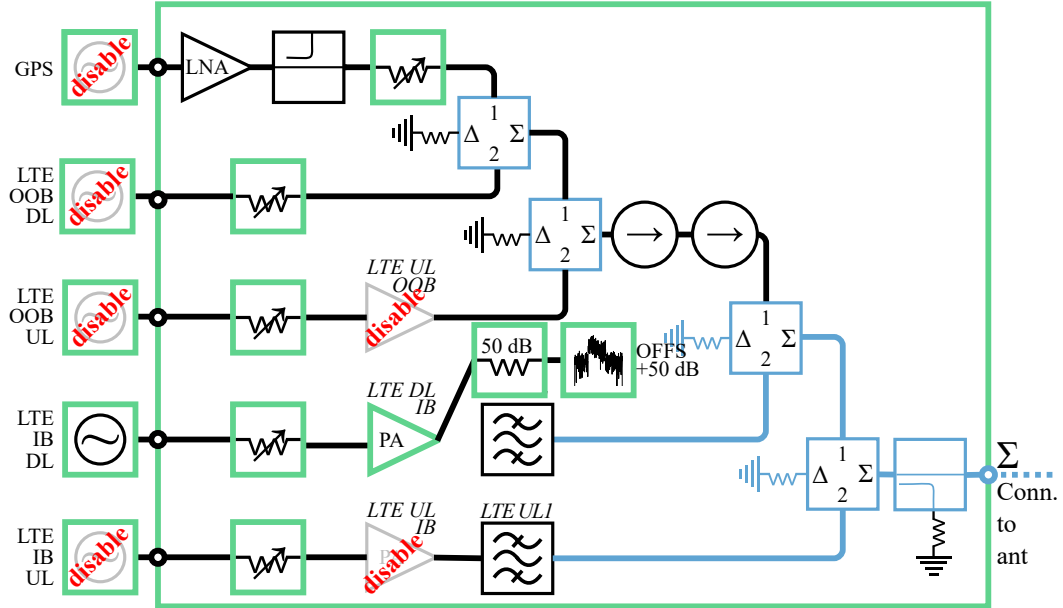
Date: 9.NOV.2016 11:55:29

(b) Forward power at LTE IB UL amplifier output

Figure D.6: LTE IB UL2 isolation tests: Comparison of forward and reverse power spectra

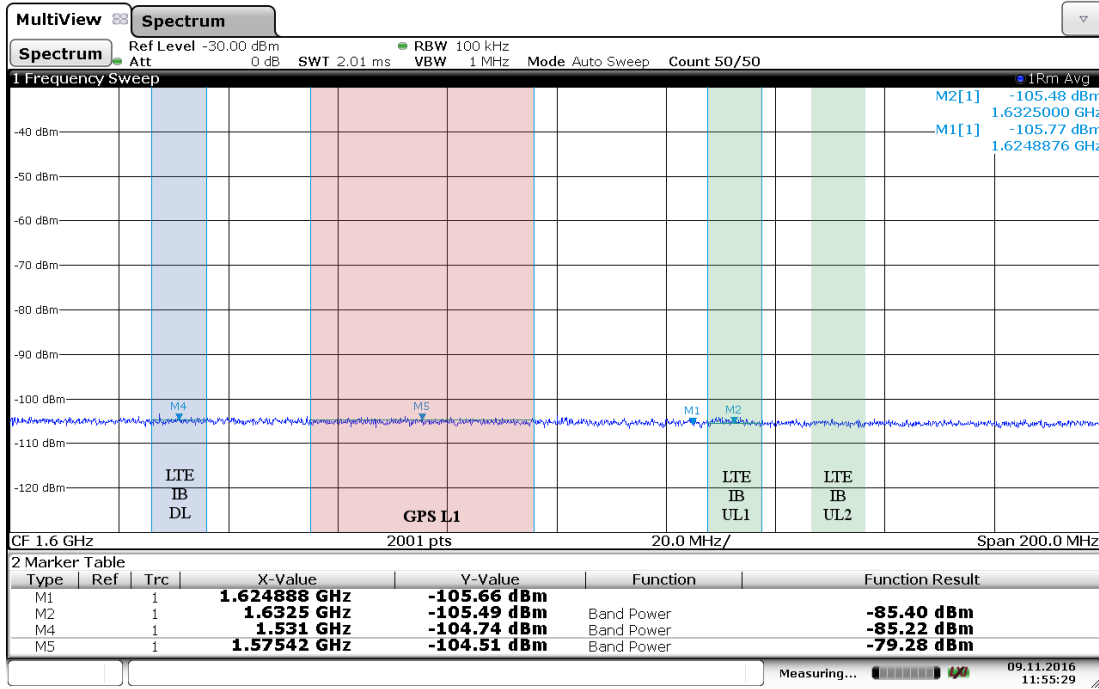


(a) Reverse coupled power



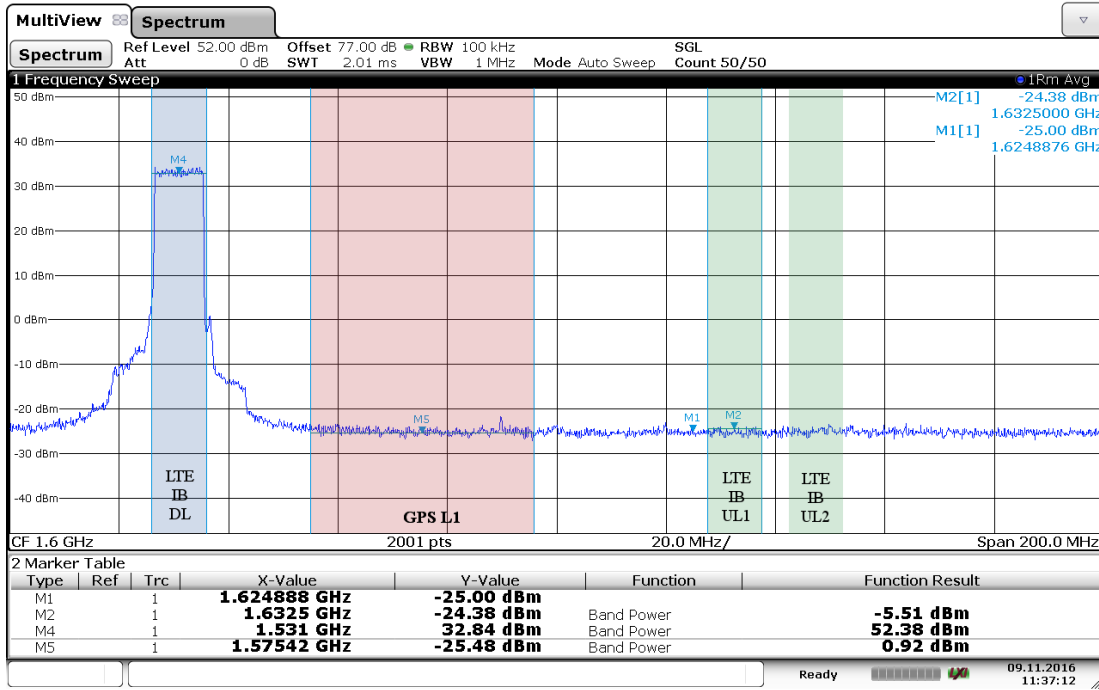
(b) Forward power

Figure D.7: LTE IB DL isolation tests: Test circuit for comparing reverse coupled power against forward power



Date: 9.NOV.2016 11:55:29

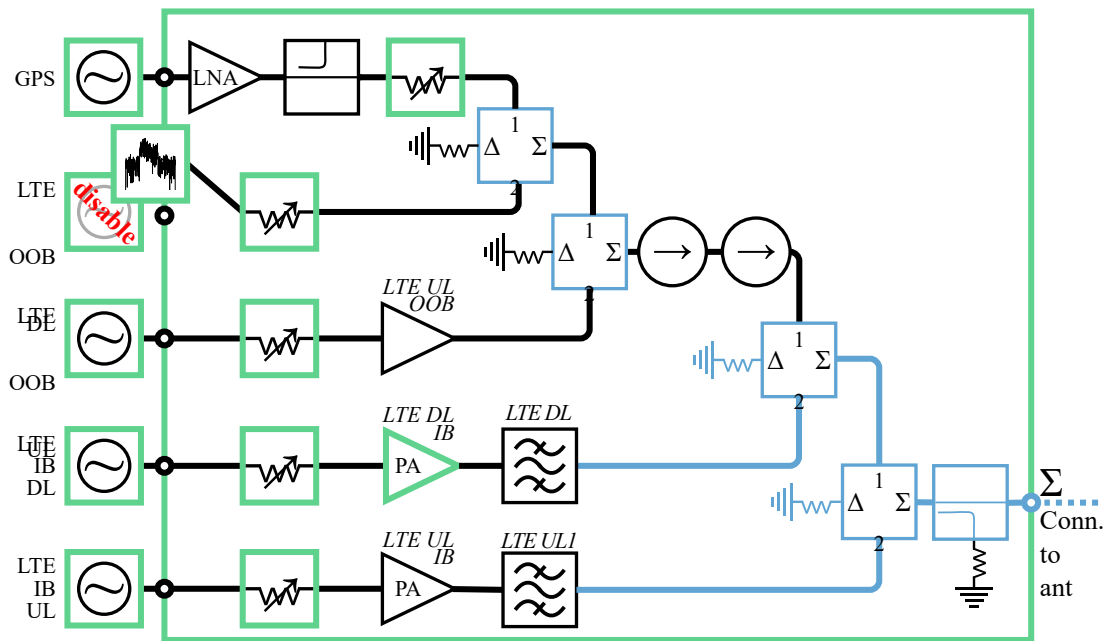
(a) Reverse coupled power at LTE IB DL amplifier output, all other LTE signals at maximum



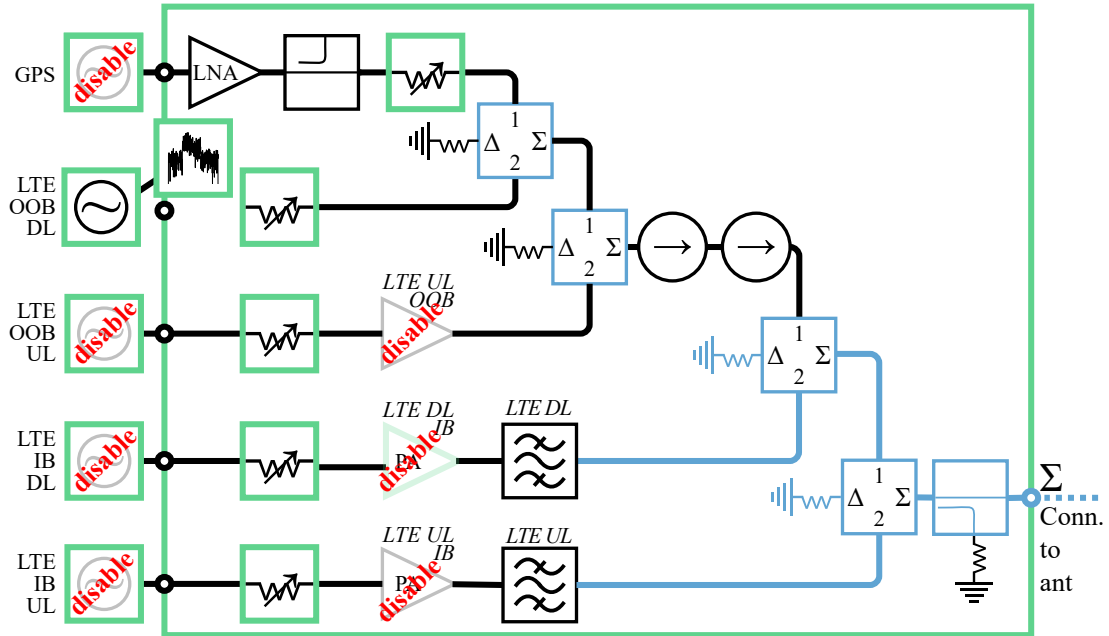
Date: 9.NOV.2016 11:37:12

(b) Forward power at LTE IB DL amplifier output

Figure D.8: LTE IB DL isolation tests: Comparison of forward and reverse power spectra

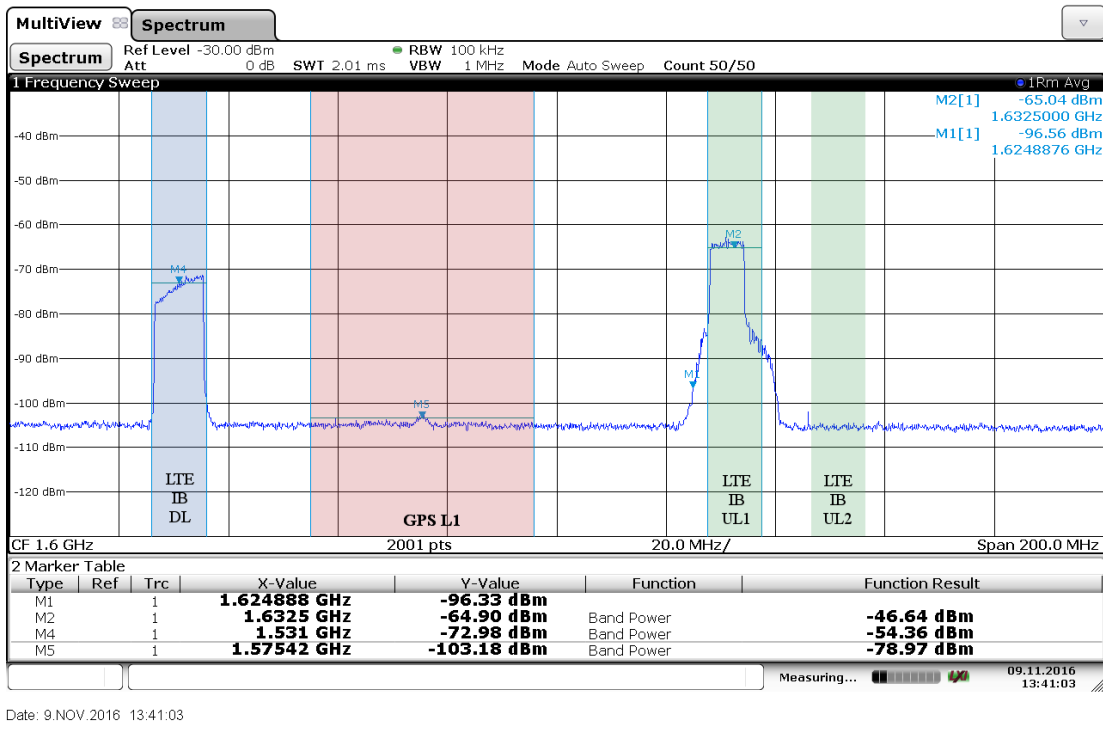


(a) Reverse coupled power

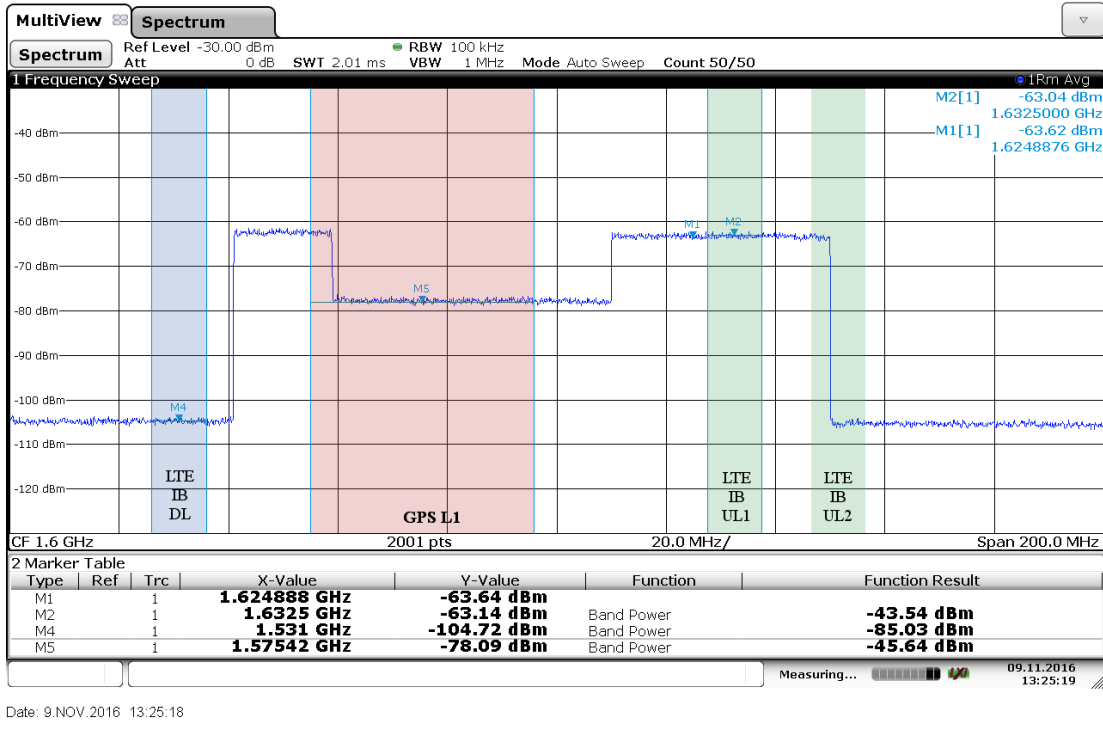


(b) Forward power

Figure D.9: LTE OOB DL isolation tests: Test circuit for comparing reverse coupled power against forward power

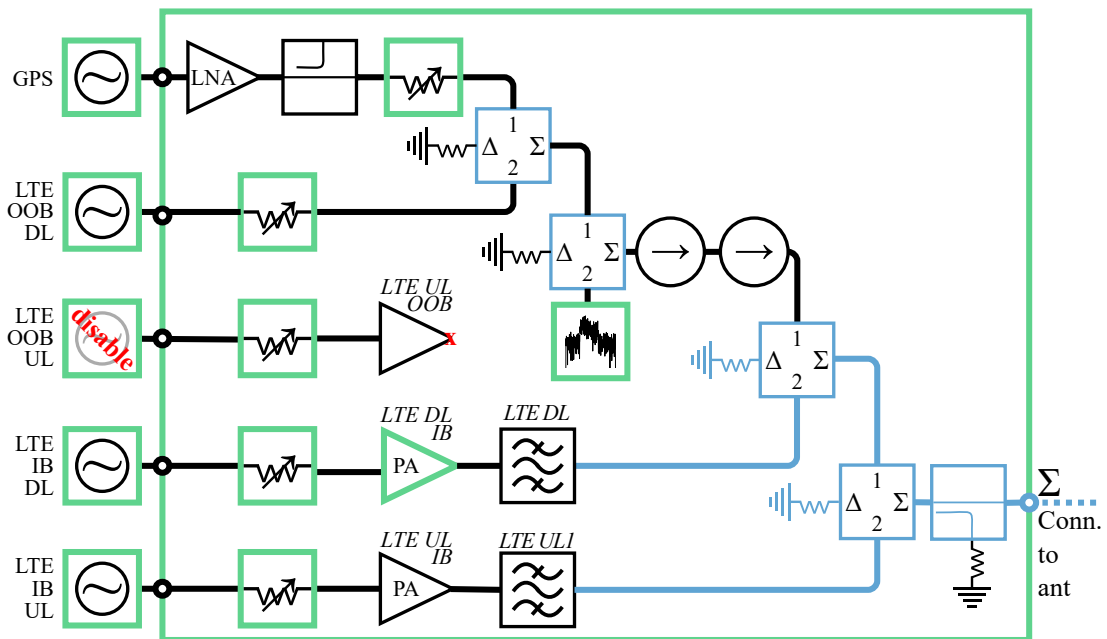


(a) Reverse coupled power at LTE OOB DL signal generator output, all other LTE signals at maximum

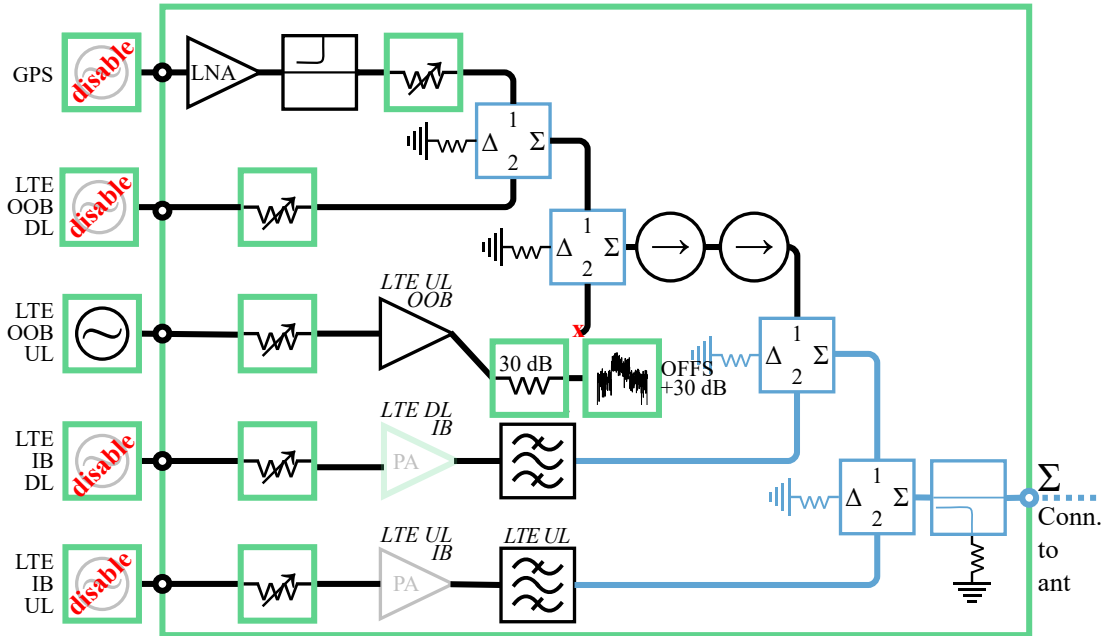


(b) Forward power at LTE OOB DL signal generator output

Figure D.10: LTE OOB DL isolation tests: Comparison of forward and reverse power spectra

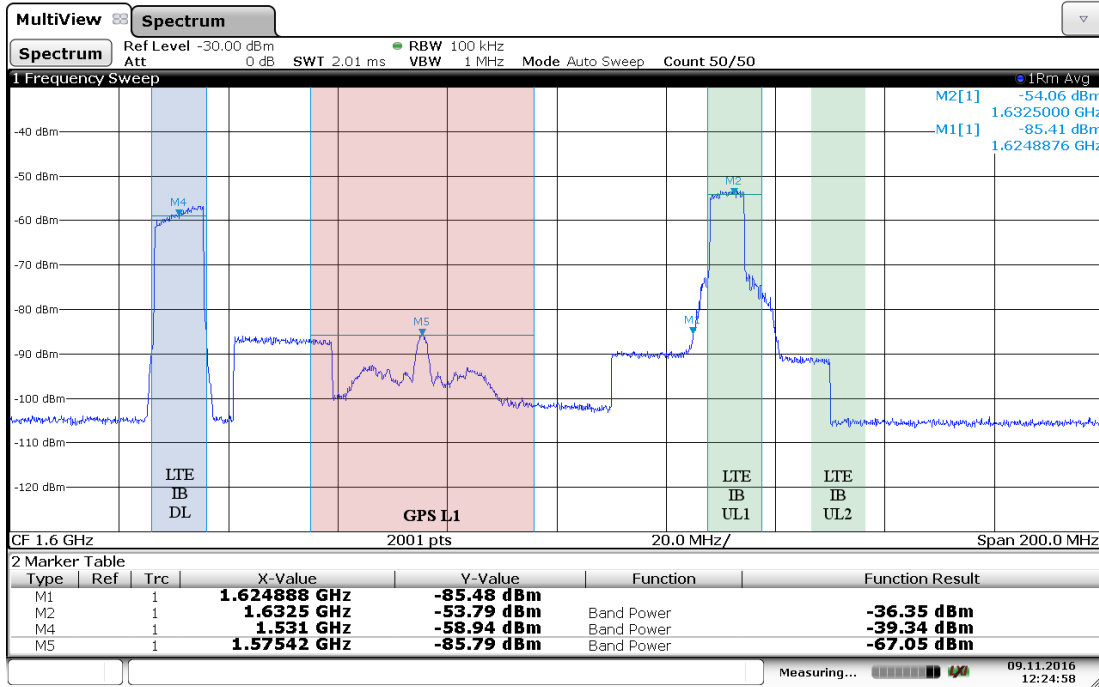


(a) Reverse coupled power



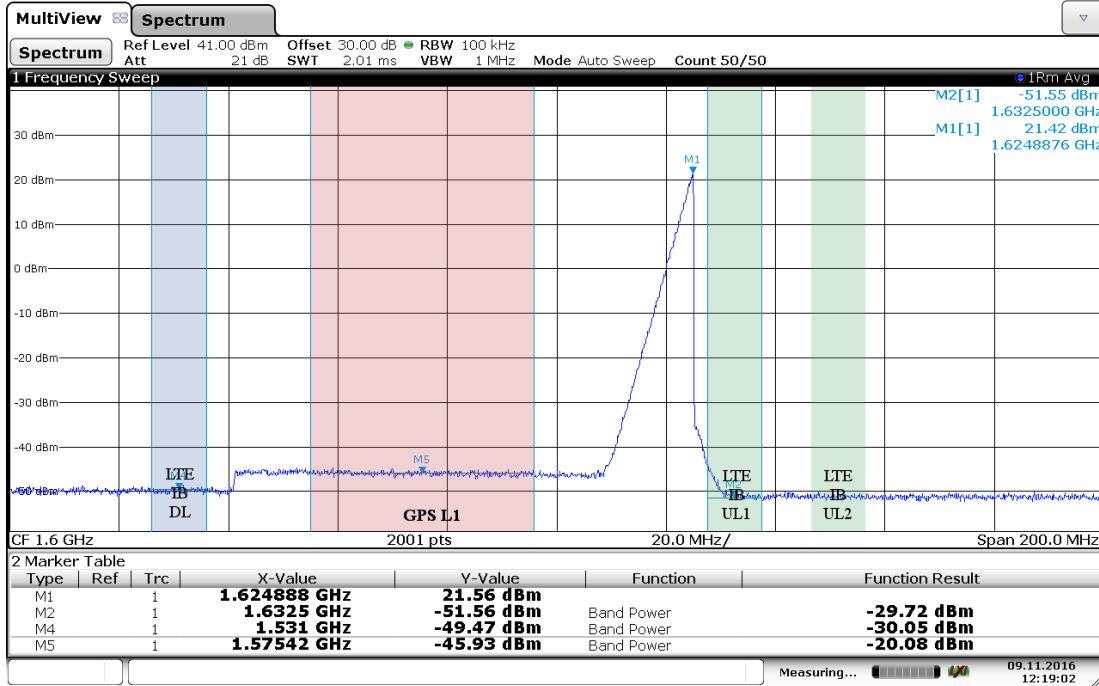
(b) Forward power

Figure D.11: LTE OOB UL isolation tests: Test circuit for comparing reverse coupled power against forward power



Date: 9.NOV.2016 12:24:58

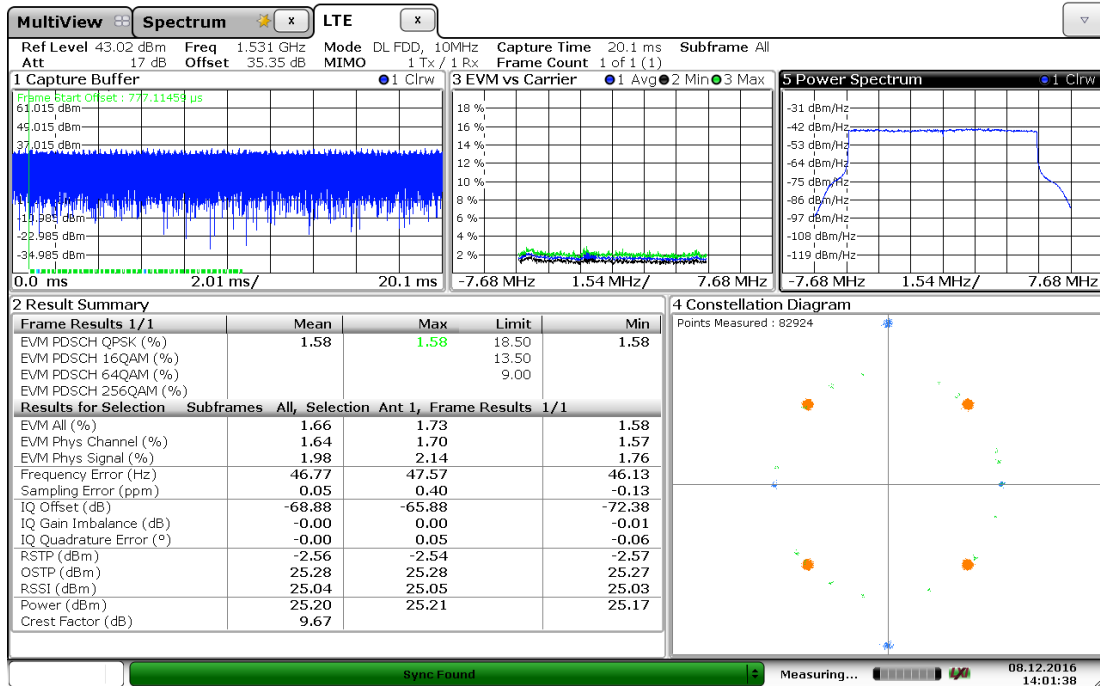
(a) Reverse coupled power at LTE OOB UL amplifier output, all other LTE signals at maximum



Date: 9.NOV.2016 12:19:01

(b) Forward power at LTE OOB UL amplifier output

Figure D.12: LTE OOB UL isolation tests: Comparison of forward and reverse power spectra. Note that “reverse power” scale in (a) is 70 dB weaker than that of the forward power (b).



Date: 8 DEC. 2016 14:01:37

Figure D.13: Spectrum analyzer capture of LTE Evaluation Suite. DL signal drive level 20 dB below maximum, low-distortion amplifier response.

### D.3 Signal Fidelity of LTE Output Modulation

To ensure that the LTE signals that we generated are representative of actual LTE signals with acceptable levels of noise and distortion, we used the LTE analysis tools built into the spectrum analyzer to evaluate LTE modulation fidelity. This tool included several windows, each of which evaluated a different characteristic of the LTE signal.

#### D.3.1 In-Band Downlink

An example of an LTE DL signal with low-distortion performance and a drive level 20 dB below the maximum is shown in Figure D.13. Here, Window 1 (top left) shows the capture buffer, which does not provide much insight for our application. Window 2 (lower left) shows a summary of signal parameters. The most important of these are:

- The error vector magnitude (EVM) indicates the quality of digital modulation. Low EVM — a few percent up to about 20% — is “acceptable.” It measures the distortion in a signal constellation (described below).
- Power indicates the average LTE power to the transmitting antenna
- Crest factor, also known as PAR, indicates the amount by which the peak transmitted power exceeds the average power and should be approximately 10 dB for the downlink signal and 6

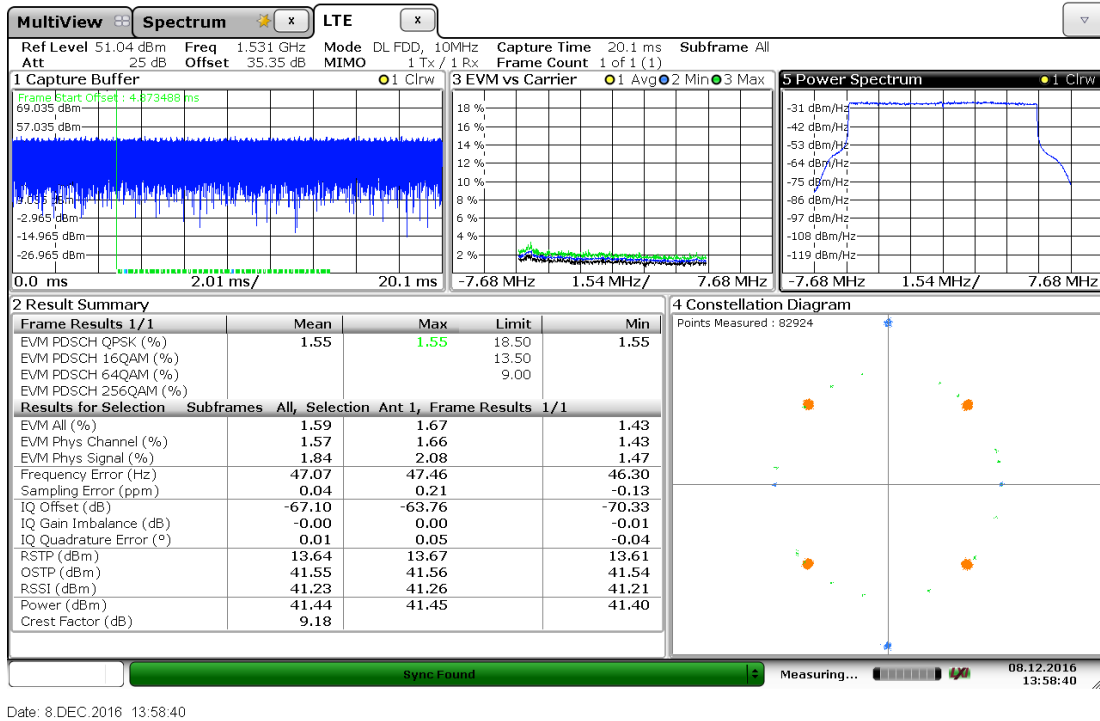


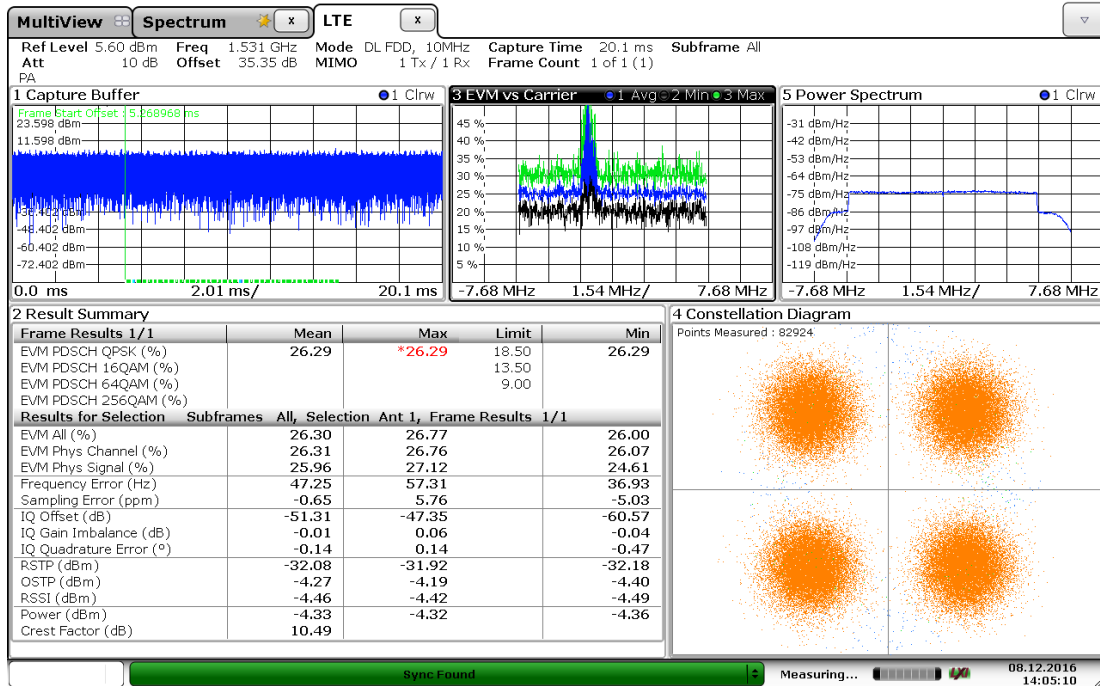
Figure D.14: Spectrum analyzer capture of LTE Evaluation Suite. DL signal drive level at maximum, distorted amplifier response.

dB for the uplink signal. Window 3 (top center) shows EVM vs carrier.

Narrowband interference can affect the EVM of individual carriers, but allows communication on others. Again, lower values indicate less distortion than higher values. Window 4 (lower right) shows the constellation diagram. Here, the orange points indicate the observed constellation. Larger “clouds” correspond to larger EVMs. Finally, Window 5 (top right) shows the power spectrum, which should be relatively flat with sharp rolloff on the edges.

As the drive power increases, there was a risk that the associated amplifier could be overdriven into a nonlinear region. This was indicated by 1) an increase in EVM, and therefore the size of the orange “clouds” in Window 4, 2) a decrease in crest factor, and 3) possibly a distortion in the shape of the power spectrum. An example display for the DL LTE signal driven at maximum system power is shown in Figure D.14. Here there was essentially no significant degradation, although the crest factor decreased marginally.

At lower drive power, amplifier noise became a significant issue. This is more apparent for high-power amplifiers such as those used for the LTE DL. Figure D.15 shows the case where the drive power was 50 dB below maximum. Here there was significant degradation in performance, with an EVM that exceeded the limit of 18.5%, with significant distortion just below midband in Window 3. This was due to spurious signals generated by the amplifier. The orange blobs in Window 4 became much larger.



Date: 8 DEC.2016 14:05:09

Figure D.15: Spectrum analyzer capture of LTE Evaluation Suite. DL signal drive level 50 dB below maximum, dominated by amplifier noise.

### D.3.2 In-Band Uplink

Characteristics of the LTE UL are shown for 1) a drive power of 10 dB below maximum as an example lower distortion performance in Figure D.16, 2) at the maximum for an example of a distorted signal in Figure D.17, and 3) 60 dB below the maximum for an example of noise-floor distortions in Figure D.18. Notice that in all cases, the EVM was below the test limit, which indicates an acceptable LTE performance. At maximum UL power, the crest factor was reduced, and rolloff at the edge of the band was reduced. For the low-power case, the crest factor was unaffected, but the rolloff at the edge appears reduced, although this was most likely due to the noise floor of the spectrum analyzer.

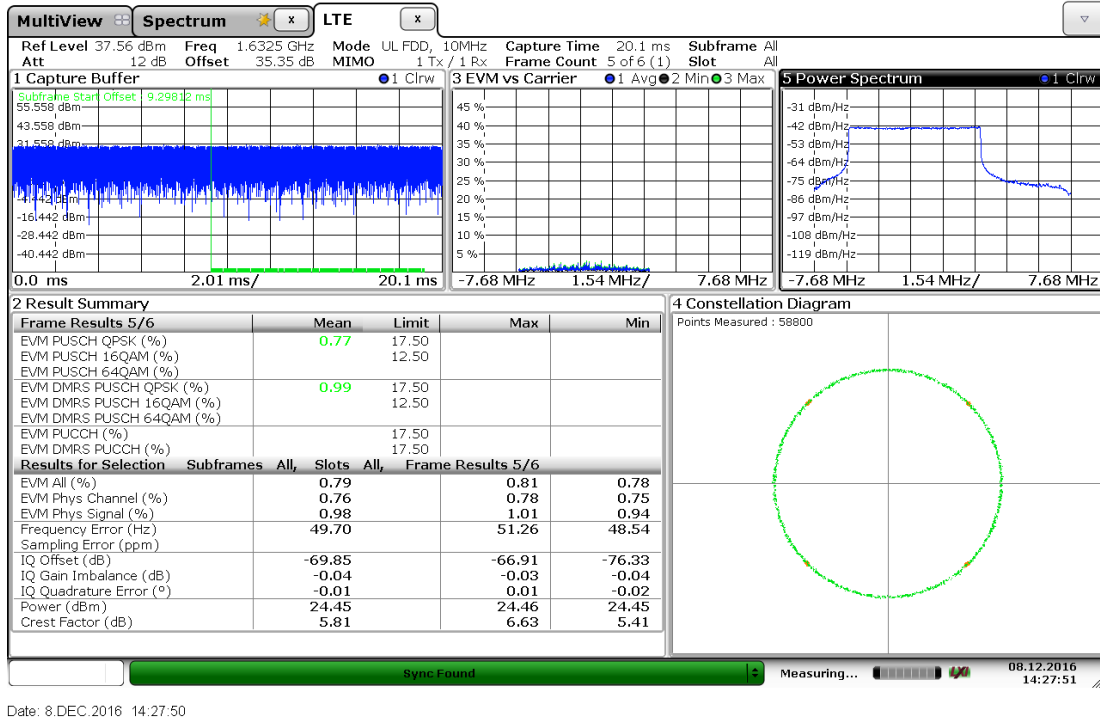


Figure D.16: Spectrum analyzer capture of LTE Evaluation Suite. UL signal drive level 10 dB below maximum, low-distortion amplifier response.

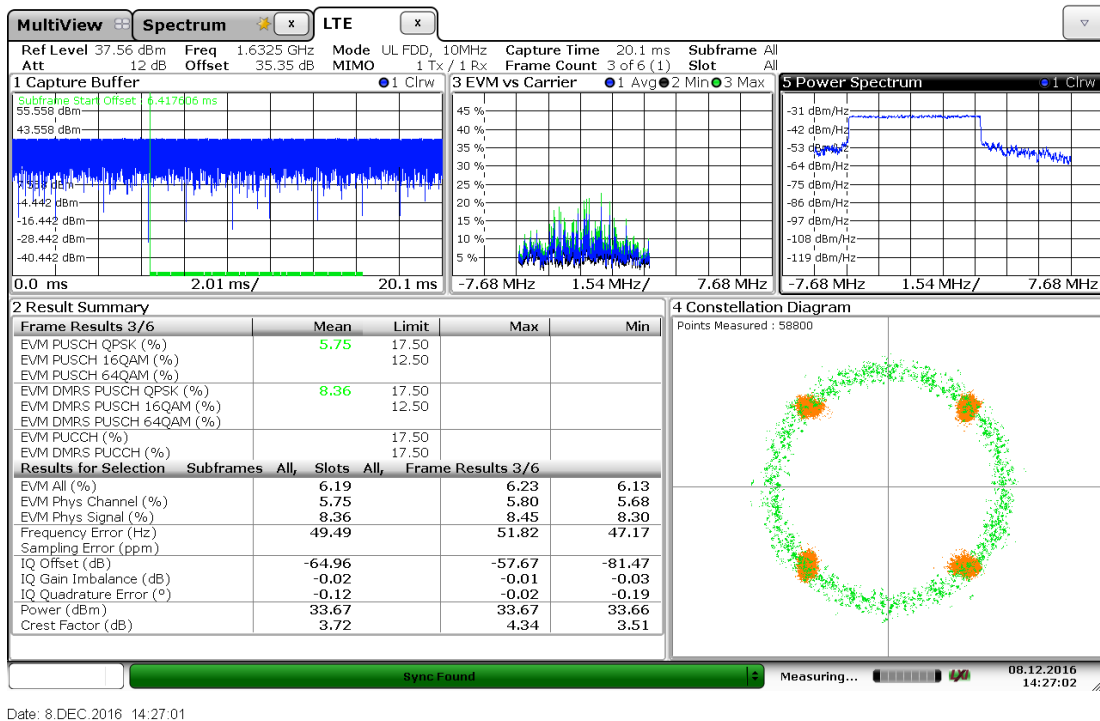


Figure D.17: Spectrum analyzer capture of LTE Evaluation Suite. UL signal drive level at maximum, distorted amplifier response.

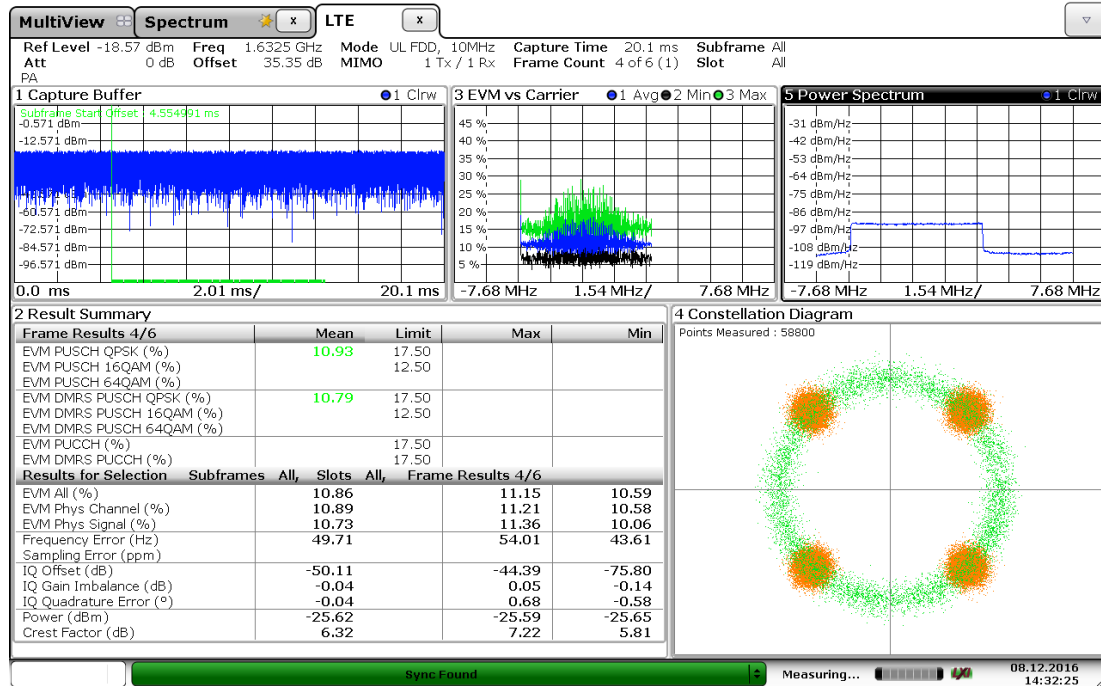


Figure D.18: Spectrum analyzer capture of LTE Evaluation Suite. UL signal drive level 60 dB below maximum, dominated by amplifier noise.

#### D.4 Conducted Testbed Noise Floor Output

The test setup for checking the noise floor of signal paths at the testbed output is shown in Figure D.19. The spectrum analyzer is connected directly to the output of the testbed in order to maximize sensitivity to low noise levels. In each test, the amplifiers and signal generators of signal paths that were *not* under test were disabled (illustrated in detail later in this section).

A summary of the conducted noise levels output by the testbed from each signal path is listed in Table D.4. The measurement result for each path is listed at what is felt to be the most impactful frequency: the output band center for LTE IB paths, and the GPS band center for the wideband GPS and LTE OOB outputs.

The spectrum analyzer imposes a noise floor on the test itself. The noise floor is determined in part by the signal level of the testbed output noise. The spectrum analyzer capture is shown in Figure D.20. The internal attenuator of the spectrum analyzer was set to 5 dB for these tests.

The GPS output noise floor test result is shown in Figure D.21. The GPS attenuator is at the calibrated level for DUT exposure at -128.5 dBm EIRP. The resulting GPS spectrum was too weak to measure.

The LTE IB and OOB DL output noise floor test results are shown in Figure D.22. There was no

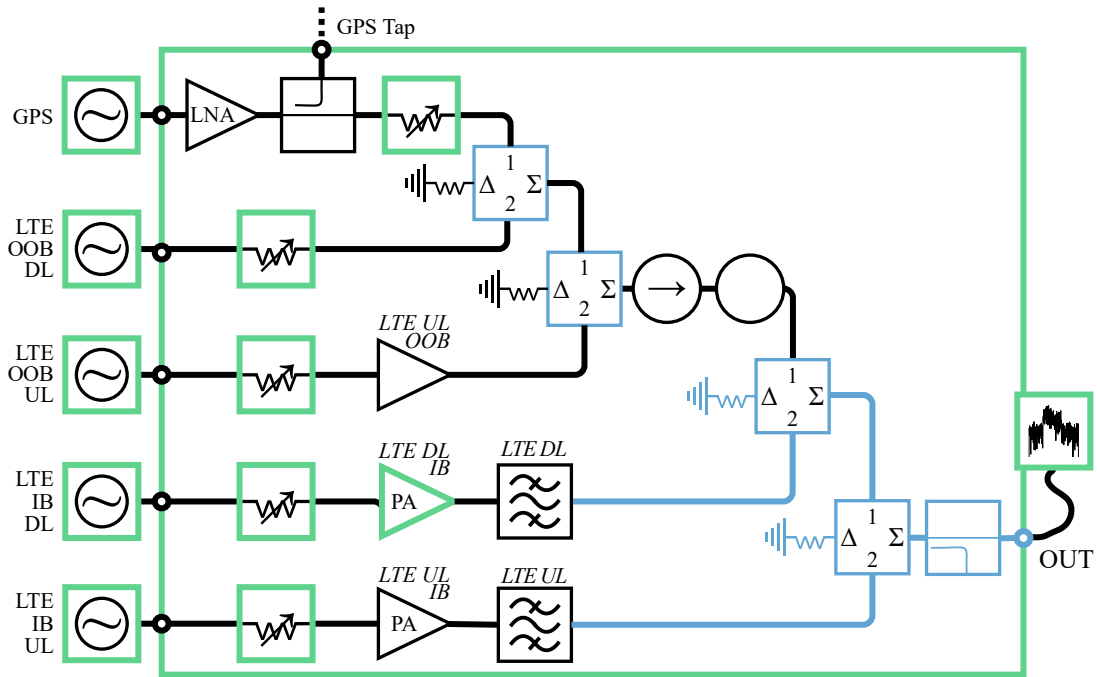
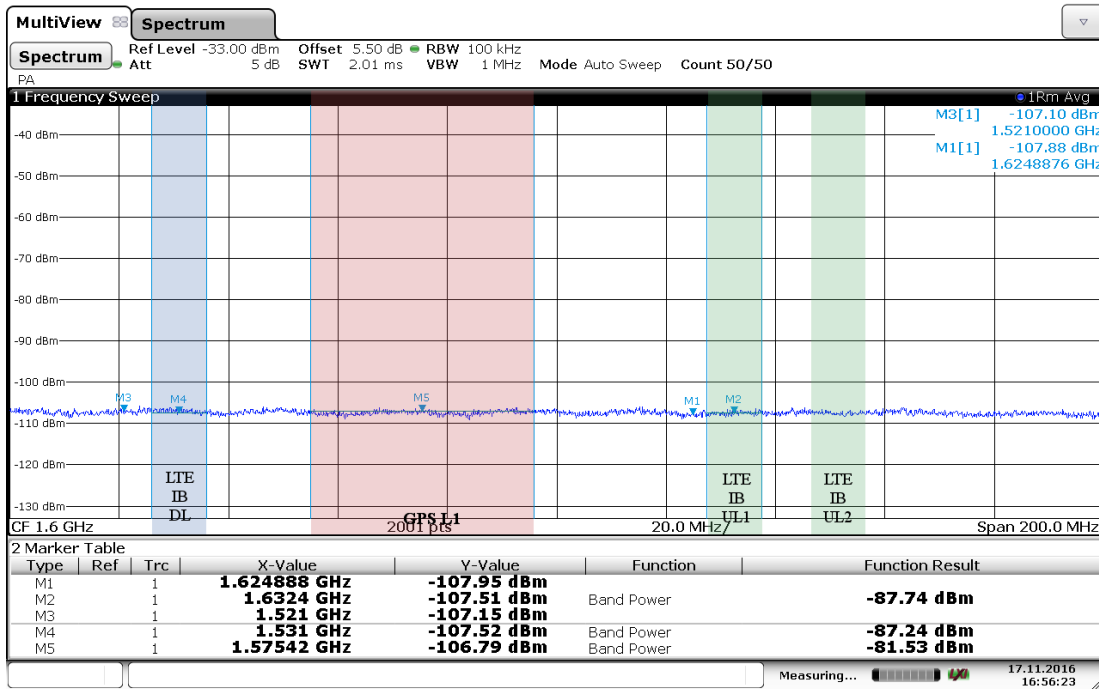


Figure D.19: Test setups for testbed noise floor



Date: 17.NOV.2016 16:56:23

Figure D.20: Noise floor of the spectrum analyzer used to measure noise floor

Table D.4: Summary of Output Noise Floor Test Results by Signal Path

	Measurement Frequency		Noise Output	
	Center <i>MHz</i>	Bandwidth <i>MHz</i>	Band Power <i>dBm</i>	Average PSD <i>dBW/MHz</i>
<b>GPS</b>	1575.42	40.92	max. -81.5	max. -127.6
<b>LTE IB DL</b>	1531	10.00	-7.6	-47.6
<b>LTE IB UL1</b>	1632.5	10.00	-34.0	-74.0
<b>LTE IB UL2</b>	1651.5	10.00	-34.0	-74.0
<b>LTE OOB DL</b>	1575.42	40.92	max. -81.5	max. -127.6
<b>LTE OOB UL</b>	1575.42	40.92	-74.0	-120.1

detectable change in the LTE OOB DL noise output outside of the desired signal when its output was enabled (compared to no signal). The IB amplifier, in contrast, is specified by the manufacturer to have 60 dB gain, and produces the strongest of the measured noise floors: -7.6 dBm band power.

The LTE IB and OOB UL output noise floor test results are shown in Figure D.23. There was no detectable change in the LTE OOB DL noise output outside of the desired signal when its output was enabled (compared to no signal). The IB amplifier noise floor output (referenced at the testbed output) is therefore -34.0 dBm/10 MHz across the full filter output bandwidth.

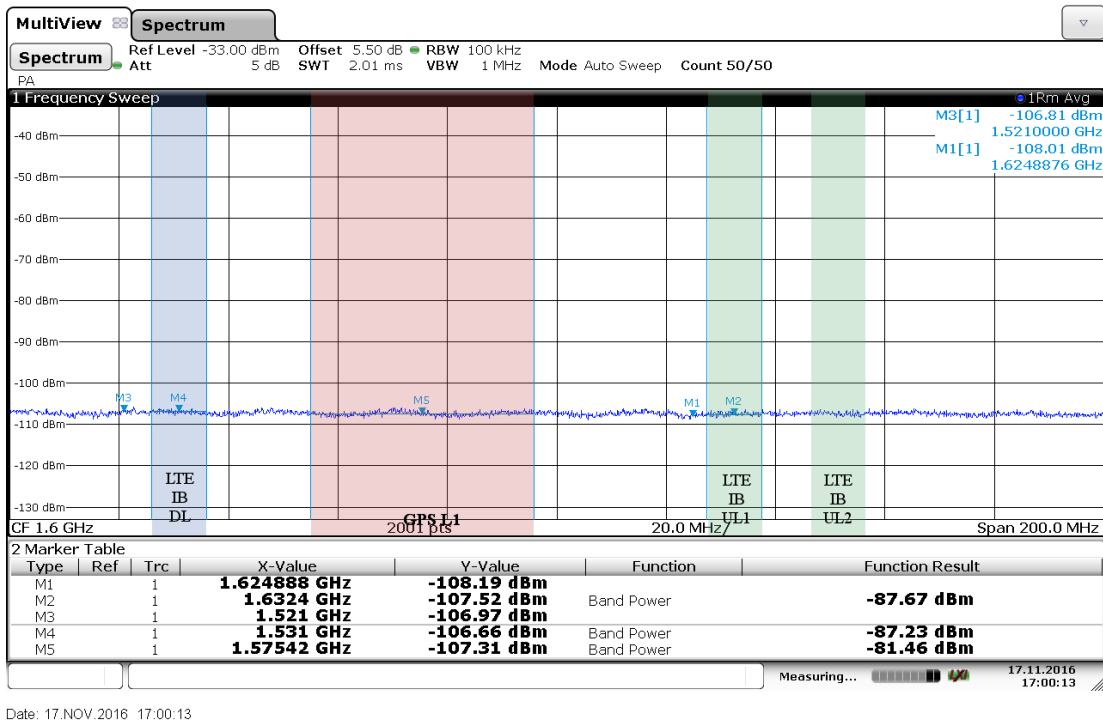
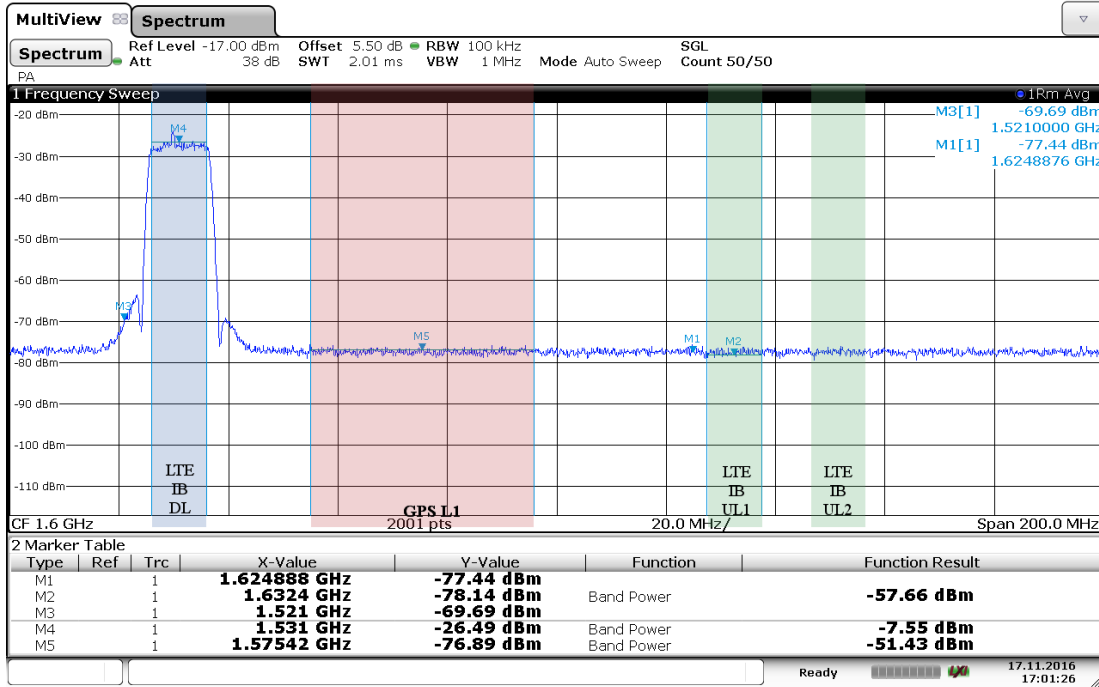
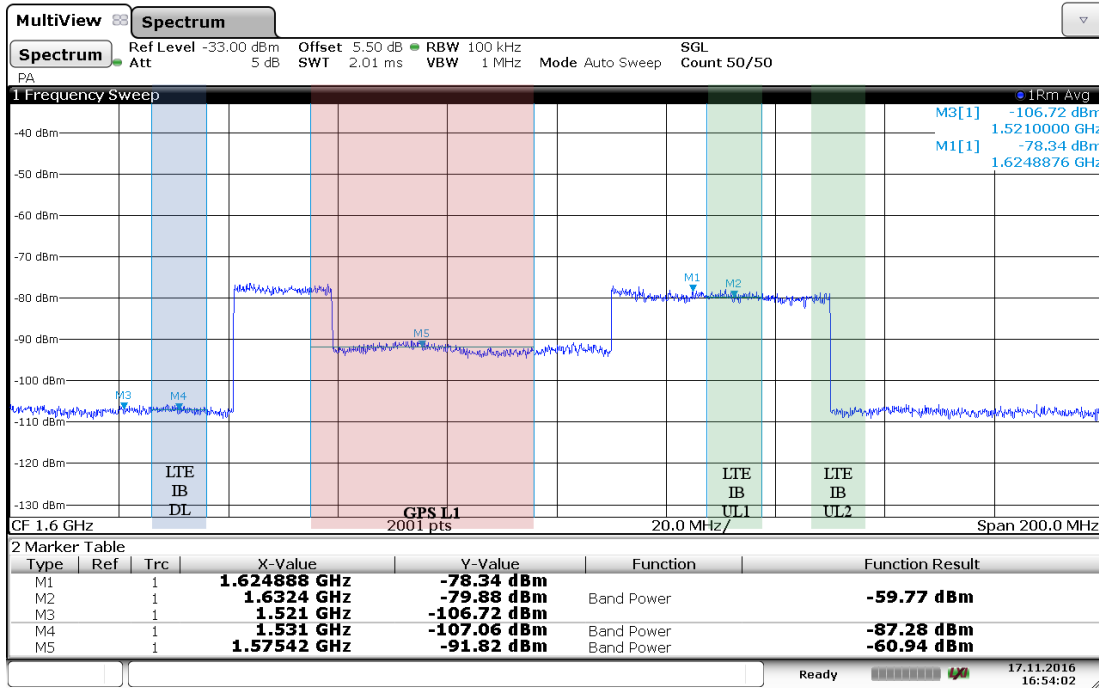


Figure D.21: Spectrum analyzer capture of GPS noise floor test (amplifier on, signal off, attenuator at nominal operating level). Output signals and amplifiers in other paths were disabled.



Date: 17.NOV.2016 17:01:26

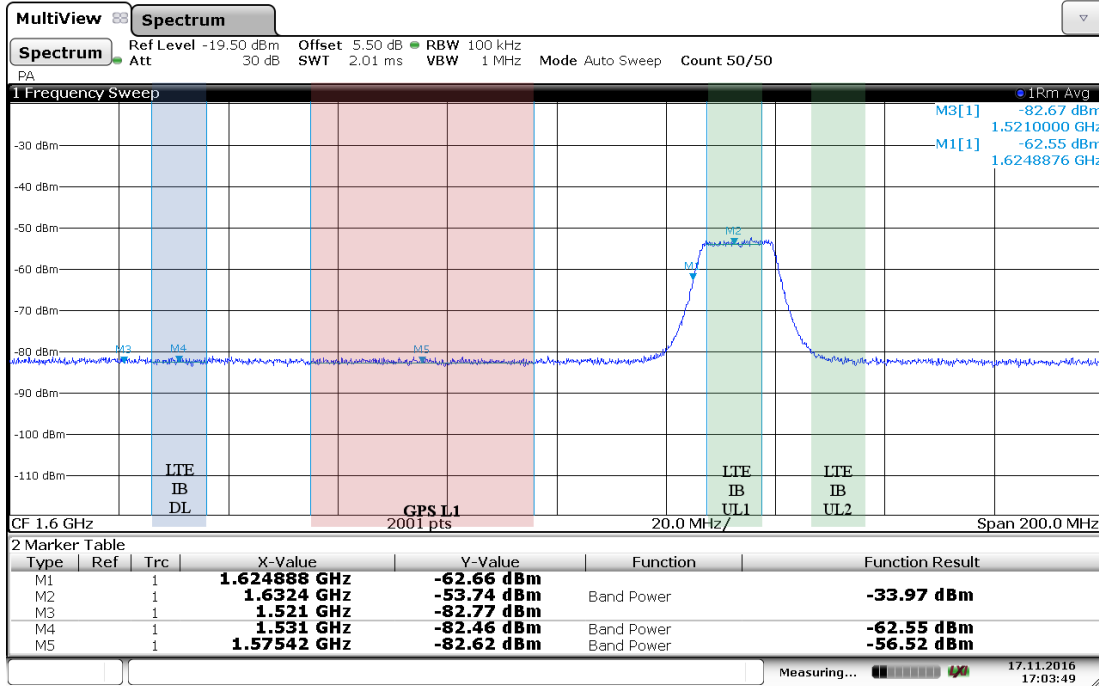
(a) LTE IB DL (amplifier on at maximum gain; signal off)



Date: 17.NOV.2016 16:54:02

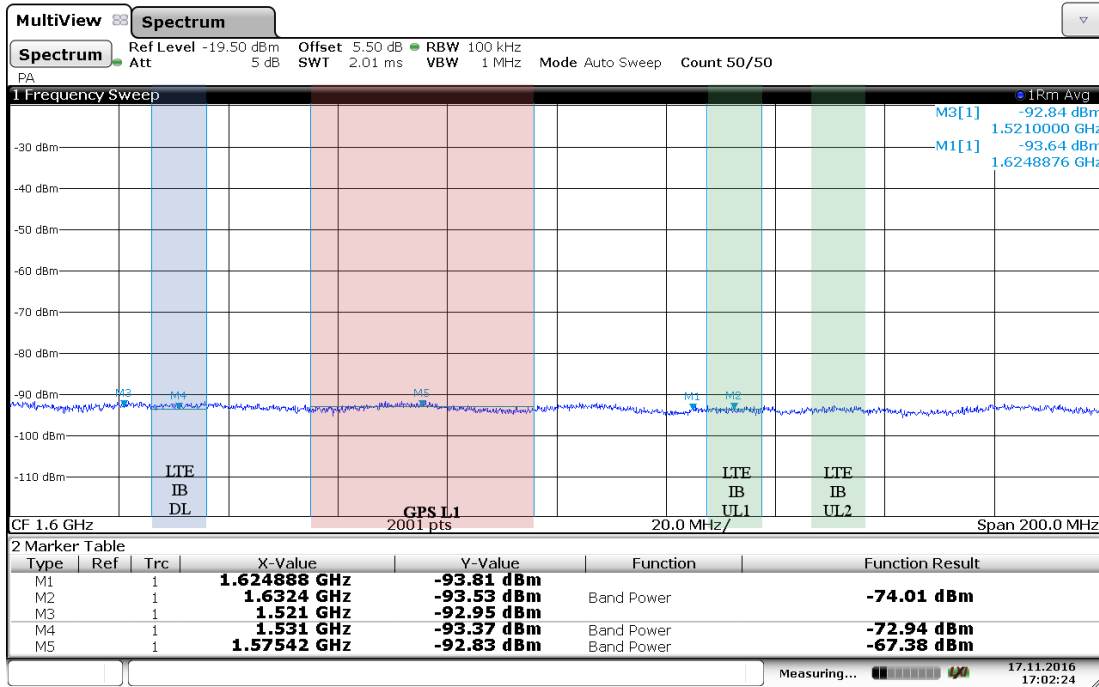
(b) LTE OOB DL (signal on, level corresponds to maximum DL output of testbed)

Figure D.22: Testbed LTE DL output noise floors. All outputs of non-indicated paths are disabled.



Date: 17.NOV.2016 17:03:49

(a) LTE IB UL (amplifier on; signal off)



Date: 17.NOV.2016 17:02:24

(b) LTE OOB UL (amplifier on, signal off)

Figure D.23: Testbed LTE UL output noise floors. All outputs of non-indicated paths are disabled. This was the strongest output noise floor measured, and motivated the use of the medium power amplifier for low power levels. The LTE OOB DL output spectrum shown is shown for comparison.

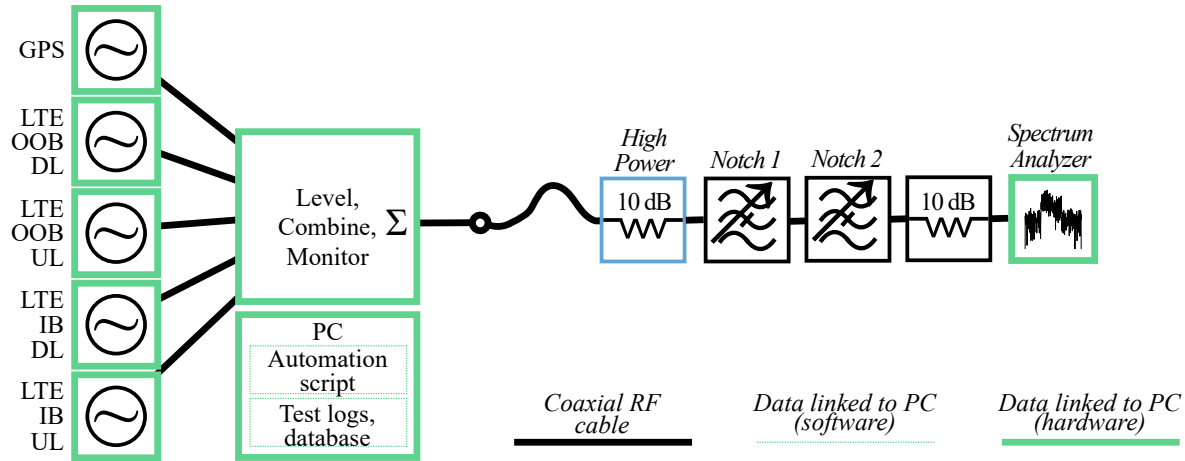


Figure D.24: Two-tone intermodulation test setup.

Table D.5: Summary of Two-Tone IMD3 Test Tone Inputs and Output Products

Input tones		IMD3 product output tones	
$f_1$ (MHz)	$f_2$ (MHz)	$2f_1 - f_2$ (MHz)	$2f_2 - f_1$ (MHz)
1531	1632.5	1429.5	1734
1526	1536	1516	1546
1627.5	1634.5	1620.5	1641.5

## D.5 Tests for Testbed Intermodulation

### D.5.1 Two-Tone Excitation

The two signals at the testbed output power levels with the greatest power levels are DL and UL1, in the combo LTE scenario.

A conducted intermodulation distortion (IMD) test setup is shown in Figure D.24. The output of the testbed feeds directly into a low-PIM attenuator. The attenuator serves two functions:

1. help ensure matching between the testbed output, the filters, and the spectrum analyzer at the notch filter frequencies, and
2. reduce the input level by 10 dB in order to reduce the passive intermodulation (PIM) output of the downstream filters and attenuators by 30 dB.

The two manually-controlled variable notch filters allow the test operator to selectively reject the input tones. These filters selectively attenuated the input tones by 60 to 70 dB, leaving the spectrum analyzer with a clear view of the (weaker) IMD products below its own IMD measurement dynamic range. The remaining downstream attenuators serve to protect the input of the spectrum analyzer.

Tests were performed to study two-tone response at

1. LTE IB DL and UL1 band centers ( $f_1 = 1531$  MHz and  $f_2 = 1632.5$  MHz “wideband response”),
2. LTE IB DL transmit spectrum edges ( $f_1 = 1526$  MHz and  $f_2 = 1536$  MHz), and
3. LTE IB UL1 transmit spectrum ( $f_1 = 1627.5$  MHz and  $f_2 = 1634.5$  MHz).

The IMD3 products of each two-tone test is listed in Table D.5. The test method was the same for each scenario:

1. The generator(s) in the corresponding paths are configured to transmit two tones instead of LTE modulation.
2. Generators in *other* paths are disabled
3. Tune the filter notches away from the input tone frequencies
4. Capture a spectrum analyzer trace of the high-power output of these tones (as a reference to compute IMD3 in dBc)
5. Tune the filter notches to minimize the PSD at the two input frequencies
6. Capture a spectrum analyzer trace to find PSD generated at intermodulation frequencies

The result of these IMD measurements is output-referenced.

#### **D.5.1.1 DL+UL1**

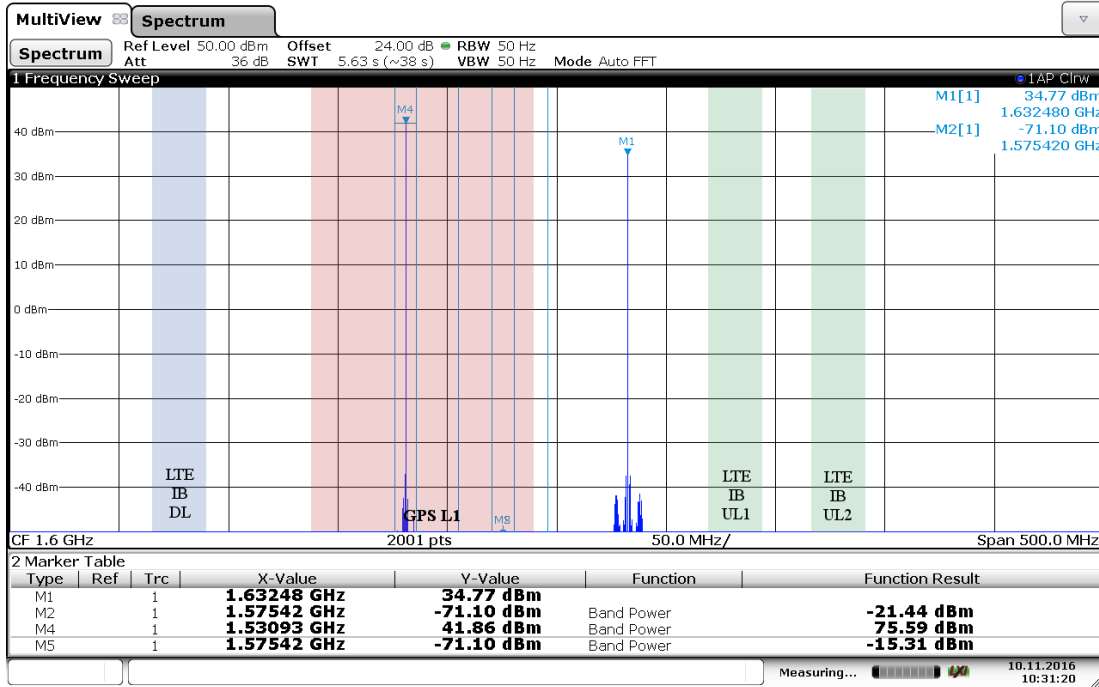
The results of the wideband test are shown in Figure D.25. The displayed power levels are offset to correspond with levels at the input (the equivalent conducted power that would be delivered to the testbed transmit antenna). Third-order products appear at the expected frequencies 1429.5 MHz and 1734 MHz (input tones  $\pm$  their frequency separation, 101.5 MHz), far outside the range of interest of this study.

#### **D.5.1.2 DL**

Results of the LTE IB DL test are shown in Figure D.26. Several measurable two-tone products are visible between the DL and GPS bands. These levels are related to the detectable energy output from an LTE input signal in the next subsection.

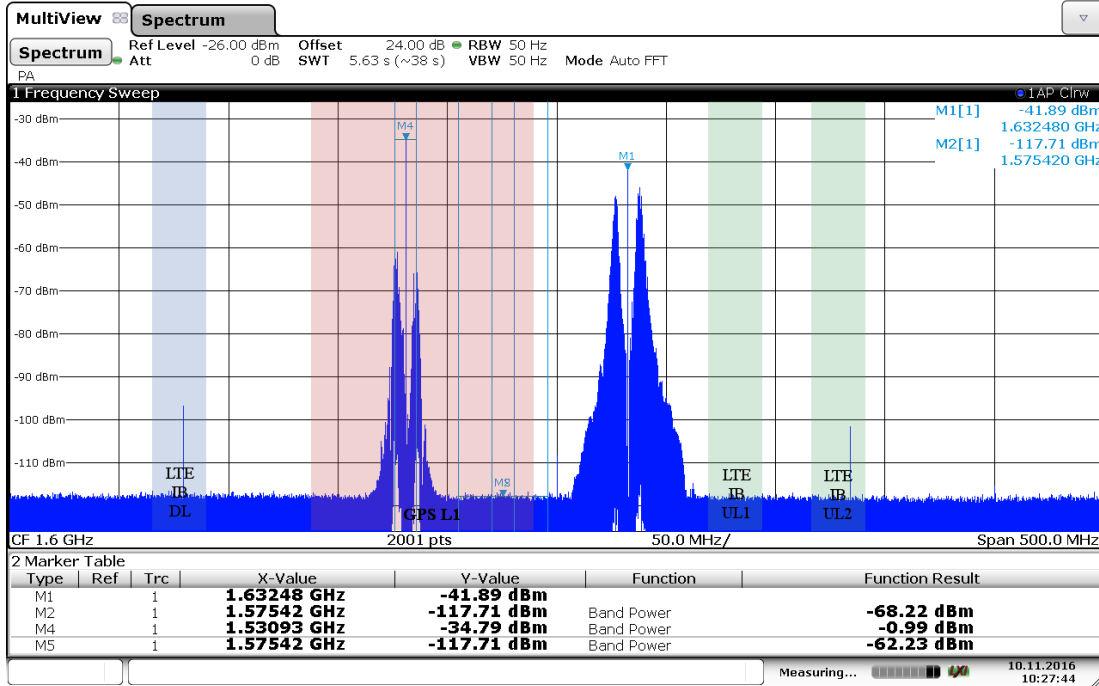
#### **D.5.1.3 UL1**

Results of the LTE IB UL1 test are shown in Figure D.27. Several measurable two-tone products are visible between the UL and GPS bands. These levels are stronger than those in the DL tests.



Date: 10.NOV.2016 10:31:21

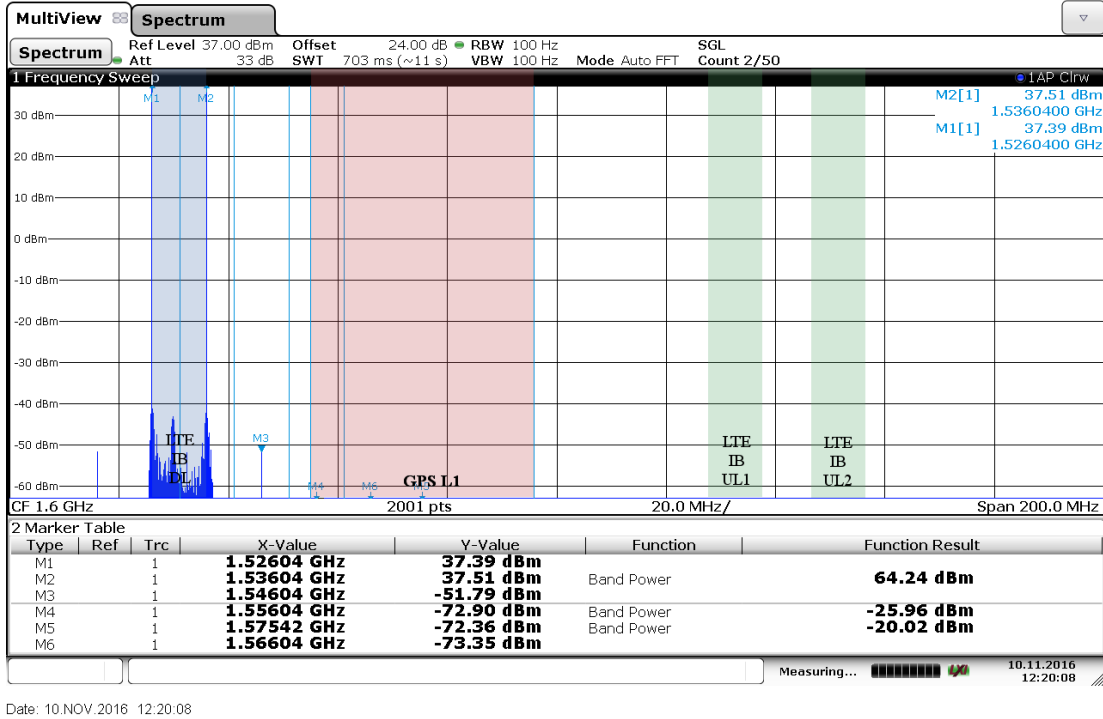
(a) No output filtering; display DL level 41.9 dBm, display UL1 power 34.8 dBm



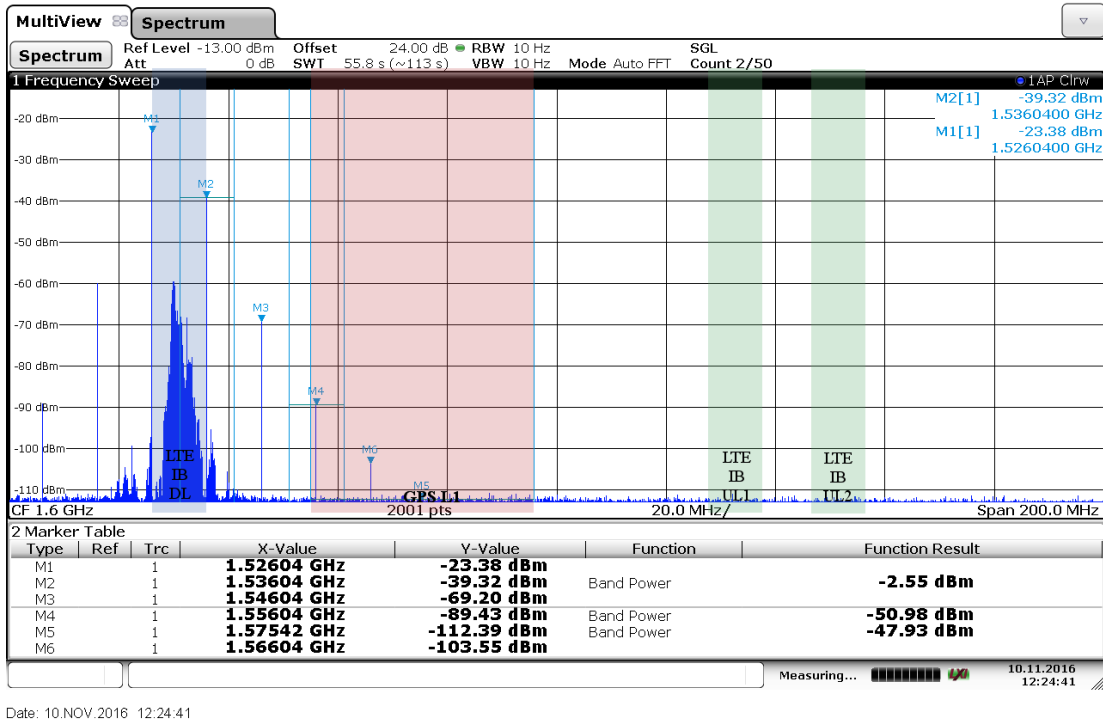
Date: 10.NOV.2016 10:27:45

(b) Notch filters remove input tones; IMD3 products at -138 dBc (lower) and -136 dBc (upper)

Figure D.25: Wideband tests of two-tone intermodulation for input tones at the DL band center (1536 MHz) and UL1 band center (1632.5 MHz).

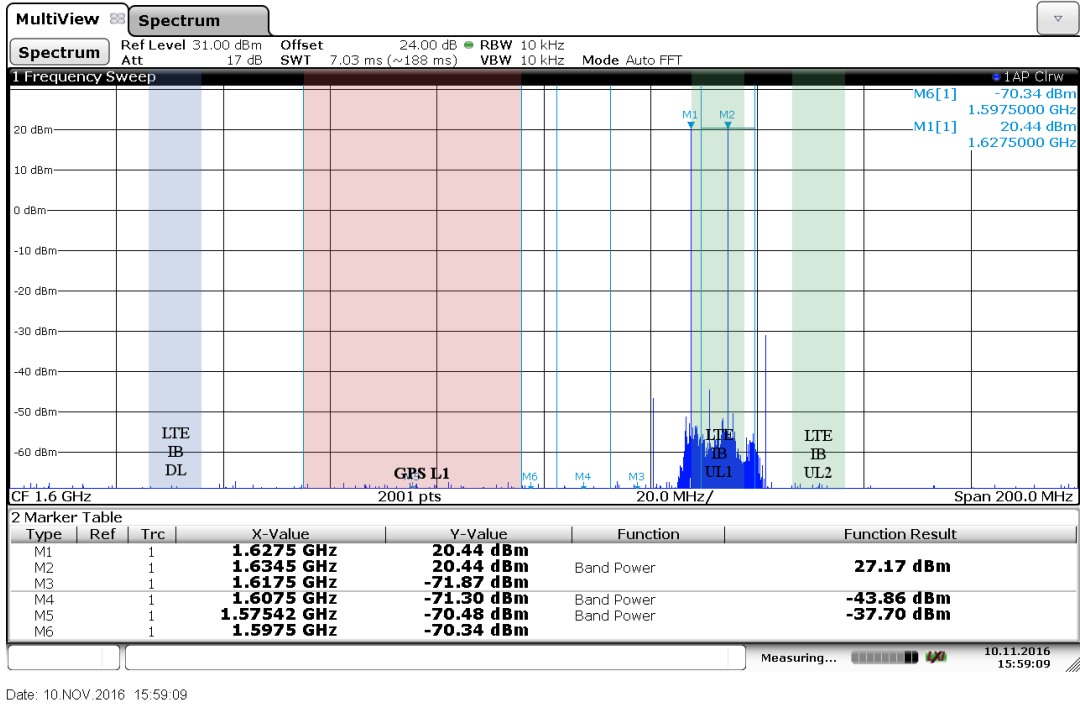


(a) Unfiltered: input tone levels 40.5 dBm

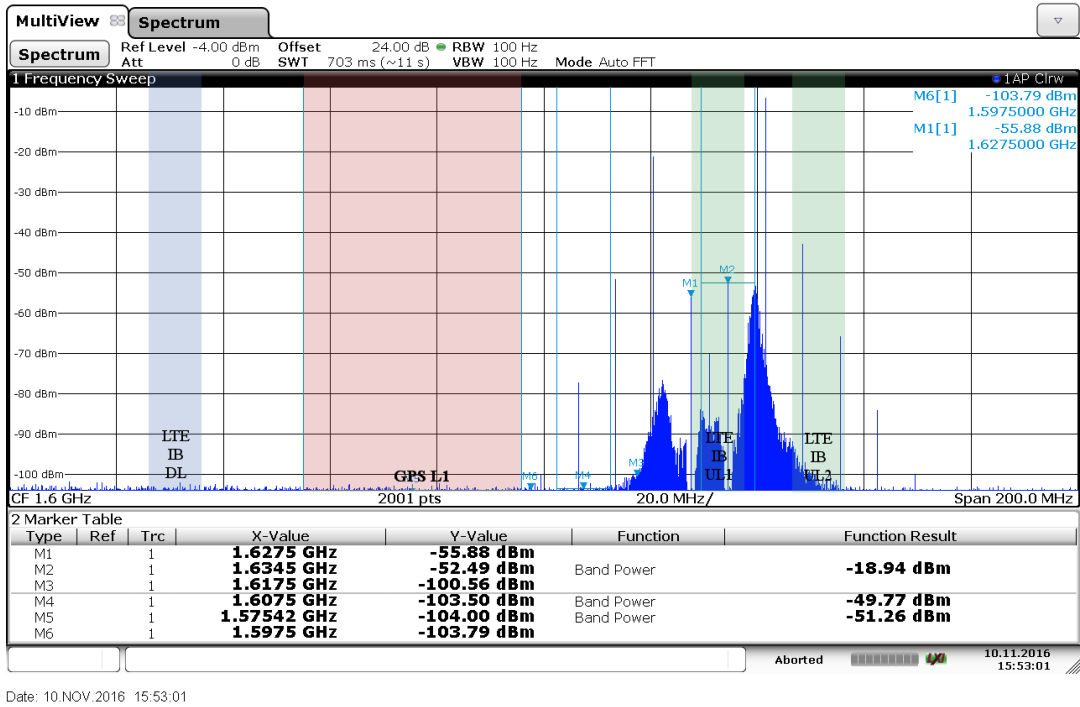


(b) Filtered: IMD levels -109.7 dBc ± 1.5 dB at 1646 MHz, -129.9 dBc ± 1.5 dB at 1656 MHz, and -152.8 dBc ± 1.5 dB at 1666 MHz.

Figure D.26: Two-tone IMD tests of LTE IB DL output. Output is at maximum tested power split between 1531 MHz ± 5 MHz.

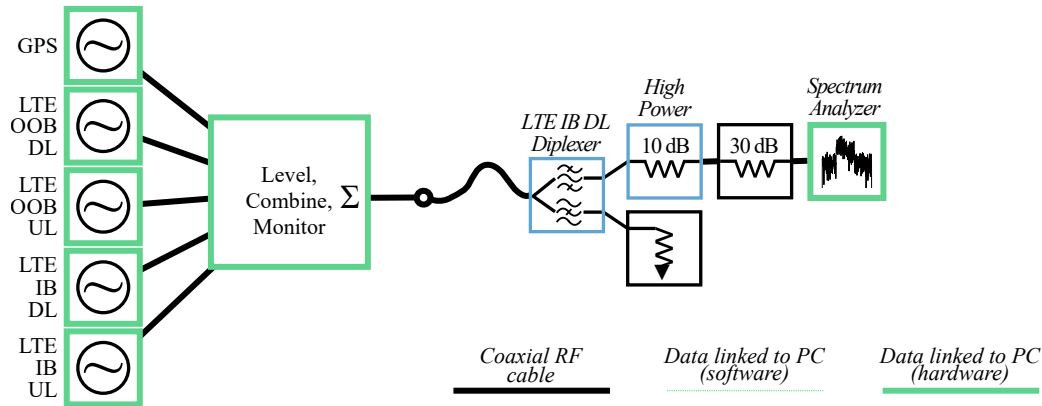


(a) Unfiltered: input tone levels 20.4 dBm

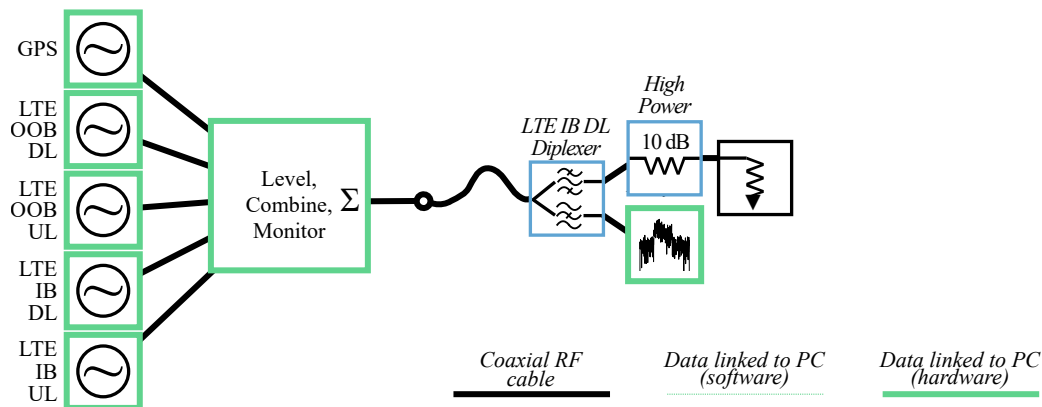


(b) Filtered: IMD levels -43 dBc  $\pm$  1.5 dB at 1620.5 MHz, -75 dBc  $\pm$  1.5 dB at 1613.5 MHz, and -101 dBc  $\pm$  1.5 dB at 1606.5 MHz.

Figure D.27: Two-tone intermodulation tests of the LTE IB UL1. The testbed output tones split maximum testbed output power between 1627.5 MHz and 1634.5 MHz. 7 MHz bandwidth corresponds with 70% resource block loading across the proposed 10 MHz channel.



(a) Setup to measure testbed LTE IB DL output inside of the intended band



(b) Setup to measure testbed LTE IB DL output outside of the intended band

Figure D.28: Two-tone intermodulation tests of the LTE IB DL output. Output tones are at maximum testbed power, split between 1526 MHz and 1536 MHz.

## D.5.2 LTE Excitation

### D.5.2.1 DL

While two-tone tests are the standard practice in microwave measurements of IMD, the real concern for this test application is the impact of intermodulation upon spectral regrowth for the LTE IB DL and UL signals.

The test team obtained a low-PIM bandpass/bandstop diplexer that enables direct measurement of the undesired OOB components output by the LTE IB DL path. A diplexer was not available to test the LTE IB UL paths in time for the testing. The test setup, illustrated in Figure D.28, shows how the diplexer routes a high-sensitivity measurement path for weak OOB signaling in the chain through its bandstop filter, and high-power measurements of the desired in-band signal through its bandpass filter.

Matching and insertion loss performance of the diplexer are shown in Figure D.29. The pass-

band in the bandpass branch (and bandstop in the bandstop branch) spans approximately 1526-1546 MHz. Therefore, the only directly visible OOB signals through the bandstop path are those below 1526 MHz. In post-processing, the spectrum above 1536 MHz are estimated under the assumption of symmetry about 1531 MHz.

The transmit spectrum of each test is shown in Figure D.30. The testbed is excited with LTE IB DL at full power; all other signals are off. The level offset in the spectrum analyzer is chosen here to reflect actual testbed output in the passband only.

The network analyzer test data allows us to de-embed the output spectra back to the diplexer input. This allows us to find PSD at frequencies where the diplexer attenuates at both outputs (such as 1520 MHz — 1526 MHz). The correction for either output path is

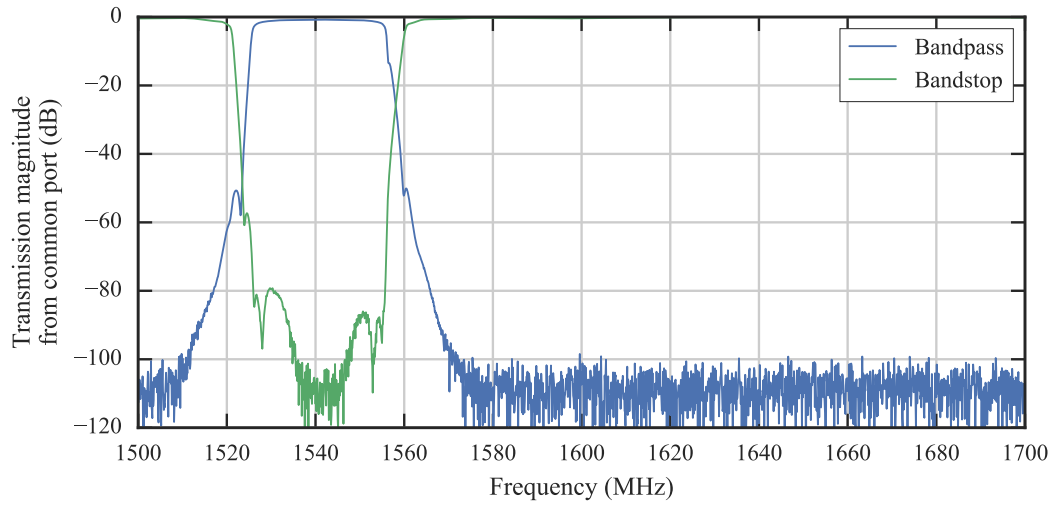
$$\text{PSD}_{\text{in}} \text{ in (dBW/MHz)} = \text{PSD}_{\text{out}} \text{ in (dBW/MHz)} - 20 \log_{10} |S_{21}|. \quad (\text{D.1})$$

The diplexer branch transmission magnitude in dB,  $20 \log_{10} |S_{21}|$ , is the curve plotted in Figure D.29.

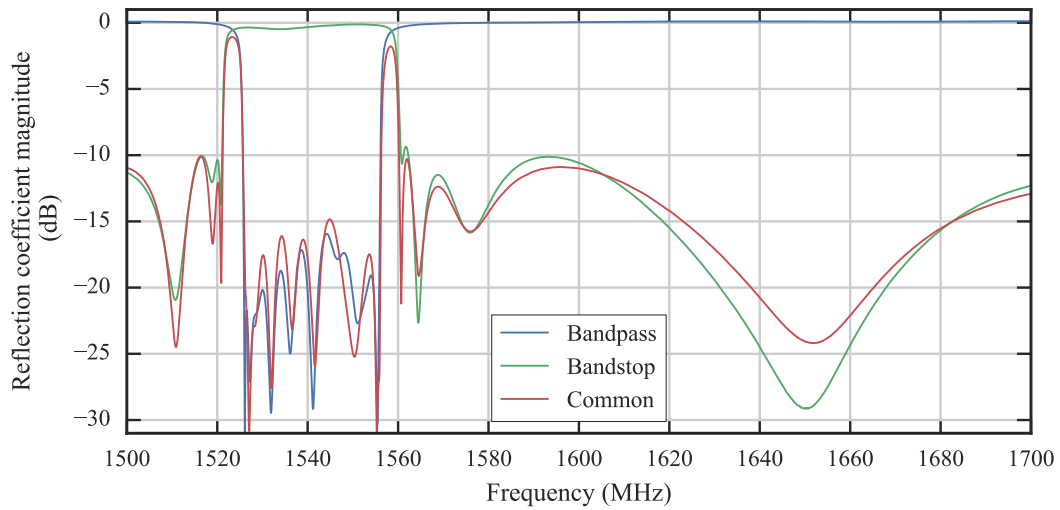
The spectra are plotted on the same axes in Figure D.31. Only data at frequencies at least 5 dB above the noise floor are plotted. These results, and the estimate for values between 1538 MHz - 1555 MHz, are the curves superimposed over the desired downlink signal spectra in Figure 3.10. The estimate at 1538 MHz - 1555 MHz is the result of mirroring the bandstop data about the downlink center frequency, 1531 MHz.

#### **D.5.2.2 UL**

The test team did not have a test diplexer available for either LTE uplink band. Therefore, the only type of IMD results are two-tone test data.

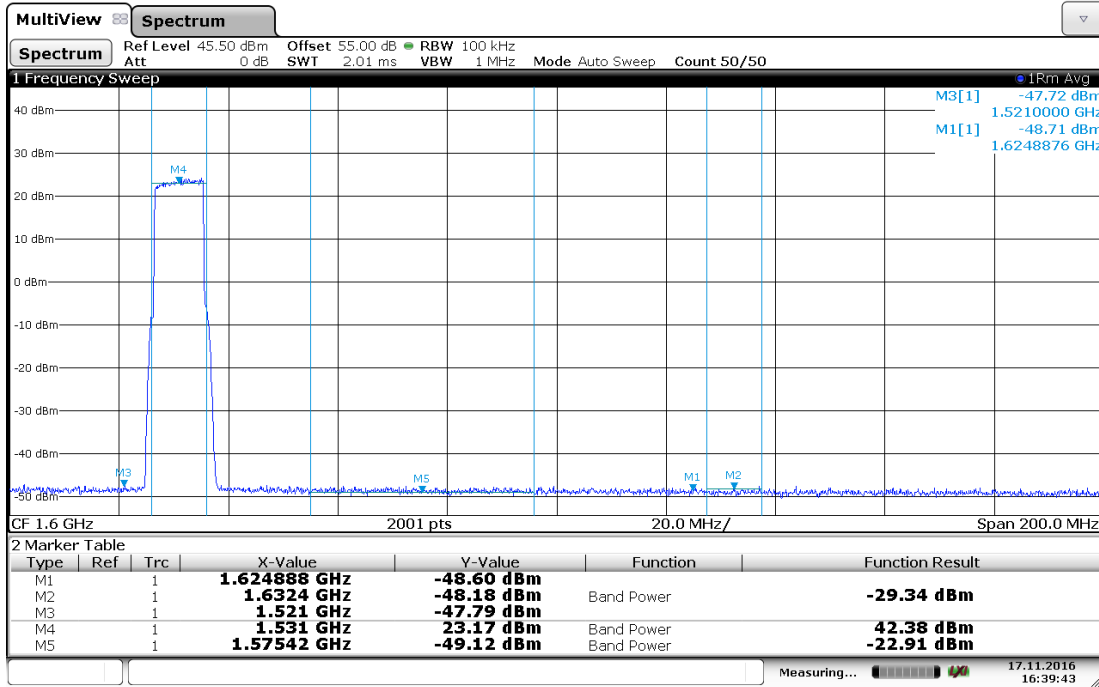


(a) Transmission



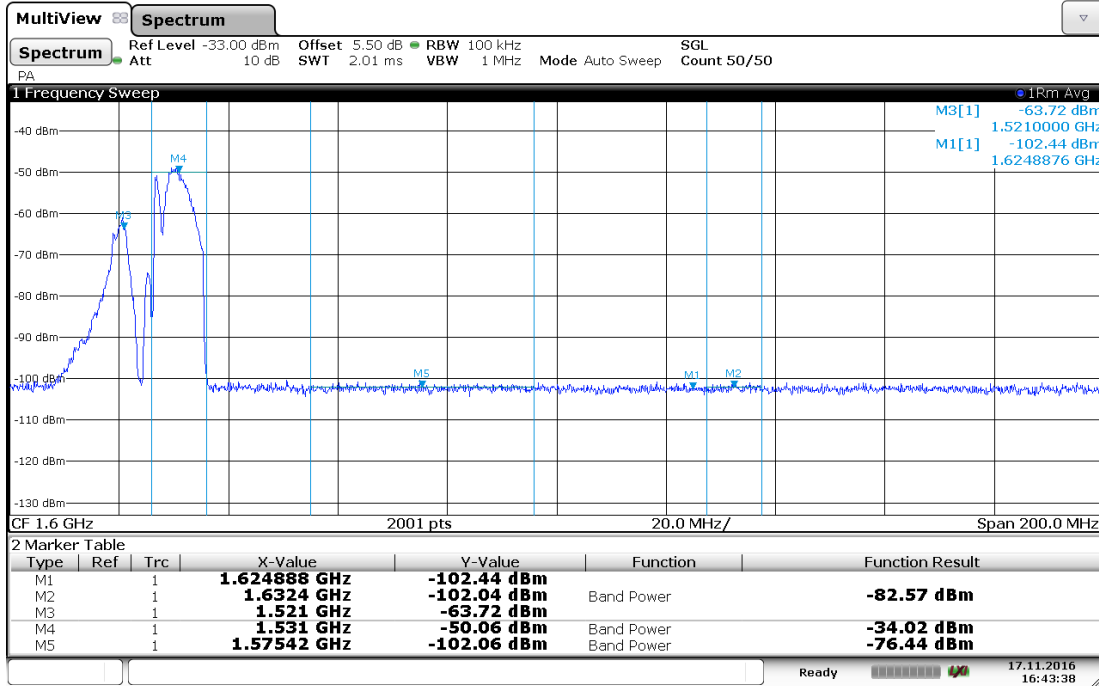
(b) Matching

Figure D.29: Transmission and matching characteristics of the low-PIM diplexer used for high-dynamic range tests of LTE DL outputs



Date: 17.NOV.2016 16:39:43

(a) Measurements of testbed LTE IB DL output inside of the intended band



Date: 17.NOV.2016 16:43:38

(b) Measurements of testbed LTE IB DL output outside of the intended band

Figure D.30: Spectrum analyzer captures of spectra detected from the two diplexer tests of LTE IB DL performed according to Figure D.28.

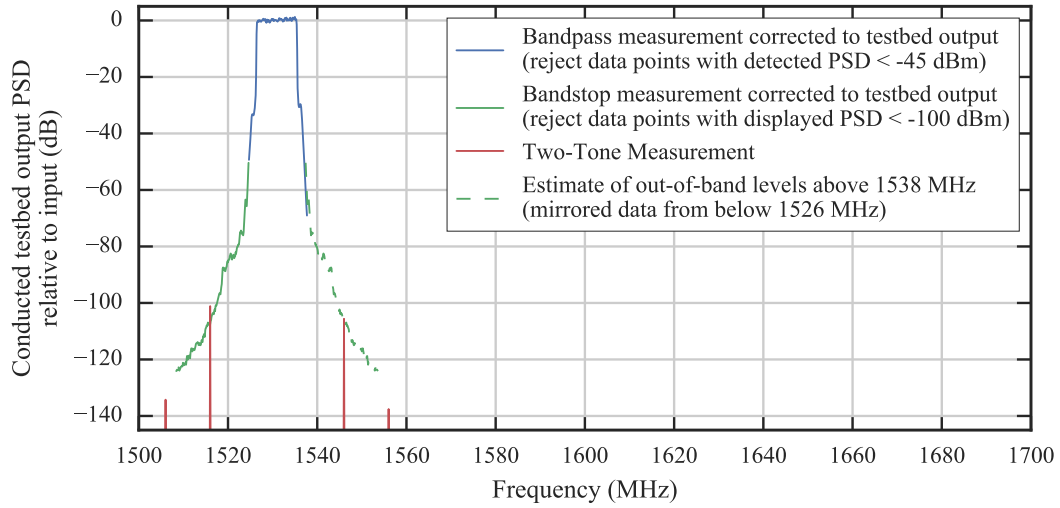


Figure D.31: Measurements of testbed LTE IB DL performed by diplexer output spectra (Figure D.30) with network analyzer data of (Figure D.29). Levels are normalized to average in-band PSD.

## D.6 Components

### D.6.1 Testbed Filters

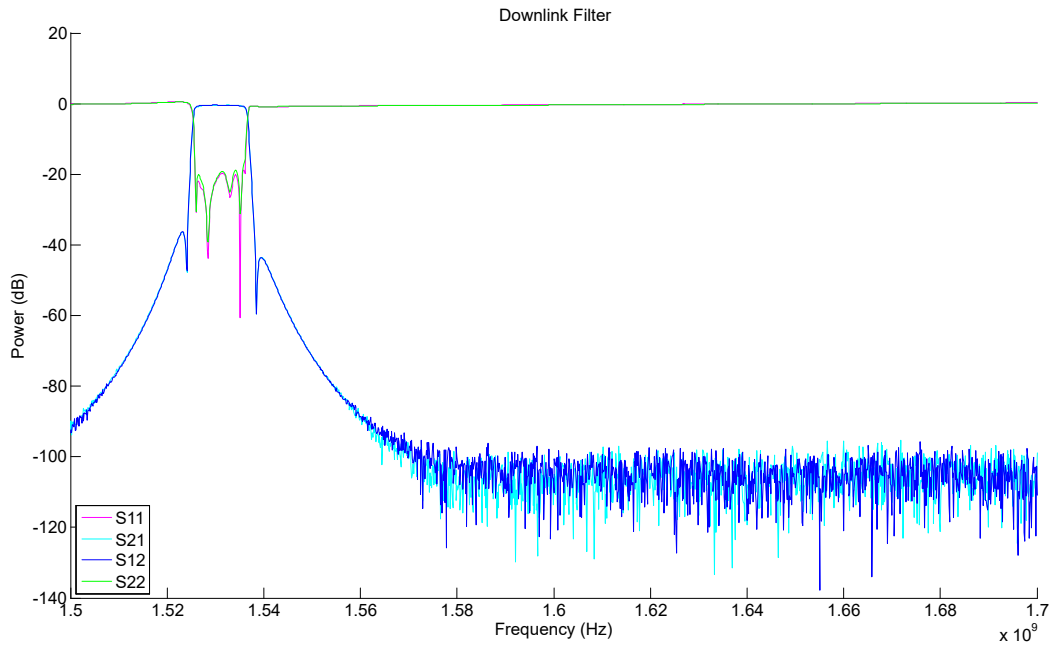


Figure D.32: Full 2-port S-parameter measurements of LTE IB DL bandpass cavity filter.

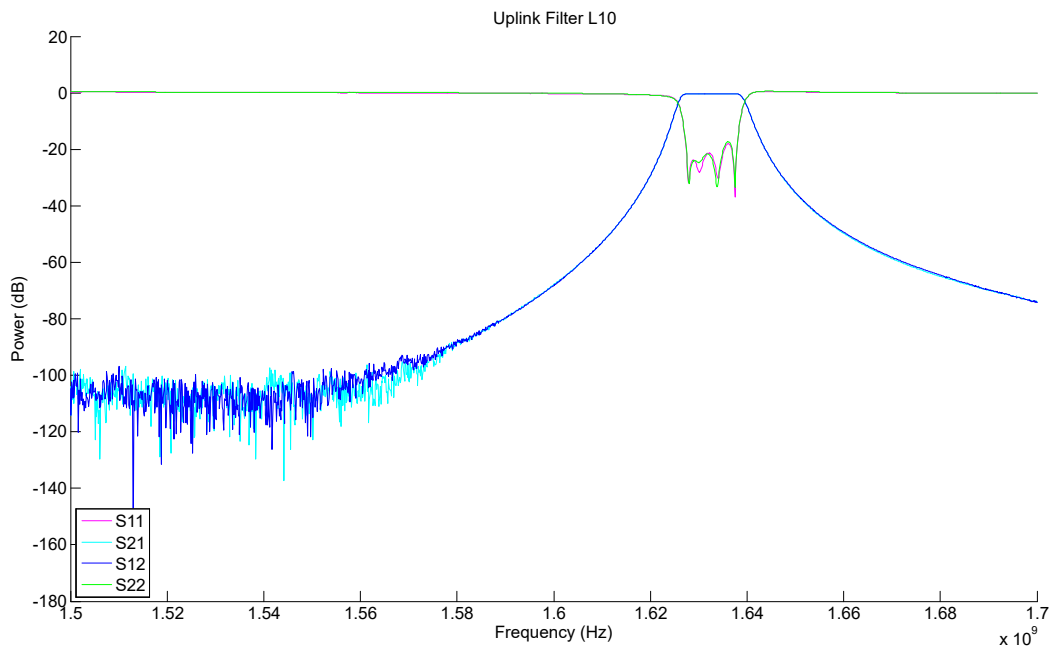


Figure D.33: Full 2-port S-parameter measurements of LTE IB UL1 bandpass cavity filter.

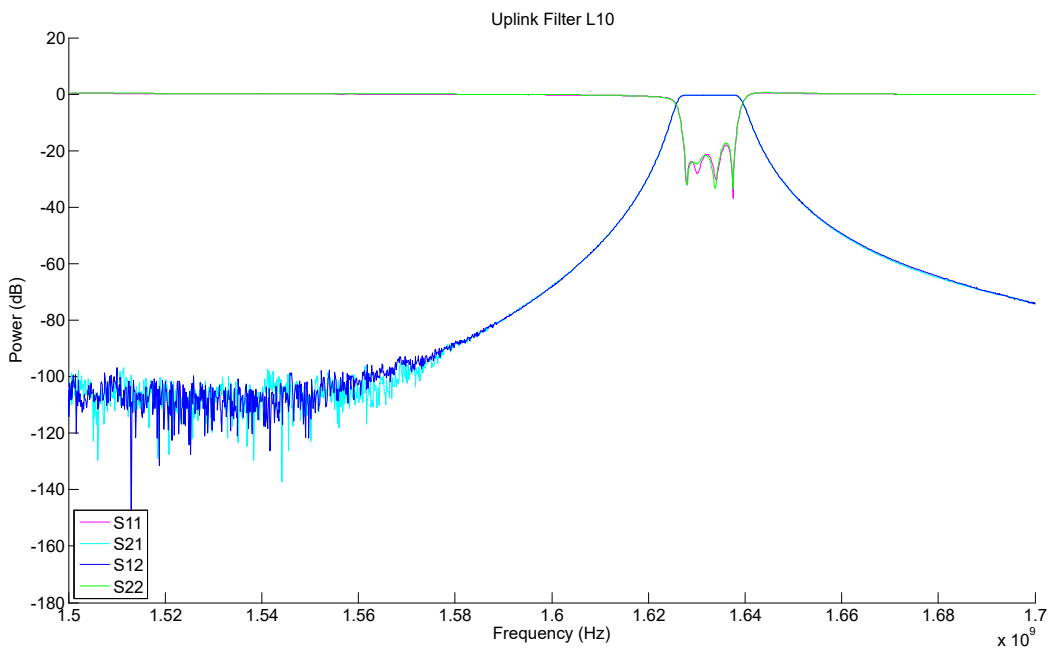


Figure D.34: Full 2-port S-parameter measurements of LTE IB UL2 bandpass cavity filter.

## E Validation of Radiated Chamber Performance

### E.1 Chamber Performance

In an ideal test configuration, measurements would not be affected by reflections from the test chamber, fixtures, antennas or other scatterers. To check possible limitations of our test setup, we performed a wideband multipath check test as shown in Figure E.1. In this test, frequency-domain data were acquired using a vector network analyzer (VNA) and then converted to the time domain. This gave the approximate impulse response of the measurement setup. In a perfect setup, the impulse response would consist of a single desired impulse that corresponds to the LOS component. The location (in time) of this impulse depends on the separation distance between the transmitting and receiving antennas. The shape of the impulse is a function of the measurement bandwidth and the impulse response of the antennas. Reflections from the measurement environment will contribute to the time domain response as lower-level signals after the initial impulse. Furthermore, multiple reflections coming from (for example) insufficient separation between measurement antennas, would become apparent in the measurement.

In order to understand locations of NLOS reflection components, we use the rough guide of 1 ns time delay per 30 cm in path length. As the LOS path from the transmitting antenna to the receiving antenna is the shortest possible path, undesired NLOS paths can be characterized by their difference in path length with respect to LOS.

In a wideband multipath check it is important to give consideration to the polarization of the measurement antennas. When the transmitting and receiving antennas are both circularly polarized and complimentary (e.g., RHCP antennas), the impulse response of an initial reflection is reduced, because refraction introduces a phase change that reverses the circular polarization — an RHCP wave becomes an LHCP wave. For this reason, we used an RHCP transmitting antenna, and a linearly-polarized receiving antenna. Two sets of measurements were performed, once with the receiving antenna aligned for horizontal polarization, and once aligned for vertical polarization. The result shows the presence of any cross-polarized components in the reflection, and leads to the axial ratio of the RHCP antenna.

There is very little information about the setup that occurs before the initial impulse, therefore all measurement traces were shifted so that the initial LOS impulse begins at 0 ns.

The multipath response from our setup at the NTS semi-anechoic measurement environment is shown in Figure E.2. Here, the initial rise of the impulse is very fast, followed by a much more gradual decay, consistent with log-spiral antennas. For the first 3 ns, the H-Pol and V-Pol responses

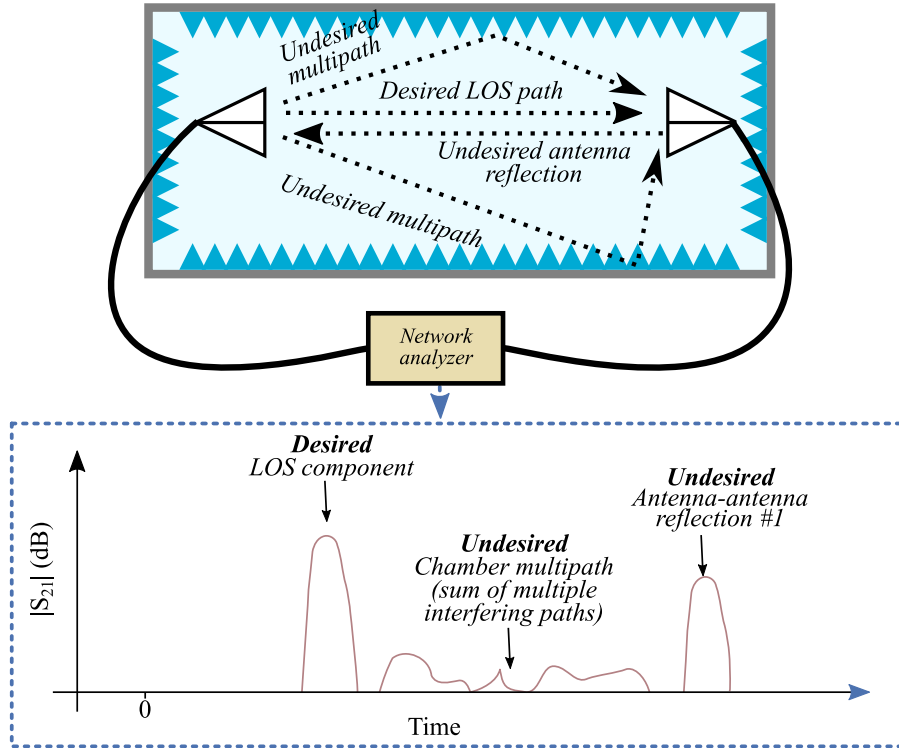


Figure E.1: Test method for wideband multipath check in the anechoic chamber.

are nearly identical, and remain similar for the entire time span with minor exceptions. The principal deviations from a simple monotonic decay occur around 3 ns, 5 ns, 10 ns, and 23 ns, and all are well below (> 15 dB) the LOS component. This implies that multipath reflection effects are insignificant and can be accounted for by the uncertainty analysis given in Appendix C.

It is interesting to compare the impulse response in the NTS chamber with the impulse response in the NBIT chamber Figure E.3. Here, the same minor deviations around 3 ns and 5 ns are present, indicating they are probably artifacts of the measurement antennas, but the deviations at 10 ns and 23 ns are either missing or greatly reduced. This implies that differences between the chamber or antenna mounting are likely sources. This is not surprising, since the NTS chamber is semi-anechoic with spot loading on the floor between antennas, and the NBIT chamber is fully anechoic with absorber covering all chamber surfaces.

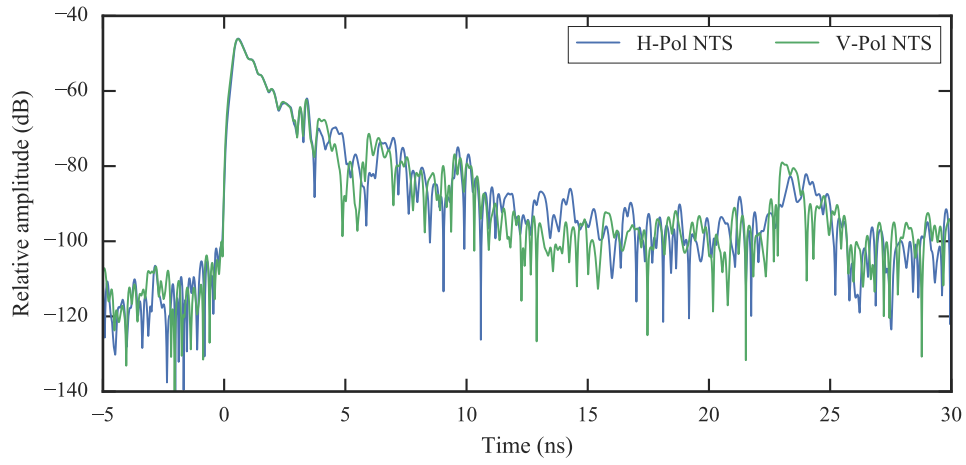


Figure E.2: Multipath response (both H-Pol and V-Pol) in the NTS chamber.

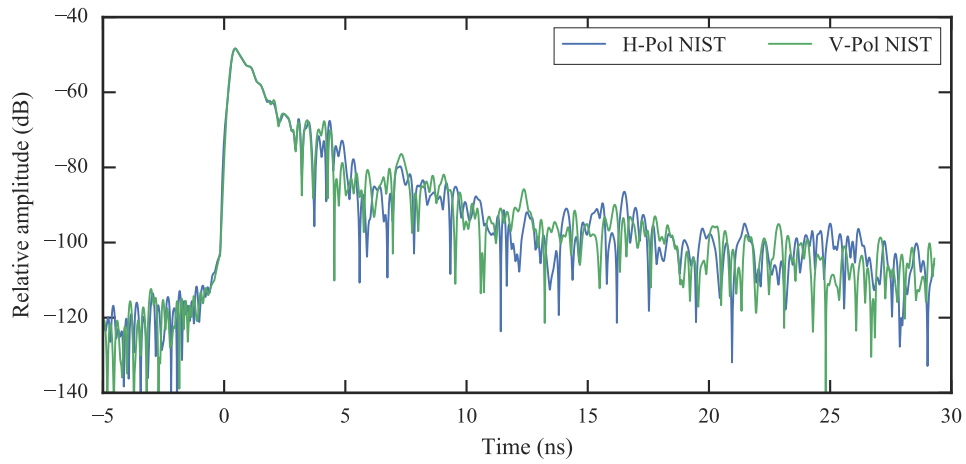


Figure E.3: Multipath response (both H-Pol and V-Pol) in the NIST NBIT chamber.

## E.2 Chamber Environmental Stability

Temperature and relative humidity readings were taken throughout the test campaign. The measurements were performed at the test-stand inside the chamber, 100 cm below the plane of the DUT. Measurement intervals were taken every 6 minutes. The variation in chamber performance can be attributable to the type of chamber, semi-anechoic at NTS versus anechoic at NIST in addition to climate control in the building (these RF chambers do not have their own systems).

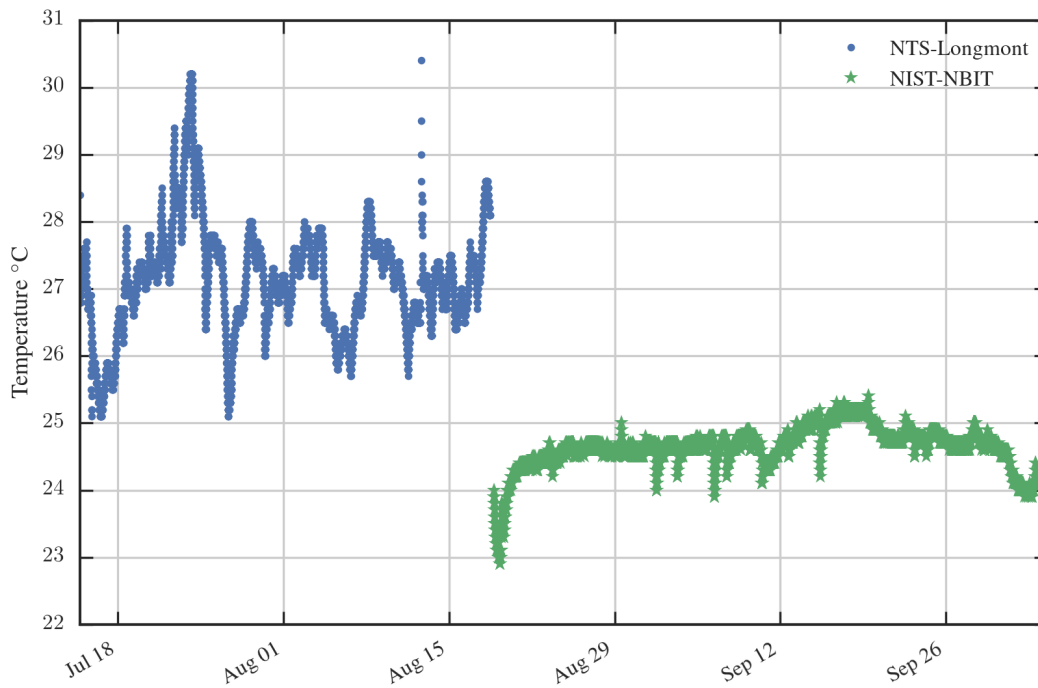


Figure E.4: Temperature fluctuations during the test campaign at the NTS and NBIT facilities.

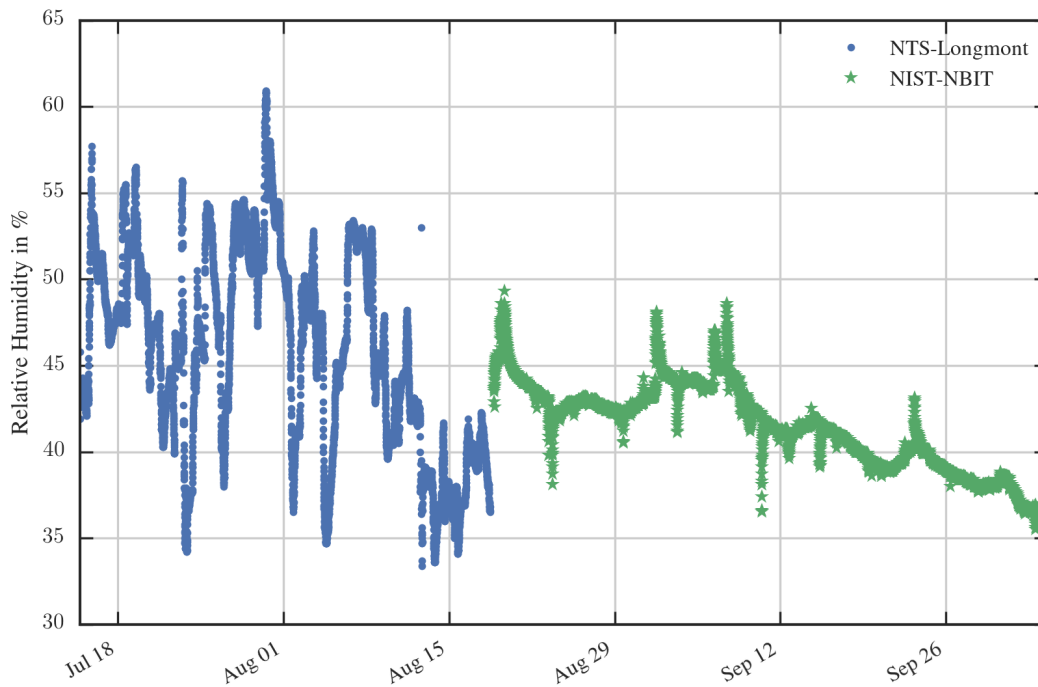


Figure E.5: Humidity variability during the test campaign at the NTS and NBIT facilities.

### E.3 DUT Test Locations

Some DUTs were tested in both locations (NTS in Longmont, CO and NBIT in Boulder, CO). Table E.1 outlines the test locations for the affected DUTs and corresponding test conditions. For all other DUTs tests were performed at NBIT.

Table E.1: DUT Test Locations ▲ Denotes NTS Longmont and ▼ Denotes NBIT Boulder.

Device	Type	GPS Scenario	Test Sweep	LTE Waveform			
				DL	UL 1	UL 2	DL + UL 1
DUT 1	GLN	Nominal	LTE power	▲▼	▲▼	▼	▼
		TTFR	TTFR	▼	▼	—	—
		Limited	LTE power	▼	▼	—	—
DUT 2	GLN	Nominal	LTE power	▲▼	▲▼	▼	▼
		TTFR	TTFR	▼	▼	—	—
		Limited	LTE power	▼	▼	—	—
DUT 4	GLN	Nominal	LTE power	▲▼	▲▼	—	—
		TTFR	TTFR	—	—	—	—
		Limited	LTE power	—	—	—	—

Table E.1: DUT Test Locations ▲ Denotes NTS Longmont and ▼ Denotes NBIT Boulder.

Device	Type	GPS Scenario	Test Sweep	LTE Waveform			
				DL	UL 1	UL 2	DL + UL 1
DUT 5	GLN	Nominal	LTE power	▼	▲	—	—
		TTFR	TTFR	—	—	—	—
		Limited	LTE power	—	—	—	—
DUT 7	HPP	Nominal	LTE power	▲▼	▲▼	▼	▼
		TTFF	TTFF	▲▼	▲▼	—	—
		Limited	LTE power	▼	▼	—	—
DUT 8	HPP	Nominal	LTE power	▼	▲▼	▼	▼
		TTFF	TTFF	▲▼	▲▼	—	—
		Limited	LTE power	▼	▼	—	—
DUT 11, Ant A	RTK	Nominal	LTE power	▼	▲▼	▼	▼
		TTFF	TTFF	▼	▲▼	—	—
		Limited	LTE power	▼	▼	—	—

## F Supplemental Test Results: Development Board Devices (DEV)

### F.1 Development Board Setup

Development board devices DEVs were tested with the same methodology as the high-performance positioning (HPP) DUT. And in the case of the Ublox M8F 1 PPS timing performance was tested in the same manor as for GPS-disciplined oscillator (GPSDO) DUT. The main difference between the DEV tests and other device under test (DUT) tests was in the long-term evolution (LTE) emissions mask for LTE in-band (IB) uplink bands (UL) and LTE out-of-band (OOB) UL. For the DEV tests, the LTE OOB UL was 3 dB higher with respect to the emissions mask discussed in Subsection 2.3.2. The test matrix for the DEV DUTs follows the same methodology as previously presented DUTs (see Table F.1).

As DEV DUT placement inside the chamber followed the same methodology as for HPP units. The external antenna was mounted boresight with the signaling antenna. Initial system level checks and setups required using the Ublox U-Center software to select relevant National Marine Electronics Association (NMEA) streams and baudrate. The settings were saved to the nonvolatile memory of the DEV DUT. After the intial setup, interfacing with the DEV DUTs was straightforward and followed the programming steps outlined in Section 4.1. The relevant driver settings are in Table F.2 and an example of the data stream output is in Figure F.1.

We solely collected NMEA data for the DEV and used the previously discussed parsing and data analysis techniques. While the DUTs were able to provide binary “UBX” formatted data it did not offer an advantage over the NMEA streams (this was based on inspecting the UBX data outputs with the manufacturers U-center software suite).

The DEV test results are presented in the following sections.

```

$GNRMC,015208.00,A,3135.89366,N,11016.67083,W,0.002,,080716,,,A*73
$GNVTG,,T,,M,0.002,N,0.003,K,A*3C
$GNGGA,015208.00,3135.89366,N,11016.67083,W,1,11,0.77,1380.5,M,-28.4,M,,*49
$GNGSA,A,3,12,13,02,29,05,15,18,20,21,25,26,,1.42,0.77,1.20*1A
$GNGSA,A,3,,,,,,,,,,,,,1.42,0.77,1.20*18
$GPGSV,3,1,11,02,14,076,42,05,40,043,43,12,14,179,42,13,29,101,43*7B
$GPGSV,3,2,11,15,33,143,43,18,30,225,43,20,07,278,43,21,36,294,43*7C
$GPGSV,3,3,11,25,35,211,42,26,13,316,43,29,79,025,43*4C
$GLGSV,1,1,00*65
$GNLL,3135.89366,N,11016.67083,W,015208.00,A,A*60
$GNZDA,015208.00,08,07,2016,00,00*7C
    
```

Figure F.1: 1 second capture of the Ublox EVK-M8F NMEA data stream.

Table F.1: DEV Test Matrix. The DEV DUTs were Evaluated for the Following GPS and LTE Signal Combinations.

Device	Type	GPS Scenario	Test Sweep	LTE Waveform			
				DL	UL 1	UL 2	DL + UL 1
DUT 16	DEV	Nominal	LTE power	☑	☑	☑	☑
DUT 17	DEV	Nominal	LTE power	☑	☑	☑	☑
DUT 18	DEV	Timing	LTE power	☑	☑	—	—
DUT 16	DEV	TTFB	TTFB	☑	☑	—	—
DUT 17	DEV	TTFB	TTFB	☑	☑	—	—
DUT 16	DEV	Limited	LTE power	☑	☑	—	—
DUT 17	DEV	Limited	LTE power	☑	☑	—	—

Table F.2: Development Board Interfacing, Initialization Commands and NMEA Strings Collected. *Italicized NMEA strings* are Used for Data Analysis

Device <sup>1</sup>	Model ID	Type	Interface	Reset Commands	NMEA Strings
UBlox EVK-7M	s/n: 63 f/w: 1.0 (59842) h/w: 00070000	DEV	Serial ASCII 9600 baud	“CFG-RST\r\n”	GPRMC, GPVTG, <i>GPGGA</i> , GPGSA, <i>GPGSV</i> , GPGLL
UBlox EVK-M8F	s/n: 143 f/w: 2.20 (81289) h/w: 00080000	DEV	Serial ASCII 9600 baud	“CFG-RST\r\n”	GNRMC, GNVTG, <i>GNGGA</i> , GNGSA, <i>GPGSV</i> , GLGSV, GNGLL, GNZDA

<sup>1</sup>Certain commercial equipment, instruments, or materials are identified in this report in order to specify the experimental procedure adequately. Such identification is not intended to imply recommendation or endorsement by National Institute of Standards and Technology (NIST) nor is it intended to imply that the materials or equipment identified are necessarily the best available for the purpose.

Table F.3: The Fix Flag Indicators, Leap Second Accounting, and Source of the Timestamp are Shown Below

DUT <sup>1</sup>	Initialization time	Leap Seconds	Fix Quality	Data	Fix Indicator
Ublox EVK-7M	01:35:01 UTC	+17	“GPS fix”	GPGGA	1
Ublox EVK-M8F	01:35:01 UTC	+17	“GPS fix”	GPGGA	1

<sup>1</sup>Certain commercial equipment, instruments, or materials are identified in this report in order to specify the experimental procedure adequately. Such identification is not intended to imply recommendation or endorsement by NIST nor is it intended to imply that the materials or equipment identified are necessarily the best available for the purpose.

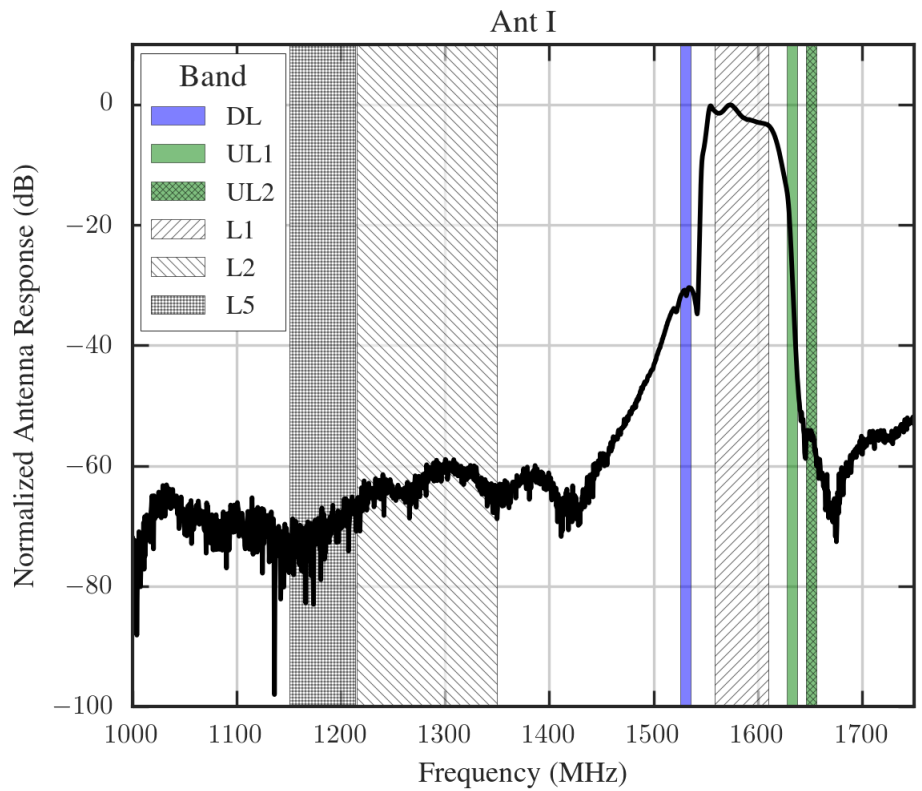


Figure F.2: Normalized  $S_{21}$  S-parameter responses of external DUT antennas.

## F.2 LTE Power Level Sweeps (Nominal GPS Scenario)

Refer to previous parts of this report address the definition and execution of these tests:

- The development board (DEV) GPS receivers under test are listed in Table F.2.
- The incident power condition, effective isotropic incident power (EIIP), is defined in Subsection 2.1.4.
- The simulated GPS signal parameters are listed in Section 2.2.
- The simulated GPS constellation parameters in the nominal power scenario are listed in Subsubsection 2.2.2.1.
- The radiated LTE waveforms are listed in Section 2.3.
- The signal level of each LTE power sweep is defined by Subsection 2.4.1.
- The transmission system that creates the test conditions is detailed in Chapter 3.
- Each DUT under test is positioned according to Section 4.2.
- The test procedure for LTE power level sweeps is detailed by Subsection 4.3.1.
- Data acquisition from each DUT is described by Section 4.4.
- Data parsing and statistical postprocessing is described in Chapter 5.

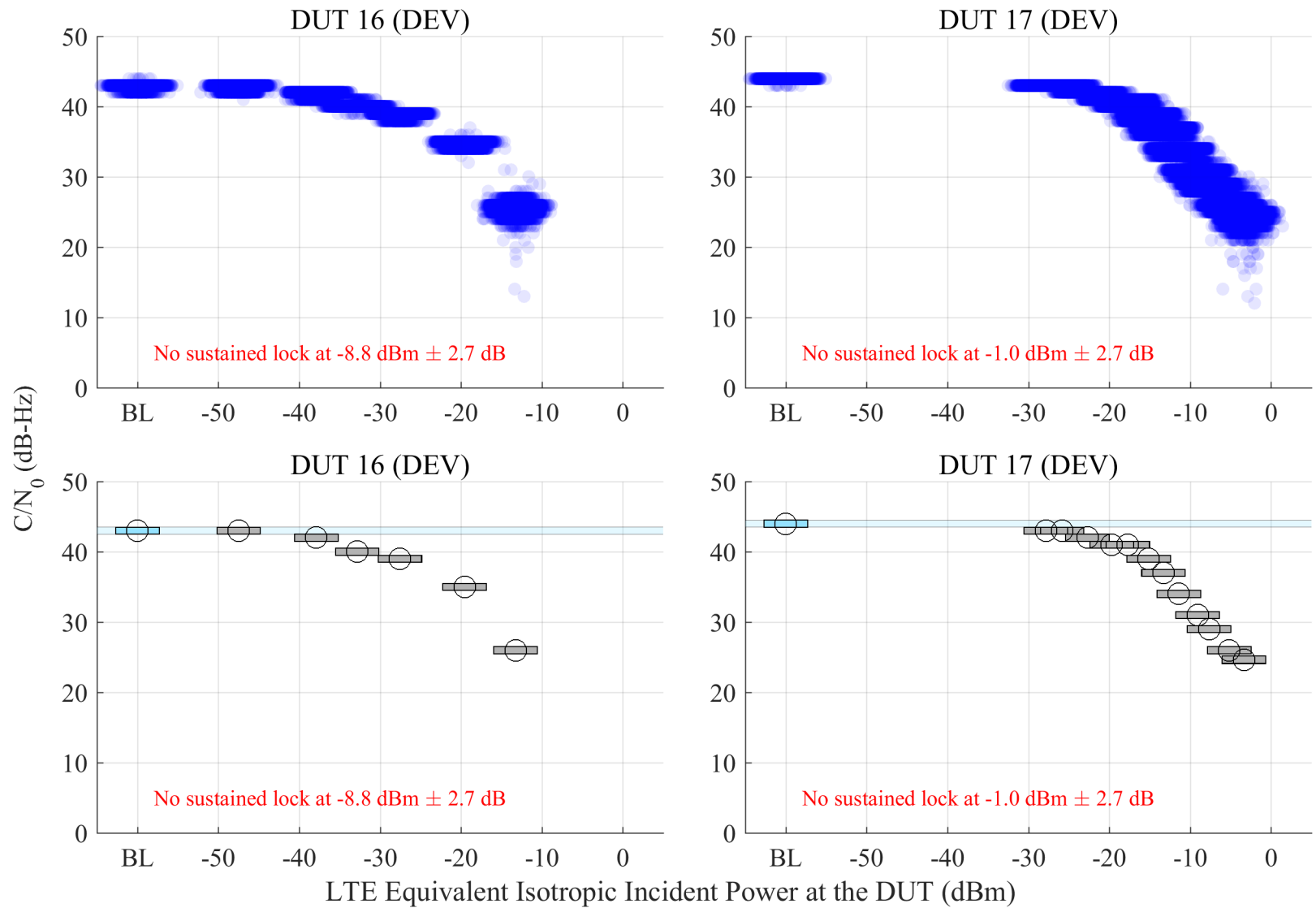


Figure F.3: Scatterplots of reported  $C/N_0$ , and estimated 95% confidence regions of the median of reported  $C/N_0$  from DEV receivers, swept with LTE power level. The GPS scenario is nominal, and the type of incident LTE is DL.

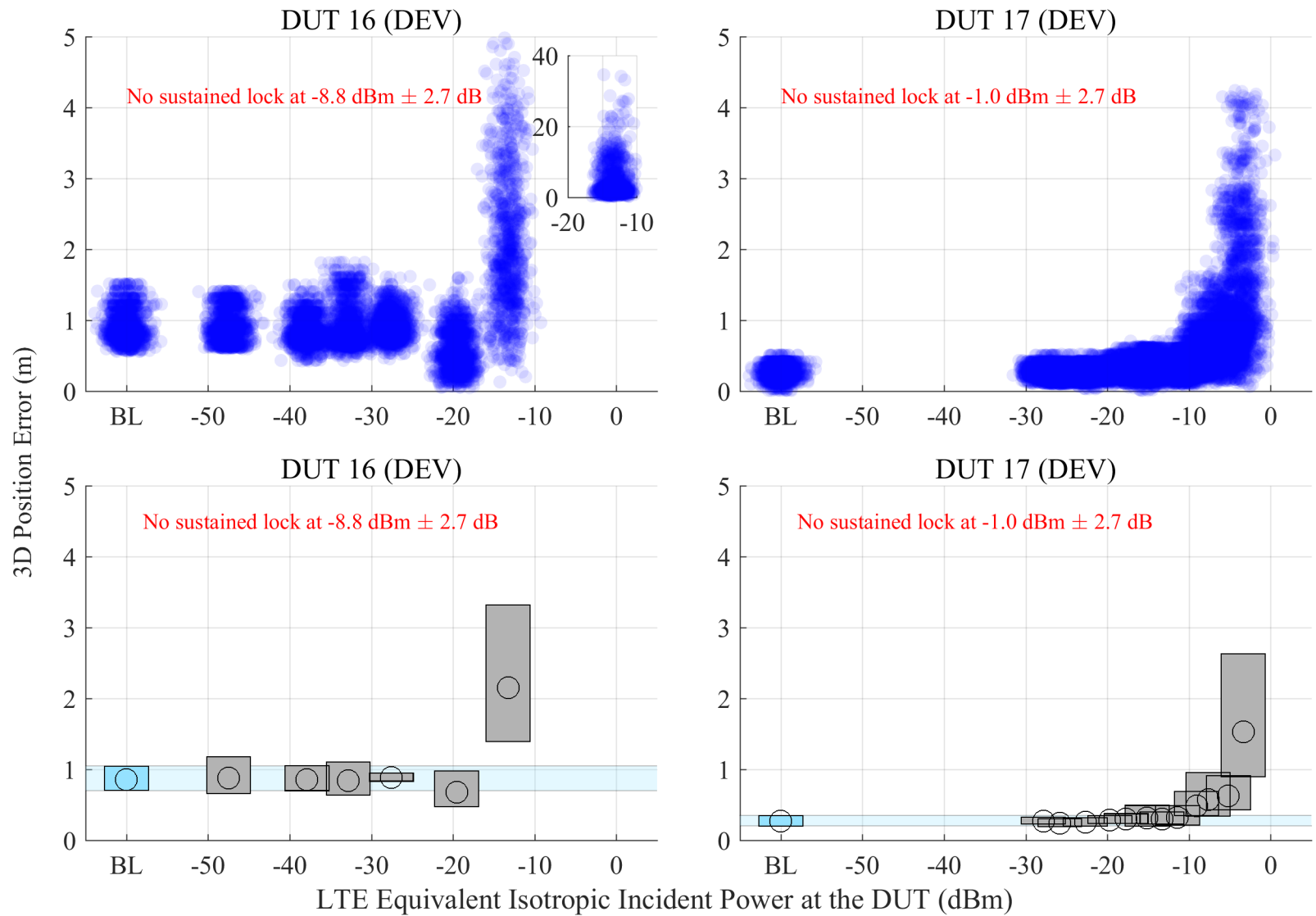


Figure F.4: Scatterplots of error in reported 3-D position compared to simulator truth, and estimated 95% confidence regions of the median error in reported 3-D position from DEV receivers, swept with LTE power level. The GPS scenario is nominal, and the type of incident LTE is DL.

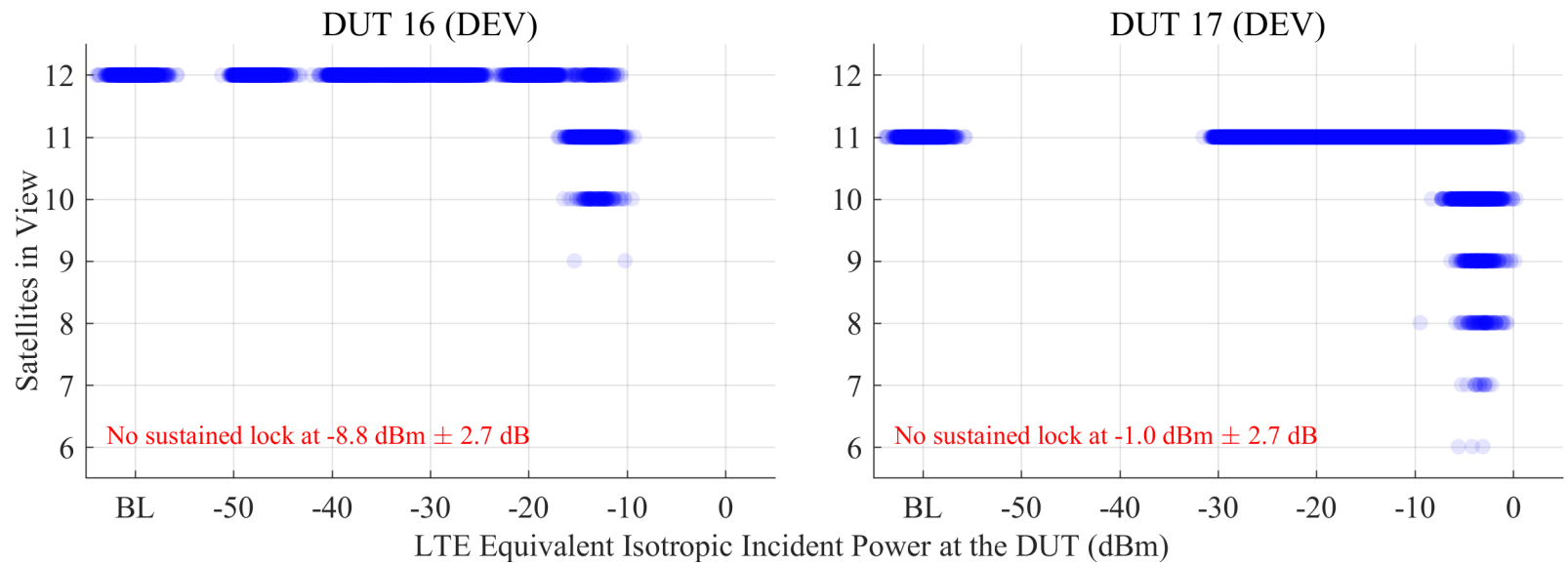


Figure F.5: Scatterplots of the number of satellites in view from DEV receivers, swept with LTE power level. The GPS scenario is nominal, and the type of incident LTE is DL.

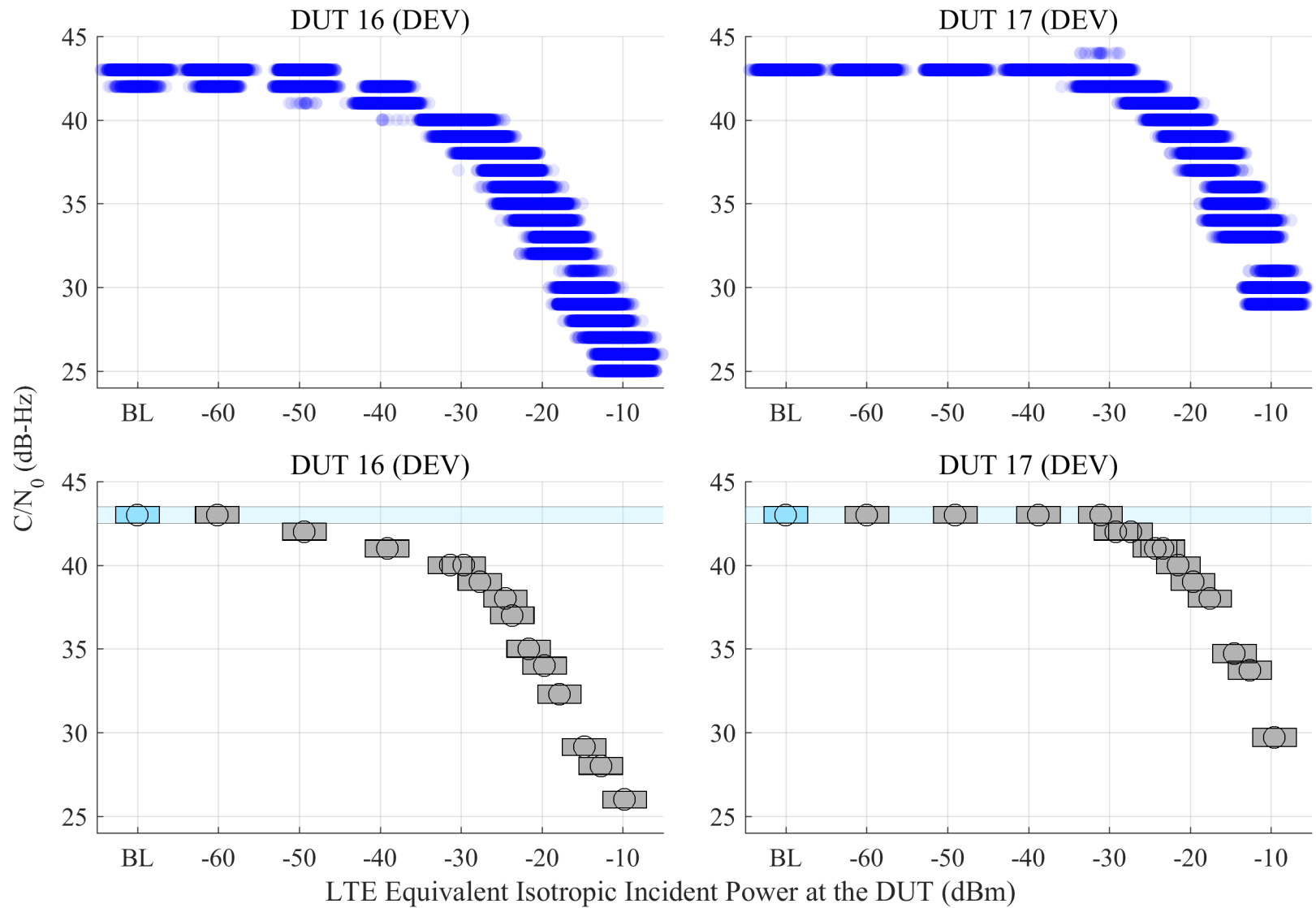


Figure F.6: Scatterplots of reported  $C/N_0$ , and estimated 95% confidence regions of the median of reported  $C/N_0$  from DEV receivers, swept with LTE power level. The GPS scenario is nominal, and the type of incident LTE is UL1.

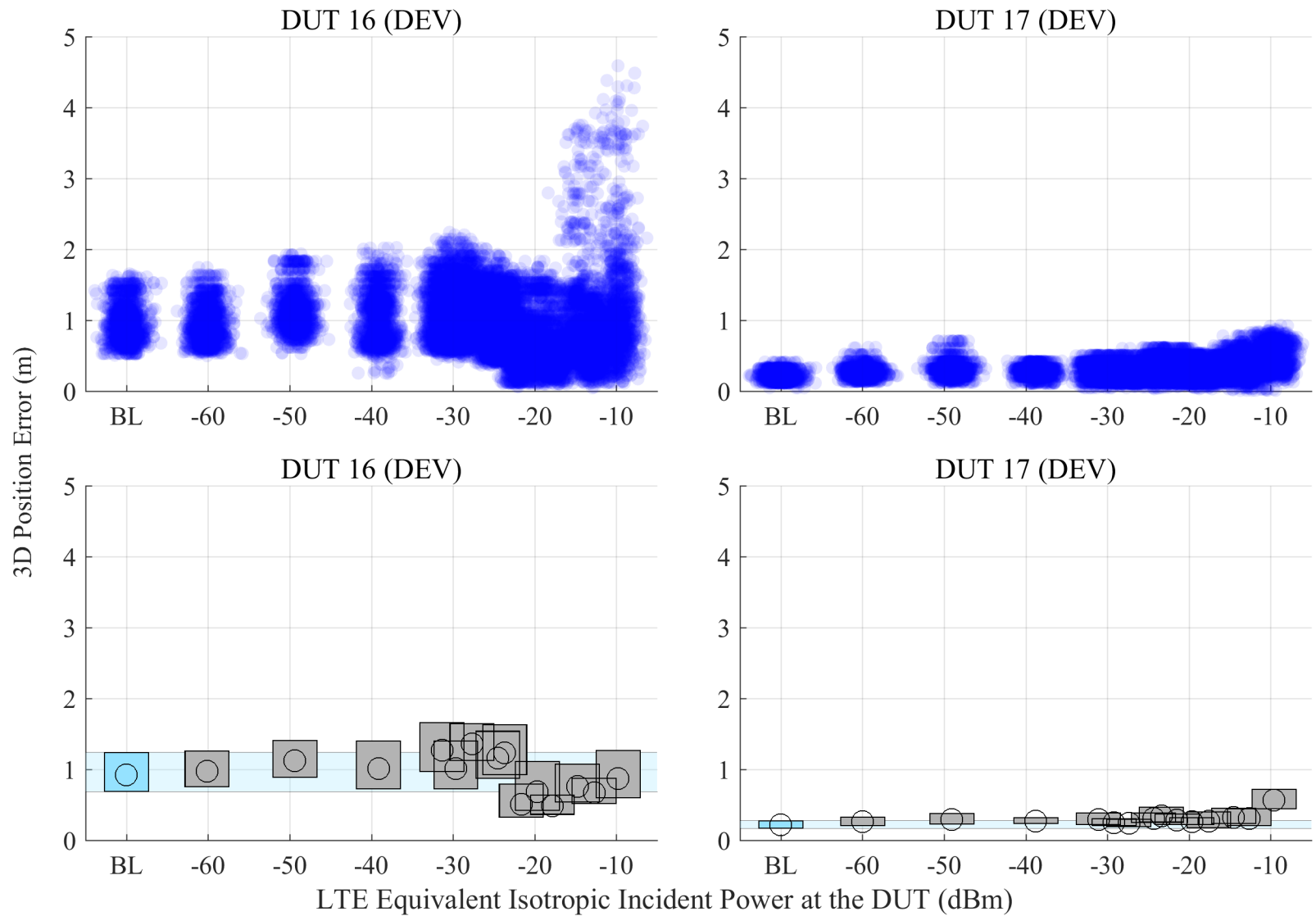


Figure F.7: Scatterplots of error in reported 3-D position compared to simulator truth, and estimated 95% confidence regions of the median error in reported 3-D position from DEV receivers, swept with LTE power level. The GPS scenario is nominal, and the type of incident LTE is UL1.

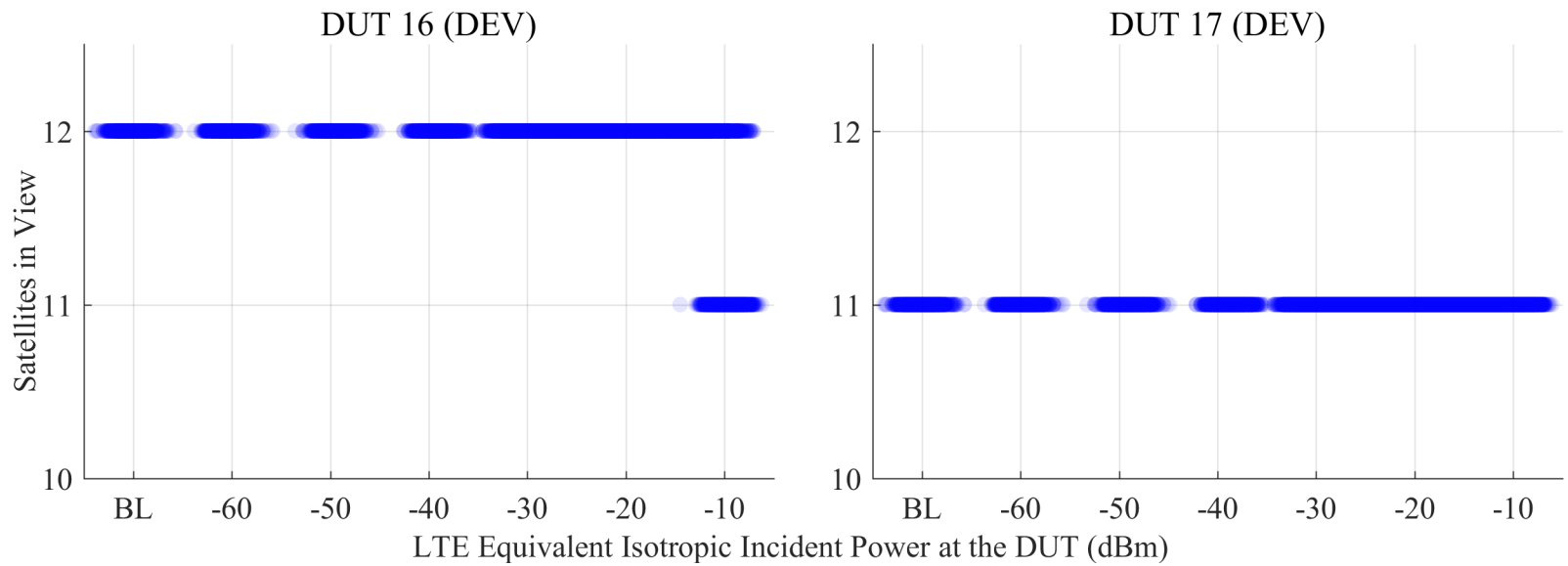


Figure F.8: Scatterplots of the number of satellites in view from DEV receivers, swept with LTE power level. The GPS scenario is nominal, and the type of incident LTE is UL1.

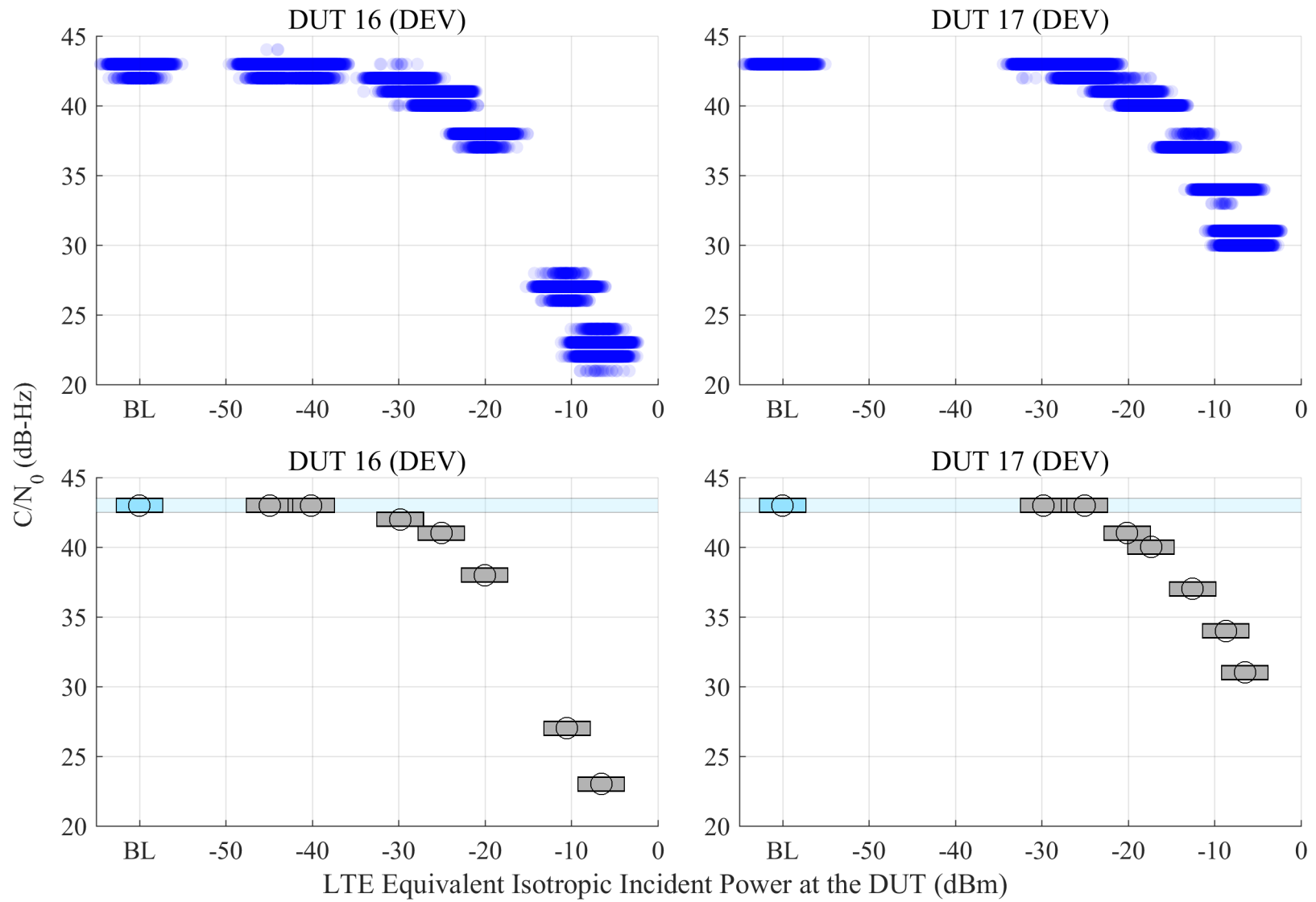


Figure F.9: Scatterplots of reported  $C/N_0$ , and estimated 95% confidence regions of the median of reported  $C/N_0$  from DEV receivers, swept with LTE power level. The GPS scenario is nominal, and the type of incident LTE is UL2.

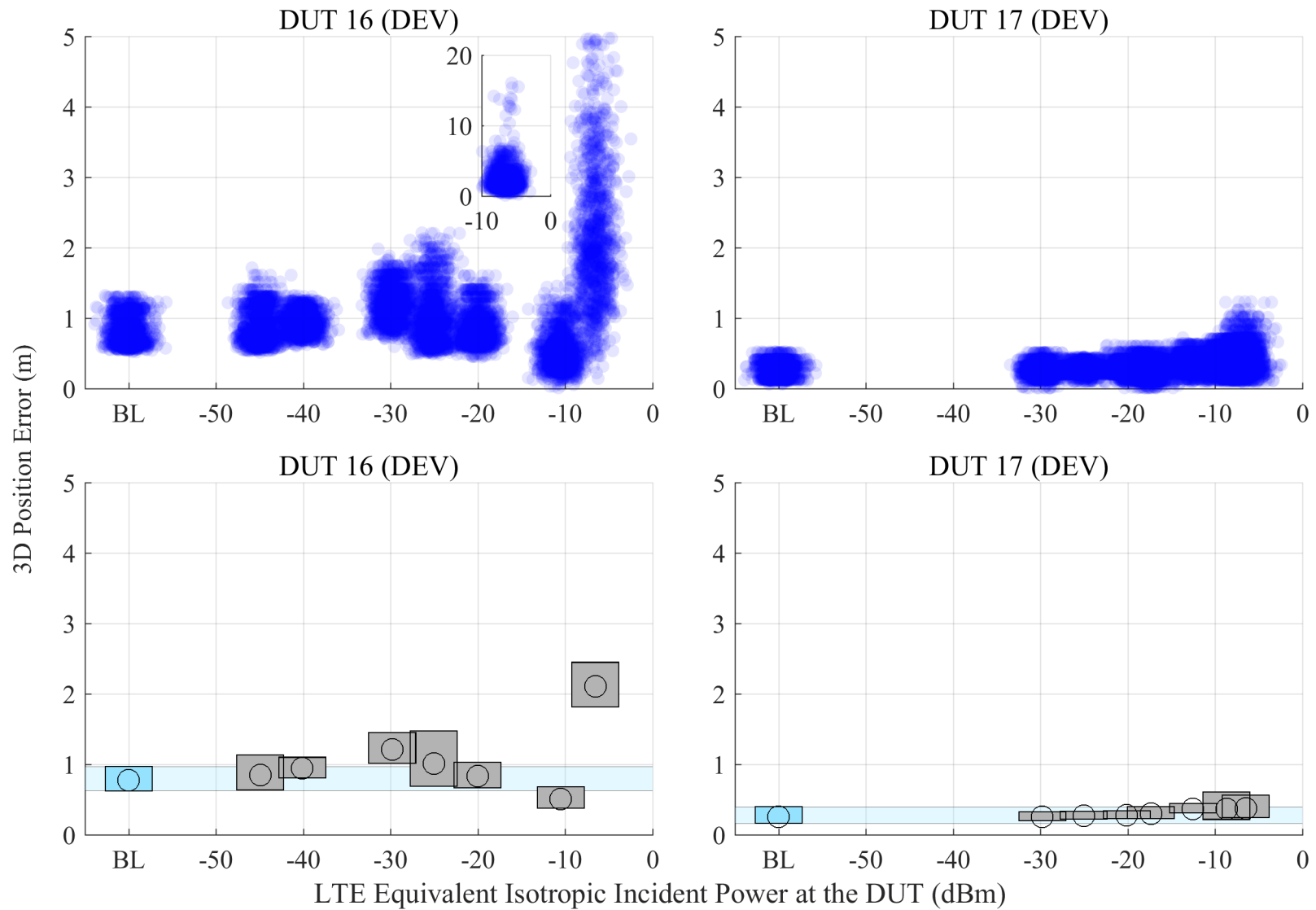


Figure F.10: Scatterplots of error in reported 3-D position compared to simulator truth, and estimated 95% confidence regions of the median error in reported 3-D position from DEV receivers, swept with LTE power level. The GPS scenario is nominal, and the type of incident LTE is UL2.

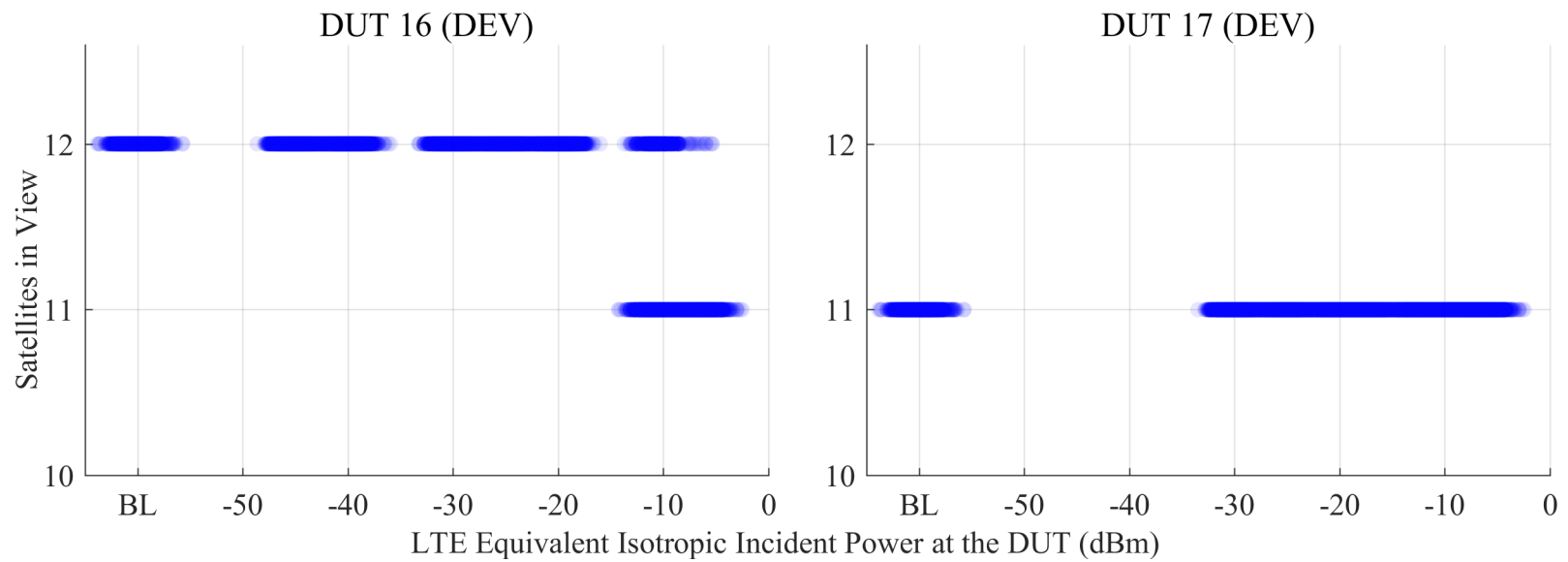


Figure F.11: Scatterplots of the number of satellites in view from DEV receivers, swept with LTE power level. The GPS scenario is nominal, and the type of incident LTE is UL2.

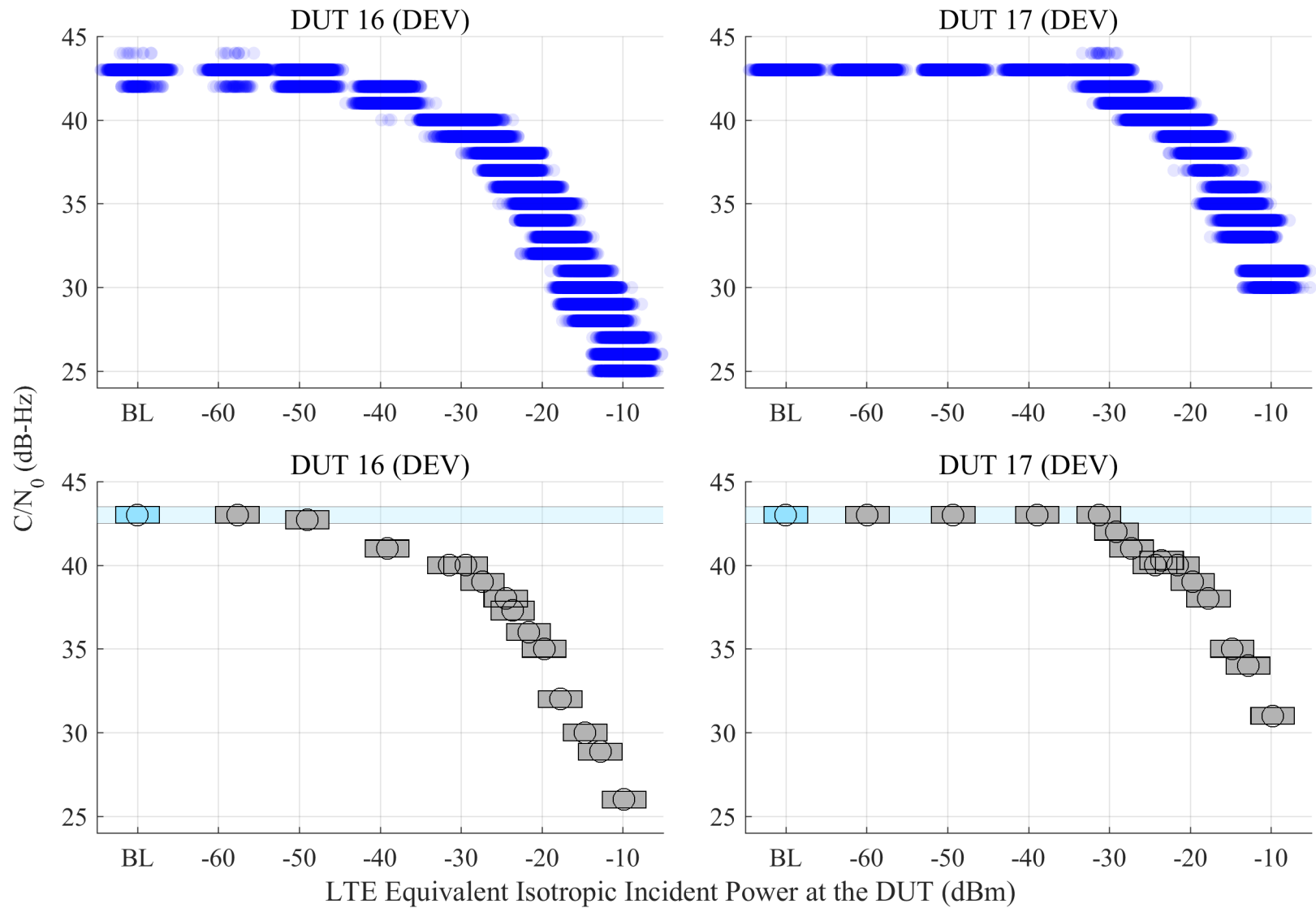


Figure F.12: Scatterplots of reported  $C/N_0$ , and estimated 95% confidence regions of the median of reported  $C/N_0$  from DEV receivers, swept with LTE power level. The GPS scenario is nominal, and the type of incident LTE is DL + UL1. The UL level was swept, and the DL level was fixed at -50 dBm EIIP unless otherwise annotated. The horizontal axis reports the linear sum of DL and UL power.

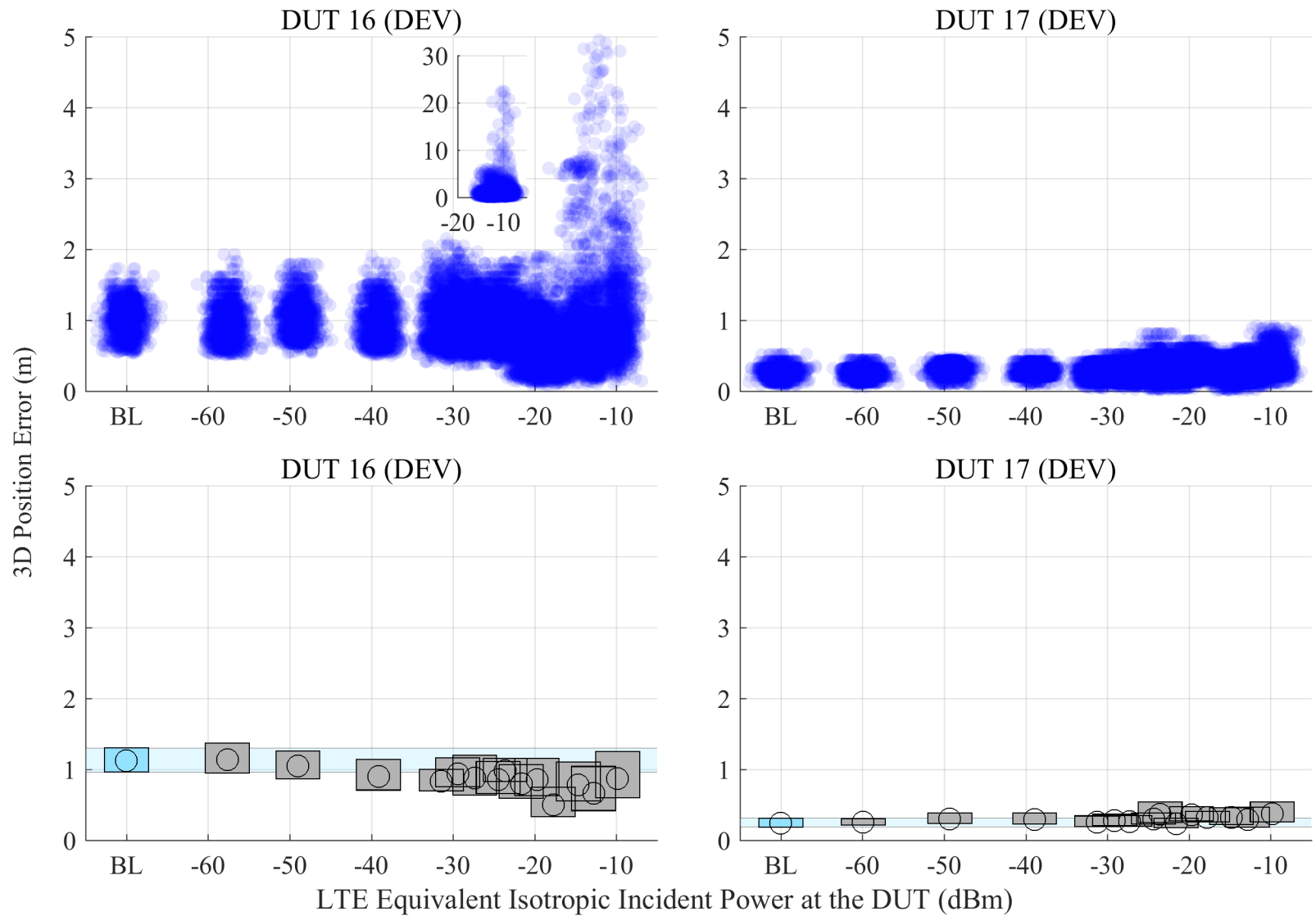


Figure F.13: Scatterplots of error in reported 3-D position compared to simulator truth, and estimated 95% confidence regions of the median error in reported 3-D position from DEV receivers, swept with LTE power level. The GPS scenario is nominal, and the type of incident LTE is DL + UL1. The UL level was swept, and the DL level was fixed at -50 dBm EIIIP unless otherwise annotated. The horizontal axis reports the linear sum of DL and UL power.

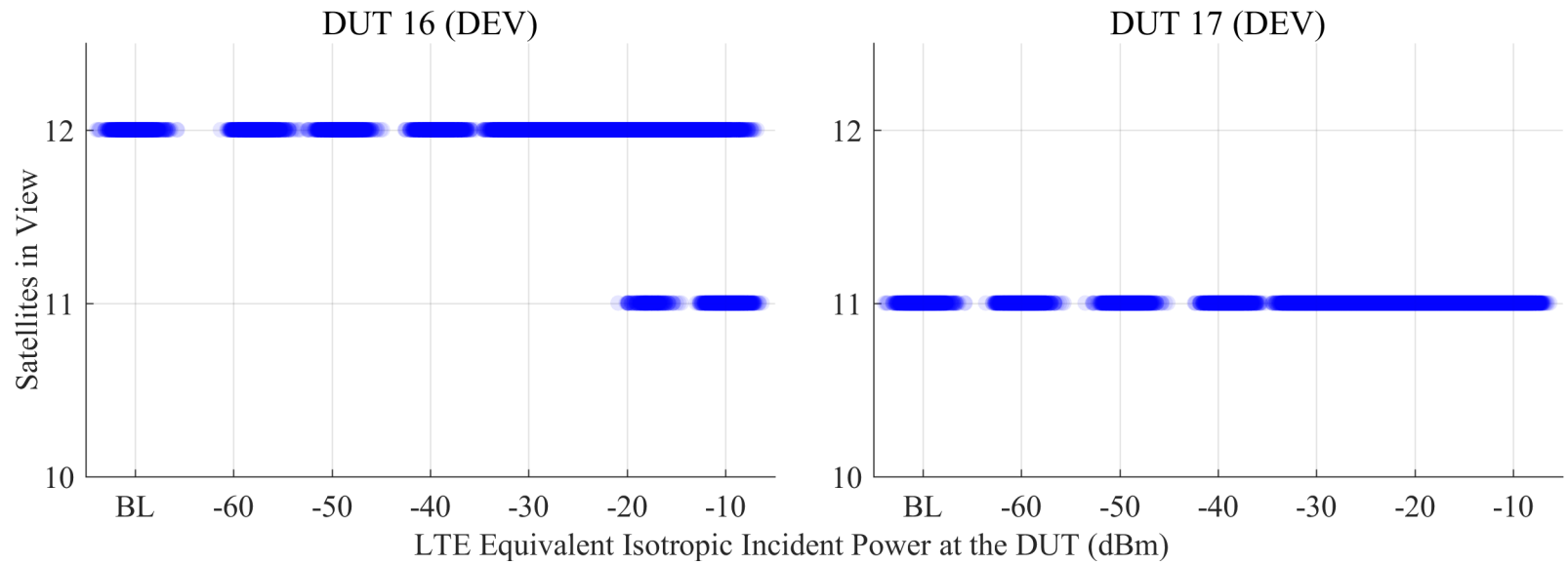


Figure F.14: Scatterplots of the number of satellites in view from DEV receivers, swept with LTE power level. The GPS scenario is nominal, and the type of incident LTE is DL + UL1. The UL level was swept, and the DL level was fixed at -50 dBm EIIP unless otherwise annotated. The horizontal axis reports the linear sum of DL and UL power.

Table F.4: LTE Powers by DUT for the Timing Test. The Uncertainty Corresponds to the 97.5% Confidence Interval.

<b>Device</b>	<b>UL 1 (dBm)</b>	<b>DL (dBm)</b>	<b>DL + UL 1 (dBm)</b>	<b>UL 2 (dBm)</b>
DUT 18	-25.4 ± 2.7 dB	-25.5 ± 2.7 dB	-25.5 ± 2.7 dB	—
	-20.7 ± 2.7 dB	-19.5 ± 2.7 dB	-20.5 ± 2.7 dB	—
	-16.9 ± 2.7 dB	-14.7 ± 2.7 dB	-16.8 ± 2.7 dB	—
	—	-10.4 ± 2.7 dB	—	—

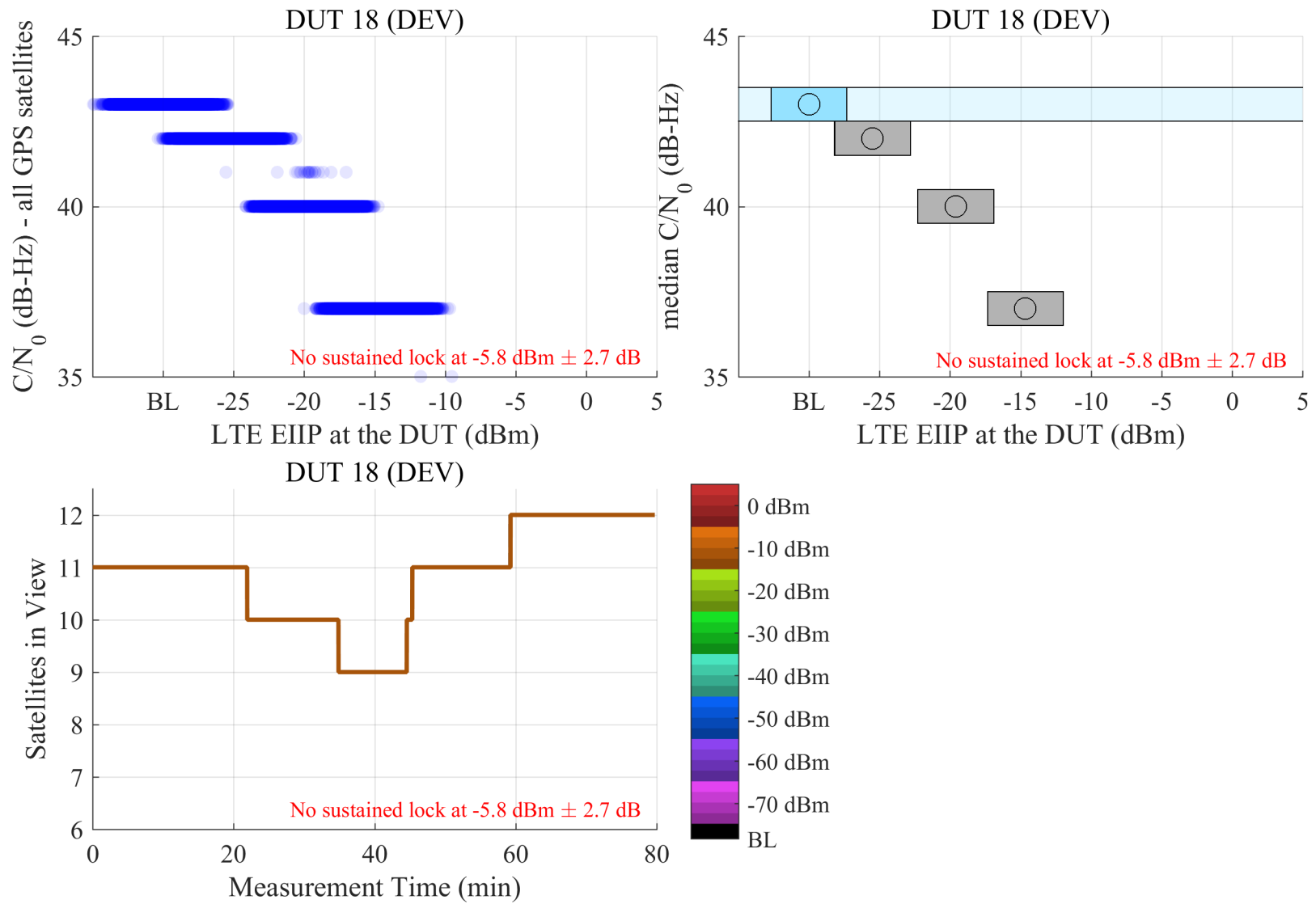


Figure F.15:  $C/N_0$  scatter plots and median, estimated 95% confidence region of the median, and number of satellites in view from DEV receivers, swept with LTE power level. The GPS scenario is timing, and the type of incident LTE is DL.

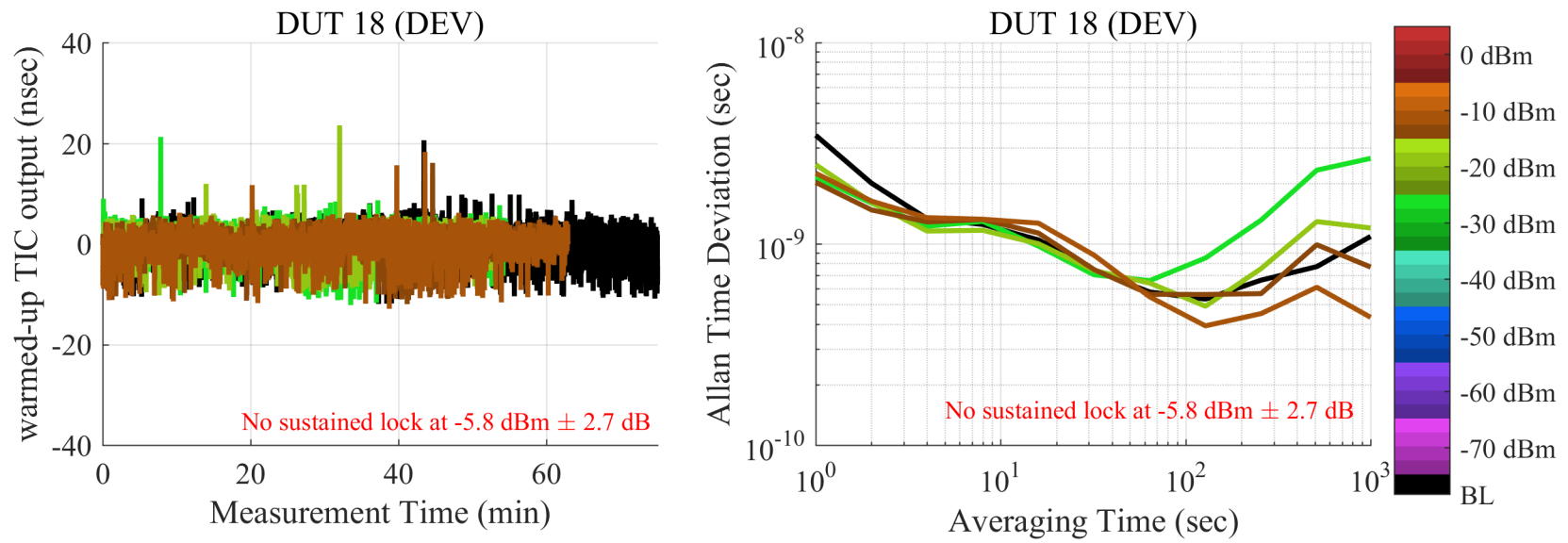


Figure F.16: Plots of stability of GPSDO receiver 1 PPS output measured against the GPS simulator, and Allan time deviation plots from DEV receivers, swept with LTE power level. The GPS scenario is timing, and the type of incident LTE is DL.

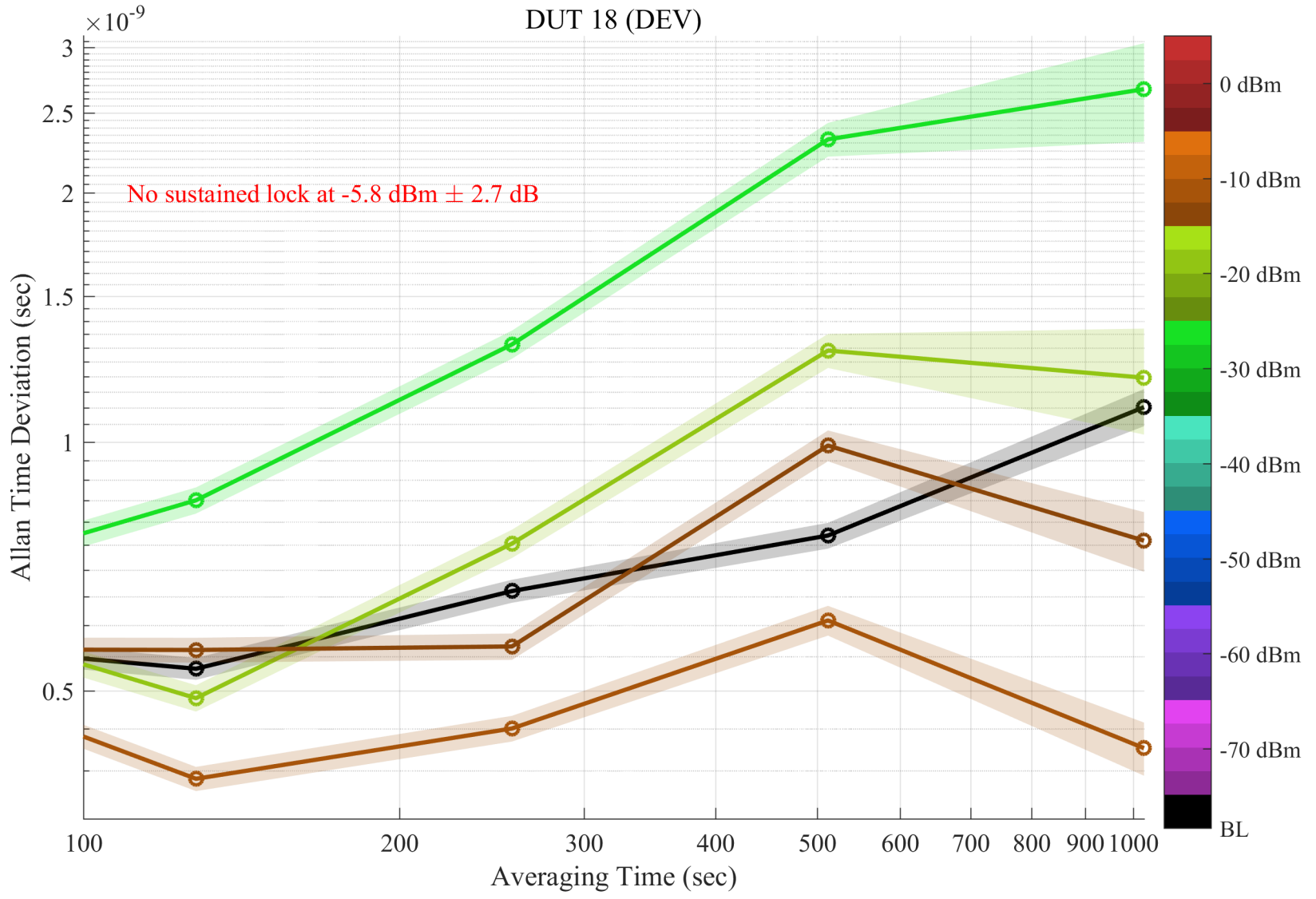


Figure F.17: Zoom of Allan time deviation for DUT 18. Shaded regions indicate pointwise 95% confidence bands. Each curve corresponds to a tested LTE power level. The GPS scenario is timing, and the type of incident LTE is DL.

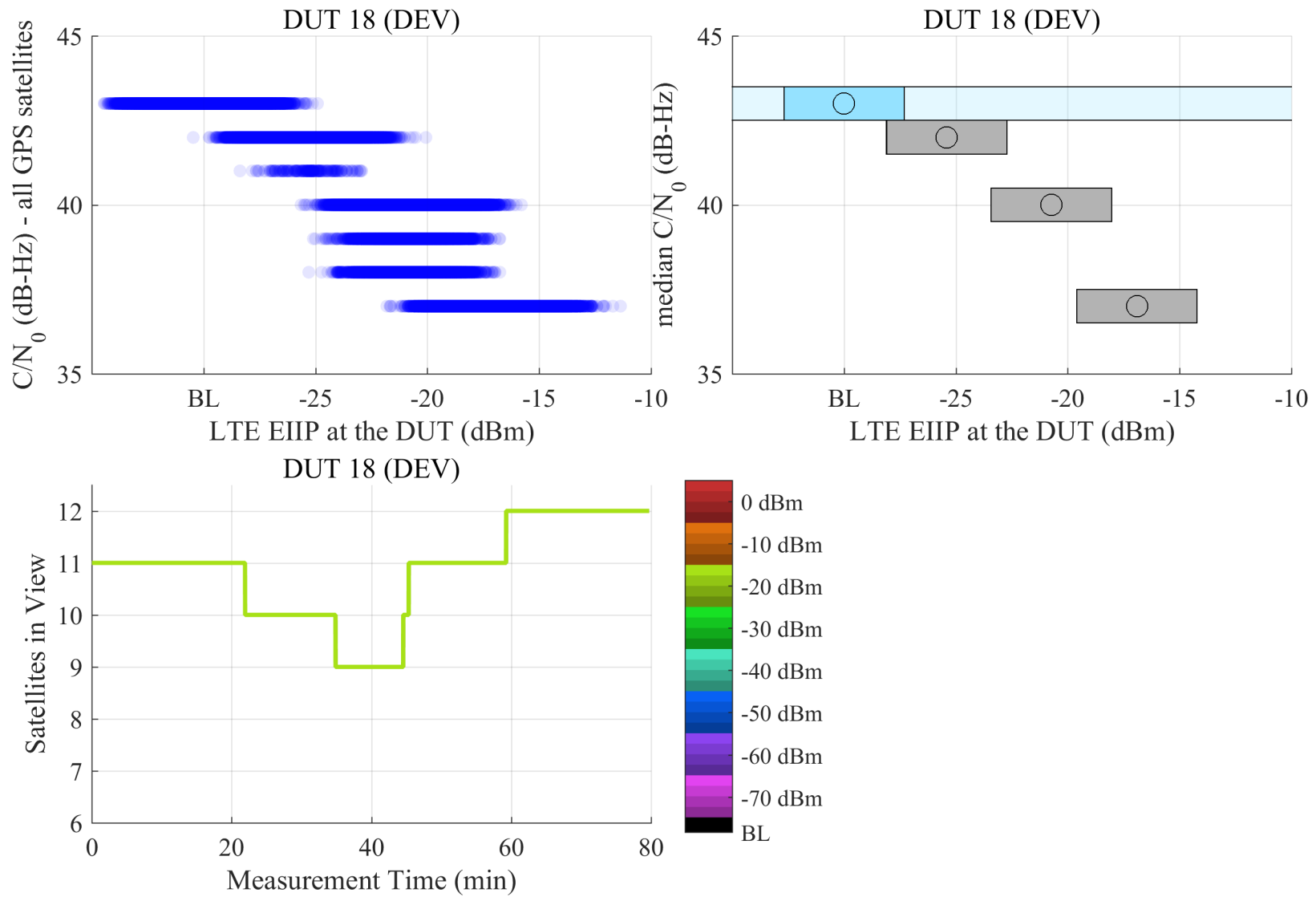


Figure F.18:  $C/N_0$  scatter plots and median, estimated 95% confidence region of the median, and number of satellites in view from DEV receivers, swept with LTE power level. The GPS scenario is timing, and the type of incident LTE is UL1.

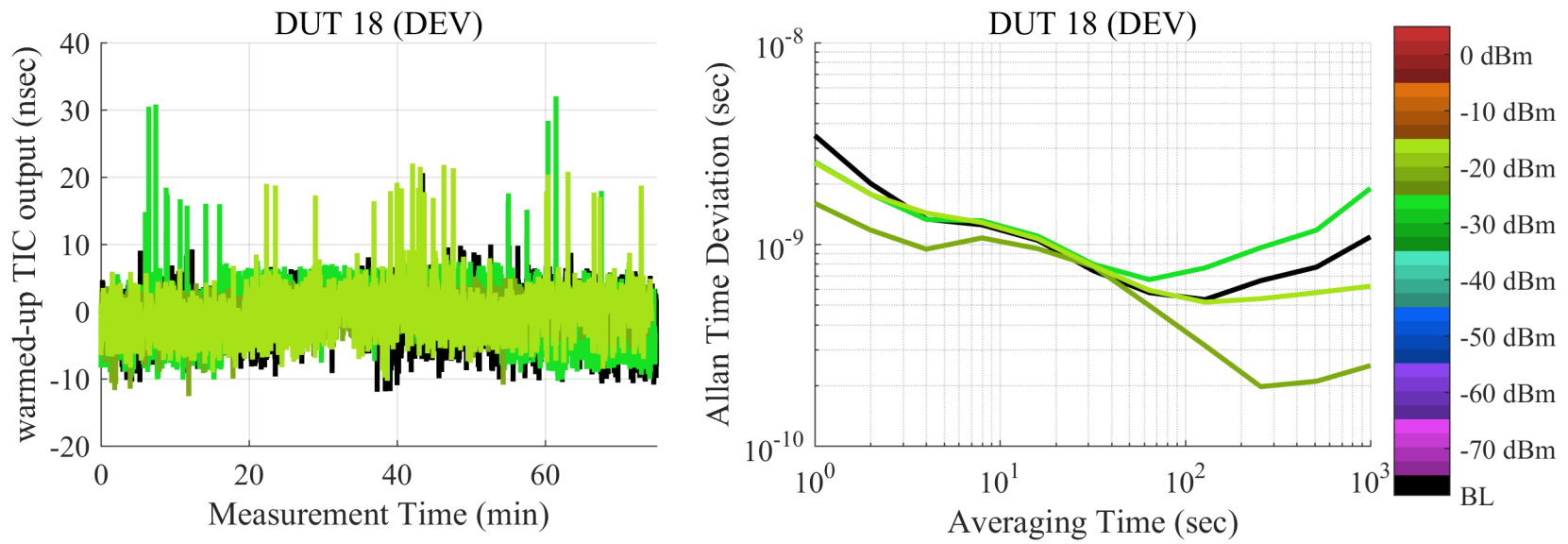


Figure F.19: Plots of stability of GPSDO receiver 1 PPS output measured against the GPS simulator, and Allan time deviation plots from DEV receivers, swept with LTE power level. The GPS scenario is timing, and the type of incident LTE is UL1.

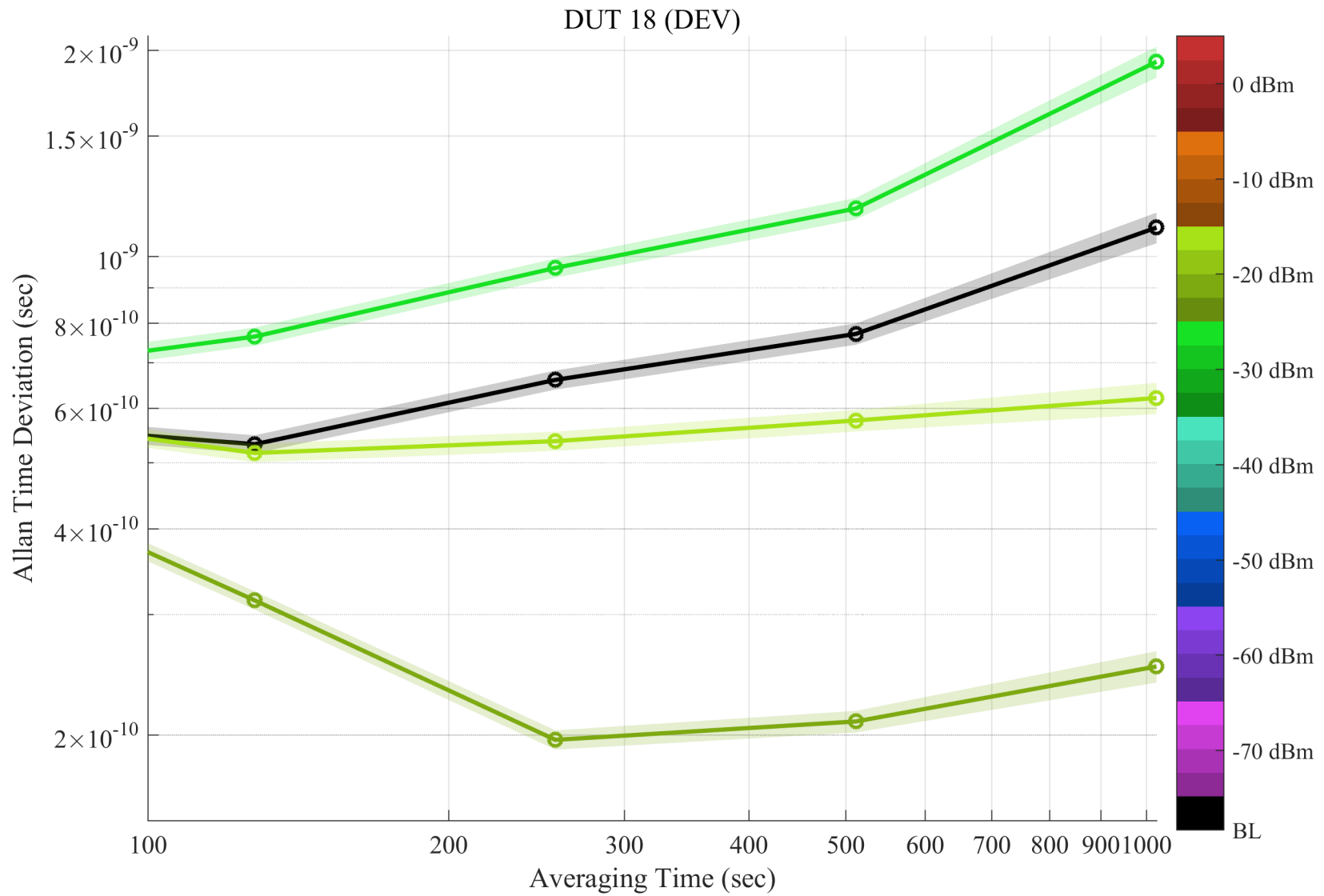


Figure F.20: Zoom of Allan time deviation for DUT 18. Shaded regions indicate pointwise 95% confidence bands. Each curve corresponds to a tested LTE power level. The GPS scenario is timing, and the type of incident LTE is UL1.

Table F.5: LTE Power by DUT for the Time-to-First-Fix Test. The Uncertainty Corresponds to the 97.55% Confidence Interval.

Device	Type	UL 1 (dBm)	DL (dBm)
DUT 16	DEV	-29.5 ±2.7 dB	-27.6 ±2.7 dB
		-23.7 ±2.7 dB	—
		-18.9 ±2.7 dB	—
DUT 17	DEV	-29.3 ±2.7 dB	-27.7 ±2.7 dB
		-23.4 ±2.7 dB	-19.9 ±2.7 dB
		-18.6 ±2.7 dB	-15.5 ±2.7 dB

### F.3 TTFF and TTFR (Nominal GPS Scenario)

Refer to previous parts of this report address the definition and execution of these tests:

- The GPS receivers under test are listed in Subsection 2.1.1.
- The incident power condition, EIIP, is defined in Subsection 2.1.4.
- The simulated GPS signal parameters are listed in Section 2.2.
- The simulated GPS constellation parameters are listed in Subsubsection 2.2.2.1.
- The radiated LTE waveforms are listed in Section 2.3.
- The signal level of each LTE power sweep is defined by Subsection 2.4.2.
- The transmission system that creates the test conditions is detailed in Chapter 3.
- Each DUT under test is positioned according to Section 4.2.
- The test procedure for time to first reacquisition (TTFR) and time to first fix (TTFF) power level sweeps are detailed by Subsection 4.3.2 and Subsection 4.3.3.
- Data acquisition from each DUT is described by Section 4.4.
- Data parsing and statistical postprocessing is described in Chapter 5.

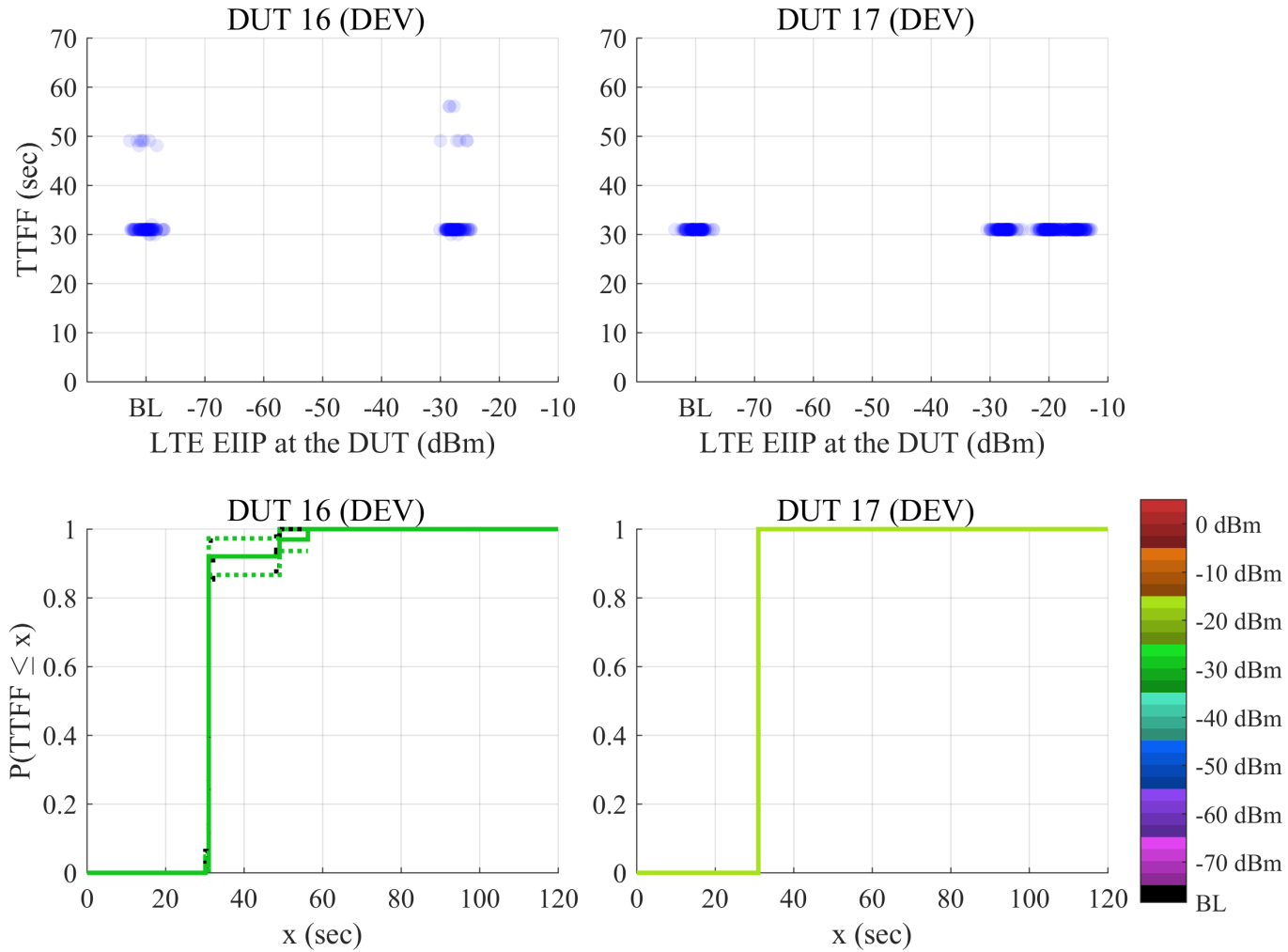


Figure F.21: TTF CDF plots and TTF scatterplots of TTF from lock acquisition reported by DEV receivers at different LTE power levels. The GPS scenario is TTF, and the type of incident LTE is DL.

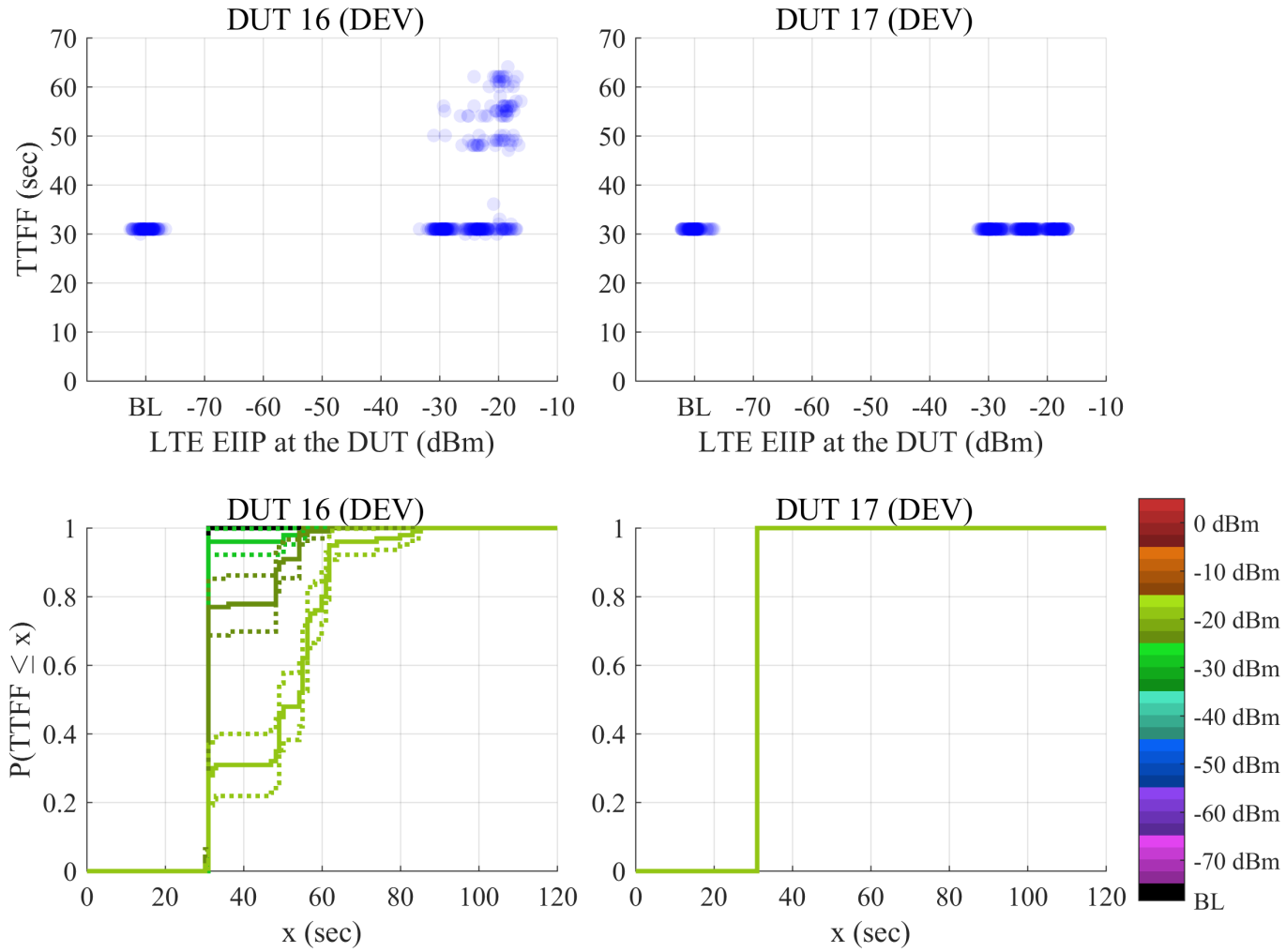


Figure F.22: TTFB CDF plots and TTFB scatterplots of TTFB from lock acquisition reported by DEV receivers at different LTE power levels. The GPS scenario is TTFB, and the type of incident LTE is UL1.

#### **F.4 LTE Power Level Sweeps (Limited GPS Scenario)**

Refer to previous parts of this report address the definition and execution of these tests:

- The GPS receivers under test are listed in Subsection 2.1.1.
- The incident power condition, EIIP, is defined in Subsection 2.1.4.
- The simulated GPS signal parameters are listed in Section 2.2.
- The simulated GPS constellation parameters in the limited scenario are listed in Subsubsection 2.2.2.2.
- The radiated LTE waveforms are listed in Section 2.3.
- The signal level of each LTE power sweep is defined by Subsection 2.4.1.
- The transmission system that creates the test conditions is detailed in Chapter 3.
- Each DUT under test is positioned according to Section 4.2.
- The test procedure for LTE power level sweeps is detailed by Subsection 4.3.1.
- Data acquisition from each DUT is described by Section 4.4.
- Data parsing and statistical postprocessing is described in Chapter 5.

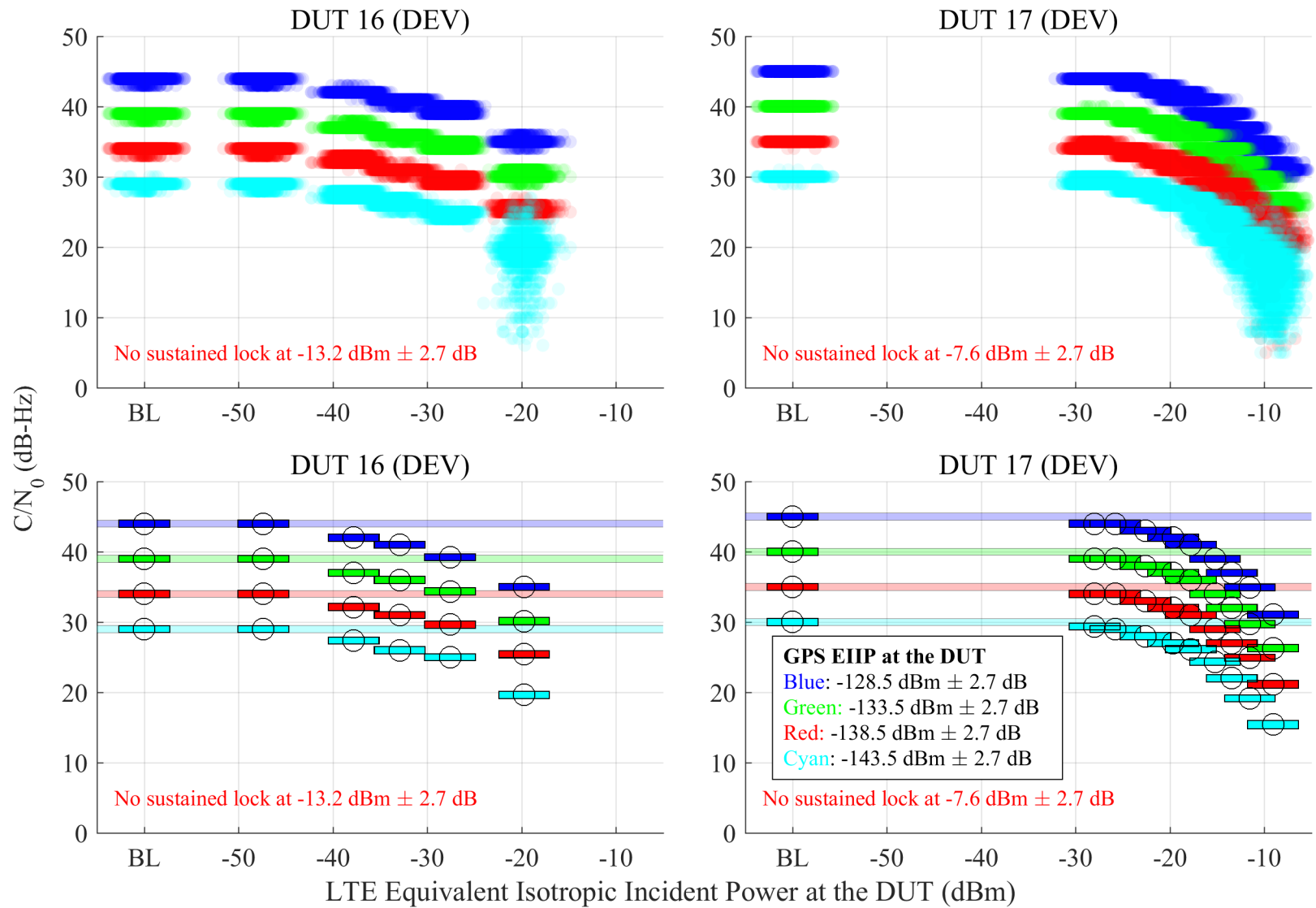


Figure F.23: Scatterplots of reported  $C/N_0$ , and estimated 95% confidence regions of the median of reported  $C/N_0$  from DEV receivers, swept with LTE power level. The GPS scenario is limited, and the type of incident LTE is DL.

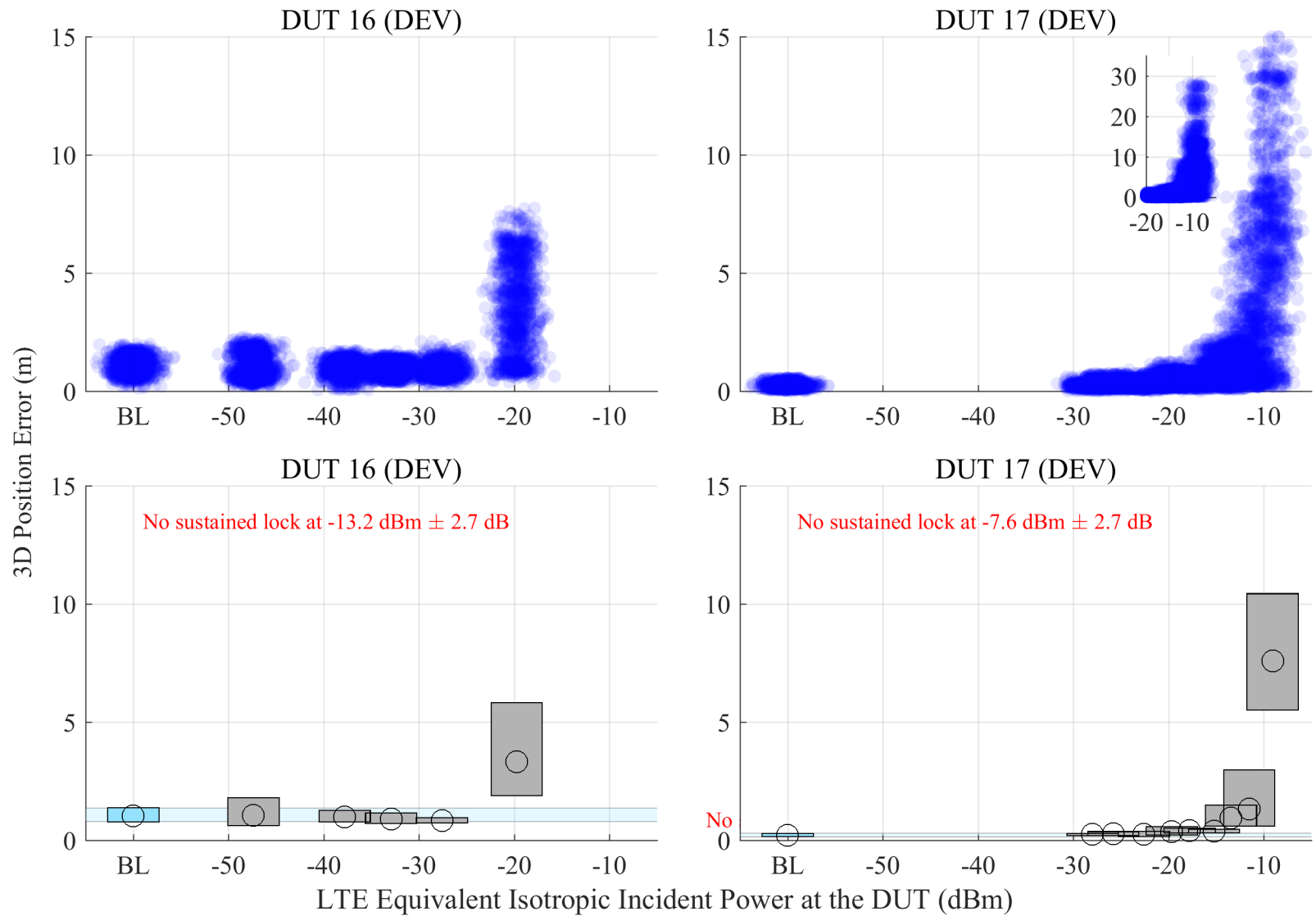


Figure F.24: Scatterplots of error in reported 3-D position compared to simulator truth, and estimated 95% confidence regions of the median error in reported 3-D position from DEV receivers, swept with LTE power level. The GPS scenario is limited, and the type of incident LTE is DL.

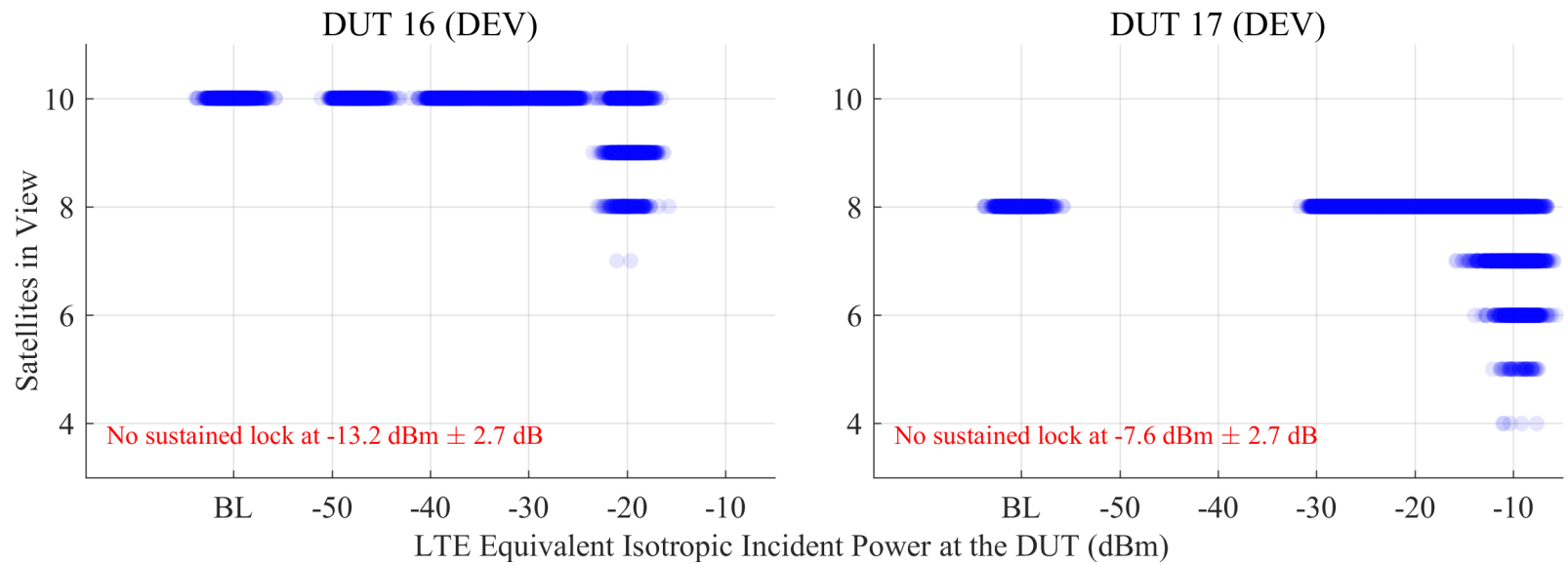


Figure F.25: Scatterplots of the number of satellites in view from DEV receivers, swept with LTE power level. The GPS scenario is limited, and the type of incident LTE is DL.

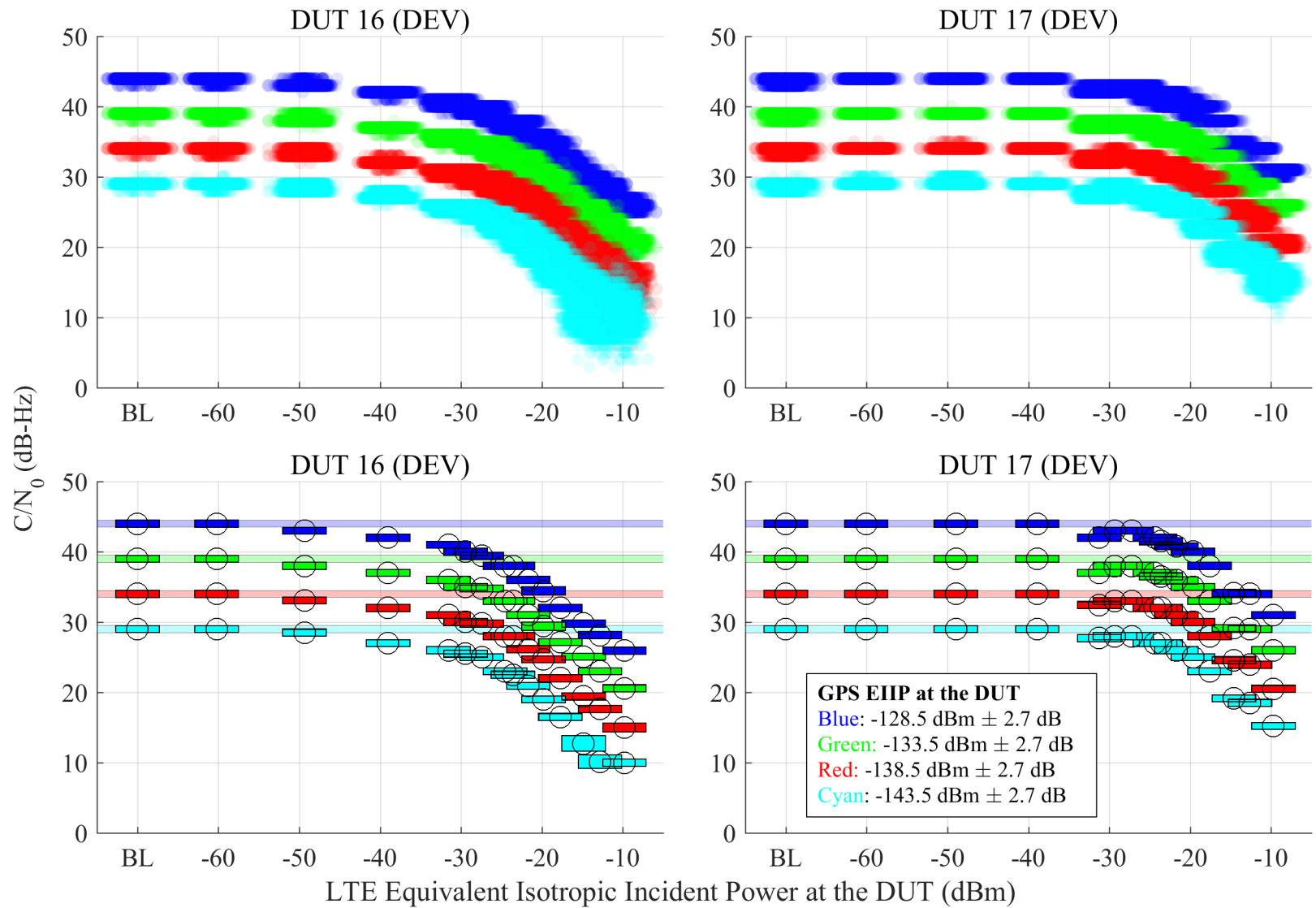


Figure F.26: Scatterplots of reported  $C/N_0$ , and estimated 95% confidence regions of the median of reported  $C/N_0$  from DEV receivers, swept with LTE power level. The GPS scenario is limited, and the type of incident LTE is UL1.

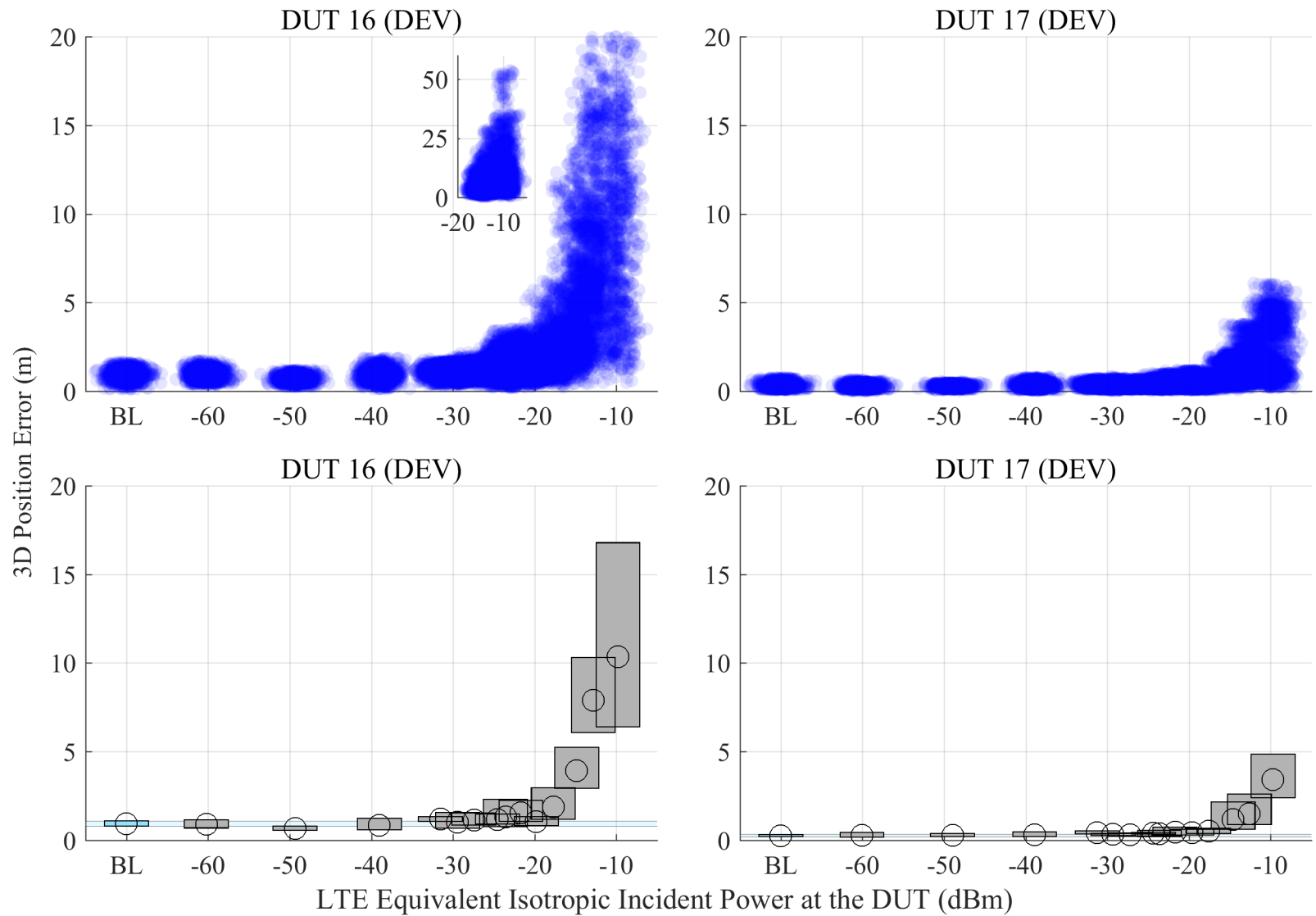


Figure F.27: Scatterplots of error in reported 3-D position compared to simulator truth, and estimated 95% confidence regions of the median error in reported 3-D position from DEV receivers, swept with LTE power level. The GPS scenario is limited, and the type of incident LTE is UL1.

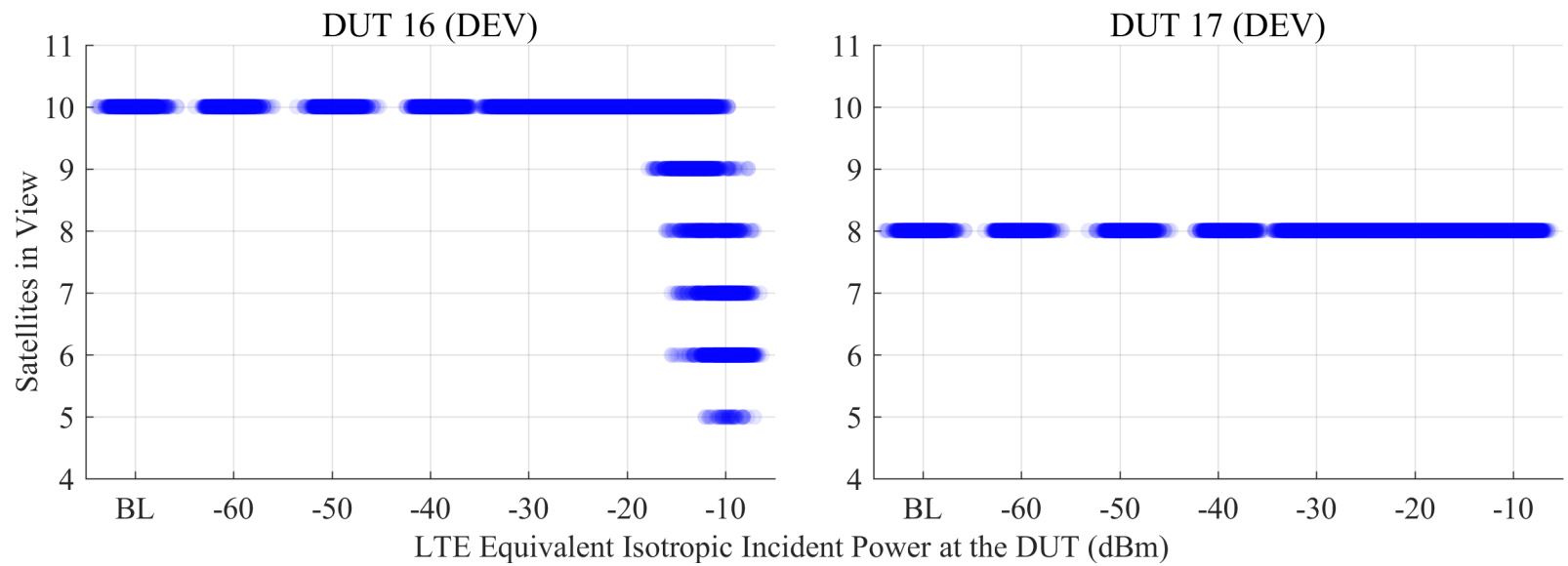


Figure F.28: Scatterplots of the number of satellites in view from DEV receivers, swept with LTE power level. The GPS scenario is limited, and the type of incident LTE is UL1.



## References

- [1] “The National Advanced Spectrum and Communications Test Network (NASCTN) Capability (Memorandum of Agreement),” Mar. 2015 (cit. on pp. vii, 4).
- [2] “GPS Technical Working Group Final Report,” GPS Working Group, 2011 (cit. on pp. x, 3, 4, 17, 44, 45).
- [3] R. Erickson, D. Bunce, “Follow-on Assessment of LightSquared Ancillary Terrestrial Component Effects on GPS Receivers,” National Space-Based Positioning, Navigation, and Timing Systems Engineering Forum (NPEF), Washington, D.C., Jan. 2012 (cit. on pp. x, 3, 4, 44, 45).
- [4] Roberson and Associates, LLC, “GPS Sensitivity Measurement Plan,” Federal Communications Commission, Washington, D.C., IB 12-340, 2015 (cit. on pp. x, 4, 17, 44, 45).
- [5] “Test Plan to Develop Interference Tolerance Masks for GNSS Receivers in the L1 Radiofrequency Band (1559-1610 MHz),” U.S. Department of Transportation, Washington, D.C., IB 12-340, Mar. 2016 (cit. on pp. x, 4).
- [6] B. Taylor, “NIST Technical Note 1297: guidelines for evaluating and expressing the uncertainty of NIST measurement results,” 1994 (cit. on pp. 14, 52, 307).
- [7] “User Equipment (UE) Conformance Specification for UE Positioning; Part 1: Conformance Test Specification,” 3GPP, TS 37.571-1, 2016 (cit. on pp. 17, 267).
- [8] “IEEE 802 LAN/MAN Standards Committee 802.22 WG on WRANs (Wireless Regional Area Networks),” Institute of Electrical and Electronics Engineers, New York, NY, Tech. Rep. 802.22.1, 2011 (cit. on p. 17).
- [9] “Measurements of radiated performance for MIMO and multi-antenna reception for HSPA and LTE terminals,” 3GPP, Tech. Rep. TR 37.976 v11.0.0, 2012 (cit. on pp. 17, 267).
- [10] H. Friis, “A Note on a Simple Transmission Formula,” *Proc. IRE*, vol. 34, no. 5, pp. 254–256, 1946 (cit. on pp. 17, 291).
- [11] “Comment Sought on Ligado’s Modification Applications (Public Notice DA 16-442),” Federal Communications Commission, Washington, D.C., Apr. 2016, pp. 10–12 (cit. on pp. 25, 27, 61).
- [12] “NMEA 0183 - Standard for Interfacing Marine Electronics Devices,” National Marine Electronics Association, Severna Park, MD, USA, version 4.10, Jun. 2012, [http://www.nmea.org/content/nmea\\_standards/nmea\\_standards.asp](http://www.nmea.org/content/nmea_standards/nmea_standards.asp) (cit. on pp. 93, 96).
- [13] R. B. Langley, “NMEA 0183: A GPS Receiver Interface Standard,” *GPS World*, pp. 54–57, Jul. 1995 (cit. on pp. 93, 96).
- [14] “BINEX: Binary Exchange Format,” UNAVCO, <http://binex.unavco.org/binex.html> (cit. on p. 93).
- [15] “RINEX: The Receiver Independent Exchange Format Version 2.11,” International GNSS Service, <ftp://igs.org/pub/data/format/rinex211.txt> (cit. on p. 99).
- [16] L. H. Estey and C. M. Meertens, “TEQC: the multi-purpose toolkit for GPS/GLONASS data,” *GPS Solutions*, vol. 3, no. 1, pp. 42–49, 1999 (cit. on p. 99).

- [17] *SQLite documentation*, <https://sqlite.org/docs.html> (cit. on p. 100).
- [18] E. Kaplan and C. Hegarty, Eds., *Understanding GPS: Principles and Applications*, 2nd ed. Artech House, 2005 (cit. on p. 104).
- [19] K. Hoad, S. Robinson, and R. Davies, “Automating warm-up length estimation,” *Journal of the Operational Research Society*, vol. 61, pp. 1389–1403, 2010 (cit. on p. 105).
- [20] K. Hoad and S. Robinson, “Implementing MSER-5 in commercial simulation software and its wider implications,” in *Proceedings of the 2011 Winter Simulation Conference*, IEEE, 2011, pp. 495–503 (cit. on p. 105).
- [21] P. Heidelberger and P. A. W. Lewis, “Quantile estimation in dependent sequences,” *Operations Research*, vol. 32, no. 1, pp. 185–208, 1984 (cit. on p. 105).
- [22] E. L. Kaplan and P. Meier, “Nonparametric estimation from incomplete observations,” *Journal of the American Statistical Association*, vol. 53, no. 282, pp. 457–481, Jun. 1958 (cit. on p. 107).
- [23] M. Greenwood, “A report on the natural duration of cancer,” *Reports on Public Health and Medical Subjects*, vol. 33, pp. 1–26, 1926 (cit. on p. 107).
- [24] W. N. Venables and B. D. Ripley, *Modern Applied Statistics with S*, 4th ed. New York: Springer, 2013 (cit. on p. 107).
- [25] W. J. Riley, “Handbook of frequency stability analysis,” NIST, Tech. Rep. SP 1065, 2008 (cit. on p. 107).
- [26] G. Casella and R. L. Berger, *Statistical Inference*, 2nd ed. Pacific Grove, CA: Duxbury/Thomson Learning, 2002 (cit. on p. 108).
- [27] “IEEE Std 139-1952 Recommended Practice for Measurement of Field Intensity Above 300 Me from Scientific , and Medical Equipments,” Institute of Electrical and Electronics Engineers, New York, NY, Tech. Rep., 1952 (cit. on p. 267).
- [28] A. A. Smith, R. F. German, and J. B. Pate, “Calculation of Site Attenuation From Antenna Factors.,” *IEEE Trans. Electromagn. Compat.*, vol. EMC-24, no. 3, pp. 301–316, 1982 (cit. on p. 267).
- [29] C. R. Paul, *Introduction to Electromagnetic Compatibility*, 2nd. Hoboken, NJ: Wiley & Sons, 2006 (cit. on p. 267).
- [30] J. C. Schelling, “Some Problems in Short-Wave Telephone Transmission,” *Proc. Inst. Radio Eng.*, vol. 18, no. 6, pp. 913–938, 1930 (cit. on p. 267).
- [31] J. McPetrie and B. Pressey, “A Method of Using Horizontally Polarized Waves for the Calibration of Short-Wave Field-Strength Measuring Sets by Radiation,” *J. Inst. Electr. Eng.*, vol. 13, no. 39, pp. 267–272, 1938 (cit. on p. 267).
- [32] F. Colebrook and A. Gordon-Smith, “The Design and Construction of a Short-Wave Field-Strength Measuring Set,” *J. Inst. Electr. Eng.*, vol. 84, no. 507, pp. 388–398, 1939 (cit. on p. 267).
- [33] K. Bullington, “Radio Propagation at Frequencies above 30 Megacycles,” *Proc. IRE*, vol. 35, no. 10, pp. 128–136, 1947 (cit. on p. 267).
- [34] E. W. Allen, “Very-High-Frequency and Ultra-High-Frequency Signal Ranges as Limited by Noise and Co-channel Interference,” *Proc. Inst. Radio Eng.*, vol. 35, no. 2, pp. 128–136, 1947 (cit. on p. 267).
- [35] D. G. Kuester, D. R. Novotny, and J. R. Guerrieri, “Forward and Reverse Link Constraints in UHF RFID with Passive Tags,” in *Proc. 2010 IEEE Symp. Electromagn. Compat.*, 2010, pp. 680–685 (cit. on p. 267).

- [36] D. Kuester, D. Novotny, J. Guerrieri, R. Direen, and Z. Popovic, "Reference Modulation for Calibrated Measurements of Tag Backscatter," in *Proc. IEEE Conf. RFID*, 2011, pp. 154–161 (cit. on p. 267).
- [37] D. R. Novotny, D. G. Kuester, and J. R. Guerrieri, "A reference modulated scatterer for ISO18000-6 UHF tag testing," *IEEE Electromagn. Compat. Mag.*, vol. 1, no. 3, pp. 103–106, Jul. 2012 (cit. on p. 267).
- [38] P. V. Nikitin and K. V. S. Rao, "Antennas and Propagation in UHF RFID Systems," in *2008 IEEE Int. Conf. RFID*, 2008, pp. 277–288 (cit. on p. 267).
- [39] S. Saunders and A. Aragón-Zavala, *Antennas and Propagation for Wireless Communication Systems*, 2nd. John Wiley & Sons, 2007, p. 90 (cit. on p. 267).
- [40] A. Saakian, *Radio Wave Propagation Fundamentals*. Artech House, 2011, p. 120 (cit. on p. 267).
- [41] "IEEE Standard for Definitions of Terms for Antennas," IEEE Standards Association, Tech. Rep., 2013 (cit. on p. 268).
- [42] E. Falletti, M. Pini, and L. L. Presti, "Low complexity carrier-to-noise ratio estimators for gnss digital receivers," *IEEE Transactions on Aerospace and Electronic Systems*, vol. 47, no. 1, pp. 420–437, Jan. 2011 (cit. on pp. 271, 272).
- [43] "Electromagnetic Interference Measurement Antennas; Standard Calibration Method," Society of Aerospace Engineers, SAE ARP 958 Rev D, Feb. 2003 (cit. on p. 291).
- [44] M. Alexander, M. Salter, D. Gentle, D. Knight, B. Loader, and K. Holland, "Calibration and use of antennas, focusing on EMC applications," U.K. National Physical Laboratory, Good Practice Guide No. 73, Dec. 2004 (cit. on pp. 291, 295).
- [45] T. Hertel and G. Smith, "Analysis and design of two-arm conical spiral antennas," *IEEE Transactions on Electromagnetic Compatibility*, vol. 44, no. 1, pp. 1389–1403, 2002 (cit. on p. 292).
- [46] *Rohde and Schwarz FSW signal and spectrum analyzer specifications, version 19.00*, [https://cdn.rohde-schwarz.com/pws/dl\\_downloads/dl\\_common\\_library/dl\\_brochures\\_and\\_datasheets/pdf\\_1/service\\_support\\_30/FSW\\_dat-sw\\_en\\_5214-5984-22\\_v1900.pdf](https://cdn.rohde-schwarz.com/pws/dl_downloads/dl_common_library/dl_brochures_and_datasheets/pdf_1/service_support_30/FSW_dat-sw_en_5214-5984-22_v1900.pdf), Aug. 2016 (cit. on p. 293).